COORDINATION AND REDOX CHEMISTRIES OF THE RARE EARTHS WITHIN REDOX ACTIVE NITROXIDE LIGAND FRAMEWORKS

Justin A. Bogart

A DISSERTATION

in

Chemistry

Presented to the Faculties of the University of Pennsylvania

in

Partial Fulfillment of the Requirements for the
Degree of Doctor of Philosophy

2015

Supervisor of Dissertation

_____

Prof. Eric J. Schelter, Associate Professor of Chemistry

Graduate Group Chairperson

_____

Prof. Gary Molander, Hirschmann-Makineni Professor of Chemistry

Dissertation Committee:
Prof. Donald H. Berry, Professor of Chemistry
Prof. Ivan J. Dmochowski, Professor of Chemistry
Prof. Daniel J. Mindiola, Presidential Professor

COORDINATION AND REDOX CHEMISTRIES OF THE RARE EARTHS WITHIN REDOX ACTIVE NITROXIDE LIGAND FRAMEWORKS

Dedication

To my loving grandpa, Fred Ezra Tawil, for always believing in me and guiding me in my pursuit of knowledge. I know you are still looking down on me from above and I hope to continue to make you proud.

Acknowledgements

First and foremost I would like to thank my advisor, Professor Eric J. Schelter, who has been a mentor to me for the past five years and whom I hope will continue to be a mentor as I pursue a career in academia. I would also like to thank my committee members, Professors Donald H. Berry, Ivan J. Dmochowski, Daniel J. Mindiola, and So-Jung Park, for their helpful suggestions on where to take my research and how to fix the problems that inevitably arose. Thanks also to the wonderful staff, Drs. Patrick J. Carroll, Jun Gu, and George Furst, who run our top-of-the-line X-ray crystallography and NMR facilities. Without them there would have been very little data to put in this dissertation. And, thanks to Professor Christopher Graves for his as always helpful discussions.

Thanks also to my amazing colleagues past and present (there have been too many of them to list) who have been more than willing to listen to me ramble on and on about my chemistry over the past five years; this dissertation would not have been possible without their support and I apologize for forcing them to put up with my incessant singing and dancing in the laboratory. Thanks, particularly, to the people with whom I have had the pleasure to directly collaborate, Dr. Corwin H. Booth, Dr. David Weinberger, Dr. Nicolas Piro, Dr. Andrew Lewis, Bren Cole, Michael Boreen, Connor Lippincott, and Heui Beom Lee; without their hard work and dedication to the chemistry, none of this would have been possible.

Thanks to my ever supportive family whose positive energy and calming presence has helped me through the thick and thin. And, thanks to my Penn Quidditch and New Deck karaoke “families” who have helped keep me sane these past few years.

Finally, thanks to Jessica Levin and Peter Nopachinda who were kind enough to put a roof over my head as I finished up this dissertation.

ABSTRACT

COORDINATION AND REDOX CHEMISTRIES OF THE RARE EARTHS WITHIN REDOX ACTIVE NITROXIDE LIGAND FRAMEWORKS

Justin A. Bogart

Eric J. Schelter

The rare earth elements, La–Lu, Sc and Y, are vital components of many technologies. Production processes of these ions, however, involve inefficient and costly separations steps that are associated with large amounts of waste. This work develops the coordination and redox chemistries of the rare earth ions within nitroxide ligand frameworks with particular emphasis on improving the current state of separations. The synthesis and characterization of a family of *N*-*tert*-butyl-*N*-2-pyridyl hydroxylamines are described. These were used as ligands and oxidants towards cerium and a series of highly stabilized Ce^{IV} complexes were formed. These established the basis of a ligand field series for the 4f-block using combinations of solution electrochemistry and DFT techniques. Modification of the pyridyl nitroxide system led to the development of a tripodal nitroxide ligand, whose coordination chemistry to the rare earth ions was exploited for early/late rare earth separations. The redox chemistry of the rare earth ions within this tripodal nitroxide ligand environment was also explored. The techniques established with these projects were applied to the understanding of the newly discovered biological role of the rare earths for methanol dehydrogenase reactivity.

Table of Contents

List of Tables

CHAPTER 1

CHAPTER 2

CHAPTER 3

CHAPTER 4

CHAPTER 5

CHAPTER 6

List of Figures

CHAPTER 1

CHAPTER 2

CHAPTER 3

CHAPTER 4

CHAPTER 5

CHAPTER 6

List of Schemes

CHAPTER 3

CHAPTER 4

CHAPTER 5

Chapter 1

Outline and Introduction to the Dissertation

1.1 Outline

The research described in this dissertation focuses on the coordination chemistry of the 4f-block elements with redox active ligands, in particular compounds with nitroxide ($R_2N–O$) moieties. Our hypothesis and motivation for the work was that nitroxides, which are persistent and stable in both the oxidized, neutral radical, and reduced, closed shell, anionic redox form, could act as both oxidants and ligands towards supporting high oxidation state rare earth (La–Lu, Y and Sc) complexes. Synthesizing and characterizing the complexes would advance the coordination chemistry of this underexplored group of elements with the ultimate goal of exploiting unique redox properties toward new methods for rare earth metal separations. Development of new separations methods was accomplished through rational ligand design enabled by the use of cyclic voltammetry, X-ray crystallography, and density functional theory (DFT). The work reported herein sets the groundwork for targeted rare earth separations, Lewis acid catalysis, and furthering our understanding of the recently discovered biological role of the rare earth elements.[1]

In **Chapter 2**, the development of methods for the synthesis of a family of *N-tert*-butyl-*N*-2-pyridyl nitroxide radicals with varying pyridyl substituents is described. By modifying a previously published procedure for the parent compound, 2-(^{t}BuNOH)py, we achieved higher yields for these compounds, simplified their purification, and extended the chemistry to pyridyl hydroxylamines with 5–CF_3, 5–Me, 5–MeS, 3–OMe, 4–NMe_2, and 5–NMe_2 substituents. These substitutions allowed for the fine-tuning of the oxidative ability of these compounds. Through the combined use of solution electrochemistry and DFT, we established a methodology for predicting the redox properties of new derivatives within this class of compounds.

In **Chapter 3**, we describe the use of these pyridyl nitroxide compounds as ligands towards cerium. Homoleptic dimers of cerium(III) and homoleptic monomers of cerium(IV) were reported

and fully characterized for the 5–CF_3, 5-H, 5–Me, 3–OMe, 4–NMe_2, and 5–NMe_2-2-(^{t}BuNO)py derivatives. Within the series of complexes, an unprecedented stabilization of the tetravalent oxidation state of cerium was observed, which could be tuned by 500 mV across the series. The properties of the system that conferred the unprecedented stabilization were described. The combination of data from experimental electrochemistry and theoretical calculations for the series of cerium(IV)-pyridyl nitroxide complexes provided the basis for a semi-empirical correlation between experimentally and computationally determined $Ce^{IV/III}$ redox potentials that could be extended to include nine compounds from the literature of varying ligand field strengths. This work established a ligand field series for the 4f-block where conventional spectroscopic techniques could not be used due to the unique bonding properties of the valence 4f orbitals.

In **Chapter 4**, a new tripodal nitroxide ligand, $[(2\text{-}^t\text{BuNO})C_6H_4CH_2)_3N]^{3-}$ ($TriNOx^{3-}$), was developed and used to coordinate the trivalent rare earth ions. The rationale behind the design of this ligand was to mitigate facile ligand redistribution pathways observed with the pyridyl nitroxide systems by increasing chelation to the metal center. Controlled coordination and redox chemistries on the series of rare earth complexes were performed. Due to the unique sterics imposed by the $TriNOx^{3-}$ ligand, a self-association equilibrium between dimeric and monomeric species was observed that was highly sensitive to subtle differences in the ionic radius of the coordinated rare earth cation. The position of the equilibrium could be shifted through varying solvent polarity and ligand oxidation state. Differences in solubility between the dimeric and monomeric species were exploited for targeted separations of the rare earths. A complete separations cycle was achieved for mixtures of neodymium and dysprosium which has potential applications in magnet recycling, offering a simpler and more cost effective method than the liquid-liquid extractions currently in use.[2]

In **Chapter 5**, the controlled redox chemistry of cerium within the $TriNOx^{3-}$ ligand framework was explored. The single coordination site available for substrate binding and reduced ligand reorganization upon metal oxidation imposed by the tethered and bulky $TriNOx^{3-}$ ligand allowed for the isolation and crystallographic characterization of rare cationic complexes of cerium(IV). A

complete Ce^{IV}-halide series supported by the $TriNOx^{3-}$ ligand framework was also reported where trends in the solution chemistries of the complexes based on halide size were observed. These results highlight the unique coordination complexes of cerium that are possible using the $TriNOx^{3-}$ supporting ligand.

In **Chapter 6**, the computational methodology established by us through the study of the pyridyl nitroxide systems was used to model a cerium metal site within the active site of the newly discovered, rare earth dependent, XoxF-type methanol dehydrogenase (MDH) enzyme. Through a similar correlation of experimentally and computationally determined $Ce^{IV/III}$ redox potentials of model complexes under aqueous conditions, the redox potential of the cerium in the active site was predicted as a gauge for the Lewis acidic properties of the rare earth metal within the protein environment. By comparing the results obtained from replacing the Ce^{III} cation with Ca^{II}, where Ca^{II} typically plays a physiological role within MDH enzymes, insight was gained into how the rare earths provide a competitive advantage to XoxF-type dehydrogenase reactivity. This work is expected to aid in the development of biomimetic rare earth containing complexes that show catalytic activity towards alcohol and carbonyl oxidation.

A brief introduction to the fundamental properties of the rare earth elements is given in the ensuing sections of this chapter.

1.2 Introduction

The rare earth metals are a group of 17 elements consisting of the 15 lanthanoids, La–Lu, and the group III transition metals, Y and Sc. These elements are commonly grouped together due to their similar physical and chemical properties. They have found ubiquitous use in diverse technology as permanent magnetic materials in hybrid-electric automobiles and wind turbines, Lewis acid catalysts in catalytic converters and fluid catalytic cracking units, and phosphors in fluorescent light bulbs.[3] In fact, these broad uses of the rare earth elements, and their supply risks, have led the Department of Energy to classify these elements as “critical” for clean energy technologies (Figure 1.2.1).[4]

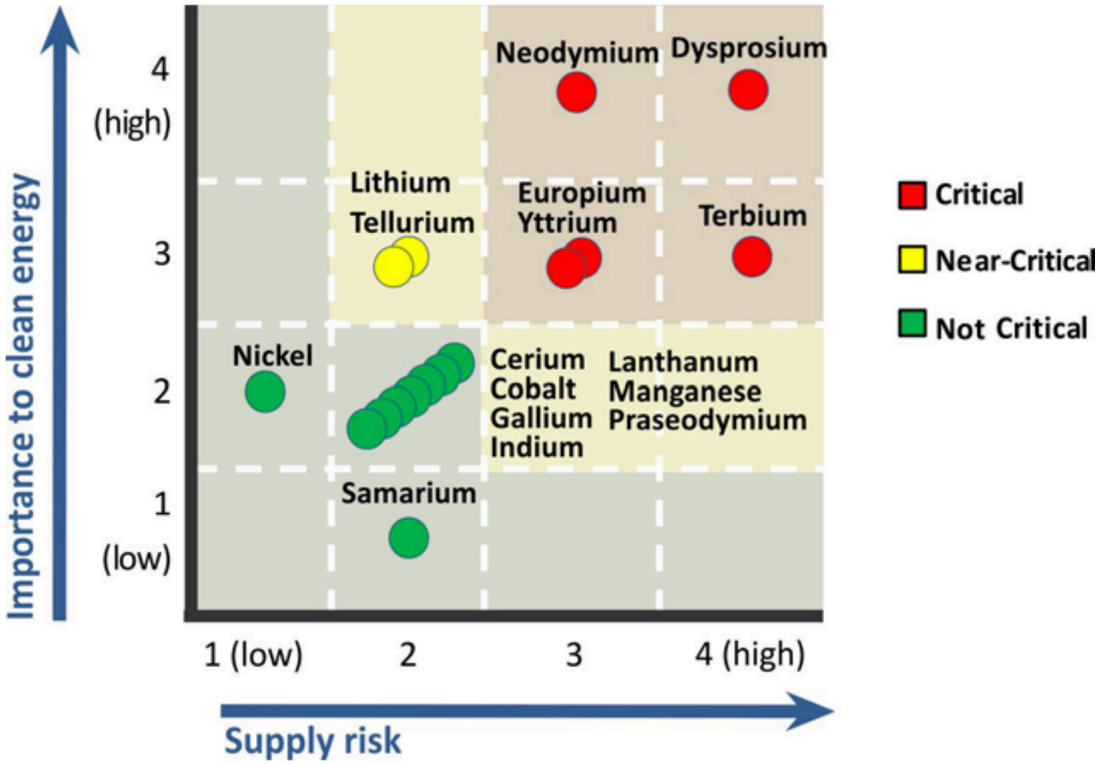

Figure 1.2.1. Medium-term criticality matrix (US Department of Energy, Critical Materials Strategy, 2011). Figure reproduced with permission of the US Department of Energy © 2011.

Contrary to their name, the rare earth elements are not rare and have abundances in the earth's crust ranging from 60 ppm for Ce to 0.5 ppm for Th and Lu. For reference, these values are similar to that of 50 ppm for copper (Figure 1.2.2).[5] The concentrations of the rare earths in their natural ore deposits, however, are quite low, which complicates the extractive metallurgy of these elements.[6] The production process is therefore associated with low efficiencies and large amounts of waste.[7] These complications have led to potential supply risks of these critical elements in recent years.

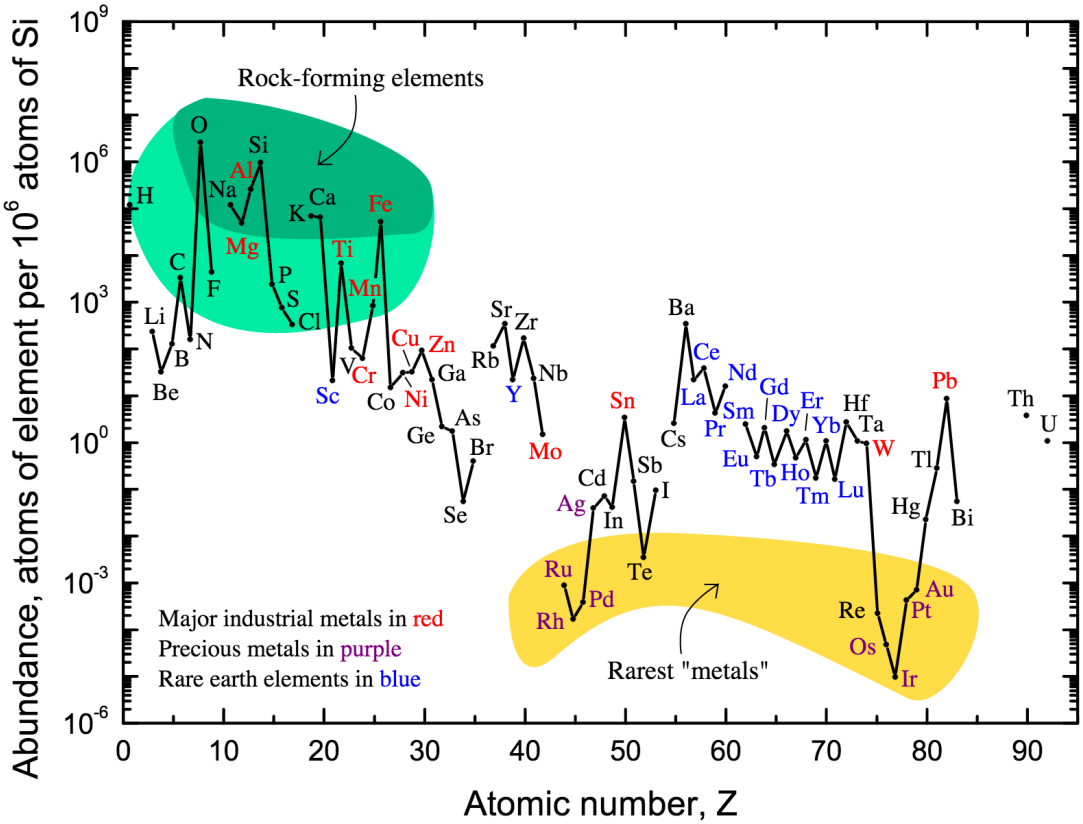

Figure 1.2.2. Natural abundance of the elements in the earth's crust (Haxel, G. B., et al. US Geological Survey, Fact Sheet 087-02, 2005). Figure adapted with permission of the USGS © 2005.

The members of the lanthanide series, La–Lu, predominantly exist in nature in the 3+ oxidation state. The first and second ionization energies remove the two valence 6s electrons and removal of a third electron is favored because of the increased stabilization achieved through more favorable interactions of the ligand donors with the 3+ ions relative to their 2+ congeners. Hence, the lanthanide ions in their tripositive oxidation states all have electronic configurations consisting of a xenon core and an incrementally increasing number of 4f electrons, $[Xe]4f^n$. [8]

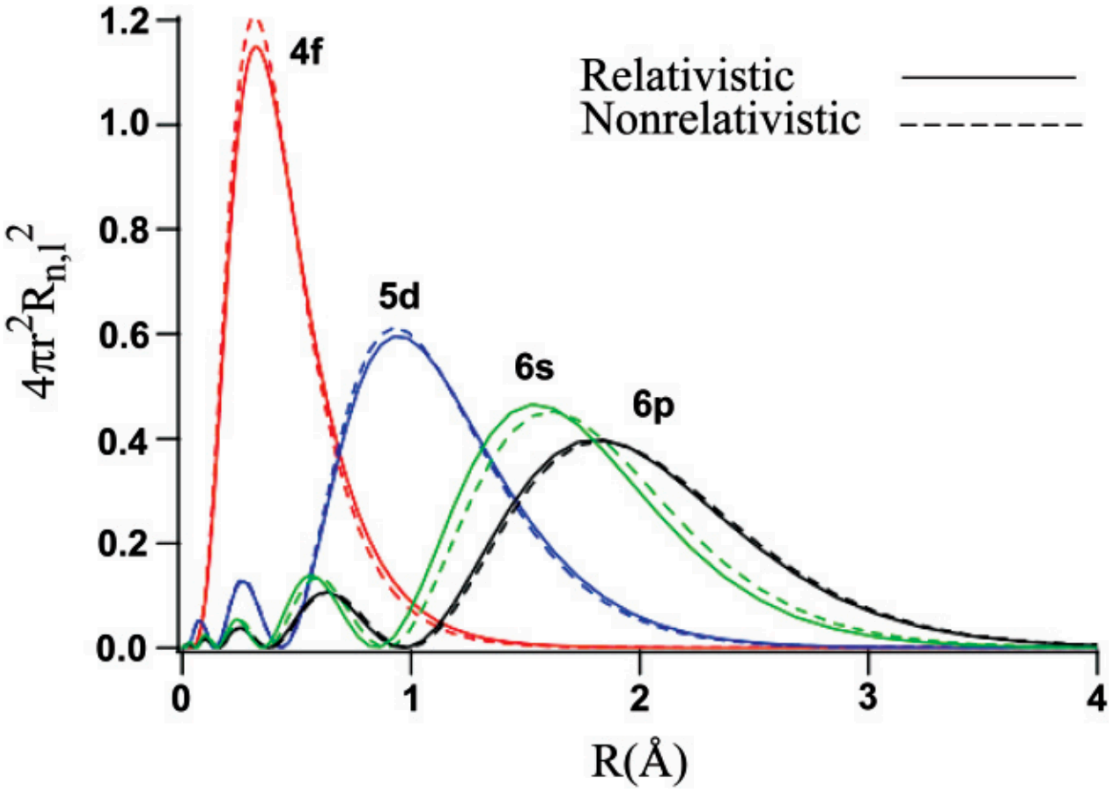

Figure 1.2.3. Calculated radial distribution functions for Sm^{3+} highlighting the affect of relativistic effects. Figure reprinted with permission of the Royal Society of Chemistry © 2004.

These elements comprise the first instance on the periodic table where the f-orbitals are filled, which gives them their unique properties. In contrast to the valence d-orbitals of the transition block, the 4f orbitals are "core-like" and do not have significant radial probability extending past ~1.3 Å (Figure 1.2.3).[9] This minimal radial extent of the 4f-orbitals leads to important differences in the bonding characteristics of the 4f-block versus the d-block elements (Table 1.2.1). For example, the 4f orbitals are less involved in bonding and their energies are significantly less perturbed by the crystal field imposed by the surrounding ligands. The bonding picture for the rare earth elements is, therefore, largely ionic and nondirectional.[10] As a result, the rare earth ions are highly oxophilic, coordination numbers of eight or nine are typical, and coordination geometries are determined by the steric demands of the ligands; as is observed with the aquo complexes, for example (Figure 1.2.4, left).[10-11] In contrast, the aquo complexes for the transition

metals typically exist in octahedral geometries with coordination numbers of six (Figure 1.2.4, right).[10, 12]

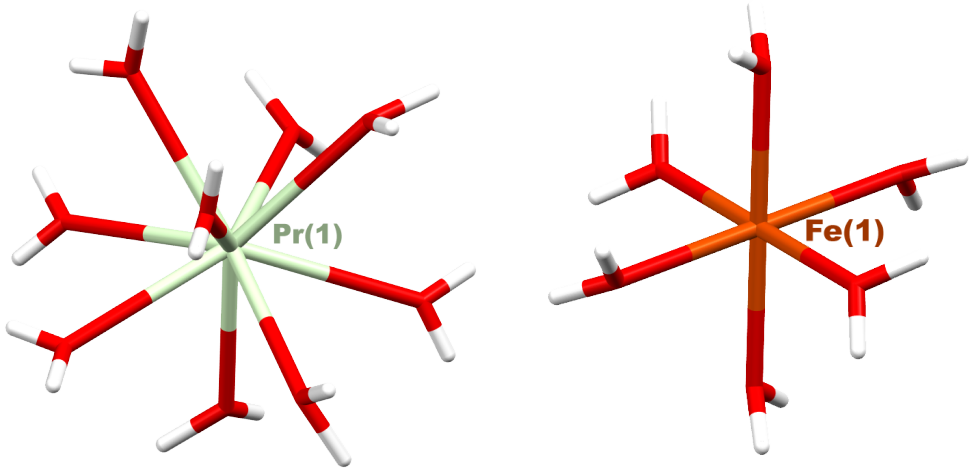

Figure 1.2.4. Molecular structures of $[Pr(H_2O)_9]^{3+}$ (left) and $[Fe(H_2O)_6]^{3+}$ (right). Counter anions omitted for clarity.

Table 1.2.1. Comparison of the properties of the lanthanides and transition metals. Reprinted with permission of John Wiley & Sons Inc. © 2006.

	Lanthanides, 4f	**Transition Metals, 3d**
Stable Oxidation States	Usually 3+	Variable
Coordination Numbers in Complexes	Commonly 8–10	Usually 6
Coordination polyhedral in complexes	Minimize repulsion	Directional
Hydration energy	High	Usually moderate
Crystal field effects in complexes	Weak	Strong
Bonding in organometallic compounds	Usually ionic, some with covalent character	Covalent
Magnetic properties	Independent of environment	Depends on ligand field
Electronic spectra	Typically sharp lines	Typically broad lines

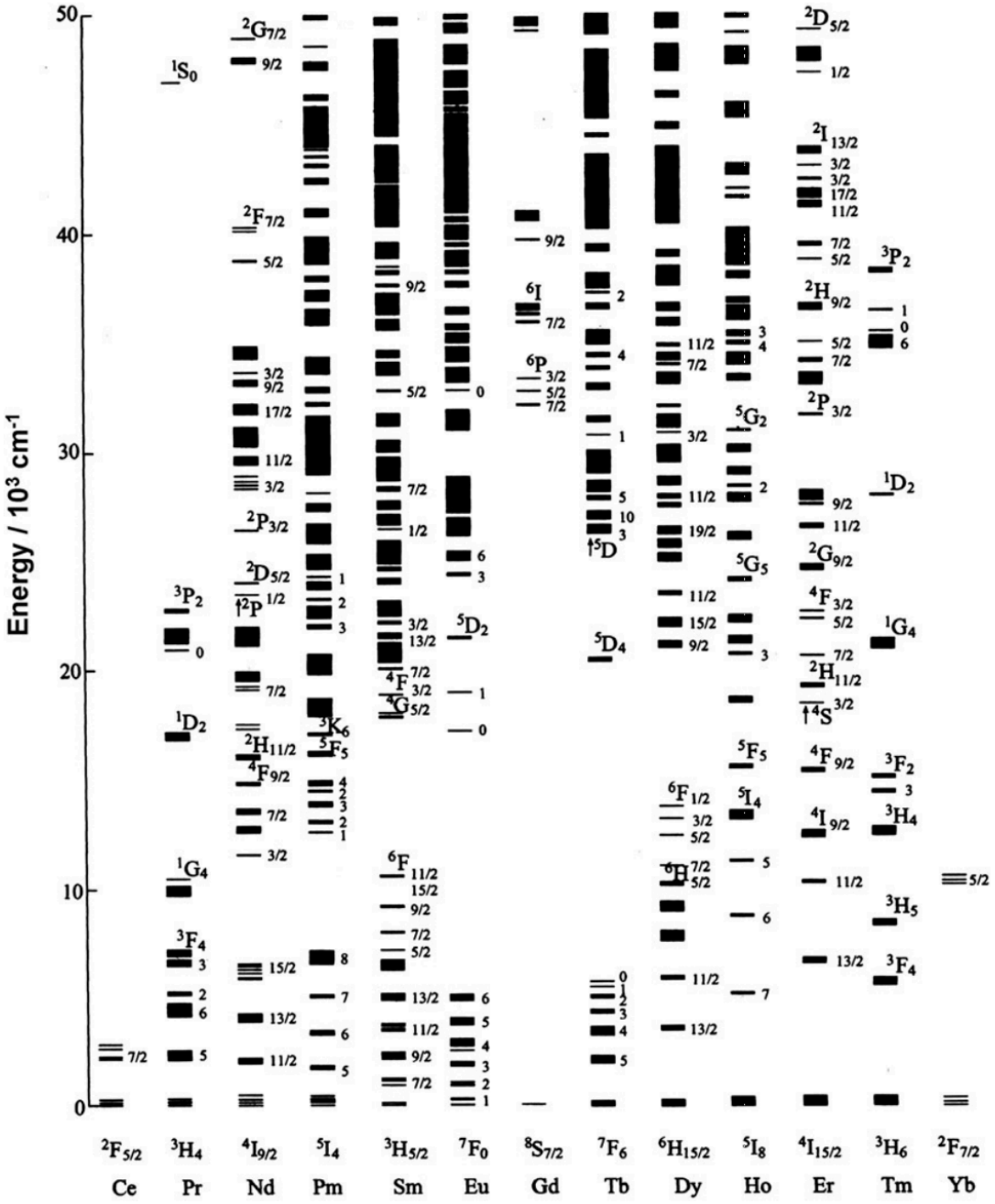

Figure 1.2.5. Energy level structures of Ln^{3+}:LaF_3. Reprinted with permission of AIP Publishing LLC © 1989.

The lack of large crystal field splittings of the 4f-orbitals leads to a set of degenerate orbitals that are related by rotational symmetry. Thus, the orbital angular momentum of the 4f electrons remains largely unquenched, leading to large spin-orbit coupling effects in their electronic

structures.[13] The spin orbit coupling constants for these ions are on the order of 10^3 cm^{-1}. The magnitudes of the spin-orbit coupling constants are compared to the crystal field splittings that are on the order of 10^2 cm^{-1}, which leads to energy diagrams for the ions where crystal field levels are secondary perturbations to the overall spin-orbit manifold (Figure 1.2.5).[14] These minimal perturbations to the overall electronic structures by crystal fields have implications in both the magnetic and optical properties of the rare earth cations.

The poor shielding of the 4f-orbitals also creates important trends across the lanthanide series. As the series is traversed, there is a systematic decrease in ionic radius known as the "Lanthanoid Contraction."[15] This decrease in ionic radius is concomitant with a systematic increase in Lewis acidity and hydration enthalpy (Figure 1.2.6).[8]

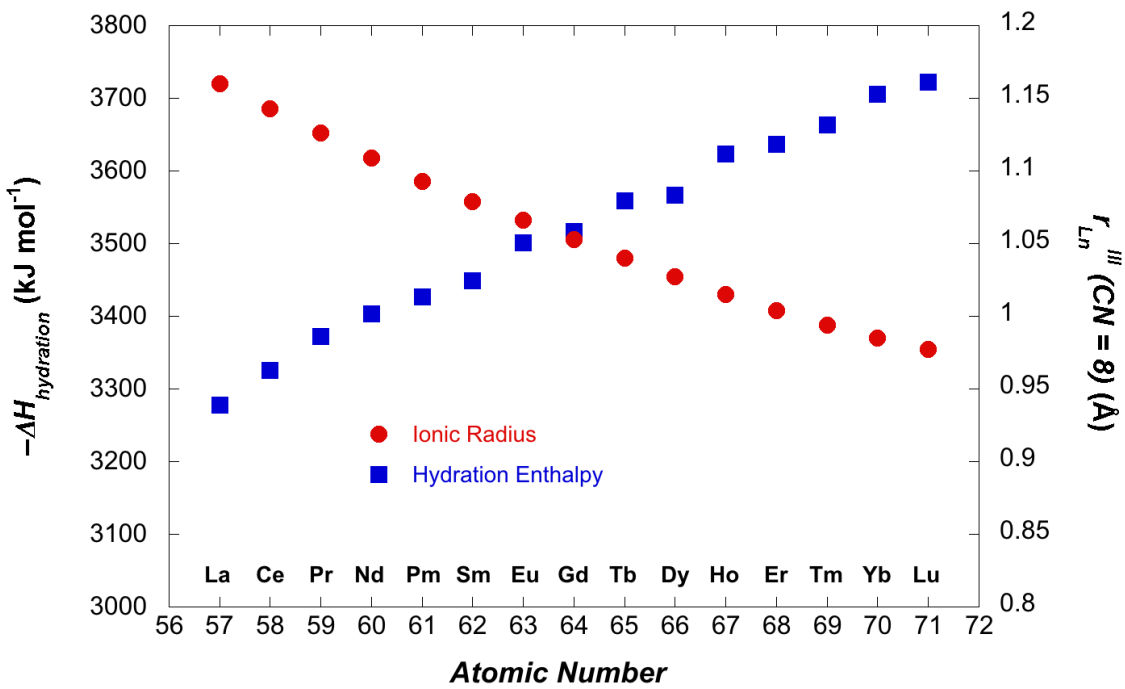

Figure 1.2.6. Systematic changes in ionic radius (red circles) and hydration enthalpy (blue squares) plotted for the trivalent lanthanide ions.

These gradual changes in ionic radii and Lewis acidities across the series have been exploited for rare earth separations. Methods for rare earth separations include fractional crystallization, ion exchange, solvent extraction, and chemical separations.[10] Historically, separation by fractional

crystallization was achieved through slight differences in the solubilities of the lanthanide bromate salts, $Ln(BrO_3)_3 \cdot 9H_2O$. This method was used in 1911 by C. James to achieve pure thulium by performing ~15,000 successive recrystallizations.[16] In 1947, the separations of rare earth ions was revolutionized by Spedding and coworkers with the application of ion exchange chromatography.[17] Through a series of studies, they established a method where the ions would be adsorbed onto Amberlite IR-1 or Amberlite IR-100 exchange resins and eluted with citric acid ammonium citrate solutions. Complications arose, however, when using very large rare earth cation loadings. In such cases, significant amounts of overlap were observed between eluted fractions.

As a result, current commercial separation systems almost exclusively use liquid-liquid extraction methods pioneered in the 1960s.[18] In these systems, the rare earth containing ore is leached with dilute acid, which forms an aqueous solution of the trivalent rare earth ions.[6, 19] This aqueous feed is combined in a mixer settler unit with an immiscible organic solvent, such as kerosene, containing an added extractant. The later (heavy) rare earth ions have slightly higher binding affinities to the added extractant than the early (light) rare earth ions.[20] This creates an organic phase with slightly higher concentrations of heavy rare earths and an aqueous phase with slightly higher concentration of light rare earths. This process is repeated many times to achieve purities up to 99.99%.[21] For certain applications, purities of up to 99.999% (phosphor grade) are required and a final ion exchange chromatography step is utilized.[10]

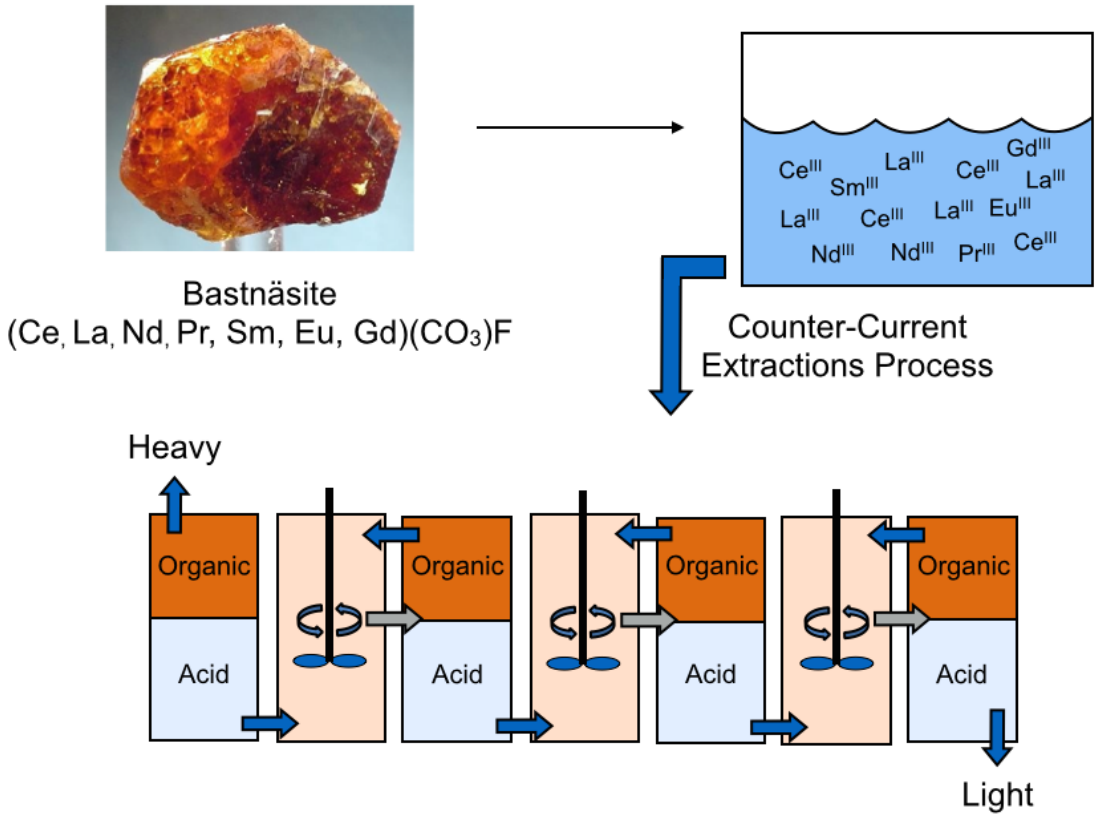

Figure 1.2.7. Schematic of the counter-current extractions process used in industrial liquid-liquid extractions processes for the separations of trivalent rare earth ions. Adapted with permission from Molycorp, Inc. © 2013.

A few lanthanide elements have accessible oxidation states other than 3+ that allow for more efficient separations using chemical based methods. These include cerium, which can be oxidized to Ce^{IV} upon roasting of the rare earth containing ore. The tetravalent cerium ions are not leached into the dilute acid with the other trivalent rare earth ions.[6] Conversely, europium, samarium, and ytterbium can be reduced to the 2+ oxidation state and separated as the divalent ions.[6] For example, Marsh successfully separated these ions from mixtures of rare earths through targeted reductive extraction into dilute sodium amalgam.[22] These select examples demonstrate the use of new redox based separations methods for the complete series of rare earths could have profound and beneficial effects on the processing of these materials.

In this vein, fundamental research on the rare earths in recent years have advanced our understanding of the redox properties of these ions.[23] Previously, it was thought that only europium, ytterbium, samarium, thulium, dysprosium, and neodymium, had accessible divalent oxidation states in molecular chemistry due to their relatively small standard reduction potentials, $E_{1/2} \leq -2.6$ V vs. NHE, and the electronic structures of their solid state chlorides, $[Xe]4f^{n}5d^{0}6s^{0}$, compared to $[Xe]4f^{n+1}5d^{1}6s^{0}$ ("$M^{3+}e^{-}$") for the metallic solid state iodides of La, Ce, Pr, and Gd.[24] However, through the initial work of Lappert and coworkers and the ensuing efforts of Evans and coworkers, molecular complexes of the divalent lanthanides, $[K(2.2.2.\text{-cryptand})][Cp'_3Ln^{II}]$ where $Cp' = C_5H_4SiMe_3$, have been isolated for the complete set of lanthanide ions.[25] As with the solid state halides, however, the molecular divalent lanthanide complexes of La–Pr, Gd, Tb, Ho, Er, and Lu have $5d^1$ electron configurations while those of Sm, Eu, Tm, and Yb have $5f^{n+1}$ configurations.[25] Surprisingly, the spectroscopic data for the molecular complexes of Nd and Dy were consistent with $5d^1$ configurations despite these ions belonging to the traditional six group of lanthanide elements, implicating ligand field effects in the electronic configurations.

A similar complete series of molecular complexes of the tetravalent lanthanides is not known. Currently, only cerium has a well-defined tetravalent oxidation state in molecular chemistry.[26] However, the tetravalent oxidation state is known for Pr, Tb, Nd, and Dy in the solid-state. These include the binary oxides of Pr and Tb as well as the perovskite-type oxides of Nd and Dy.[27] Furthermore, Pr^{IV} and Tb^{IV} have been observed by Hobart and coworkers in basic carbonate solutions.[28] By furthering our understanding of the coordination chemistry of the rare earth ions, particularly in environments that stabilize the 4+ oxidation states, we expect to advance the boundaries of our understanding of these ions and exploit their properties for use in technologies.

1.3 References

[1] a) J. Keltjens, A. Pol, J. Reimann, H. M. Op den Camp, *Appl. Microbiol. Biotechnol.* **2014**, *98*, 6163-6183; b) A. Pol, T. R. M. Barends, A. Dietl, A. F. Khadem, J. Eygensteyn, M. S. M. Jetten, H. J. M. Op den Camp, *Environ. Microbiol.* **2014**, *16*, 255-264.

[2] R. F. Sebenik, "The Optimization of a Solvent Extraction Plant to Process Monazite Rare Earth Nitrates", **1968**. *Retrospective Theses and Dissertations. Paper 3261.*

[3] a) O. Gutfleisch, M. A. Willard, E. Brück, C. H. Chen, S. G. Sankar, J. P. Liu, *Adv. Mater.* **2011**, *23*, 821-842; b) K. Binnemans, P. T. Jones, B. Blanpain, T. Van Gerven, Y. Yang, A. Walton, M. Buchert, *J. Clean Prod.* **2013**, *51*, 1-22; c) M. Shibasaki, K.-I. Yamada, N. Yoshikawa, in *Lewis Acids in Organic Synthesis*, Wiley-VCH Verlag GmbH, **2008**, pp. 911-944; d) M. Humphries, Rare Earth Elements: The Global Supply Chain, **2013**, pp. 1-26.

[4] U.S. Department of Energy, Critical Materials Strategy, Washington, D. C., **2011**, pp. 1-191.

[5] a) G. B. Haxel, J. B. Hedrick, G. J. Orris, U.S. Geological Survey, Fact Sheet 087-02, **2005**; b) J. Gambogi, Rare Earths, 2012 Minerals Yearbook, U.S. Geological Survey, **2012**.

[6] C. K. Gupta, N. Krishnamurthy, *Int. Mater. Rev.* **1992**, *37*, 197-248.

[7] C. Sonich-Mullin, Rare Earth Elements: A Review of Production, Processing, Recycling and Associated Issues, Cincinatti, OH, **2012**.

[8] D. A. Atwood, *The Rare Earth Elements: Fundementals and Applications*, John Wiley & Sons, **2012**.

[9] a) G. R. Giesbrecht, J. C. Gordon, *Dalton Trans.* **2004**, 2387-2393; b) H. G. Friedman, G. R. Choppin, D. G. Feuerbacher, *J. Chem. Educ.* **1964**, *41*, 354.

[10] S. Cotton, in *Lanthanide and Actinide Chemistry*, John Wiley & Sons Inc., Hoboken, NJ, **2006**.

[11] a) P. G. Eller, R. A. Penneman, *J. Less-Common Met.* **1987**, *127*, 19-33; b) A. Chatterjee, E. N. Maslen, K. J. Watson, *Acta Crystallogr., Sect. B: Struct. Sci* **1988**, *44*, 381-386; c) S. A. Cotton, in *Encyclopedia of Inorganic and Bioinorganic Chemistry*, John Wiley & Sons, Ltd, **2011**.

[12] C. Nitschke, M. Köckerling, *Inorg. Chem.* **2011**, *50*, 4313-4321.

[13] C. H. Huang, *Rare earth coordination chemistry: fundamentals and applications*, John Wiley& Sons, Hoboken, NJ, **2010**.

[14] a) S. Gao, *Molecular Nanomagnets and Related Phenomena*, Springer - Verlag Berlin Heidelberg, New York, **2015**; b) W. T. Carnall, G. L. Goodman, K. Rajnak, R. S. Rana, *J. Chem. Phys.* **1989**, *90*, 3443-3457.

[15] a) E. A. Quadrelli, *Inorg. Chem.* **2002**, *41*, 167-169; b) R. Shannon, *Acta Crystallogr. Sect. A* **1976**, *32*, 751-767.

[16] C. James, *J. Am. Chem. Soc.* **1911**, *33*, 1332-1344.

[17] a) F. H. Spedding, E. I. Fulmer, T. A. Butler, E. M. Gladrow, M. Gobush, P. E. Porter, J. E. Powell, J. M. Wright, *J. Am. Chem. Soc.* **1947**, *69*, 2812-2818; b) F. H. Spedding, A. F. Voigt, E. M. Gladrow, N. R. Sleight, *J. Am. Chem. Soc.* **1947**, *69*, 2777-2781; c) F. H. Spedding, A. F. Voigt, E. M. Gladrow, N. R. Sleight, J. E. Powell, J. M. Wright, T. A. Butler, P. Figard, *J. Am. Chem. Soc.* **1947**, *69*, 2786-2792; d) F. H. Spedding, E. I. Fulmer, B. Ayers, T. A. Butler, J. Powell, A. D. Tevebaugh, R. Thompson, *J. Am. Chem. Soc.* **1948**, *70*, 1671-1672; e) F. H. Spedding, E. I. Fulmer, J. E. Powell, T. A. Butler, *J. Am. Chem. Soc.* **1950**, *72*, 2354-2361.

[18] F. Xie, T. A. Zhang, D. Dreisinger, F. Doyle, *Miner. Eng.* **2014**, *56*, 10-28.

[19] H. C. Aspinall, *Chemistry of the f-Block Elements,* Gordon and Breach Science Publishers, Amsterdam, The Netherlands, **2001**.

[20] a) C. K. Gupta, N. Krishnamurthy, *Extractive Metallurgy of Rare Earths*, CRC Press, New York, **2005**; b) M. Yuan, A. Luo, D. Li, *Acta Metall. Sin.* **1995**, *8*, 10-14.

[21] B. Sprecher, Y. Xiao, A. Walton, J. Speight, R. Harris, R. Kleijn, G. Visser, G. J. Kramer, *Environ. Sci. Technol.* **2014**, *48*, 3951-3958.

[22] a) J. K. Marsh, *J. Chem. Soc.* **1942**, 523-526; b) J. K. Marsh, *J. Chem. Soc.* **1942**, 398-401; c) J. K. Marsh, *J. Chem. Soc.* **1943**, 8-10.

[23] W. J. Evans, *Inorg. Chem.* **2007**, *46*, 3435-3449.

[24] a) L. J. Nugent, R. D. Baybarz, J. L. Burnett, J. L. Ryan, *J. Phys. Chem.* **1973**, *77*, 1528-1539; b) G. Meyer, H. J. Meyer, *Chem. Mater.* **1992**, *4*, 1157-1168.

[25] a) P. B. Hitchcock, M. F. Lappert, L. Maron, A. V. Protchenko, *Angew. Chem. Int. Ed.* **2008**, *47*, 1488-1491; b) M. E. Fieser, M. R. MacDonald, B. T. Krull, J. E. Bates, J. W. Ziller, F. Furche, W. J. Evans, *J. Am. Chem. Soc.* **2015**, *137*, 369-382; c) M. R. MacDonald, J. E. Bates, J. W. Ziller, F. Furche, W. J. Evans, *J. Am. Chem. Soc.* **2013**, *135*, 9857-9868; d) M. R. MacDonald, J. E. Bates, M. E. Fieser, J. W. Ziller, F. Furche, W. J. Evans, *J. Am. Chem. Soc.* **2012**, *134*, 8420-8423; e) M. R. MacDonald, J. W. Ziller, W. J. Evans, *J. Am. Chem. Soc.* **2011**, *133*, 15914-15917.

[26] N. A. Piro, J. R. Robinson, P. J. Walsh, E. J. Schelter, *Coord. Chem. Rev.* **2014**, *260*, 21-36.

[27] a) M. Oishi, K. Yashiro, K. Sato, J. Mizusaki, N. Kitamura, K. Amezawa, T. Kawada, Y. Uchimoto, *Solid State Ionics* **2008**, *179*, 529-535; b) G. Brauer, H. Kristen, *Z. Anorg. Allg. Chem.* **1979**, *456*, 41-53; c) D. Han, T. Uda, Y. Nose, T. Okajima, H. Murata, I. Tanaka, K. Shinoda, *Adv. Mater.* **2012**, *24*, 2051-2053; d) F. A. Cotton, G. Wilkinson, in *Advanced Inorganic Chemistry, Third Edition*, John Wiley & Sons, New York, **1972**, pp. 1056-1076.

[28] D. E. Hobart, K. Samhoun, J. P. Young, V. E. Norvell, G. Mamantov, J. R. Peterson, *Inorg. Nucl. Chem. Lett.* **1980**, *16*, 321-328.

Chapter 2

Fine-Tuning the Oxidative Ability of Persistent Radicals: Electrochemical and Computational Studies of Substituted 2-Pyridylhydroxylamines

Abstract

Due to their persistence in their neutral free radical forms, nitroxides find use in organic, inorganic, materials, and medicinal chemistry. Their ubiquitous use underlines the need for tuning the redox potentials of these compounds. Towards this goal, *N*-*tert*-Butyl-*N*-2-pyridyl hydroxylamines were synthesized from 2-halopyridines and 2-methyl-2-nitrosopropane using magnesium-halogen exchange reactions. The use of Turbo Grignard reagent generated the metallo-2-pyridyl intermediate more reliably than alkyllithium reagents. The resulting hydroxylamines were characterized using NMR, electrochemistry, and density functional theory. Substitution of the pyridyl ring in the 3-, 4-, and 5-positions was used to vary the potential of the nitroxyl/oxoammonium redox couple by 0.95 V. DFT computations of the electrochemical properties agreed with experiment and provided a toolset for the predictive design of pyridyl-nitroxides.

2.1 Introduction

Nitroxides are important compounds in a wide variety of chemical disciplines, ranging from organic to inorganic to medicinal and materials chemistries, due to their stabilities in multiple redox forms.[1] In their neutral state, these compounds exist as π-radicals with spin density primarily located on the N–O moiety. These radicals can either be oxidized to their cationic oxoammonium forms or reduced to the anionic nitroxides, both of which have closed shell electronic configurations (Figure 2.1.1).[2] The electrochemical potentials for these transformations fall into chemically accessible ranges, which makes them desirable reagents for the synthetic chemist. For example, derivatives of the well-known nitroxide, 2,2,6,6-tetramethylpiperidine-*N*-oxyl (TEMPO), have been used in organic chemistry as catalysts in the oxidation of primary and secondary alcohols to aldehydes and ketones. TEMPO can also be activated towards oxidation chemistry through coordination to a Lewis acid such as Cu(II),[1a-c] Fe(III),[1d] and Al(III).[1d]

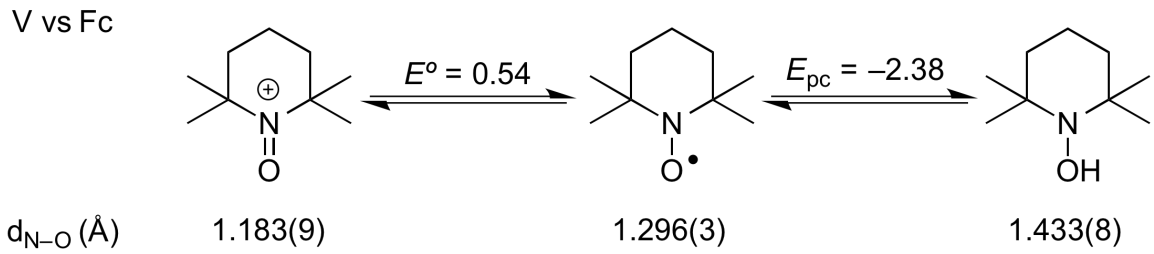

Figure 2.1.1. The redox states of TEMPO and their N–O bond distances. Potentials are shown in V versus Fc, which were adjusted from the reported experimental values collected in 0.1 M CH_3CN/TBAF solution at a Pt working electrode versus Ag/AgCl at a scan rate of 0.15 V s^{-1}.[2] The N–O distances are typical for each redox form.[3]

In medicinal chemistry, nitroxide radicals have been used as spin probes,[1e] and multiple studies have shown that these reagents can act as superoxide dismutase mimics.[1f-h] The superoxide dismutase chemistry involves initial reactivity between the nitroxide radical, O_2^-, and two equivalents of H^+ to form the respective oxoammonium cation and H_2O_2. Subsequent reaction between the oxoammonium cation and another molecule of O_2^- regenerates the nitroxide radical catalyst and a molecule of O_2.[1h]

Due to their open shell character, nitroxide radicals also find use in materials chemistry as redox mediators in dye-sensitized solar cells and as building blocks in the synthesis of molecular-based magnetic materials.[1i-o] For the former, nitroxides are promising alternatives to the more common I^-/I_3^- redox mediator due to the better matching of their redox potentials with that of the TiO_2 semiconductor, their less corrosive properties toward the electrode metals, and their weaker visible absorptive characteristics.[1i] For the latter, purely organic ferromagnets have been produced based on substituted phenyl nitronyl nitroxides and substituted benzylideneamino-TEMPO radicals, though their Curie temperatures remain low, ranging from 0.09 K – 0.60 K and 0.18 K – 0.4 K, respectively.[1k] The α-phase of 1,3,5,7-tetramethyl-2,6-diazaadamane-*N*,*N'*-dioxyl has a T_c of 1.48 K, which is one of the largest T_c values for a purely organic ferromagnet based on nitroxide radicals.[1k] Ishida et al. have also studied molecular ferromagnetic behavior in Cu(II) and Ni(II) complexes of pyridyl nitroxide radicals.[1l-n]

In inorganic chemistry, these nitroxide compounds can act as both oxidants and ligands toward a metal cation. In work performed by Evans and coworkers, free TEMPO was reacted with two equivalents of $Sm(C_5Me_5)_3$ to form the bimetallic homoleptic samarium complex, $[(\eta^1\text{-}ONC_5H_6\text{-}Me_4)_2Sm(\mu\text{-}\eta^1\text{:}\eta^2\text{-}ONC_5H_6Me_4)]_2$, where the two Sm(III) cations were surrounded by six fully reduced $TEMPO^-$ anions.[1p]

All of these applications of nitroxide radicals arise from their persistence in the open-shell form as well as the electrochemical reversibility of their oxidation and reduction events. Their performance is also highly dependent on the matching of their redox potentials with those of other redox active components within the systems, which indicates the need for methods to tune their electrochemical properties. Methods for shifting these potentials that existed prior to this work focused mostly on substitutions of an aliphatic backbone.[2, 4] For example, Blinco et al. performed an extensive study on substituent effects of isoindoline nitroxides and discovered a correlation between oxidation potential and Hammett parameter, σ, with a slope of 0.11 (Figure 2.1.2).[2]

A few studies, in particular those conducted by Xu and coworkers on a series of *N*-(4-R-phenyl)hydroxamic acids, have focused on substituent effects on redox potentials of aromatic

nitroxides.[5] In the case of the substituted *N*-(4-R-phenyl)hydroxamic acids, a similar correlation between E_{pa} of the second oxidation and Hammett parameter, σ^+, of the substituents was evident with a slope of 0.22.[6] This result suggested that substitution of π-conjugated aromatic nitroxides could be a more effective way of tuning the redox potentials of these nitroxide compounds.

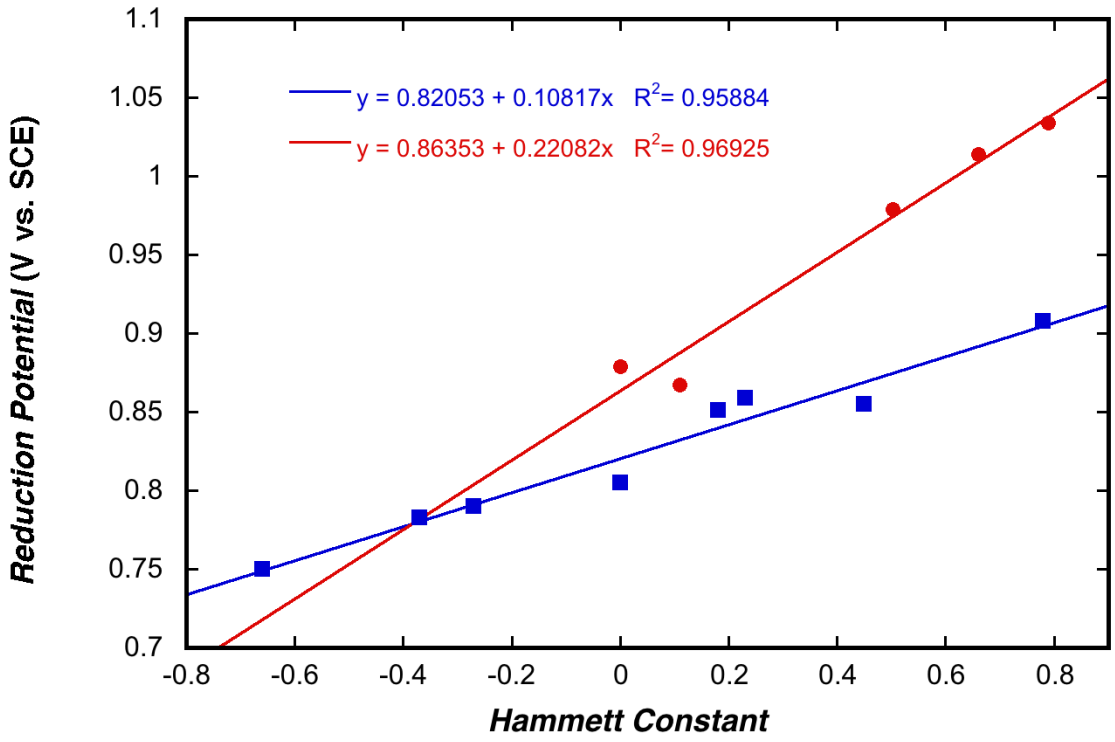

Figure 2.1.2. Hammett plots of reduction potential versus σ for the series of isoindoline derivatives (blue squares) and reduction potential of the second redox event versus σ^+ for the series of *N*-(4-R-phenyl)hydroxamic acids (red circles). Reproduced using data from references [2] and [5d].

To the best of our knowledge, previous reports on aromatic nitroxides did not include both electrochemical and theoretical studies. We hypothesized that 1) such studies could benefit from a more detailed approach that incorporated both experimental and computational findings and 2) substituent effects in aromatic nitroxides would be more significant compared to those in aliphatic nitroxides due to direct π-conjugation between the substituents and the redox active N–O moiety. Towards this goal, we examined substitutions of the pyridyl ring of a series of *N*-*tert*-butyl-*N*-(2-pyridyl)nitroxides where the substituents would be in direct conjugation with the heterocyclic ring system.

Herein, we report on our electrochemical and computational studies of a series of substituted *N-tert*-butyl-*N*-(2-pyridyl)nitroxides. Through a modified literature procedure, we prepared the parent unsubstituted pyridylhydroxylamine as well as seven derivatives that had the pyridyl ring substituted with 5–CF_3, 6-Br, 5–Me, 4–NMe_2, 5–MeS, 3–OMe, and 5–NMe_2 groups. The solution electrochemistry of the hydroxylamines, R-2-(^{t}BuNOH)py with R = 5–CF_3, 5–Me, 4–NMe_2, 5–MeS, 3–OMe, and 5–NMe_2, revealed a highly tunable radical to oxoammonium redox couple, with $E_{1/2}$ values ranging from 0.24 V to 1.17 V vs. SCE. A semi-empirical correlation between redox potential and Hammett parameter, σ^+, was formed, indicating that bond resonance between the substituents and the N–O moiety played an important role in adjusting the redox potentials of these nitroxide compounds. Computational studies revealed the SOMOs of the nitroxide radicals had electron density delocalized over the entire π-system and allowed for the determination of calculated free energy changes (ΔG) between the oxoammonium and neutral radical forms. These ΔG values could be correlated to the experimentally determined values, providing a toolset for predictive design of persistent radicals based on the pyridyl nitroxide system with varying redox potentials.

2.2 Results/Discussion

2.2.1 Synthesis and Characterization

The synthesis of the parent unsubstituted pyridyl hydroxylamine, 2-(^{t}BuNOH)py, had been reported previously in 41% yield by Ishida and coworkers (Figure 2.2.1).[1n] In our hands, however, attempts to produce the 2-lithiopyridine intermediate using ^{n}BuLi at the reported temperature of –78 ºC failed due to the production of butylated addition products. To prevent such addition products from forming, we turned to the use of the isopropylmagnesium chloride lithium chloride complex (Turbo Grignard), a reagent pioneered by Knochel et al. for metal-halogen exchange reactions.[7] We hypothesized that the secondary carbon of the isopropyl group would be less nucleophilic, which would make attack of the pyridine ring less favorable. Being less reactive, Turbo Grignard would also allow for the use of milder reaction conditions. Indeed, the reaction of 2-bromopyridine with Turbo Grignard at 0 ºC cleanly afforded the 2-

pyridylmagnesium chloride complex *in situ*, which could be converted into 2-(^{t}BuNOH)py upon addition of 2-methyl-2-nitrosopropane dimer and quenching with degassed $NH_4Cl_{(aq)}$.

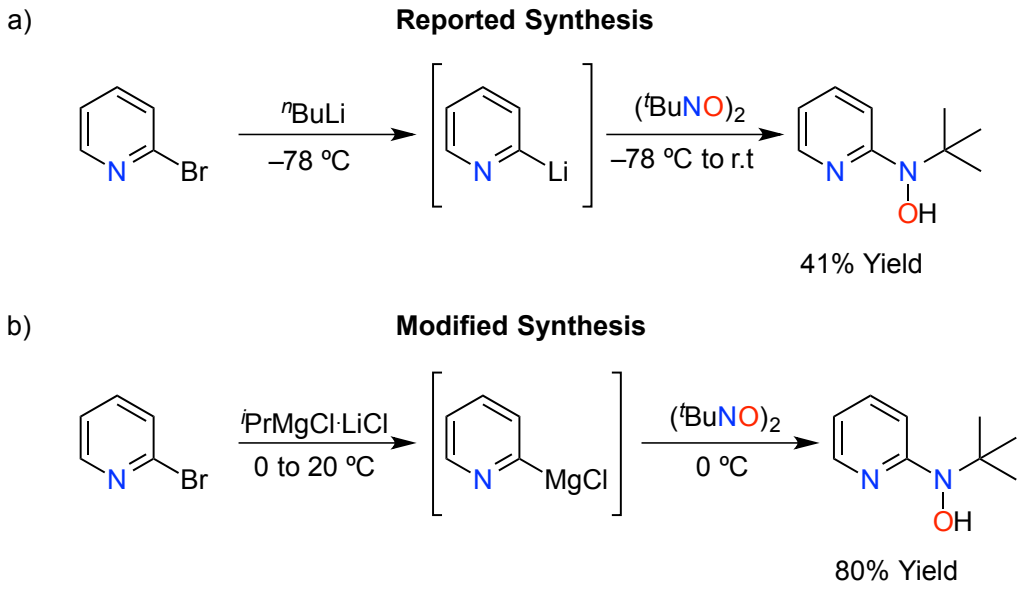

Figure 2.2.1.1. Schematics of a) the reported synthesis according to reference [1n] and b) our improved modified synthesis of 2-(^{t}BuNOH)py. Adapted with permission of the American Chemical Society © 2013.

Similar magnesium-halogen exchange reactions were performed to afford the pyridyl hydroxylamines derivatives, R-2-(^{t}BuNOH)py, where R = 5–CF_3, 6-Br, 5–Me, 4–NMe_2, 5–MeS, and 3–OMe, indicating that both electron withdrawing and electron donating substituents were tolerated by this modified route. We noticed, however, that cooling the magnesium-halogen exchange reaction to –78 ºC was required for the 5–CF_3 substituted derivative in order to prevent the formation of a complex mixture of products. Turbo Grignard could also be used to form the 2-pyridylmagnesium chloride species of the 5–NMe_2 substituted 2-bromopyridine, albeit in only 50% conversion. To synthesize 5-NMe_2-2-(^{t}BuNOH)py in good yield the use of ^{n}BuLi was required. Addition of ^{n}BuLi at –100 ºC cleanly afforded the 2-lithiopyridine species in good conversion free of butylated addition products. The addition of 2-methyl-2-nitrosopropane dimer to this 2-lithiopyridine species produced the desired 5-NMe_2-2-(^{t}BuNOH)py upon quenching with degassed $NH_4Cl_{(aq)}$.

Table 2.2.1.1. Reaction conditions and percent yields for the syntheses of the *N-tert*-butyl-*N*-2-pyridylhydroxylamine derivatives. Table adapted with permission of the American Chemical Society © 2013.

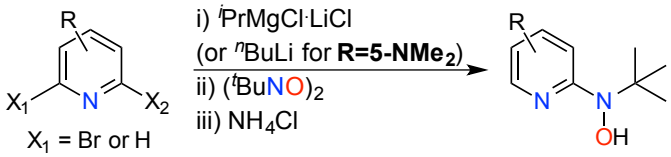

X_1 = Br or H
X_2 = Br or I

R=5-CF_3, 6-Br, H, 5-Me, 5-MeS, 3-OMe, 4-NMe_2, or 5-NMe_2

Precursor	Product	Time[a], h	Temp[a], ºC	Yield[b], %
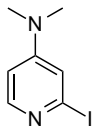	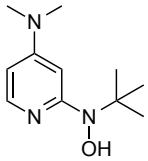	3 / 3	0→20 / 0	68
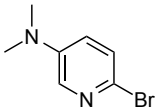	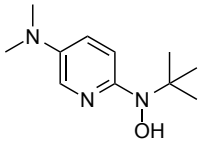	3 / 3	–100 / –100→20	64
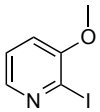	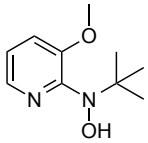	14 / 3	0→20 / 0	69
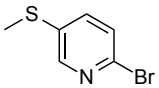	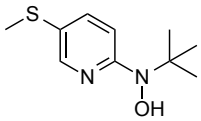	3 / 3	0→20 / 0	63
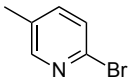	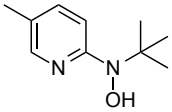	3 / 3	0→20 / 0	62
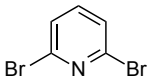	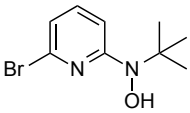	0.33 / 1	20 / 20	42
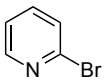	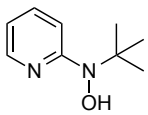	1 / 3	0→20 / 0	80
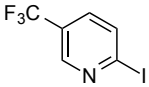	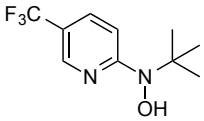	2 / 3	–78 / –78[c]	74

[a]Values are for reaction conditions during the first/second steps. [b]Isolated yields. [c]A complex mixture resulted if the reaction was not cooled to –78 ºC.

The pyridyl hydroxylamines, R-2-(^{t}BuNOH)py, where R = 5–CF_3, 6-Br, 5–Me, 4–NMe_2, 5–MeS, and 3–OMe, could be conveniently purified in good recoveries by crystallization or sublimation. This allowed for the isolation of higher yields and eliminated the waste associated with column chromatography, which was used in the reported procedure for the purification of 2-(^{t}BuNOH)py. All of the pyridyl hydroxylamines were air-sensitive and oxidized to their neutral radical forms upon exposure to O_2. They could be stored indefinitely, however, as solids under a strictly N_2 atmosphere.

Confirmation of the solid state structures of these complexes came from X-ray crystallography of the 6-Br-2-(^{t}BuNOH)py derivative. X-ray quality crystals of this compound were grown by cooling a saturated chloroform solution to –30 ºC. As shown in Figure 2.2.1.2, the thermal ellipsoid plot revealed a *trans* disposition between the pyridyl nitrogen atom and the nitroxide oxygen atom. This conformation was expected to be lower in energy than the *cis* congener due to large steric interactions between the hydrogen attached to C3 of the pyridyl ring and the large *tert*-butyl group in the latter. The N–OH bond distance of 1.4476(11) Å falls within the range of a fully reduced nitroxide moiety and supports our assignment of the compound in its hydroxylamine form. As indicated, these hydroxylamine compounds pack in the solid state to maximize intermolecular hydrogen bonding between the N–OH groups.

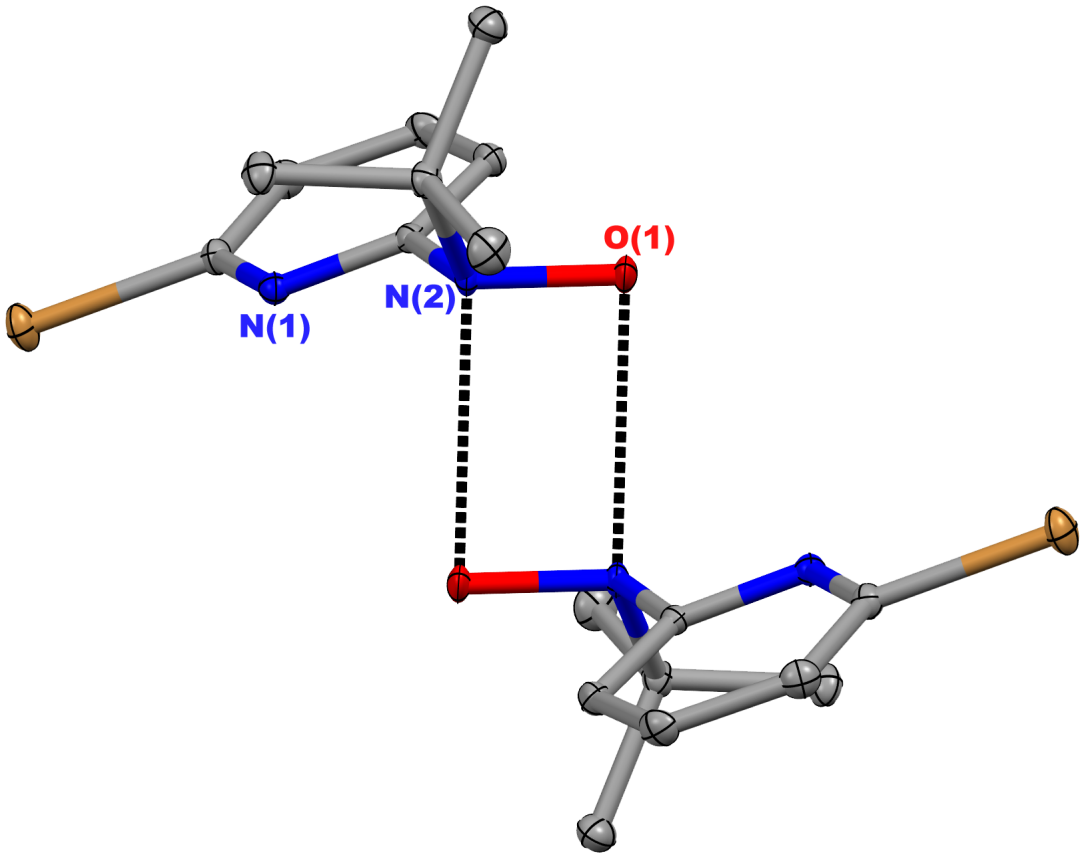

Figure 2.2.1.2. Thermal Ellipsoid plot of 6-Br-2-(^{t}BuNOH)py. H atoms omitted for clarity. Dotted lines indicate H-bonding contacts. Selected distances in Å: N(2)–O(1) 1.4476(11).

2.2.2 Solution Electrochemistry

With the series of R-2-(^{t}BuNOH)py in hand, we turned to evaluation of their redox properties through solution electrochemistry experiments. Figure 2.2.2.1 shows the cyclic voltammogram (CV) of 5-MeS-2-(^{t}BuNOH)py, which served as a representative example of the series of pyridyl hydroxylamines. Based on the open circuit potential of –0.24 V, the three waves centered at 0.27 V, 0.76 V, and 1.30 V were assigned as oxidation events. Electrochemical data for nitroxides typically include two primary processes corresponding to the [N–O$^\bullet$]/[N–OH] and [N=O$^+$]/[N–O$^\bullet$] redox couples. As indicated in the figure, these two redox events were assigned to the first two oxidation waves, respectively, and were also present in the CVs of the other hydroxylamine derivatives. The third oxidation feature was unique to the CV of 5-MeS-2-(^{t}BuNOH)py and was assigned as a sulfide based oxidation process.[8]

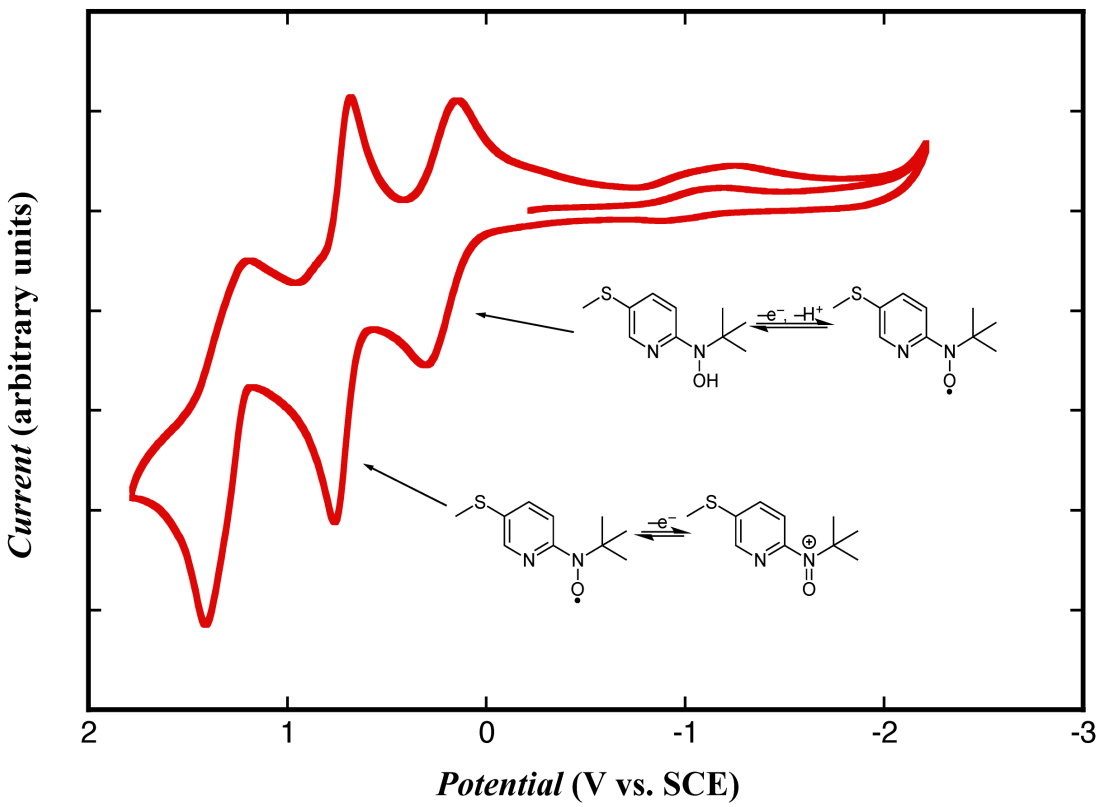

Figure 2.2.2.1. Cyclic Voltammogram of 5-MeS-2-(^{t}BuNOH) recorded in 0.1 M [^{n}Bu$_4$N][PF$_6$] in CH$_3$CN. Figure reprinted with permission of the American Chemical Society © 2013.

In general, the [N–O$^\bullet$]/[N–OH] redox couple is irreversible in acidic media due to complexity arising from an associated proton transfer. Indeed, we observed that the first oxidation events of these pyridyl hydroxylamines were poorly defined in the electrochemical experiments. The [N=O$^+$]/[N–O$^\bullet$] redox couple, on the other hand, was better defined in the electrochemical experiments and served as the basis for our assessment of the relative energetics of the series of pyridyl hydroxylamine derivatives.

Table 2.2.2.1 shows the electrochemical data for the [N=O$^+$]/[N–O$^\bullet$] redox couple in the series of pyridyl hydroxylamines. As expected, the $E_{1/2}$ values shift towards more negative potentials with increasing electron donating ability of the pyridyl substituents into the ^{t}BuNO moiety. This result indicated that the nitroxide radicals adjacent to more electron rich pyridyl ring π-systems were easier to oxidize. We also observed a similar trend in the current ratio, i_{pa}/i_{pc}, which trended

towards unity with the more electron rich substituents. This observation was noteworthy because the ratio, i_{pa}/i_{pc}, could be used to assess the stability of the oxoammonium cation formed during the voltammetric scan, as shown in the reported work by Rychnovsky et al, with values closer to 1.00 indicating increased stability of the oxoammonium species.[9]

Table 2.2.2.1. Redox Potentials in V vs SCE for the [N=O$^+$]/[N–O$^\bullet$] Couples. Table reprinted with permission of the American Chemical Society © 2013.

Compound	E_{pa}	E_{pc}	$E_{1/2}$	ΔE	i_{pa}/i_{pc}
4-NMe$_2$-2-(^{t}BuNOH)py	0.91	–	–	–	–
5-NMe$_2$-2-(^{t}BuNOH)py	0.29	0.19	0.24	0.10	1.08
3-OMe-2-(^{t}BuNOH)py	0.79	0.72	0.76	0.07	1.36
5-MeS-2-(^{t}BuNOH)py	0.83	0.73	0.78	0.10	1.07
5-Me-2-(^{t}BuNOH)py	0.90	0.84	0.87	0.06	1.52
2-(^{t}BuNOH)py	1.05	0.95	1.00	0.10	2.02
5-CF$_3$-2-(^{t}BuNOH)py	1.23	1.10	1.17	0.13	2.55

As shown in Figure 2.2.2.2, we observed a roughly linear relationship between the potentials for the [N=O$^+$]/[N–O$^\bullet$] redox couple with the Hammett constant, σ^+,[10] of the *para*-substituents for the series of 5-substituted pyridyl nitroxides; though a slight negative curvature was evident. However, if these redox potentials were instead plotted versus the Hammett constant, σ,[10] the linear relationship completely broke down and a pronounced negative curvature was observed. This result indicated that bond resonance between the substituent in the 5-position and the ^{t}BuNO moiety played a significant role in shifting the potentials of the [N=O$^+$]/[N–O$^\bullet$] redox events of these compounds. Therefore, it was evident that the σ^+ values provide the most useful linear free energy model for the pyridyl nitroxide system.[10]

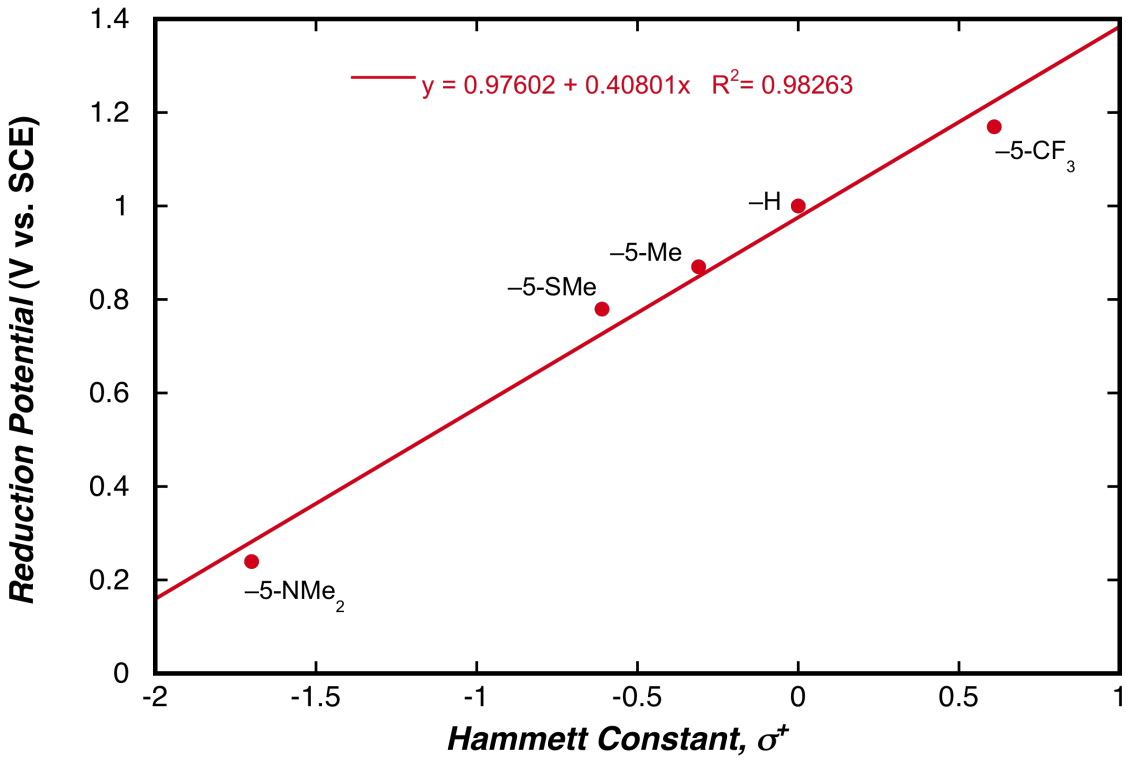

Figure 2.2.2.2. Hammett plot of the redox potential for the [N=O$^+$]/[N–O$^\bullet$] couple of the *para*-substituted pyridyl hydroxylamines versus the constants σ^+ for the *para*-substituents. Figure reprinted with permission of the American Chemical Society © 2013.

The slope of 0.41 given by the linear fit of these data provided a metric for the sensitivity of the nitroxide redox potential to pyridyl substitution. This compared favorably to the slopes of 0.11 and 0.22 obtained in the cases of the aliphatic isoindoline compounds and aromatic substituted *N*-phenylhydroxamic acids, respectively.[2, 5d] Therefore, these results provide definitive evidence that the redox potentials of the pyridyl nitroxide system are ~4 times more sensitive to substituent effects than the isoindoline system and ~2 times more sensitive to substituent effects than the *N*-phenylhydroxamic acid system.

2.2.3 DFT Calculations

Having determined the redox properties of these pyridyl hydroxylamines, we looked into whether DFT calculations in conjunction with experiment could be used to develop a toolset for the predictive design of new pyridyl nitroxides. Methods for estimating the half-wave oxidation potentials of aliphatic nitroxyl radicals have been previously reported with great accuracy and we

used these as the bases of our calculations.[2, 4a] The use of a solvent continuum in the calculations has also been shown to improve the accuracy of these predictions.[9] Therefore, for our calculations, we used a B3LYP hybrid DFT method. Geometry optimizations and frequency calculations were carried out using the 6-31g* basis set and a CPCM solvent continuum with acetonitrile as solvent.[11]

Figure 2.2.3.1 shows the calculated singly occupied molecular orbitals (SOMOs) for the neutral radical forms of the pyridyl nitroxide derivatives. As is evident from these plots, there is significant electron delocalization into the pyridyl ring system, particularly in the 1-, 3-, and 5-positions. This suggested that substituents at the 3- and 5-positions would have a significant effect on the energies of these SOMO orbitals, which would explain the shift in redox potentials observed in the electrochemical results.

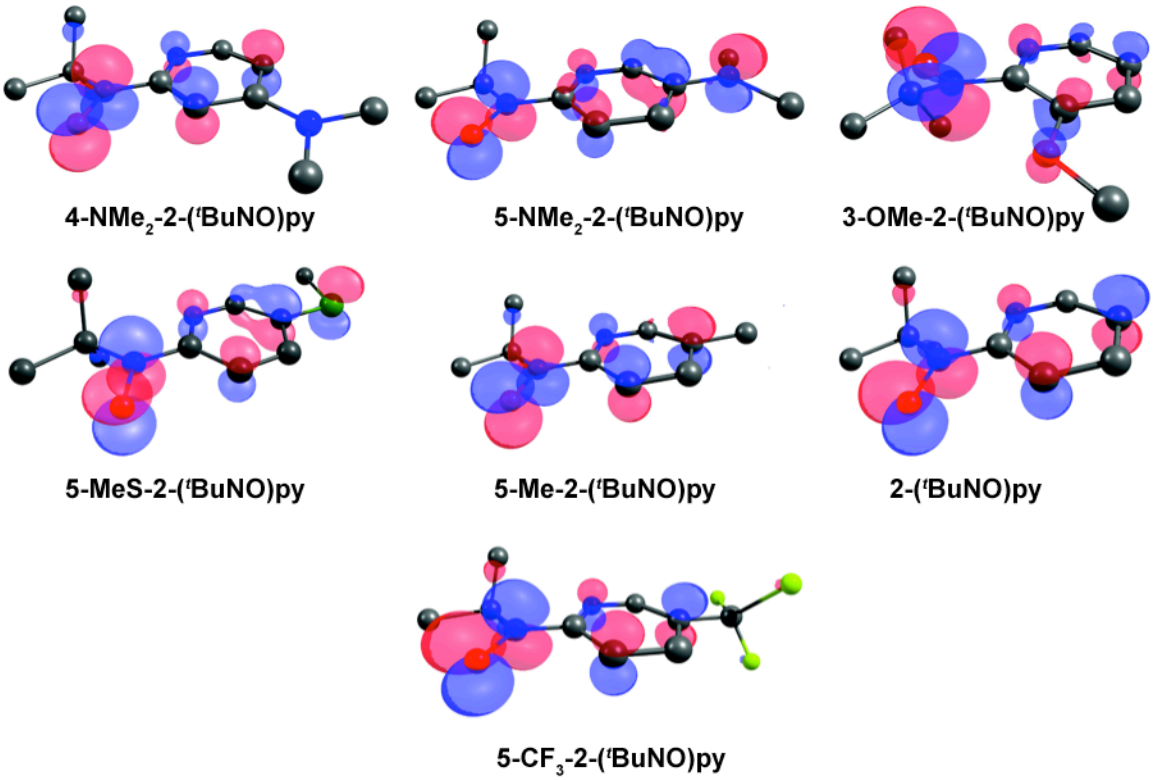

Figure 2.2.3.1. Singly occupied molecular orbitals for the optimized pyridyl nitroxides in their neutral radical forms. Figure reprinted with permission of the American Chemical Society © 2013.

Inspired by the extensive work of Gillmore and co-workers where they correlated the free energy changes between oxidized and reduced forms to redox potential for a diverse group of organic compounds,[12] we set out to form a similar correlation in our pyridyl nitroxide case. In addition to calculations on the neutral radical forms, we performed calculations on the oxidized oxoammonium cation forms of these compounds; the free energy, G, values for both species were determined from frequency calculations. These results are summarized in Table 2.2.3.1 and plotted against the experimentally determined redox potentials (Figure 2.2.3.2).

Table 2.2.3.1. Calculated total free energies, G, of the neutral radical and oxoammonium cation forms of the isolated pyridyl hydroxylamines. Table reprinted with permission of the American Chemical Society © 2013.

Compound	Radical Form G (eV)	Radical Form G (eV)	ΔG (eV)
4-NMe$_2$-2-(^{t}BuNOH)py	–18209.70719	–18204.51814	–5.189
5-NMe$_2$-2-(^{t}BuNOH)py	–18209.50661	–18204.97997	–4.524
3-OMe-2-(^{t}BuNOH)py	–17681.15268	–17676.15735	–4.994
5-MeS-2-(^{t}BuNOH)py	–26470.25567	–26465.18752	–5.152
5-Me-2-(^{t}BuNOH)py	–15635.07860	–15629.88766	–5.177
2-(^{t}BuNOH)py	–14565.83596	–14560.51733	–5.318
5-CF$_3$-2-(^{t}BuNOH)py	–23737.11922	–23731.56225	–5.573

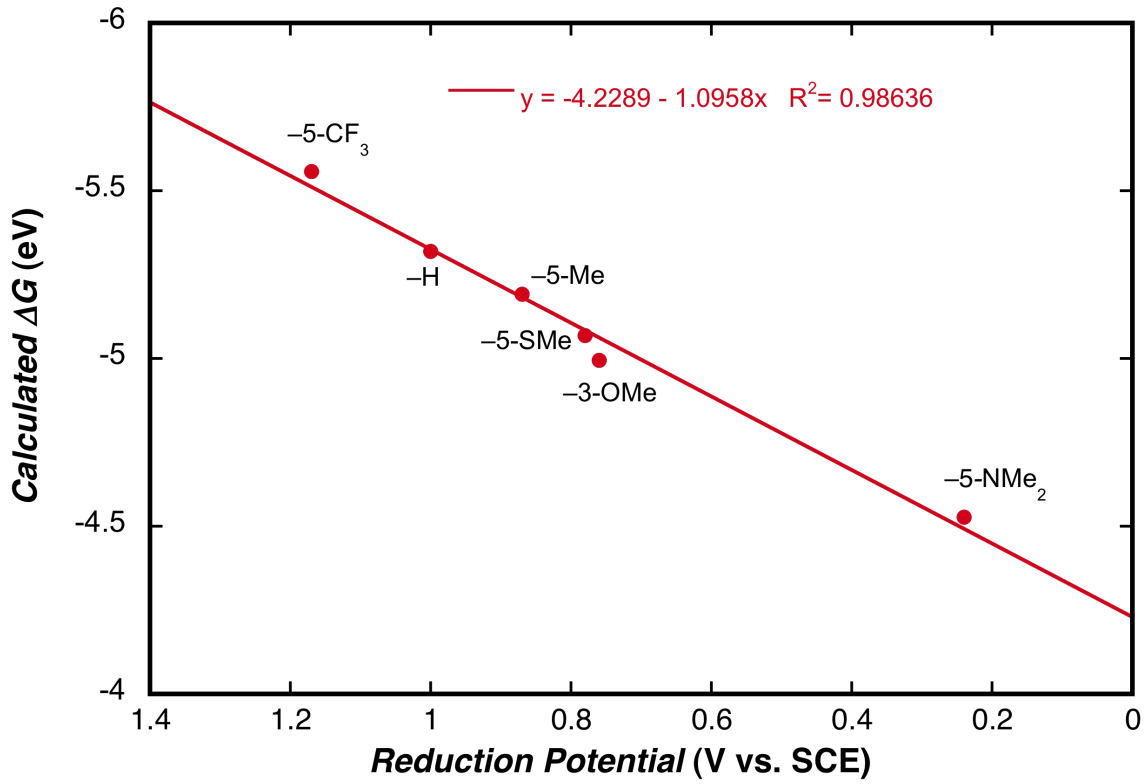

Figure 2.2.3.2. Correlation between calculated free energy differences between the *N*-oxoammonium cation and nitroxide radical forms and observed redox potential. Figure reprinted with permission of the American Chemical Society © 2013.

A remarkably good correlation was formed between the ΔG values and the reduction potentials as indicated by the R^2 value of 0.986. Furthermore, for the calculated half wave potentials, a mean absolute deviation (MAD) of 30 mV from the experimentally determined values was obtained,[4b] which supports the validity of the applied computational model for the pyridyl nitroxide system. It is noteworthy that the linear regression obtained here for the pyridyl nitroxide case is similar to those obtained by Gillmore and coworkers in their study.

The 4-NMe_2-2-(^{t}BuNO)py nitroxide compound was not included in the correlation because the $E_{1/2}$ value of its [N=O$^+$]/[N–O$^\bullet$] redox event could not be accurately determined as a result of the irreversibility of this wave in the CV scan. Nevertheless, the calculated ΔG value obtained for this compound was similar to that of the 5-Me-2-(^{t}BuNO)py, which was in agreement with their similar σ^+ Hammett parameters and similar E_{pa} values. Therefore, the semiempirical correlation

established here provides a basis for the prediction of the pyridyl-based nitroxide oxidation potentials.

2.2.3 Unsuccessful Synthetic Pursuits

Compelled by our results we examined whether we could extend the redox potentials of the pyridyl nitroxides further in the positive direction by incorporating strong resonance withdrawing substituents. We chose the incorporation of 5–NO_2 and 5–SO_2CH_3 as our initial targets. The incorporation of a 5–NO_2 group, which has a σ^+ Hammett parameter of 0.79,[10] was expected to shift the redox potential of the nitrixide moiety to 1.30 versus SCE based on our semi-empirical results, a +130 mV shift from the 5-CF_3-2-(^{t}BuNOH)py derivative. To the best of our knowledge, there is no tabulated σ^+ value for a 5–SO_2CH_3 group, but based on the Hammett parameter, σ_p, of 0.72,[10] it was expected to shift the redox potential by a similar amount.

Attempts to cleanly synthesize these compounds using similar metal-halogen exchange reactions failed. For the 5–SO_2CH_3 substituted derivative, we initially tried adding Turbo Grignard to a THF solution of the known 2-Br-5-$MeSO_2$-py precursor[13] at –78 ºC. Monitoring this step of the reaction indicated that no reaction was occurring at this temperature despite reaction times of 4 h. Furthermore, increasing the number of equivalents of Turbo Grignard by 5-fold had no effect on the conversion of this step. Even when this reaction was performed at 0 ºC or 20ºC, only starting material and minor impurities were observed.

Because no metal halogen exchange reactivity was occurring with Turbo Grignard, we switched to the use of the more reactive ^{n}BuLi reagent. Addition of ^{n}BuLi to 2-Br-5-$MeSO_2$-py at –78 ºC followed by the addition of 2-methyl-2-nitrosopropane led to non-productive reactivity and a mixture of products as determined by ^{1}H-NMR spectroscopy.

To enhance the metal-halogen exchange reactivity of the 2-Br-5-$MeSO_2$-py precursor in an attempt to make it susceptible to magnesium exchange with Turbo Grignard, we converted the 2-bromo precursor to the 2-iodo congener.[14] Briefly, this result was achieved by reacting the 2-Br-5-$MeSO_2$-py with the nucleophilic iodide source, NaI•$2H_2O$, in glacial acetic acid at 100 ºC.[15] This reaction yielded pure 2-I-5-$MeSO_2$-py in 56% isolated yield. Unlike the reaction with the 2-Br-

5-$MeSO_2$-py precursor, the metal-halogen exchange reaction with Turbo Grignard and 2-I-5-$MeSO_2$-py led to significant conversion to the 2-pyridylmagnesium chloride intermediate. Addition of 2-methyl-2-nitroso propane dimer to this intermediate afforded the desired 5-$MeSO_2$-2-(^{t}BuNOH)py product in a 6:1 ratio with undesired side products. However, we were unable to purify the product by simple sublimation or recrystallization.

For the 5–NO_2 substituted derivative, similar approaches were taken starting from the commercially available 2-Cl-5-NO_2-py. Because the 2-I-5-$MeSO_2$-py compound was the most promising starting material for the 5–$MeSO_2$ derivative, we first converted the 2-Cl-5-NO_2-py to its 2-iodo congener with NaI in refluxing glacial acetic acid.[15] The reaction of this 2-I-5-NO_2-py compound with Turbo Grignard in THF at room temperature led to a dark brown solution, which remained dark brown upon addition of 2-methyl-2-nitrosopropane dimer. There were no identifiable resonances in the ^{1}H-NMR corresponding to the desired product. If this reaction was carried out at –78 ºC, a dark red solution was formed immediately upon addition of Turbo Grignard to 2-I-5-NO_2-py. This solution turned dark green upon addition of 2-methyl-2-nitrosopropane dimer. However, quenching with degassed $NH_4Cl_{(aq)}$ produced a red solution and a viscous red oil was isolated. No usable product could be isolated from this mixture.

In light of these results, an alternate route for the isolation of the 5–NO_2 derivative was envisioned where commercially available 2-NH_2-5-NO_2-py would be oxidized to the nitroso compound, 2-NO-5-NO_2-py, and reacted with ^{t}BuMgCl;[16] an acid quench would theoretically form the desired hydroxylamine. Therefore, we attempted to form the 2-NO-5-NO_2-py precursor through modifications of previously reported procedures.[16a, 16b] We were successful in forming the 2-$NS(CH_3)_2$-5-NO_2 intermediate. In our hands, however, reaction of this intermediate with mCPBA to form the 2-NO-5-NO_2-py product did not proceed with appreciable conversion and led to the formation of mixtures of minor products based on ^{1}H NMR spectroscopy. This negative result prevented us from continuing with this synthetic route.

2.3 Conclusions

With these studies, we have demonstrated reliable syntheses for a series of pyridyl-appended hydroxylamine compounds using metal-halogen exchange reactions. Our results also showed that both electron withdrawing and electron donating substituents were tolerated by our modified synthetic route. The use of Turbo Grignard instead of ^{n}BuLi allowed for the synthesis of R-2-(^{t}BuNOH)py where R = 5-CF_3, 6-Br, H, 5-Me, 4–NMe_2, 5–MeS, and 3–OMe without the potential for the formation of butylated addition products. In general, this method allowed for milder reaction conditions. The highly electron donating 5-NMe_2 substituted pyridyl hydroxylamine compound, however, required the use of the conventional ^{n}BuLi reagent to be produced in high yield. These compounds were purified by recrystallization or sublimation, which eliminated the large amounts of solvent waste associated with column chromatography.

Solution electrochemistry experiments indicated that these simple substitutions could tune the oxidative ability of these pyridyl nitroxide radicals over a 0.90 V range. A simple Hammett analysis revealed that the [N=O^{+}]/[N–O$^{\bullet}$] redox potential displayed a 4-fold greater sensitivity to substituent effects compared to the aliphatic nitroxides, and that resonance effects played a significant role in the shifting of these potentials.

DFT calculations on these compounds reproduced the sensitivity of the nitroxide oxidation potential to substituent effects. Calculated free energy changes between the oxidized and neutral forms were correlated to experimental $E_{1/2}$ values in very good agreement (MAD = 0.03 V), providing a predictive toolset for the design of new pyridyl nitroxides in silico.

2.4 Experimental Section

General Methods. Unless otherwise noted, all reactions and manipulations were performed under an inert atmosphere (N_2) using standard Schlenk techniques or in a drybox equipped with a molecular sieves 13X / Q5 Cu–0226S catalyst purifier system. Glassware was oven-dried for at least 3 h at 150 °C prior to use. Chemical shifts were recorded in units of parts per million downfield from residual proteo solvent for ^{1}H–NMR and from characteristic solvent peaks for ^{13}C–NMR. ^{19}F–NMR chemical shifts were referenced using an external $CFCl_3$ reference (0 ppm).

Infrared spectra were collected on samples prepared as KBr pellets. HRMS data were obtained on a TOF mass spectrometer. Cyclic voltammetry data were processed using CHI software v 9.24.

Materials. All solvents were sparged for 20 min with dry N_2 and dried using a commercial two-column solvent purification system comprising columns packed with Q5 reactant and neutral alumina respectively (for hexanes and pentane), or two columns of neutral alumina (for THF, Et_2O, CH_2Cl_2 and CH_3CN). Deuterated solvents were stored over potassium mirror overnight prior to use. Isopropyl magnesium chloride lithium chloride solution (1.3 M in THF) was used as received. 2-iodo-4-(dimethylamino)pyridine,[17] 2-bromo-5-(dimethylamino)pyridine,[18] 2-iodo-3-methoxypyridine,[19] and 2-bromo-5-(methylthio)pyridine[13] were synthesized according to the literature procedures. 2-iodo-5-(trifluoromethyl)pyridine was synthesized starting from 2-chloro-5-(trifluoromethyl)pyridine by modifying a previously published procedure (vide infra).[15, 20] 2-bromopyridine and 2-bromo-5-methylpyridine were available commercially. The [^{n}Bu$_4$N][PF$_6$] electrolyte was synthesized and purified by a slight modification of a reported procedure; [^{n}Bu$_4$N][PF$_6$] was precipitated as a white solid on mixing aqueous solutions of [^{n}Bu$_4$N]Br and [NH$_4$]PF$_6$. The mixture was heated to 40ºC and stirred for 30 min. The white solid was isolated by vacuum filtration and recrystallized three times from hot ethanol.

Synthetic Details and Characterization

Modified Synthesis of 2-iodo-5-(trifluoromethyl)pyridine. A 250 mL round-bottom flask was charged with 2-chloro-5-(trifluoromethyl)pyridine (5.01 g, 27.6 mmol, 1 equiv) and sodium iodide (41.21 g, 275 mmol, 10 equiv). Glacial acetic acid (50 mL) was added, and the solution was refluxed for 3 hours while stirring at 100°C under an N_2 atmosphere. The dark brown solution was cooled to room temperature and poured over frozen distilled water (~200 mL). An off-white solid precipitated, which was isolated by vacuum filtration and rinsed with distilled water. The resulting white solid was dried under reduced pressure and purified by sublimation at 70°C and 0.l Torr. Yield 3.56 g, 47%. m.p. 86.1–86.4 °C. ^{1}H NMR (500 MHz, $CDCl_3$): δ 8.63 (d, J = 2.0 Hz, 1H), 7.89 (d, J = 8.5 Hz, 1H), 7.54 (dd, J = 8.5, 2.0 Hz); ^{13}C NMR (125.8 MHz, $CDCl_3$): δ 147.6 (q,

J = 4.0 Hz), 135.2, 134.4 (q, J = 4.0 Hz), 126.5 (q, J = 34.0 Hz), 123.5 (q, J = 273.0 Hz), 122.3 (q, J = 2.5 Hz); ^{19}F NMR (282.2 MHz, $CDCl_3$): δ –62.7 ppm.

Reaction of 2-halopyridines with 2-methyl-2-nitroso-propane dimer. General Procedure. An N_2 purged Schlenk flask equipped with a magnetic stirrer was charged with halopyridine (1 equiv) and cooled to 0 ºC. A 1.3 M solution of isopropyl magnesium chloride lithium chloride complex in THF (1.1–2 equiv) was added and the reaction was allowed to slowly warm to room temperature where it was reacted for 3 h. The solution was cooled back down to 0 ºC and a clear blue THF solution of 2-methyl-2-nitrosopropane dimer (1 equiv) was added. After reacting for another 3 h, the reaction was quenched with a degassed saturated aqueous NH_4Cl solution. The organic layer was extracted under an N_2 atmosphere with Et_2O by syringing the Et_2O layer into a separate N_2 purged Schlenk flask. The organic extracts were dried over $MgSO_4$ and the organic layer isolated by cannula filtration into another N_2 purged Schlenk flask. Volatiles were removed under reduced pressure and *N-tert*-butyl-*N*-2-pyridylhydroxylamine was isolated by sublimation or recrystallization in 60–80% yield.

***N-tert*-butyl-*N*-2-[4-dimethylamino-pyridyl]hydroxylamine.** A 50 mL Schlenk flask was charged with a solution of 2-iodo-4-(dimethylamino)pyridine (1.00 g, 4.03 mmol, 1 equiv) in THF (5 mL). A 1.3 M solution of isopropylmagnesium chloride lithium chloride complex in THF (3.8 mL, 4.94 mmol, 1.23 equiv) was added dropwise at 0 °C and the mixture was slowly warmed to room temperature. The mixture was stirred at room temperature for 3 h. A separate Schlenk flask was charged with a solution of 2-methyl-2-nitroso-propane dimer (0.77 g, 4.4 mmol, 1.1 equiv) in THF (10 mL). The resulting blue solution was added to the reaction flask by cannula transfer at 0 °C and the mixture was stirred for 3 hours. A saturated, degassed, aqueous solution of ammonium chloride (~25 mL) was added to quench the reaction. The aqueous layer was extracted with degassed CH_2Cl_2 and the organic extracts were syringed into an N_2 purged Schlenk flask. The extracts were dried over $MgSO_4$ and filtered by cannula transfer into an N_2 purged Schlenk flask. The filtrate was concentrated under reduced pressure to yield a crude tan solid. 4-NMe_2-2-(^{t}BuNOH)py was isolated as colorless crystals by layering hexane onto a saturated DME solution

at –35 ºC. The crystals were isolated by filtration and dried under reduced pressure. Yield 0.57 g, 68%. m.p. decomposes above 115 °C; ^{1}H NMR (500 MHz, C_6D_6) δ 8.49 (s, 1H), 8.01 (d, *J* = 5.9 Hz, 1H), 6.35 (d, *J* = 2.4 Hz, 1H), 5.87 (dd, *J* = 5.9, 2.4 Hz, 1H), 2.27 (s, 6H), 1.42 (s, 9H); ^{13}C NMR (125.8 MHz, C_6D_6) δ 163.9, 155.7, 146.9, 104.3, 100.1, 61.8, 38.9, 27.5; FT-IR (KBr, cm^{-1}) 3295, 2984, 1598, 1531, 1512, 1449, 1369, 1224, 1158, 1006, 962, 843, 809, 631; HRMS (ESI) *m/z* calcd for $C_{11}H_{20}N_3O$ (M+H) 210.1606, found 210.1605.

Synthesis of N-*tert*-butyl-N-2-[5-(dimethylamino)pyridyl]hydroxylamine. A 50 mL Schlenk flask was charged with a solution of 2-bromo-5-(dimethylamino)pyridine (0.33 g, 1.6 mmol, 1 equiv) in Et_2O (10 mL) and cooled to –100 ºC in an Et_2O/dry ice bath. To this colorless slurry, a solution of ^{n}BuLi in hexanes (1.0 mL, 1.6 mmol, 1 equiv) was added dropwise. The resulting yellow slurry was allowed to stir for 3 h. 2-methyl-2-nitrosopropane (0.285 g, 1.6 mmol, 1 equiv) dissolved in Et_2O was added dropwise and the reaction turned orange. This mixture was slowly brought to room temperature and stirred for 3 hours producing a green solution. The reaction was quenched with a degassed, saturated aqueous solution of ammonium chloride, producing a red solution. The aqueous layer was extracted with degassed Et_2O and the organic extracts were syringed into an N_2 purged Schlenk flask. The extracts were dried over $MgSO_4$ and filtered by cannula transfer into an N_2 purged Schlenk flask. The filtrate was concentrated under reduced pressure to yield a crude tan solid. 5-NMe_2-2-(^{t}BuNOH)py was isolated as colorless crystals by layering hexane onto a saturated DME solution at –35 ºC. The crystals were isolated by filtration and dried under reduced pressure Yield 0.21 g, 64%. m.p. decomposes above 103 °C; ^{1}H NMR (500 MHz, C_6D_6) δ 8.00 (s, 1H), 7.79 (d, *J* = 3.2 Hz, 1H), 7.04 (d, *J* = 8.9 Hz, 1H), 6.55 (dd, *J* = 8.9, 3.2 Hz, 1H), 2.32 (s, 6H), 1.34 (s, 9H); ^{13}C NMR (125.8 MHz, C_6D_6) δ 153.3, 144.4, 131.7, 121.4, 119.0, 61.6, 40.3, 27.0; FT-IR (KBr, cm^{-1}) 3196, 2974, 1593, 1555, 1497, 1446, 1388, 1360, 1272, 1215, 1125, 1062, 1010, 944, 875, 829, 809, 756, 682, 638, 538; HRMS (ESI) *m/z* calcd for $C_{11}H_{20}N_3O$ (M+H) 210.1606, found 210.1605.

Synthesis of *N-tert*-butyl-*N*-2-[3-methoxypyridyl]hydroxylamine. A 250 mL Schlenk flask was charged with a solution of 2-iodo-3-methoxypyridine (2.02 g, 8.6 mmol, 1 equiv) in THF (20

mL). A 1.3 M solution of isopropylmagnesium chloride lithium chloride complex in THF (7.3 mL, 9.5 mmol, 1.1 equiv) was added dropwise at 0 °C and the mixture was allowed to slowly warm to room temperature over 12 h. A separate Schlenk flask was charged with a solution of 2-methyl-2-nitroso-propane dimer (1.00 g, 5.7 mmol, 0.67 equiv) in THF (10 mL). The resulting blue solution was added to the reaction flask via cannula at 0 °C and slowly warmed to room temperature. Stirring was continued for 3 h at room temperature. A saturated, degassed, aqueous solution of ammonium chloride (5 mL) was added to quench the reaction. The volatiles were removed under reduced pressure, and the organic product was extracted with THF. The filtrate was concentrated under reduced pressure to yield a creamy yellow solid. This solid was suspended in toluene and stirred with gentle heating until dissolved. This saturated solution was then cooled to –35 ºC, resulting in the precipitation of 3-OMe-2-(^{t}BuNOH)py as a white powder. The solid was isolated by filtration over a medium porosity fritted filter. Yield 1.16 g, 69%. m.p. decomposes above 130 °C; ^{1}H NMR (500 MHz, C_6D_6): δ 7.84 (dd, J = 4.5, 1.5 Hz, 1H), 7.21 (s, 1H), 6.49 (dd, *J* = 8.0, 4.5 Hz, 1H), 6.41 (dd, *J* = 8.0, 1.5 Hz, 1H), 3.10 (s, 3H), 1.45 (s, 9H); ^{13}C NMR (125.8 MHz, C_6D_6): δ 153.7, 150.4, 138.5, 121.2, 119.6, 62.2, 55.4, 26.5; FT-IR (KBr, cm^{-1}) 3611, 2977, 1591, 1577, 1465, 1430, 1370, 1283, 1227, 1193, 1126, 1018, 806; HRMS (ESI) *m/z* calcd for $C_{10}H_{16}N_2O_2$ (M+H) 197.1290, found 197.1291.

Synthesis of *N-tert*-butyl-*N*-2-[5-(methylthio)pyridyl] hydroxylamine. 2-bromo-5-(methylthio)pyridine (0.58 g, 2.8 mmol, 1 equiv) dissolved in THF (5 mL) was added to an N_2-purged Schlenk flask and cooled to 0 ºC. A 1.3 M solution of isopropylmagnesium chloride lithium chloride complex in THF (4.3 mL, 5.6 mmol, 2 equiv) was added dropwise at this temperature. The flask was removed from the ice bath and allowed to slowly warm to room temperature where it was reacted for 3 h. The flask was then cooled back down to 0 ºC and a THF solution (5 mL) of 2-methyl-2-nitrosopropane dimer (0.74 g, 4.2 mmol, 1.5 equiv) was added. After 3 h, the reaction was quenched with degassed aqueous NH_4Cl. The aqueous layer was extracted with 3 × 20 mL Et_2O under an N_2 atmosphere. The organic extracts were dried with $MgSO_4$, which was filtered off by cannula filtration, and the solvent was removed under reduced pressure, yielding a crude tan

solid. Layering of pentane onto an Et_2O solution of this crude solid lead to the deposition of colorless crystals of 5-MeS-2-(^{t}BuNOH)py**,** which were collected by filtration. Yield 0.37 g, 63%. m.p. 61.8–62.9 °C; ^{1}H NMR (500 MHz, C_6D_6) δ 8.18 (dd, J = 2.5 , 0.9 Hz, 1H), 7.33 (s, 1H), 7.11 (dd, *J* = 8.6, 2.5 Hz, 1H), 6.93 (dd, *J* = 8.6, 0.9 Hz, 1H), 1.86 (s, 3H), 1.29 (s, 9H); ^{13}C NMR (125.8 MHz, C_6D_6) δ 161.2, 146.3, 137.5, 129.4, 117.1, 62.3, 27.3, 17.1; FT-IR (KBr, cm^{-1}) 3086, 3929, 1571, 1553, 1477, 1432, 1393, 1366, 1260, 1199, 1108, 1013, 964, 950, 921, 846, 834, 741, 665, 626, 549, 473; HRMS (ESI) *m/z* calcd for $C_{10}H_{17}N_2OS$ (M+H) 213.1062, found, 213.1069.

Synthesis of *N-tert*-butyl-*N*-2-[5-methylpyridyl] hydroxylamine. 5-Me-2-(^{t}BuNOH)py was synthesized from the action of 2-bromo-5-methylpyridine (1.0 g, 5.8 mmol, 1 equiv) with a 1.3 M THF solution of isopropylmagnesium chloride lithium chloride complex in THF (5.4 mL, 7.0 mmol, 1.2 equiv) at 0 ºC. The solution was allowed to warm to room temperature and react for 3 h. The reaction was placed back into the 0 ºC ice bath and a THF solution (10 mL) of 2-methyl-2-nitrosopropane dimer was then added (1.01 g, 5.8 mmol, 1 equiv). The reaction was quenched after an additional 3 h with a saturated aqueous ammonium chloride solution that had been sparged with N_2 prior to addition. The organic layer was removed and the aqueous layer was extracted under an N_2 atmosphere with 3 × 15 mL Et_2O. The combined organic extracts were dried with $MgSO_4$, and the organic layer isolated by cannula filtration. Solvents were removed *in vacuuo* and the crude tan solid was sublimed at 50 ºC and 0.1 torr. Yield 0.65 g, 62%. m.p. 64.1–65.5 °C; ^{1}H NMR (500 MHz, C_6D_6) δ 7.97 (s, 1H), 7.75 (s, 1H), 6.92 (d, *J* = 8.2 Hz, 1H), 6.84 (d, *J* = 8.2 Hz, 1H), 1.77 (s, 3H), 1.31 (s, 9H); ^{13}C NMR (125.8 MHz, C_6D_6) δ 160.9, 146.9, 137.7, 117.3, 62.0, 27.2, 17.7; FT-IR (KBr, cm^{-1}) 3190, 2990, 1597, 1474, 1359, 1210, 1026, 957, 855, 675; HRMS (ESI) *m/z* calcd for $C_{10}H_{17}N_2O$ (M+H) 181.1341, found, 181.1336.

Synthesis of *N-tert*-butyl-*N*-[2-pyridyl] hydroxylamine. 2-(^{t}BuNOH)py was synthesized by modification of a previously reported procedure.[1n] A 50 mL Schlenk flask was charged with 2-bromopyridine (0.8 mL, 8.4 mmol, 1 equiv). A 1.3 M solution of isopropylmagnesium chloride lithium chloride complex in THF (8.8 mL, 11.4 mmol, 1.35 equiv) was added dropwise at 0 ºC and

the reaction was allowed to warm to room temperature. The solution was stirred at RT for 1 h. A separate Schlenk flask was charged with a solution of 2-methyl-2-nitroso-propane dimer (0.89 g, 5.1 mmol, 0.6 equiv) in THF (10 mL). The resulting blue solution was added to the reaction flask via cannula at 0 °C and stirred for 3 h. A saturated, degassed, aqueous solution of ammonium chloride (5 mL) was added under N_2 to quench the reaction. The organic layer was removed and the aqueous layer was extracted under an N_2 atmosphere with 3 × 15 mL Et_2O. The combined organic extracts were dried with $MgSO_4$, and the organic layer isolated by cannula filtration. The organic layer was concentrated under reduced pressure to yield a crude tan solid. 2-(^{t}BuNOH)py was isolated as colorless crystals after sublimation at 35 °C and 0.2 torr. Yield 1.12 g, 80%. m.p. 44.7–45.4 ºC (lit. 40–42 ºC); ^{1}H NMR (500 MHz, C_6D_6) δ 8.08 (ddd, *J* = 4.9, 2.0, 0.5 Hz, 1H), 7.66 (s, 1H), 6.99 (ddd, *J* = 8.6, 6.6, 2.0 Hz, 1H) 6.97 (ddd, *J* = 8.6, 1.5, 0.5 Hz, 1H), 6.40 (ddd, *J* = 6.6, 4.9, 1.5 Hz, 1H), 1.30 (s, 9H); ^{13}C NMR (125.8 MHz, C_6D_6) δ 163.6, 147.0, 137.1, 118.9, 117.2, 62.2, 27.3; FT-IR (KBr, cm^{-1}) 2972, 1597, 1465, 1429, 1360, 1273, 1200, 1027, 932, 748, 702; HRMS (ESI) *m/z* calcd for $C_9H_{15}N_2O$ (M+H) 167.1184, found 167.1183.

Synthesis of *N-tert*-butyl-*N*-2-[5-(trifluoromethyl)pyridyl] hydroxylamine. A 50 mL Schlenk flask was charged with a solution of 2-iodo-5-(trifluoromethyl)pyridine (0.29 g, 1.07 mmol, 1 equiv) in THF (~5 mL). A 1.3 M solution of isopropylmagnesium chloride lithium chloride complex in THF (1.2 mL, 1.56 mmol, 1.45 equiv) was added dropwise at –78 °C and stirred for 2 hours. A separate Schlenk flask was charged with a solution of 2-methyl-2-nitroso-propane dimer (0.35 g, 2 mmol, 2 equiv) in THF (5 mL). The resulting blue solution was added to the reaction flask via cannula at –78 °C and reacted for 3 h. A saturated, degassed, aqueous solution of ammonium chloride (5 mL) was added to quench the reaction. All volatiles were removed under reduced pressure, and the organic product was extracted with Et_2O. The filtrate was concentrated under reduced pressure to yield a creamy yellow solid. 5-CF_3-2-(^{t}BuNOH)py was isolated as a white solid after sublimation at 50 °C and 0.2 torr. Yield 0.19 g, 74%. m.p. 78.8–79.7 ^{o}C; ^{1}H NMR (500 MHz, C_6D_6): δ 8.33 (dd, *J* = 2.5, 1.0 Hz, 1H), 7.22 (dd, *J* = 8.8, 2.5 Hz, 1H), 6.74 (dd, *J* = 8.8, 1.0 Hz), 6.02 (s, 1H), 1.30 (s, 9H); ^{13}C NMR (125.8 MHz, C_6D_6): δ 165.4, 144.5 (q, *J* = 4.3 Hz),

134.3 (q, *J* = 3.3 Hz), 125.2 (q, *J* = 271.2 Hz), 119.9 (q, *J* = 32.9 Hz), 113.8, 63.0, 27.6; ^{19}F NMR (282.2 MHz, C_6D_6): δ –61.2 ppm; FT-IR (KBr, cm^{-1}) 3233, 2984, 1607, 1575, 1484, 1392, 1338, 1162, 1080, 854; HRMS (ESI) *m/z* calcd for $C_{10}H_{14}F_3N_2O$ (M+H) 235.1058, found 235.1059.

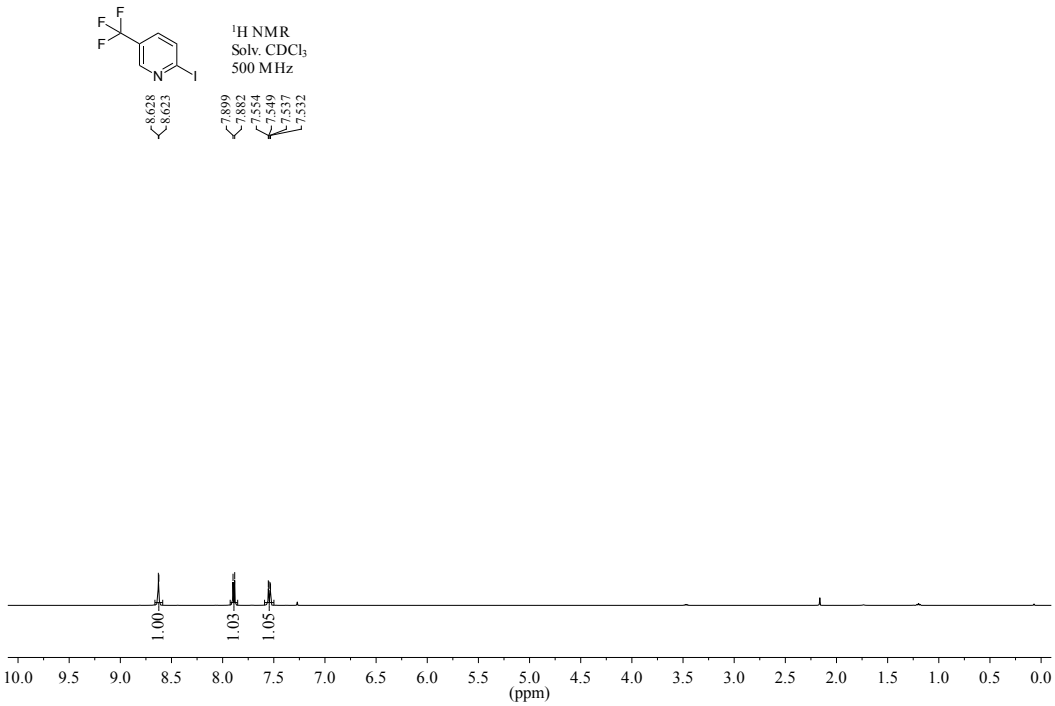

Figure 2.4.1. ^{1}H NMR spectrum of 2-I-5-CF_3-py.

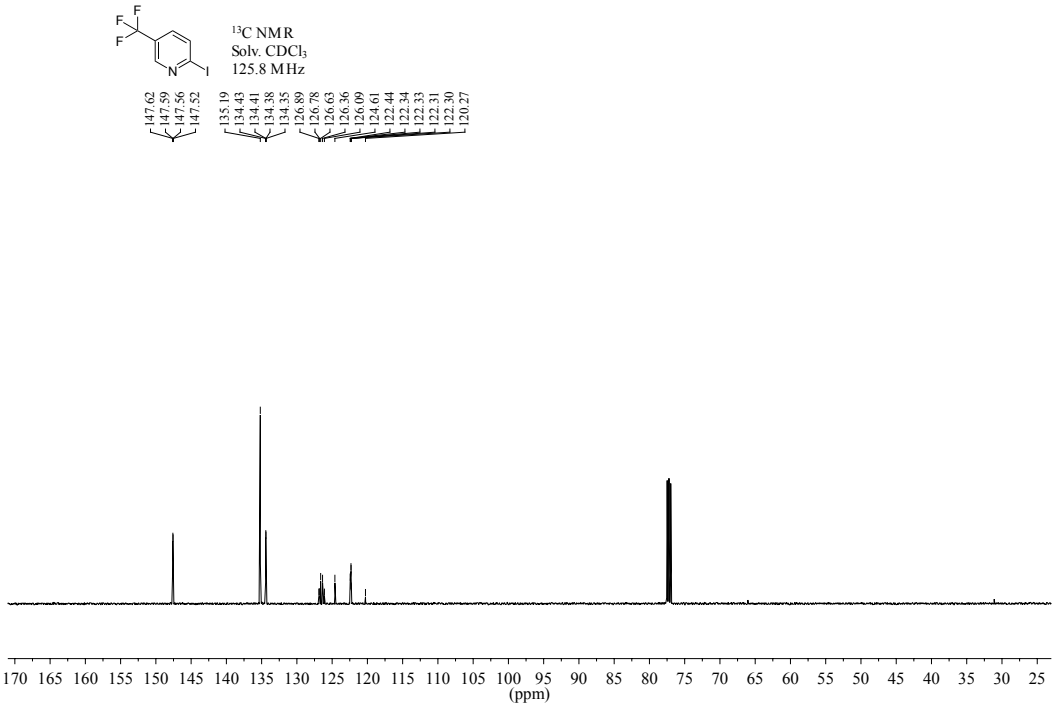

Figure 2.4.2. ^{13}C{^{1}H} NMR of 2-I-5-CF_3-py.

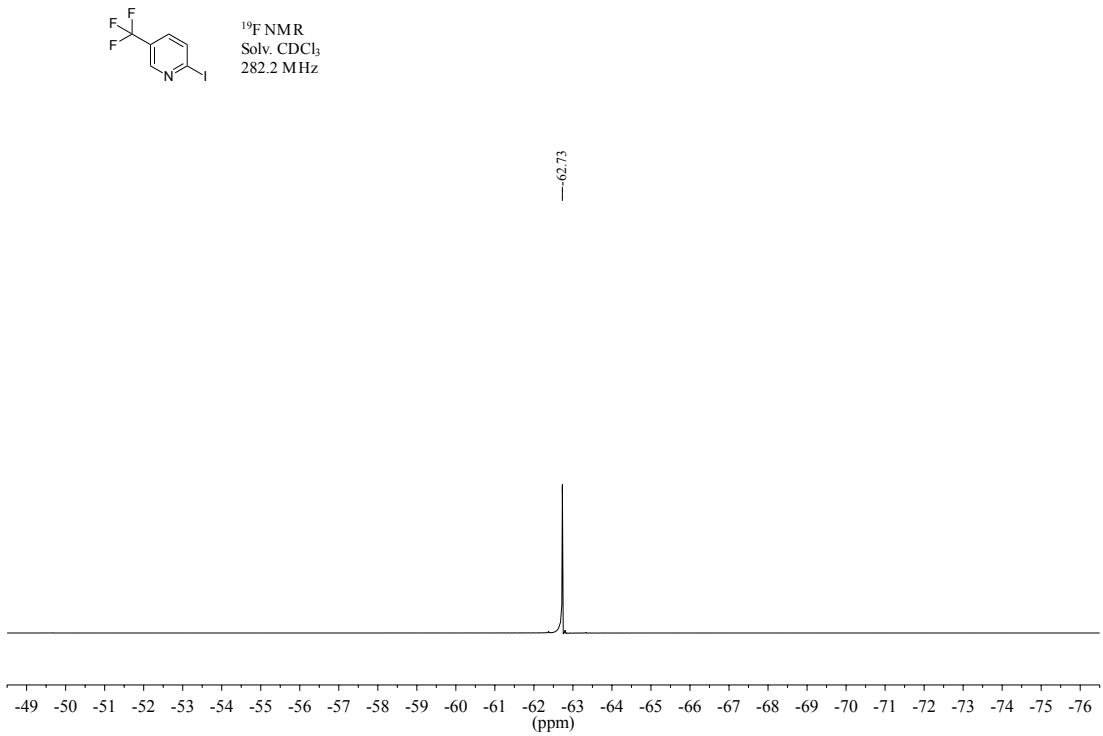

Figure 2.4.3. $^{19}F\{^{1}H\}$ NMR of 2-I-5-CF_3-py.

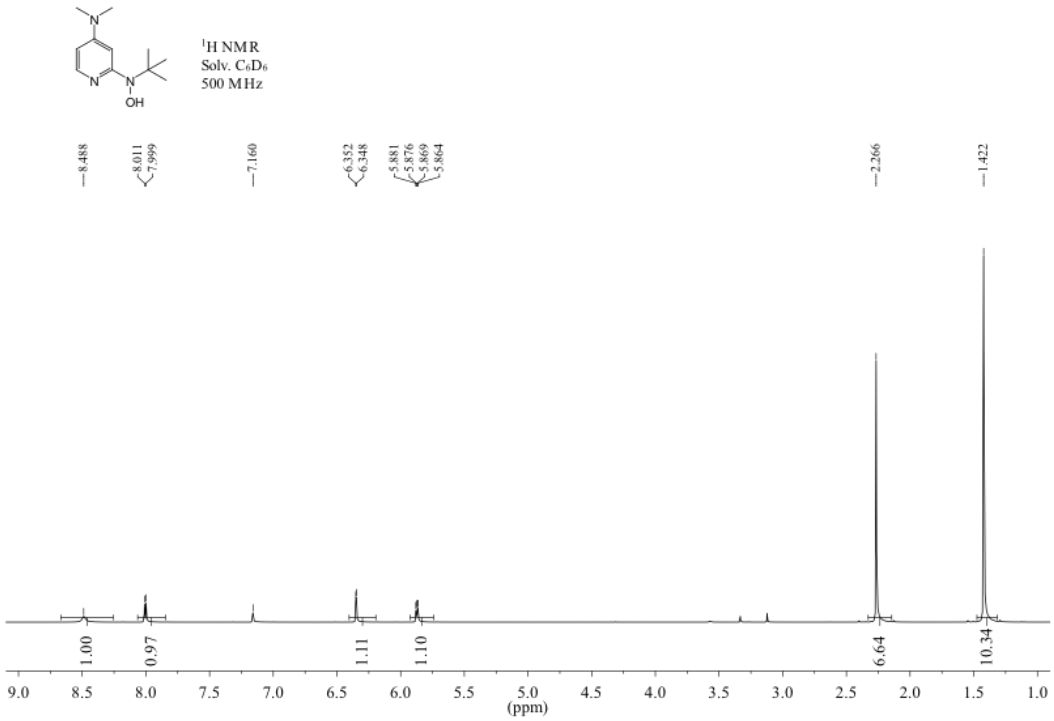

Figure 2.4.4. ^{1}H NMR of 4-NMe_2-2-(^{t}BuNOH)-py.

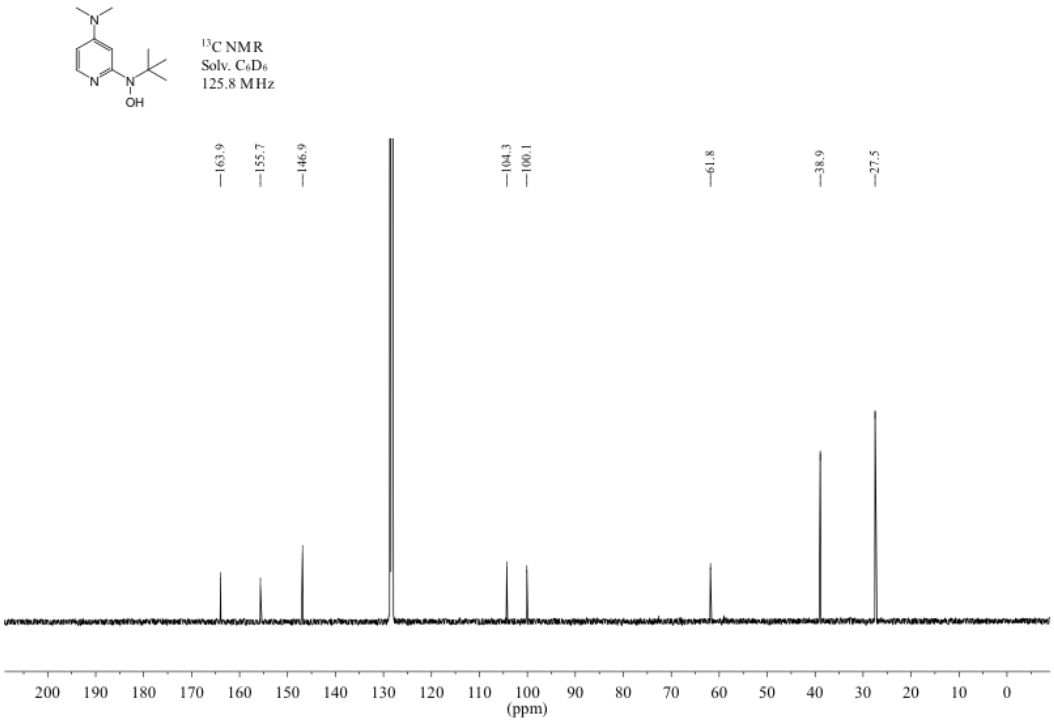

Figure 2.4.5. $^{13}C\{^{1}H\}$ NMR of 4-NMe_2-2-(^{t}BuNOH)-py.

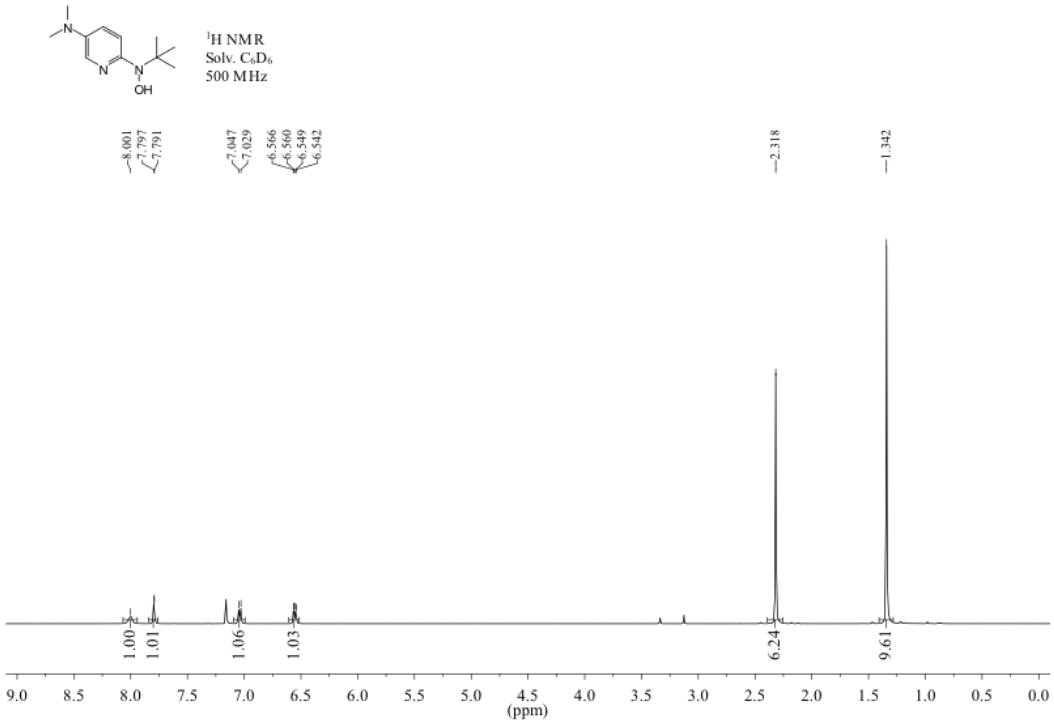

Figure 2.4.6. ^{1}H NMR of 5-NMe_2-2-(^{t}BuNOH)-py.

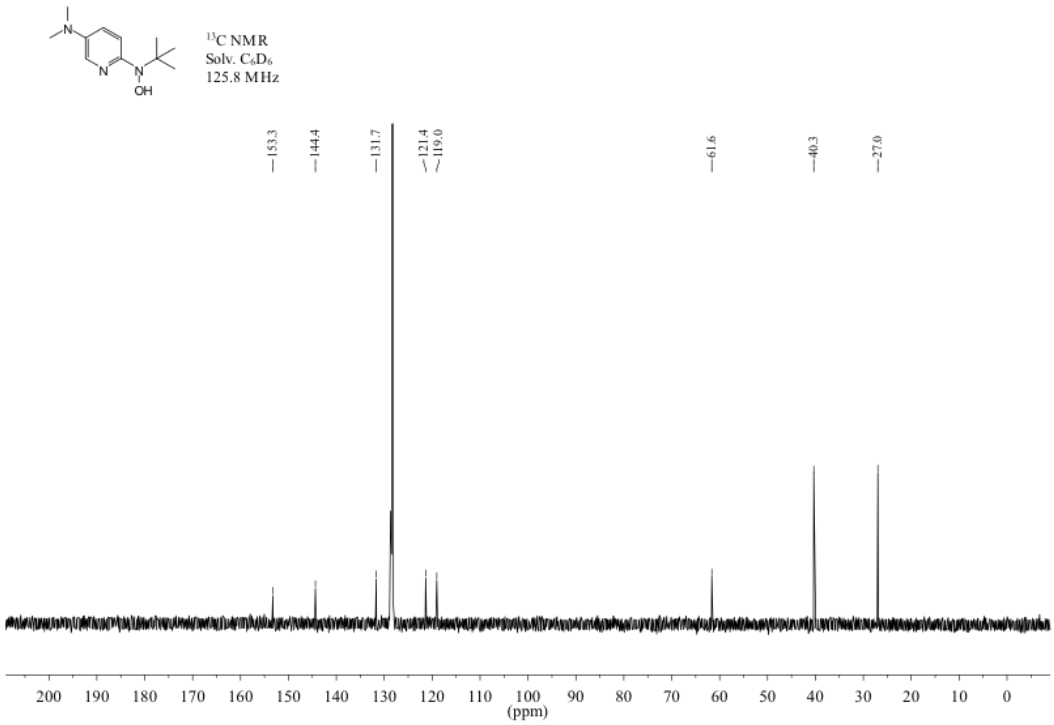

Figure 2.4.7. $^{13}C\{^{1}H\}$ NMR of 5-NMe_2-2-(^{t}BuNOH)-py.

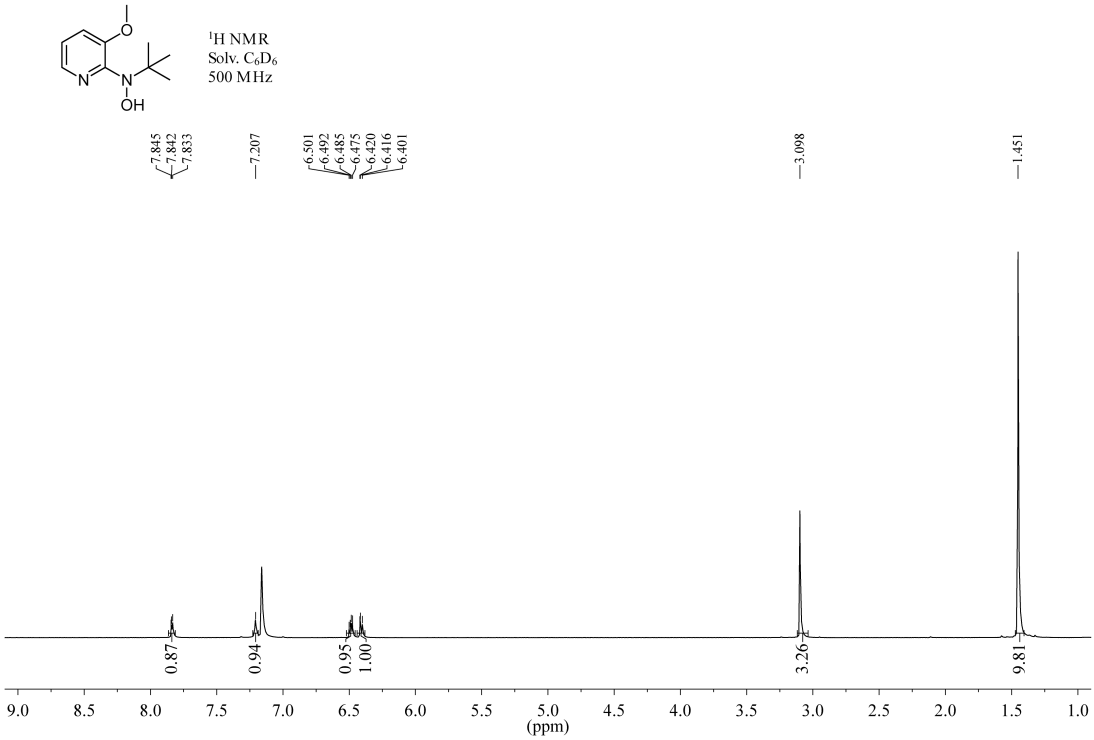

Figure 2.4.8. ^{1}H NMR of 3-OMe-2-(^{t}BuNOH)-py.

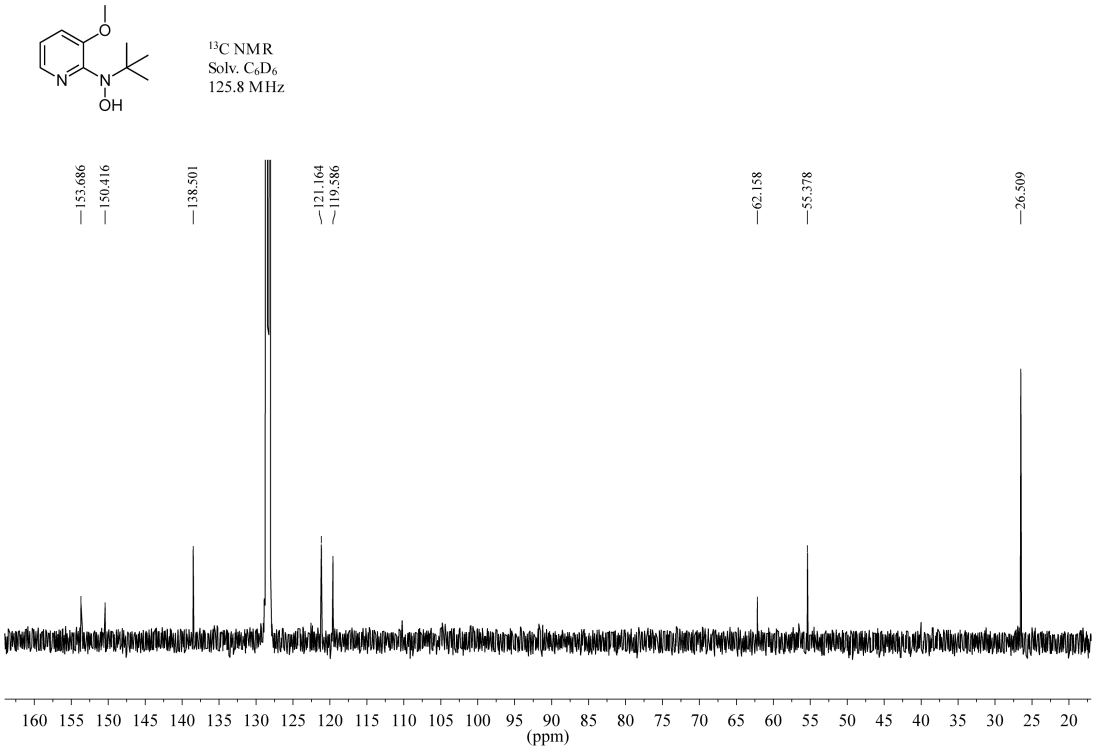

Figure 2.4.9. $^{13}C\{^{1}H\}$ NMR of 3-OMe-2-(^{t}BuNOH)-py.

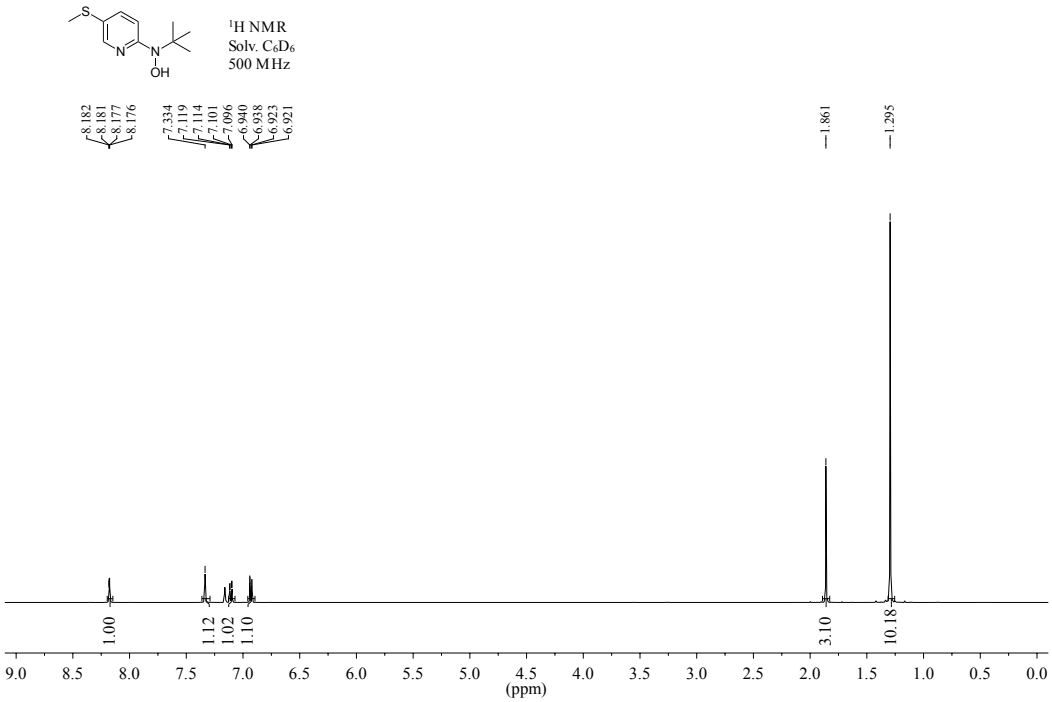

Figure 2.4.10. ^{1}H NMR of 5-MeS-2-(^{t}BuNOH)-py.

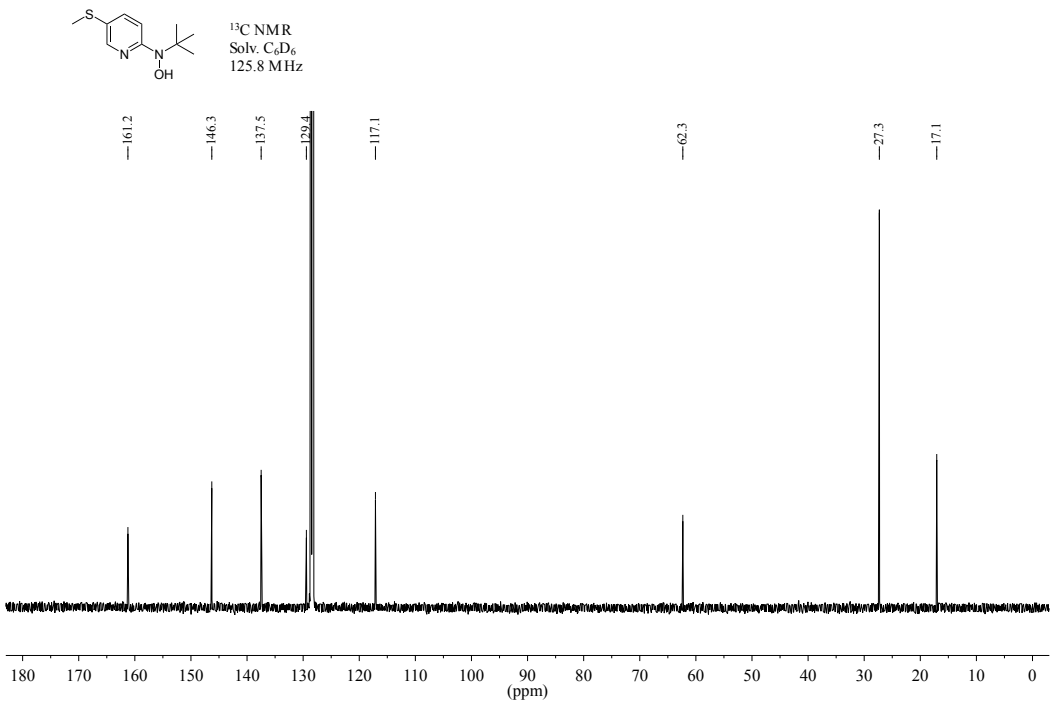

Figure 2.4.11. $^{13}C\{^{1}H\}$ NMR of 3-MeS-2-(^{t}BuNOH)-py.

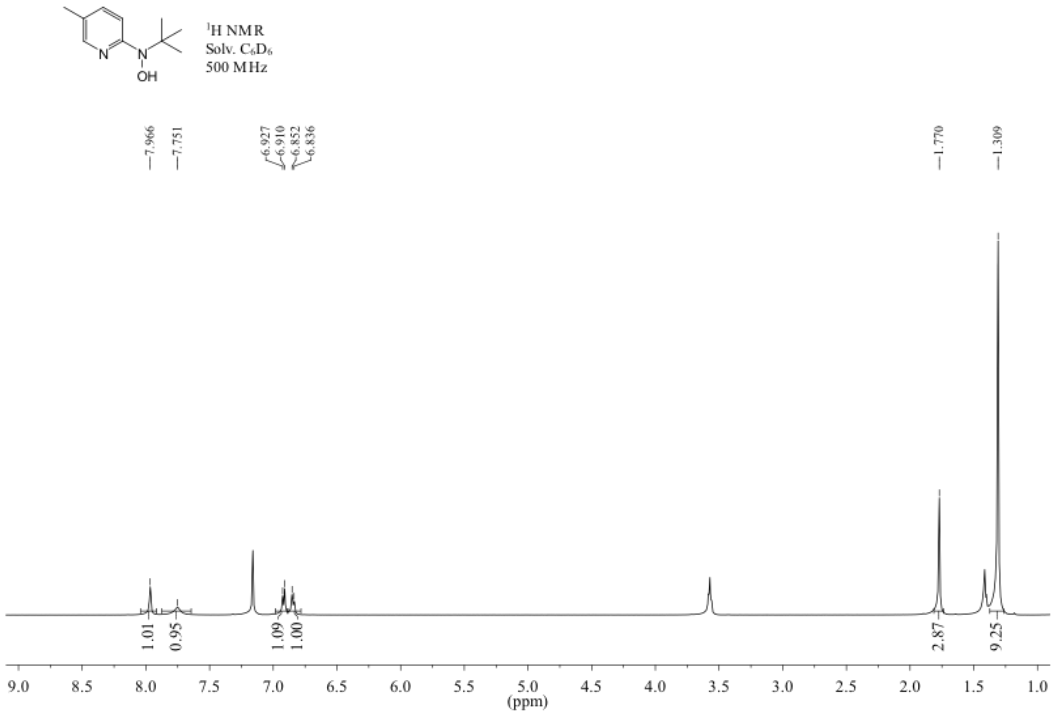

Figure 2.4.12. ^{1}H NMR of 5-Me-2-(^{t}BuNOH)-py.

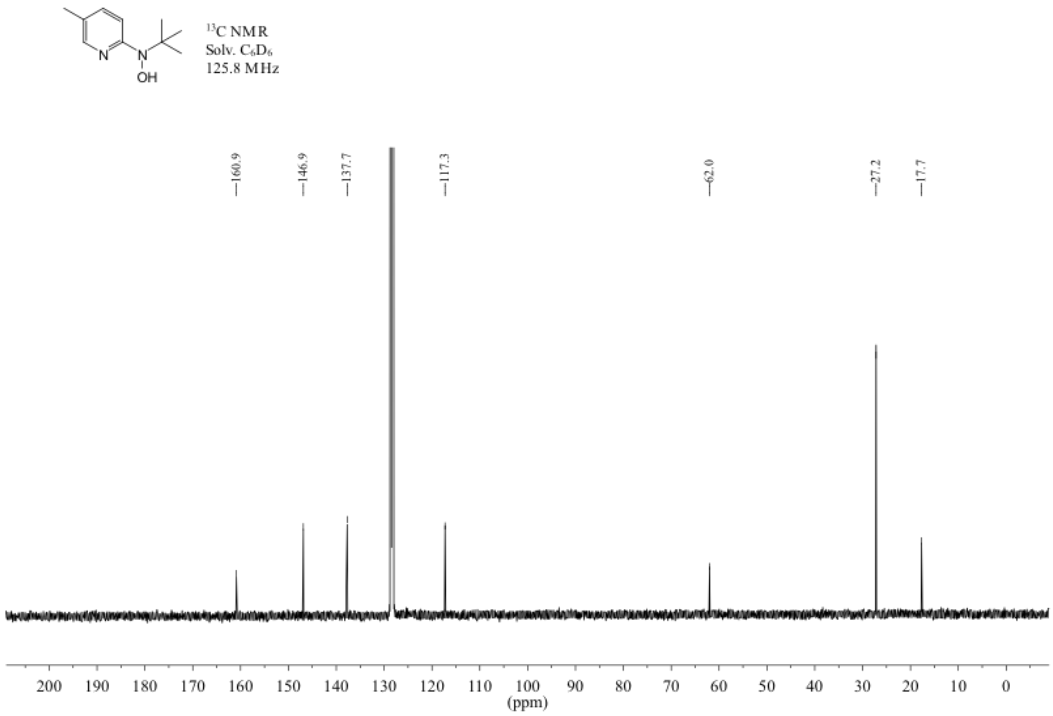

Figure 2.4.13. $^{13}C\{^{1}H\}$ NMR of 5-MeS-2-(^{t}BuNOH)-py.

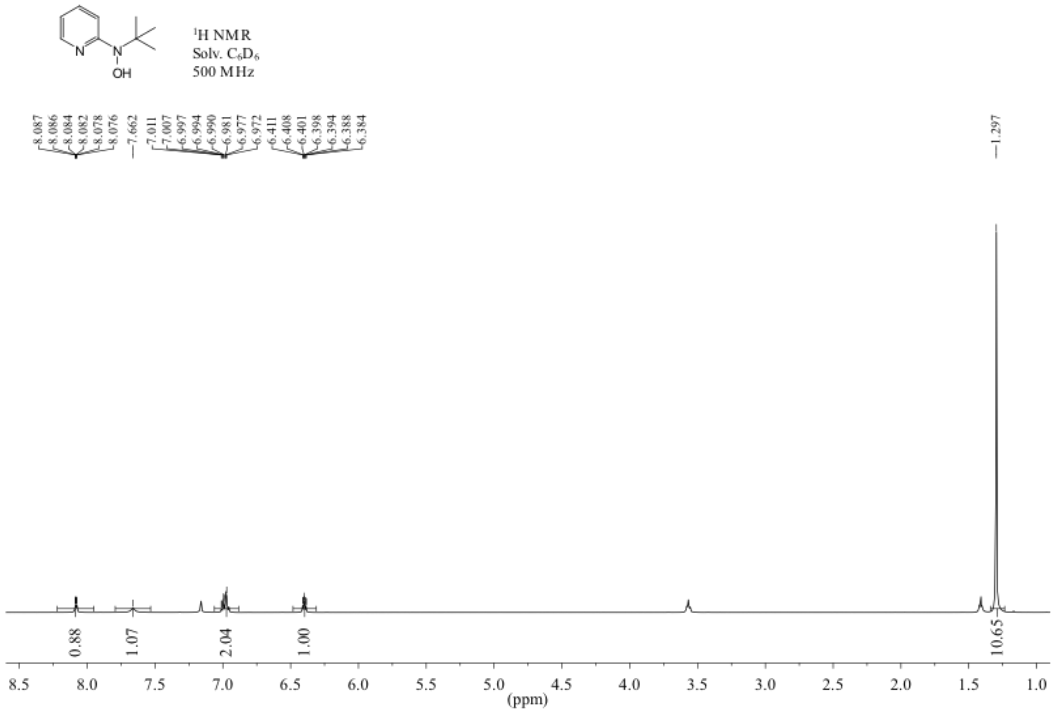

Figure 2.4.14. ^{1}H NMR of 2-(^{t}BuNOH)-py.

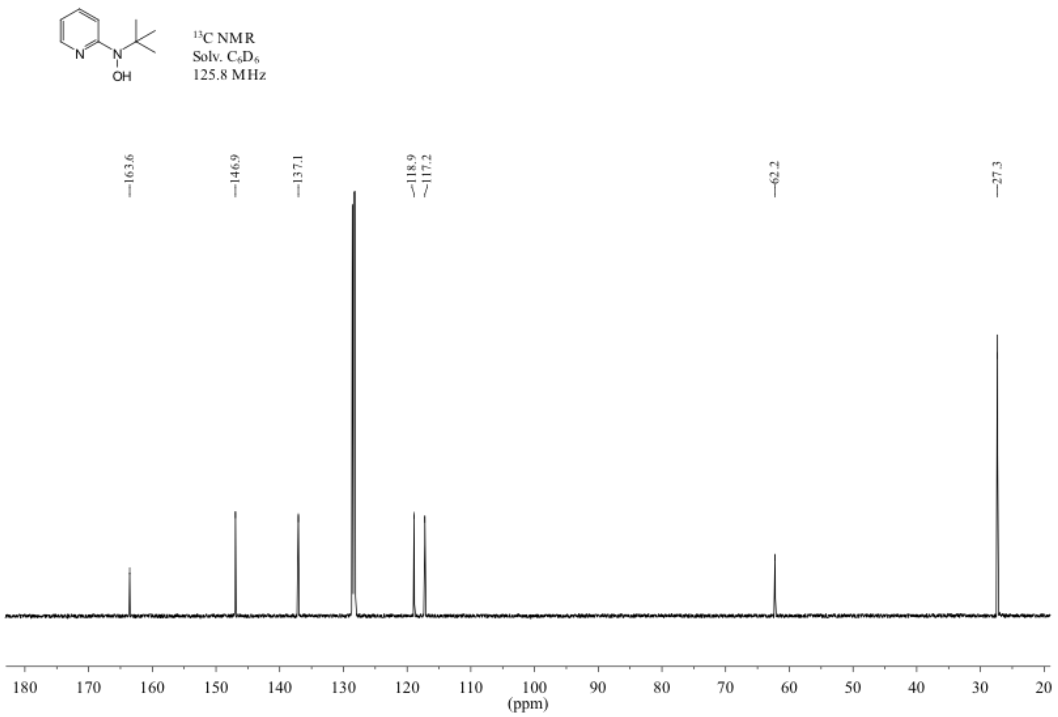

Figure 2.4.15. $^{13}C\{^{1}H\}$ NMR of 2-(^{t}BuNOH)-py.

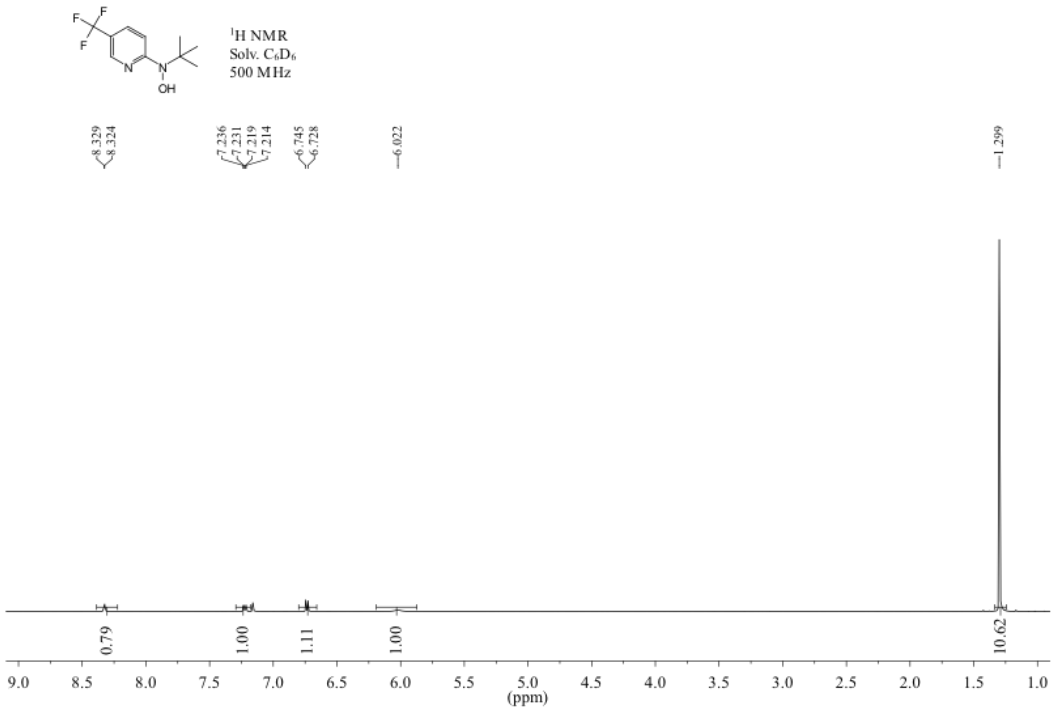

Figure 2.4.16. ^{1}H NMR of 5-CF_3-2-(^{t}BuNOH)-py.

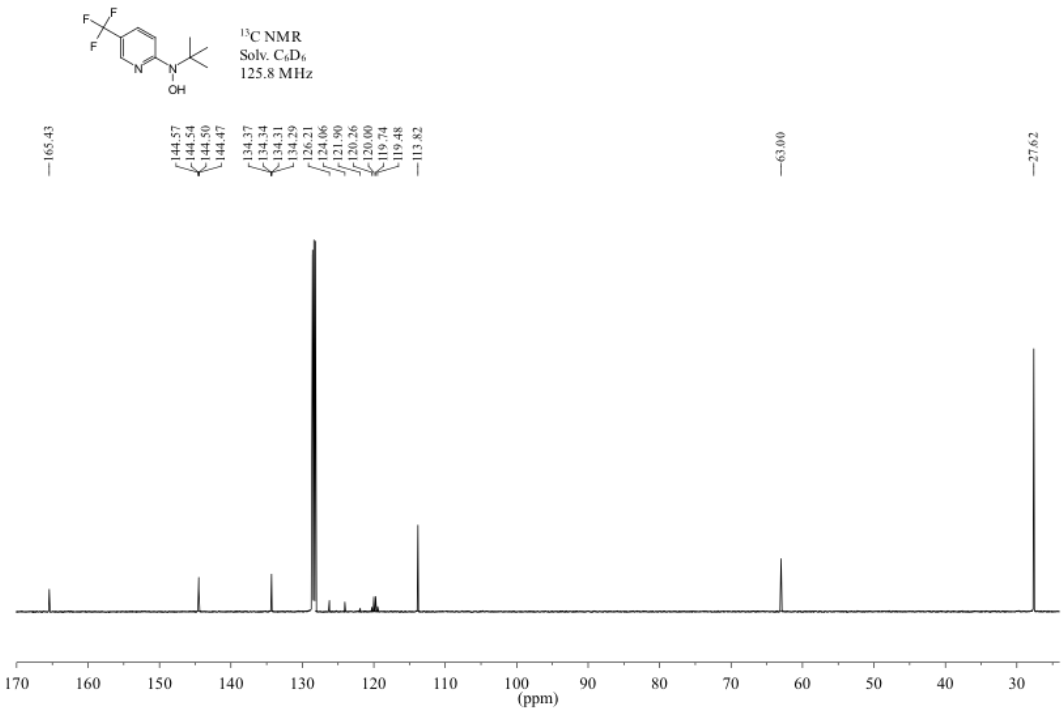

Figure 2.4.17. $^{13}C\{^{1}H\}$ NMR of 5-CF_3-2-(^{t}BuNOH)-py.

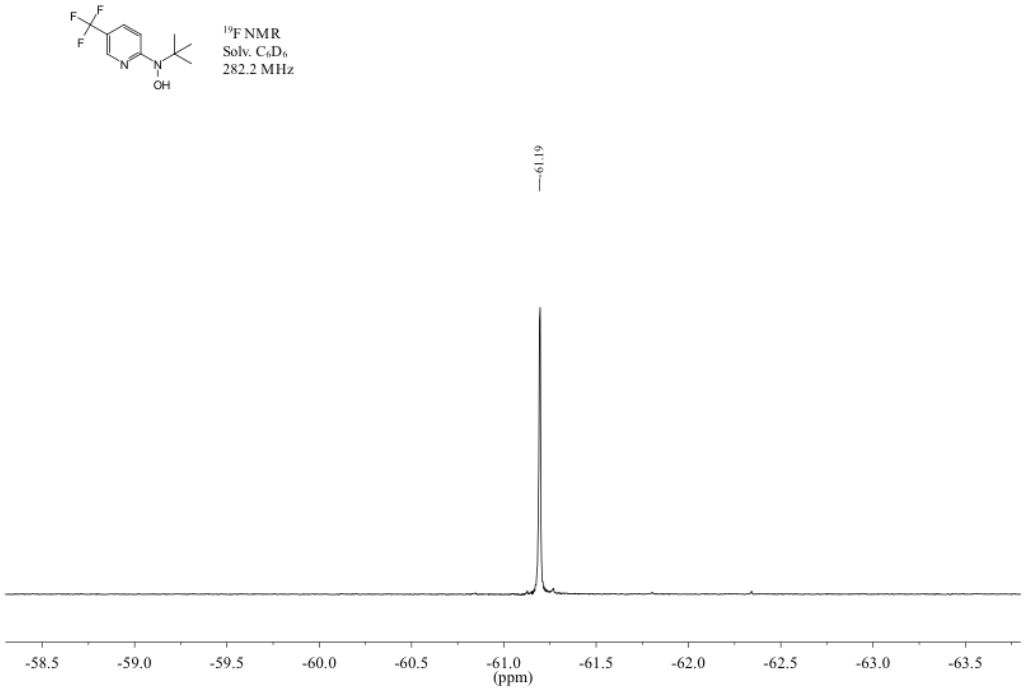

Figure 2.4.18. $^{19}F\{^{1}H\}$ NMR of 5-CF_3-2-(^{t}BuNOH)-py.

X-ray Crystallography. X-ray intensity data were collected on a Bruker APEXII CCD area detector employing graphite-monochromated Mo-Ka radiation (l=0.71073 Å) at a temperature of 143(1)K. Rotation frames were integrated using SAINT,[21] producing a listing of unaveraged F^2 and s(F^2) values which were then passed to the SHELXTL[22] program package for further processing and structure solution. The intensity data were corrected for Lorentz and polarization effects and for absorption using SADABS.[23]

The structure was solved by direct methods (SHELXS-97).[24] Refinement was by full-matrix least squares based on F2 using SHELXL-97.[24] All reflections were used during refinement. Non-hydrogen atoms were refined anisotropically and hydrogen atoms were refined using a riding model.

Crystallographic data and structure refinement information for **6-Br-2-(^{t}BuNOH)py** (Penn4064) are summarized in Tables 2.4.1.

Table 2.4.1. Crystallographic parameters for 6-Br-2-(^{t}BuNOH)py.

	6-Br-2-(^{t}BuNOH)py (Penn4064)
Empirical formula	$C_9H_{13}N_2OBr$
Formula weight	245.12
Temperature	143(1) K
Wavelength	0.71073 Å
Crystal system	triclinic
Space group	$P\bar{1}$
Cell constants:	
a	6.2902(5) Å
b	9.7633(8) Å
c	9.9781(9) Å
α	62.314(3)°
β	73.204(3)°
γ	75.961(3)°
Volume	515.22(7) $Å^3$
Z	2
Density (calculated)	1.580 Mg/m^3
Absorption coefficient	3.953 mm^{-1}
F(000)	248
Crystal size	0.50 x 0.15 x 0.15 mm^3
Theta range for data collection	2.36 to 27.52°
Index ranges	$-8 \leq h \leq 8$, $-12 \leq k \leq 12$, $-12 \leq l \leq 12$
Reflections collected	20449
Independent reflections	2317 [R(int) = 0.0251]
Completeness to theta = 27.52°	97.8 %
Absorption correction	Semi-empirical from equivalents
Max. and min. transmission	0.7456 and 0.4518
Refinement method	Full-matrix least-squares on F^2
Data / restraints / parameters	2317 / 0 / 123
Goodness-of-fit on F^2	1.050
Final R indices [I>2sigma(I)]	R1 = 0.0142, wR2 = 0.0365
R indices (all data)	R1 = 0.0148, wR2 = 0.0368
Largest diff. peak and hole	0.288 and -0.261 e.$Å^{-3}$

Electrochemistry. All experiments were performed under an inert atmosphere (N_2) using standard Schlenk techniques with electrochemical cells that consisted of a 10 mL vial, glassy carbon disk (3 mm diameter) working electrode, a platinum wire counter electrode, and a silver wire plated with AgCl as a quasi-reference electrode. The working electrode surfaces were polished prior to each set of experiments. Potentials recorded in CH_3CN were referenced versus ferrocene, which was added as an internal standard for calibration at the end of each run. These values were reported vs. SCE using the formal reduction potential for Fc of $E_{1/2}$ = +0.40 V vs. SCE, tabulated by Geiger and Connelly.[25] Solutions employed during CV studies were ~3 mM in analyte and 100 mM in [$^{n}Bu_4N$][PF_6]. All data were collected in a positive-feedback IR compensation mode. The CH_3CN solution cell resistances were measured prior to each run to insure resistances ≤ ~500 Ω.[26] Scan rate dependences of 50–1000 mV/s were performed to determine electrochemical reversibility.

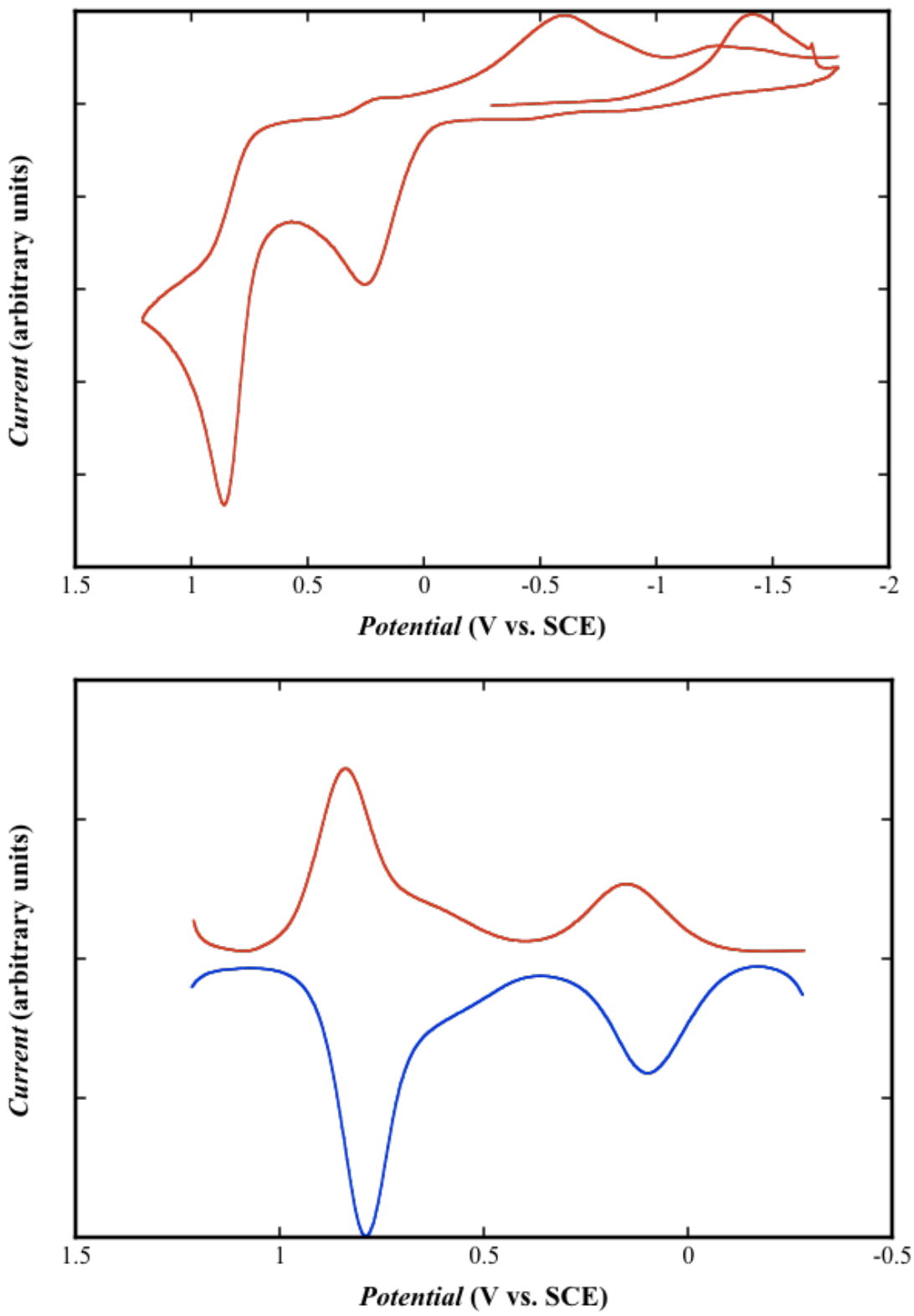

Figure 2.4.19. Cyclic voltammogram (top) and differential pulse voltammogram (bottom) of 4-NMe_2-2-(^{t}BuNOH)py.

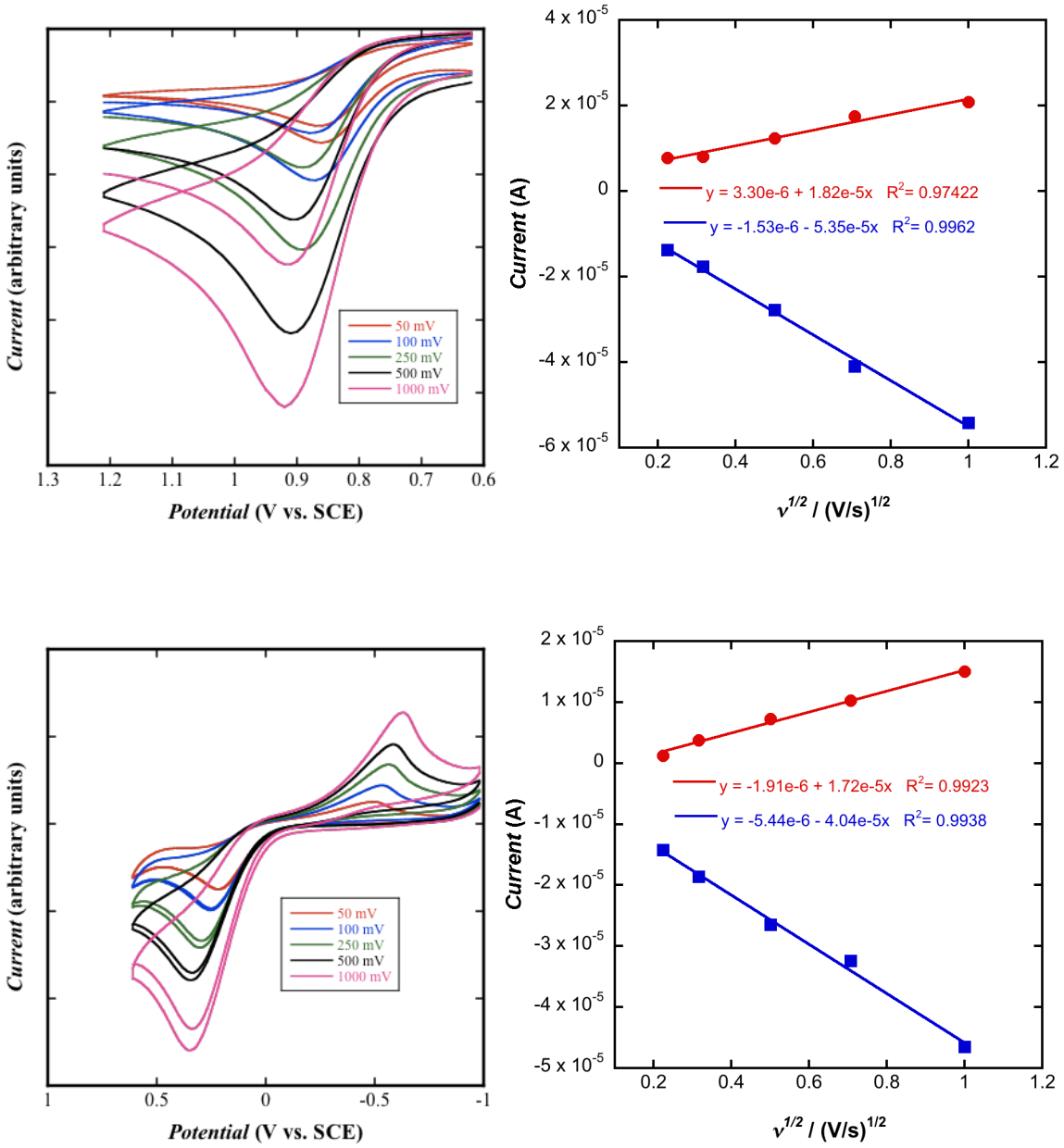

Figure 2.4.20. Scan rate dependence for the [N=O$^+$]/[N–O$^\bullet$] (top) and [N–O$^\bullet$]/[N–O$^-$] (bottom) redox couples of 4-NMe$_2$-2-(^{t}BuNOH)py.

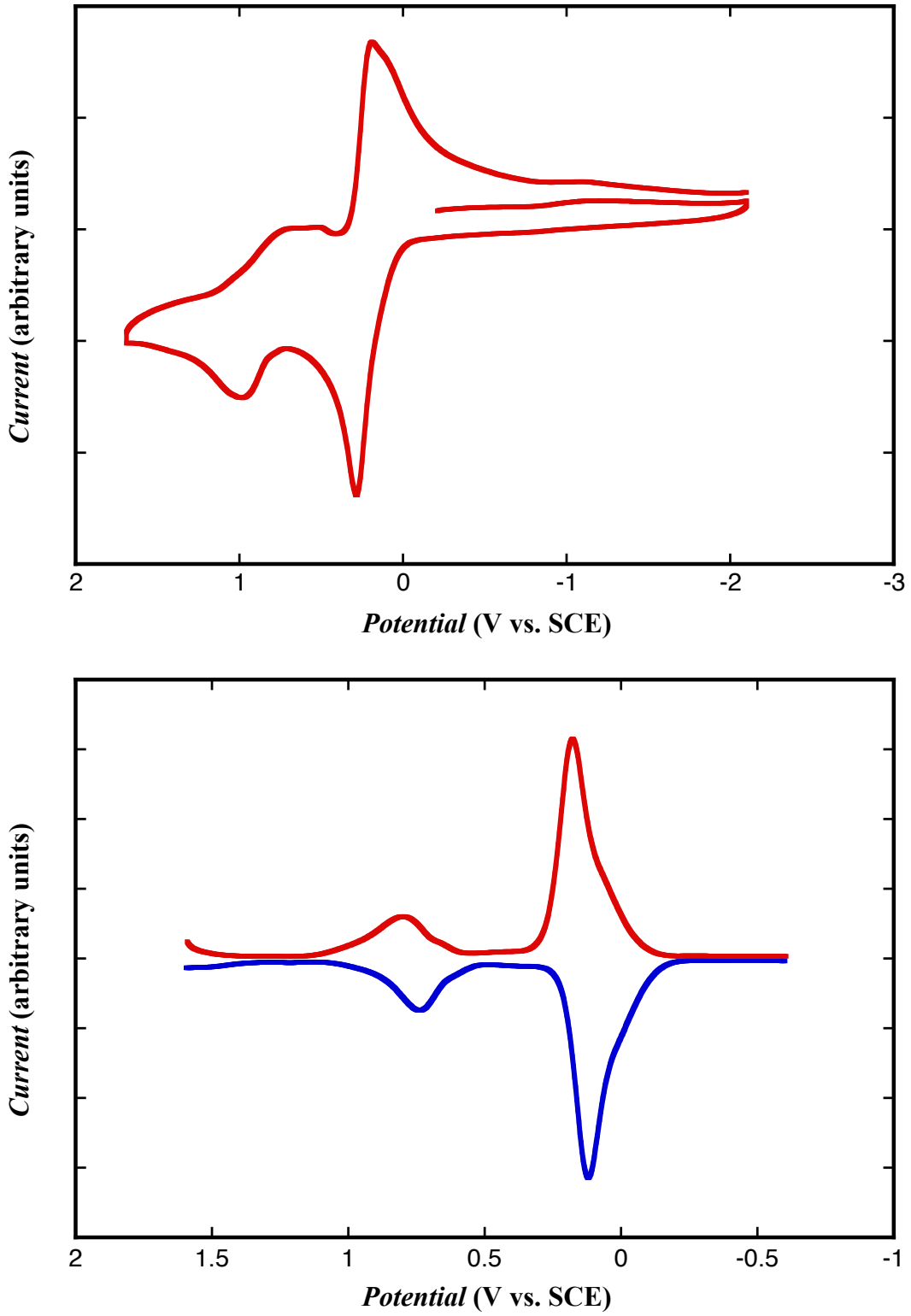

Figure 2.4.21. Cyclic voltammogram (top) and differential pulse voltammogram (bottom) of 5-NMe_2-2-(^{t}BuNOH)py.

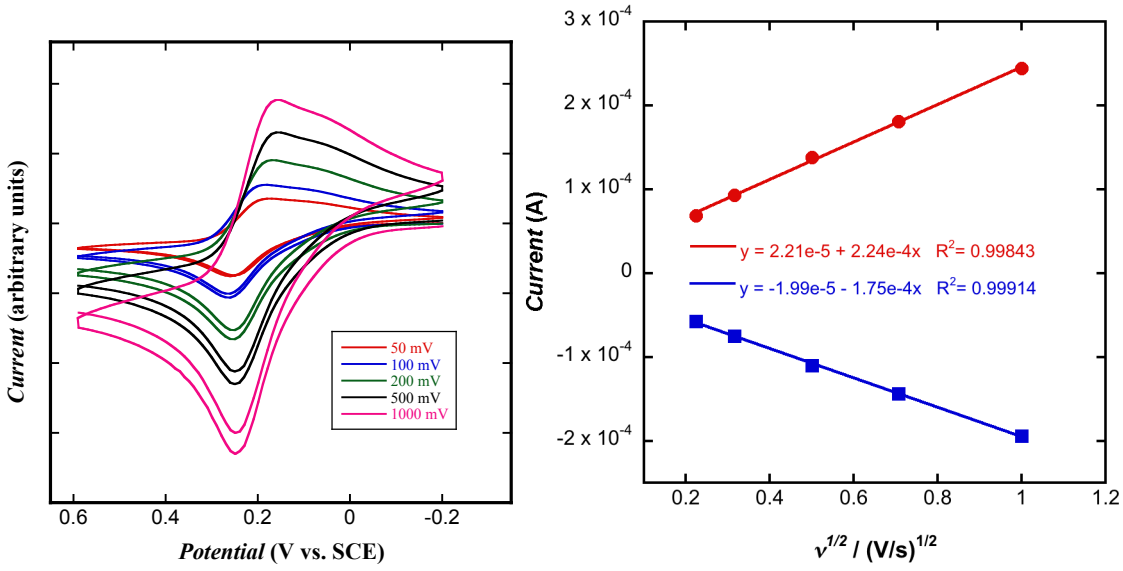

Figure 2.4.22. Scan rate dependence for the [N=O$^+$]/[N–O$^\bullet$] redox couple of 5-NMe$_2$-2-(^{t}BuNOH)py.

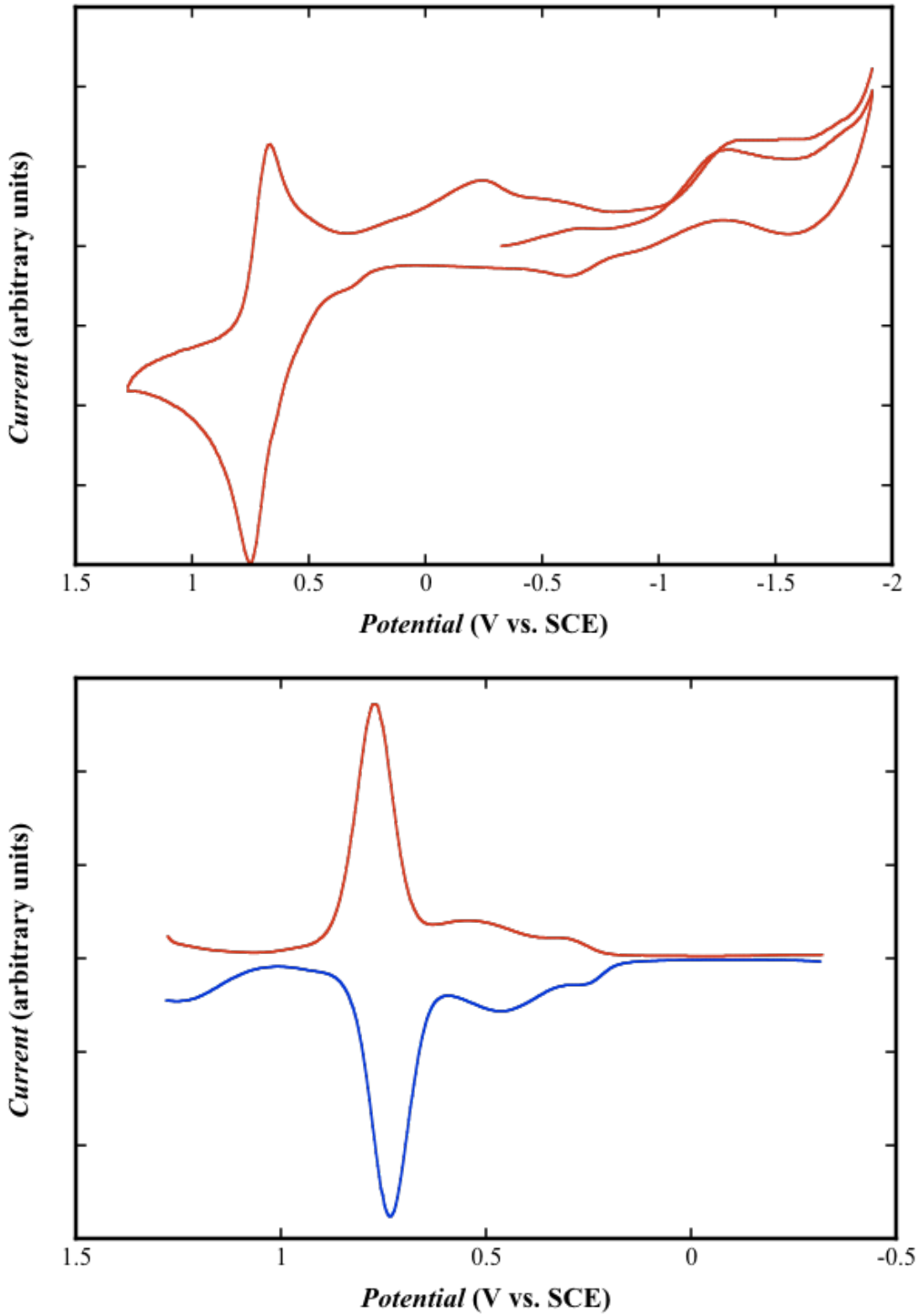

Figure 2.4.23. Cyclic voltammogram (top) and differential pulse voltammogram (bottom) of 3-OMe-2-(^{t}BuNOH)py.

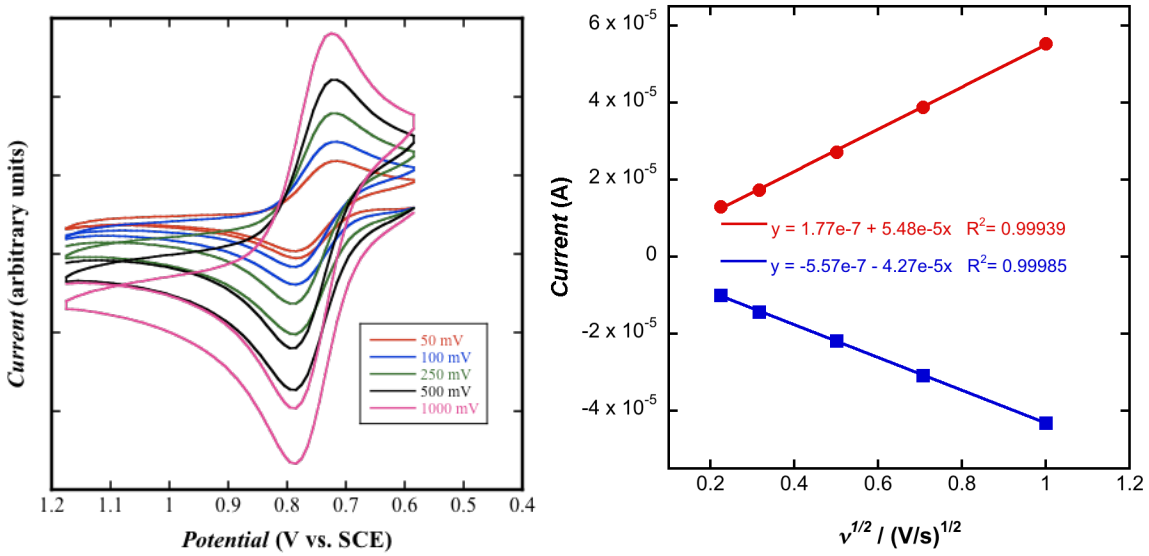

Figure 2.4.24. Scan rate dependence for the [N=O^{+}]/[N–O$^{\bullet}$] redox couple of 3-OMe-2-(^{t}BuNOH)py.

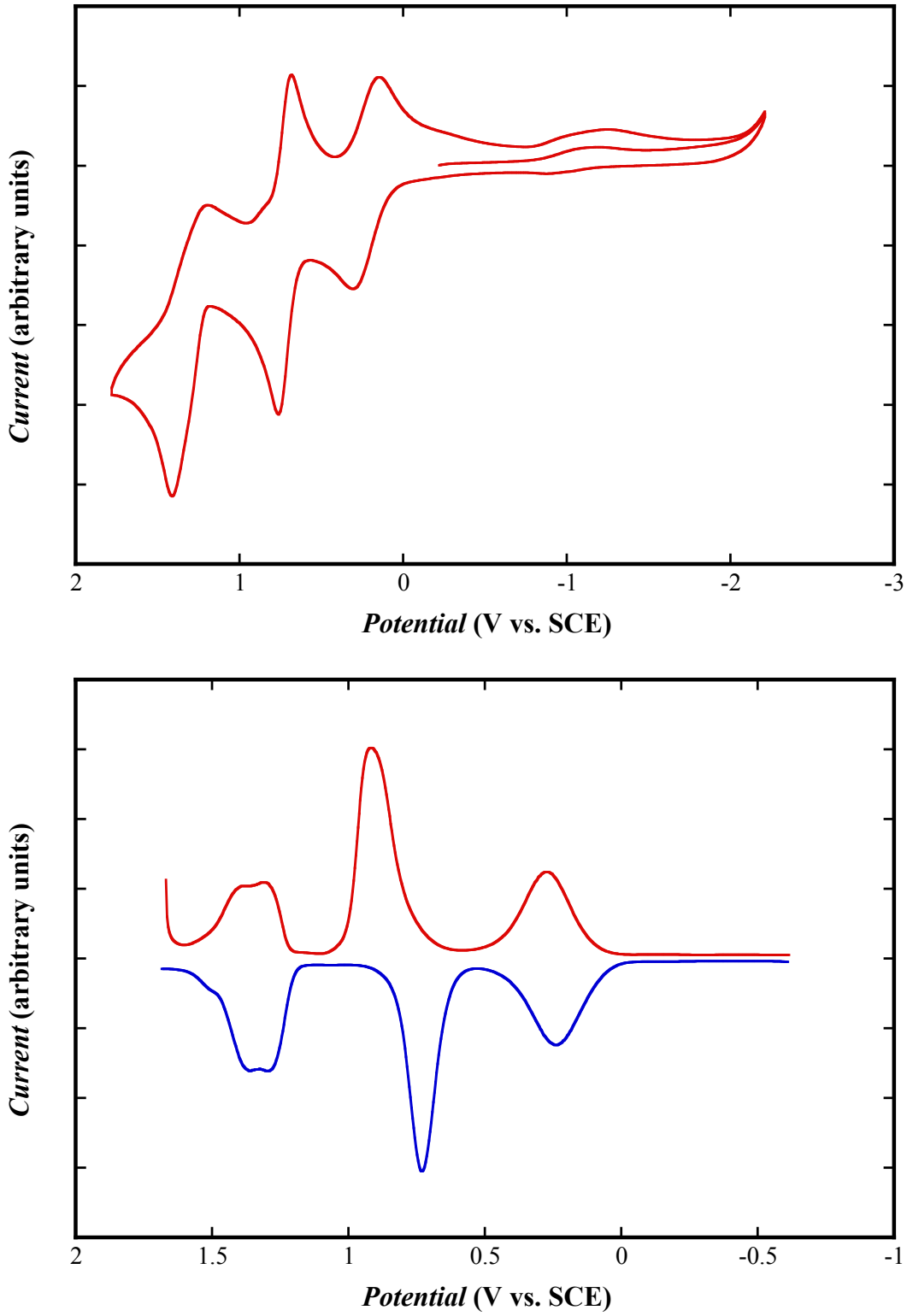

Figure 2.4.25. Cyclic voltammogram (top) and differential pulse voltammogram (bottom) of 5-MeS-2-(^{t}BuNOH)py.

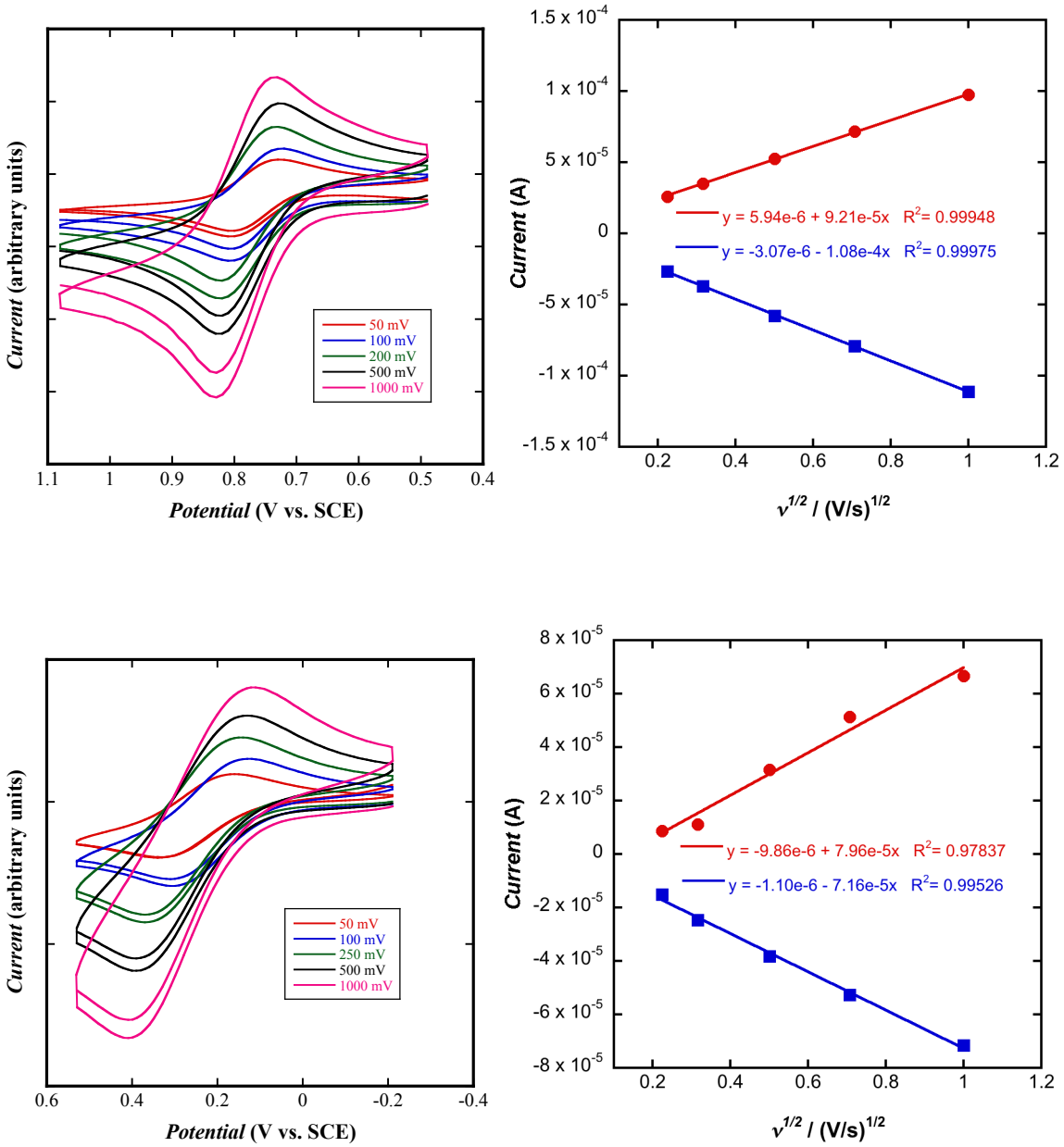

Figure 2.4.26. Scan rate dependence for the [N=O$^+$]/[N–O$^\bullet$] (top) and [N–O$^\bullet$]/[N–O$^-$] (bottom) redox couples of 5-MeS-2-(^{t}BuNOH)py.

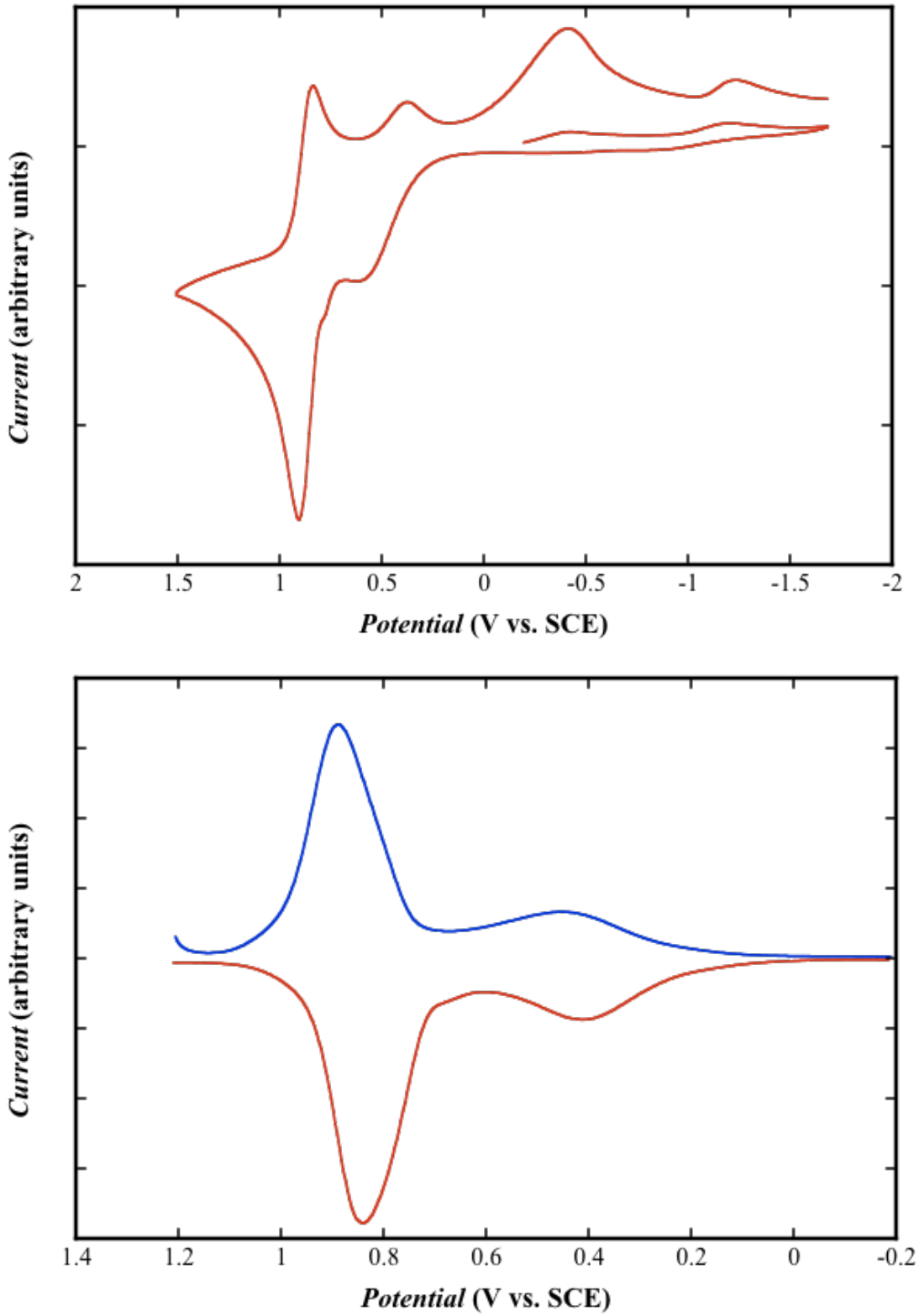

Figure 2.4.27. Cyclic voltammogram (top) and differential pulse voltammogram (bottom) of 5-Me-2-(^{t}BuNOH)py.

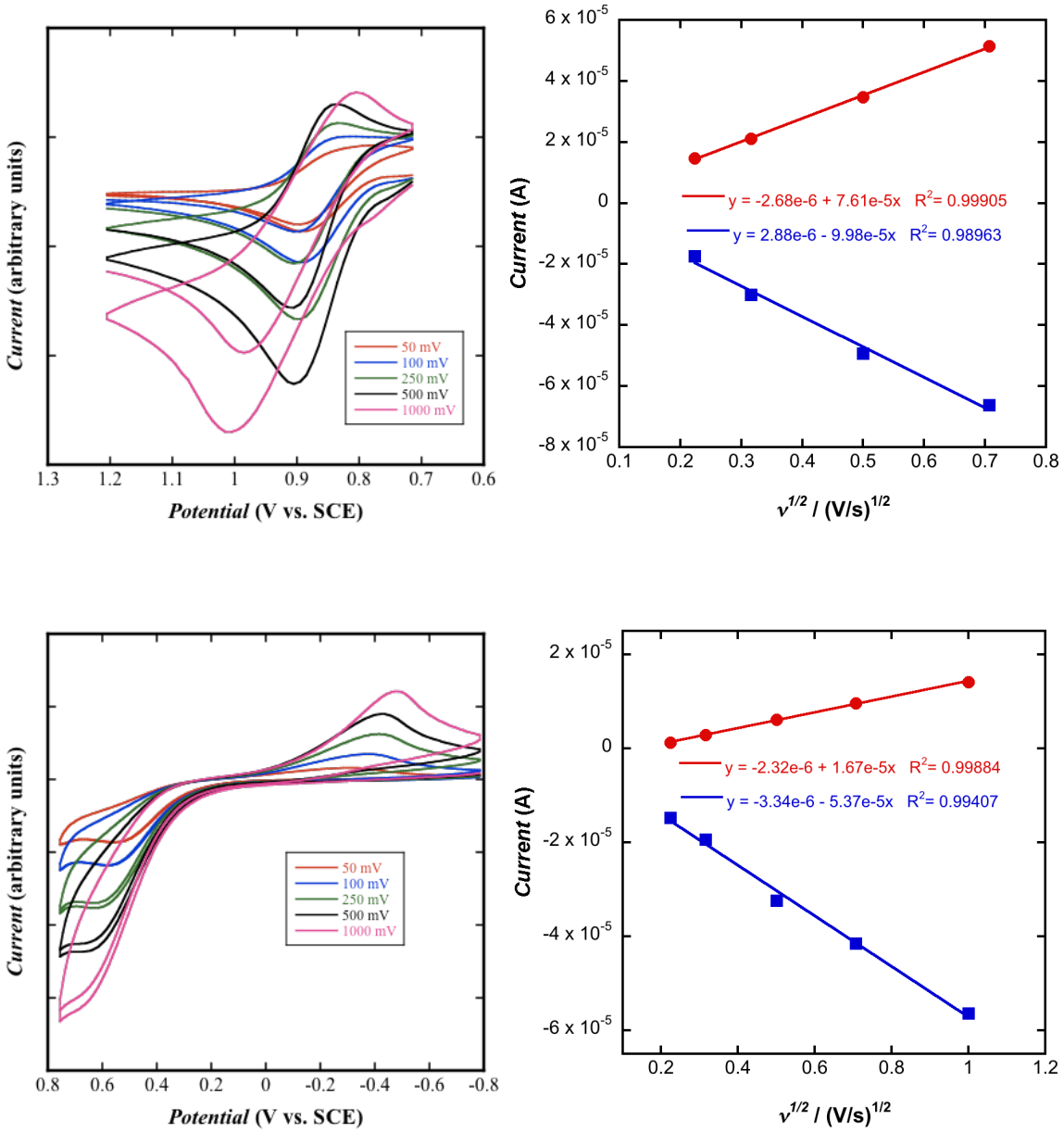

Figure 2.4.28. Scan rate dependence for the [N=O^{+}]/[N–O$^{\bullet}$] (top) and [N–O$^{\bullet}$]/[N–O^{-}] (bottom) redox couples of 5-Me-2-(^{t}BuNOH)py.

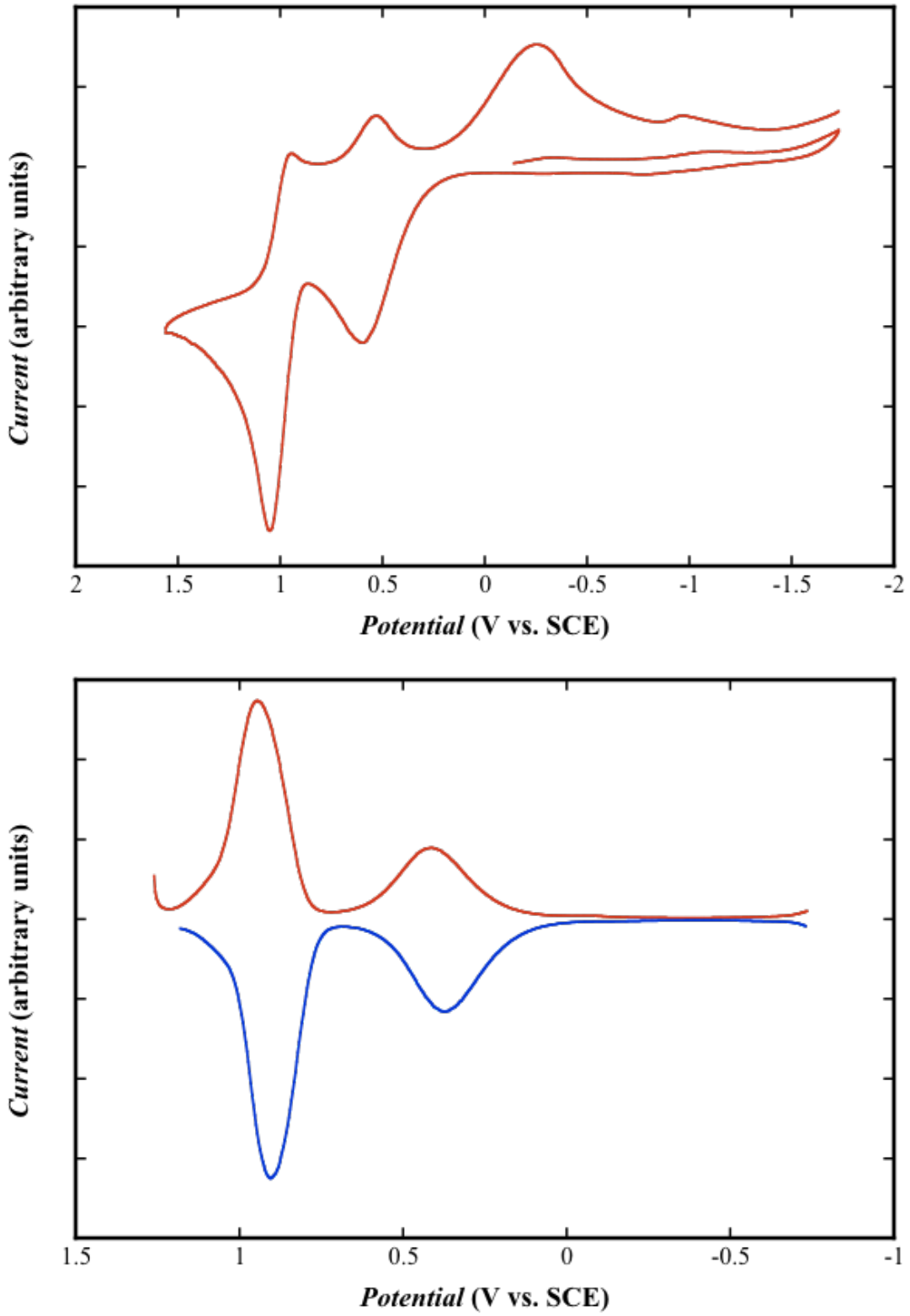

Figure 2.4.29. Cyclic voltammogram (top) and differential pulse voltammogram (bottom) of 2-(^{t}BuNOH)py.

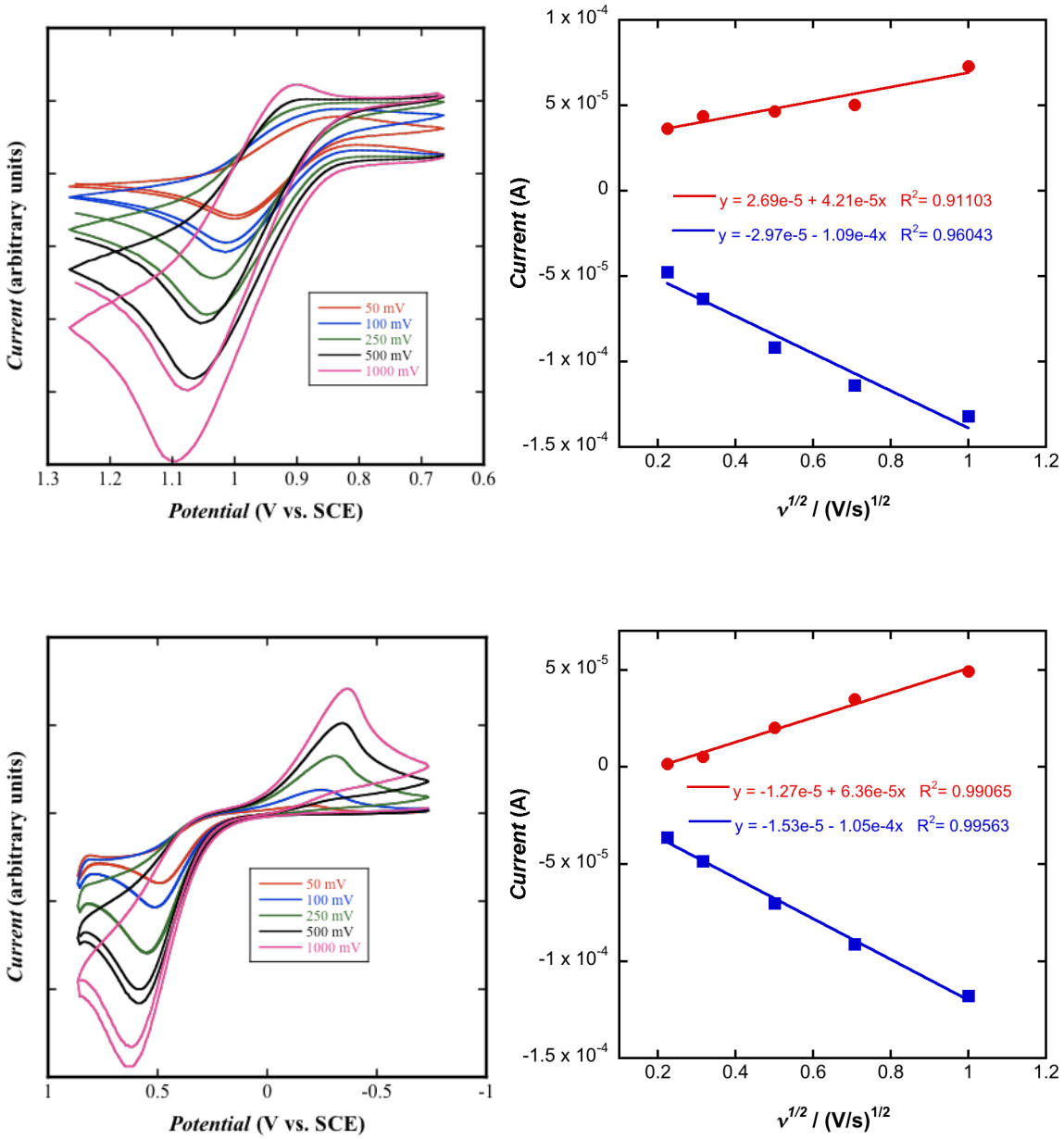

Figure 2.4.30. Scan rate dependence for the [N=O$^+$]/[N–O$^\bullet$] (top) and [N–O$^\bullet$]/[N–O$^-$] (bottom) redox couples of 2-(^{t}BuNOH)py.

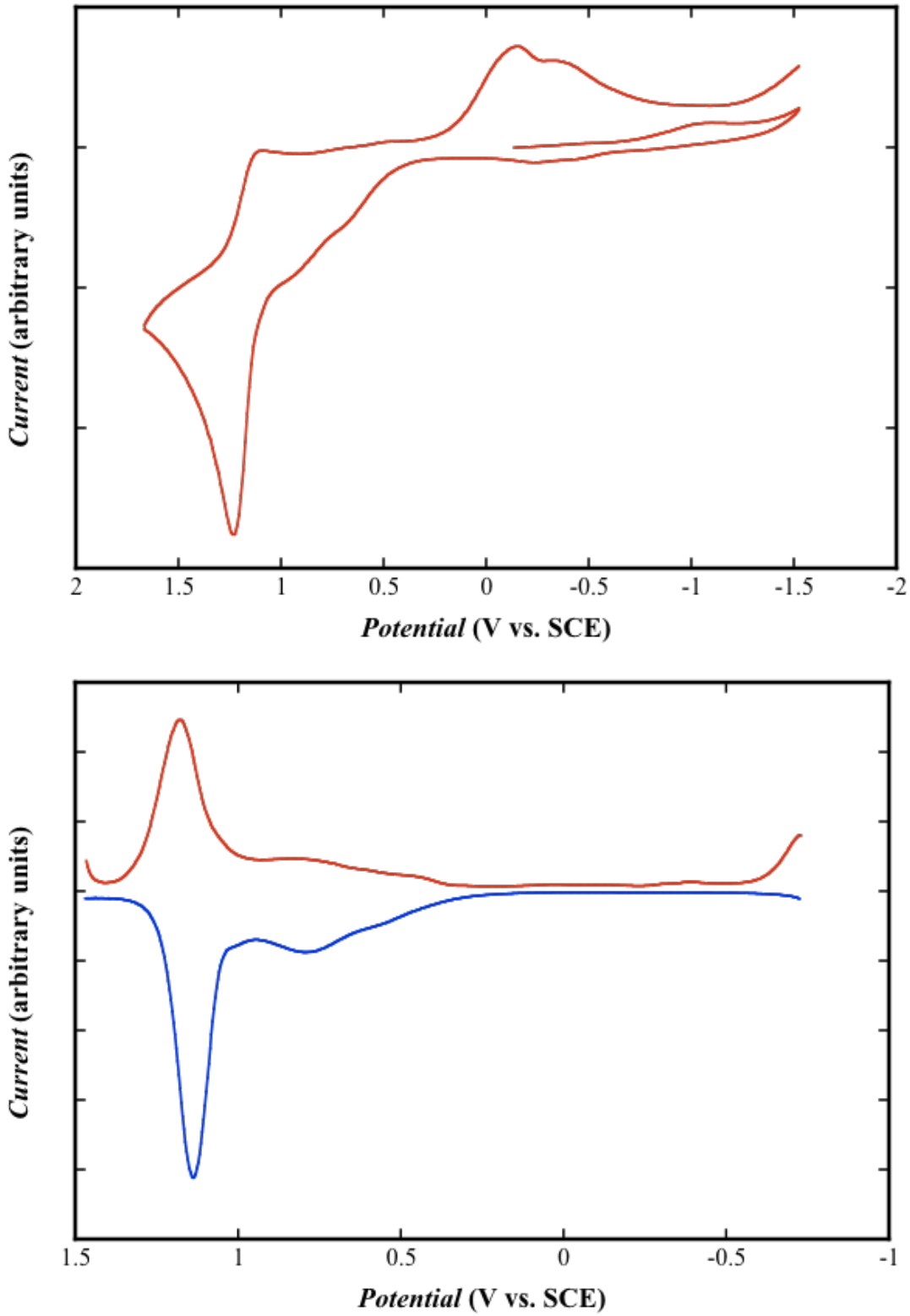

Figure 2.4.31. Cyclic voltammogram (top) and differential pulse voltammogram (bottom) of 5-CF_3-2-(^{t}BuNOH)py.

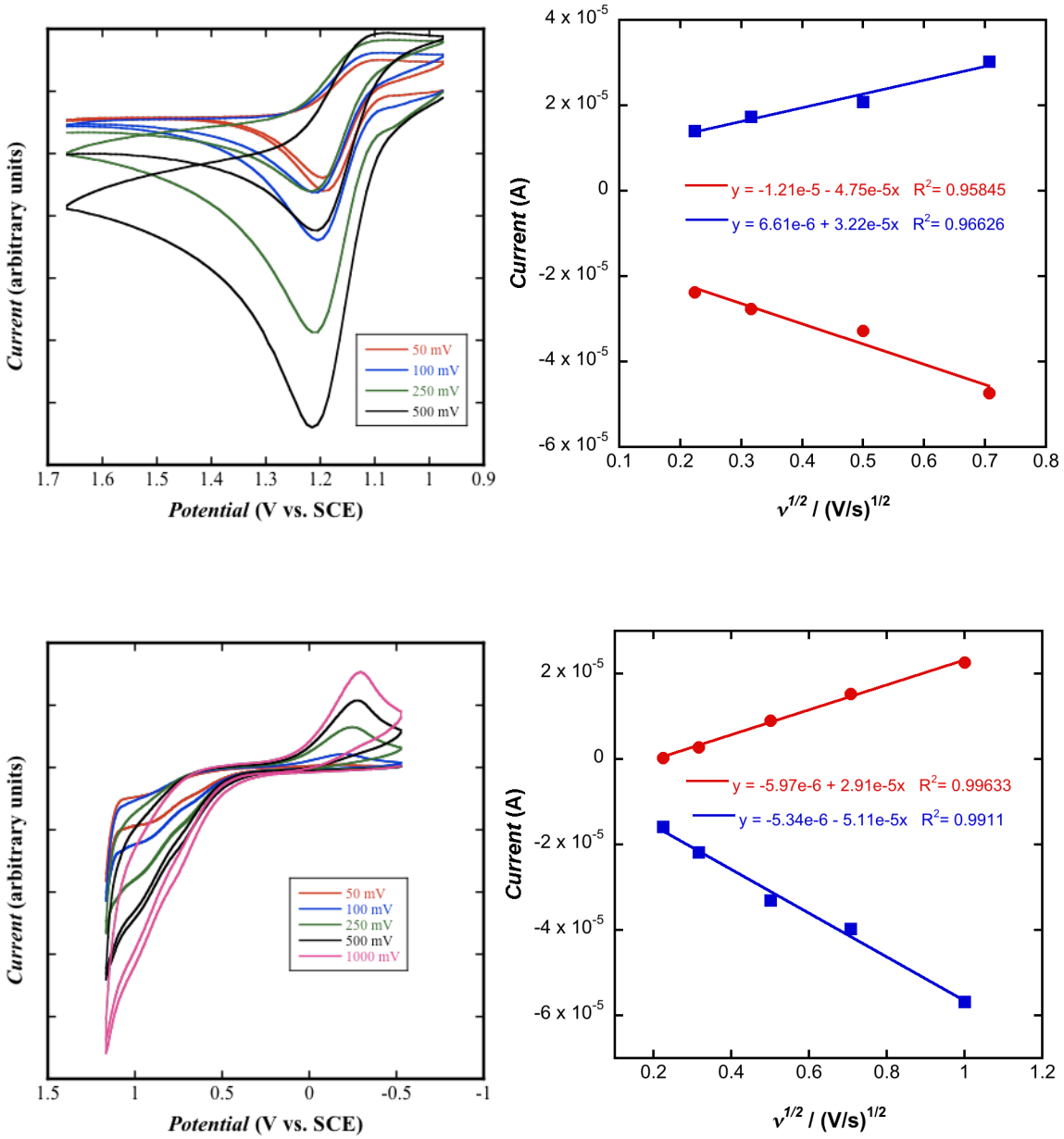

Figure 2.4.32. Scan rate dependence for the [N=O$^+$]/[N–O$^\bullet$] (top) and [N–O$^\bullet$]/[N–O$^-$] (bottom) redox couples of 5-CF_3-2-(^{t}BuNOH)py.

Table 2.4.2. Redox Potentials in V vs SCE for the [N–O•]/[N–O¯] Couples.

	Reduction (V vs SCE)				
Compound	E_{pa}	E_{pc}	$E_{1/2}$	ΔE	i_{pa}/i_{pc}
4-NMe$_2$-2-(^{t}BuNOH)py	0.35	–0.59	–0.12	0.94	3.15
5-NMe$_2$-2-(^{t}BuNOH)py	–	–	–	–	–
3-OMe-2-(^{t}BuNOH)py	–	–0.25	–	–	–
5-MeS-2-(^{t}BuNOH)py	0.40	0.13	0.27	0.27	1.32
5-Me-2-(^{t}BuNOH)py	0.62	–042	0.10	1.04	3.54
2-(^{t}BuNOH)py	0.60	–0.25	0.17	0.85	2.62
5-CF$_3$-2-(^{t}BuNOH)py	–	–0.28	–	–	–

Computational details. All calculations were performed with Gaussian '09,[11a] with the B3LYP hybrid DFT method. Geometry optimizations were carried out using the 6-31g* basis set and the CPCM SCRF method with acetonitrile as the solvent. The default UFF radii were used. The change in the free energy of reaction $\Delta G_{rxn} = \Sigma(G_{product}) + \Sigma(G_{reactant})$ was obtained through use of the zero-point energy corrected free energy values obtained from frequency calculations. All frequency calculations found no imaginary frequencies, supporting that the optimized structures are energy minima. Molecular orbital analysis was performed using Chemcraft.[27]

Table 2.4.3. Optimized coordinates of 4-NMe_2-2-(^{t}BuNO)py.

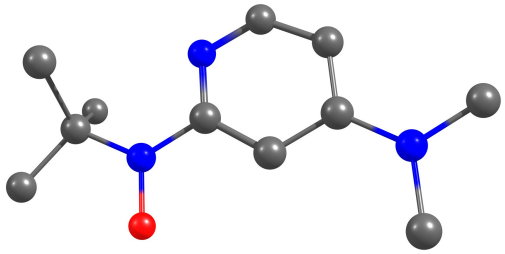

C	2.897484880	-0.051195554	0.000005667
C	3.104309247	0.788077821	-1.275383158
H	2.431224631	1.645248856	-1.302402779
H	4.138345346	1.149806857	-1.301784140
H	2.937726709	0.175504329	-2.168687198
C	3.104293969	0.788067185	1.275404003
H	4.138330630	1.149793273	1.301822103
H	2.431211206	1.645239754	1.302421211
H	2.937697472	0.175486999	2.168700846
C	3.889967807	-1.221673885	0.000006657
H	4.902751624	-0.805848128	0.000014727
H	3.773149411	-1.850743600	0.885872809
H	3.773160370	-1.850735753	-0.885866528

N	1.497552257	-0.642982838	-0.000005258
C	0.295587693	0.120885285	-0.000008160
C	-0.920543899	-0.569970370	-0.000015976
C	-2.127204248	0.163297413	-0.000023251
C	-2.007319497	1.578478329	-0.000008261
C	-0.741849188	2.143307551	0.000000331
N	0.411019161	1.457922247	-0.000000780
H	-0.644446701	3.227850248	0.000010544
H	-2.876162831	2.223743001	-0.000001121
N	-3.345080312	-0.458468629	-0.000046049
C	-3.422372248	-1.914058542	0.000020837
H	-2.942712353	-2.344170111	-0.888872673
H	-2.942820400	-2.344097105	0.889010460
H	-4.469947025	-2.215326897	-0.000034105
C	-4.570382379	0.331596583	0.000027574
H	-4.639720765	0.971406072	0.889380281
H	-4.639702276	0.971570837	-0.889205261
H	-5.427590276	-0.341734442	-0.000047725
H	-0.903453427	-1.648308357	-0.000015498
O	1.383336021	-1.921356526	-0.000013612

Table 2.4.4. Optimized coordinates of 5-NMe_2-2-(^{t}BuNO)py.

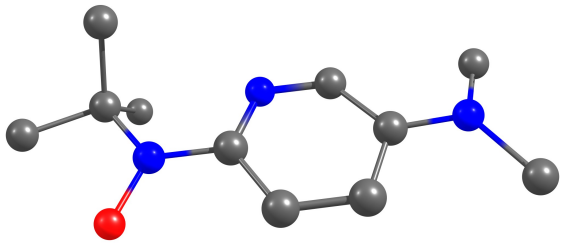

C	-2.930414274	-0.413180883	0.010085073
C	-2.793429461	-1.261097161	-1.269232219
H	-1.834618601	-1.779169848	-1.305370771
H	-3.596480628	-2.006233836	-1.292888585
H	-2.891002782	-0.630067601	-2.159840752
C	-2.767780843	-1.271116323	1.279673146
H	-3.570457686	-2.016248728	1.313870347
H	-1.808606513	-1.789600953	1.292149621
H	-2.846975007	-0.647084925	2.177012067
C	-4.311625786	0.255354514	0.026594762
H	-5.070438946	-0.533989370	0.030759731
H	-4.449776492	0.874412613	0.916381947
H	-4.467357030	0.882036142	-0.854908505
N	-1.889049789	0.690921826	0.003883314
C	-0.491905568	0.474218821	-0.012251237
C	0.377993263	1.581721423	-0.010476226
C	1.742609701	1.361551471	-0.028640392
C	2.256530029	0.040826396	-0.058036853
C	1.284816092	-0.990464412	-0.038929120
N	-0.031411991	-0.782627396	-0.021202027
H	1.588229250	-2.032585355	-0.036669304
N	3.607856325	-0.226321250	-0.108854934

C	4.560578217	0.861026710	0.071902677
H	5.572042806	0.466051033	-0.030774022
H	4.425776674	1.633475593	-0.693971278
H	4.473606709	1.337870916	1.059889721
C	4.075342979	-1.597112750	0.050042054
H	3.810720122	-2.021321463	1.030353846
H	3.657264620	-2.246793189	-0.727452762
H	5.161145250	-1.615306292	-0.050833855
H	2.410123641	2.214846970	-0.018253033
H	-0.026459070	2.584596941	0.010460394
O	-2.295598026	1.912616534	0.012363842

Table 2.4.5. Optimized coordinates of 3-OMe-2-(^{t}BuNO)py.

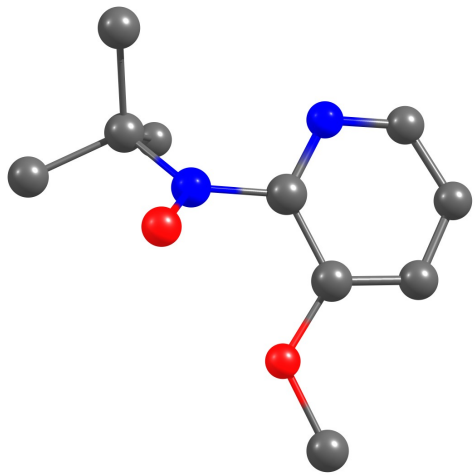

C	-0.320338819	0.365975676	-0.223103788
C	-1.549829027	-0.319415298	-0.029854956
C	-2.702867866	0.459627747	0.094518259
C	-2.597828944	1.851540727	0.046148928
C	-1.342044426	2.425191064	-0.115258068
N	-0.227512881	1.692215167	-0.255644402
H	-3.670134057	-0.005186918	0.243367424

H	-1.215758371	3.504610420	-0.143213612
O	0.859402347	-1.287193241	-1.331959488
C	2.206309865	-0.031406823	0.213486270
C	2.954682062	0.941237307	-0.716977471
H	2.410799485	1.884573775	-0.808254122
H	3.954410711	1.145812998	-0.317716817
H	3.065612938	0.499765462	-1.713111176
C	1.982404218	0.582960168	1.603269055
H	2.955646381	0.731495353	2.082467291
H	1.478504448	1.549412220	1.547520179
H	1.392429509	-0.087246053	2.238587116
C	2.993419149	-1.344520886	0.355508426
H	3.961336985	-1.128813258	0.818884478
H	2.456777564	-2.055863111	0.992530505
H	3.166531569	-1.811201217	-0.615615384
N	0.881573625	-0.380382040	-0.418093816
H	-3.482057478	2.473192859	0.143452987
O	-1.515588232	-1.669072601	0.056321041
C	-2.738893496	-2.359519617	0.320708081
H	-3.465389067	-2.202434917	-0.484594892
H	-2.473437714	-3.415858150	0.370153528
H	-3.174287419	-2.044985031	1.276149185

Table 2.4.6. Optimized coordinates of 5-MeS-2-(^{t}BuNO)py.

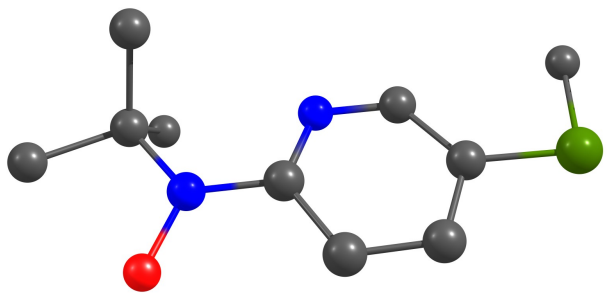

C	0.514619860	0.551879477	0.000060148
C	-0.254384398	1.734534514	0.000124617
C	-1.631674761	1.619917553	0.000025287
C	-2.231881339	0.345721840	-0.000134067
C	-1.373727887	-0.761415802	-0.000181910
N	-0.039632166	-0.664896735	-0.000090435
H	-2.246766016	2.515775562	0.000070658
H	0.234372208	2.698813072	0.000248406
H	-1.765366302	-1.773945054	-0.000298372
O	2.424648096	1.835799116	0.000152845
C	2.877701864	-0.531829057	0.000239415
C	2.658558246	-1.367698034	1.275447813
H	1.662743704	-1.811364304	1.297957479
H	3.401478007	-2.172322376	1.306819695
H	2.792951196	-0.747921629	2.168974526
C	2.658911308	-1.367617001	-1.275084364
H	3.401853194	-2.172226257	-1.306317781
H	1.663108948	-1.811295262	-1.297883219
H	2.793527756	-0.747774301	-2.168531758

C	4.305302869	0.030412117	0.000453208
H	5.001412187	-0.814422683	0.000547577
H	4.499368909	0.640009931	-0.885446096
H	4.499108835	0.639991230	0.886424572
N	1.924944210	0.653183836	0.000142125
S	-4.007017126	0.263653340	-0.000250002
C	-4.361683752	-1.526898491	-0.000624352
H	-3.969530072	-2.011159979	-0.897894748
H	-3.969707331	-2.011509210	0.896534598
H	-5.451102362	-1.605547470	-0.000744852

Table 2.4.7. Optimized coordinates of 5-Me-2-(^{t}BuNO)py.

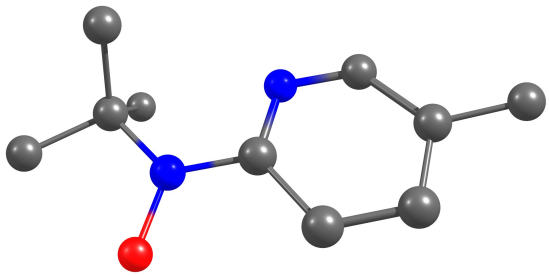

C	0.252477943	0.399723861	0.000038264
C	1.172077822	1.467354027	-0.000798963
C	2.523700393	1.162175005	-0.000866175
C	2.952932046	-0.175755314	-0.000038189
C	1.946023726	-1.145399573	0.000814065
N	0.633782658	-0.882109084	0.000895833
H	3.255102521	1.966831648	-0.001583554
H	0.815646437	2.488144450	-0.001397217
H	2.213373180	-2.201426903	0.001536529
O	-1.472932725	1.927483007	0.001807060
C	-2.236472761	-0.358767397	-0.000306270

C	-2.130379655	-1.217304326	-1.275023572
H	-1.201487831	-1.787597117	-1.298262857
H	-2.972887082	-1.917039937	-1.303757976
H	-2.183932917	-0.585974166	-2.168967218
C	-2.132407171	-1.216113693	1.275377660
H	-2.974665615	-1.916187051	1.303341323
H	-1.203287193	-1.785992372	1.300648874
H	-2.187689361	-0.583935653	2.168619030
C	-3.577728729	0.386421578	-0.001856255
H	-4.378635829	-0.359951183	-0.002183022
H	-3.691538849	1.016552639	0.883709570
H	-3.689896563	1.015585049	-0.888339881
N	-1.134947687	0.689353117	0.000348511
C	4.412404661	-0.550016127	-0.000060339
H	4.926144185	-0.149342398	-0.882361835
H	4.926576713	-0.147712853	0.881244080
H	4.543025588	-1.636434726	0.000905913

Table 2.4.8. Optimized coordinates of 2-(^{t}BuNO)py.

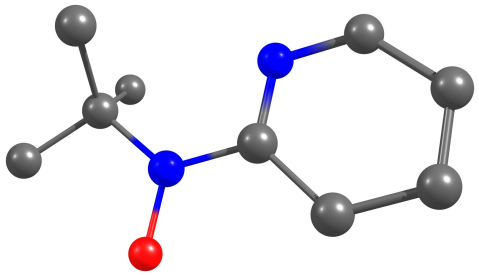

C	0.696801212	0.287854054	-0.000252049
C	1.697265159	1.280022059	-0.000270070
C	3.022297891	0.867105766	-0.000159535

C	3.318634404	-0.500043714	0.000066885
C	2.251937617	-1.396852505	0.000224117
N	0.966164561	-1.024212924	0.000083999
H	3.818844337	1.605570643	-0.000258529
H	1.420807644	2.325074363	-0.000397875
H	2.432715355	-2.469967158	0.000398845
O	-0.895685285	1.952303706	0.000489103
C	-1.849079243	-0.260719186	-0.000047817
C	-1.815721592	-1.124706462	-1.274939671
H	-0.939649076	-1.773410452	-1.296065279
H	-2.715481113	-1.749010237	-1.305392181
H	-1.812532997	-0.491129434	-2.168841168
C	-1.816115749	-1.124147370	1.275245848
H	-2.715787390	-1.748580022	1.305660114
H	-0.939918417	-1.772673499	1.296973394
H	-1.813334436	-0.490155631	2.168858091
C	-3.121678172	0.596559214	-0.000489954
H	-3.983343112	-0.078595227	-0.000660277
H	-3.180572097	1.233782238	0.885397714
H	-3.180056668	1.233577558	-0.886562264
N	-0.662465155	0.690922831	-0.000005476
H	4.341845199	-0.860313315	0.000160409

Table 2.4.9. Optimized coordinates of 5-CF_3-2-(^{t}BuNO)py.

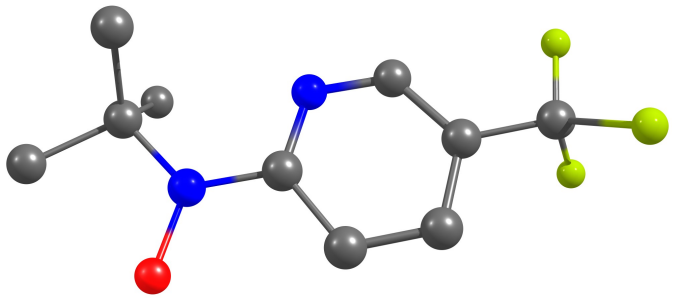

C	-0.742552163	0.475329168	-0.000349932
C	0.110859201	1.599824349	-0.000943071
C	1.475257025	1.378190534	-0.000922512
C	1.957605755	0.061055218	-0.000153615
C	1.030275549	-0.979796601	0.000564804
N	-0.290895951	-0.785103327	0.000512283
H	2.164094776	2.217392905	-0.001525391
H	-0.306055647	2.596738553	-0.001466688
H	1.361311098	-2.014254502	0.001202758
O	-2.543744008	1.898840632	0.001858072
C	-3.184062423	-0.425770625	-0.000228961
C	-3.030344259	-1.275185341	-1.275817682
H	-2.075884188	-1.801732796	-1.297963348
H	-3.838223522	-2.014215105	-1.306933193
H	-3.112323996	-0.646261610	-2.169127437
C	-3.032116304	-1.273882523	1.276453689
H	-3.839468279	-2.013518782	1.306891430
H	-2.077243486	-1.799634095	1.300722292
H	-3.116099279	-0.644104710	2.168979082
C	-4.561969805	0.248796185	-0.001673996
H	-5.321885268	-0.538937241	-0.002132768

H	-4.708718345	0.871385963	0.884287706
H	-4.707056718	0.870806217	-0.888344268
N	-2.139689693	0.683411504	0.000234397
C	3.433748014	-0.194524157	0.000049613
F	4.034892040	0.352921797	1.084499246
F	3.730005928	-1.511490342	-0.000150241
F	4.035257686	0.353372512	-1.083965841

Table 2.4.10. Optimized coordinates of [4-NMe_2-2-(^{t}BuNO)py]$^+$.

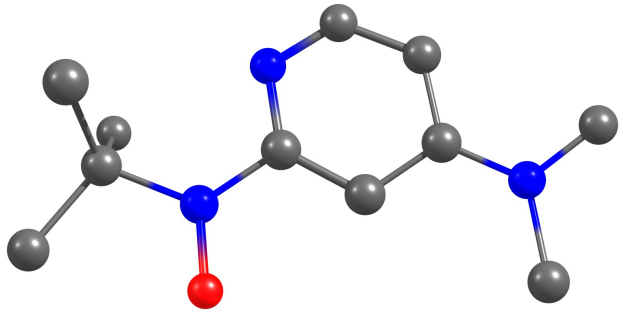

C	-2.920560924	-0.048585593	0.000000948
C	-3.081173596	0.786568216	1.286196848
H	-2.440392098	1.666259441	1.282478515
H	-4.127214409	1.104826378	1.331656804
H	-2.873633364	0.182310246	2.174506772
C	-3.081176967	0.786569841	-1.286193477
H	-4.127218008	1.104827759	-1.331650433
H	-2.440395681	1.666261214	-1.282475531
H	-2.873638725	0.182313077	-2.174504677
C	-3.893671471	-1.228258628	0.000001506
H	-4.903867897	-0.810478381	0.000003796
H	-3.780582901	-1.853346803	-0.889215077
H	-3.780579578	-1.853348571	0.889216437

N	-1.488773000	-0.659778554	-0.000001405
C	-0.276488264	0.111453937	-0.000001079
C	0.928392058	-0.592545320	-0.000001001
C	2.137081913	0.150501505	-0.000000650
C	1.980390333	1.563553435	-0.000000945
C	0.707592930	2.134576602	-0.000001038
N	-0.430419286	1.440320553	-0.000000925
H	0.609598670	3.216452135	-0.000001086
H	2.840107816	2.220390017	-0.000000994
N	3.348913408	-0.450424116	-0.000000129
C	3.445033650	-1.910125252	0.000001027
H	2.973629052	-2.339926019	0.891781126
H	2.973628766	-2.339927321	-0.891778258
H	4.496291368	-2.194001514	0.000001041
C	4.568351805	0.357997483	0.000001565
H	4.624424849	0.993603613	-0.891618319
H	4.624422473	0.993603476	0.891621706
H	5.430716179	-0.306960171	0.000002610
H	0.920079033	-1.671971571	-0.000001025
O	-1.404506524	-1.867743689	-0.000003556

Table 2.4.11. Optimized coordinates of [5-NMe_2-2-(^{t}BuNO)py]$^+$.

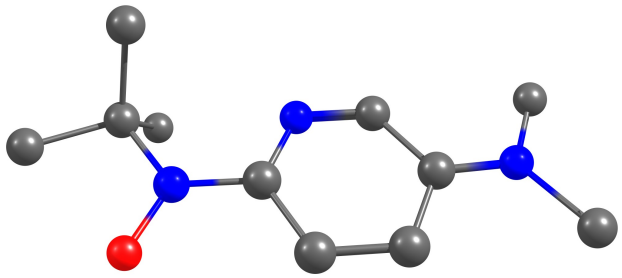

C	-2.914767084	-0.427474909	0.000000027
C	-2.740519214	-1.260287097	-1.282703987
H	-1.802806767	-1.814533107	-1.286441275
H	-3.570403175	-1.972278353	-1.331332307
H	-2.790434080	-0.623167135	-2.171531314
C	-2.740519208	-1.260286240	1.282704569
H	-3.570403339	-1.972277263	1.331333672
H	-1.802806958	-1.814532605	1.286442005
H	-2.790433625	-0.623165696	2.171531500
C	-4.284110855	0.257435269	-0.000000260
H	-5.041287947	-0.531747362	0.000000047
H	-4.431323123	0.876470488	0.888049791
H	-4.431323049	0.876469763	-0.888050823
N	-1.850952567	0.709995564	-0.000000284
C	-0.486075916	0.497442542	0.000000049
C	0.394286677	1.613863697	0.000000445
C	1.742908739	1.393204949	0.000000532
C	2.238970822	0.050715415	0.000000328
C	1.241768724	-1.002822256	0.000000020
N	-0.043327014	-0.781509520	-0.000000144
H	1.549746825	-2.042346300	-0.000000386

N	3.544348276	-0.232686580	0.000000747
C	4.539927572	0.849303735	-0.000000765
H	5.535168518	0.410747510	0.000000352
H	4.429995926	1.472084756	-0.892822071
H	4.429995508	1.472087560	0.892818520
C	4.022137064	-1.624918051	-0.000000156
H	3.675479160	-2.152610783	0.893182790
H	3.675483891	-2.152608148	-0.893186536
H	5.109720572	-1.619331431	0.000002877
H	2.421802308	2.235215479	0.000000857
H	-0.008239193	2.618176095	0.000000731
O	-2.277807024	1.871210996	-0.000000686

Table 2.4.12. Optimized coordinates of [3-OMe-2-(^{t}BuNO)py]$^+$.

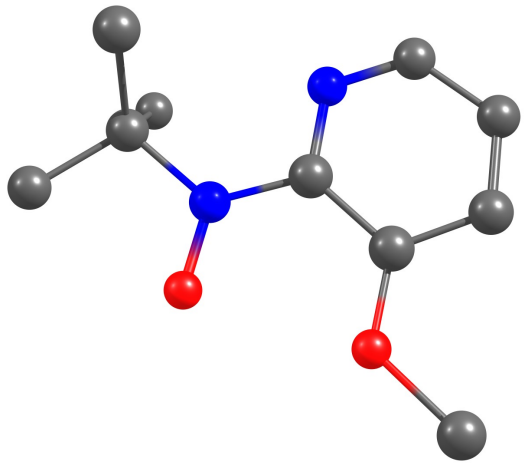

C	-0.299013855	0.268669326	0.000244925
C	-1.643550556	-0.248179317	0.000111216
C	-2.681692706	0.714013131	-0.000099417
C	-2.365511115	2.053038892	-0.000111016
C	-1.005157606	2.452383244	0.000043411

N	-0.020285008	1.584838690	0.000186614
H	-3.716333740	0.396987257	-0.000240787
H	-0.737393553	3.504744963	0.000079272
O	0.647344899	-1.795439334	0.000111328
C	2.303697434	-0.083031581	-0.000078903
C	2.542514353	0.728589424	-1.285614525
H	1.993582627	1.668615317	-1.285712090
H	3.614152301	0.944864801	-1.338145506
H	2.273452234	0.147244302	-2.173091038
C	2.542980352	0.728061708	1.285708693
H	3.614662682	0.944096753	1.338104792
H	1.994141279	1.668150805	1.286326946
H	2.274037096	0.146399086	2.173034675
C	3.170462642	-1.344052167	-0.000497902
H	4.213120425	-1.014938595	-0.000652768
H	3.004143428	-1.957310204	0.888276549
H	3.003791795	-1.956965519	-0.889438421
N	0.813187261	-0.586725423	0.000239958
H	-3.149059264	2.803100630	-0.000264144
O	-1.848792212	-1.548927722	0.000159264
C	-3.197731299	-2.077759095	-0.000160224
H	-3.727466745	-1.759596587	-0.900849213
H	-3.067728912	-3.157905255	-0.000231437
H	-3.727824834	-1.759745561	0.900374880

Table 2.4.13. Optimized coordinates of [5-MeS-2-(^{t}BuNO)py]$^+$.

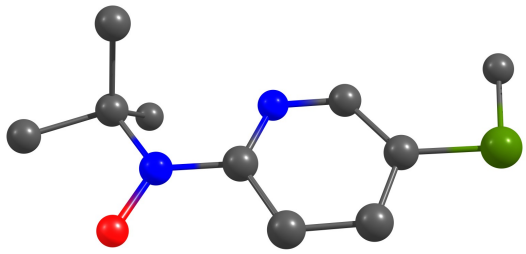

C	-0.499654643	0.576192097	-0.000062786
C	0.268674964	1.763074562	-0.000043780
C	1.638945540	1.642005803	0.000046811
C	2.223405015	0.353647874	0.000129064
C	1.342434562	-0.771684699	0.000103035
N	0.032760096	-0.657466272	0.000009725
H	2.264215826	2.528553456	0.000046686
H	-0.212095872	2.732265684	-0.000112111
H	1.734840125	-1.782314759	0.000127022
O	-2.407838828	1.787270874	-0.000077877
C	-2.868108457	-0.547933868	-0.000107788
C	-2.617419467	-1.360885338	-1.284069958
H	-1.637945485	-1.836918623	-1.281590286
H	-3.387168832	-2.137161517	-1.333890535
H	-2.716199296	-0.730217480	-2.173034353
C	-2.617786848	-1.360481152	1.284194711
H	-3.387613436	-2.136675097	1.334118071
H	-1.638339658	-1.836568736	1.282118796
H	-2.716724510	-0.729505737	2.172923432
C	-4.285824167	0.027421584	-0.000417071
H	-4.977684684	-0.819143939	-0.000347449
H	-4.481932963	0.632520115	0.888053654

H	-4.481712244	0.632179235	-0.889164376
N	-1.900176042	0.672648367	-0.000189884
S	3.950244625	0.249646276	0.000181388
C	4.326261426	-1.536500962	0.000125031
H	3.943403327	-2.018463207	0.901278889
H	3.943482534	-2.018396907	-0.901097593
H	5.416615881	-1.588069920	0.000168465

Table 2.4.14. Optimized coordinates of [5-Me-2-(^{t}BuNO)py]$^+$.

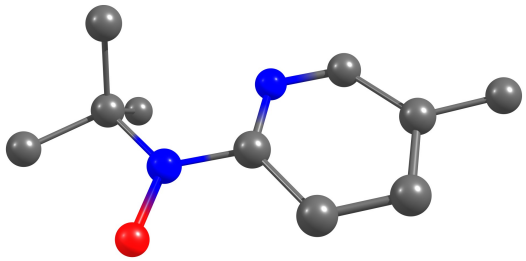

C	-2.247249668	-0.369053928	0.001747544
C	-2.107252456	-1.204517625	-1.286057574
H	-1.198992798	-1.804670974	-1.287973666
H	-2.973550924	-1.871642810	-1.328305270
H	-2.129436931	-0.565339053	-2.173860562
C	-2.100414612	-1.211232683	1.284406303
H	-2.965898519	-1.879370862	1.327193141
H	-1.191728327	-1.810753321	1.278844861
H	-2.118944235	-0.576844588	2.175723012
C	-3.572806127	0.393028817	0.007156287
H	-4.371602984	-0.353270777	0.007078258
H	-3.684548264	1.015580297	0.898318524
H	-3.689026511	1.020453961	-0.880023279

N	-1.122052886	0.709238619	0.001736178
C	0.271627184	0.419342825	-0.002295649
C	1.183256072	1.489983250	-0.003831438
C	2.532675954	1.171607632	-0.008626817
C	2.932573767	-0.172392872	-0.009438013
C	1.908321149	-1.155323154	-0.012318938
N	0.617499869	-0.873371573	-0.007559851
H	2.172705956	-2.209593679	-0.021016196
C	4.374176309	-0.572283245	0.013194507
H	4.990154566	0.132980809	-0.551972480
H	4.741618401	-0.568935833	1.048715693
H	4.518843955	-1.579828307	-0.385192396
H	3.274955325	1.963051835	-0.013638293
H	0.839949495	2.516289652	-0.004061969
O	-1.466509058	1.873233776	0.005914884

Table 2.4.15. Optimized coordinates of [2-(^{t}BuNO)py]$^+$.

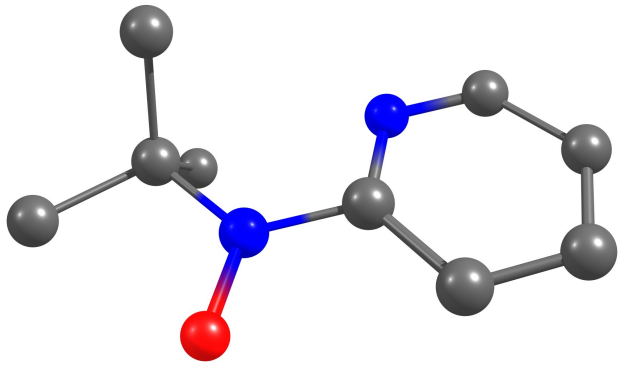

C	0.719606392	0.299890233	-0.000309217
C	1.709486857	1.294863237	0.000326061
C	3.032750184	0.863437255	0.000538681
C	3.292410819	-0.505633539	0.000139327

C	2.212689324	-1.410236556	-0.000418364
N	0.946207165	-1.016529609	-0.000588710
H	3.841501749	1.585429649	0.001016188
H	1.450086598	2.345330761	0.000665661
H	2.388043355	-2.481736642	-0.000731792
O	-0.895000371	1.896120147	-0.001008018
C	-1.869452519	-0.266201393	0.000228887
C	-1.794066632	-1.113628750	-1.285998952
H	-0.941340136	-1.790207866	-1.280305650
H	-2.715030164	-1.702643584	-1.331386029
H	-1.755300065	-0.476974220	-2.174989345
C	-1.793105048	-1.113553480	1.286412551
H	-2.714253951	-1.702193540	1.332752804
H	-0.940604675	-1.790394549	1.280022371
H	-1.753300108	-0.476835093	2.175339306
C	-3.124355380	0.607080305	0.000693549
H	-3.984272093	-0.067801607	0.001609563
H	-3.183955312	1.240009242	0.889724124
H	-3.185273106	1.239198616	-0.888809621
N	-0.656396572	0.710265196	-0.000384557
H	4.309242699	-0.882395316	0.000294318

Table 2.4.16. Optimized coordinates of [5-CF_3-2-(^{t}BuNO)py]$^+$.

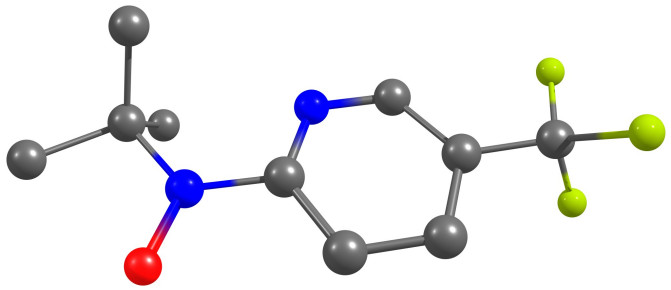

C	-3.198365883	-0.436738777	0.000429885
C	-3.000095556	-1.264821304	-1.286843476
H	-2.060662717	-1.814691617	-1.280794414
H	-3.828764468	-1.977960182	-1.329004149
H	-3.053527350	-0.630589899	-2.176496865
C	-2.997377813	-1.267656641	1.285456640
H	-3.826180930	-1.980615509	1.328033157
H	-2.058159661	-1.817833432	1.276013319
H	-3.048495118	-0.635358738	2.176619671
C	-4.565251085	0.246641106	0.002611234
H	-5.318422703	-0.545299417	0.002619065
H	-4.714745711	0.862498309	0.893014860
H	-4.716738370	0.864351292	-0.886176478
N	-2.140878585	0.702175521	0.000410378
C	-0.709981573	0.495747667	-0.001085233
C	0.120626857	1.624296320	-0.001364653
C	1.491002678	1.389968782	-0.002379751
C	1.945492427	0.071633636	-0.002655666
C	1.013937318	-0.981645408	-0.003002023
N	-0.295927951	-0.769015597	-0.002215119
H	1.341903353	-2.015217075	-0.004156171

C	3.433278575	-0.201791396	0.000474330
F	4.005959020	0.320064064	1.102331747
F	3.703033769	-1.517816036	-0.026680144
F	4.019901121	0.368120915	-1.069692888
H	2.186905348	2.221436269	-0.003223414
H	-0.284809847	2.627200626	-0.000999021
O	-2.540037111	1.840354438	0.001713438

2.5 References

[1] a) L. De Luca, G. Giacomelli, A. Porcheddu, *Org. Lett.* **2001**, *3*, 3041-3043; b) P. Gamez, I. W. C. E. Arends, J. Reedijk, R. A. Sheldon, *Chem. Commun.* **2003**, 2414-2415; c) T. Fey, H. Fischer, S. Bachmann, K. Albert, C. Bolm, *J. Org. Chem.* **2001**, *66*, 8154-8159; d) J. J. Scepaniak, A. M. Wright, R. A. Lewis, G. Wu, T. W. Hayton, *J. Am. Chem. Soc.* **2012**, *134*, 19350-19353; e) P. Nguyen, P. Z. Qin, *Wiley Interdiscip. Rev. RNA*, *3*, 62-72; f) A. T. Hoye, J. E. Davoren, P. Wipf, M. P. Fink, V. E. Kagan, *Acc. Chem. Res.* **2008**, *41*, 87-97; g) S. Goldstein, G. Merenyi, A. Russo, A. Samuni, *J. Am. Chem. Soc.* **2002**, *125*, 789-795; h) B. P. Soule, F. Hyodo, K.-i. Matsumoto, N. L. Simone, J. A. Cook, M. C. Krishna, J. B. Mitchell, *Free Radic. Biol. Med.* **2007**, *42*, 1632-1650; i) F. Kato, A. Kikuchi, T. Okuyama, K. Oyaizu, H. Nishide, *Angew. Chem. Int. Ed.*, *51*, 10177-10180; j) F. Kato, N. Hayashi, T. Murakami, C. Okumura, K. Oyaizu, H. Nishide, *Chem. Lett.*, *39*, 464-465; k) G. Likhtenshtein, J. Yamauchi, S. Nakatsuji, A. I. Smirnov, R. Tamura, *Nitroxides: Applications in Chemistry, Biomedicine, and Materials Science*, Wiley-VCH, Weinheim, **2008**; l) A. Okazawa, Y. Nagaichi, T. Nogami, T. Ishida, *Inorg. Chem.* **2008**, *47*, 8859-8868; m) K. Osanai, A. Okazawa, T. Nogami, T. Ishida, *J. Am. Chem. Soc.* **2006**, *128*, 14008-14009; n) A. Okazawa, T. Nogami, T. Ishida, *Chem. Mater.* **2007**, *19*, 2733-2735; o) S. Kanegawa, S. Karasawa, M. Maeyama, M. Nakano, N. Koga, *J. Am. Chem. Soc.* **2008**, *130*, 3079-3094; p) W. J. Evans, J. M. Perotti, R. J. Doedens, J. W. Ziller, *Chem. Commun.* **2001**, 2326-2327.

[2] J. P. Blinco, J. L. Hodgson, B. J. Morrow, J. R. Walker, G. D. Will, M. L. Coote, S. E. Bottle, *J. Org. Chem.* **2008**, *73*, 6763-6771.

[3] a) Y. Yonekuta, K. Oyaizu, H. Nishide, *Chem. Lett.* **2007**, *36*, 866-867; b) S. Stefan, F. Belaj, T. Madl, R. Pietschnig, *Eur. J. Inorg. Chem.*, *2010*, 289-297; c) L. Balloch, A. M. Drummond, P. García-Álvarez, D. V. Graham, A. R. Kennedy, J. Klett, R. E. Mulvey, C. T. O'Hara, P. J. A. Rodger, I. D. Rushworth, *Inorg. Chem.* **2009**, *48*, 6934-6944.

[4] a) G. Gryn'ova, J. M. Barakat, J. P. Blinco, S. E. Bottle, M. L. Coote, *Chem. Eur. J.* **2012**, *18*, 7582-7593; b) J. L. Hodgson, M. Namazian, S. E. Bottle, M. L. Coote, *J. Phys. Chem. A.* **2007**, *111*, 13595-13605.

[5] a) L. Marx, B. Schollhorn, *New J. Chem.* **2006**, *30*, 430-434; b) R. Ziessel, G. Ulrich, R. C. Lawson, L. Echegoyen, *J. Mater. Chem.* **1999**, *9*, 1435-1448; c) T. Suga, Y.-J. Pu, K. Oyaizu, H. Nishide, *Bull. Chem. Soc. Jpn.* **2004**, *77*, 2203-2204; d) F. Xu, H.-J. W. Deussen, B. Lopez, L. Lam, K. Li, *Eur. J. Biochem.* **2001**, *268*, 4169-4176.

[6] Xu and coworkers report a slope of 0.14 for the correlation of anodic peak potentials for the second oxidation to sigma minus values. Replotting these potentials verus the set of sigma plus values, however, a slope of 0.22 is obtained.

[7] a) C. Despotopoulou, R. C. Bauer, A. Krasovskiy, P. Mayer, J. M. Stryker, P. Knochel, *Chem. Eur. J.* **2008**, *14*, 2499-2506; b) F. Kopp, S. Wunderlich, P. Knochel, *Chem. Commun.* **2007**, 2075-2077; c) A. Krasovskiy, P. Knochel, *Angew. Chem. Int. Ed.* **2004**, *43*, 3333-3336; d) W. Lin, L. Chen, P. Knochel, *Tetrahedron* **2007**, *63*, 2787-2797; e) C.-Y. Liu, P. Knochel, *Org. Lett.* **2005**, *7*, 2543-2546; f) C.-Y. Liu, H. Ren, P. Knochel, *Org. Lett.* **2006**, *8*, 617-619; g) H. Ren, P. Knochel, *Chem. Commun.* **2006**, 726-728; h) H. Ren, A. Krasovskiy, P. Knochel, *Chem. Commun.* **2005**, 543-545; i) A. H. Stoll, A. Krasovskiy, P. Knochel, *Angew. Chem. Int. Ed.* **2006**, *45*, 606-609.

[8] This assignment was made based on DFT calculations on the triply oxidized compound.

[9] S. D. Rychnovsky, R. Vaidyanathan, T. Beauchamp, R. Lin, P. J. Farmer, *J. Org. Chem.* **1999**, *64*, 6745-6749.

[10] C. Hansch, A. Leo, R. W. Taft, *Chem. Rev.* **1991**, *91*, 165-195.

[11] a) Gaussian 09, Revision D.01, Frisch, M. J.; Trucks, G. W.; Schlegel, H. B.; Scuseria, G. E.; Robb, M. A.; Cheeseman, J. R.; Scalmani, G.; Barone, V.; Mennucci, B.; Petersson, G. A.; Nakatsuji, H.; Caricato, M.; Li, X.; Hratchian, H. P.; Izmaylov, A. F.; Bloino, J.; Zheng, G.; Sonnenberg, J. L.; Hada, M.; Ehara, M.; Toyota, K.; Fukuda, R.; Hasegawa, J.; Ishida, M.; Nakajima, T.; Honda, Y.; Kitao, O.; Nakai, H.; Vreven, T.; Montgomery, Jr., J. A.;

Peralta, J. E.; Ogliaro, F.; Bearpark, M.; Heyd, J. J.; Brothers, E.; Kudin, K. N.; Staroverov, V. N.; Kobayashi, R.; Normand, J.; Raghavachari, K.; Rendell, A.; Burant, J. C.; Iyengar, S. S.; Tomasi, J.; Cossi, M.; Rega, N.; Millam, N. J.; Klene, M.; Knox, J. E.; Cross, J. B.; Bakken, V.; Adamo, C.; Jaramillo, J.; Gomperts, R.; Stratmann, R. E.; Yazyev, O.; Austin, A. J.; Cammi, R.; Pomelli, C.; Ochterski, J. W.; Martin, R. L.; Morokuma, K.; Zakrzewski, V. G.; Voth, G. A.; Salvador, P.; Dannenberg, J. J.; Dapprich, S.; Daniels, A. D.; Farkas, Ö.; Foresman, J. B.; Ortiz, J. V.; Cioslowski, J.; Fox, D. J. Gaussian, Inc., Wallingford CT, 2009; b) V. Barone, M. Cossi, *J. Phys. Chem. A.* **1998**, *102*, 1995-2001; c) M. Cossi, N. Rega, G. Scalmani, V. Barone, *J. Comput. Chem.* **2003**, *24*, 669-681.

[12] E. J. Lynch, A. L. Speelman, B. A. Curry, C. S. Murillo, J. G. Gillmore, *J. Org. Chem.* **2012**, *77*, 6423-6430.

[13] J. Li, M. P. Lynch, K. L. DeMello, S. M. Sakya, H. Cheng, R. J. Rafka, B. S. Bronk, B. H. Jaynes, C. Kilroy, D. W. Mann, M. L. Haven, N. L. Kolosko, C. Petras, S. B. Seibel, L. A. Lund, *Bioorg. Med. Chem.* **2005**, *13*, 1805-1809.

[14] L. Shi, Y. Chu, P. Knochel, H. Mayr, *Org. Lett.* **2012**, *14*, 2602-2605.

[15] H. S. Radeke, A. Purohit, T. D. Harris, K. Hanson, R. Jones, C. Hu, P. Yalamanchili, M. Hayes, M. Yu, M. Guaraldi, M. Kagan, M. Azure, M. Cdebaca, S. Robinson, D. Casebier, *ACS Med. Chem. Lett.*, *2*, 650-655.

[16] a) O. A. Rakitin, O. G. Vlasova, L. I. Khmel'nitskii, I. F. Falyakhov, T. N. Sobachkina, *Chem. Heterocycl. Compd.* **1990**, *26*, 1281-1283; b) E. C. Taylor, C. P. Tseng, J. B. Rampal, *J. Org. Chem.* **1982**, *47*, 552-555; c) R. Dalpozzo, L. Grossi, F. Ganazzoli, *Tetrahedron* **1991**, *47*, 1091-1094.

[17] M. Jaric, B. A. Haag, S. M. Manolikakes, P. Knochel, *Org. Lett.*, *13*, 2306-2309.

[18] a) M. A. Matulenko, C.-H. Lee, M. Jiang, R. R. Frey, M. D. Cowart, E. K. Bayburt, S. DiDomenico, G. A. Gfesser, A. Gomtsyan, G. Z. Zheng, J. A. McKie, A. O. Stewart, H. Yu, K. L. Kohlhaas, K. M. Alexander, S. McGaraughty, C. T. Wismer, J. Mikusa, K. C. Marsh,

R. D. Snyder, M. S. Diehl, E. A. Kowaluk, M. F. Jarvis, S. S. Bhagwat, *Bioorg. Med. Chem.* **2005**, *13*, 3705-3720; b) A. E. Felten, G. Zhu, Z. D. Aron, *Org. Lett.*, *12*, 1916-1919.

[19] a) P. W. Sheldrake, L. C. Powling, P. K. Slaich, *J. Org. Chem.* **1997**, *62*, 3008-3009; b) A. Yoshimura, C. T. Banek, M. S. Yusubov, V. N. Nemykin, V. V. Zhdankin, *J. Org. Chem.*, *76*, 3812-3819; c) K. J. Edgar, S. N. Falling, *J. Org. Chem.* **1990**, *55*, 5287-5291.

[20] F. Cottet, M. Marull, O. Lefebvre, M. Schlosser, *Eur. J. Org. Chem.* **2003**, *2003*, 1559-1568.

[21] Bruker (2009) SAINT. Bruker AXS Inc., Madison, Wisconsin, USA.

[22] Bruker (2009) SHELXTL. Bruker AXS Inc., Madison, Wisconsin, USA.

[23] Sheldrick, G.M. (2007) SADABS. University of Göttingen: Göttingen, Germany.

[24] G. Sheldrick, *Acta Crystallogr. Sect. A* **2008**, *64*, 112-122.

[25] N. G. Connelly, W. E. Geiger, *Chem. Rev.* **1996**, *96*, 877-910.

[26] R. K. Thomson, B. L. Scott, D. E. Morris, J. L. Kiplinger, *C. R. Chimie* **2010**, *13*, 790-802.

[27] Chemcraft. www.chemcraftprog.com.

Chapter 3

Significant Stabilization of the Ce^{4+} Oxidation State by Tetrakis Pyridyl Nitroxide Ligand Frameworks and the Establishment of a Ligand Field Series for the 4f-Block

Abstract

Understanding the sensitivity of $Ce^{IV/III}$ reduction potential to ligand field strength has yet to benefit from systematic variations of the ligand environment. Detailed analyses for a series of seven cerium(IV) tetrakis(pyridyl-nitroxide) compounds and their cerium(III) analogs in varying ligand field strengths are presented. Electrochemical, spectroscopic, and computational results reveal a close correlation of electronic properties with ligand substituents. Together with electrochemical data for reported eight-coordinate compounds, DFT calculations reveal a broad range of cerium(IV/III) redox potentials correlated to ligand field strengths, establishing a semi-empirical, predictive model for the modulation of cerium redox thermodynamics and ligand field strengths. Applications over a variety of scientific disciplines make use of the fundamental redox thermodynamics of cerium. Such applications will benefit from a combined experimental and theoretical approach for assessing thermodynamic redox cycling of cerium compounds. Attempts to extend this chemistry to lanthanides other than cerium as well as actinides such as uranium were also explored.

3.1 Introduction

Cerium is a unique member of the lanthanide series with an accessible, established molecular chemistry in both the tervalent and tetravalent redox forms.[1] The accessibility of the Ce^{IV} state arises from the $4f^0$ configuration achieved upon removal of the $4f^1$ electron in Ce^{III}. The rich redox chemistry that results from the accessibility of this $Ce^{IV/III}$ redox couple has found use in many applications. Due to the chemical reversibility of the Ce_2O_3/CeO_2 redox cycle, for example, CeO_2 is used as an active support in 3-way catalytic converters that both stores and provides oxygen equivalents for the oxidation of CO to CO_2.[2] The redox properties of ceria are also used in medicinal chemistry where CeO_2 nanoparticles have been proposed as radical scrubbers for the treatment of ischemic stroke.[3] The reversibility of oxygen transport to and from these solid state materials is understood to derive from localized electronic structure, where an electron is transferred to a nonbonding Ce 4f orbital concomitant with reorganization of the metal–oxide lattice.[4] Studies have shown, however, that single-crystalline cubic CeO_2, which provides the thermodynamic parentage for oxygen transport, exhibits a remarkable and peculiar resistance to reduction.[5]

The redox properties of cerium also find use in synthetic chemistry, where ceric ammonium nitrate (CAN) is widely used as a potent oxidant for the oxidation of alcohols to carbonyls.[6] CAN also finds use in energy applications as a terminal oxidant in the catalytic oxidation of water. In such cases, 4 equivalents of CAN accept the four electrons needed to oxidize two molecules of H_2O to O_2.[7]

Previous work in our laboratory provided evidence that hydroxamate collectors used in the beneficiation of light rare earth ores induce oxidation of cerium at ore particle surfaces. This implies that collector efficiency is related to cerium redox chemistry.[8] Similarly, separations of cerium from rare-earth metal concentrates also benefit from $Ce^{IV/III}$ redox chemistry. Roasting of the rare-earth mixture oxidizes Ce_2O_3 to CeO_2, which prevents leaching of cerium into the dilute HCl solution.[9]

In these cases and many others, cerium redox chemistry plays a pivotal role. In this context, it was of interest to 1) further push the boundaries of $Ce^{IV/III}$ redox potentials by synthesizing complexes with electronic structures mimicking that of single-crystalline cubic CeO_2 and 2) develop methods for predicting $Ce^{IV/III}$ redox potentials across a wide variety of compounds and ligand environments. Towards these goals, we first devoted efforts into further understanding the relationship between crystal field strength and cerium redox chemistry. A survey of the literature conducted by previous members of our research group revealed that the $Ce^{IV/III}$ redox couple was highly sensitive to ligand environment, spanning a range of over 2 V under either aqueous or non-aqueous conditions.[10]

This sensitivity of $Ce^{IV/III}$ redox potential to crystal field strength was appealing as a potential probe of rare earth metal electronic structures in novel ligand environments. Common probes of metal electronic structures in transition metal complexes, such as optical transitions or CO stretching frequencies, cannot be applied to complexes of the rare earth metals because of the core-like nature of the 4f orbitals and the ionic nature of their bonding.[11] Because of the integral relationship between metal electronic structure and complex reactivity, we believed that the establishment of a ligand field series for the 4f-block based on $Ce^{IV/III}$ redox potentials would have a broad impact to chemists across diverse fields.

In this regard, we decided to expand on our previous efforts with pyridyl nitroxides and explore their coordination chemistry with cerium. We hypothesized that four nitroxide ligands, due to their potential for redox activity and role as anionic oxygen-donor ligands,[12] could coordinatively saturate and electronically stabilize the cerium cation to act as effective surrogates for the eight-coordinate ligand field in CeO_2. Furthermore, we expected that coordination through the pyridine nitrogen atom would lend structural stability to these complexes. The functional pyridyl nitroxide derivatives, $[R\text{-}2\text{-}(^{t}BuNO)py]^{-}$ where R = 5-CF_3, H, 5-Me, 3-OMe, 5-NMe_2, and 4-NMe_2, would allow for the development of a series of compounds within a conserved ligand framework where ligand substituent effects could be used to probe the sensitivity of the $Ce^{IV/III}$ redox couple.

Combining these experimental results with DFT would then form the basis for the ligand field series for the 4f-block.

Similar studies have been performed by Batista, et al. on 3, 4, and 5d transition metal complexes[13] and by Ephritikhine, et al. on uranium in the 5f-block.[14] For example, in one study, Batista and coworkers performed gas-phase DFT optimizations on $[MCp_2]^{0/+}$ (M = Co, Ni, Ru, and Os), $[MCp^*_2]^{0/+}$ (M = Fe, Co, Ni, Ru, and Os), and $[M(bpy)_3]^{2+/3+}$ (M = Fe, Co, Os, and Ir) in both indicated redox forms. Single point calculations employing a solvent continuum then completed the thermochemical cycle needed to correlate calculated $E_{1/2}$ values with experimentally observed $E_{1/2}$ values.[13a] Similarly, Ephritikhine and coworkers performed geometry optimizations on a series of L_3UCl complexes, L = tmp, TMSCp, Cp, ^{t}BuCp, and MeCp, and Cp*, using a solvent continuum model in both the neutral and singly reduced forms and computed their electron affinities. Using a correlation of electron affinities and experimental reduction potentials for these complexes, they were able to predict the half-wave potential for the Cp^*_3UCl complex, whose electrochemistry had not been reported in the literature.[14a] These studies provided the inspiration for our extensive cerium study and served as the bases of our approach.

Herein, we report on the successful syntheses of a series of structurally related complexes of the general formula, $[Ce^{III}(\mu\text{-(R-2-(}^t\text{BuNO)py))(R-2-(}^t\text{BuNO)py)}_2]_2$ (**3.1-X**) and $Ce^{IV}[\text{R-2-(}^t\text{BuNO)py}]_4$ (**3.2-X**), respectively, where R = 5-CF_3 (**3.1-CF$_3$**, **3.2-CF$_3$**), 5-Me (**3.1-Me**, **3.2-Me**), 3-OMe (**3.1-OMe**, **3.2-OMe**), 5-NMe_2 (**3.1-*p*NMe$_2$**, **3.2-*p*NMe$_2$**), and 4-NMe_2 (**3.1-*m*NMe$_2$**, **3.2-*m*NMe$_2$**). Solution electrochemistry experiments indicated a significant stabilization of the 4+ oxidation state of Ce as indicated by the highly shifted metal based redox couples. We were also able to tune the $Ce^{IV/III}$ redox potential by 500 mV over the series. DFT B3LYP calculations on both the neutral and anionic forms were used to understand the underlying nature of this stabilization as well as correlate the experimentally determined redox potentials with calculated $E_{1/2}$ $Ce^{IV/III}$ values. We expanded this correlation to include nine cerium compounds from the literature. Overall, these results comprise a new method for organizing donor types into a ligand field series for cerium; they are important steps in using combined computational chemistry and

experimental approaches to understand and predict redox chemistry of cerium in novel ligand environments.

3.2 Results/Discussion

3.2.1 Complex Syntheses

Layering or gently mixing 1 equivalent of $Ce[N(SiMe_3)_2]_3$ with 3 equivalents of R-2-(^{t}BuNOH)py led to the deposition of X-ray quality crystals of isostructural dimeric cerium(III) complexes of general forumulae, $[Ce^{III}(\mu\text{-(R-2-(}^t\text{BuNO)py))(R-2-(}^t\text{BuNO)py)}_2]_2$ where R = 5-CF_3, H, 5-Me, 3-OMe, 5-NMe_2, and 4-NMe_2 (**3.1-X**). Complexes **3.1-X** were all sparingly soluble in common organic solvents, which prevented their solution characterization by ^{1}H NMR spectroscopy. Their compositions, however, were confirmed by elemental analysis and X-ray crystallography.

Reaction of **3.1-X** with 2 equivalents of neutral R-2-(^{t}BuNO)py radical, formed *in situ* from the oxidation of R-2-(^{t}BuNOH)py with excess PbO_2, immediately produced dark red to dark purple solutions. Following work up, the homoleptic, monomeric cerium(IV) complexes of general formula, $Ce^{IV}[\text{R-2-(}^t\text{BuNO)py}]_4$ where R = 5-CF_3, H, 5-Me, 3-OMe, 5-NMe_2, and 4-NMe_2 (**3.2-X**), were isolated.

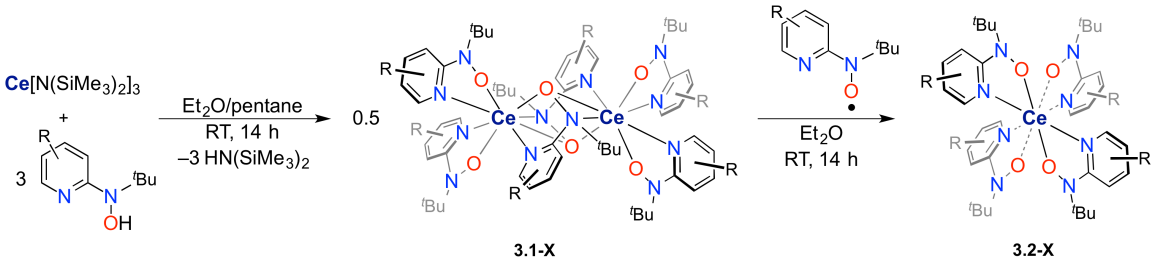

Scheme 3.2.1.1. Syntheses of **3.1-X** and **3.2-X** (**X = -CF_3, -H, -Me, -OMe, -*p*NMe_2, and –*m*NMe_2**). Figure adapted with permission of the American Chemical Society © 2013.

Complexes **3.2-X** were unreactive towards oxygen. Indeed, **3.2-H** was alternatively synthesized in good yield by addition of 1 equivalent of 2-(^{t}BuNOH)py to a THF suspension of **3.1-H** with exposure of the suspension to dry O_2. The solubilities of these monomeric **3.2-X** complexes in common organic solvents were drastically different than those of the dimeric **3.1-X** complexes. This allowed us to determine their solution phase structures using ^{1}H NMR

spectroscopy. The ^{1}H NMR spectra showed a highly symmetric ligand environment with resonances in the region of 0 to 10 ppm, consistent with their solid state structures of four ligands in chemically equivalent environments surrounding a diamagnetic Ce^{IV} cation.

It is noteworthy that the dimeric **3.1-X** complexes were stable under a nitrogen atmosphere without the addition of an external oxidant. However, even without the addition of ligand, the Ce^{III} dimers would convert to their monomeric Ce^{IV} congeners upon oxidation through ligand redistribution pathways.

In this regard, we were interested in whether we could isolate reduced forms of **3.2-X** or whether these complexes would revert back to the Ce^{III} dimers upon reduction. Reaction of a THF solution of **3.2-H** with potassium mirror led to the formation of a new soluble Ce^{III} complex, which we putatively assigned as the K[Ce(2-^{t}BuNO)py)$_4$] complex, though attempts to crystallize this complex from this route were unsuccessful. However, the exceedingly oxygen sensitive complex, [K(18-crown-6)(py)$_2$][Ce(2-(^{t}BuNO)py)$_4$] (**3.3-Ce**), was ultimately prepared in 57% isolated crystalline yield following reaction of 1 equivalent K[2-(^{t}BuNO)py], 3 equivalents 2-(^{t}BuNOH)py, and 1 equivalent 18-crown-6 with 1 equivalent Ce[N(SiMe$_3$)$_2$]$_3$. This suggested that the ligand frameworks around the central Ce^{IV} cation would be conserved upon redox cycling of the cerium. Therefore, we focused on the series of Ce^{IV} complexes for the ensuing electrochemistry and computational studies.

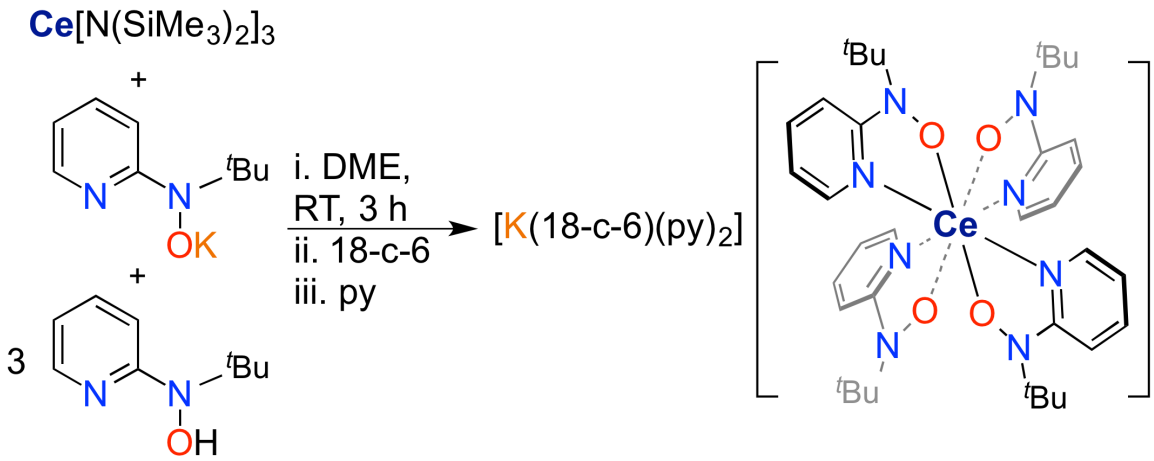

Scheme 3.2.1.2. Synthesis of **3.3-Ce**. Figure reprinted with permission of the American Chemical Society © 2013.

3.2.2 X-ray Structural Analyses

Complexes **3.1-CF$_3$**, **3.1-H**, **3.1-Me**, **3.1-OMe**, **3.1-*m*NMe$_2$**, and **3.1-*p*NMe$_2$** were isostructural in the solid state. Figure 3.2.2.1 shows the thermal ellipsoid plot of **3.1-H**, which serves as a representative example of the series of complexes. The bonding metrics from the X-ray structures of **3.1-X** were consistent with a formally Ce^{III}/Ce^{III} complex with reduced nitroxide ligands. Two bonding modes of the [R-2-(^{t}BuNO)py]$^-$ anion were observed. The chelating nitroxide ligands exhibited average N–O bond lengths ranging from 1.358(4) Å in **3.1-CF$_3$** to 1.391(5) Å in **3.1-*p*NMe$_2$** while the bridging nitroxide ligands exhibited slightly longer average N–O bond lengths ranging from 1.418(4) Å in **3.1-*p*NMe$_2$** to 1.430(6) Å in **3.1-OMe** as a result of the μ-(N,O) bonding mode. For comparison, the reported N–O bond lengths in La(hfac)$_3$(bpybNO), bpybNO = 2,2′-bipyridine-6,6′-diyl bis(*tert*-butyl nitroxide), with the bpybNO ligand in its neutral, biradical form, were significantly shorter at 1.282(5) Å and 1.276(6) Å,[15] and the N–O bond lengths in [(η^1-$ONC_5H_6Me_4)_2Sm(\mu\text{-}\eta^1{:}\eta^2\text{-}ONC_5H_6Me_4)]_2$, which has fully reduced TEMPO$^-$ ligands, were 1.431(8) Å.[16]

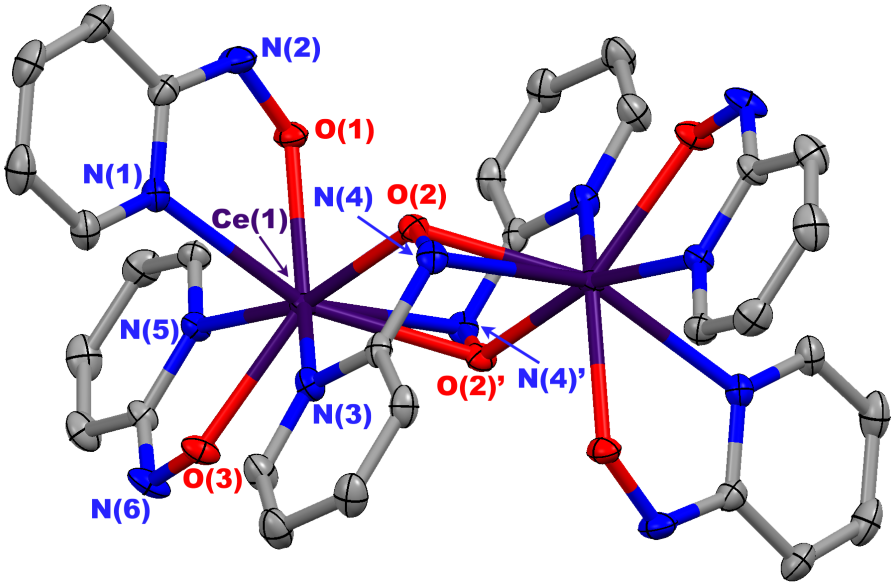

Figure 3.2.2.1. Thermal ellipsoid plot of [Ce^{III}(μ-2-(^{t}BuNO)py)(2-(^{t}BuNO)py)$_2$]$_2$ (**3.1-H**) at 30% probability as a representative example of the coordination environment of the series of **3.1-X** complexes. Hydrogen atoms and *tert*-butyl groups are omitted for clarity. Figure reprinted with permission of the American Chemical Society © 2013.

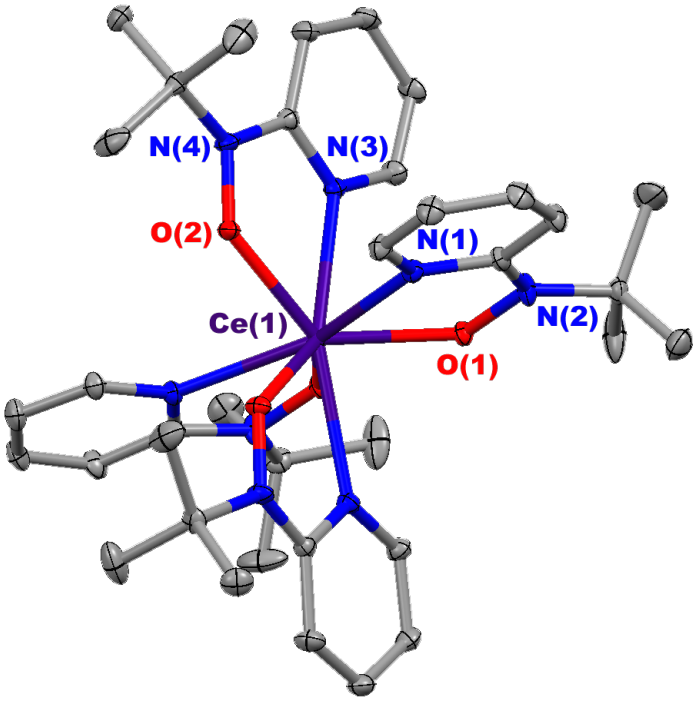

Figure 3.2.2.2. Thermal ellipsoid plot of Ce[2-(^{t}BuNO)py]$_4$ (**3.2-H**) at 30% probability as a representative example of the approximate D_{2d} coordination environment of the series of **3.2-X** complexes. Hydrogen atoms are omitted for clarity. Figure reprinted with permission of the American Chemical Society © 2013.

Similarly, X-ray analysis of **3.2-CF$_3$**, **3.2-H**, **3.2-Me**, **3.2-*p*NMe$_2$**, and **3.2-*m*NMe$_2$** revealed a conserved coordination environment with approximate D_{2d} symmetry. Figure 3.2.2.2 shows the thermal ellipsoid plot of **3.2-H**, which serves as a representative example of this D_{2d} coordination environment. Alternatively, the geometry of **3.2-OMe** differed from the others, exhibiting approximate S_4 symmetry. Calculations on optimized structures of complex **3.2-OMe** in approximate D_{2d} symmetry and approximate S_4 symmetry, however, indicated that there was negligible difference in energy between the two geometries.

It was evident from the crystal structure of complex **3.2-OMe** that the ^{t}BuNO moieties were significantly pyramidalized at the nitrogen atom as well as rotated out of plane with the pyridyl ring. This was to be compared to the structure of complex **3.2-CF$_3$** in which the ^{t}BuNO groups were coplanar with the pyridine ring (Figure 3.2.2.3). The degree of out of plane rotation was

assessed by averaging the N_{pyr}–C–N^{t}_{BuNO}–C torsion angles, while the average of the sums of the angles about the hydroxylamine nitrogen atoms (ΣY–N^{t}_{BuNO}–Z) was used to assess the degree of pyramidalization. These angles as well as selected bond distances for the series of Ce^{IV} complexes are listed in Table 3.2.2.1.

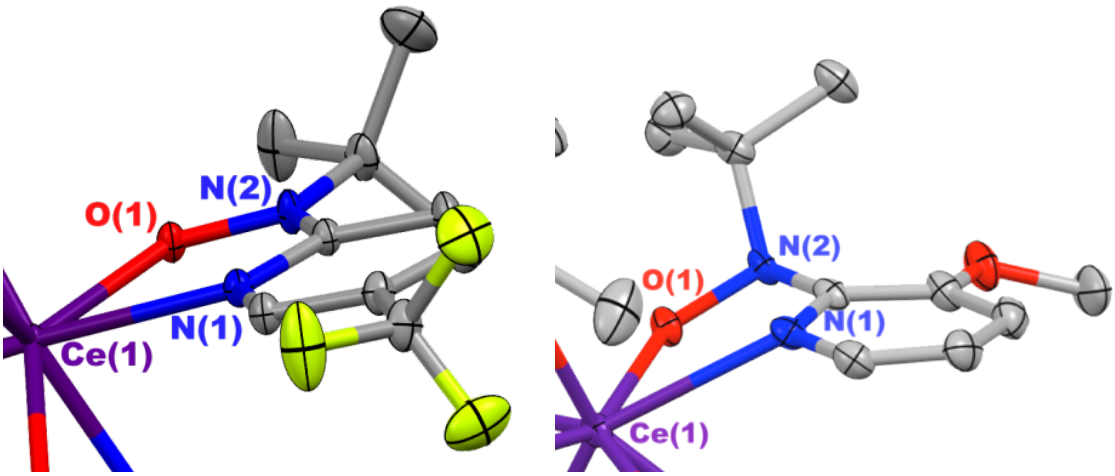

Figure 3.2.2.3. Partial thermal ellipsoid plots of **3.2-CF$_3$** (left) and **3.2-OMe** (right) indicating the relative increase in pyramidalization by comparison at N(2). Figure reprinted with permission of the American Chemical Society © 2015.

Table 3.2.2.1. Experimental structural metrics of the series of **3.2-X** complexes. Table adapted with permission of the American Chemical Society © 2015.

	N–O (Å)	Ce–O (Å)	Ce–N_{pyr} (Å)	ΣY–N^{t}_{BuNO}–Z angles (°)	N_{pyr}–C–N^{t}_{BuNO}–C torsion angle (°)
3.2-CF$_3$	1.368(2)	2.2318(14)	2.5416(16)	359.9(2)	2.51
3.2-H	1.375(2)	2.2356(13)	2.5434(17)	358.6(2)	7.49
3.2-Me	1.392(3)	2.2201(18)	2.566(2)	348.7(2)	29.65
3.2-OMe (S$_4$)	1.410(6)	2.193(4)	2.633(4)	337.9(7)	66.15
3.2-*p*NMe$_2$	1.4092(17)	2.2039(10)	2.5829(14)	337.17(15)	49.17
3.2-*m*NMe$_2$	1.399(2)	2.2269(14)	2.5415(17)	349.39(19)	29.23

The N–O bond lengths in the series of **3.2-X** complexes were similar to those for the chelating ligands in the **3.1-X** complexes, suggesting that all of the nitroxide ligands were fully reduced. Following the criterion articulated by Parkin,[17] the bond distances supported assignment of formal Ce^{IV} oxidation states in **3.2-X**. Decreases in the Ce–O bonds by ~0.1 Å between the chelating nitroxides in **3.1-X** and those in **3.2-X** were also consistent with the smaller ionic radius of the Ce^{IV} ion.[18]

The inter-planar torsion angles increased incrementally from 2.51° for complex **3.2-CF$_3$** to 66.15° for complex **3.2-OMe**. This increase correlated with the electron donating ability of the substituents on the pyridyl rings into the ^{t}BuNO moieties. A similar trend was observed with the degree of pyramidalization, which decreased from 359.9(2)° in complex **3.2-CF$_3$** to 337.17(15) in complex **3.2-*p*NMe$_2$**. Based on the Hammett parameters for substituents in the para position (σ_p^+ = –0.78 for OMe and –1.70 for NMe_2),[19] we expected the degree of rotation in complex **3.2-*p*NMe$_2$** to be greater than that in complex **3.2-OMe**. The unexpected *smaller* torsion angles observed in the solid state structure of **3.2-*p*NMe$_2$** were attributed to decreased steric repulsion from the smaller *ortho*-H group in the former relative to the larger *ortho*-OMe group in the latter.

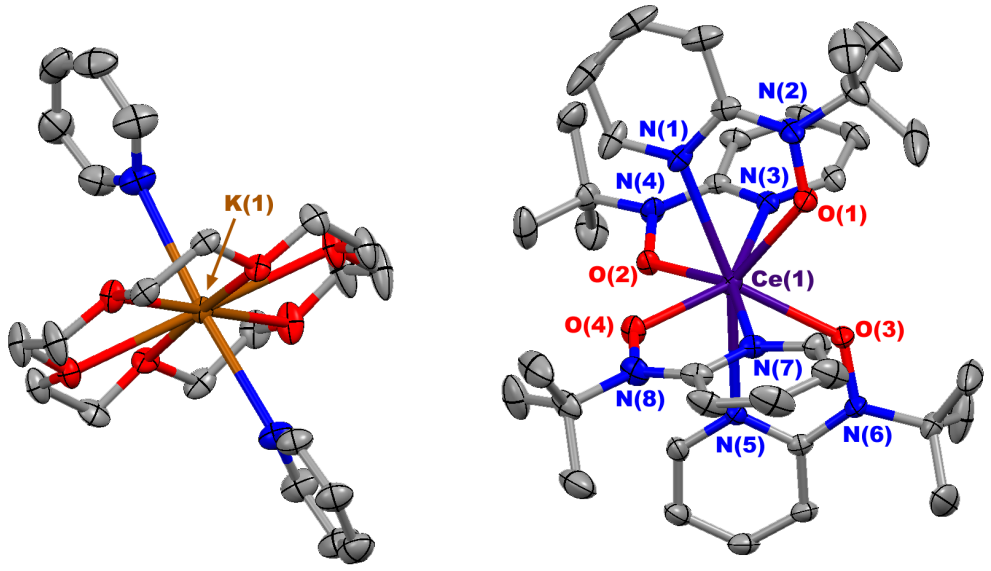

Figure 3.2.2.4. Thermal ellipsoid plot for [K(18-crown-6)(py)$_2$][Ce(2-(^{t}BuNO)py)$_4$] (**3.3-Ce**) at 30% probability. Hydrogen atoms are omitted for clarity. Figure reprinted with permission of the American Chemical Society © 2013.

Complex **3.3-Ce** crystallized in the monoclinic space group $P2_1/c$ (Figure 3.2.2.4). Again, the X-ray structure of **3.3-Ce** revealed average N–O and Ce–O bond distances of 1.367(5) Å and 2.384(3) Å, respectively, that were consistent with a Ce^{III} complex, as discussed for the series of complexes, **3.1-X**. To compare the structures of **3.2-H** and **3.3-Ce**, we determined the shape parameters associated with each complex.[20] These were compared to the shape parameters of regular trigonal dodecahedron and regular square anti-prism geometries, corresponding to pure D_{2d} and D_{4d} point group symmetry, respectively. Shape parameters for **3.3-Ce** were somewhat changed from those observed for **3.2-H**, but both were still largely consistent with distorted trigonal dodecahedral geometries. These data are tabulated in Table 3.2.2.2.

Table 3.2.2.2. Shape parameters for complexes **3.2-H** and **3.3-Ce**. Table reprinted with permission of the American Chemical Society © 2013.

	ϕ_1	ϕ_2	d_1	d_2	d_3	d_4	θ_A	θ_B
3.2-H	7.8	11.0	30.7	30.9	49.0	49.5	49.4	77.2
3.3-Ce	11.8	15.9	24.2	25.3	48.3	49.2	48.4	78.6
$\mathbf{D_{2d}}^a$	0.0	0.0	29.5	29.5	29.5	29.5	35.2	73.5
$\mathbf{D_{4d}}^a$	24.5	24.5	0.0	0.0	52.4	52.4	57.3	57.3

[a]A rigorous D_{2d} geometry corresponds to a regular trigonal dodecahedron while D_{4d} corresponds to a regular square anti-prism.

3.2.3 Spectroscopic Characterization

To confirm the Ce^{III} oxidation state of **3.1-X**, we performed magnetic susceptibility measurements on **3.1-H**, which served as a representative example of the series of complexes. The temperature dependence of the magnetic moment for **3.1-H** was measured from 2–300 K in the presence of a 1.0 T field (Figure 3.2.3.1). The χT value for **3.1-H** was 1.46 emu K mol^{-1} at 300 K, which was consistent with expected values for two isolated J = 5/2 Ce^{III} ions. The variable temperature χT response for **3.1-H** was also consistent with reported Ce^{III} complexes;[21] the χT product decreased from 1.46 to 1.0 emu K mol^{-1} at 5 K. Below 5 K the χT product decreased

precipitously due to depopulation of the three Kramer's doublets that arise from ligand field splitting within the J = 5/2 manifold of the Ce^{III} ions, though antiferromagnetic coupling between the Ce^{III} moments cannot be ruled out. The field dependent data at 2 K saturated and achieved a value of 2.17 μB at 7 T. Overall these data were consistent with assignment of the series of **3.1-X** complexes as formally Ce^{III}/Ce^{III} dimers with fully reduced nitroxide ligands.

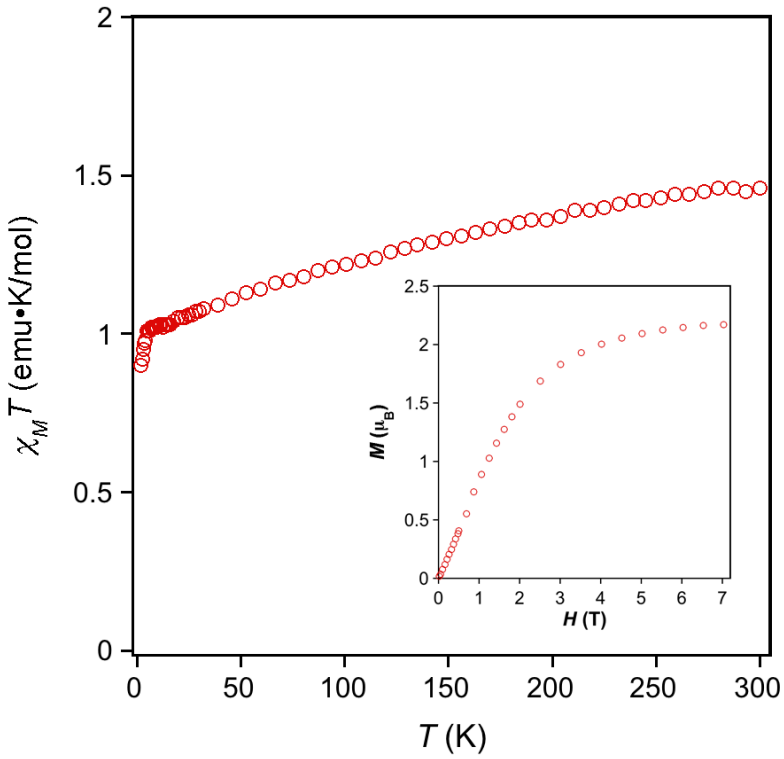

Figure 3.2.3.1. Temperature and field (inset) dependent magnetic data of compound **3.1-H**. Figure reprinted with permission of the American Chemical Society © 2013.

In order to confirm the Ce^{IV} oxidation state in the series of **3.2-X** complexes, Ce L_{III} edge X-ray absorption spectroscopy was performed on the **3.1-X** and **3.2-X**, X = **-**CF_3, -H and –*p*NMe_2, congeners. Cerium(IV) compounds are known to exhibit valence instability;[22] multi-configurational ground states have been previously observed for organo-cerium(IV) compounds bearing redox non-innocent ligands.[23] Such phenomena arise from the mixing of electronic states that reflect transfer of electrons from low-lying ligand π* orbitals to energetically close metal 4f acceptor orbitals. In such cases, low energy LMCT bands are visible in the electronic

absorption spectrum.[24] The canonical multi-configurational organocerium compound is cerocene: $Ce(COT)_2$, COT = cyclooctatetraene;[23b, 25] the lowest energy, formally LMCT band for cerocene was reported at 2.18 eV.[26] While many spectroscopic techniques such as ^{1}H NMR spectroscopy and gas phase photoelectron spectroscopy suggested the presence of a Ce^{IV} cation,[26-27] the presence of a high percentage of Ce^{III} character was clearly evident in the Ce L_{III} edge X-ray absorption spectrum of this complex.[23b, 25] As shown in Figure 3.2.3.2, the data for the series of **3.2-X** compounds, however, revealed two absorption features, consistent with the core hole excitation of the Ce^{IV} ion. In this case, the pair of transitions corresponded to final states $\bar{2}p4f^1\bar{L}5d^1$ and $\bar{2}p4f^0 5d^1$, where $\bar{L}$ indicates a ligand hole, and the f^1 contribution indicates the degree of covalency. For comparison, the data for the cerium(III) **3.1-X** compounds revealed single white line absorbances at energies consistent with cerium(III) cations.[23b] The data supported assignment of **3.2-X** as true cerium(IV) complexes and indicated that tuning the ligand redox potential for this system did not introduce multi-configurational character into the ground state of the resulting cerium(IV) complexes.

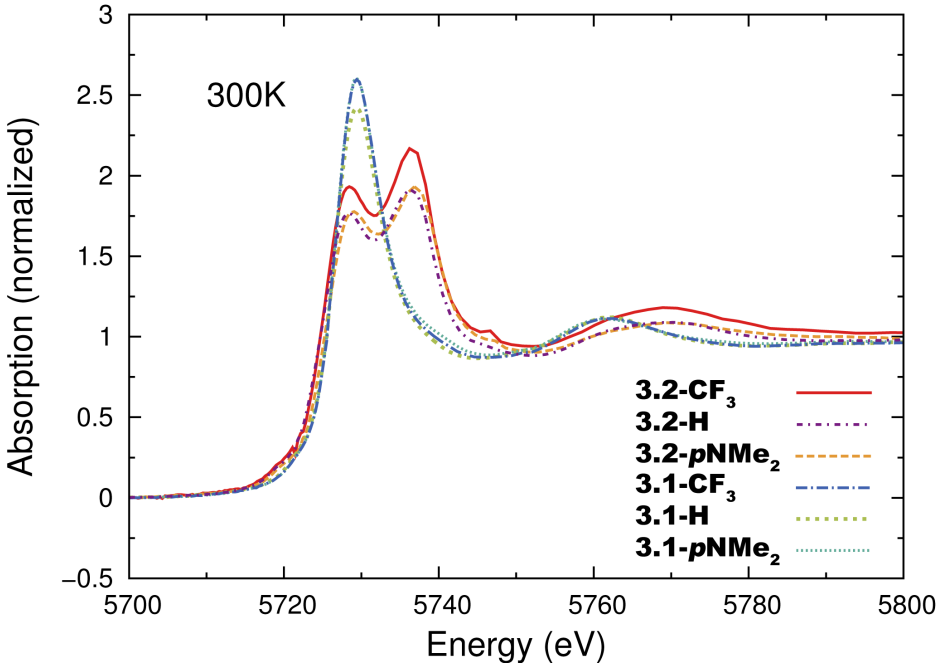

Figure 3.2.3.2. Ce L_{III} edge XAS data for the cerium(III) compounds **3.1-H**, **3.1-CF$_3$** and **3.1-*p*NMe$_2$** and their cerium(IV) congeners **3.2-H**, **3.2-CF$_3$** and **3.2-*p*NMe$_2$**. Figure reprinted with permission of the American Chemical Society © 2015.

All of the monomeric complexes, **3.2-X**, exhibited characteristic intense, dark red to dark purple colors. Ce^{IV} complexes typically have dark colors due to allowed ligand-to-metal charge transfer (LMCT) transitions in the visible region. These LMCT transitions span a range of wavelengths depending on ligand environment.[28] The electronic absorption spectra revealed a set of two broad transitions in all of the complexes except **3.2-*m*NMe$_2$**, which only showed the lower energy transition (Figure 3.2.3.3).

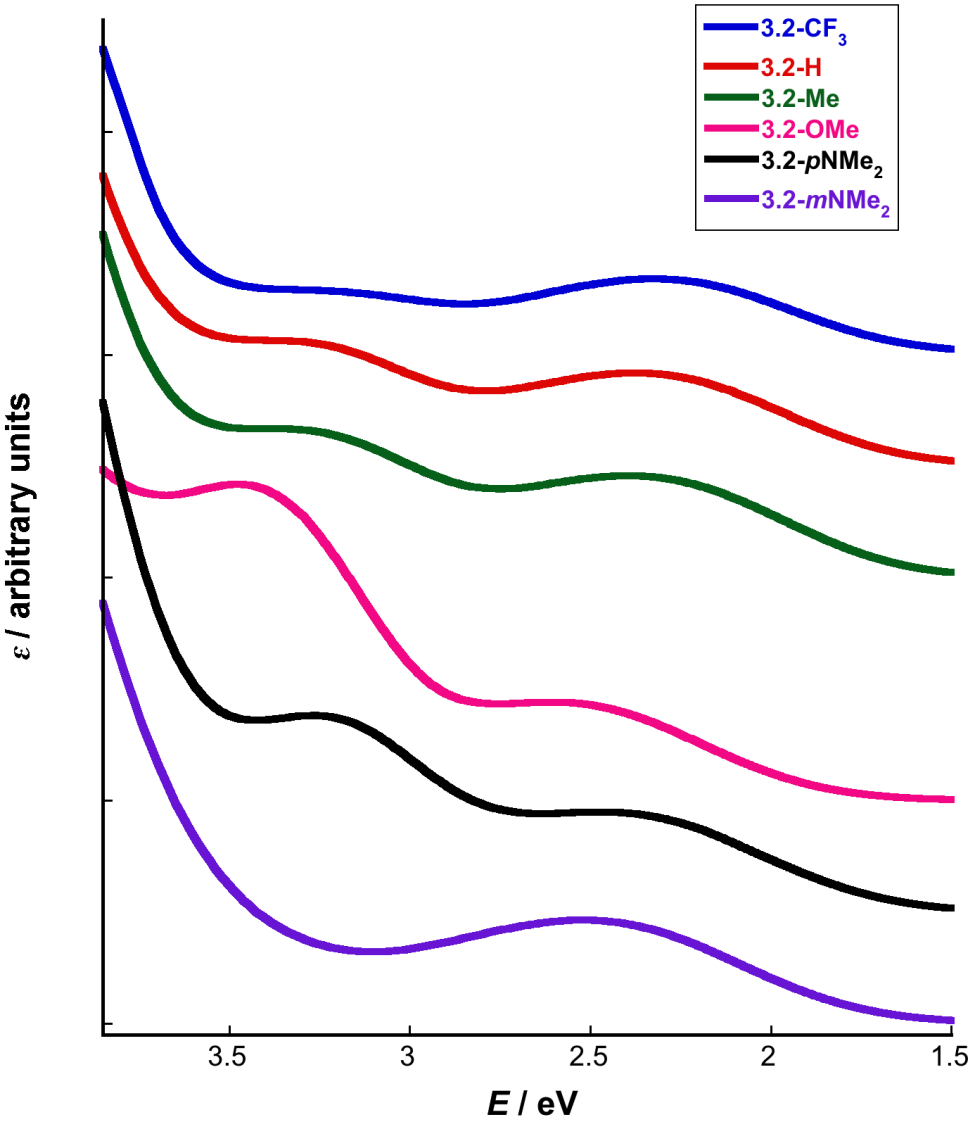

Figure 3.2.3.3. Experimental electronic absorption spectra for the **3.2-X** complexes. Figure reprinted with permission of the American Chemical Society © 2015.

To definitively assign the electronic transitions, we prepared the complex [K(18-crown-6)(py)$_2$][La(2-(^{t}BuNO)py)$_4$] (**3.3-La**) through a similar route to the analogous cerium(III) complex. In this context, transitions that have metal character, such as LMCT, would occur at significantly different energies within complexes **3.2-H** and **3.3-La.** The UV-Vis spectrum of **3.3-La** displayed a single broad absorption at 3.08 eV. The absence of a second broad band provided support for assignment of the 2.0–2.5 eV bands of **3.2-X** as LMCT. On this basis, we could also assign the higher energy of the two features in **3.2-X** as excitations localized on the pyridyl nitroxide ligand.

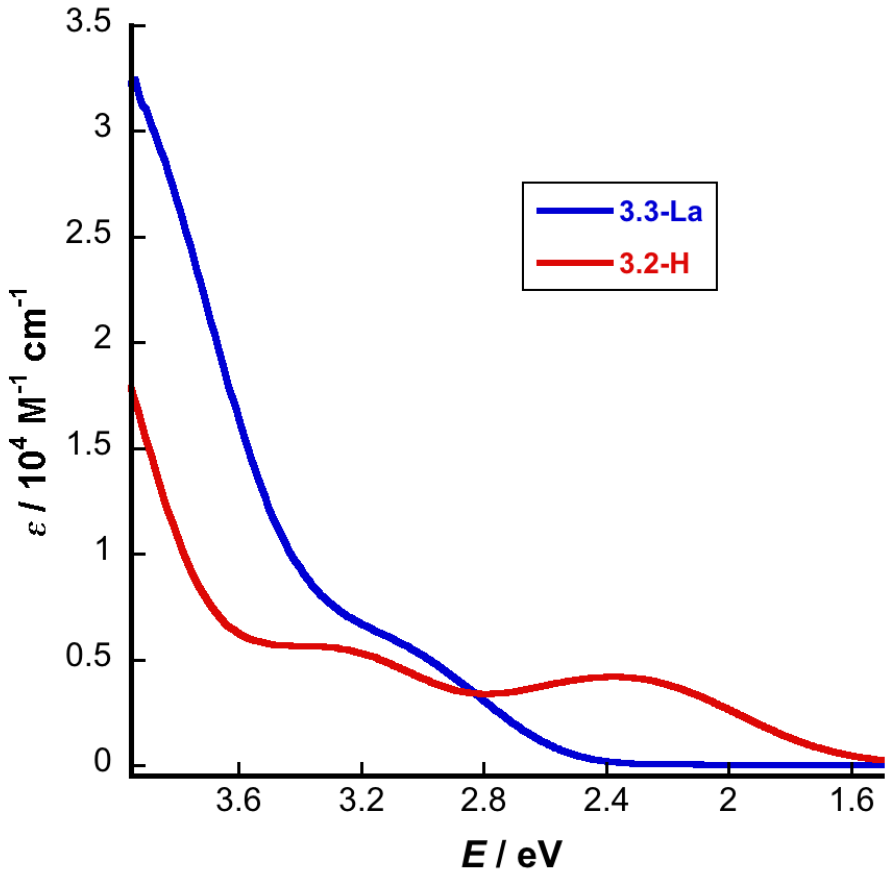

Figure 3.2.3.4. Experimental electronic absorption spectra for **3.3-La** and **3.2-H** indicating the absence of a second, low-energy, broad band in the **3.3-La** compound. Figure adapted with permission of the American Chemical Society © 2015.

To corroborate the UV-Vis band assignments we turned to TD-DFT, a method that has been used successfully to predict the absorption spectra of lanthanide complexes.[29] Representative TD-DFT calculations incorporating acetonitrile solvation revealed vertical excitations at 2.07 eV

for **3.2-H** and 2.16 eV for **3.2-CF$_3$**, characterized as transitions from an occupied nitroxide π* orbital to vacant cerium 4f orbitals, indicating LMCT character. TD-DFT also supported the nature of the higher energy feature as a ligand-based nitroxide π* to pyridyl π* excitation (Figure 3.2.3.5).

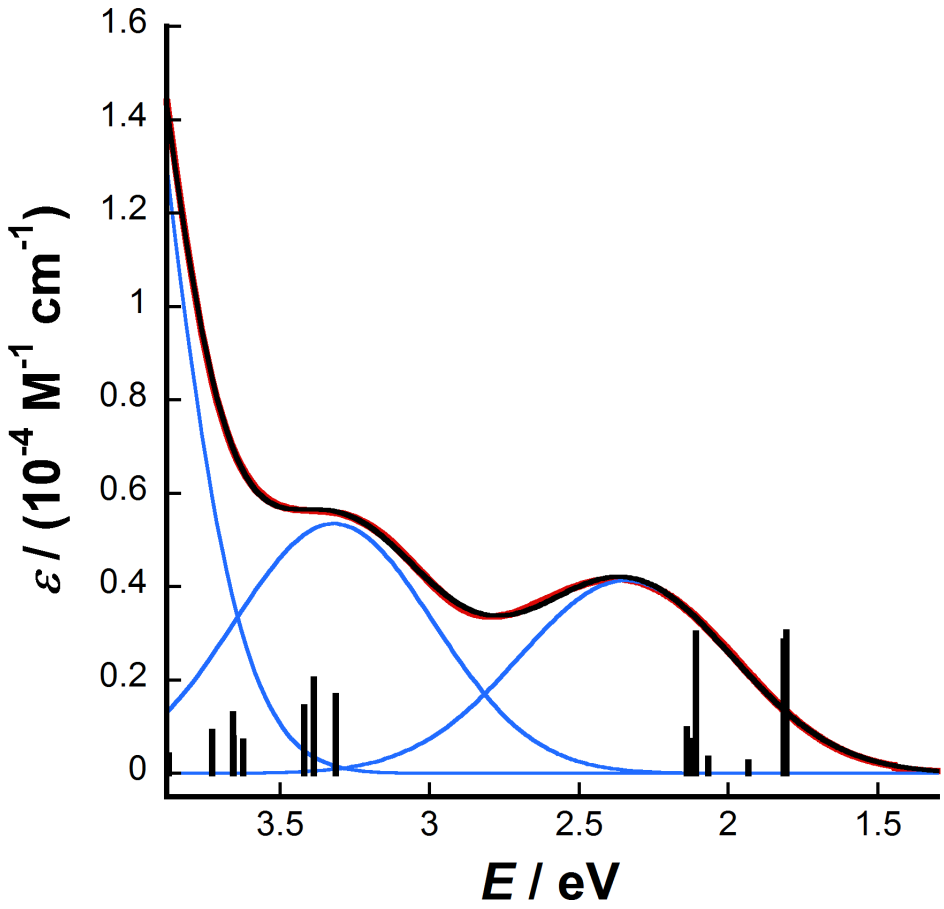

Figure 3.2.3.5. TD-DFT calculated excitation profile for **3.2-H**. Figure reprinted with permission of the American Chemical Society © 2015.

3.2.4 Solution Electrochemistry

Having established the true valence electronic structures across the series, we next examined the purely metal based electrochemistry of the compounds. To begin this study, a variety of oxidants were used to probe the instability of complex **3.3-Ce** in the +3 oxidation state. Upon reaction of **3.3-Ce** with ferrocenium hexafluorophosphate, 1,4-benzoquinone, or cobaltocenium

triflate, **3.2-H** was produced in quantitative yield based on ^{1}H NMR spectroscopy. Attempts to produce **3.2-H** from **3.3-Ce** with decamethylcobaltocenium triflate or benzophenone yielded mixtures of products, though the reaction with decamethylcobaltocenium triflate clearly produced decamethylcobaltocene through single electron transfer. Together with the observed reduction of **3.2-H** using potassium mirror, these oxidation reactions indicated that **3.3-Ce** was a potent outer sphere reductant and placed the $Ce^{III/IV}$ redox potential chemically between –1.33 V and about –2.00 V versus ferrocene,[30] which prompted detailed evaluation of the electrochemistry of the system.

Solution cyclic voltammetry measurements were therefore performed on **3.2-H** as well as 2-(^{t}BuNOH)py in DCM in order to evaluate the relative stability of the formal Ce^{IV} oxidation state in this complex. As shown in Figure 3.2.4.1, the cyclic voltammogram of **3.2-H** exhibited four redox couples, with quasi-reversible oxidation waves at E_{pa} = –1.80 V, E_{pa} = –0.49 V, and E_{pa} = +0.18 V versus Fc and an irreversible oxidation wave at E_{pa} = +0.52 V. The cyclic voltammogram of 2-(^{t}BuNOH)py displayed the corresponding oxidation waves at E_{pa} = –0.07 V and E_{pa} = +0.41 V, indicative of oxidation to the neutral radical and oxoammonium compound, respectively. Given the measured rest potential of –0.89 V, we attributed the features in **3.2-H** at E_{pa} = –1.80 V and E_{pc} = –2.09 V to the $Ce^{III/IV}$ redox couple. Solution cyclic voltammetry measurements of complex **3.3-Ce** could not be performed in DCM as the compound slowly oxidized to complex **3.2-H** under these conditions. Instead, it was measured in a 0.1 M [^{n}Pr$_4$N][BAr$^F_4$] THF/MeCN (1:4) solution. The addition of THF was necessary to dissolve the complex, which was only slightly soluble in neat MeCN solution. Given a measured rest potential of –1.59 V, the metal based oxidation feature of **3.3-Ce** was observed at E_{pa} = –1.43 V and E_{pc} = –1.68 V. For comparative purposes, complex **3.2-H** was also measured in the THF/MeCN (1:4) solution, where the metal based $Ce^{III/IV}$ redox couple was observed at E_{pa} = –1.70 V and E_{pc} = –1.89 V.

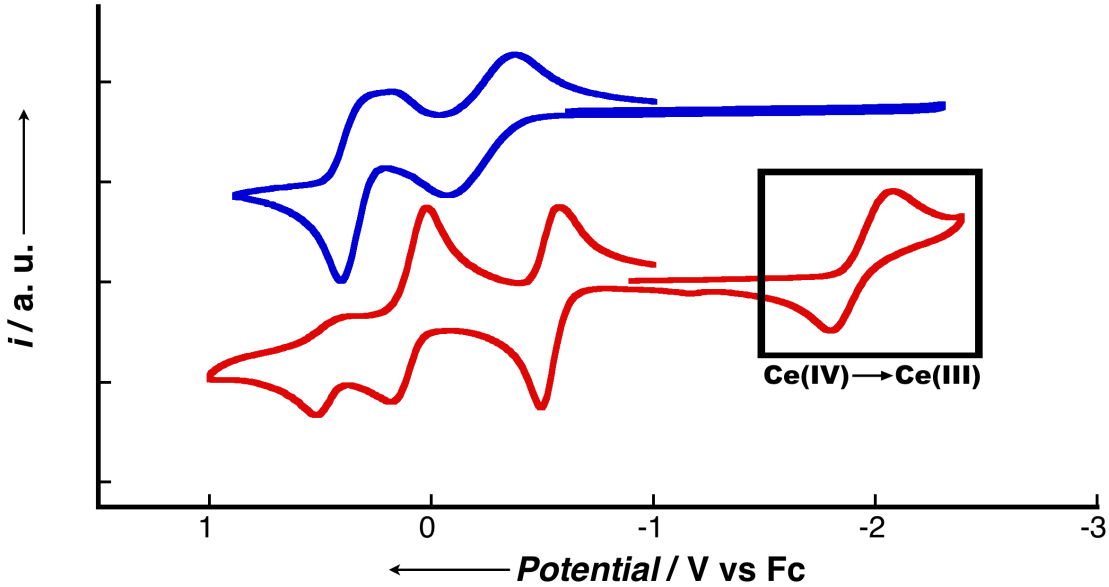

Figure 3.2.4.1. Cyclic voltammogram of complex **3.2-H** and 2-(^{t}BuNOH)py measured in 0.1 M [^{n}Pr$_4$N][BAr$^F{}_4$]/DCM versus an internal ferrocene standard. The rest potentials were measured at –0.79 V for 2-(^{t}BuNOH)py and at –0.89 V for **3.2-H**. Figure reprinted with permission of the American Chemical Society © 2013.

The value of –1.80 V versus Fc in MeCN was shifted by +3.10 versus the standard aqueous potential for the reduction of cerium(IV).[31] However, due to the difference in dielectric constants between water and acetonitrile, a more effective comparison was to that of the reduction potential of [^{n}Bu$_4$N]$_2$[Ce(NO$_3$)$_6$] at +0.62 V versus Fc in acetonitrile.[32] In this context, a +2.42 V shift for the cerium(IV) reduction potential in acetonitrile was observed when complexed by four [2-(^{t}BuNO)py]$^-$ ligands. This was greater than the 2.15 V shift observed by Raymond and co-workers for the [Ce(O$_2$C$_6$H$_4$)$_4$]$^{4-}$ anion and represented a 10^{41}-fold difference in the formation constants for **3.2-H** compared to the anion of **3.3-Ce** in reference to [^{n}Bu$_4$N]$_2$[Ce(NO$_3$)$_6$] in acetonitrile.[33] The reduction potential for compound **3.2-H** was also lower than that reported for cerocene,[27b] and for Ce(omtaa)$_2$.[34] These results indicated the Ce^{IV} ion was stabilized in the nitroxide ligand framework to an unprecedented degree. This was a noteworthy observation considering that the catecholate ligands of the benchmark complex Ce[(O$_2$C$_6$H$_4$)$_4$]$^{4-}$ have two anionic, oxygen donor sites.

Having established that **3.2-H** was the most stable cerium(IV) complex to date based on the potential of the metal based redox couple in the cyclic voltammetry measurements, we looked at whether the $Ce^{IV/III}$ redox potential could be tuned across the series of **3.2-X** complexes. These solution electrochemistry experiments were performed in 0.1 M [$^{n}Pr_4N$][BAr^{F}_4] THF/MeCN (1:4) solutions, as these conditions yielded the smallest anodic (E_{pa}) to cathodic (E_{pc}) wave separation for the quasi-reversible $Ce^{IV/III}$ redox couples across the series. Again, the addition of THF was necessary to dissolve the complexes. The $E_{1/2}$ values obtained from these experiments are listed in Table 3.2.5.2.

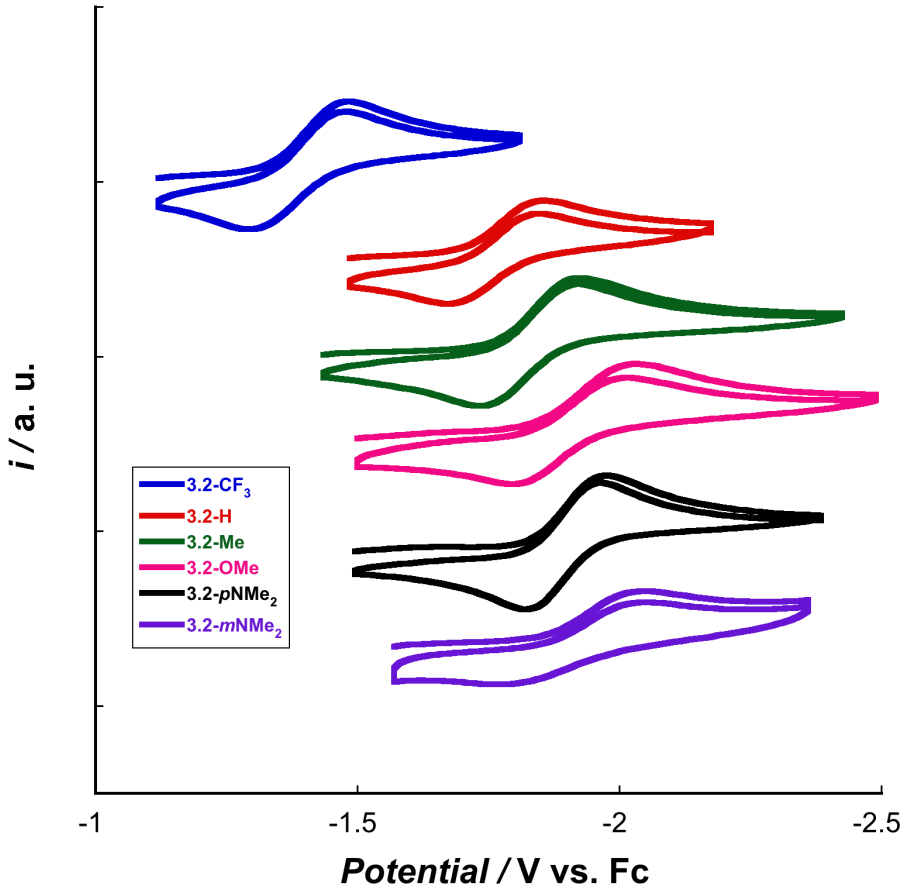

Figure 3.2.4.2. Cyclic voltammograms of the isolated $Ce^{IV/III}$ reduction features in the **3.2-X** complexes. Figure reprinted with permission of the American Chemical Society © 2015.

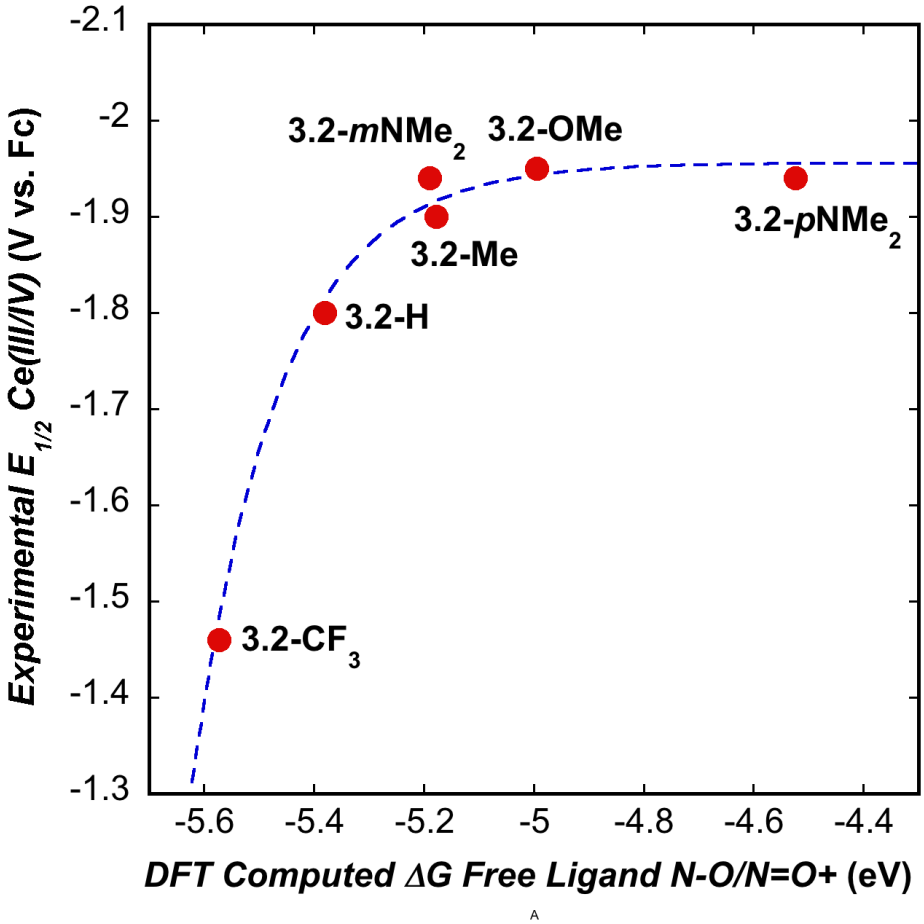

Figure 3.2.4.3. Correlation between metal redox potentials in the **3.2-X** complexes and DFT computed free energy changes for the free ligand N-O/N=O$^+$ redox event. Figure reprinted with permission of the American Chemical Society © 2015.

As expected, the potential of the $Ce^{IV/III}$ redox event shifted to more negative potentials with the more electron-rich pyridyl-nitroxide ligands coordinated to the central cerium cation (Figure 3.2.4.2). We were surprised, however, that despite the increasing of substituent donating ability from –Me to –OMe to –*p*-NMe_2, there was not a significant shift in the reduction potential of Ce^{IV} in the respective complexes (Figure 3.2.4.3). As discussed in Chapter 2, we had observed a linear dependence of the radical to oxo-ammonium redox potentials on substituent donating abilities in the solution electrochemistry of the nitroxide ligands alone. We attributed this smaller than expected substituent effect in these complexes to the pyramidalization and rotation of the nitroxide moieties, which reduced the conjugation with the pyridyl π system. As such, electron

donating substituents beyond –Me showed a negligible effect on cerium oxidation potential due to the inferred electronic feedback/distortion of the nitroxide-pyridyl ring system. We next turned to solution phase DFT calculations to corroborate these experimental observations.

3.2.5 DFT Studies

While lanthanide-ligand bonding has been traditionally viewed as primarily ionic with insignificant 4f orbital contribution,[35] recent work has explored the possibility for lanthanide complexes to exert stabilization through covalent interactions at the extremes of bonding.[36] Therefore, in order to determine whether covalent interactions were playing a role in the stabilization of the tetravalent oxidation state of cerium in the series of **3.2-X** complexes, we first explored the electronic structures of **3.2-H** and **3.3-Ce** using hybrid B3LYP DFT methods.

Both the calculated structures for the Ce^{IV} and Ce^{III} states accurately predicted the Ce–O bond lengths within 0.011 Å and 0.012 Å, respectively. The calculated $Ce–N_{(pyr)}$ bond lengths were longer than those experimentally observed but were still within 0.088 Å and 0.065 Å from the experimentally determined values for **3.2-H** and **3.3-Ce**.

In the formally Ce^{IV} state of **3.2-H**, the HOMO had significant electron density located on the 2-(^{t}BuNO)py ligands with 8.3% Ce 4f character. While there is a tendency for DFT to overemphasize such delocalization, the most striking feature of this orbital was that the N–O bonds of the nitroxide ligands were oriented around the Ce^{IV} ion with the correct symmetry for multiple π bonding interactions between the four filled N–O π* orbitals and the $f_{z(x^2-y^2)}$ atomic orbital of Ce. In fact, the LUMO of **2**, calculated to be 2.65 eV above the HOMO, had the correct symmetry for the corresponding π* antibonding interactions. Despite the rather small overlap of the core-like 4f orbitals with the ligand based π*-orbitals, this arrangement possessed the correct symmetry to impose a stabilizing influence on the electronic structure of the complex. In contrast, in the calculated result of **3.3-Ce**, with Ce in the +3 oxidation state, the HOMO consisted of a single unpaired electron residing solely in a non-bonding cerium 4f orbital. These results were similar to those observed for $[Li(thf)_4][Ce(COT)_2]$, which showed the largest single 4f orbital contribution to the SOMO was $4f_z^3$.[37]

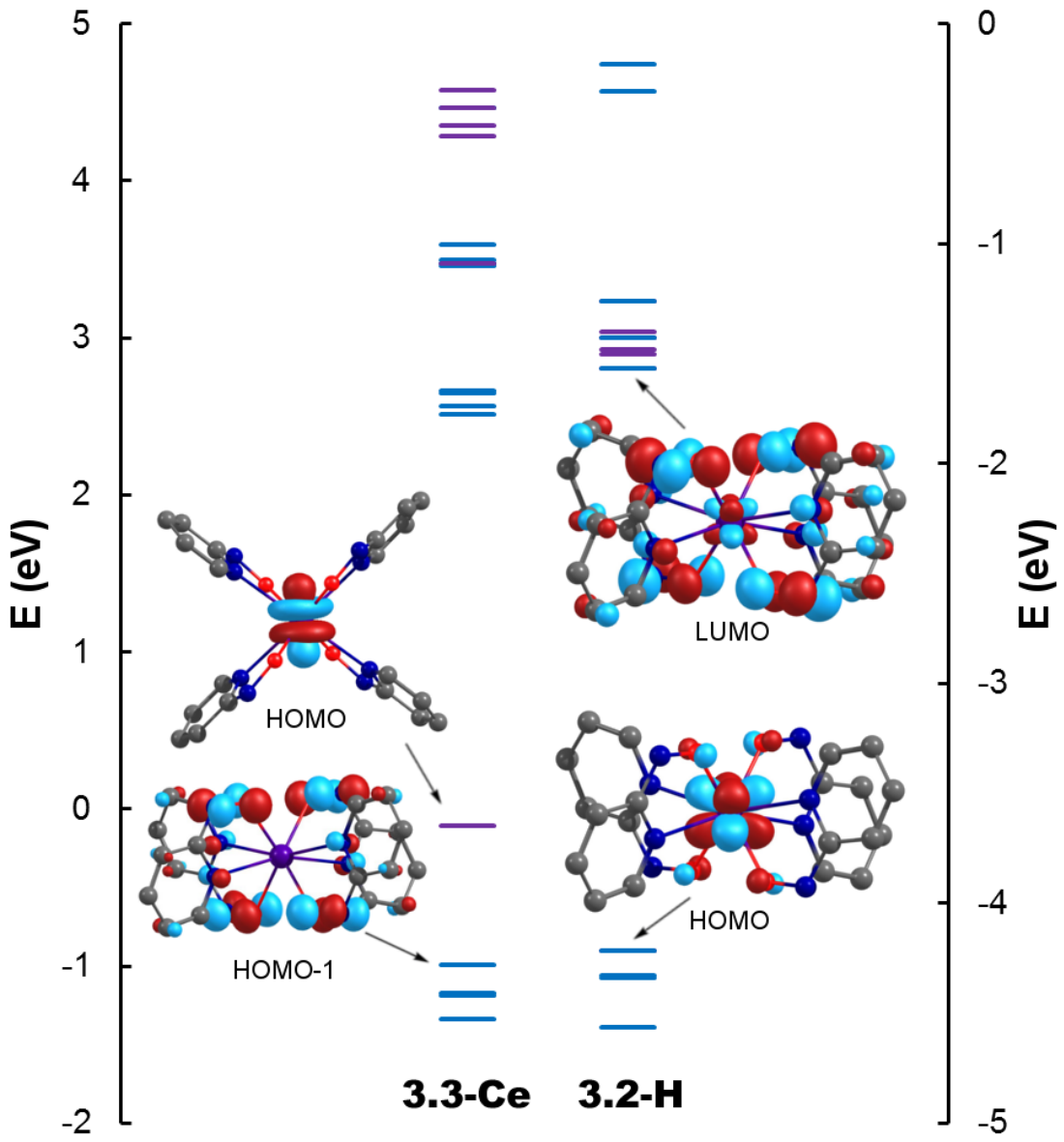

Figure 3.2.5.1. Energy level diagrams for **3.3-Ce** and **3.2-H**. The differing energy scales at left and right should be noted. Hydrogen atoms and tert-butyl groups are omitted from the inset molecular orbitals for clarity. Figure reprinted with permission of the American Chemical Society © 2013.

Unlike the Ce^{IV} state in **3.2-H**, only minor cerium 4f (< 2%) and 5d (< 6%) character was observed in other filled orbitals in **3.3-Ce**. The symmetric arrangement of nitroxide π* orbitals that comprised the HOMO of **3.2-H** was present as the HOMO-1 in **3.3-Ce**, without the cerium 4f contribution. The HOMO-1 of **3.3-Ce** was calculated to be 0.88 eV below the HOMO. We propose

that oxidation of **3.3-Ce** to **3.2-H** lowered the energy of the cerium 4f orbitals, which provided a closer energetic matching with the nitroxide N–O π* orbitals and lead to greater symmetry-allowed mixing of these metal and ligand orbitals. This effect was further illustrated by fragment molecular orbital analysis. Figure 3.2.5.1 highlights the isolated $4f_z^3$ HOMO and non-interacting N–O π* fragments of **3.3-Ce**, while mixing of the N–O π* fragments with the $4f_{z(x^2-y^2)}$ atomic orbital of Ce^{IV} is clearly observed in the HOMO of **3.2-H**.

The role of ligand to metal electron donation in the stabilization of **3.2-H** in the +4 oxidation state was examined through population analyses. A comparison of the natural bond orbital analyses of **3.2-H** and **3.3-Ce** with several reported formally Ce^{IV} complexes is shown in Table 3.2.5.1. The natural charge on cerium, q_{ce}, in **3.2-H** was essentially unchanged relative to **3.3-Ce**, despite the higher formal oxidation state. A smaller natural charge to formal charge ratio was due to greater donation of nitroxide ligand electron density into unfilled cerium 4f, 5d, and to some extent 6s orbitals. This difference was also reflected in the Mayer bond order, which increased dramatically from 3.11 to 4.56 upon oxidation. Notably, the calculated natural charge in **3.2-H** was significantly smaller than the reported Ce^{IV} complexes, indicative of a higher degree of electron donation to the Ce^{IV} cation in this compound.

Table 3.2.5.1. Natural charges (q_{Ce}), natural populations (6s, 5d, and 4f), and Mayer bond orders (MBO) of **3.2-H** and **3.3-Ce**, compared to other formally Ce^{IV} complexes. Table reprinted with permission of the American Chemical Society © 2013.

	3.3-Ce (Ce^{III})	**3.2-H** (Ce^{IV})	Cp_2CeO (Ce^{IV})[a]	CeN^*_2LCl (Ce^{IV})[b]	$Ce(COT)_2$ ($Ce^{III/IV}$)[c]
q_{Ce}	1.71	1.74	2.42	2.53	2.41
6s	0.16	0.17	0.09	0.16	[c]
5d	0.92	1.17	0.45	0.36	[c]
4f	0.14	0.87	1.01	0.95	[c]
MBO[d]	3.11	4.56	–	–	–

[a]Similar results were obtained for a series of $Cp_2Ce^{IV}Z$ (Z = F^+, O, NH, CH^-, CH_2) compounds.[38] [b]N* = $–N(SiMe_3)_2$, L = $–OCMe_2CH_2(CNCH_2CH_2NDipp)$, Dipp = 2,6-^{i}Pr$_2C_6H_3$.[39] [c]Individual populations not reported.[37] [d]Sum of metal-ligand MBOs.

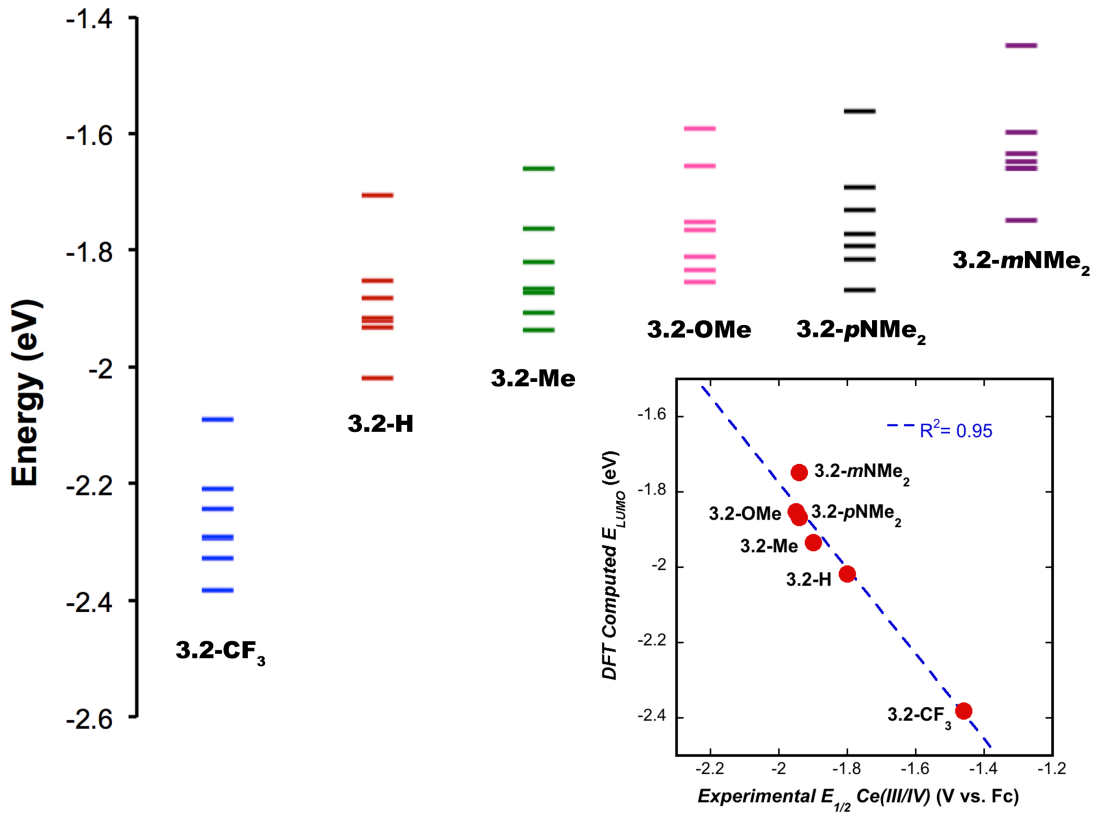

Figure 3.2.5.2. Energy level diagrams for the **3.2-X** complexes highlighting the destabilization of the LUMO through LUMO+6 virtual orbitals and correlation between LUMO energy and $Ce^{IV/III}$ reduction potential (inset). Figure adapted with permission of the American Chemical Society © 2015.

The electronic structures of the functional derivatives of **3.2-H** were then explored through solution DFT methods for comparison, revealing a systematic variation in the frontier molecular orbitals. Notably, the LUMO through LUMO+6 virtual orbitals, of predominantly Ce 4f character, exhibited a trend in destabilization directly related to the experimentally observed $Ce^{IV/III}$ reduction potential (Figure 3.2.5.2). This destabilization of the LUMO orbital was consistent with increased symmetry allowed donation from the N–O π* orbitals into the Ce $4f_{z(x^2-y^2)}$ orbital lending stability to the tetravalent oxidation state of cerium in these complexes. The addition of more electron rich pyridyl nitroxide ligands was expected to raise the N–O π* orbitals closer to the Ce $4f_{z(x^2-y^2)}$ to allow for better energy matching. The better energy matching of these orbitals would explain the increase in destabilization of the LUMO across the series. In fact, a linear correlation was

established between the calculated energy of the LUMO and the experimentally determined $Ce^{IV/III}$ redox potentials (Figure 3.2.5.2).

In addition to the computations on the cerium(IV) **3.2-X** complexes, unrestricted B3LYP DFT calculations on isostructural anionic complexes with cerium in the 3+ oxidation state were performed in order to calculate the $Ce^{IV/III}$ $E_{1/2}$ values from computed $\Delta G_{(soln)}$ values (Figure 3.2.5.3).[40] Complete geometry optimizations were performed in all cases. After an empirical correction factor of 0.30 V was applied to the calculated $E_{1/2}$ values to account for systematic errors arising from the use of ferrocene as a reference for cerium complexes, these DFT computed redox potentials correlated well with experiment, as shown in Table 3.2.5.2 and Figure 3.2.5.4. It is also noteworthy that Batista and coworkers observed systematic errors in their calculations when ferrocene was used as a reference for the second or third row transition metal complexes.[13a] Thus, the combination of X-ray structural, electrochemical and DFT analyses were validated for our series of six pyridyl-nitroxide complexes, **3.2-X**, spanning an $E_{1/2}$ range of ~500 mV.

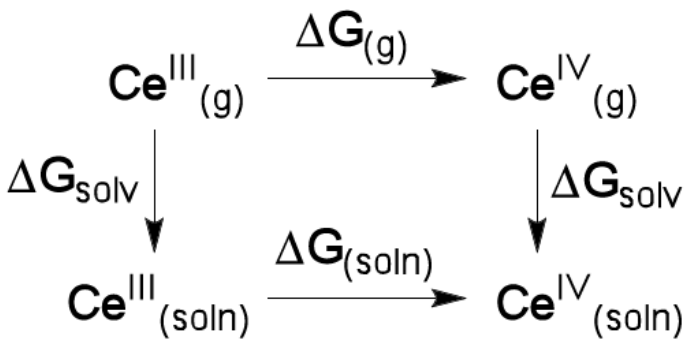

Figure 3.2.5.3. Thermodynamic cycle used for the calculation of $\Delta G_{(soln)}$ between the Ce^{III} and Ce^{IV} states. Figure reprinted with permission of the American Chemical Society © 2015.

Following our successes with the **3.2-X** series, we were interested in applying the approach more broadly to cerium compounds in general. As a limiting factor, we examined complexes with similar coordination geometries but varying ligand field strengths. A natural extension was to

cerium hydroxamate complexes. Hydroxamates are key agents in the froth flotation separation unit operations for isolation of lanthanides from their ores,[41] creating a broad interest in the ability to predict their ligand field strengths through simple calculations. Furthermore, the crystal structure of the $Ce(HA)_4$ complex (where HA = N-phenyl-pivalohydroxamate) revealed a similar D_{2d} geometry.[8] Based on the reported electrochemistry of this complex, however, the hydroxamate ligands imposed a weaker ligand field around the central cerium cation than the pyridyl-nitroxide system. The calculated $Ce^{IV/III}$ redox potential of –1.28 V for $Ce(HA)_4$ was within 20 mV of the experimentally determined $E_{1/2}$ value as estimated by averaging the anodic and cathodic wave potentials in the cyclic voltammogram.

We also examined the aryl oxide ligand frameworks in the reported $Ce(OMeSALEN)_2$, $Ce(SALEN)_2$, $Ce(BrSALEN)_2$, and $Ce(OQ)_4$ (where OQ = 8-hydroxyquinolinate), complexes as well as the carbon-based framework of COT^{2-} in cerocene, the oxygen-based framework of $acac^-$ in $Ce(acac)_4$, and the nitrogen-based framework of $omtaa^{2-}$ in $Ce(omtaa)_2$ for comparison.[27b, 34, 42] Again, the DFT computed $E_{1/2}$ $Ce^{IV/III}$ values matched well with experiment.

Finally, we examined whether the redox potential of $[^nBu_4N]_2[Ce(NO_3)_6]$ could be predicted despite the different geometry imposed by the six bidentate nitrate ligands.[32] The counter ions, two $[Et_4N]^+$ groups, were included in the calculations to account for ion pairing effects with the highly charged $[Ce(NO_3)_6]^{2-}$ unit. The ^nBu groups were reduced to Et groups to simplify the calculations. The compound $[^nBu_4N]_2[Ce(NO_3)_6]$ also fit the correlation very well, lending credence to the predictive power of this method over a range > 2.5 V.

Table 3.2.5.2. Calculated and experimental electrochemical data. Units are in V vs. Fc. Table reprinted with permission of the American Chemical Society © 2013.

	$E_{1/2}$		Ref
	Exp.	**Calc.**[a]	
3.2-CF_3	–1.46	–1.43	This work
3.2-H	–1.80	–1.81	This work
3.2-Me	–1.90	–1.93	This work
3.2-OMe	–1.95	–1.91	This work
3.2-*p*NMe_2	–1.94	–1.90	This work
3.2-*m*NMe_2	–1.94	–2.12	This work
[^{n}Bu_4N]$_2$[$Ce(NO_3)_6$]	+0.62	+0.49	[32]
Ce(acac)$_2$[b]	–0.38	–0.42	[42b]
Ce(BrSALEN)$_2$[c]	–0.92	–0.55	[42a]
Ce(SALEN)$_2$	–1.08	–0.92	[42a]
Ce(OMeSALEN)$_2$	–1.18	–1.03	[42a]
Ce(OQ)$_2$[d]	–0.61	–0.78	This work
Ce(HA)$_4$[e]	–1.30	–1.28	[8]
Ce(C_8H_8)$_2$	–1.40	–1.25	[27b]
Ce(omtaa)$_2$[f]	–1.63	–1.21	This work
MAD[g]		–0.13	

[a]All potentials were adjusted by 0.30 mV to account for systematic error. [b]acac = acetylacetonate. [c]SALEN = 2,2'-ethylenebis(nitrilomethylidene)diphenol. [d] OQ = 8-hydroxyquinolinate. [e]HA = *N*-phenyl-pivalohydroxamate. [f]omtaa = octamethyltetraazaanulene. [g]MAD = mean absolute deviation.

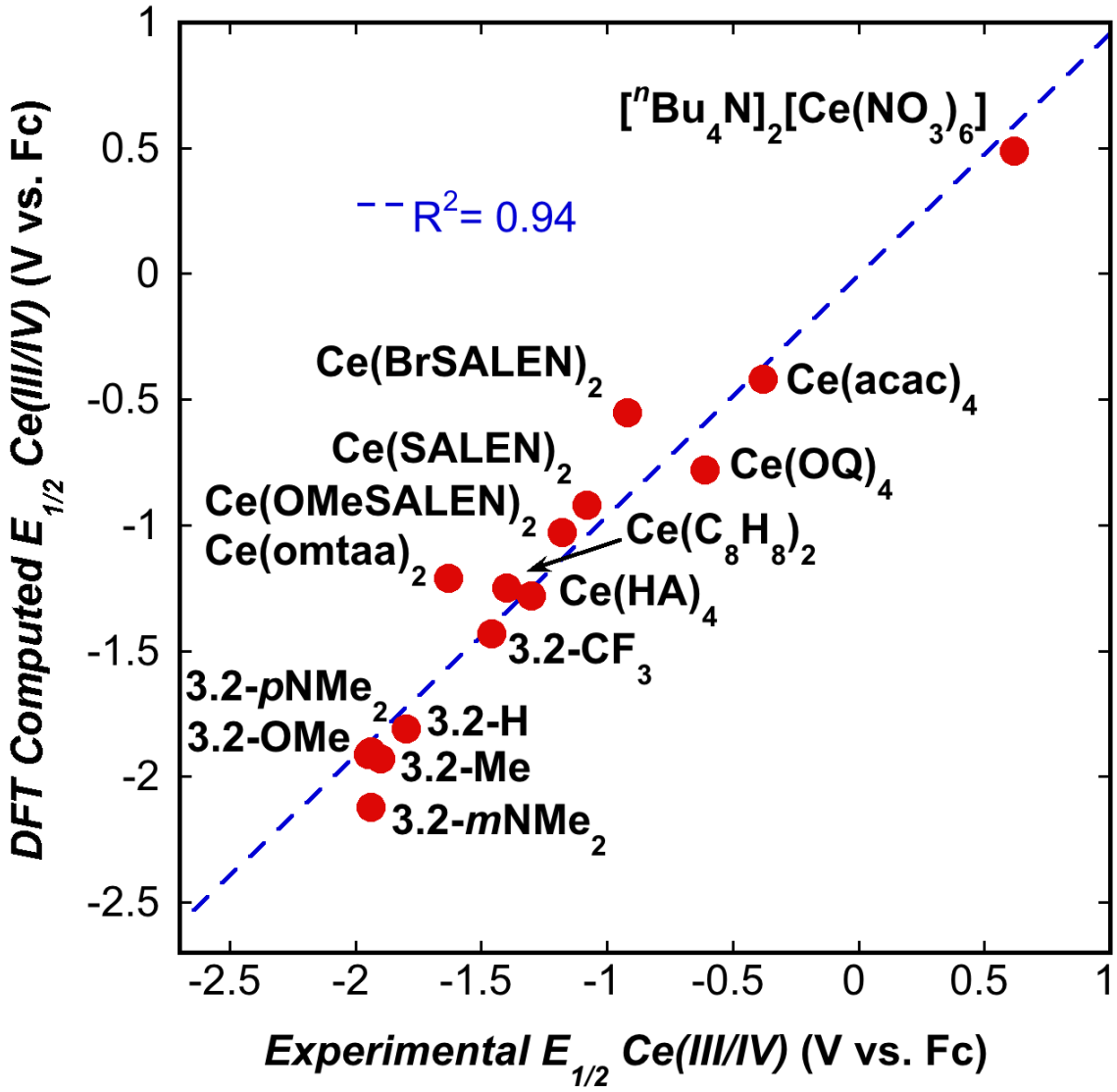

Figure 3.2.5.4. Correlation between calculated and experimental $Ce^{IV/III}$ reduction potentials. Figure reprinted with permission of the American Chemical Society © 2015.

3.2.6 Extension to RE = Pr, Tb, Dy, and Y

Compelled by the observations of stabilization imposed by the tetrakis(pyridyl nitroxide) framework on the tetravalent oxidation state of cerium, we explored whether this chemistry could be extended to praseodymium (Pr) or terbium (Tb) and allow for the isolation of high valent complexes of these elements. Based on the standard $Ln^{IV/III}$ reduction potentials of the ions, Pr and Tb would be the next easiest to oxidize after Ce with values of 2.8 ± 0.2 and 2.7 ± 0.2 V vs.

ferrocene respectively.[1] Theoretically, the tetrakis pyridyl nitroxide framework could impose a similar stabilization on the tetravalent oxidation state of these metals and shift their metal based $Ln^{IV/III}$ redox potentials into chemically accessible ranges.

We were also interested in the magnetic properties of these materials, which prompted us to look into whether we could also synthesize the Dy analog. This necessitated the synthesis of the diamagnetic Y analog for solid-state dilutions. Indeed **3.3-La** could serve as the diamagnetic analog, but due to the better size matching between Y and Dy or Tb, **3,3-Y** was chosen for the solid-state dilutions.

We successfully synthesized the complexes $[K(18\text{-crown-}6)(py)_2][RE(2\text{-}(^tBuNO)py)_4]$ (**3.3-RE**), where RE = Pr**,** Tb, Dy, and Y through similar routes to the **3.3-Ce** and **3.3-La** complexes. Compounds **3.3-La**, **3.3-Ce**, **3.3-Pr**, **3.3-Tb**, and **3.3-Pr** were crystallographically characterized and isostructural in the solid state. As listed in Table 3.2.6.1, average Ce–O bond distances decreased steadily across the series from 2.402(2) Å in **3.3-La** to 2.2714(12) Å in **3.3-Tb**. The average Ce–N bond distances also decreased steadily across the series from 2.688(3) Å in **3.3-La** to 2.4912(14) Å in **3.3-Tb** These decreases in bond distances were in accordance with the decrease in ionic radius of the central trivalent metal cation.[18]

Table 3.2.6.1. Experimental structural metrics of the series of **3.3-RE** complexes.

	N–O (Å)	**RE–O (Å)**	**RE–N_{pyr} (Å)**	**ΣY–N^t_{BuNO}–Z angles (°)**	**N_{pyr}–C–N^t_{BuNO}–C torsion angle (°)**
3.3-La	1.369(3)	2.402(2)	2.688(3)	359.6(4)	5.38
3.3-Ce	1.367(5)	2.384(3)	2.651(3)	359.6(5)	4.80
3.3-Pr	1.370(3)	2.366(2)	2.630(3)	359.4(4)	4.91
3.3-Tb	1.3652(18)	2.2714(12)	2.4912(14)	359.37(18)	8.47
3.3-Dy	1.3736(18)	2.2840(12)	2.5048(14)	359.41(16)	8.39

DFT studies were performed on the theoretical oxidized form of **3.3-Pr** in order to gain insight into its electronic structure. As shown in Figure 3.2.6.1, the spin density plot of **3.3-Pr** suggested that an electron would preferentially be removed from the ligand framework, leading to a complex characterized by a Pr^{III} cation surrounded by a delocalized ligand hole. These results prompted us to perform solution electrochemistry experiments on **3.3-Pr** and **3.3-Tb**.

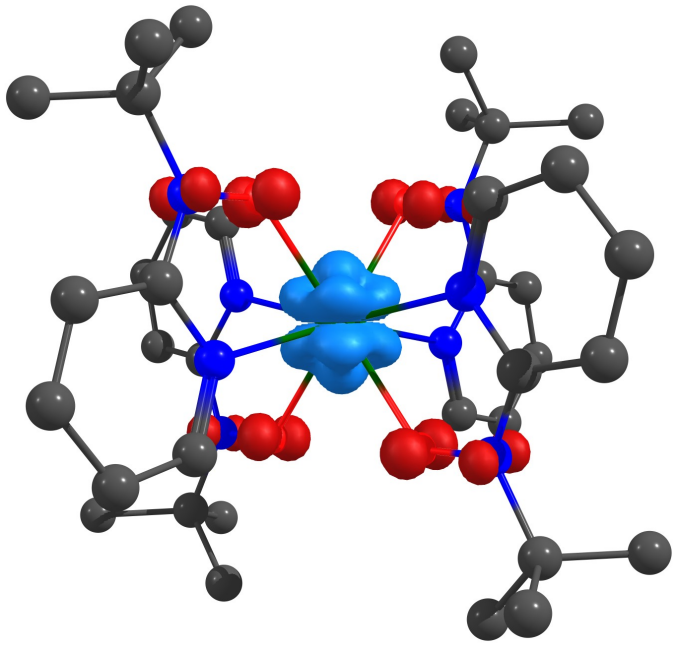

Figure 3.2.6.1. Spin Density Plot for the calculated oxidized form of **3.3-Pr**. Spin densities: 2.03 on Pr and –0.23 on each N–O moiety.

The solution electrochemistry experiments on **3.3-Pr** and **3.3-Tb** were run in 0.1 M [$^{n}Pr_4N$][BAr^{F}_4] DCM solutions. The diamagnetic **3.3-La** analog was also analyzed for comparison. Based on the similarities between the cyclic voltammograms of **3.3-Pr** and **3.3-Tb** with that of **3.3-La**, we assigned the four irreversible oxidation features between –1 V – 0.5 V versus Fc as purely ligand based oxidations (Figure 3.2.6.2). These results also indicated that only mild oxidants, $E_{1/2}$ > –0.7 V versus Fc, would be required to remove an electron from the ligand framework and potentially form the theoretical neutral analogs of **3.3-RE**, though the irreversibility of the waves were discouraging.

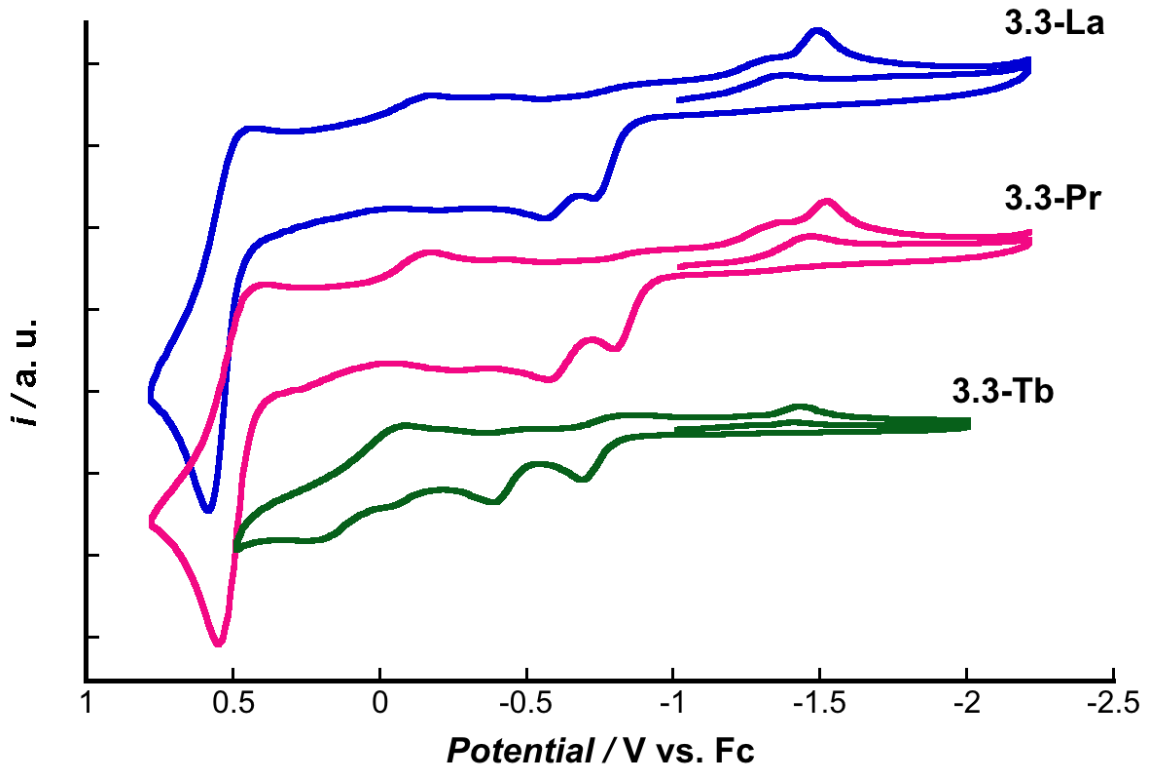

Figure 3.2.6.2. Cyclic voltammograms of **3.3-RE**, RE = La, Pr, and Tb.

Indeed, attempts to isolate chemically oxidized forms of **3.3-Pr** and **3.3-Tb** were unsuccessful. Reaction with either AgOTf or 1,4-benzoquinone led to electron transfer as indicated by the deposition of Ag^0 or K[1,4-benzoquinone] in the reaction mixtures. After workup, these reactions led to the formation of red oils, similar to what was observed in the reactions to form oxidized 2-(^{t}BuNO)py radical. Based on these observations, we postulated that oxidation of **3.3-RE** led to the formation of an instable complex, which decomposed back to the trivalent RE(III) dimers, $[RE^{III}(\mu\text{-}(R\text{-}2\text{-}(^t BuNO)py))(R\text{-}2\text{-}(^t BuNO)py)_2]_2$ (RE = Pr and Tb), through dissociation of the weak 2-(^{t}BuNO)py radical ligand (Scheme 3.2.6.1).

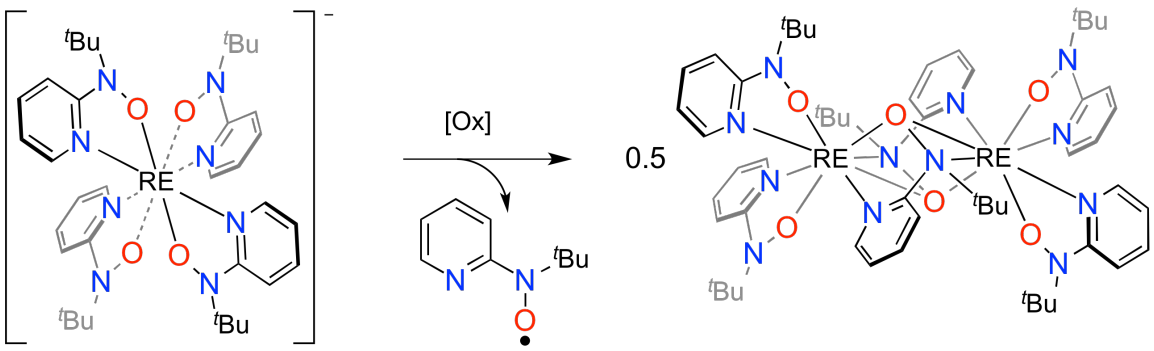

RE = Pr and Tb [Ox] = AgOTf or 1,4-benzoquinone

Scheme 3.2.6.1. Hypothesized chemistry involved in the reactions of **3.3-RE**, RE = Pr and Tb, with AgOTf or 1,4-benzoquinone.

This chemistry is to be contrasted with that reported by the Ishida group, where successful isolation of the rare earth complexes, La(hfac)$_3$(bpybNO),[15] Tb(hfac)$_3$(2-(^{t}BuNO)py),[43] Gd(hfac)$_3$(2-(^{t}BuNO)py),[44] and Gd(hfac)$_3$(6bpyNO),[45] which contained a coordinated neutral pyridyl nitroxide ligand was reported. However, we hypothesize that the stability of these complexes was a result of the use of weak, electron poor, hfac ancillary ligands, which were less likely to displace the nitroxide radical and form bridging dimers.

The temperature dependence of the magnetic susceptibilities of compounds **3.3-Tb**, **3.3-Dy**, and their solid-state dilutions, [K(18-crown-6)(py)$_2$][RE(2-(^{t}BuNO)py)$_4$]$_{0.05}$[Y(2-(^{t}BuNO)py)$_4$]$_{0.95}$ (RE = Tb and Dy), were performed from 2 – 300 K. AC measurements of the magnetic susceptibilities between 2 – 10 K were also performed. As shown in Figure 3.2.6.3, the concentrated samples exhibited ferromagnetic behavior below 150 K. This ferromagnetic response seemed also to be present in the solid-state dilution of the Dy sample but not in that of the Tb sample, though definitive results could not be obtained. Moreover, the slight out of phase signal for **3.3-Dy** in the AC measurements indicated that this complex was a weak single molecule magnet with a small barrier to magnetic relaxation. In contrast, there was negligible out of phase signal for the **3.3-Tb** complex (Figure 3.2.6.4).

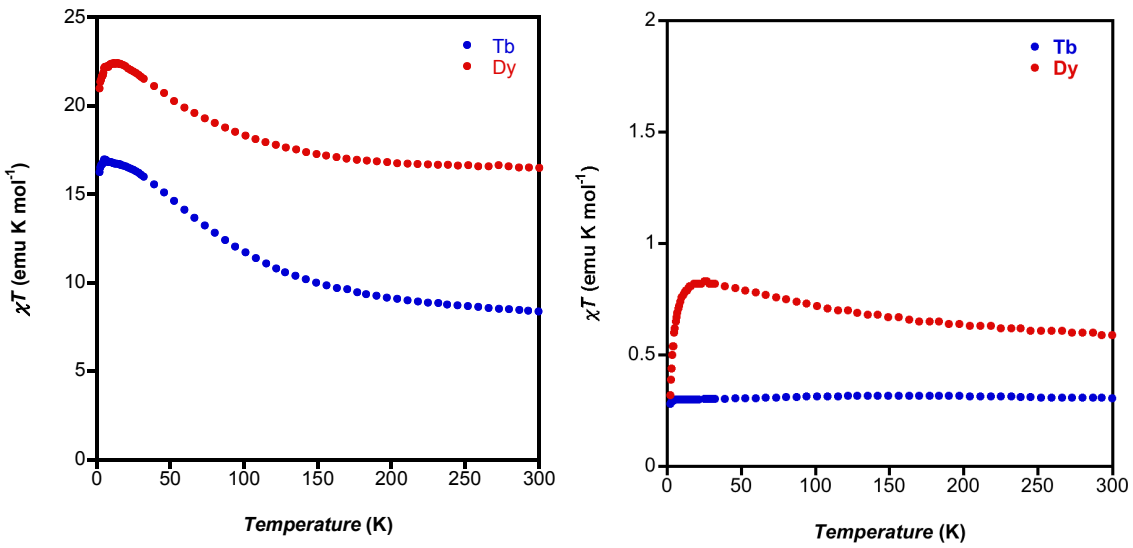

Figure 3.2.6.3. Temperature dependent magnetic data of compounds **3.3-Tb** and **3.3-Dy** (left) and their solid-state dilutions $[K(18\text{-crown-}6)(py)_2][Tb(2\text{-}(^tBuNO)py)_4]_{0.05}[Y(2\text{-}(^tBuNO)py)_4]_{0.95}$ and $[K(18\text{-crown-}6)(py)_2][Dy(2\text{-}(^tBuNO)py)_4]_{0.05}[Y(2\text{-}(^tBuNO)py)_4]_{0.95}$ (right).

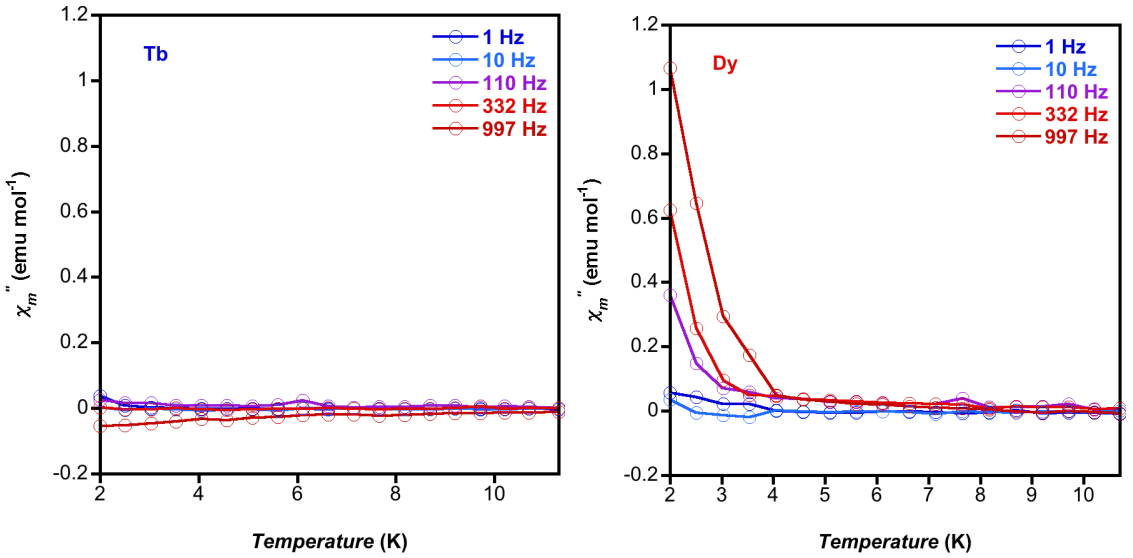

Figure 3.2.6.4. χ″ versus T plots for **3.3-Tb** (left) and **3.3-Dy** (right) highlighting the out-of-phase signal in the Dy compound but not in the Tb compound.

3.2.7 Extension to U

Due to the similarities between the ionic radii of Ce^{IV} and U^{IV} (0.97 Å for Ce^{IV} and 1.00 Å for U^{IV})[18] and the relative stability of the U^{IV} oxidation state relative to U^{III},[9a] we examined whether

we could form the analogous U[2-(^{t}BuNO)py]$_4$ complex. Layering of $U^{III}[N(SiMe_3)_2]_3$ with 3 or 4 equivalents of 2-(^{t}BuNOH)py in THF led to the formation of dark red crystals, suggestive of spontaneous oxidation to a U^{IV} product. X-ray crystallography confirmed the formation of the U[2-(^{t}BuNO)py]$_4$ complex. As shown in Figure 3.2.7.1, this complex was isostructural to the cerium(IV) analog.

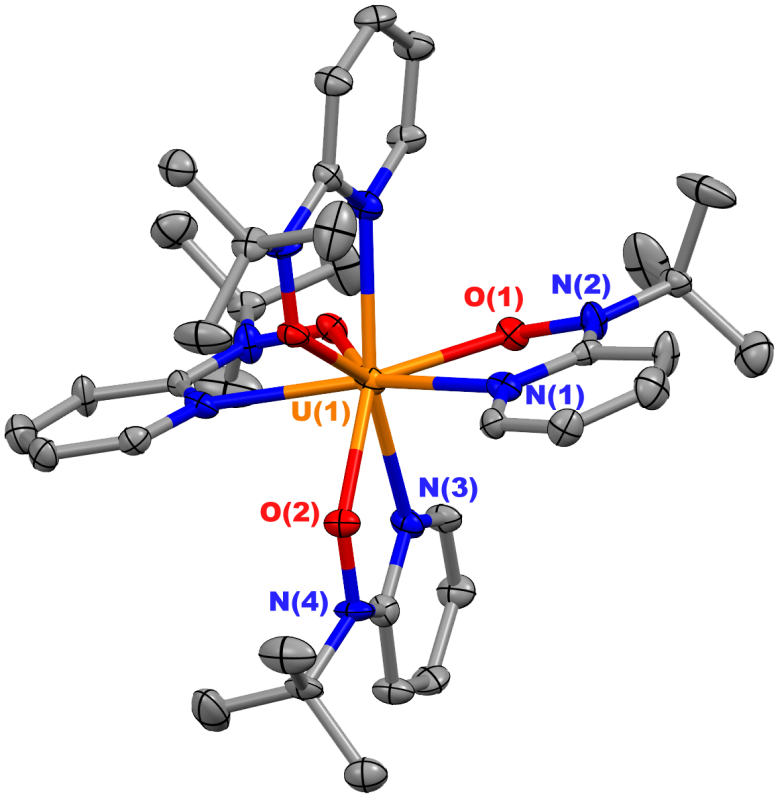

Figure 3.2.7.1. Thermal ellipsoid plot for U[2-(^{t}BuNO)py]$_4$ at 30% probability. Hydrogen atoms are omitted for clarity.

3.3 Conclusions

We demonstrated the facile oxidation of a series of Ce^{III}-nitroxide complexes to homoleptic Ce^{IV}-nitroxide complexes through the use of redox-active nitroxide ligands. The resulting cerium complexes showed unprecedented levels of stabilization to the 4+ oxidation state. Based on the spectroscopic and computational evidence, we attributed the stabilization of the 4+ oxidation state in the series of Ce^{IV}-nitroxide complexes to the following factors: the use of hard, anionic

nitroxide ligands, the symmetry allowed mixing of the nitroxide π* orbitals with the Ce^{IV} 4f orbitals provided by the D_{2d} complex symmetry, and the effective energy matching of the nitroxide π* orbitals with the Ce^{IV} 4f orbitals.

The large negative reduction potentials required to reduce the series of **3.2-X** complexes supported the claim that the geometrical positioning of ligands around cerium has a dramatic effect on the redox chemistry of the ion, in particular through a δ-bonding combination between the Ce^{IV} cation and ligand field. A similar effect on the stability of the Ce^{IV} oxidation state due to the local site symmetry at cerium was observed in ceria, CeO_2, where the cubic site symmetry of the fluorite structure was proposed to be critical for stabilizing the higher oxidation state.[5a] In this context, the partially covalent, pseudo-cubic coordination environments of **3.2-X** captured the fundamental bonding interactions found in CeO_2, in particular the strong thermodynamic preference against reduction for the defect free material.[5a]

Furthermore, our results indicated that functionalization of the pyridyl group of the 2-(^{t}BuNO)py ligand with electron withdrawing and electron donating groups provided an ~500 mV range in reduction potentials across the series of homoleptic cerium(IV) complexes. DFT calculations successfully reproduced the trend in experimental $Ce^{IV/III}$ reduction potentials, which were extended to eight other 8-coordinate cerium complexes as well as CAN. This approach established the predictive power of simple DFT methods to unknown cerium redox chemistry. An advantage of our approach was that we used cyclic voltammetry together with X-ray structural data and DFT, techniques that are readily available to many chemists.

We also expect that establishing a ligand field series for cerium will contribute to diverse areas of interest for the element where charge distribution, and potentially its effect on 4f orbital energies through crystal electric fields, plays a critical role, ranging from molecular magnetism[46] to Lewis acid catalysis,[47] to reduction chemistry mimicking samarium(II) reagents[48] and to the design of MRI contrast agents.[49]

The redox chemistry observed in the series of tetrakis pyridyl nitroxide Ce^{IV} complexes was extended to uranium in the actinide series through the synthesis of the U^{IV}[2-(^{t}BuNO)py]$_4$

complex. However, this chemistry could not be extended to that of Pr^{IV} and Tb^{IV} ions due to the presence of facile ligand dissociation pathways. As discussed in the following chapter, to circumvent such issues we developed a tripodal nitroxide ligand where the chelation effect would discourage ligand dissociation.

3.4 Experimental Section

General Methods. Unless otherwise noted, all reactions and manipulations were performed under an inert atmosphere (N_2) using standard Schlenk techniques or in a Vacuum Atmospheres, Inc. Nexus II drybox equipped with a molecular sieves 13X / Q5 Cu–0226S catalyst purifier system. Glassware was oven-dried for at least 3 h at 150 °C prior to use. ^{1}H- and ^{13}C-NMR spectra were obtained on a Bruker DMX–300 Fourier transform NMR spectrometer at 300 MHz and 75.4 MHz, respectively, or a Bruker DRX-500 Fourier transform NMR spectrometer at 500 MHz and 125.6 MHz, respectively. Chemical shifts were recorded in units of parts per million downfield from residual solvent signals. ^{19}F-NMR spectra were obtained on a Bruker DRX-500 Fourier transform NMR spectrometer at 282.2 MHz with chemical shifts recorded in units of parts per million referenced to an external $CFCl_3$ reference (0 ppm). Elemental analyses were performed at the University of California, Berkeley Microanalytical Facility using a Perkin-Elmer Series II 2400 CHNS analyzer.

Materials. Tetrahydrofuran, dimethoxyethane, diethyl ether, dichloromethane, toluene hexanes, and pentane were purchased from Fisher Scientific. The solvents were sparged for 20 min with dry N_2 and dried using a commercial two-column solvent purification system comprising columns packed with Q5 reactant and neutral alumina respectively (for hexanes and pentane), or two columns of neutral alumina (for THF, Et_2O and CH_2Cl_2). Deuterated solvents were purchased from Cambridge Isotope Laboratories, Inc. and stored over potassium mirror overnight prior to use. Anhydrous cerium(III) chloride (Strem Chemicals Inc.) was used as received. 2-Bromopyridine (Acros Organics) was degassed using three freeze-pump-thaw cycles and stored for 24 h over 3 Å molecular sieves prior to use. Isopropyl magnesium chloride lithium chloride solution (1.3 M in THF) was purchased from Sigma-Aldrich and used as received. The supporting

electrolyte, [^{n}Pr$_4$N][B(3,5-(CF$_3$)$_2$-C$_6$H$_3$)$_4$], was prepared according to literature procedures.[50] Ce(OQ)$_4$, and Ce(omtaa)$_2$ were prepared following the reported procedure.[32-33]

Synthetic Details and Characterization

Synthesis of [Ce^{III}(μ-(^{t}BuNO)py)(2-(^{t}BuNO)py)$_2$]$_2$ (3.1-H). White solid N-^{t}Bu-N-2-pyridylhydroxylamine (0.24 g, 1.44 mmol, 3 equivalent) was dissolved in 5 mL of Et$_2$O in a 20 mL scintillation vial to produce a clear, colorless solution. A clear, yellow pentane solution (10 mL) of Ce[N(SiMe$_3$)$_2$]$_3$ (0.30 g, 0.48 mmol, 1 equivalent) was layered upon the ether solution. The vial was set undisturbed at room temperature overnight and X-ray quality red-orange crystals formed from the mixture. The crystals were isolated by vacuum filtration, rinsed with Et$_2$O and pentane, and dried under reduced pressure, yielding **3.1-H** (0.20 g, 0.16 mmol, 67% crystalline yield). Anal. Calcd for C$_{54}$H$_{78}$O$_6$N$_{12}$Ce$_2$: C, 51.01; H, 6.18; N, 13.22. Found: C, 51.02; H, 6.25; N, 13.05.

Synthesis of Ce[2-(^{t}BuNO)py]$_4$ (3.2-H). White solid *N*-^{t}Bu-*N*-2-pyridylhydroxylamine (0.12 g, 0.72 mmol, 3 equivalent), was dissolved in 15 mL of Et$_2$O and solid PbO$_2$ (1.02 g, 4.33 mmol, 18 equivalent) was added. The suspension was stirred for 2 h to produce a red-orange solution. The mixture was filtered through a Celite-packed coarse porosity fritted filter into a 125 mL filter flask charged with **3.1-H** (0.30 g, 0.24 mmol, 1 equivalent) suspended in 40 mL Et$_2$O. Upon addition, the **3.1-H** immediately dissolved and a dark purple solution formed. The reaction was stirred for 14 h, after which the Et$_2$O was removed under reduced pressure to produce a dark powder. The powder was washed with pentane until the washings were colorless and the dark purple **3.2-H** compound was dried under reduced pressure (0.311 g, 0.39 mmol, 81% yield). X-ray quality crystals were obtained from slow evaporation of a nearly saturated THF solution of the complex. Anal. Calcd for C$_{36}$H$_{52}$O$_4$N$_8$Ce: C, 53.98; H, 6.54; N, 13.99. Found: C, 53.92; H, 6.64; N, 13.88. ^{1}H NMR (300 MHz, C$_6$D$_6$) δ 9.05 (ddd, J = 5.6, 2.0, 1.0 Hz, 1H, *Ar-H*), 6.75 (ddd, J = 8.9, 6.6, 2.0 Hz, 1H, *Ar-H*) 6.44 (dd, J = 8.9, 1.0 Hz, 1H, *Ar-H*), 6.20 (ddd, J = 6.6, 5.6, 1.0 Hz, 1H, *Ar-H*), 1.30 (s, 9H, C(C*H*$_3$)$_3$). ^{13}C NMR (125.6 MHz, C$_6$D$_6$) δ 159.2 (*Ar-C*) 148.9 (*Ar-C*), 135.0 (*Ar-C*), 110.4 (*Ar-C*), 108.9 (*Ar-C*), 61.7 (*C*(CH$_3$)$_3$), 29.0 (C(*C*H$_3$)$_3$).

Synthesis of [Ce^{III}(μ-(5-CF$_3$-2-(^{t}BuNO)py))(5-CF$_3$-2-(^{t}BuNO)py)$_2$]$_2$ (3.1-CF$_3$). A pentane solution (3 mL) of Ce[N(SiMe$_3$)$_2$]$_3$ (0.050 g, 0.08 mmol, 1 equivalent) was layered onto a pentane (3 mL) solution of 5-CF$_3$-2-(^{t}BuNOH)py (0.057 g, 0.24 mmol, 3 equivalent) and allowed to react at room temperature for 4 h, forming red crystals of **3.1-CF$_3$**. These were collected, washed with pentane, and dried under reduced pressure, yielding **3.1-CF$_3$** in 69% yield. Anal. Calcd for $C_{60}H_{72}F_{18}O_6N_{12}Ce_2$: C, 42.91; H, 4.32; N, 10.01. Found: C, 42.57; H, 4.49; N, 9.55.

Synthesis of Ce[5-CF$_3$-2-(^{t}BuNO)py]$_4$ (3.2-CF$_3$). To a THF solution (5 mL) of complex **3.1-CF$_3$** (0.039 g, 0.02 mmol, 1 equivalent) was added a THF solution (2 mL) of 5-CF$_3$-2-(^{t}BuNO•)py, formed in situ by the reaction of PbO_2 (0.10 g, 0.42 mmol, 18 equivalent) and 5-CF$_3$-2-(^{t}BuNOH)py (0.016 g, 0.07 mmol, 3 equivalent), and the reaction immediately turned dark purple. Solvents were removed under vacuum after 14 h. Excess 5-CF$_3$-2-(^{t}BuNO•)py was washed away with cold TMS_2O. The resulting purple powder was dried under reduced pressure, yielding **3.2-CF$_3$** in 60% yield. X-ray quality crystals were obtained from slow evaporation of a saturated THF solution of **3.2-CF$_3$**. Anal. Calcd for $C_{40}H_{48}F_{12}O_4N_8Ce$: C, 44.78; H, 4.51; N, 10.44. Found: C, 44.97; H, 4.54; N, 10.32. ^{1}H NMR (300 MHz, C_6D_6) δ 9.25 (d, J = 2.4 Hz, 1H, *Ar-H*), 6.75 (dd, J = 9.5, 2.4 Hz, 1H, *Ar-H*), 6.01 (d, J = 9.5 Hz, 1H, *Ar-H*), 1.32 (s, 9H, C(C*H*$_3$)$_3$). ^{13}C NMR (125.6 MHz, C_6D_6) δ 156.4 (s, *Ar-C*), 146.9 (q, J = 4.7 Hz, *Ar-C*), 126.2 (q, J = 269.1 Hz, *C*F$_3$), 110.2 (q, J = 32.7 Hz, *Ar-C*), 109.8 (s, *Ar-C*), 62.6 (s, *C*(CH$_3$)$_3$), 28.6 (s, C(*C*H$_3$)$_3$). ^{19}F NMR (282.2 MHz, C_6D_6) δ 60.5.

Synthesis of [Ce^{III}(μ-(5-Me-2-(^{t}BuNO)py))(5-Me-2-(^{t}BuNO)py)$_2$]$_2$ (3.1-Me). A pentane solution (10 mL) of Ce[N(SiMe$_3$)$_2$]$_3$ (0.20 g, 0.32 mmol, 1 equivalent) was layered onto an Et_2O (5 mL) solution of 5-Me-2-(^{t}BuNOH)py (0.176 g, 0.98 mmol, 3 equivalent) and allowed to react at room temperature for 14 h. Red crystals of **3.1-Me** were collected in 74% yield after being washed with Et_2O and pentane and dried under reduced pressure. Anal. Calcd for $C_{60}H_{90}O_6N_{12}Ce_2$: C, 53.16; H, 6.69; N, 12.40. Found: C, 52.94; H, 6.89; N, 12.70.

Synthesis of Ce[5-Me-2-(^{t}BuNO)py]$_4$ (3.2-Me). To an Et_2O suspension (10 mL) of complex **3.1-Me** (0.10 g, 0.07 mmol, 1 equivalent) was added an Et_2O solution (5 mL) of 5-Me-2-

(^{t}BuNO•)py, formed in situ by the reaction of PbO_2 (0.318 g, 1.33 mmol, 18 equivalent) and 5-Me-2-(^{t}BuNOH)py (0.040 g, 0.22 mmol, 3 equivalent), and the reaction immediately turned dark purple. Solvents were removed under vacuum after 14 h. Excess 5-Me-2-(^{t}BuNO•)py was washed away with cold pentane. The resulting purple powder was dried under reduced pressure, yielding **3.2-Me** in 78% yield. X-ray quality crystals were obtained from slow evaporation of a saturated THF solution of 2-Me. Anal. Calcd for $C_{40}H_{60}O_4N_8Ce$: C, 56.05; H, 7.06; N, 13.07. Found: C, 55.86; H, 7.07; N, 12.92. ^{1}H NMR (300 MHz, C_6D_6) δ 8.89 (dd, J = 2.3, 0.8 Hz, 1H, *Ar-H*), 6.65 (dd, J = 9.0, 2.3 Hz, 1H, *Ar-H*), 6.53 (d, J = 9.0 Hz, 1H, *Ar-H*), 2.10 (s, 3H, CH_3), 1.43 (s, 9H, C(CH_3)$_3$). ^{13}C NMR (75.4 MHz, C_6D_6) δ 159.4 (*Ar-C*), 148.2 (*Ar-C*), 136.7 (*Ar-C*), 118.1 (*Ar-C*), 110.6 (*Ar-C*), 61.9 (*C*(CH_3)$_3$), 29.1 (C(*C*H_3)$_3$), 17.6 (*C*H_3).

Synthesis of [Ce^{III}(μ-(3-OMe-2-(^{t}BuNO)py))(5-OMe-2-(^{t}BuNO)py)$_2$]$_2$ (3.1-OMe). A pentane solution (3 mL) of Ce[N(SiMe$_3$)$_2$]$_3$ (0.050 g, 0.08 mmol, 1 equivalent) was gently mixed with an Et_2O (4 mL) solution of 3-OMe-2-(^{t}BuNOH)py (0.047 g, 0.24 mmol, 3 equivalent). The reaction was allowed to stand at –25 ºC for 14 h during which x-ray quality red crystals formed. This were isolated and dried under reduced pressure, yielding **3.1-OMe** in 80% yield. Anal. Calcd for $C_{60}H_{90}O_{12}N_{12}Ce_2$: C, 49.64; H, 6.25; N, 11.58. Found: C, 49.99; H, 6.54; N, 11.63.

Synthesis of Ce[3-OMe-2-(^{t}BuNO)py]$_4$ (3.2-OMe). To a THF solution (5 mL) of complex **3.1-OMe** (0.083 g, 0.06 mmol, 1 equivalent) was added a THF solution (5 mL) of 3-OMe -2-(^{t}BuNO•)py, formed in situ by the reaction of PbO_2 (0.25 g, 1.03 mmol, 18 equivalent) and 3-OMe-2-(^{t}BuNOH)py (0.034 g, 0.17 mmol, 3 equivalent), and the reaction immediately turned dark purple. Solvents were removed under vacuum after 14 h. Excess 3-OMe-2-(^{t}BuNO•)py was washed away with cold TMS_2O. The resulting purple powder was dried under reduced pressure and recrystallized from layering TMS_2O onto a saturated pyridine solution at –25 ºC, yielding pure **3.2-OMe** in 11% yield. X-ray quality crystals of **3.2-OMe** were obtained by layering pentane on a toluene solution **3.2-OMe** at –25 ºC. Anal. Calcd for $C_{40}H_{60}O_8N_8Ce$: C, 52.16; H, 6.57; N, 12.17. Found: C, 51.95; H, 6.29; N, 11.93. ^{1}H NMR (300 MHz, C_6D_6) δ 8.83 (dd, J = 4.3, 1.2 Hz, 1H, *Ar-H*), 6.36 (dd, J = 6.6, 4.3 Hz, 1H, *Ar-H*), 6.28 (dd, J = 6.6, 1.2 Hz, 1H, *Ar-H*), 3.24 (s, 3H, CH_3),

1.54 (s, 9H, C(C*H*$_3$)$_3$). ^{13}C NMR (125.6 MHz, C_6D_6) δ 157.9 (*Ar-C*), 148.6 (*Ar-C*), 141.6 (*Ar-C*), 118.0 (*Ar-C*), 116.7 (*Ar-C*), 66.7 (*C*(CH$_3$)$_3$), 55.1 (O*C*H$_3$), 28.5 (C(*C*H$_3$)$_3$).

Synthesis of [Ce^{III}(μ-(5-NMe$_2$-2-(^{t}BuNO)py))(5-NMe$_2$-2-(^{t}BuNO)py)$_2$]$_2$ (3.1-*p*NMe$_2$). A pentane solution (3 mL) of Ce[N(SiMe$_3$)$_2$]$_3$ (0.050 g, 0.08 mmol, 1 equivalent) was gently mixed with an Et$_2$O (4 mL) solution of 5-NMe$_2$-2-(^{t}BuNOH)py (0.051 g, 0.24 mmol, 3 equivalent) and allowed to react at –25 ºC for 14 h. Red crystals were then collected, washed with pentane, and dried under reduced pressure, yielding **3.1-*p*NMe$_2$** in 70% yield. Anal. Calcd for $C_{66}H_{108}O_6N_{18}Ce_2$: C, 51.81; H, 7.12; N, 16.48. Found: C, 51.69; H, 6.89; N, 16.15.

Synthesis of Ce[5-NMe$_2$-2-(^{t}BuNO)py]$_4$ (3.2-*p*NMe$_2$). To a THF solution (5 mL) of complex **3.1-*p*NMe$_2$** (0.041 g, 0.03 mmol, 1 equivalent) was added a THF solution (5 mL) of 5-NMe$_2$-2-(^{t}BuNO•)py, formed in situ by the reaction of PbO$_2$ (0.116 g, 0.49 mmol, 18 equivalent) and 5-NMe$_2$-2-(^{t}BuNOH)py (0.016 g, 0.08 mmol, 3 equivalent), and the reaction immediately turned dark purple. Solvents were removed under vacuum after 14 h. Excess 5-NMe$_2$-2-(^{t}BuNO•)py was washed away with cold TMS$_2$O. The resulting purple powder was dried under reduced pressure, yielding **3.2-*p*NMe$_2$** in 40% yield. X-ray quality crystals were obtained from slow evaporation of a saturated Et$_2$O solution of the complex. Anal. Calcd for $C_{44}H_{72}O_4N_{12}Ce$: C, 54.30; H, 7.46; N, 17.27. Found: C, 54.37; H, 7.23; N, 17.11. ^{1}H NMR (300 MHz, C_6D_6) δ 8.82 (d, J = 3.0 Hz, 1H, *Ar-H*), 6.78 (d, J = 9.3 Hz, 1H, *Ar-H*), 6.59 (dd, J = 9.3, 3.0 Hz, 1H, *Ar-H*), 2.67 (s, 6H, N(C*H*$_3$)$_2$), 1.44 (s, 9H, C(C*H*$_3$)$_3$). ^{13}C NMR (125.6 MHz, C_6D_6) δ 158.1 (*Ar-C*), 140.2 (*Ar-C*), 134.6 (*Ar-C*), 124.5 (*Ar-C*), 113.5 (*Ar-C*), 63.0 (*C*(CH$_3$)$_3$), 42.0 (N(*C*H$_3$)$_2$, 29.1 (C(*C*H$_3$)$_3$).

Synthesis of [Ce^{III}(μ-(4-NMe$_2$-2-(^{t}BuNO)py))(4-NMe$_2$-2-(^{t}BuNO)py)$_2$]$_2$ (3.1-*m*NMe$_2$). A pentane solution (5 mL) of Ce[N(SiMe$_3$)$_2$]$_3$ (0.10 g, 0.16 mmol, 1 equivalent) was layered onto a 1:4 THF/Et$_2$O (10 mL) solution of 4-N(CH$_3$)$_2$-2-(^{t}BuNOH)py (0.10 g, 0.48 mmol, 3 equivalent) and allowed to react at room temperature for 6 h. Yellow-brown crystals formed. These were then collected, washed with cold DCM, and dried under reduced pressure, yielding **3.1-*m*NMe$_2$** in 71% yield. Anal. Calcd for $C_{66}H_{108}O_6N_{18}Ce_2$•1/2$C_5H_{12}$: C, 52.54; H, 7.34; N, 16.10. Found: C, 52.35; H, 7.17; N, 15.70.

Synthesis of Ce[4-NMe$_2$-2-(^{t}BuNO)py]$_4$ (3.2-*m*NMe$_2$). To a THF suspension (5 mL) of complex **3.1-*m*NMe$_2$** (0.088 g, 0.06 mmol, 1 equivalent) was added a THF solution (5 mL) of 4-NMe$_2$-2-(^{t}BuNO•)py, formed in situ by the reaction of PbO_2 (0.248 g, 1.04 mmol, 18 equivalent) and 4-NMe$_2$-2-(^{t}BuNOH)py (0.036 g, 0.17 mmol, 3 equivalent), and the reaction immediately turned dark purple. Solvents were removed under vacuum after 14 h. Excess 4-NMe$_2$-2-(^{t}BuNO•)py was washed away with cold Et_2O. The resulting purple powder was dried under reduced pressure, yielding **3.2-*m*NMe$_2$** in 80% yield. X-ray quality crystals were obtained from vapor diffusion of pentane into a saturated pyridine solution of **3.2-*m*NMe$_2$**. Anal. Calcd for $C_{44}H_{72}O_4N_{12}Ce$•1/2C_5H_{12}: C, 55.33; H, 7.79; N, 16.65. Found: C, 55.53; H, 8.16; N, 16.48. ^{1}H NMR (500 MHz, C_6D_6) δ 9.08 (d, J = 6.4 Hz, 1H, *Ar-H*), 5.90 (d, J = 2.2 Hz, 1H, *Ar-H*), 5.86 (dd, J = 6.4, 2.2 Hz, 1H, *Ar-H*), 2.26 (s, 6H, N(C*H*$_3$)$_2$), 1.65 (s, 9H, C(C*H*$_3$)$_3$). ^{13}C NMR (125.6 MHz, $CDCl_3$) δ 162.7 (*Ar-C*), 153.8 (*Ar-C*), 148.4 (*Ar-C*), 98.0 (*Ar-C*), 91.3 (*Ar-C*), 61.6 (*C*(CH$_3$)$_3$), 39.6 (N(*C*H$_3$)$_2$), 28.6 (C(*C*H$_3$)$_3$).

Synthesis of [K(18-crown-6)(py)$_2$][Ce(2-(^{t}BuNO)py)$_4$] (3.3-Ce). Potassium *N*-^{t}Bu-*N*-2-pyridylnitroxide (2-(^{t}BuNOK)py) was synthesized by the addition of K[N(SiMe$_3$)$_2$] (0.32 g, 1.6 mmol, 0.9 equivalent) to an Et_2O solution of *N*-^{t}Bu-*N*-2-pyridylhydroxylamine (0.30 g, 1.8 mmol, 1 equivalent). Yellow solid crashed out immediately but stirring continued for 2 h to ensure complete conversion. The solid was washed with Et_2O and dried under reduced pressure to afford potassium *N*-^{t}Bu-*N*-2-pyridylnitroxide in 93% yield.

To a mixture of *N*-^{t}Bu-*N*-2-pyridylhydroxylamine (0.040 g, 0.24 mmol, 3 equivalent) and potassium *N*-^{t}Bu-*N*-2-pyridylnitroxide (0.017 g, 0.080 mmol, 1 equivalent) dissolved in DME (5 mL) was added a DME (2 mL) solution of Ce[N(SiMe$_3$)$_2$]$_3$ (0.050 g, 0.080 mmol, 1 equivalent). The reaction immediately turned dark red. Volatiles were removed in vacuo after 3 h., leaving an orange powder. The addition of 1 equivalent of 18-crown-6 was made to this orange powder and the mixture was dissolved in 1 mL of pyridine. Layering pentane (~4 mL) at –25 ºC resulted in the formation of complex **3.3-Ce** as x-ray quality block red crystals in 57% yield. Anal. Calcd for $C_{58}H_{86}KN_{10}O_{10}Ce$: C, 55.17; H, 6.87; N, 11.09. Found: C, 55.21; H, 6.88; N, 11.06. ^{1}H NMR (500

MHz, d_5-pyridine) δ 8.44 (s, 4H, *Ar-H*), 7.17 (s, 4H, *Ar-H*), 4.07 (s, 4H, *Ar-H*), 3.43 (s, 24H, 18-crown-6), 3.07 (s, 36H, $C(CH_3)_3$), 2.05 (s, 4H, *Ar-H*), –0.1.37 (s, 4H, *Ar-H*).

Synthesis of [K(18-crown-6)(py)$_2$][La[2-(^{t}BuNO)py]$_4$] (**3.3-La**). **3.3-La** was synthesized in an identical fashion to the analogous **3.3-Ce** complex, except that $La[N(SiMe_3)_2]_3$ was used instead of $Ce[N(SiMe_3)_2]_3$. Anal. Calcd for $C_{58}H_{86}N_{10}O_{10}KLa{\bullet}C_5H_5N$: C, 56.45; H, 6.84; N, 11.49. Found: C, 56.16; H, 6.92; N, 11.38. ^{1}H NMR (500 MHz, d_8-THF) δ 8.53 (d, J = 4.1 Hz, 4H, *Ar-H*), 8.17 (s, 4H, *Ar-H*), 7.65 (t, J = 7.6 Hz, 2H, *Ar-H*), 7.24 (dd, J = 7.3, 5.4 Hz, 4H, *Ar-H*), 6.81 (m, 4H, *Ar-H*), 6.56 (d, J = 8.4 Hz, 4H, *Ar-H*), 5.85 (m, 4H, *Ar-H*), 3.53 (s, 24H, 18-crown-6), 1.37 (s, 36H, $C(CH_3)_3$). ^{13}C NMR (125.6 MHz, d_8-THF) δ 160.2 (*Ar-C*), 150.9 (*Ar-C*), 149.4 (*Ar-C*), 136.4 (*Ar-C*), 133.7 (*Ar-C*), 124.5 (*Ar-C*), 110.1 (*Ar-C*), 107.1 (*Ar-C*), 71.4 (18-crown-6), 60.7 ($C(CH_3)_3$), 29.3 ($C(CH_3)_3$).

Synthesis of [K(18-crown-6)(py)$_2$][Pr[2-(^{t}BuNO)py]$_4$] (**3.3-Pr**). **3.3-Pr** was synthesized in an identical fashion to the analogous **3.3-Ce** complex, except that $Pr[N(SiMe_3)_2]_3$ was used instead of $Ce[N(SiMe_3)_2]_3$. ^{1}H NMR (300 MHz, d_5-pyridine) δ 9.15 (s, 4H, *Ar-H*), 6.15 (s, 4H, *Ar-H*), 4.84 (s, 36H, $C(CH_3)_3$), 3.49 (s, 24H, 18-crown-6), –0.74 (s, 4H, *Ar-H*), –16.26 (s, 4H, *Ar-H*).

Synthesis of [K(18-crown-6)(py)$_2$][Tb[2-(^{t}BuNO)py]$_4$] (**3.3-Tb**). To a suspension of $TbCl_3$ (0.050 g, 0.188 mmol, 1 equivalent) in DME was added a DME solution of 2-(^{t}BuNOK)py (0.154 g, 0.754 mmol, 4 equivalents) and the mixture was stirred for 2 d. The resulting mixture was pumped down to a crude yellow solid. This product was recrystallized by layering a pentane/Et_2O (8 mL/2 mL) mixture onto a pyridine solution of the crude yellow solid in the presence of 18-crown-6 (0.20 g, 0.754 mmol, 4 equivalents). Yield: 33%. Anal. Calcd for $C_{58}H_{86}N_{10}O_{10}KTb$: C, 54.36; H, 6.77; N, 10.93. Found: C, 54.13; H, 6.73; N, 10.80. ^{1}H NMR (300 MHz, d_5-pyridine) δ 12.70 (s, 4H, *Ar-H*), 10.33 (s, 4H, *Ar-H*), 3.39 (s, 24H, 18-crown-6), 0.31 (s, 4H, *Ar-H*), –5.60 (s, 36H, $C(CH_3)_3$).

Synthesis of [K(18-crown-6)(py)$_2$][Dy[2-(^{t}BuNO)py]$_4$] (**3.3-Dy**). **3.3-Dy** was synthesized in an identical fashion to the analogous **3.3-Ce** complex, except that $Dy[N(SiMe_3)_2]_3$ was used instead of $Ce[N(SiMe_3)_2]_3$. Yield: 68%.

Synthesis of [K(18-crown-6)(py)$_2$][Y[2-(^{t}BuNO)py]$_4$] (**3.3-Y**). **3.3-Y** was synthesized in an identical fashion to the analogous **3.3-Ce** complex, except that Y[N(SiMe$_3$)$_2$]$_3$ was used instead of Ce[N(SiMe$_3$)$_2$]$_3$. Yield: 68%.

Synthesis of [K(18-crown-6)(py)$_2$][Tb[2-(^{t}BuNO)py]$_4$]$_{0.05}$[Y[2-(^{t}BuNO)py]$_4$]$_{0.95}$. To a 20 mL scintillation vial was added [K(18-crown-6)(py)$_2$][Tb[2-(^{t}BuNO)py]$_4$] (0.0056 g, 0.0044 mmol, 1 equivalent) and [K(18-crown-6)(py)$_2$][Y[2-(^{t}BuNO)py]$_4$] (0.10 g, 0.083 mmol, 19 equivalents) and the mixture was dissolved in ~5 mL pyridine. Layering a pentane/Et$_2$O (8 mL/2 mL) mixture onto the pyridine solution led to the deposition of red crystals of [K(18-crown-6)(py)$_2$][Tb[2-(^{t}BuNO)py]$_4$]$_{0.05}$[Y[2-(^{t}BuNO)py]$_4$]$_{0.95}$ in 88% yield.

Synthesis of [K(18-crown-6)(py)$_2$][Dy[2-(^{t}BuNO)py]$_4$]$_{0.05}$[Y[2-(^{t}BuNO)py]$_4$]$_{0.95}$. [K(18-crown-6)(py)$_2$][Dy[2-(^{t}BuNO)py]$_4$]$_{0.05}$[Y[2-(^{t}BuNO)py]$_4$]$_{0.95}$ was synthesized in an identical fashion to the analogous [K(18-crown-6)(py)$_2$][Tb[2-(^{t}BuNO)py]$_4$]$_{0.05}$[Y[2-(^{t}BuNO)py]$_4$]$_{0.95}$ complex, except [K(18-crown-6)(py)$_2$][Dy[2-(^{t}BuNO)py]$_4$] was used instead of [K(18-crown-6)(py)$_2$][Tb[2-(^{t}BuNO)py]$_4$]. Yield: 86%.

Synthesis of U[2-(^{t}BuNO)py]$_4$. A pentane solution (~10 mL) of U[N(SiMe$_3$)$_2$]$_3$ (0.10 g, 0.139 mmol, 1 equivalent) was layered onto an Et$_2$O solution (~4 mL) of 2-(^{t}BuNOH)py (3 or 4 equivalents) and the reaction was allowed to stand at room temperature overnight, leading to the deposition of dark red X-ray quality crystals.

Oxidation reactions of 3.3-Ce. To a 20 mL scintillation vial equipped with a magnetic stir bar, 1 equivalent. of complex **3.3-Ce** (0.020 g, 0.016 mmol, 1 equivalent) and 1 equivalent of oxidant (FcPF$_6$, 1,4-benzoquinone, or [CoCp$_2$]OTf) were dissolved in THF (2 mL). The reaction immediately turned purple and was allowed to react for 2 h. THF was removed *in vacuo* and the products were taken up in C$_6$D$_6$. The reactions were analyzed by ^{1}H NMR spectroscopy.

To a 20 mL scintillation vial equipped with a magnetic stir bar, 1 equivalent. of complex **3.3-Ce** (0.020 g, 0.016 mmol, 1 equivalent) and 1 equivalent of benzophenone (0.003 g, 0.016 mmol) were dissolved in THF (2 mL). No immediate color change to purple was observed. The reaction

was allowed to react for 2 h. THF was removed *in vacuo* and the products were taken up in C_6D_6. The reaction was analyzed by ^{1}H NMR spectroscopy.

To a 20 mL scintillation vial equipped with a magnetic stir bar, 1 equivalent. of complex **3.3-Ce** (0.020 g, 0.016 mmol, 1 equivalent) was dissolved in THF (2 mL). [CoCp*$_2$]OTf (0.008 g, 0.016 mmol, 1 equivalent) was dissolved in MeCN (2 mL) and added to the reaction mixture. No immediate color change to purple was observed. The reaction was allowed to react for 2 h. THF was removed under reduced pressure and the products were taken up in C_6D_6. The reaction was analyzed by ^{1}H NMR spectroscopy.

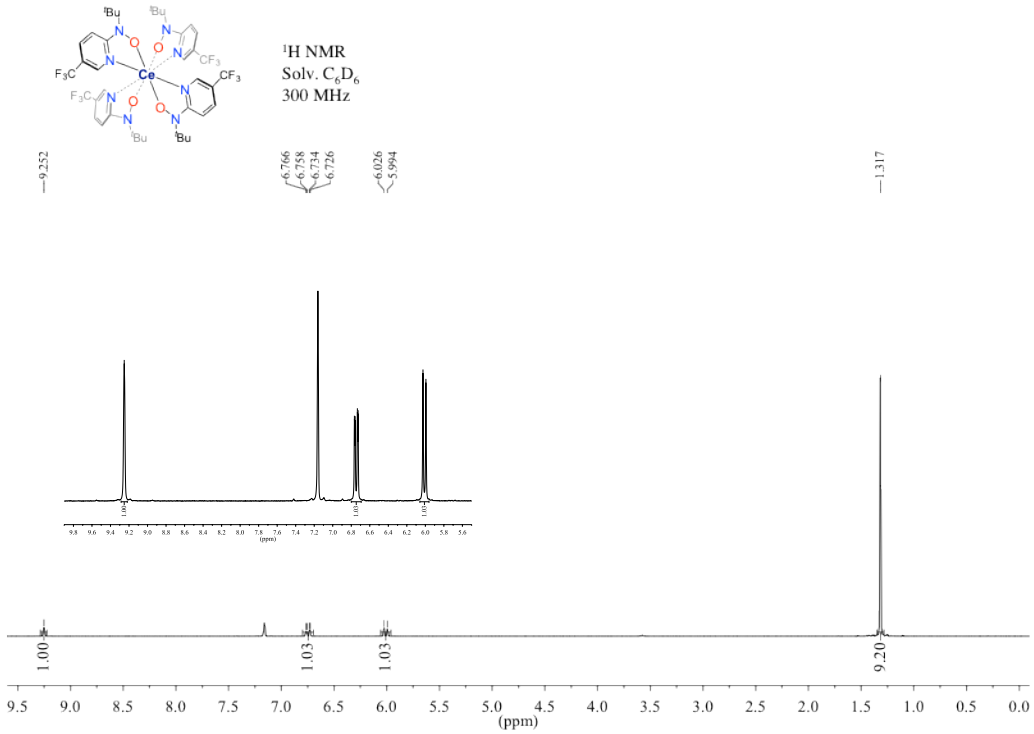

Figure 3.4.1. ^{1}H NMR spectrum of **3.2-CF$_3$**.

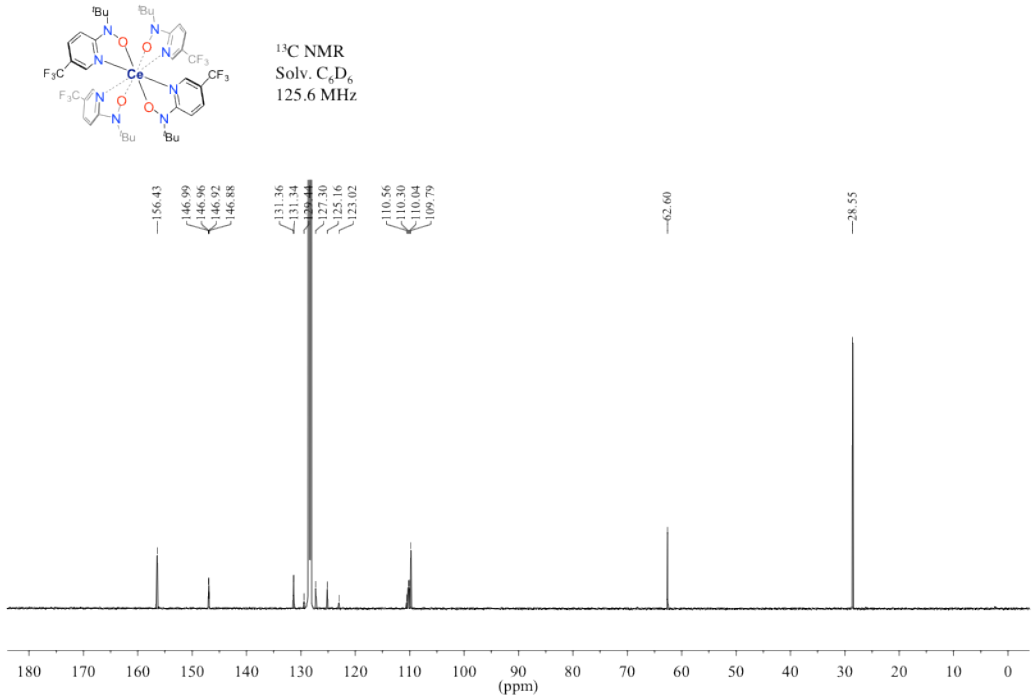

Figure 3.4.2. ^{13}C{^{1}H} NMR spectrum of **3.2-CF$_3$**.

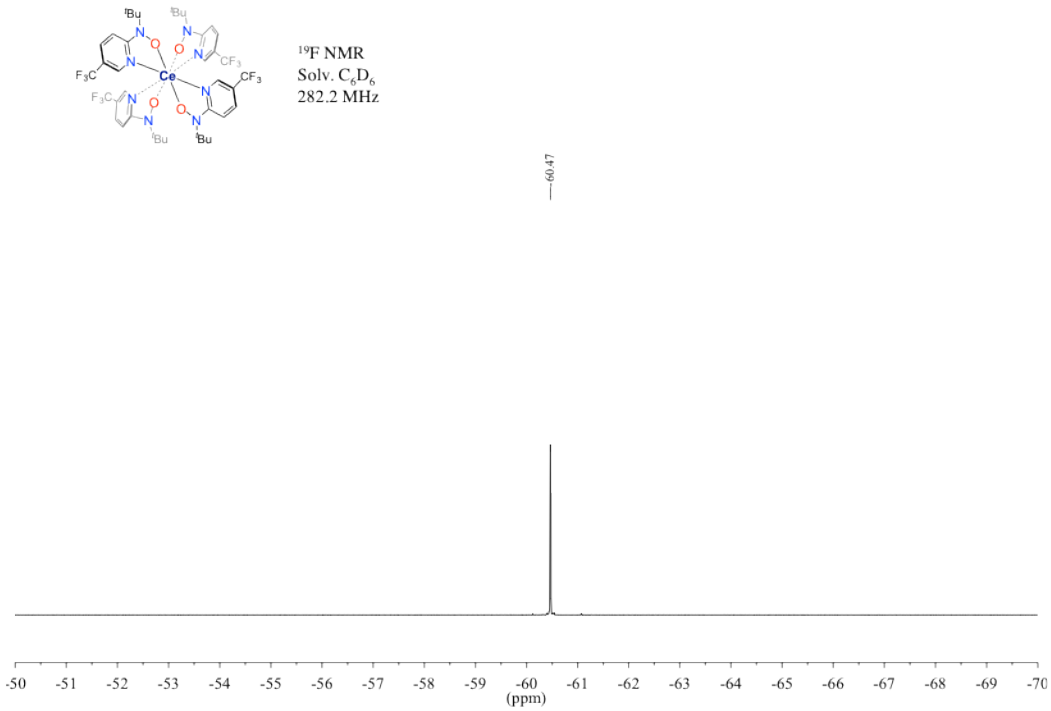

Figure 3.4.3. $^{19}F\{^1H\}$ NMR spectrum of **3.2-CF$_3$**.

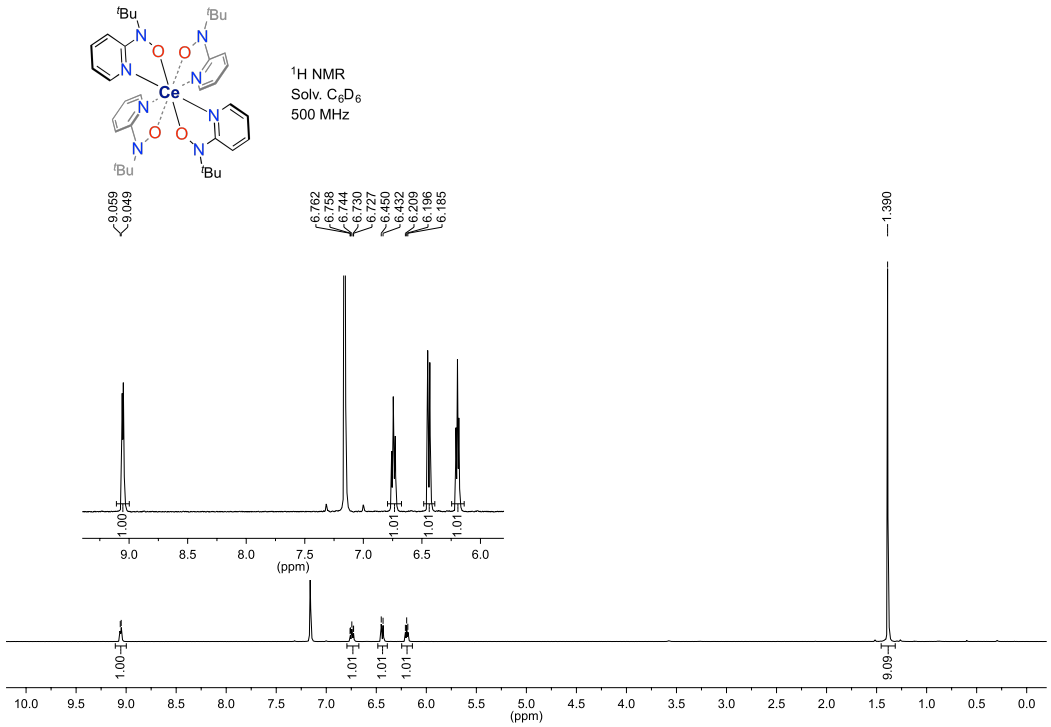

Figure 3.4.4. ^{1}H NMR spectrum of **3.2-H**.

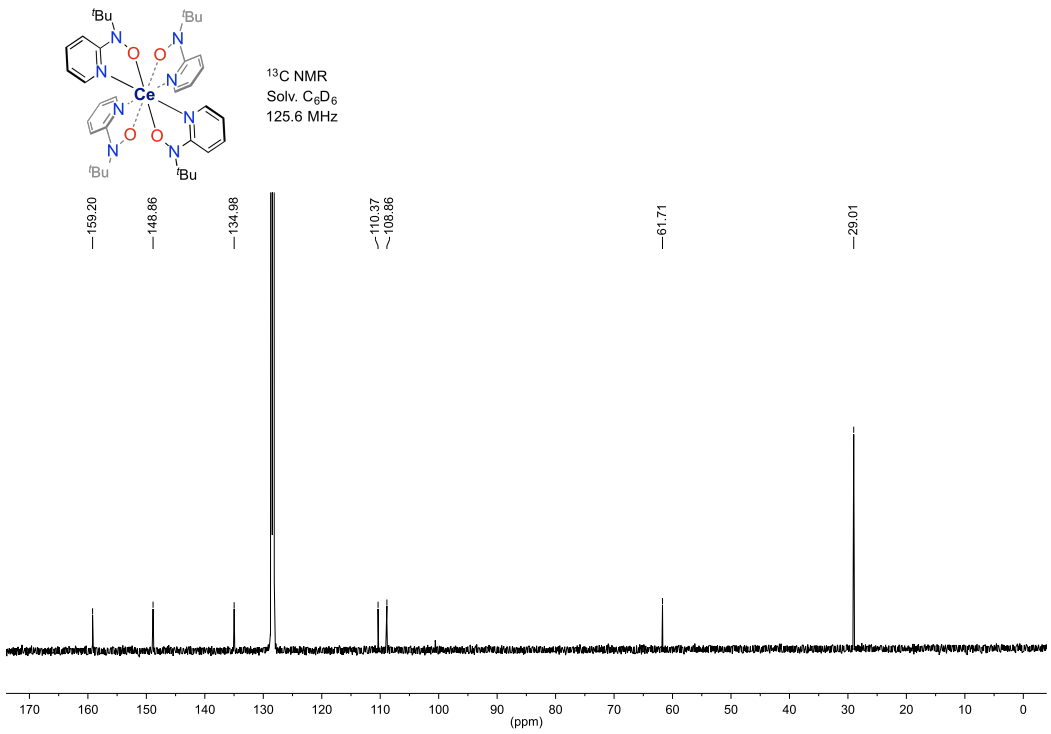

Figure 3.4.5. $^{13}C\{^1H\}$ NMR spectrum of **3.2-H**.

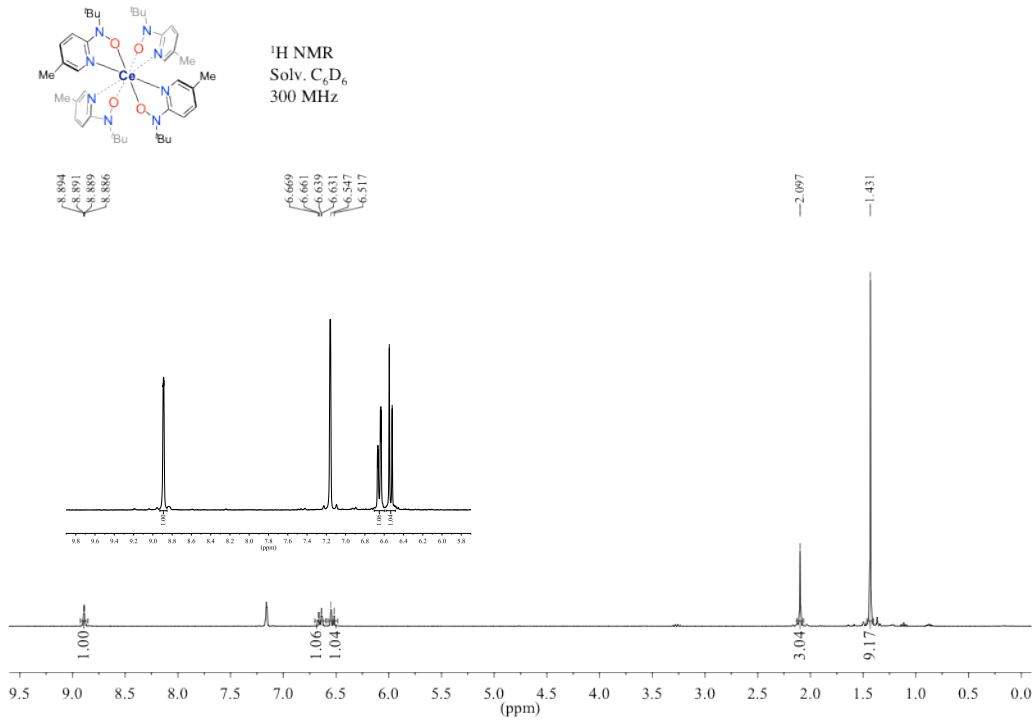

Figure 3.4.6. ^{1}H NMR spectrum of **3.2-Me**.

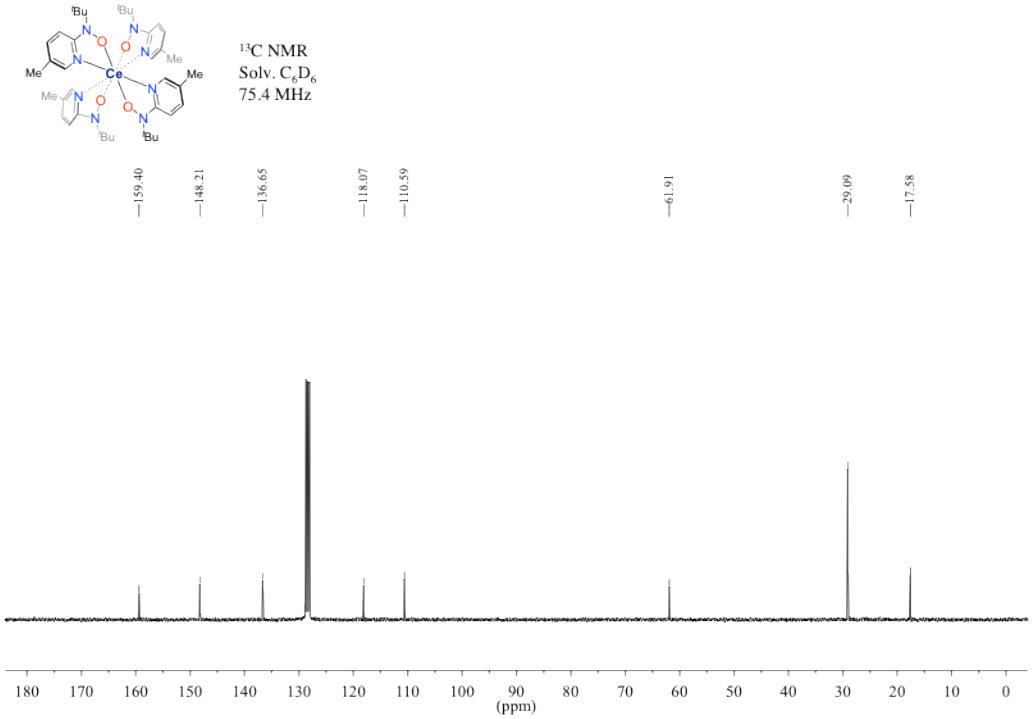

Figure 3.4.7. $^{13}C\{^1H\}$ NMR spectrum of **3.2-Me**.

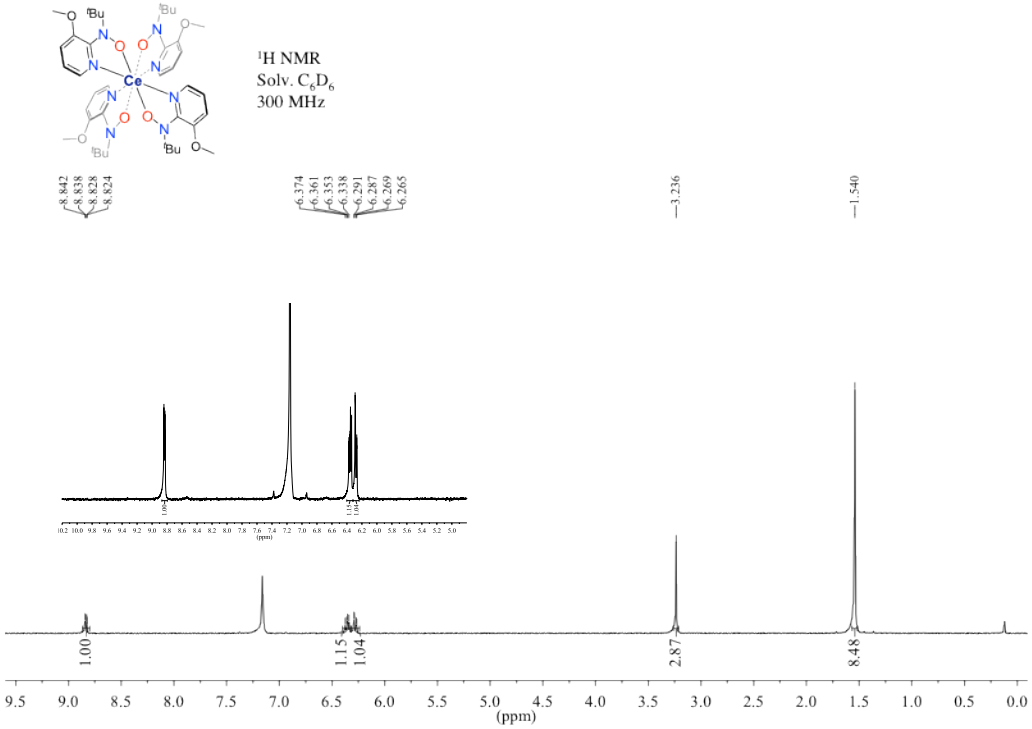

Figure 3.4.8. ^{1}H NMR spectrum of **3.2-OMe**.

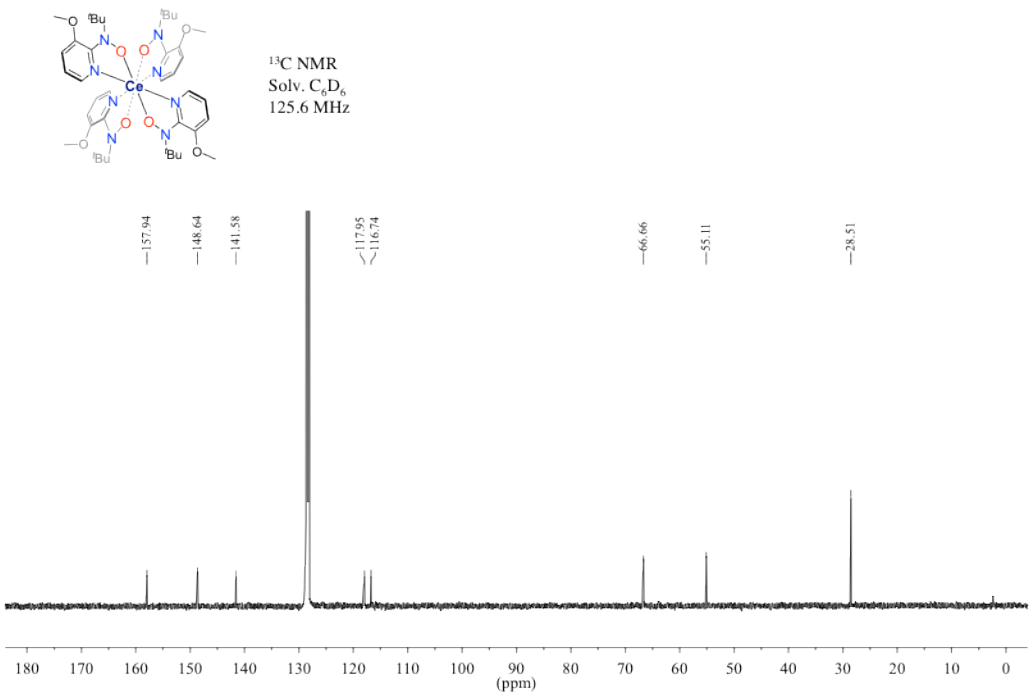

Figure 3.4.9. $^{13}C\{^{1}H\}$ NMR spectrum of **3.2-OMe**.

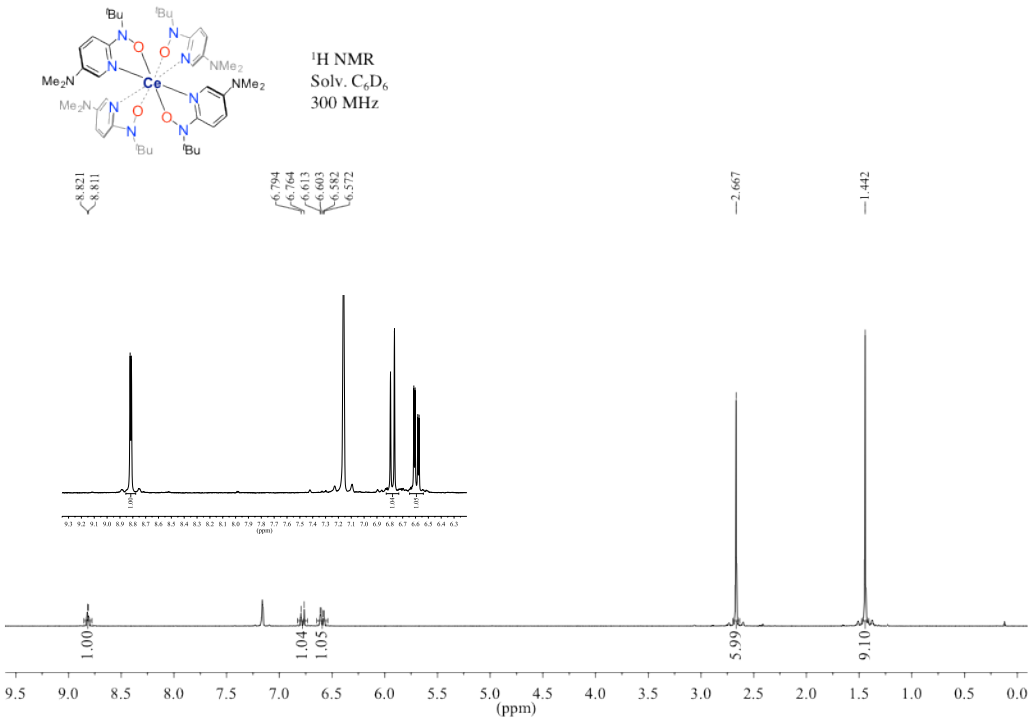

Figure 3.4.10. ^{1}H NMR spectrum of **3.2-*p*NMe$_2$**.

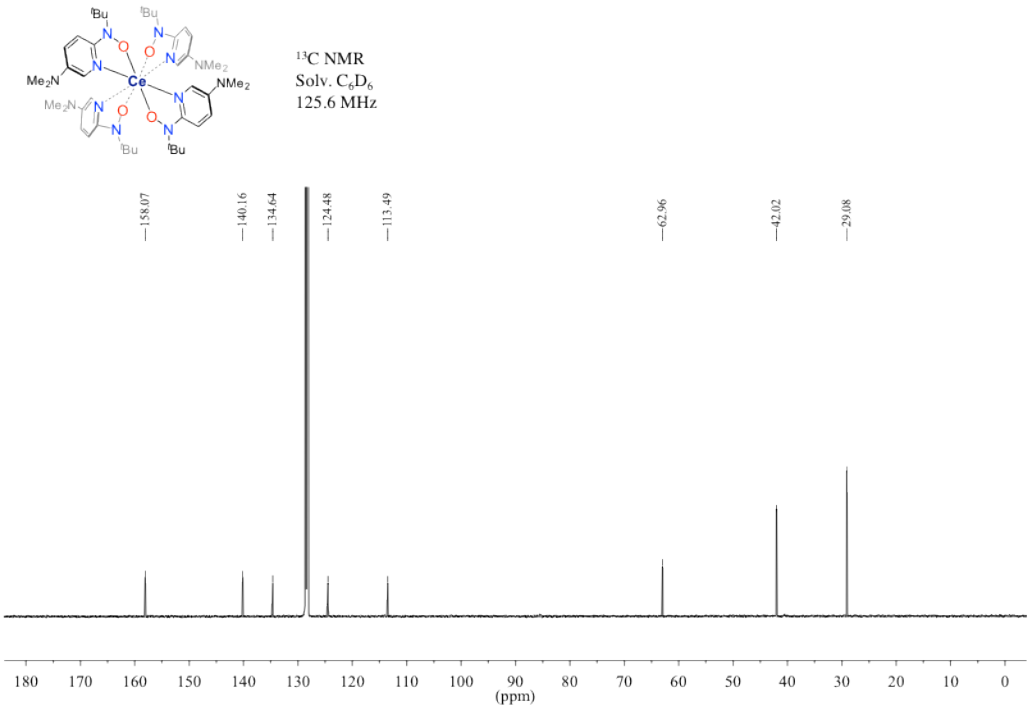

Figure 3.4.11. $^{13}C\{^{1}H\}$ NMR spectrum of **3.2-*p*NMe$_2$**.

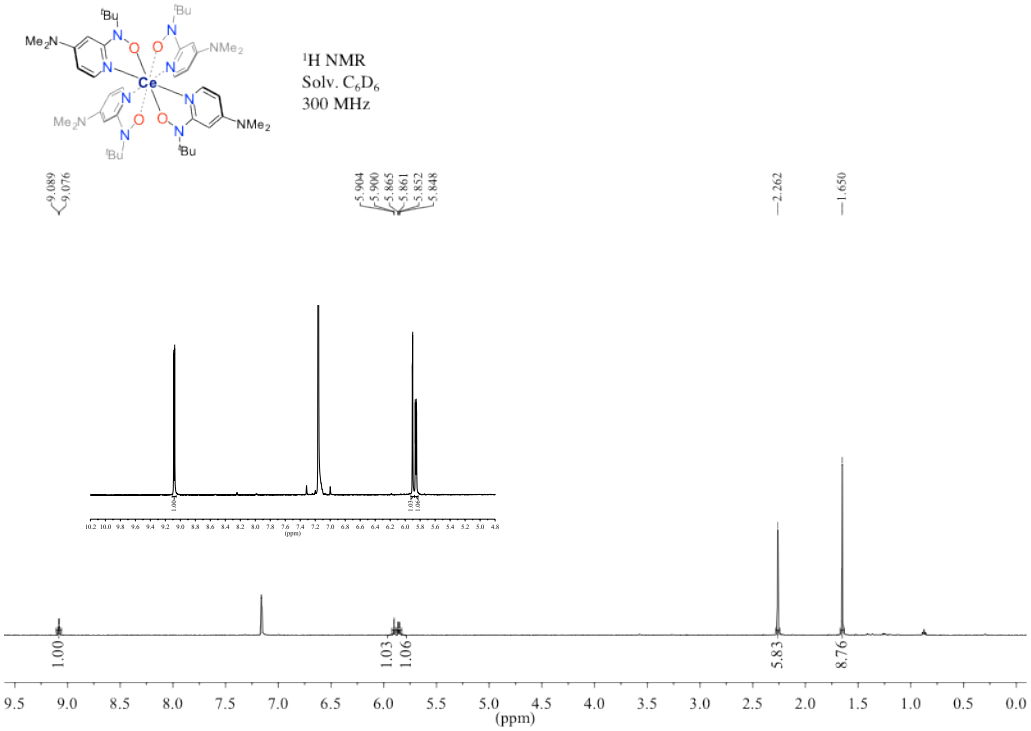

Figure 3.4.12. ^{1}H NMR spectrum of **3.2-*m*NMe$_2$**.

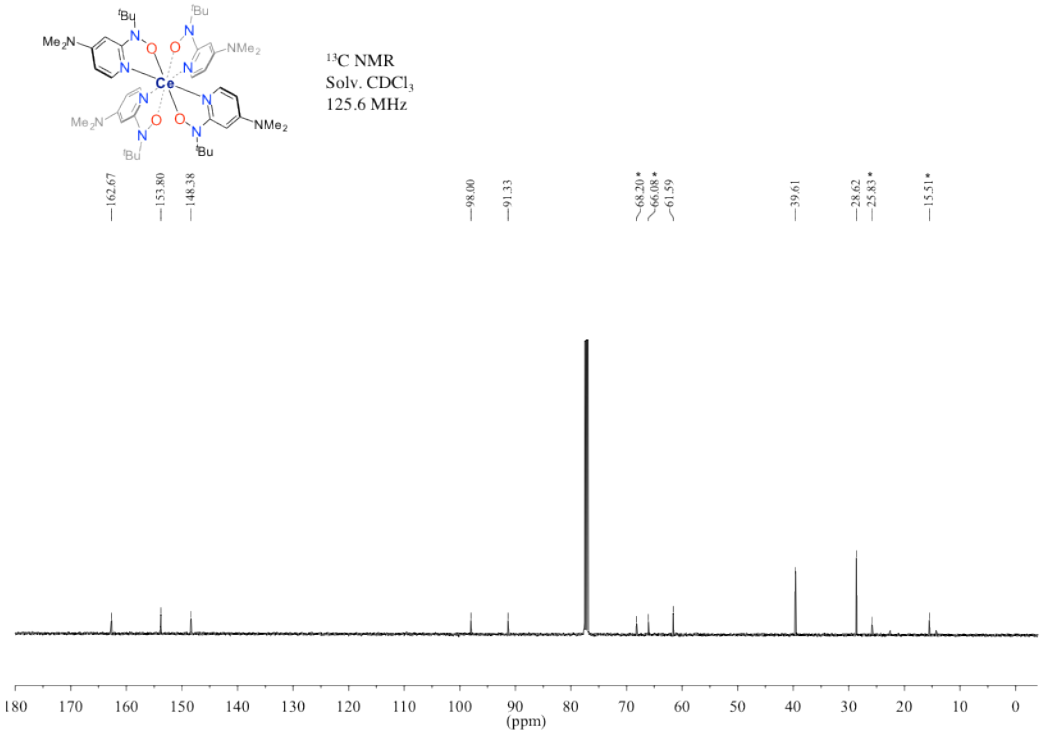

Figure 3.4.13. $^{13}C\{^{1}H\}$ NMR spectrum of **3.2-*m*NMe$_2$**.

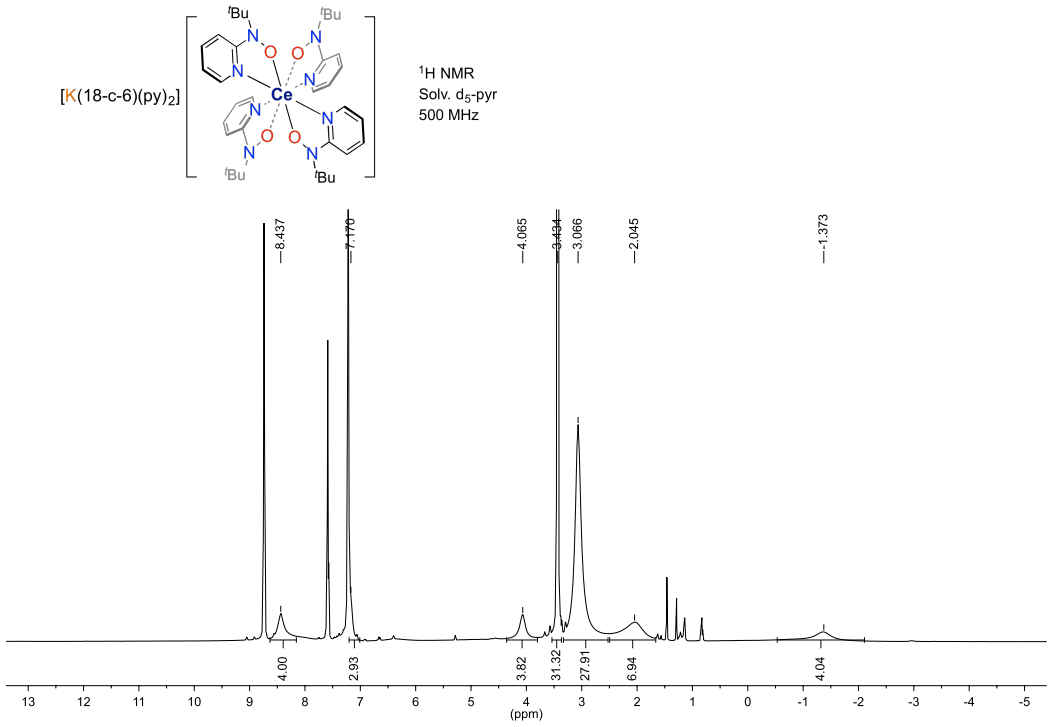

Figure 3.4.14. ^{1}H NMR spectrum of **3.3-Ce**.

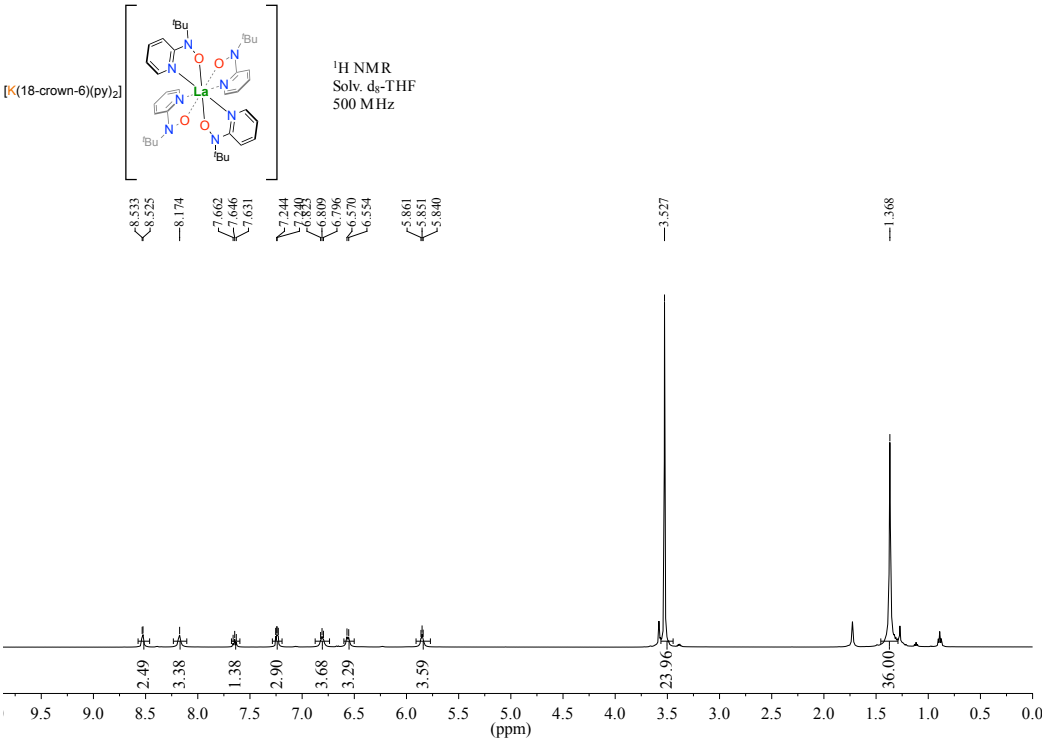

Figure 3.4.15. ^{1}H NMR spectrum of **3.3-La**.

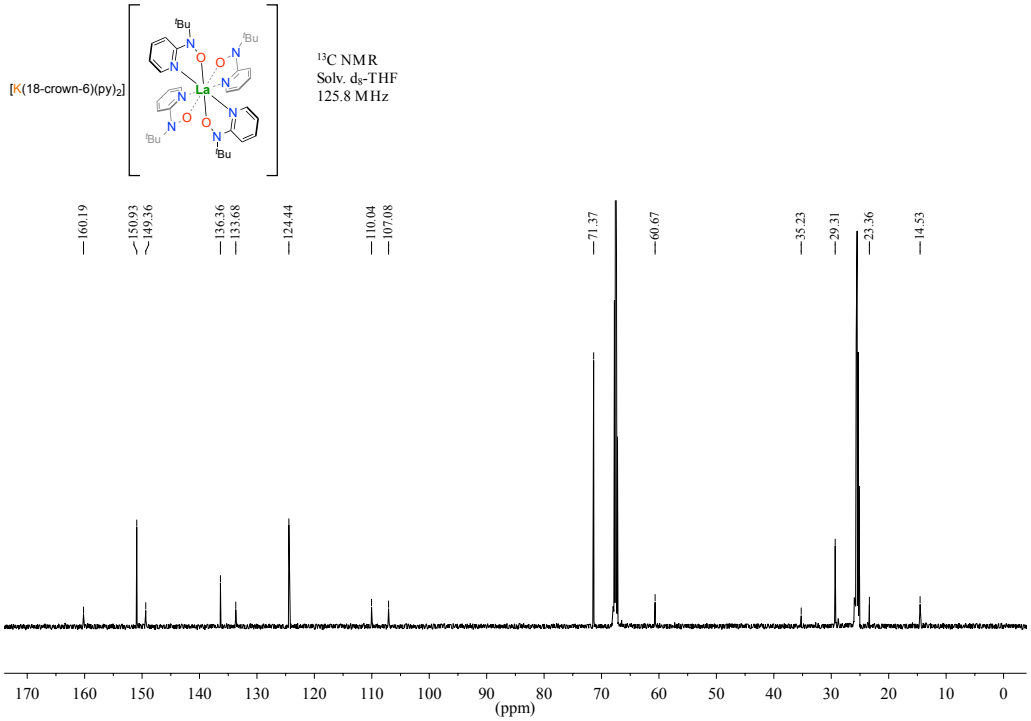

Figure 3.4.16. ^{13}C{^{1}H} NMR spectrum of **3.3-La**.

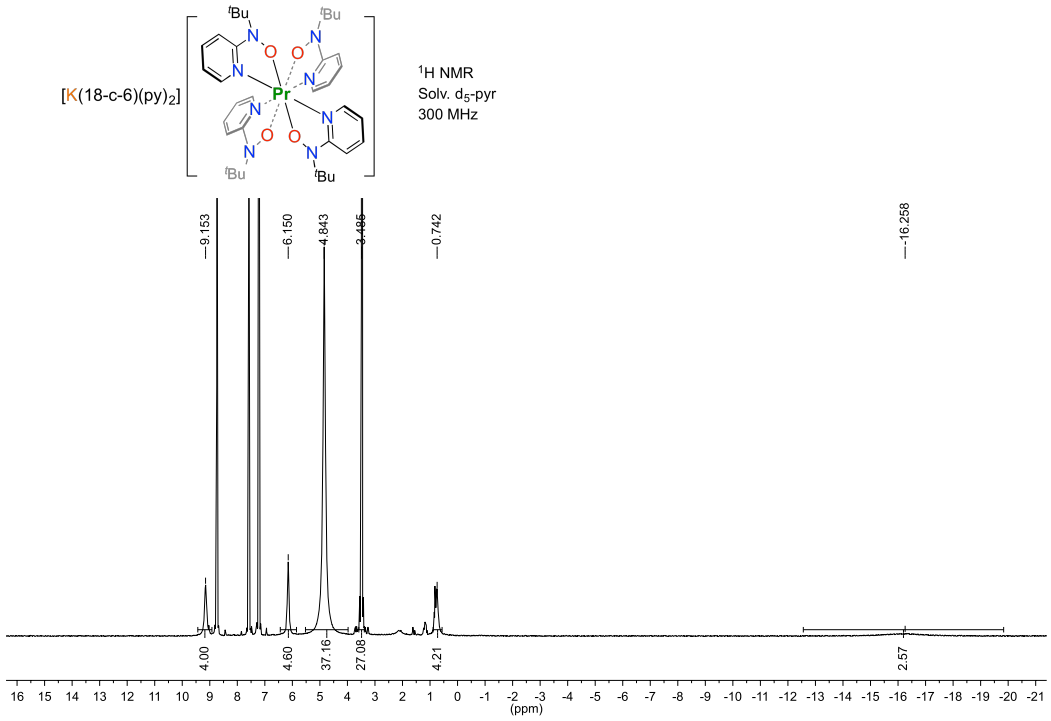

Figure 3.4.17. ^{1}H NMR spectrum of **3.3-Pr**.

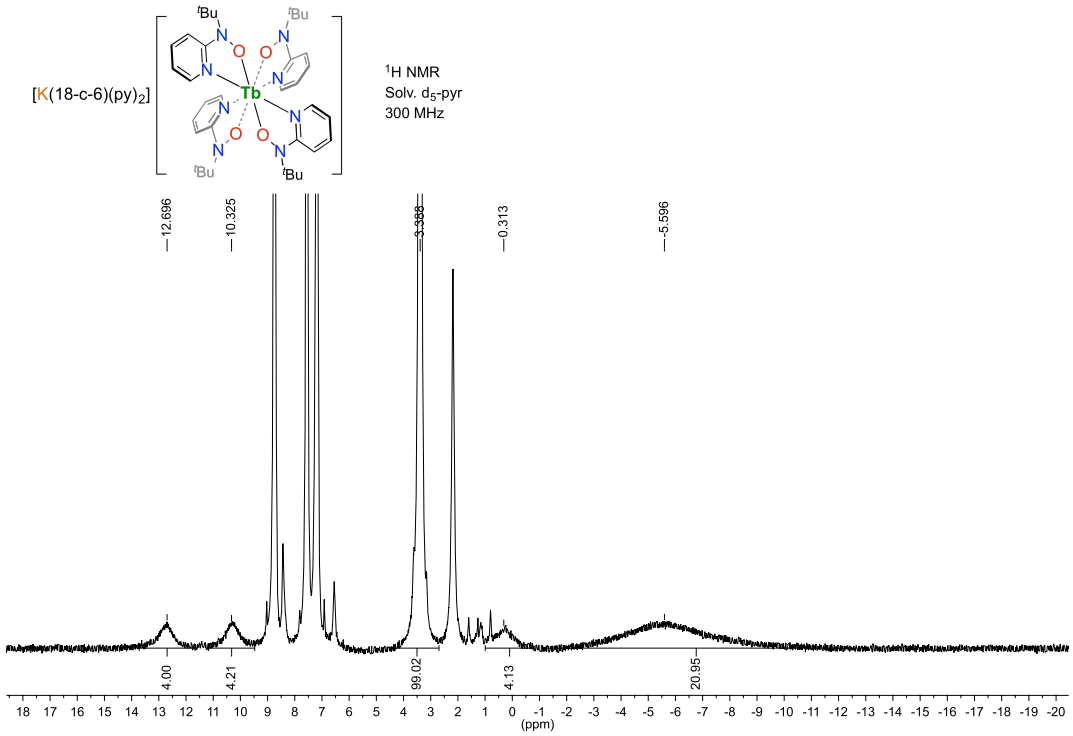

Figure 3.4.18. ^{1}H NMR spectrum of **3.3-Tb**.

X-ray Crystallography. X-ray intensity data were collected on a Bruker APEXII CCD area detector employing graphite-monochromated Mo-Kα radiation (λ=0.71073 Å) at a temperature of 143(1) K. In all cases, rotation frames were integrated using SAINT,[51] producing a listing of unaveraged F^2 and $\sigma(F^2)$ values that were then passed to the SHELXTL[52] program package for further processing and structure solution on a Dell Pentium 4 computer. The intensity data were corrected for Lorentz and polarization effects and for absorption using TWINABS[53] or SADABS.[54] The structures were solved by direct methods (SHELXS-97).[55] Refinement was by full-matrix least squares based on F^2 using SHELXL-97.[55] All reflections were used during refinements. Non-hydrogen atoms were refined anisotropically and hydrogen atoms were refined using a riding model.

Crystallographic data and structure refinement information for **3.1-X,** X= CF_3 (Penn4288), H (Penn4084), Me (Penn4150), OMe (Penn4406), *p*NMe_2 (Penn4343), *m*NMe_2 (Penn4226), **3.2-X,** X= CF_3 (Penn4284), H (Penn4130), Me (Penn4168), OMe (Penn4444), *p*NMe_2 (Penn4476), *m*NMe_2 (Penn4235), **3.3-RE**, RE = La (Penn4373), Ce (Penn4369), Pr (Penn4348), Tb (Penn4432), Dy (Penn4427), and **U[2-(^{t}BuNO)py]$_4$** (Penn4205) are summarized in Tables 3.4.3 – 3.4.20.

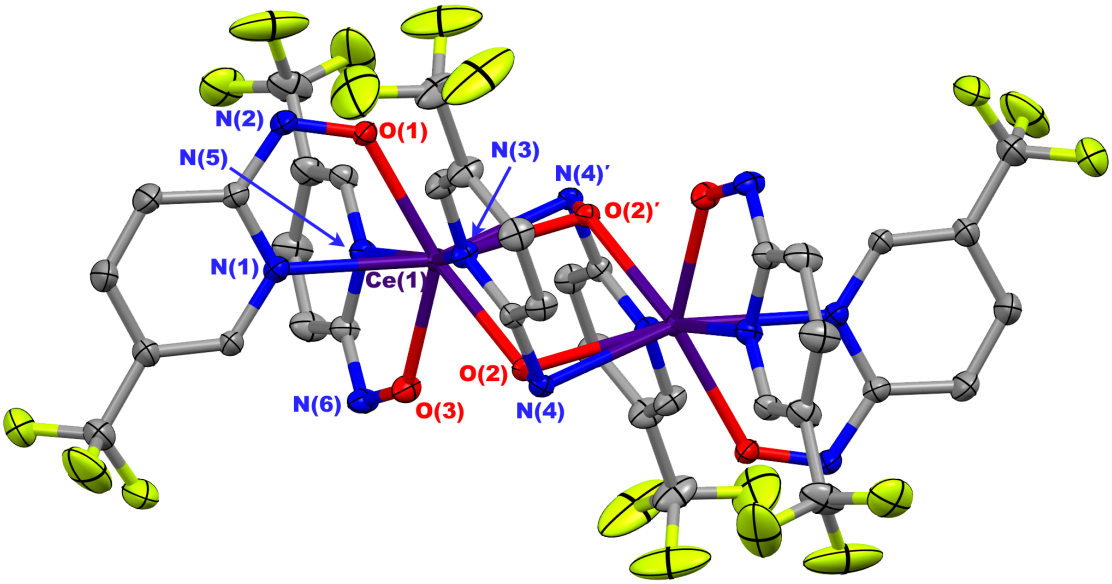

Figure 3.4.19. Thermal ellipsoid plot of **3.1-CF$_3$** at 30% probability. Hydrogen atoms and *tert*-butyl groups are omitted for clarity.

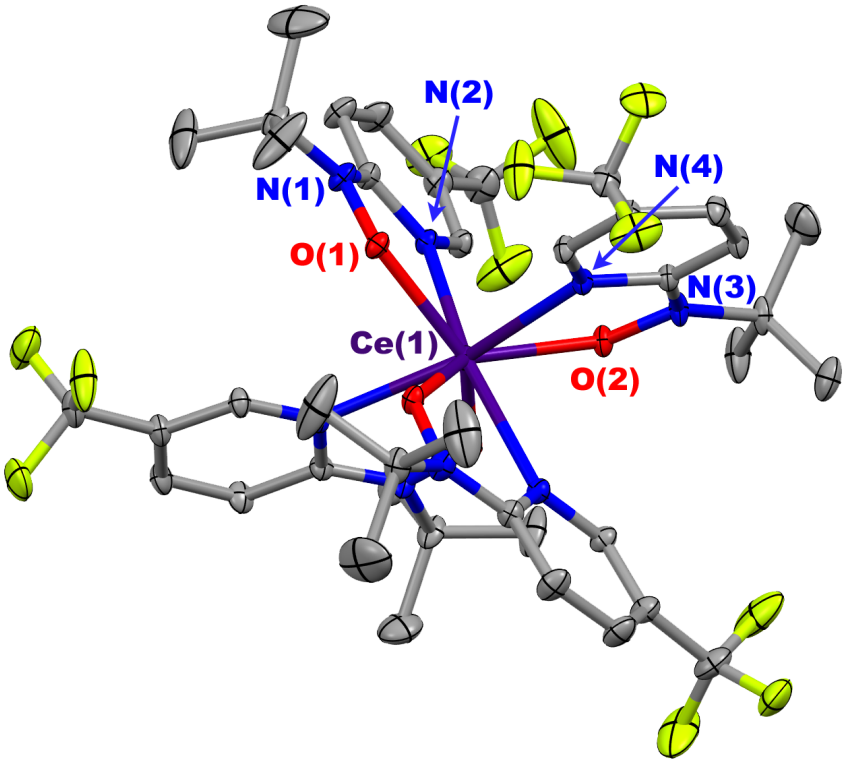

Figure 3.4.20. Thermal ellipsoid plot of **3.2-CF$_3$** at 30% probability. Hydrogen atoms are omitted for clarity.

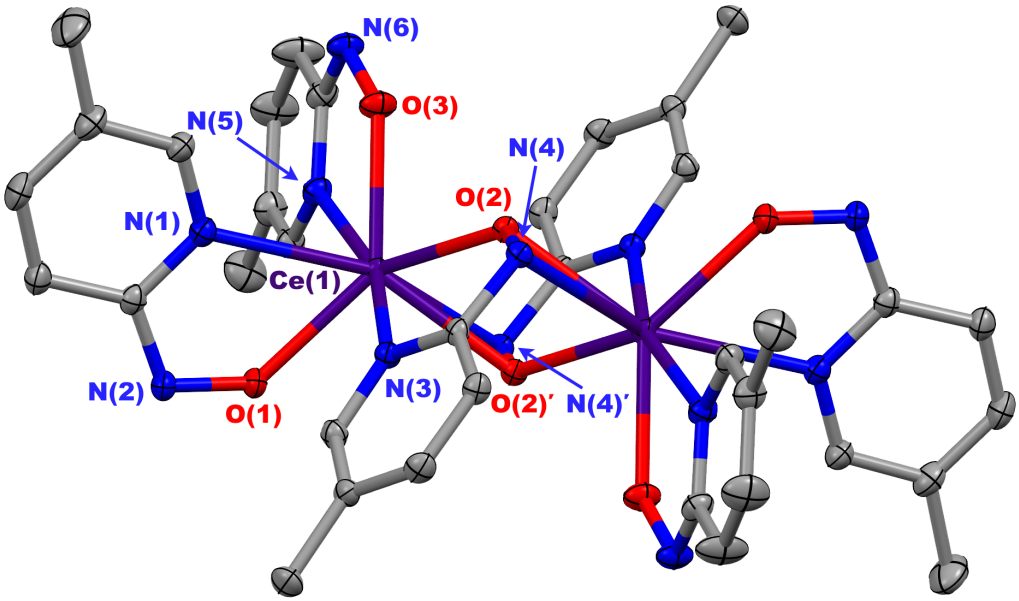

Figure 3.4.21. Thermal ellipsoid plot of **3.1-Me** at 30% probability. Hydrogen atoms and *tert*-butyl groups are omitted for clarity.

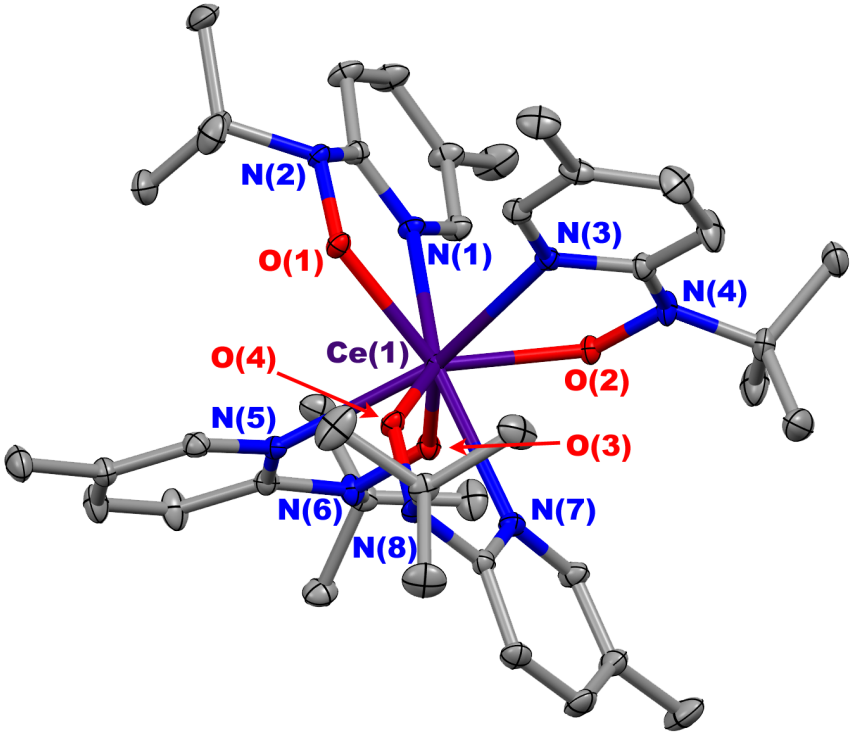

Figure 3.4.22. Thermal ellipsoid plot of **3.2-Me** at 30% probability. Hydrogen atoms are omitted for clarity.

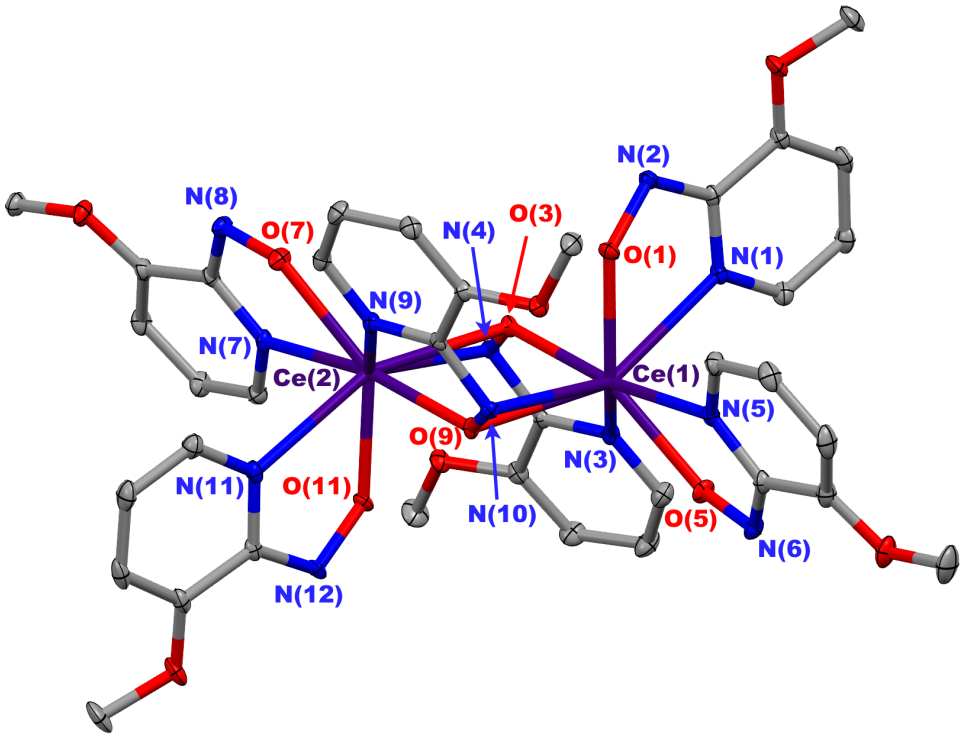

Figure 3.4.23. Thermal ellipsoid plot of **3.1-OMe** at 30% probability. Hydrogen atoms and *tert*-butyl groups are omitted for clarity.

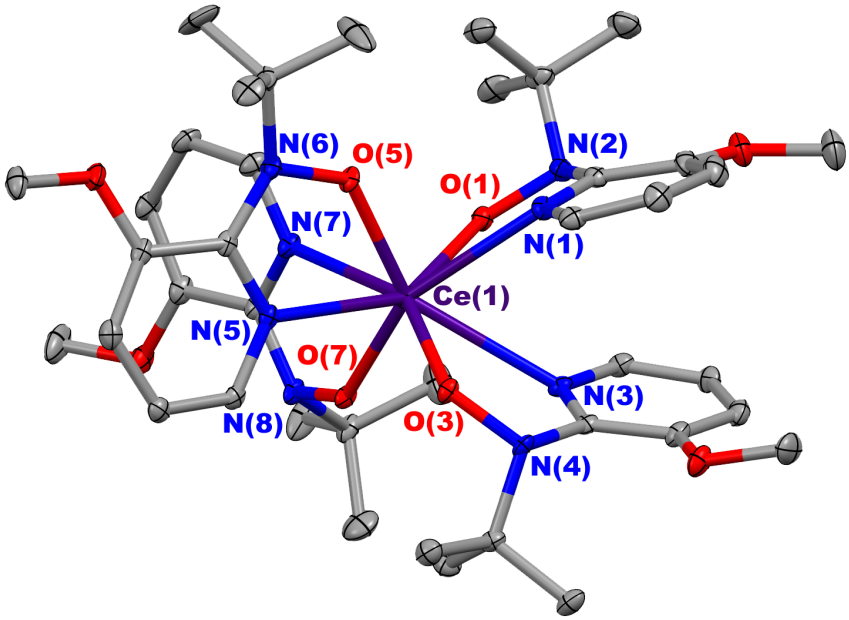

Figure 3.4.24. Thermal ellipsoid plot of **3.2-OMe** at 30% probability. Hydrogen atoms are omitted for clarity.

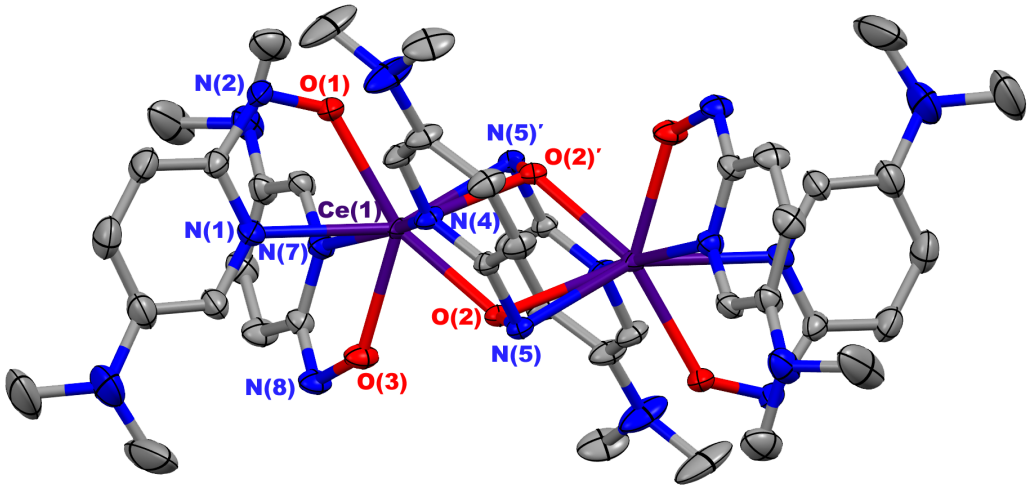

Figure 3.4.25. Thermal ellipsoid plot of **3.1-*p*NMe$_2$** at 30% probability. Hydrogen atoms and *tert*-butyl groups are omitted for clarity.

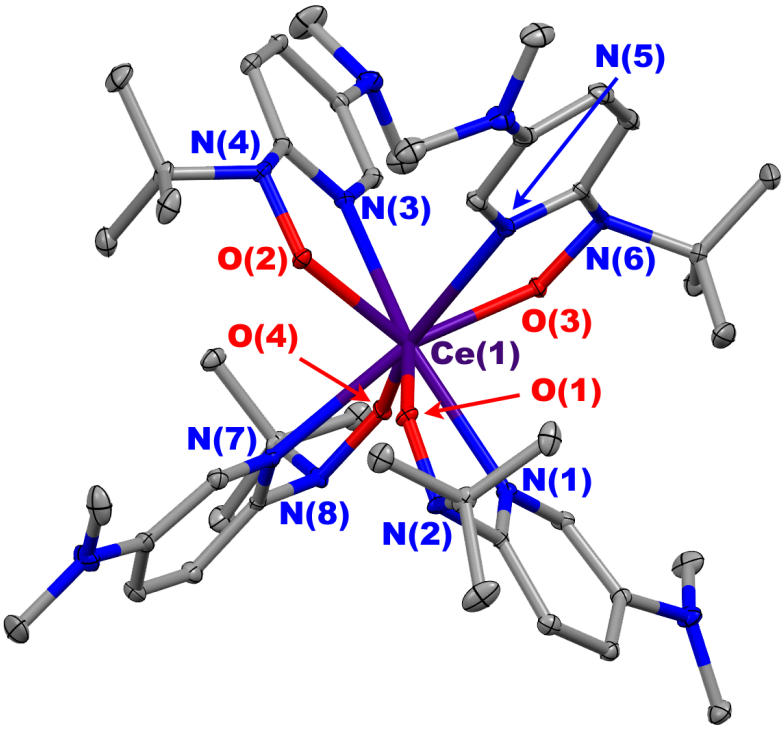

Figure 3.4.26. Thermal ellipsoid plot of **3.2-*p*NMe$_2$** at 30% probability. Hydrogen atoms are omitted for clarity.

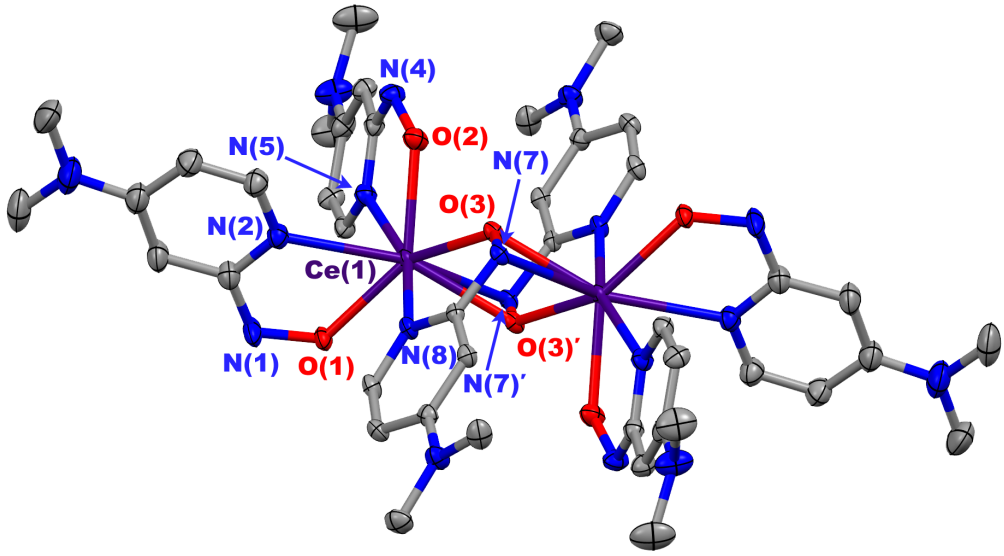

Figure 3.4.27. Thermal ellipsoid plot of **3.1-*m*NMe$_2$** at 30% probability. Hydrogen atoms and *tert*-butyl groups are omitted for clarity.

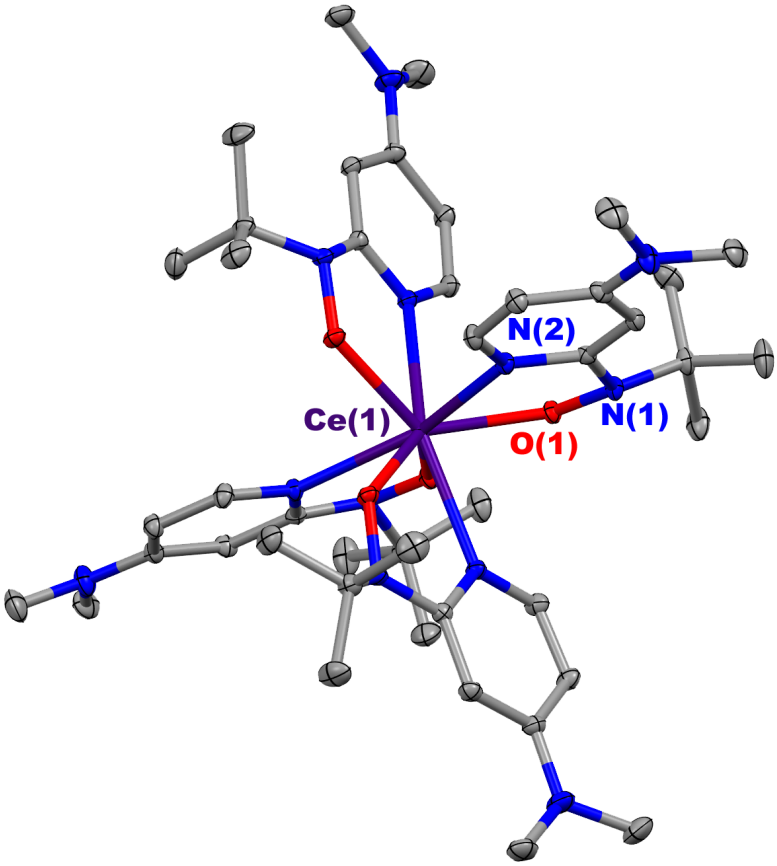

Figure 3.4.28. Thermal ellipsoid plot of **3.2-*m*NMe$_2$** at 30% probability. Hydrogen atoms are omitted for clarity.

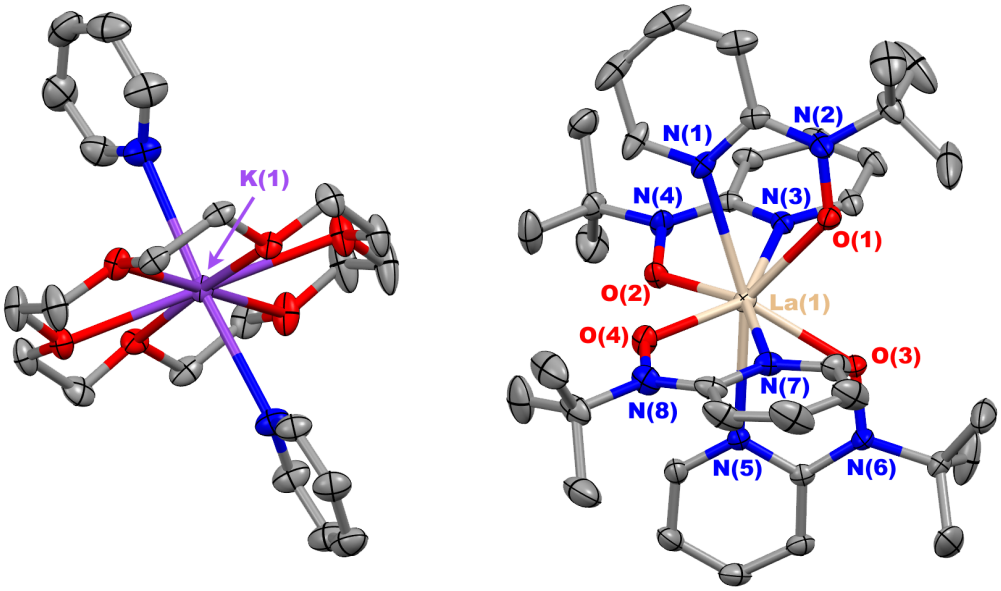

Figure 3.4.29. Thermal ellipsoid plot of **3.3-La** at 30% probability. Hydrogen atoms are omitted for clarity.

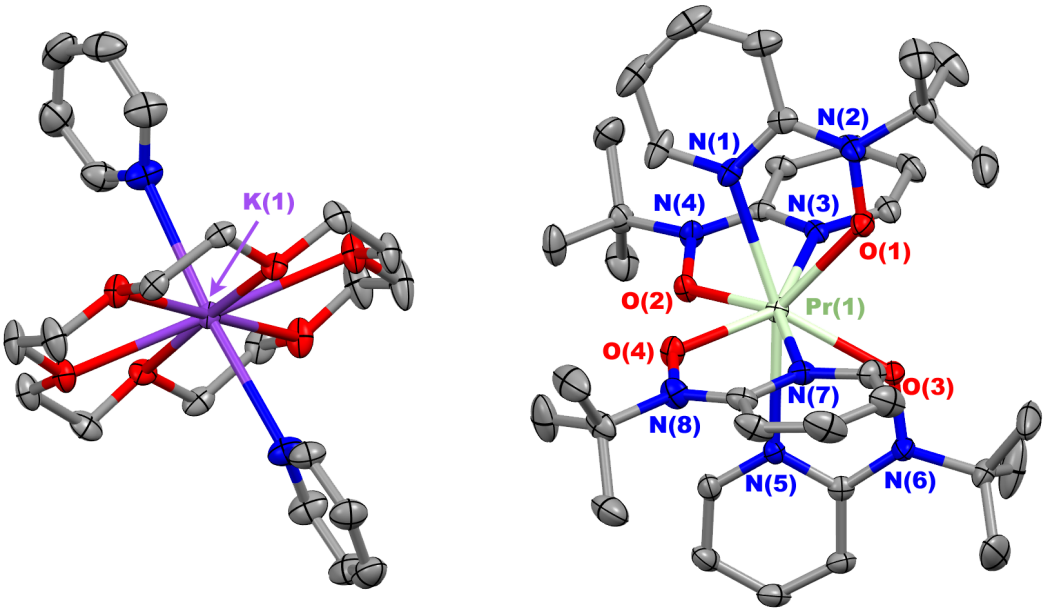

Figure 3.4.30. Thermal ellipsoid plot of **3.3-Pr** at 30% probability. Hydrogen atoms are omitted for clarity.

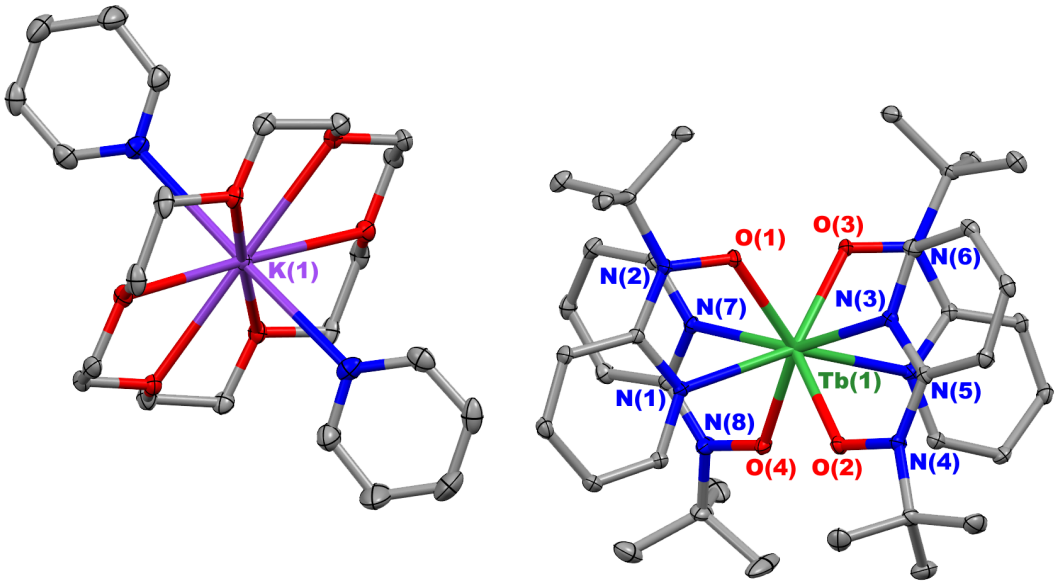

Figure 3.4.31. Thermal ellipsoid plot of **3.3-Tb** at 30% probability. Hydrogen atoms are omitted for clarity.

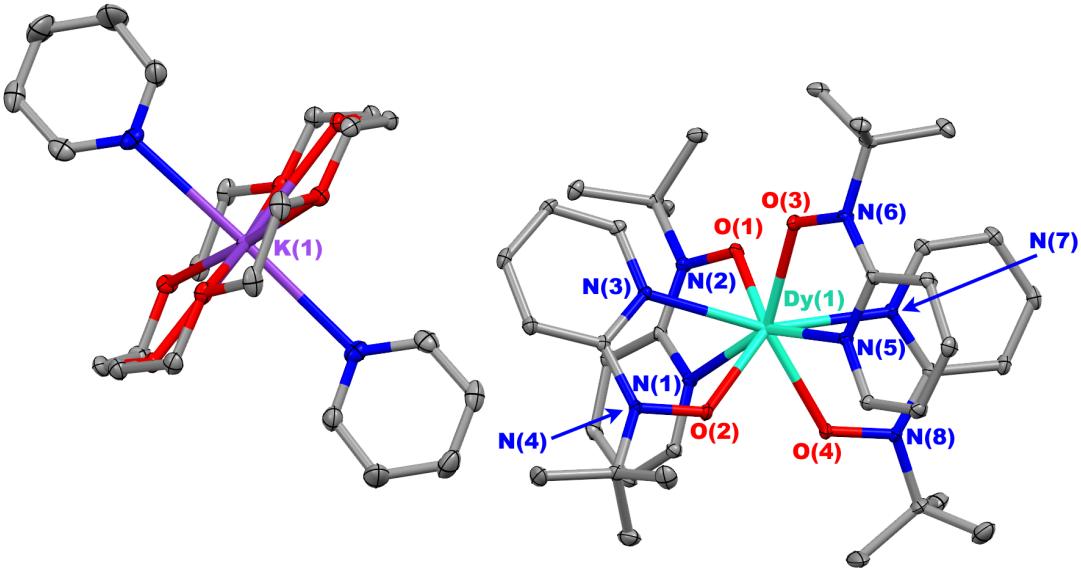

Figure 3.4.32. Thermal ellipsoid plot of **3.3-Dy** at 30% probability. Hydrogen atoms are omitted for clarity.

Table 3.4.1. Experimental structural metrics for the chelating nitroxide ligands of the series of **3.1-X** complexes. Distances are in Å and angles are in º.

	N–O exp	Ce–O exp	Ce–N_{pyr} exp	N_{pyr}–C–N^{t}_{BuNO}–C exp
3.1-CF_3	1.358(4)	2.319(2)	2.596(3)	7.22
3.1-H	1.375(3)	2.319(2)	2.606(2)	3.38
3.1-Me	1.383(3)	2.318(2)	2.624(2)	18.90
3.1-OMe	1.390(5)	2.304(3)	2.616(3)	40.68
3.1-*p*NMe_2	1.391(5)	2.306(2)	2.625(3)	35.26
3.1-*m*NMe_2	1.369(3)	2.320(2)	2.612(3)	6.92

Table 3.4.2. Experimental structural metrics for the bridging nitroxide ligands of the series of **3.1-X** complexes. Distances are in Å and angles are in º.

	N–O exp	Ce–O exp	Ce–N_{pyr} exp	N_{pyr}–C–N^{t}_{BuNO}–C exp
3.1-CF_3	1.423(3)	2.430(2)	2.708(2)	64.13
3.1-H	1.419(3)	2.4624(18)	2.707(2)	66.54
3.1-Me	1.426(2)	2.4539(17)	2.686(2)	68.13
3.1-OMe	1.430(6)	2.466(4)	2.763(4)	77.97
3.1-*p*NMe_2	1.418(4)	2.441(2)	2.706(3)	75.34
3.1-*m*NMe_2	1.427(3)	2.4389(17)	2.673(2)	69.96

Table 3.4.3. Crystallographic parameters for **3.1-CF_3.**

	3.1-CF_3 (Penn4288)
Empirical formula	$C_{60}H_{72}N_{12}O_6F_{18}Ce_2$
Formula weight	1679.54
Temperature	143(1) K
Wavelength	0.71073 Å
Crystal system	triclinic
Space group	$P\bar{1}$
Cell constants:	
a	10.8967(15) Å
b	14.6519(19) Å
c	14.732(3) Å
α	114.162(7)°
β	96.636(8)°
γ	111.145(5)°
Volume	1903.4(5) $Å^3$
Z	1
Density (calculated)	1.465 Mg/m^3
Absorption coefficient	1.276 mm^{-1}
F(000)	842
Crystal size	0.28 x 0.12 x 0.04 mm^3
Theta range for data collection	1.59 to 27.52°
Index ranges	$-13 \leq h \leq 14$, $-18 \leq k \leq 19$, $-19 \leq l \leq 19$
Reflections collected	76895
Independent reflections	8650 [R(int) = 0.0202]
Completeness to theta = 27.52°	98.8 %
Absorption correction	Semi-empirical from equivalents
Max. and min. transmission	0.7456 and 0.6696
Refinement method	Full-matrix least-squares on F^2
Data / restraints / parameters	8650 / 0 / 452
Goodness-of-fit on F^2	1.090
Final R indices [I>2sigma(I)]	R1 = 0.0332, wR2 = 0.0899
R indices (all data)	R1 = 0.0344, wR2 = 0.0909
Largest diff. peak and hole	1.323 and -0.750 e.$Å^{-3}$

Table 3.4.4. Crystallographic parameters for **3.2-CF_3.**

	3.2-CF_3 (Penn4284)
Empirical formula	$C_{40}H_{48}N_8O_4F_{12}Ce$
Formula weight	1072.98
Temperature	143(1) K
Wavelength	0.71073 Å
Crystal system	Monoclinic
Space group	C2/c
Cell constants:	
a	26.8816(12) Å
b	11.1429(5) Å
c	21.1312(16) Å
β	126.9870(10)°
Volume	5055.9(5) $Å^3$
Z	4
Density (calculated)	1.410 Mg/m^3
Absorption coefficient	0.989 mm^{-1}
F(000)	2168
Crystal size	0.32 x 0.28 x 0.28 mm^3
Theta range for data collection	1.90 to 27.61°
Index ranges	$-34 \leq h \leq 34$, $-14 \leq k \leq 14$, $-27 \leq l \leq 27$
Reflections collected	63453
Independent reflections	5832 [R(int) = 0.0200]
Completeness to theta = 27.61°	99.5 %
Absorption correction	Semi-empirical from equivalents
Max. and min. transmission	0.7456 and 0.6681
Refinement method	Full-matrix least-squares on F^2
Data / restraints / parameters	5832 / 0 / 301
Goodness-of-fit on F^2	1.070
Final R indices [I>2sigma(I)]	R1 = 0.0234, wR2 = 0.0615
R indices (all data)	R1 = 0.0237, wR2 = 0.0617
Largest diff. peak and hole	0.966 and -0.576 e.$Å^{-3}$

Table 3.4.5. Crystallographic parameters for **3.1-H.**

	3.1-H (Penn4084)
Empirical formula	$C_{54}H_{78}N_{12}O_6Ce_2$
Formula weight	1271.52
Temperature	143(1) K
Wavelength	0.71073 Å
Crystal system	monoclinic
Space group	$P2_1/n$
Cell constants:	
a	13.0570(8) Å
b	16.7150(10) Å
c	13.6361(8) Å
β	101.858(3)°
Volume	2912.5(3) $Å^3$
Z	2
Density (calculated)	1.450 Mg/m^3
Absorption coefficient	1.600 mm^{-1}
F(000)	1300
Crystal size	0.44 x 0.32 x 0.24 mm^3
Theta range for data collection	1.95 to 27.55°
Index ranges	$-16 \leq h \leq 16$, $-21 \leq k \leq 21$, $-17 \leq l \leq 17$
Reflections collected	75441
Independent reflections	6691 [R(int) = 0.0456]
Completeness to theta = 27.55°	99.6 %
Absorption correction	Semi-empirical from equivalents
Max. and min. transmission	0.7456 and 0.6238
Refinement method	Full-matrix least-squares on F^2
Data / restraints / parameters	6691 / 0 / 344
Goodness-of-fit on F^2	1.189
Final R indices [I>2sigma(I)]	R1 = 0.0296, wR2 = 0.0676
R indices (all data)	R1 = 0.0375, wR2 = 0.0757
Largest diff. peak and hole	1.403 and -0.974 $e.Å^{-3}$

Table 3.4.6. Crystallographic parameters for **3.2-H.**

	3.2-H (Penn4130)
Empirical formula	$C_{36}H_{52}N_8O_4Ce$
Formula weight	800.98
Temperature	143(1) K
Wavelength	0.71073 Å
Crystal system	monoclinic
Space group	C2/c
Cell constants:	
a	25.7533(13) Å
b	10.0788(5) Å
c	17.7825(9) Å
β	125.134(2)°
Volume	3774.7(3) $Å^3$
Z	4
Density (calculated)	1.409 Mg/m^3
Absorption coefficient	1.254 mm^{-1}
F(000)	1656
Crystal size	0.35 x 0.28 x 0.18 mm^3
Theta range for data collection	1.93 to 27.50°
Index ranges	$-33 \leq h \leq 25$, $-13 \leq k \leq 13$, $-21 \leq l \leq 23$
Reflections collected	44577
Independent reflections	4323 [R(int) = 0.0196]
Completeness to theta = 27.50°	99.8 %
Absorption correction	Semi-empirical from equivalents
Max. and min. transmission	0.7456 and 0.6643
Refinement method	Full-matrix least-squares on F^2
Data / restraints / parameters	4323 / 0 / 229
Goodness-of-fit on F^2	1.136
Final R indices [I>2sigma(I)]	R1 = 0.0186, wR2 = 0.0508
R indices (all data)	R1 = 0.0210, wR2 = 0.0528
Largest diff. peak and hole	1.098 and -0.285 $e.Å^{-3}$

Table 3.4.7. Crystallographic parameters for **3.1-Me.**

	3.1-Me (Penn4150)
Empirical formula	$C_{60}H_{90}N_{12}O_6Ce_2$
Formula weight	1355.68
Temperature	143(1) K
Wavelength	0.71073 Å
Crystal system	triclinic
Space group	$P\bar{1}$
Cell constants:	
a	10.8521(11) Å
b	11.1870(11) Å
c	13.6250(13) Å
α	94.766(4)°
β	95.119(4)°
γ	96.179(4)°
Volume	1630.7(3) $Å^3$
Z	1
Density (calculated)	1.380 Mg/m^3
Absorption coefficient	1.433 mm^{-1}
F(000)	698
Crystal size	0.25 x 0.10 x 0.10 mm^3
Theta range for data collection	1.84 to 27.50°
Index ranges	$-14 \leq h \leq 14$, $-14 \leq k \leq 14$, $-16 \leq l \leq 16$
Reflections collected	38626
Independent reflections	7142 [R(int) = 0.0190]
Completeness to theta = 27.50°	95.2 %
Absorption correction	Semi-empirical from equivalents
Max. and min. transmission	0.7456 and 0.6433
Refinement method	Full-matrix least-squares on F^2
Data / restraints / parameters	7142 / 0 / 374
Goodness-of-fit on F^2	1.165
Final R indices [I>2sigma(I)]	R1 = 0.0263, wR2 = 0.0645
R indices (all data)	R1 = 0.0298, wR2 = 0.0681
Largest diff. peak and hole	1.087 and -0.856 e.$Å^{-3}$

Table 3.4.8. Crystallographic parameters for **3.2-Me.**

	3.2-Me (Penn4168)
Empirical formula	$C_{40}H_{60}N_8O_4Ce$
Formula weight	857.08
Temperature	143(1) K
Wavelength	0.71073 Å
Crystal system	monoclinic
Space group	$P2_1/n$
Cell constants:	
a	9.1393(6) Å
b	21.1201(13) Å
c	22.2592(14) Å
β	101.433(3)°
Volume	4211.3(5) $Å^3$
Z	4
Density (calculated)	1.352 Mg/m^3
Absorption coefficient	1.129 mm^{-1}
F(000)	1784
Crystal size	0.42 x 0.20 x 0.15 mm^3
Theta range for data collection	1.87 to 27.58°
Index ranges	$-11 \leq h \leq 11$, $-27 \leq k \leq 27$, $-28 \leq l \leq 28$
Reflections collected	163944
Independent reflections	9709 [R(int) = 0.0240]
Completeness to theta = 27.58°	99.6 %
Absorption correction	Semi-empirical from equivalents
Max. and min. transmission	0.7456 and 0.7033
Refinement method	Full-matrix least-squares on F^2
Data / restraints / parameters	9709 / 0 / 495
Goodness-of-fit on F^2	1.217
Final R indices [I>2sigma(I)]	R1 = 0.0299, wR2 = 0.0629
R indices (all data)	R1 = 0.0361, wR2 = 0.0676
Largest diff. peak and hole	1.340 and -0.798 $e.Å^{-3}$

Table 3.4.9. Crystallographic parameters for **3.1-OMe.**

	3.1-OMe (Penn4406)
Empirical formula	$C_{140}H_{230}N_{24}O_{29}Ce_4$
Formula weight	3273.96
Temperature	100(1) K
Wavelength	0.71073 Å
Crystal system	monoclinic
Space group	$P2_1/n$
Cell constants:	
a	14.7521(6) Å
b	24.8495(10) Å
c	21.3962(8) Å
β	90.013(2)°
Volume	7843.5(5) $Å^3$
Z	2
Density (calculated)	1.386 Mg/m^3
Absorption coefficient	1.213 mm^{-1}
F(000)	3404
Crystal size	0.25 x 0.25 x 0.12 mm^3
Theta range for data collection	1.64 to 27.56°
Index ranges	$-19 \leq h \leq 19$, $-32 \leq k \leq 32$, $-27 \leq l \leq 27$
Reflections collected	312581
Independent reflections	18097 [R(int) = 0.0475]
Completeness to theta = 27.56°	99.8 %
Absorption correction	Semi-empirical from equivalents
Max. and min. transmission	0.7456 and 0.6572
Refinement method	Full-matrix least-squares on F^2
Data / restraints / parameters	18097 / 46 / 923
Goodness-of-fit on F^2	1.200
Final R indices [I>2sigma(I)]	R1 = 0.0439, wR2 = 0.0867
R indices (all data)	R1 = 0.0623, wR2 = 0.1009
Largest diff. peak and hole	2.167 and -1.103 $e.Å^{-3}$

Table 3.4.10. Crystallographic parameters for **3.2-OMe.**

	3.2-OMe (Penn4444)
Empirical formula	$C_{40}H_{60}N_8O_8Ce$
Formula weight	921.08
Temperature	100(1) K
Wavelength	0.71073 Å
Crystal system	monoclinic
Space group	$P2_1/n$
Cell constants:	
a	20.0600(11) Å
b	12.0199(6) Å
c	36.536(2) Å
β	92.954(3)°
Volume	8797.8(8) $Å^3$
Z	8
Density (calculated)	1.391 Mg/m^3
Absorption coefficient	1.092 mm^{-1}
F(000)	3824
Crystal size	0.50 x 0.08 x 0.08 mm^3
Theta range for data collection	1.78 to 27.88°
Index ranges	$-26 \leq h \leq 26$, $-15 \leq k \leq 15$, $-47 \leq l \leq 47$
Reflections collected	207539
Independent reflections	20630 [R(int) = 0.0489]
Completeness to theta = 27.88°	98.2 %
Absorption correction	Semi-empirical from equivalents
Max. and min. transmission	0.7456 and 0.6225
Refinement method	Full-matrix least-squares on F^2
Data / restraints / parameters	20630 / 54 / 1054
Goodness-of-fit on F^2	1.281
Final R indices [I>2sigma(I)]	R1 = 0.0616, wR2 = 0.1266
R indices (all data)	R1 = 0.0734, wR2 = 0.1323
Largest diff. peak and hole	2.393 and -3.457 $e.Å^{-3}$

Table 3.4.11. Crystallographic parameters for **3.1-*p*NMe$_2$.**

	3.1-*p*NMe$_2$ (Penn4343)
Empirical formula	$C_{71}H_{120}N_{18}O_6Ce_2$
Formula weight	1602.09
Temperature	143(1) K
Wavelength	0.71073 Å
Crystal system	triclinic
Space group	$P\bar{1}$
Cell constants:	
a	12.7510(12) Å
b	17.9395(17) Å
c	19.958(3) Å
α	70.026(4)°
β	89.891(7)°
γ	85.221(5)°
Volume	4274.1(9) Å^3
Z	2
Density (calculated)	1.245 Mg/m^3
Absorption coefficient	1.106 mm^{-1}
F(000)	1672
Crystal size	0.35 x 0.25 x 0.10 mm^3
Theta range for data collection	1.60 to 27.61°
Index ranges	-16 ≤ h ≤ 16, -23 ≤ k ≤ 23, -25 ≤ l ≤ 26
Reflections collected	126422
Independent reflections	19608 [R(int) = 0.0335]
Completeness to theta = 27.61°	98.7 %
Absorption correction	Semi-empirical from equivalents
Max. and min. transmission	0.7456 and 0.6793
Refinement method	Full-matrix least-squares on F^2
Data / restraints / parameters	19608 / 0 / 860
Goodness-of-fit on F^2	1.065
Final R indices [I>2sigma(I)]	R1 = 0.0439, wR2 = 0.1133
R indices (all data)	R1 = 0.0582, wR2 = 0.1210
Largest diff. peak and hole	2.059 and -0.964 e.Å^{-3}

Table 3.4.12. Crystallographic parameters for **3.2-*p*NMe$_2$.**

	3.2-*p*NMe$_2$ (Penn4476)
Empirical formula	$C_{48}H_{82}N_{12}O_5Ce$
Formula weight	1047.38
Temperature	100(1) K
Wavelength	0.71073 Å
Crystal system	monoclinic
Space group	$P2_1$
Cell constants:	
a	9.7931(6) Å
b	22.6748(14) Å
c	11.7718(7) Å
β	94.030(3)°
Volume	2607.5(3) Å^3
Z	2
Density (calculated)	1.334 Mg/m^3
Absorption coefficient	0.928 mm^{-1}
F(000)	1104
Crystal size	0.50 x 0.20 x 0.12 mm^3
Theta range for data collection	1.80 to 27.58°
Index ranges	$-12 \leq h \leq 12$, $-29 \leq k \leq 29$, $-15 \leq l \leq 15$
Reflections collected	69397
Independent reflections	11984 [R(int) = 0.0227]
Completeness to theta = 27.58°	100.0 %
Absorption correction	Semi-empirical from equivalents
Max. and min. transmission	0.7456 and 0.6522
Refinement method	Full-matrix least-squares on F^2
Data / restraints / parameters	11984 / 1 / 618
Goodness-of-fit on F^2	1.044
Final R indices [I>2sigma(I)]	R1 = 0.0144, wR2 = 0.0351
R indices (all data)	R1 = 0.0151, wR2 = 0.0352
Absolute structure parameter	-0.010(4)
Largest diff. peak and hole	0.348 and -0.327 e.Å^{-3}

Table 3.4.13. Crystallographic parameters for **3.1-*m*NMe$_2$.**

	3.1-*m*NMe$_2$ (Penn4226)
Empirical formula	$C_{33}H_{54}N_9O_3Ce$
Formula weight	764.97
Temperature	143(1) K
Wavelength	0.71073 Å
Crystal system	triclinic
Space group	$P\bar{1}$
Cell constants:	
a	11.8816(6) Å
b	12.3754(7) Å
c	15.7354(10) Å
α	101.944(3)°
β	99.040(3)°
γ	115.595(3)°
Volume	1960.20(19) Å^3
Z	2
Density (calculated)	1.296 Mg/m^3
Absorption coefficient	1.203 mm^{-1}
F(000)	794
Crystal size	0.35 x 0.15 x 0.01 mm^3
Theta range for data collection	1.92 to 27.59°
Index ranges	-15 ≤ h ≤ 15, -16 ≤ k ≤ 16, -20 ≤ l ≤ 20
Reflections collected	94921
Independent reflections	8908 [R(int) = 0.1281]
Completeness to theta = 27.59°	97.9 %
Absorption correction	Semi-empirical from equivalents
Max. and min. transmission	0.7456 and 0.6908
Refinement method	Full-matrix least-squares on F^2
Data / restraints / parameters	8908 / 0 / 430
Goodness-of-fit on F^2	1.038
Final R indices [I>2sigma(I)]	R1 = 0.0329, wR2 = 0.0850
R indices (all data)	R1 = 0.0402, wR2 = 0.0871
Largest diff. peak and hole	2.014 and -0.609 e.Å^{-3}

Table 3.4.14. Crystallographic parameters for **3.2-*m*NMe$_2$.**

	3.2-*m*NMe$_2$ (Penn4235)
Empirical formula	$C_{44}H_{72}N_{12}O_4Ce$
Formula weight	973.26
Temperature	143(1) K
Wavelength	0.71073 Å
Crystal system	tetragonal
Space group	P4/n
Cell constants:	
a	16.472(3) Å
c	9.7869(17) Å
Volume	2655.4(8) Å^3
Z	2
Density (calculated)	1.217 Mg/m^3
Absorption coefficient	0.905 mm^{-1}
F(000)	1020
Crystal size	0.45 x 0.42 x 0.25 mm^3
Theta range for data collection	2.42 to 27.52°
Index ranges	$-21 \leq h \leq 21$, $-21 \leq k \leq 21$, $-12 \leq l \leq 11$
Reflections collected	3058
Independent reflections	3054 [R(int) = 0.1619]
Completeness to theta = 27.52°	99.6 %
Absorption correction	Semi-empirical from equivalents
Max. and min. transmission	0.7456 and 0.6819
Refinement method	Full-matrix least-squares on F^2
Data / restraints / parameters	3054 / 0 / 144
Goodness-of-fit on F^2	1.073
Final R indices [I>2sigma(I)]	R1 = 0.0249, wR2 = 0.0625
R indices (all data)	R1 = 0.0335, wR2 = 0.0676
Largest diff. peak and hole	0.397 and -0.275 e.Å^{-3}

Table 3.4.15. Crystallographic parameters for **3.3-Ce.**

	3.3-Ce (Penn4369)
Empirical formula	$C_{68}H_{96}N_{12}O_{10}KCe$
Formula weight	1420.79
Temperature	143(1) K
Wavelength	0.71073 Å
Crystal system	monoclinic
Space group	$P2_1/c$
Cell constants:	
a	14.4111(8) Å
b	22.9801(14) Å
c	22.4451(13) Å
β	102.809(3)°
Volume	7248.1(7) $Å^3$
Z	4
Density (calculated)	1.302 Mg/m^3
Absorption coefficient	0.748 mm^{-1}
F(000)	2980
Crystal size	0.32 x 0.18 x 0.08 mm^3
Theta range for data collection	1.70 to 27.58°
Index ranges	$-18 \leq h \leq 18$, $-29 \leq k \leq 29$, $-29 \leq l \leq 29$
Reflections collected	141990
Independent reflections	16638 [R(int) = 0.0342]
Completeness to theta = 27.58°	99.2 %
Absorption correction	Semi-empirical from equivalents
Max. and min. transmission	0.7456 and 0.6941
Refinement method	Full-matrix least-squares on F^2
Data / restraints / parameters	16638 / 0 / 842
Goodness-of-fit on F^2	1.106
Final R indices [I>2sigma(I)]	R1 = 0.0515, wR2 = 0.1065
R indices (all data)	R1 = 0.0777, wR2 = 0.1271
Largest diff. peak and hole	2.935 and -1.121 $e.Å^{-3}$

Table 3.4.16. Crystallographic parameters for **3.3-La.**

	3.3-La (Penn4373)
Empirical formula	$C_{68}H_{96}N_{12}O_{10}KLa$
Formula weight	1419.58
Temperature	143(1) K
Wavelength	0.71073 Å
Crystal system	monoclinic
Space group	$P2_1/c$
Cell constants:	
a	14.4506(18) Å
b	23.094(3) Å
c	22.371(3) Å
β	102.673(4)°
Volume	7283.8(16) $Å^3$
Z	4
Density (calculated)	1.295 Mg/m^3
Absorption coefficient	0.706 mm^{-1}
F(000)	2976
Crystal size	0.30 x 0.12 x 0.12 mm^3
Theta range for data collection	1.69 to 27.53°
Index ranges	$-18 \leq h \leq 18$, $-29 \leq k \leq 29$, $-29 \leq l \leq 29$
Reflections collected	124724
Independent reflections	16690 [R(int) = 0.0451]
Completeness to theta = 27.53°	99.5 %
Absorption correction	Semi-empirical from equivalents
Max. and min. transmission	0.7456 and 0.6777
Refinement method	Full-matrix least-squares on F^2
Data / restraints / parameters	16690 / 0 / 842
Goodness-of-fit on F^2	1.019
Final R indices [I>2sigma(I)]	R1 = 0.0417, wR2 = 0.0957
R indices (all data)	R1 = 0.0698, wR2 = 0.1121
Largest diff. peak and hole	1.291 and -0.711 $e.Å^{-3}$

Table 3.4.17. Crystallographic parameters for **3.3-Pr.**

	3.3-Pr (Penn4348)
Empirical formula	$C_{68}H_{96}N_{12}O_{10}KPr$
Formula weight	1421.58
Temperature	143(1) K
Wavelength	0.71073 Å
Crystal system	monoclinic
Space group	$P2_1/c$
Cell constants:	
a	14.4111(9) Å
b	22.9801(16) Å
c	22.4451(16) Å
β	102.809(3)°
Volume	7248.1(9) $Å^3$
Z	4
Density (calculated)	1.303 Mg/m^3
Absorption coefficient	0.792 mm^{-1}
F(000)	2984
Crystal size	0.30 x 0.15 x 0.08 mm^3
Theta range for data collection	1.70 to 27.54°
Index ranges	$-18 \leq h \leq 17$, $-28 \leq k \leq 29$, $-29 \leq l \leq 29$
Reflections collected	149850
Independent reflections	16696 [R(int) = 0.0321]
Completeness to theta = 27.54°	99.9 %
Absorption correction	Semi-empirical from equivalents
Max. and min. transmission	0.7456 and 0.6881
Refinement method	Full-matrix least-squares on F^2
Data / restraints / parameters	16696 / 0 / 842
Goodness-of-fit on F^2	1.075
Final R indices [I>2sigma(I)]	R1 = 0.0410, wR2 = 0.0878
R indices (all data)	R1 = 0.0610, wR2 = 0.1031
Largest diff. peak and hole	1.860 and -0.756 $e.Å^{-3}$

Table 3.4.18. Crystallographic parameters for **3.3-Tb.**

	3.3-Tb (Penn4332)
Empirical formula	$C_{58}H_{86}N_{10}O_{10}KTb$
Formula weight	1281.39
Temperature	100(1) K
Wavelength	0.71073 Å
Crystal system	monoclinic
Space group	$P2_1/c$
Cell constants:	
a	12.7804(2) Å
b	19.5209(3) Å
c	25.2075(4) Å
β	103.2180(10)°
Volume	6122.28(17) $Å^3$
Z	4
Density (calculated)	1.390 Mg/m^3
Absorption coefficient	1.287 mm^{-1}
F(000)	2672
Crystal size	0.20 x 0.12 x 0.08 mm^3
Theta range for data collection	1.64 to 27.52°
Index ranges	$-12 \leq h \leq 16$, $-25 \leq k \leq 25$, $-32 \leq l \leq 32$
Reflections collected	103458
Independent reflections	14087 [R(int) = 0.0299]
Completeness to theta = 27.52°	99.8 %
Absorption correction	Semi-empirical from equivalents
Max. and min. transmission	0.7456 and 0.6471
Refinement method	Full-matrix least-squares on F^2
Data / restraints / parameters	14087 / 0 / 734
Goodness-of-fit on F^2	1.018
Final R indices [I>2sigma(I)]	R1 = 0.0196, wR2 = 0.0431
R indices (all data)	R1 = 0.0279, wR2 = 0.0466
Largest diff. peak and hole	0.640 and -0.412 $e.Å^{-3}$

Table 3.4.19. Crystallographic parameters for **3.3-Dy.**

	3.3-Dy (Penn4427)
Empirical formula	$C_{58}H_{86}N_{10}O_{10}KDy$
Formula weight	1284.97
Temperature	100(1) K
Wavelength	0.71073 Å
Crystal system	monoclinic
Space group	$P2_1/c$
Cell constants:	
a	12.7980(10) Å
b	19.5444(15) Å
c	25.2727(19) Å
β	103.355(3)°
Volume	6150.5(8) $Å^3$
Z	4
Density (calculated)	1.388 Mg/m^3
Absorption coefficient	1.346 mm^{-1}
F(000)	2676
Crystal size	0.38 x 0.32 x 0.12 mm^3
Theta range for data collection	1.64 to 27.56°
Index ranges	$-16 \leq h \leq 16$, $-25 \leq k \leq 25$, $-32 \leq l \leq 32$
Reflections collected	213717
Independent reflections	14189 [R(int) = 0.0227]
Completeness to theta = 27.56°	99.7 %
Absorption correction	Semi-empirical from equivalents
Max. and min. transmission	0.7456 and 0.6507
Refinement method	Full-matrix least-squares on F^2
Data / restraints / parameters	14189 / 0 / 734
Goodness-of-fit on F^2	1.155
Final R indices [I>2sigma(I)]	R1 = 0.0187, wR2 = 0.0468
R indices (all data)	R1 = 0.0219, wR2 = 0.0502
Largest diff. peak and hole	1.134 and -0.677 $e.Å^{-3}$

Table 3.4.20. Crystallographic parameters for **U[2-(^{t}BuNO)py]$_4$.**

	U[2-(^{t}BuNO)py]$_4$ (Penn4205)
Empirical formula	$C_{36}H_{52}N_8O_4U$
Formula weight	898.89
Temperature	143(1) K
Wavelength	0.71073 Å
Crystal system	monoclinic
Space group	C2/c
Cell constants:	
a	25.9575(16) Å
b	10.0871(6) Å
c	18.0199(11) Å
β	126.433(2)°
Volume	3796.1(4) Å^3
Z	4
Density (calculated)	1.573 Mg/m^3
Absorption coefficient	4.324 mm^{-1}
F(000)	1792
Crystal size	0.35 x 0.28 x 0.20 mm^3
Theta range for data collection	2.24 to 27.52°
Index ranges	-30 ≤ h ≤ 33, -13 ≤ k ≤ 12, -23 ≤ l ≤ 19
Reflections collected	27584
Independent reflections	4341 [R(int) = 0.0569]
Completeness to theta = 27.52°	99.5 %
Absorption correction	Semi-empirical from equivalents
Max. and min. transmission	0.7456 and 0.5989
Refinement method	Full-matrix least-squares on F^2
Data / restraints / parameters	4341 / 0 / 229
Goodness-of-fit on F^2	1.303
Final R indices [I>2sigma(I)]	R1 = 0.0755, wR2 = 0.1629
R indices (all data)	R1 = 0.0928, wR2 = 0.1716
Largest diff. peak and hole	2.283 and -2.128 e.Å^{-3}

Magnetism. Magnetic data were collected using a Quantum Design Multi-Property Measurement System (MPMS-7) with a Reciprocating Sample Option at 2 T from 2–300 K and at 2 K from 0–7 T. Two methods for sample preparations were used. *Method 1*: Quartz tubes (3 mm OD, 2 mm ID), quartz rods, and quartz wool were dried at 250 °C prior to use. The sample tubes were loaded with finely ground crystalline sample and packed on both sides with quartz wool in the N_2 atmosphere drybox. Quartz wool 'slugs' were packed into separate small lengths of quartz 'loading tubes' prior to drying to facilitate direct transfer of the slugs into the quartz tube sample holder before and after loading the sample. The quartz wool slugs were loaded into the sample tube using a quartz 'tamping' rod. The sample was loaded through a glass Pasteur pipette that acted as a funnel. Valves with Teflon stopcocks were attached to each end of the tube and the sample was removed from the glovebox. The samples were flame-sealed under dynamic vacuum on a Schlenk line. A short length of heat-shrink tubing was fitted to one end of the quartz tube and affixed to the tube by treatment with a heat gun. The open end of the heat shrink tubing was fitted to the end of the MPMS-7 plastic sample transport, without heat shrinking, by fitting a ~1 cm length of drinking straw snugly over the tubing/transport assembly. *Method 2*: Magnetism samples were placed in a heat-sealed compartment of a plastic drinking straw. The plastic drinking straws were dried under dynamic vacuum overnight prior to use. These straws were then sealed at one end (~9.5 cm from the top) by heating a pair of forceps and crimping the sides of the straw until both sides were fused together. Microcrystalline compound (~10 – 20 mg) was loaded into the straw and capped with ~10 mg of Quartz wool (dried at 250 °C prior to use) and packed in tightly using a Q-tip. The other end of the plastic drinking straw was then sealed directly above the quartz wool, forming a small compartment (< 1 cm). Samples and wool were massed four times each to the nearest 0.1 mg and the values used were the averages of these mass measurements. Corrections for the intrinsic diamagnetism of the samples were made using Pascal's constants.[56] Data were collected on two independently prepared samples to ensure reproducibility.

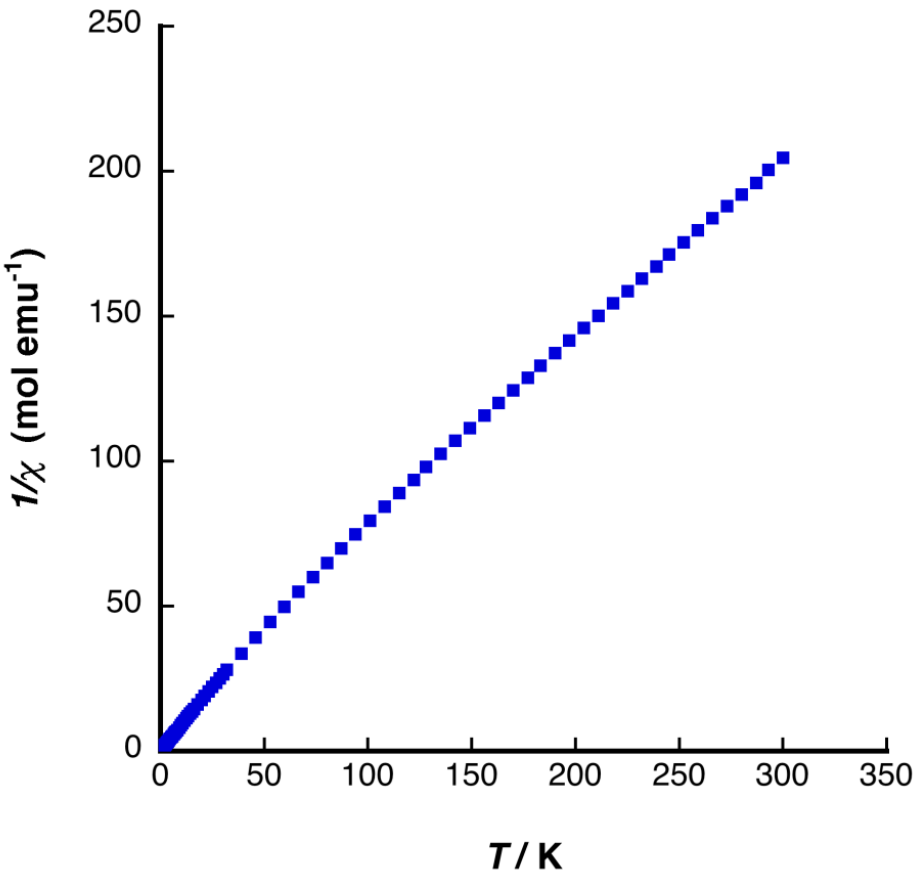

Figure 3.4.33. 1/χ versus T plot of compound **3.1-H.**

X-Ray Absorption Spectroscopy. Ce L_{III}-edge XANES data were collected at the Stanford Synchrotron Radiation Lightsource, beamline 11-2, using a Si 220 (phi=0) double monochromator that was detuned to 20% in order to reduce harmonic contamination. The resulting data have an energy resolution limited by the broadening due to the $2p_{3/2}$ corehole lifetime of 3.2 eV. Data were collected in transmission, using a CeO_2 reference to calibrate the energy scale, setting the first inflection point of the CeO_2 absorption to 5723 eV. A linear pre-edge background was subtracted and the data were subsequently normalized at 5800 eV.

The samples were prepared for these experiments using procedures outlined previously.[57] In particular, each sample was ground into a powder, mixed with dry boron nitride as a diluent, and then packed into the slots of a machined aluminum sample holder in an N_2 atmosphere drybox. Aluminized mylar was affixed to the holder with an indium-wire seal. After packaging, the samples were transported in dry, nitrogen-filled containers to the beamline. Sample holders were quickly transferred to the vacuum chamber, exposing the sealed holders to air for less than thirty seconds before pumping out the chamber and collecting the data under vacuum. Compounds **3.1-X**, where X = $-CF_3$, -H, and -*p*NMe_2, show extreme air sensitivity and have easily identifiable spectral changes upon exposure. These samples served as “canary” samples and were monitored to check for sample holder integrity. Following measurement, no significant changes in those samples were observed.

UV-Vis Spectroscopy. All UV-Vis absorption measurements were performed using a Perkin Elmer 950 UV-Vis/NIR Spectrophotometer. 1 mm path length screw cap quartz cells were used with a blank measured before each run.

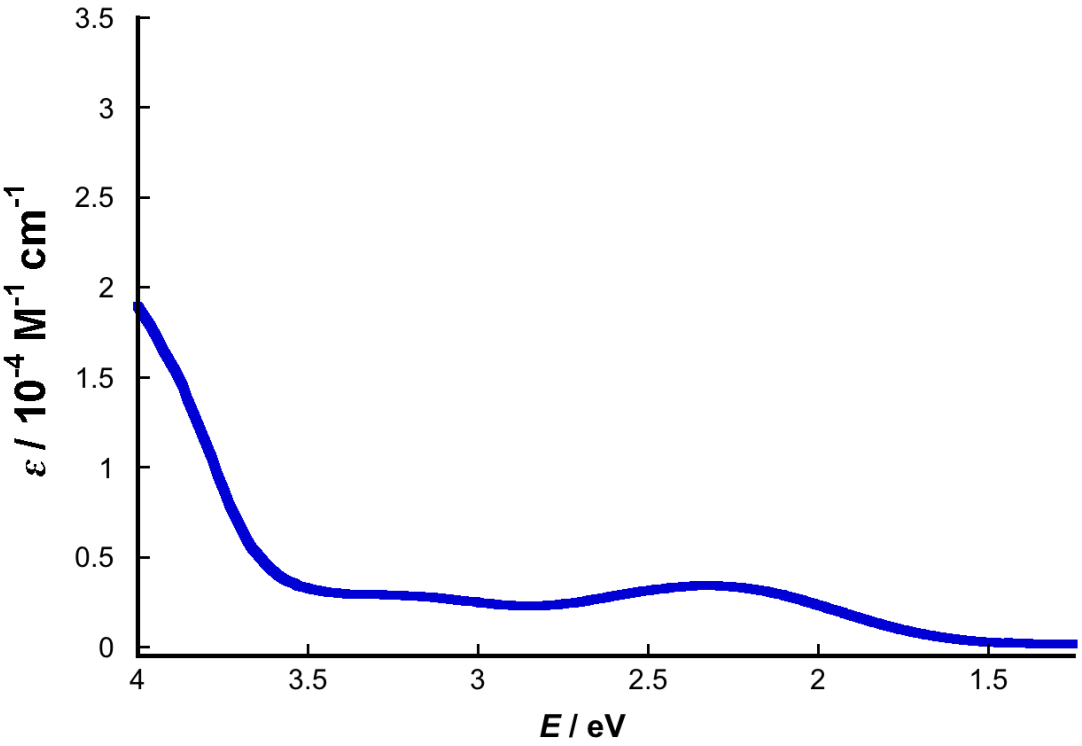

Figure 3.4.34. UV-Vis spectrum of **3.2-CF$_3$.**

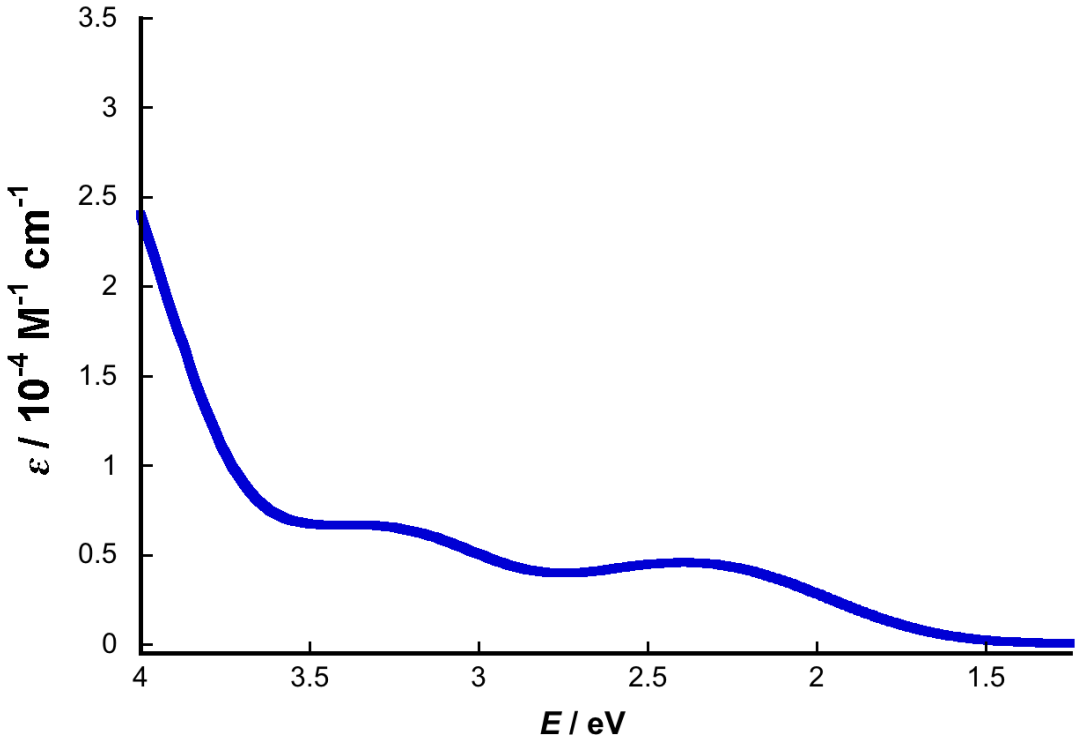

Figure 3.4.35. UV-Vis spectrum of **3.2-Me.**

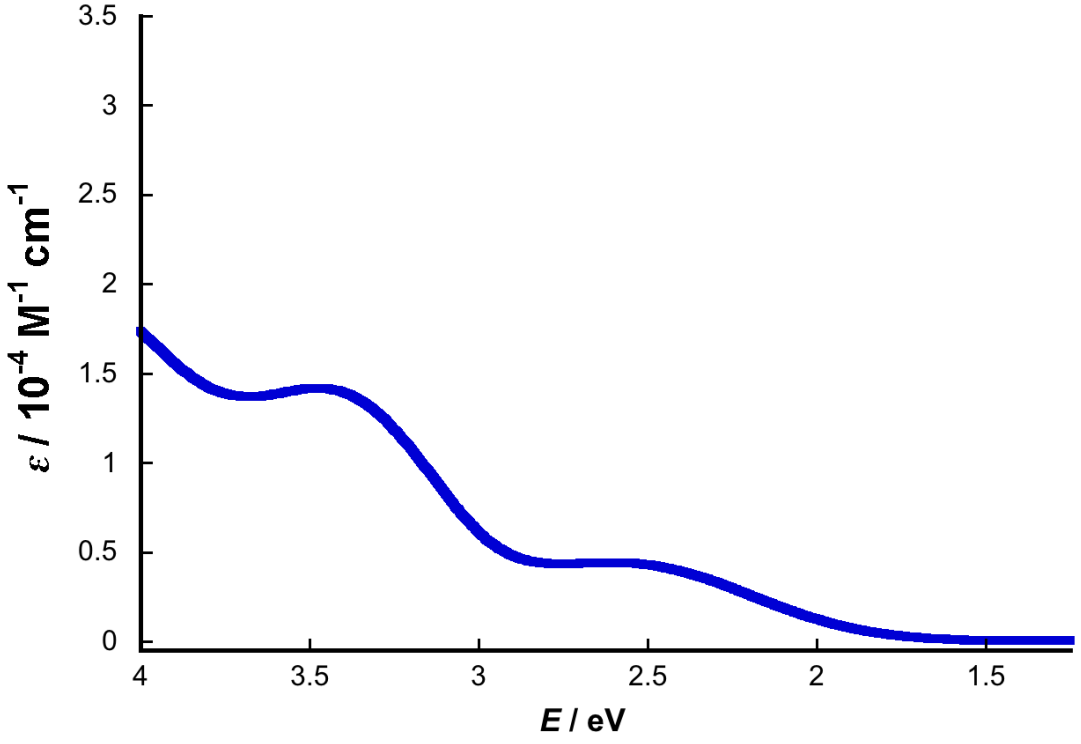

Figure 3.4.36. UV-Vis spectrum of **3.2-OMe.**

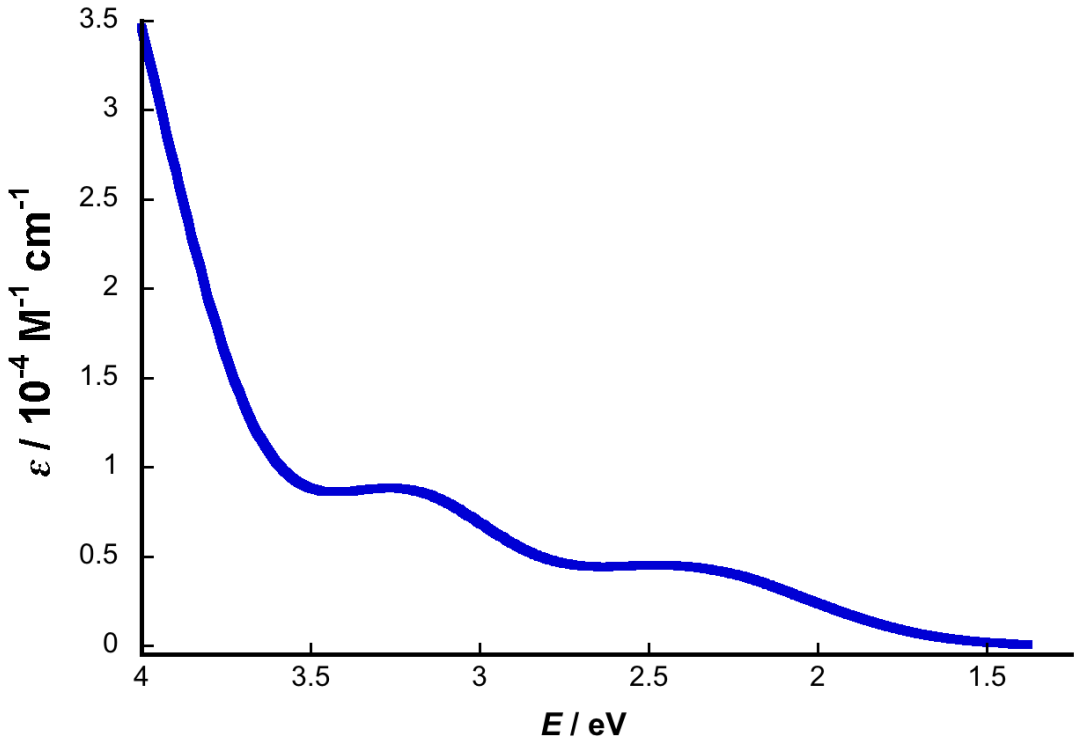

Figure 3.4.37. UV-Vis spectrum of **3.2-*p*NMe$_2$.**

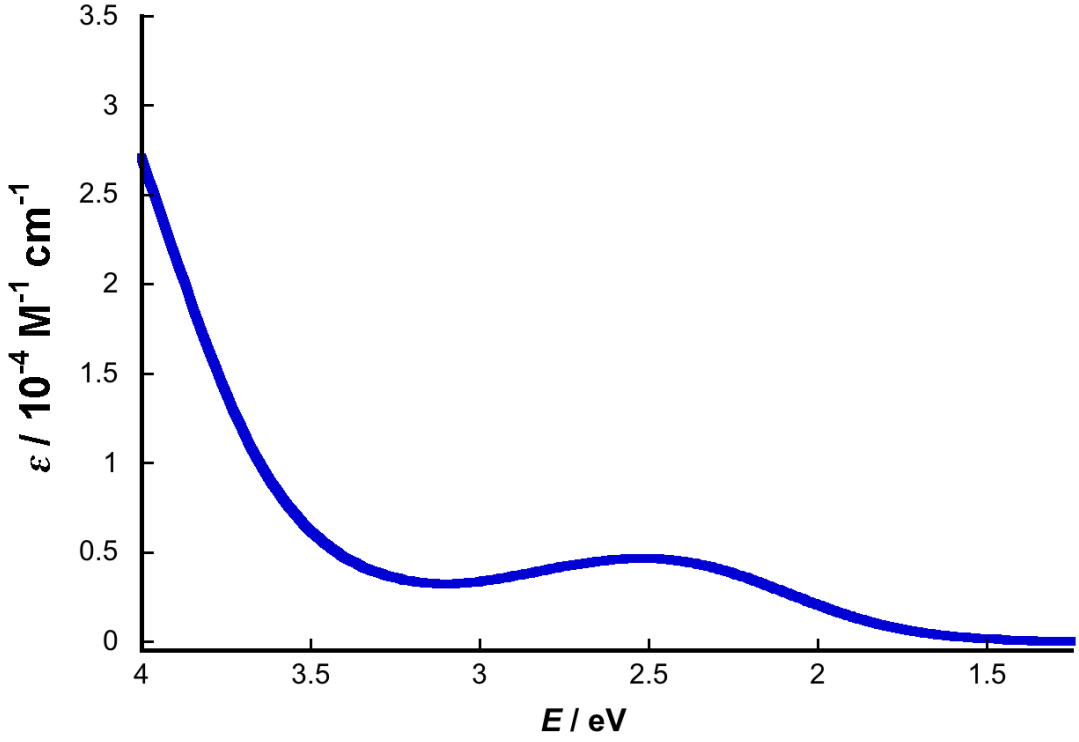

Figure 3.4.38. UV-Vis spectrum of **3.2-*m*NMe$_2$.**

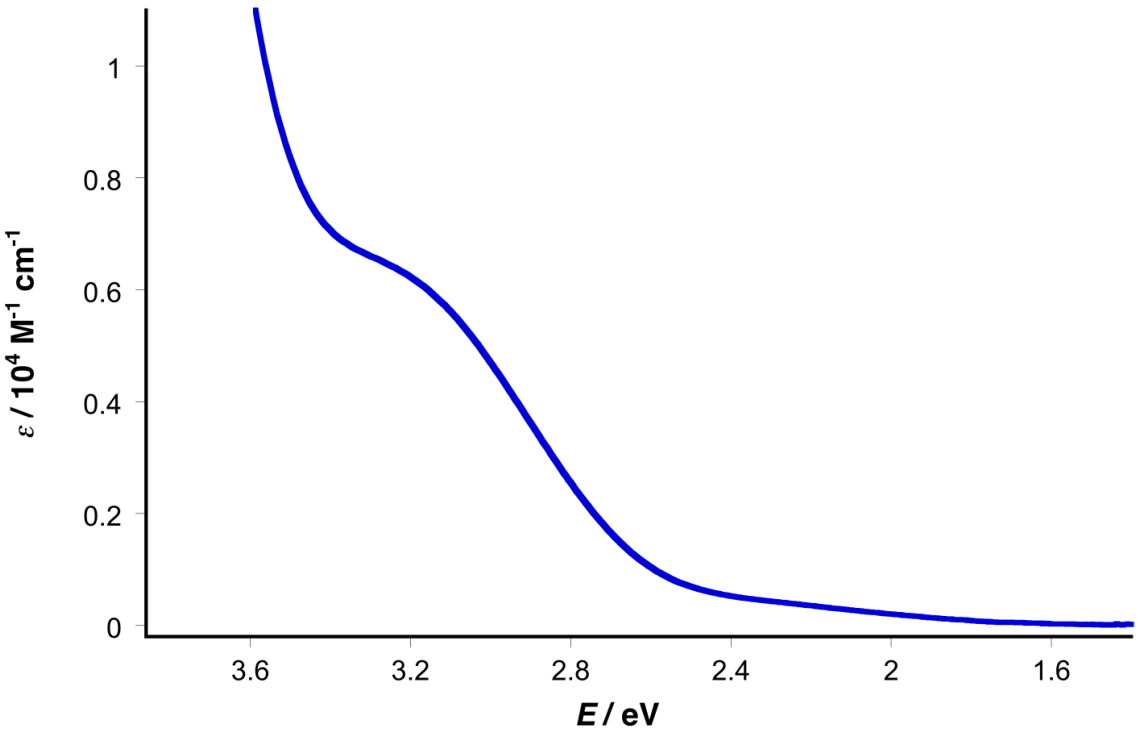

Figure 3.4.39. UV-Vis spectrum of **3.3-Ce.**

Electrochemistry. Cyclic voltammetry experiments were performed using a CH Instruments 620D Electrochemical Analyzer/Workstation and the data were processed using CHI software v 9.24. All experiments were performed in an N_2 atmosphere drybox using electrochemical cells that consisted of a 4 mL vial, glassy carbon (3 mm diameter) working electrode, a platinum wire counter electrode, and a silver wire plated with AgCl as a quasi-reference electrode. The working electrode surfaces were polished prior to each set of experiments, and were periodically replaced on scanning > 0 V versus ferrocene (Fc) to prevent the buildup of oxidized product on the electrode surfaces. Potentials were reported versus Fc, which was added as an internal standard for calibration at the end of each run. Solutions employed during CV studies were ~3 mM in analyte and 100 mM in $[^{n}Pr_4N][B(3,5\text{-}(CF_3)_2\text{-}C_6H_3)_4]$ ($[^{n}Pr_4N][BAr^{F}_4]$). All complexes were measured in 1:4 THF/AcN mixtures unless otherwise stated. The THF was necessary to dissolve the complexes in solution. All data were collected in a positive-feedback IR compensation mode. The solution cell resistances were measured prior to each run to ensure resistances ≤ ~500 Ω.[50] Scan rate dependences of 50–1000 mV/s were performed to determine electrochemical reversibility.

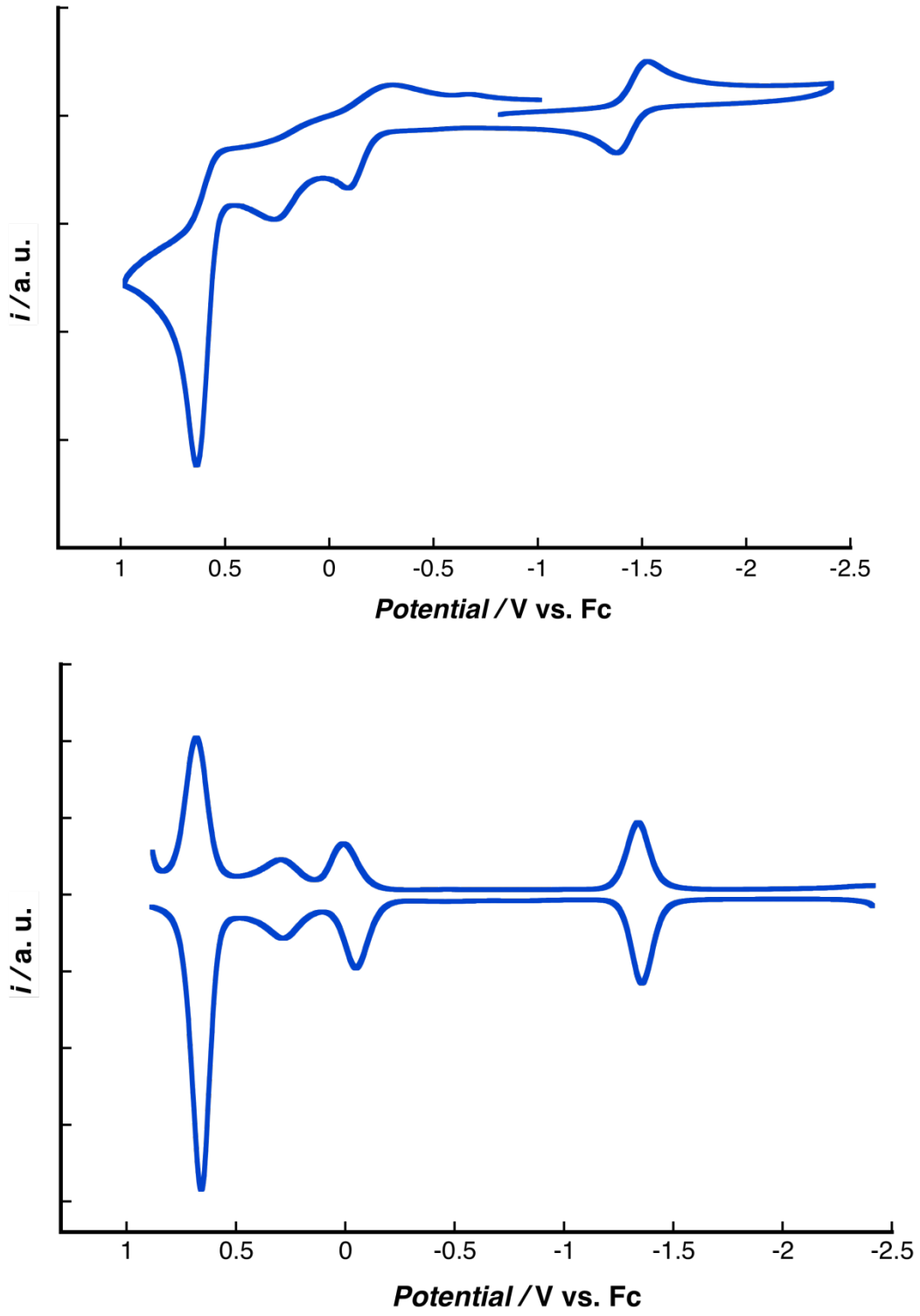

Figure 3.4.40. Cyclic voltammogram (top) and differential pulse voltammogram (bottom) of **3.2-CF_3.**

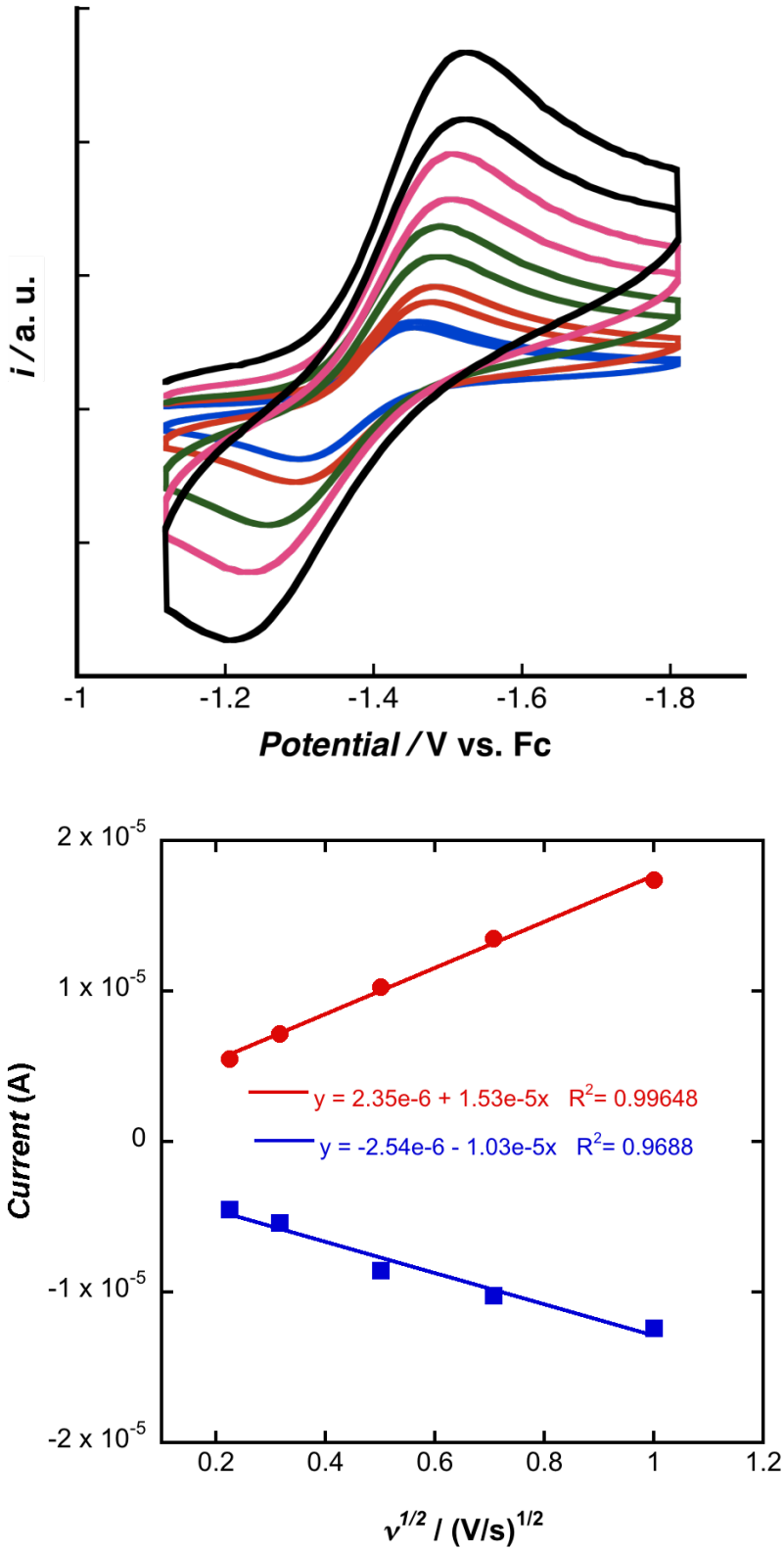

Figure 3.4.41. Scan rate dependence of the $Ce^{IV/III}$ couple of **3.2-CF$_3$**.

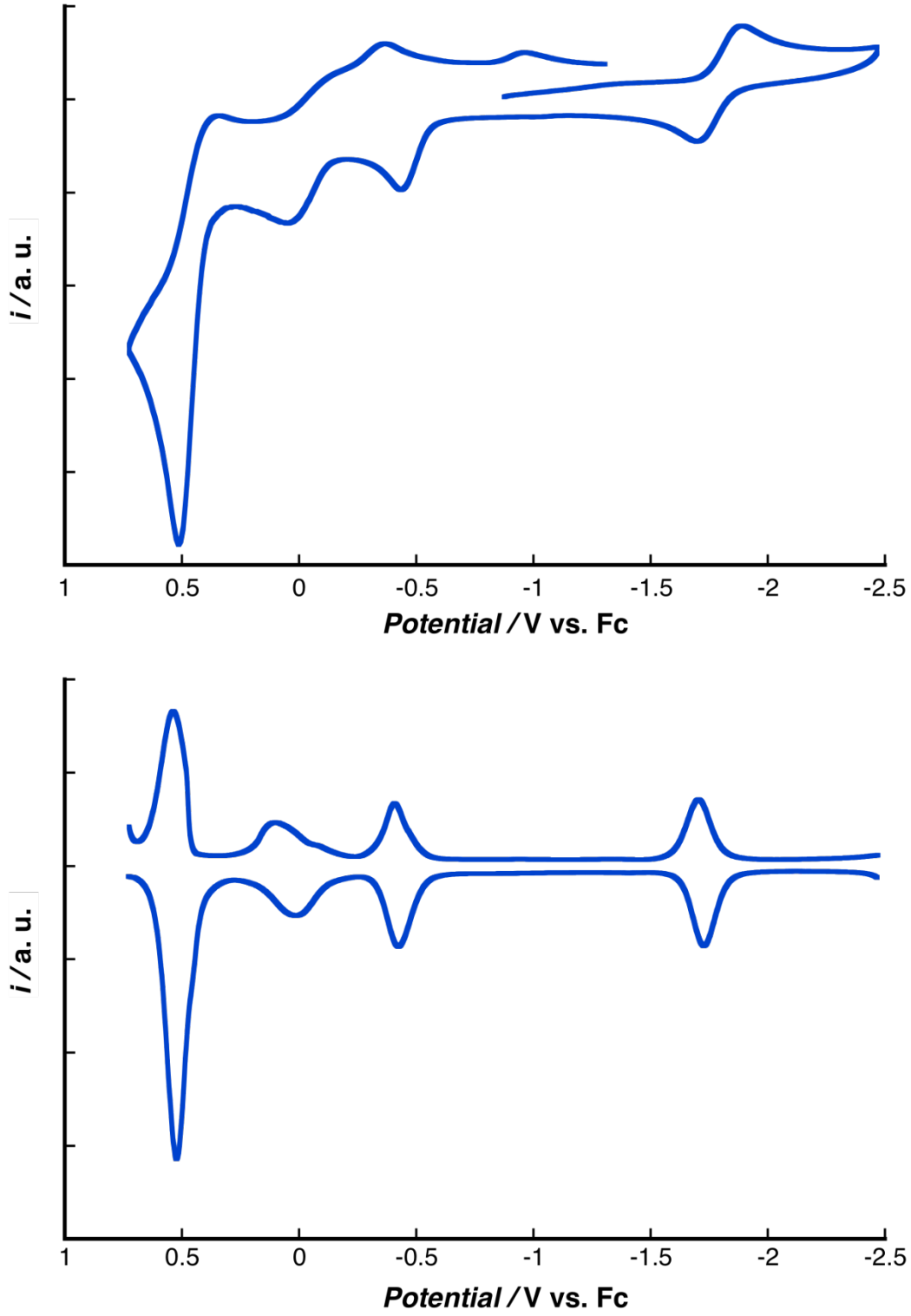

Figure 3.4.42. Cyclic voltammogram (top) and differential pulse voltammogram (bottom) of **3.2-H.**

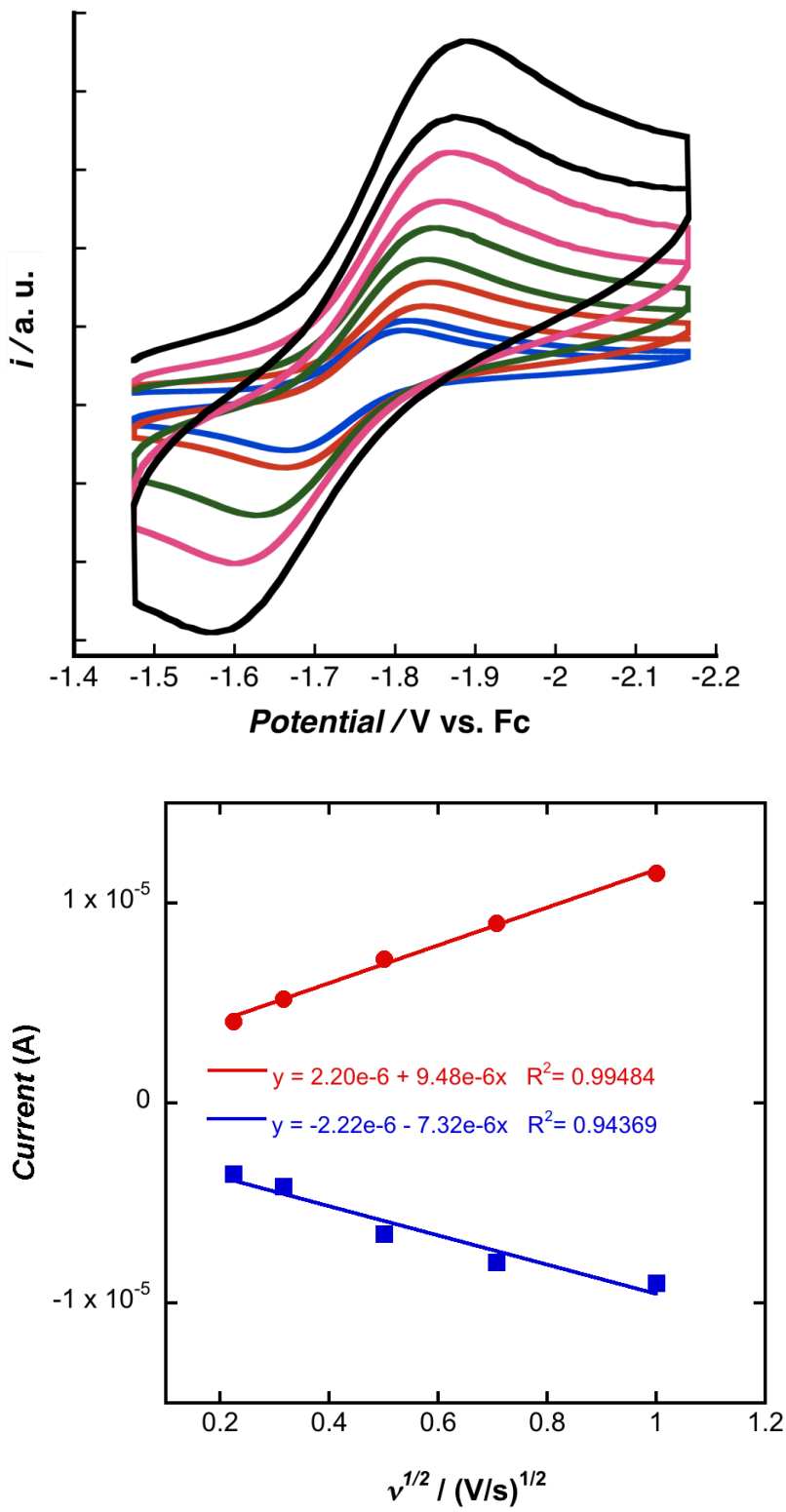

Figure 3.4.43. Scan rate dependence of the $Ce^{IV/III}$ couple of **3.2-H.**

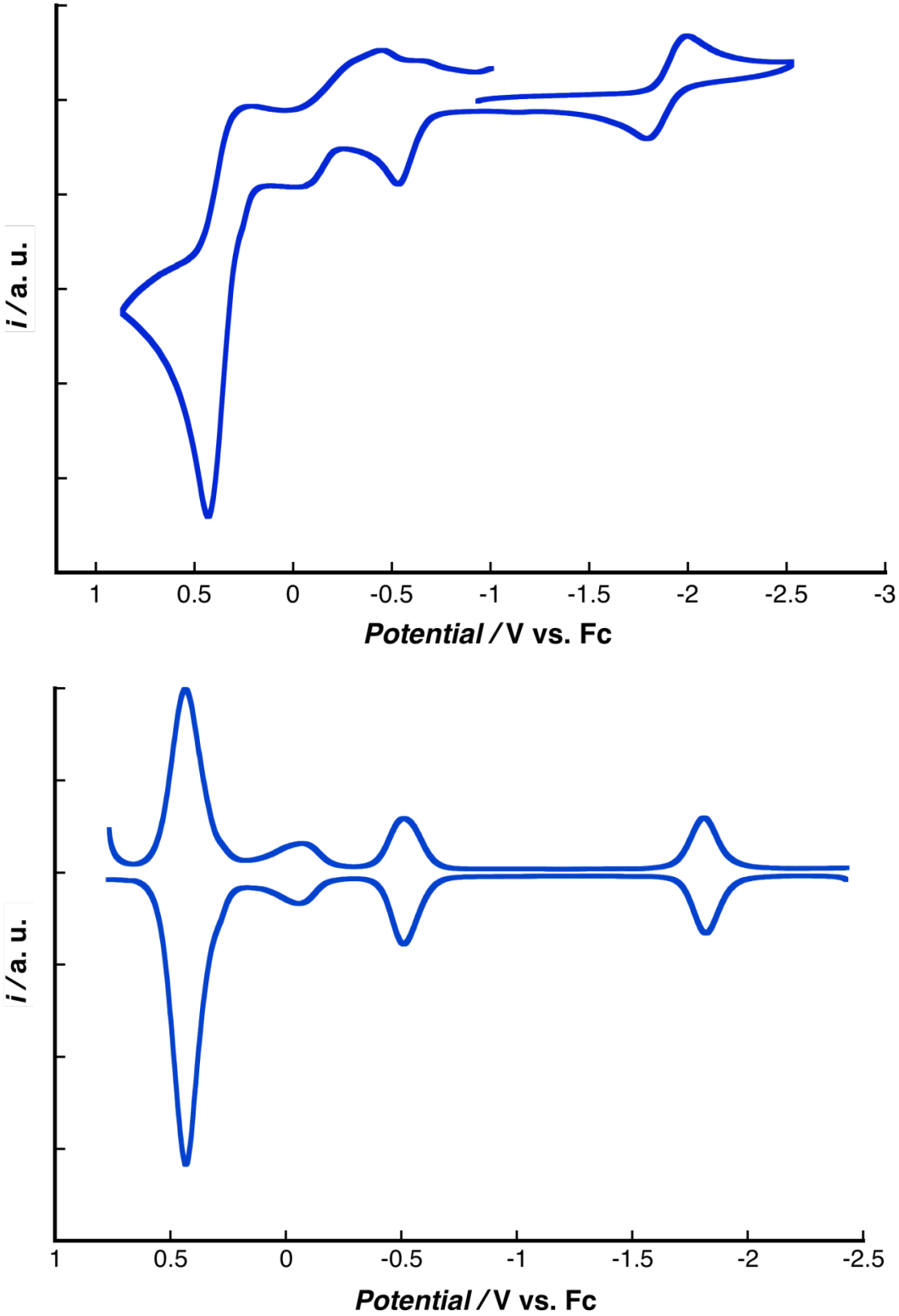

Figure 3.4.44. Cyclic voltammogram (top) and differential pulse voltammogram (bottom) of **3.2-Me.**

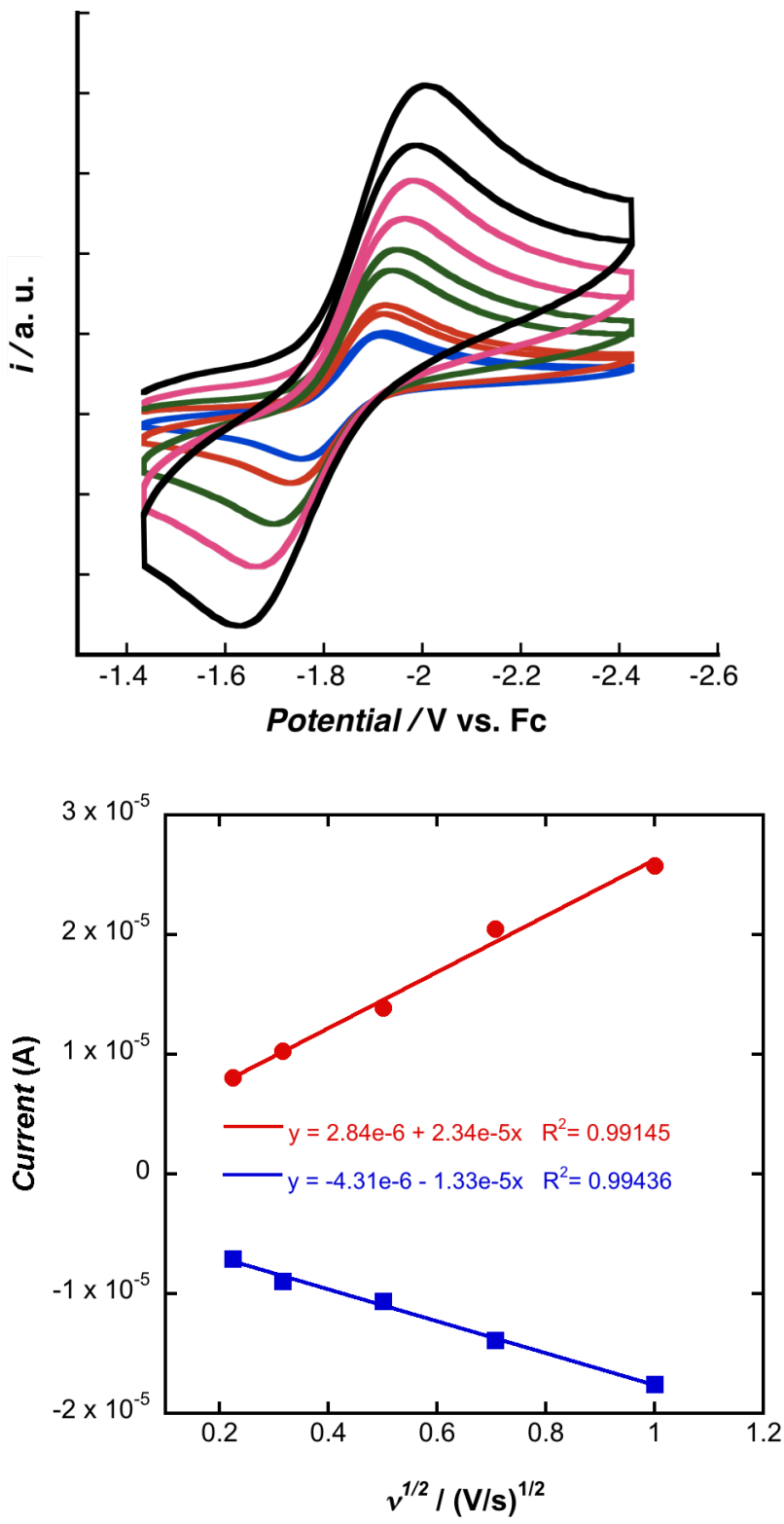

Figure 3.4.45. Scan rate dependence of the $Ce^{IV/III}$ couple of **3.2-Me.**

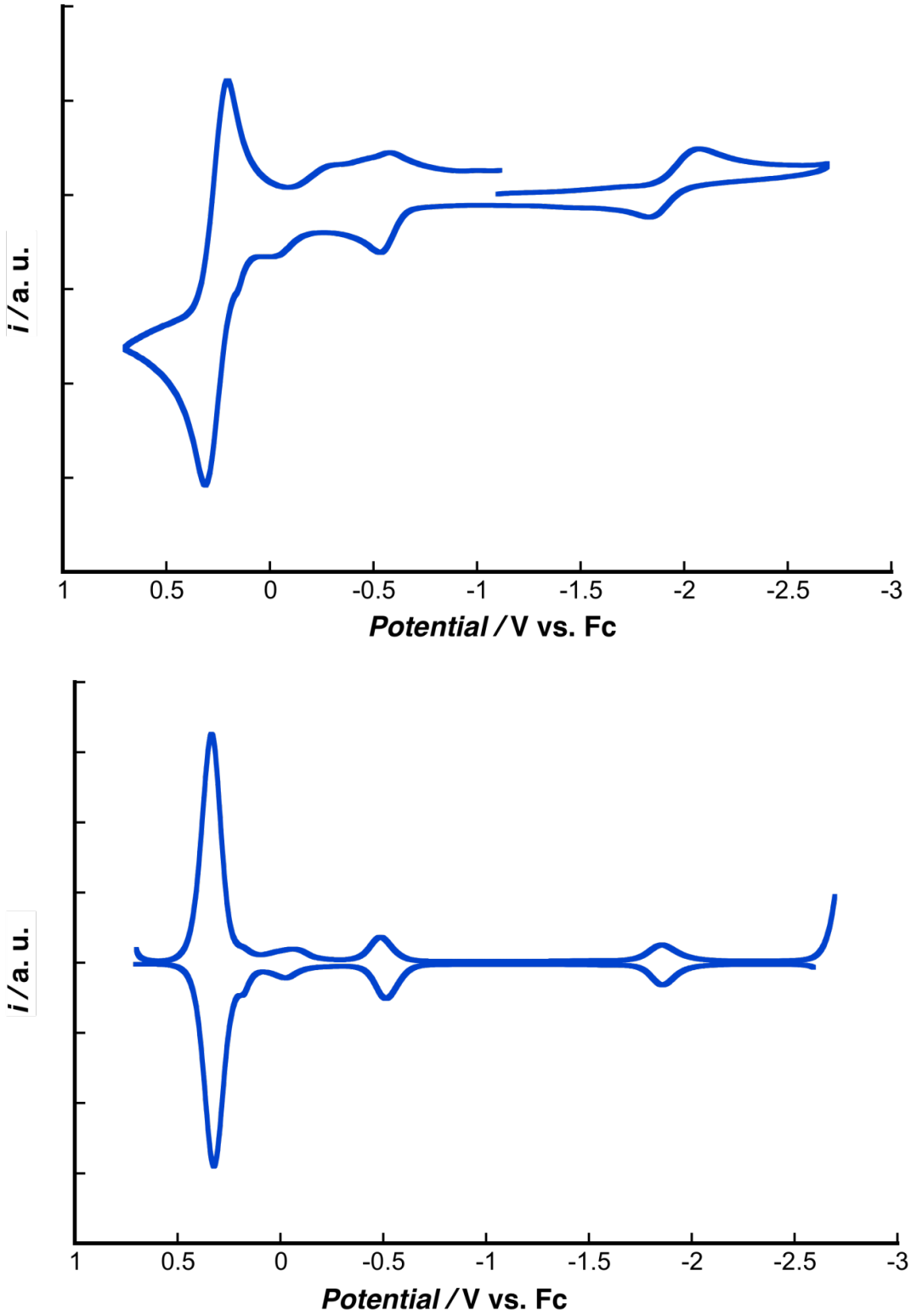

Figure 3.4.46. Cyclic voltammogram (top) and differential pulse voltammogram (bottom) of **3.2-OMe.**

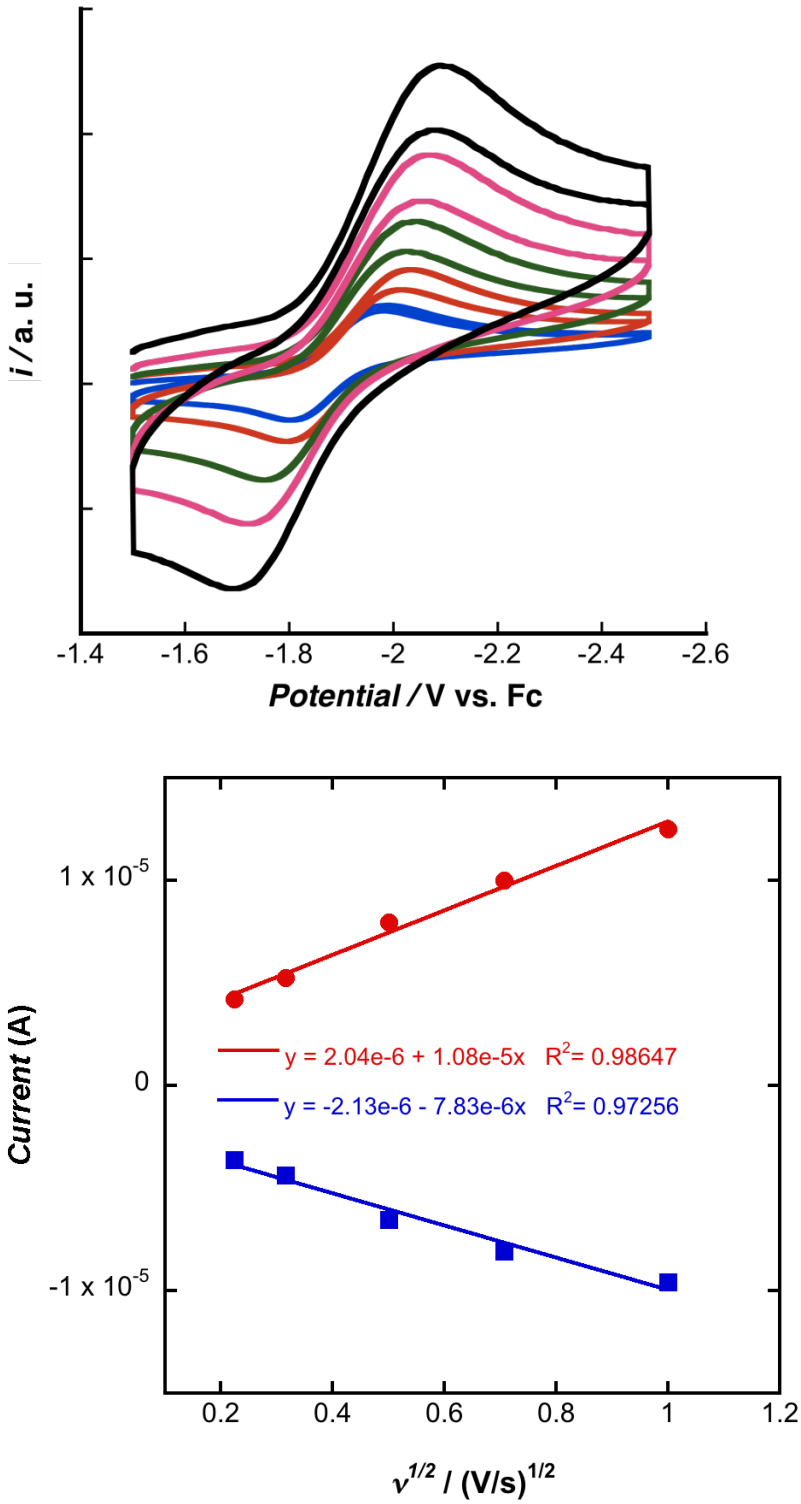

Figure 3.4.47. Scan rate dependence of the $Ce^{IV/III}$ couple of **3.2-OMe.**

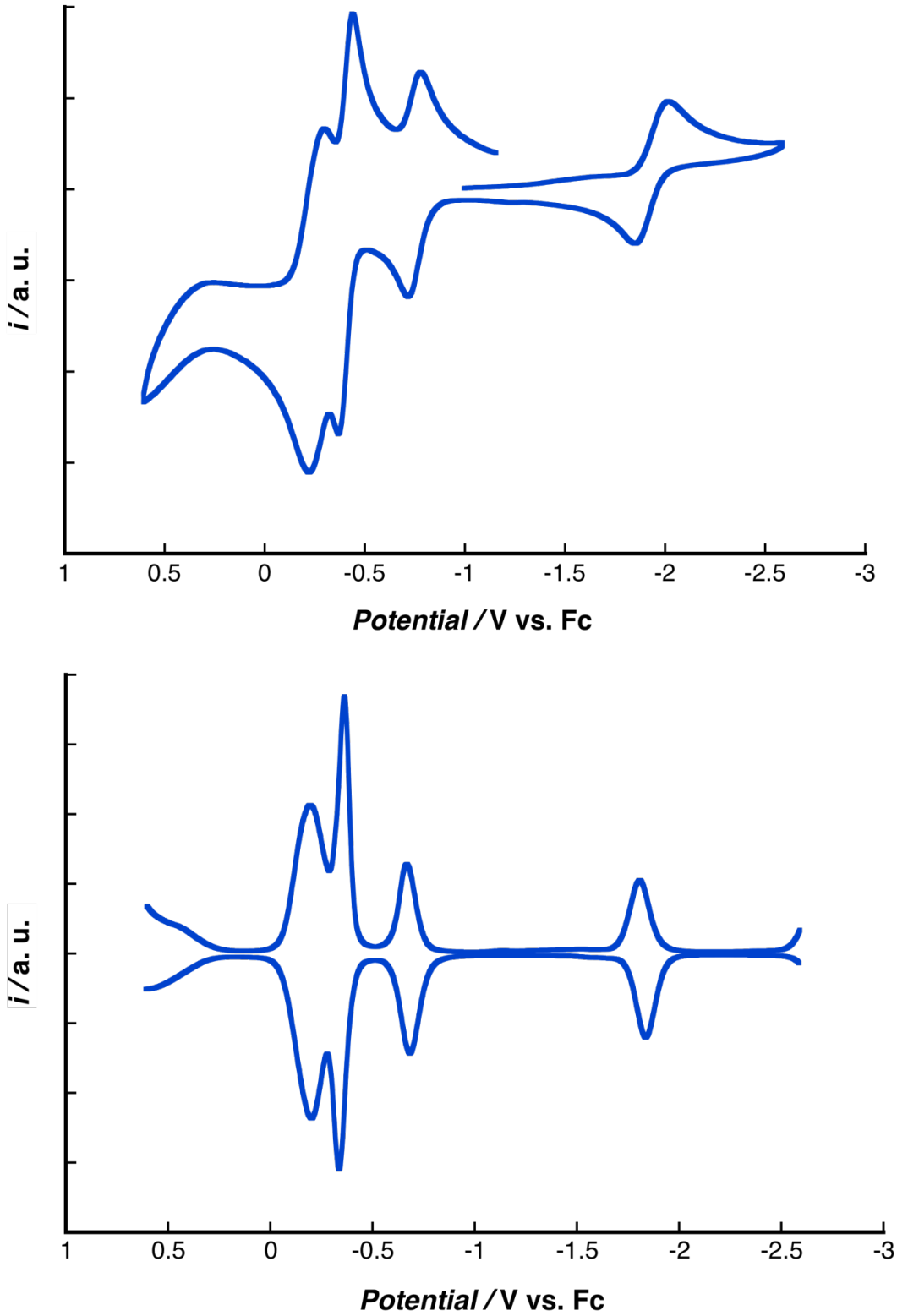

Figure 3.4.48. Cyclic voltammogram (top) and differential pulse voltammogram (bottom) of **3.2-*p*NMe$_2$**.

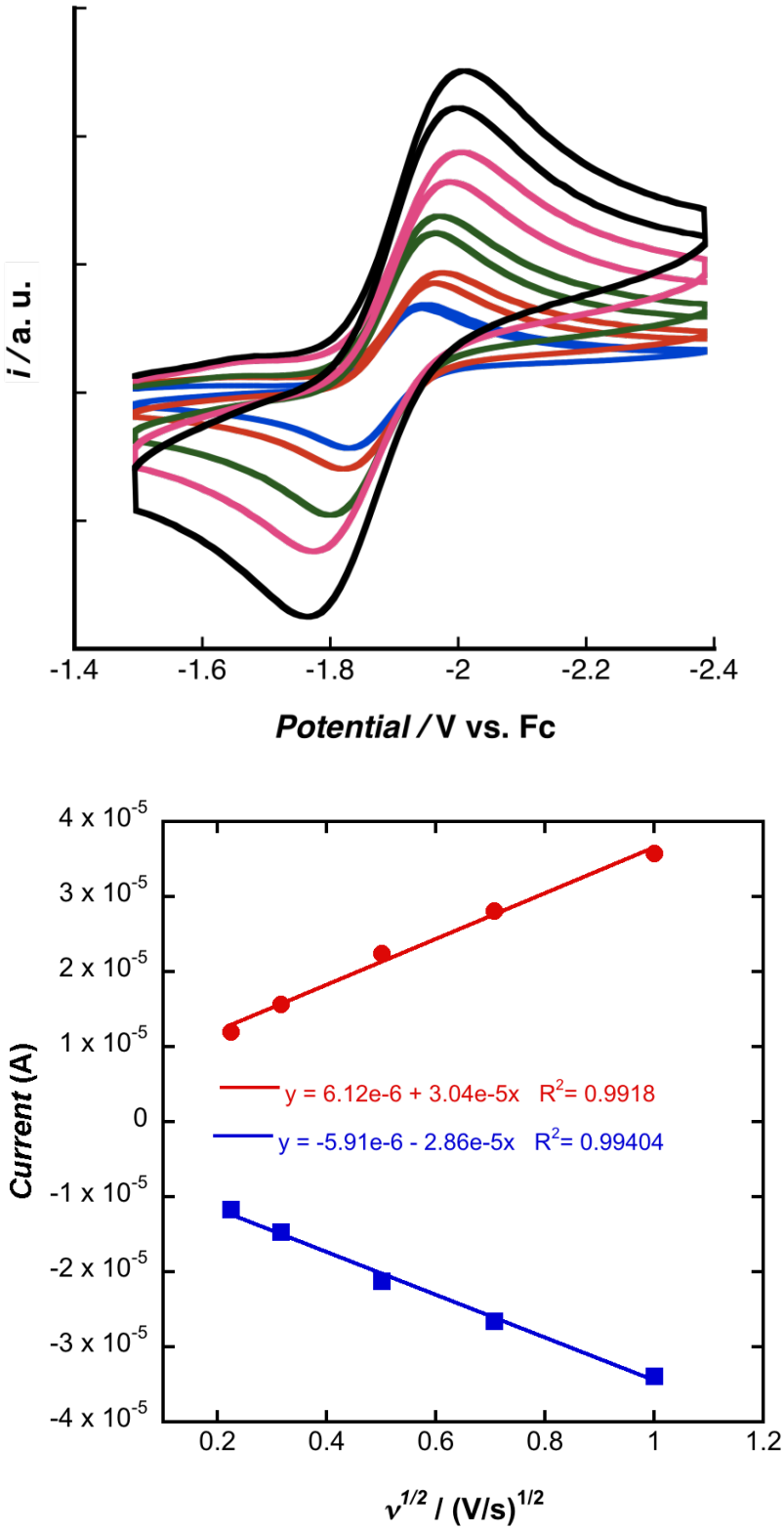

Figure 3.4.49. Scan rate dependence of the $Ce^{IV/III}$ couple of **3.2-*p*NMe$_2$**.

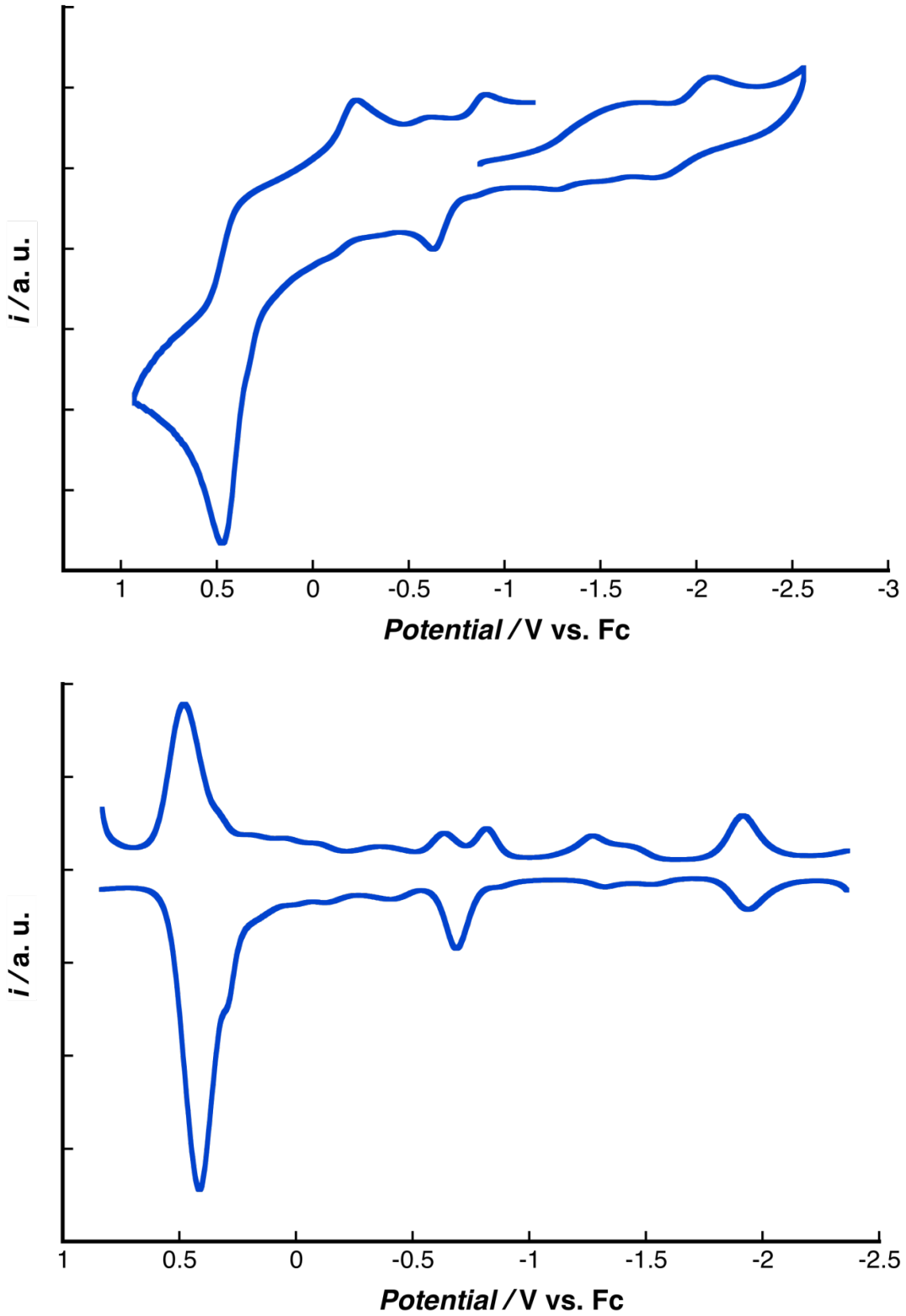

Figure 3.4.50. Cyclic voltammogram (top) and differential pulse voltammogram (bottom) of **3.2-*m*NMe$_2$.**

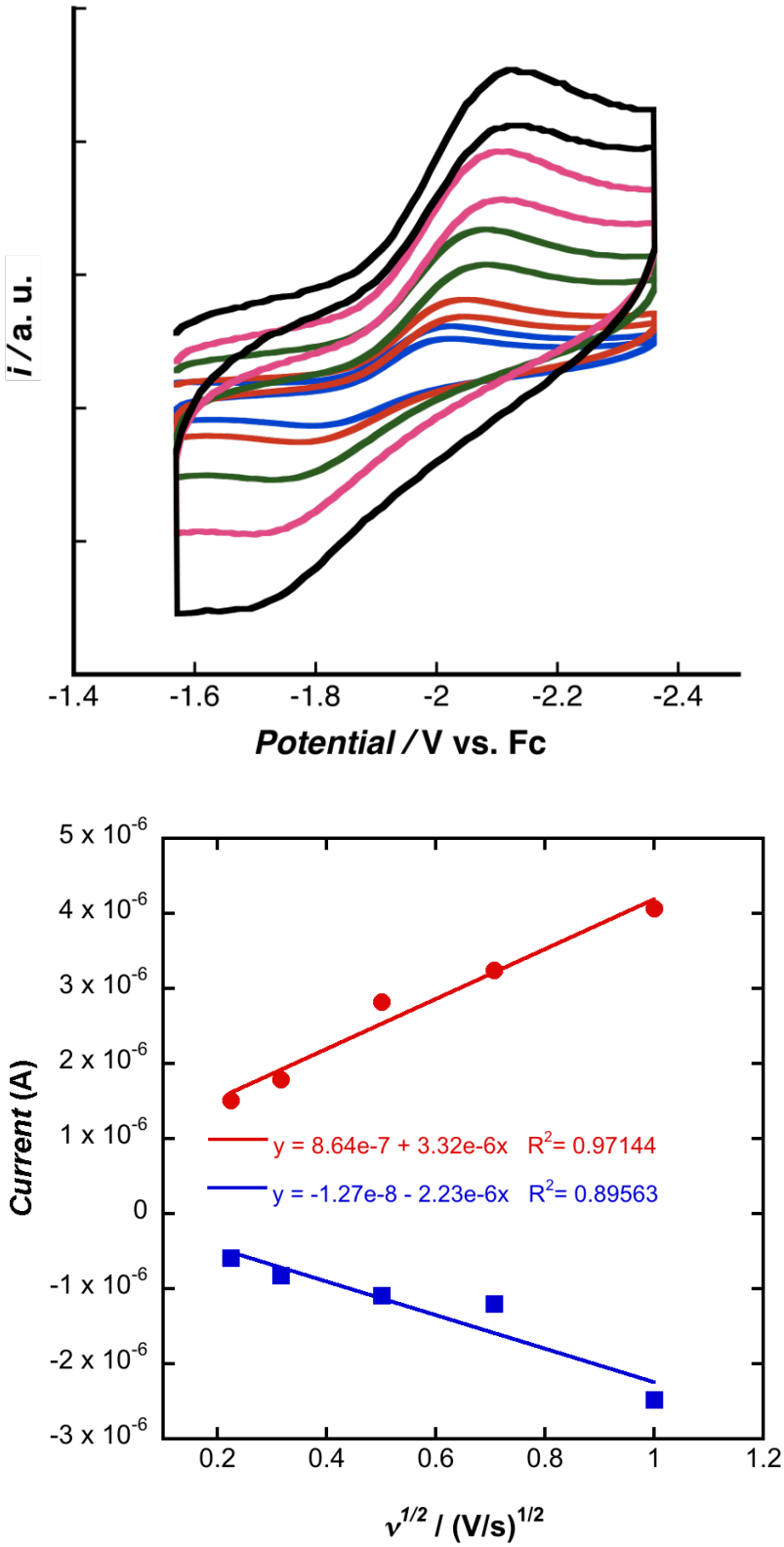

Figure 3.4.51. Scan rate dependence of the $Ce^{IV/III}$ couple of **3.2-*m*NMe$_2$.**

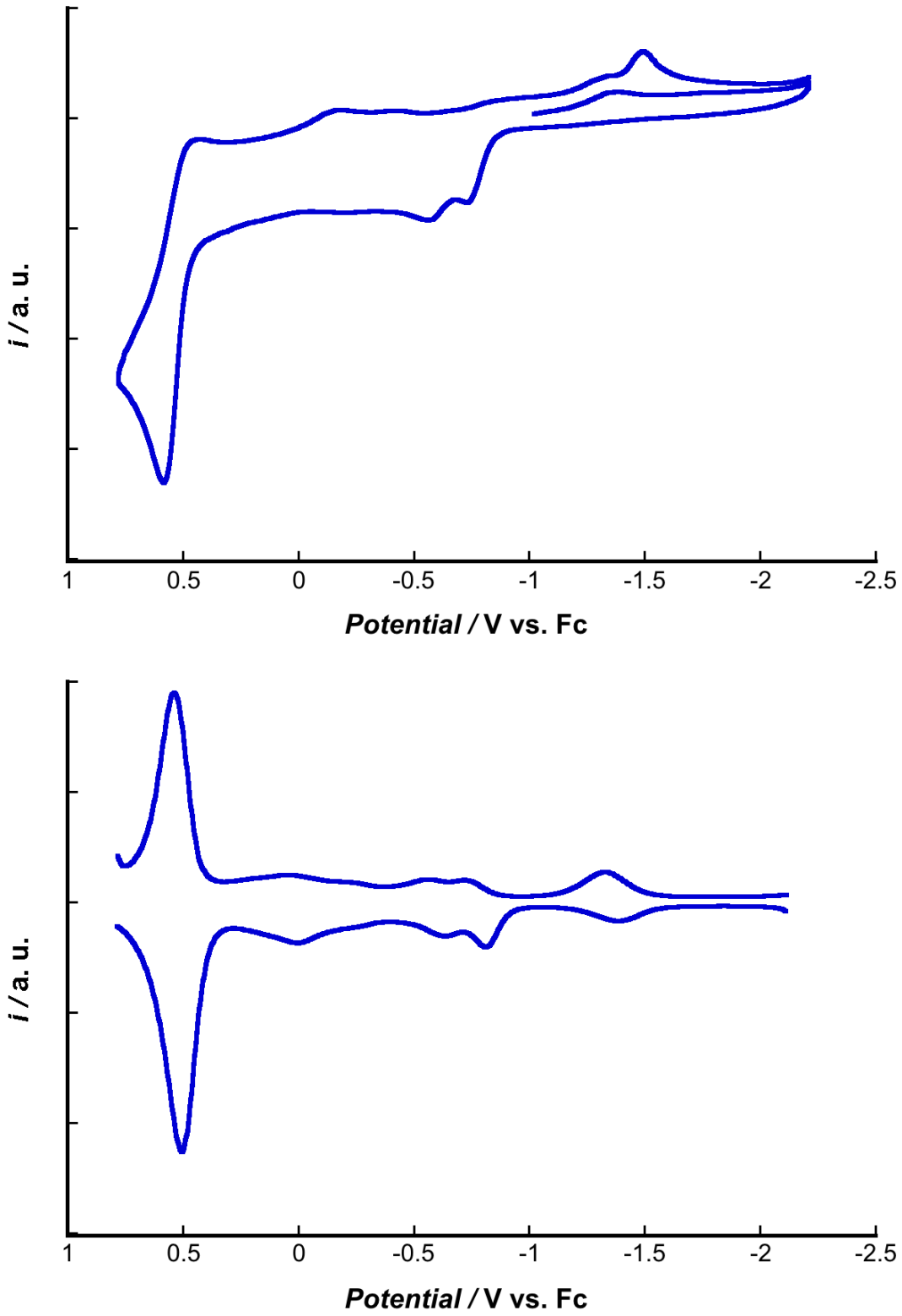

Figure 3.4.52. Cyclic voltammogram (top) and differential pulse voltammogram (bottom) of **3.3-La.** Measurements were performed in dichloromethane solutions.

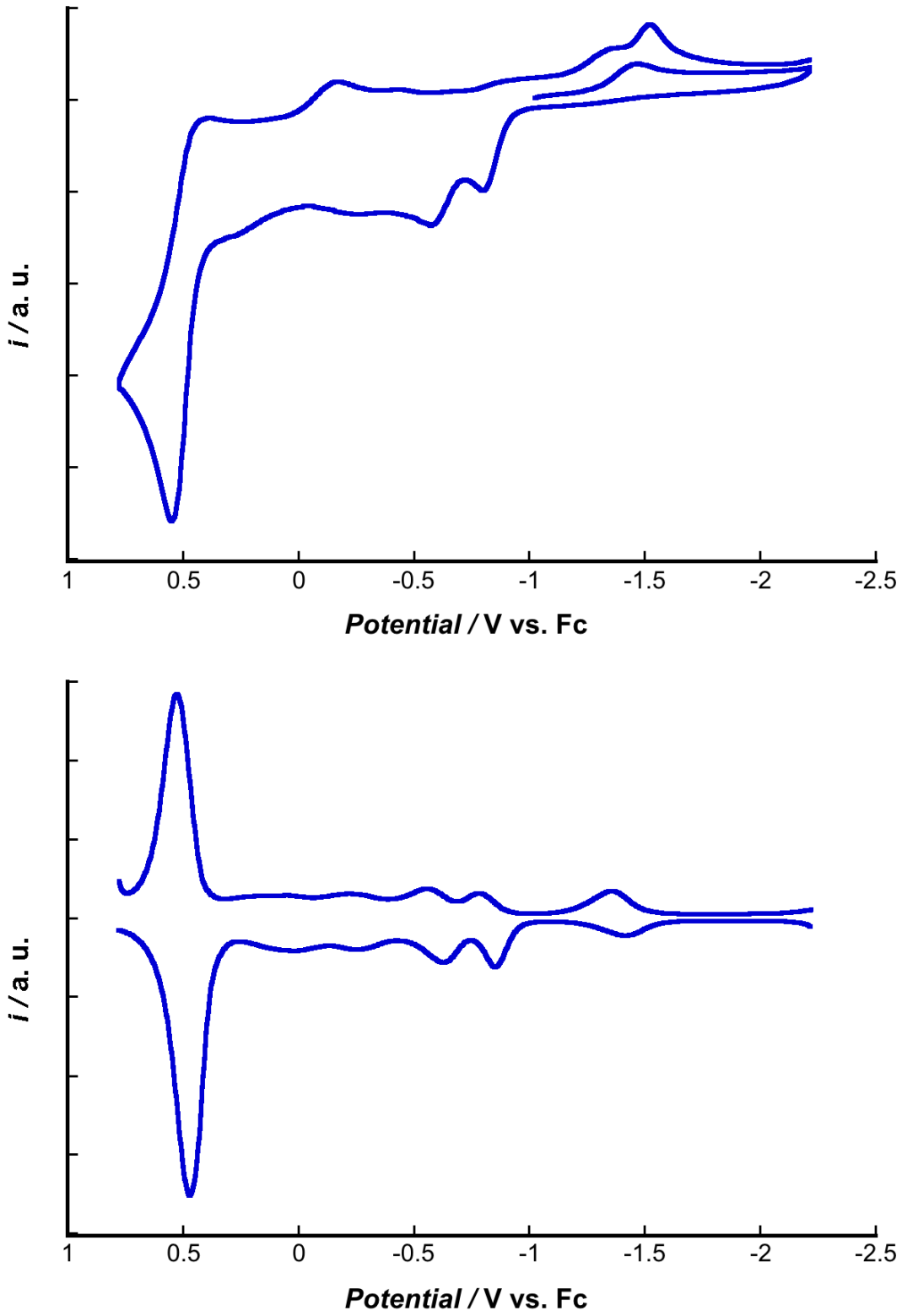

Figure 3.4.53. Cyclic voltammogram (top) and differential pulse voltammogram (bottom) of **3.3-Pr.** Measurements were performed in dichloromethane solutions.

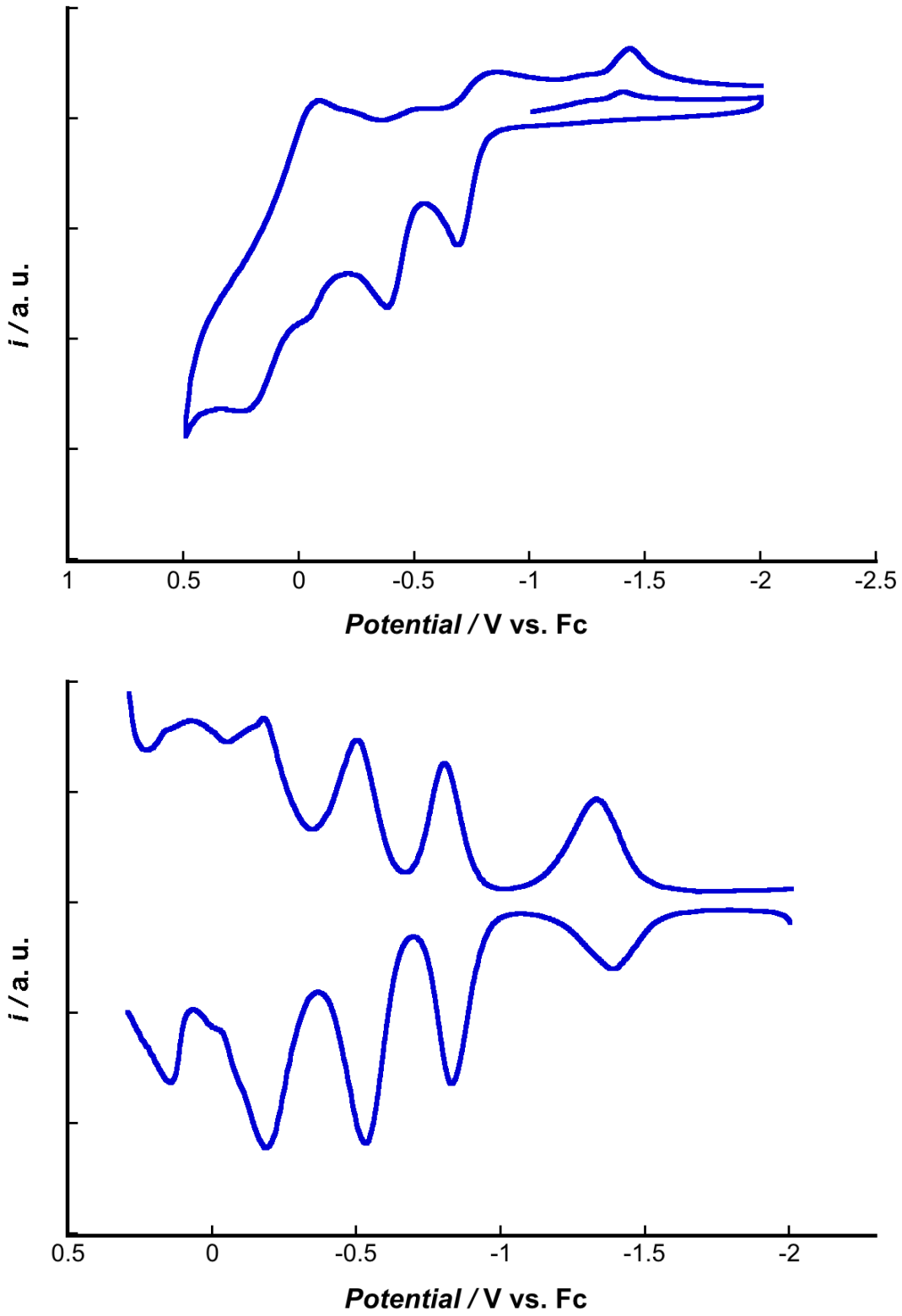

Figure 3.4.54. Cyclic voltammogram (top) and differential pulse voltammogram (bottom) of **3.3-Tb.** Measurements were performed in dichloromethane solutions.

Table 3.4.21. Calculated and experimental electrochemical data. Units are in V.

	E_{pa}	E_{pc}	ΔE	$E_{1/2}$ exp	$E_{1/2}$ calc	$E_{1/2}$ corr
3.2-CF$_3$	–1.38	–1.53	0.15	–1.46	–1.73	–1.43
3.2-H	–1.70	–1.89	0.19	–1.80	–2.11	–1.81
3.2-Me	–1.80	–2.00	0.20	–1.90	–2.23	–1.93
3.2-OMe	–1.83	–2.07	0.24	–1.95	–2.21	–1.91
3.2-*p*NMe$_2$	–1.85	–2.02	0.17	–1.94	–2.20	–1.90
3.2-*m*NMe$_2$	–1.78	–2.09	0.31	–1.94	–2.42	–2.12
$[^{n}Bu_4N]_2[Ce(NO_3)_6]$			0.08	0.62	0.19	0.49
$Ce(acac)_2$	–0.31	–0.45	0.14	–0.38	–0.72	–0.42
$Ce(BrSALEN)_2$				–0.92	–0.85	–0.55
$Ce(SALEN)_2$				–1.08	–1.22	–0.92
$Ce(OMeSALEN)_2$				–1.18	–1.33	–1.03
$Ce(OQ)_2$	–0.55	–0.67	0.12	–0.61	–1.08	–0.78
$Ce(HA)_4$	–0.94	–1.66	0.72	–1.30	–1.58	–1.28
$Ce(C_8H_8)$				–1.40	–1.55	–1.25
$Ce(omtaa)_2$				–1.63	–1.51	–1.21

Computational Details. Gaussian 09 Rev. A.02 was used in electronic structure calculations.[58] The B3LYP hybrid DFT method was employed, with a 28-electron small core pseudopotential on cerium with published segmented natural orbital basis set incorporating quasi-relativistic effects,[59] and the 6-31G* basis set on all other atoms. No restraints were imposed other than spin. Molecular orbitals were rendered with the program Chemcraft v1.6.[60] Mayer bond orders and atomic orbital contributions to individual molecular orbitals were calculated with the AOMix program[61],[62] through fragment molecular orbital analysis, with the following fragments: 1 - Ce, 2 - [R-2-(^{t}BuNO)py]$_4$. The D_{2d} calculated structure of complex **3.2-OMe** was used in the correlation rather than the crystallographically observed S_4 structure. This is because in solution it is expected that this complex has a similar structure to the other analogues due to the removal of crystal packing effects.

Table 3.4.22. Computed Thermal Free Energies, G, and ΔG values for the series of cerium complexes in their anionic Ce^{III} and neutral Ce^{IV} forms. Units are in eV.

	G_{Ce}^{III}	G_{Ce}^{IV}	$\Delta G_{Ce}^{III/IV}$
3.2-CF_3	–107887.7076	–107884.3631	–3.3445
3.2-H	–71201.9416	–71198.9758	–2.9658
3.2-Me	–75478.5763	–75475.7213	–2.8550
3.2-OMe (D_{2d})	–83662.5949	–83659.7227	–2.8722
3.2-*p*NMe_2	–85775.6384	–85772.7595	–2.8788
3.2-*m*NMe_2	–85776.5127	–85773.8531	–2.6596
$[Et_4N]_2[Ce(NO_3)_6]$	–78917.9683	–78912.6982	–5.2700
$Ce(acac)_4$	–50505.4729	–50501.1133	–4.3596
$Ce(BrSALEN)_2$	–340540.1803	–340535.9460	–4.2343
$Ce(SALEN)_2$	–60844.1802	–60840.4997	–3.6805
$Ce(OMeSALEN)_2$	–73177.3921	–73173.6389	–3.7534
$Ce(OQ)_4$	–64800.3707	–64796.3698	–4.0009
$Ce(HA)_4$	–81791.6566	–81788.1594	–3.4972
$Ce(C_8H_8)$	–29779.8317	–29776.3023	–3.5294
$Ce(omtaa)_2$	–79735.9060	–79732.3334	–3.5725

Natural Transition Orbitals of **3.2-H** from TD-DFT:

Transition 15 (1.806 eV):

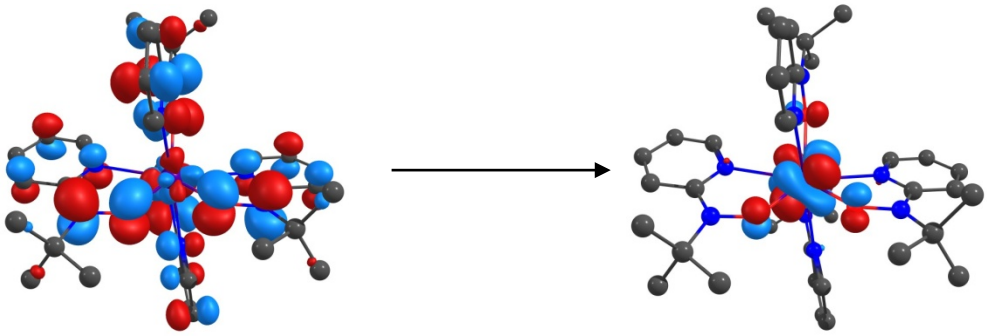

HOTO LUTO

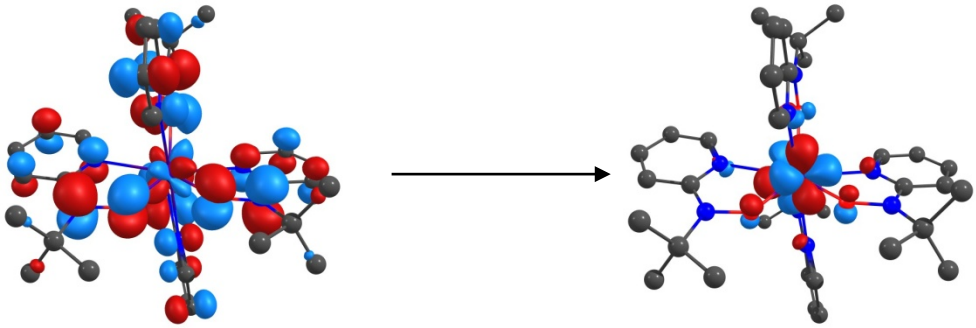

HOTO–1 LUTO+1

Transition 16 (1.814 eV):

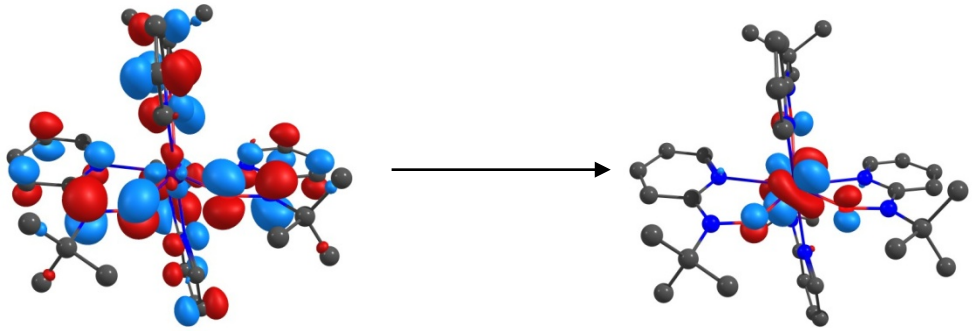

HOTO LUTO

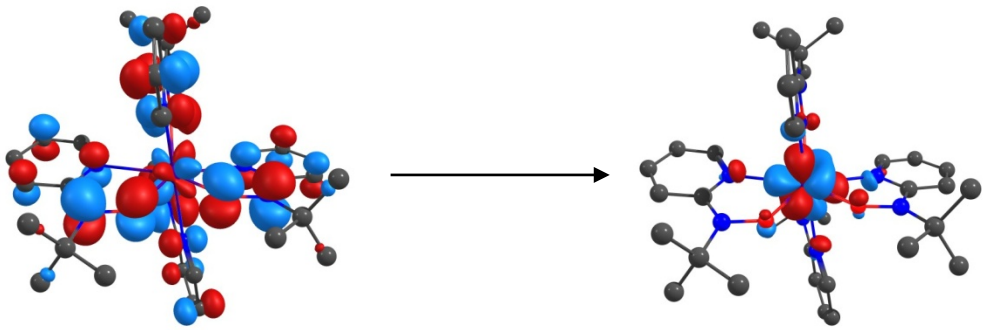

HOTO–1 LUTO+1

Transition 24 (2.108 eV):

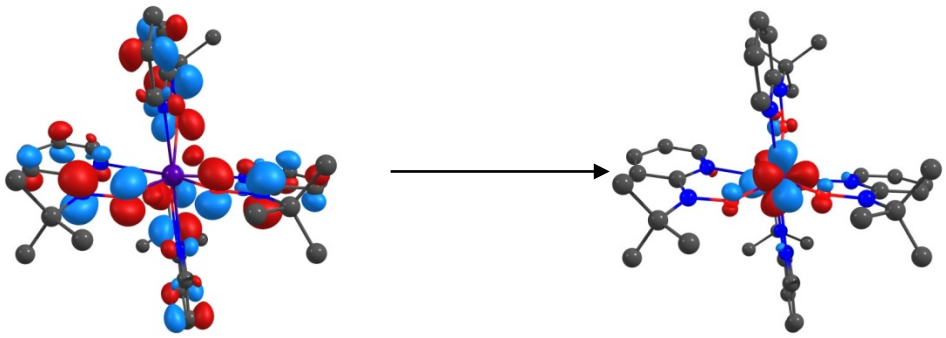

HOTO LUTO

Transition 29 (3.314 eV):

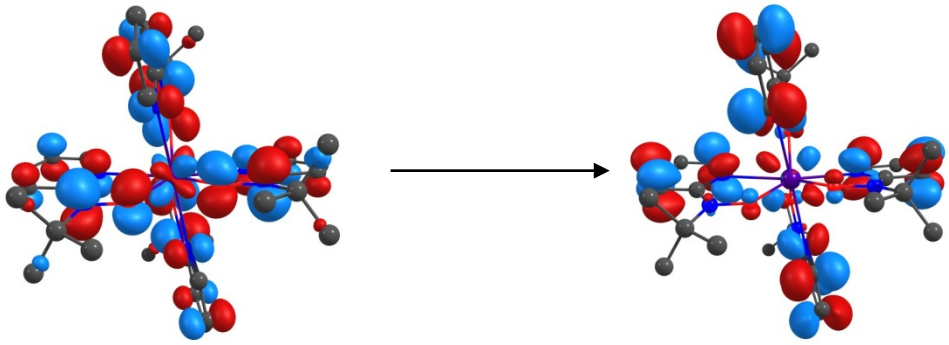

HOTO LUTO

Transition 30 (3.389 eV):

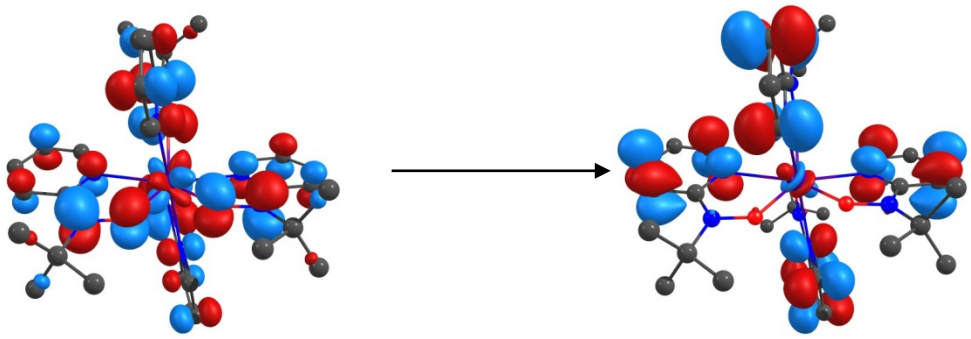

HOTO LUTO

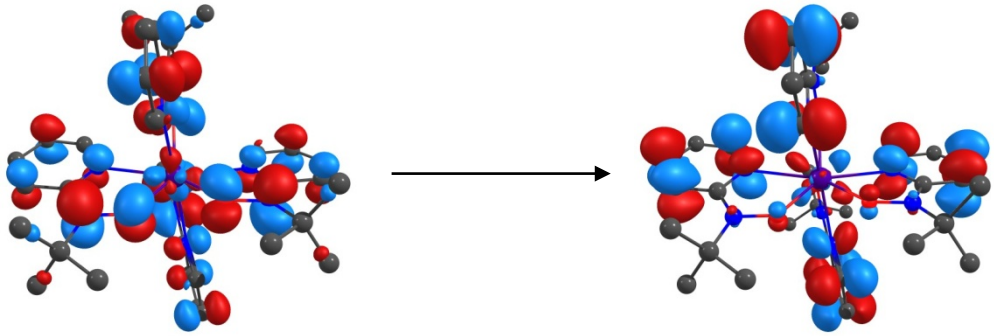

HOTO–1 LUTO+1

Transition 31 (3.420 eV):

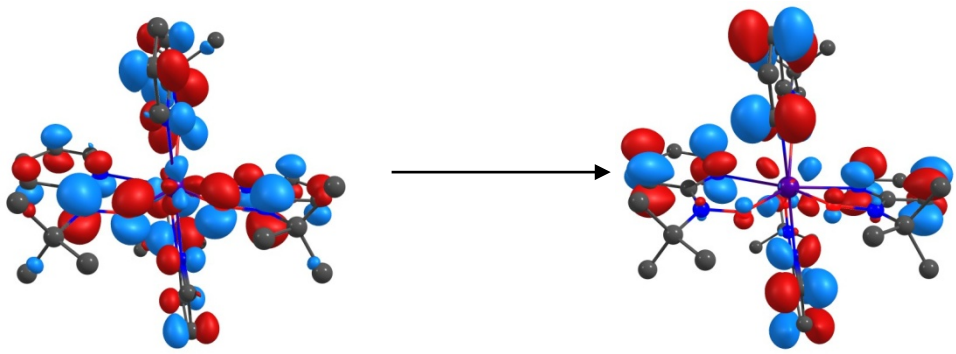

HOTO LUTO

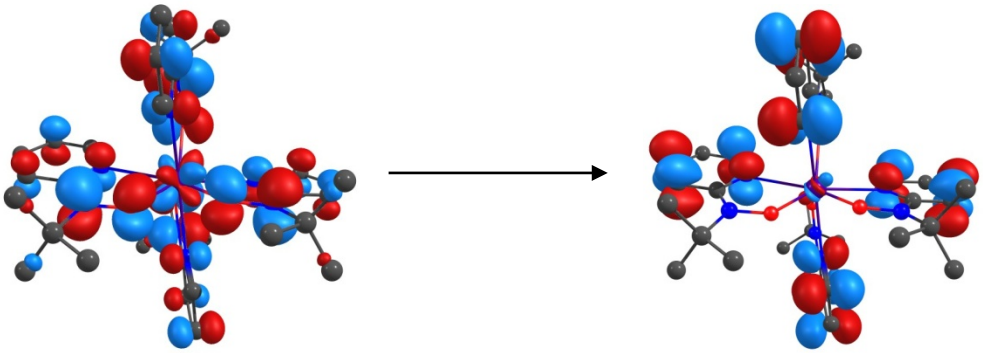

HOTO–1 LUTO+1

Table 3.4.23. Optimized coordinates of **Ce^{III}[5-CF_3-2-(^{t}BuNO)py]$_4^-$**

Ce	0.000068000	-0.000050000	0.000015000
N	2.156683000	-0.415171000	1.590381000
C	2.710821000	0.671546000	2.220986000
N	2.077821000	1.842555000	2.009886000
O	0.971641000	1.813203000	1.208872000
C	2.441254000	3.183879000	2.584990000
C	2.340254000	3.151784000	4.125814000
H	1.323408000	2.877764000	4.427805000
H	2.558948000	4.146579000	4.529479000
H	3.031303000	2.447388000	4.593417000
C	3.841844000	3.619927000	2.099840000
H	4.642160000	2.949505000	2.419430000
H	4.069345000	4.616120000	2.495246000
H	3.864069000	3.675064000	1.006589000
C	1.428879000	4.224391000	2.074078000
H	1.446924000	4.302351000	0.985326000
H	1.700575000	5.197259000	2.498389000

H	0.410841000	3.980806000	2.383809000
C	3.889067000	0.492020000	3.024801000
H	4.337661000	1.316260000	3.557110000
C	4.466401000	-0.749738000	3.111684000
H	5.364464000	-0.880908000	3.708729000
C	3.904197000	-1.848859000	2.419751000
C	2.747776000	-1.608175000	1.690087000
H	2.264106000	-2.405259000	1.132455000
C	4.508115000	-3.201034000	2.510967000
F	5.859560000	-3.172865000	2.361316000
F	4.291688000	-3.805124000	3.714330000
F	4.022908000	-4.053385000	1.570675000
N	-2.156381000	0.414710000	1.590672000
C	-2.710535000	-0.672170000	2.220981000
N	-2.077623000	-1.843155000	2.009465000
O	-0.971480000	-1.813607000	1.208411000
C	-2.441180000	-3.184671000	2.584042000
C	-1.428981000	-4.225110000	2.072629000
H	-1.447102000	-4.302608000	0.983844000
H	-1.700788000	-5.198121000	2.496544000
H	-0.410890000	-3.981800000	2.382401000
C	-2.340090000	-3.153249000	4.124876000
H	-2.558900000	-4.148185000	4.528129000
H	-3.031011000	-2.448956000	4.592823000
H	-1.323188000	-2.879501000	4.426926000
C	-3.841850000	-3.620324000	2.098770000
H	-3.864126000	-3.674986000	1.005491000

H	-4.642064000	-2.949931000	2.418680000
H	-4.069466000	-4.616657000	2.493757000
C	-3.888759000	-0.492836000	3.024870000
H	-4.337385000	-1.317219000	3.556929000
C	-4.466039000	0.748922000	3.112140000
H	-5.364086000	0.879951000	3.709238000
C	-3.903818000	1.848221000	2.420503000
C	-2.747430000	1.607705000	1.690736000
H	-2.263761000	2.404923000	1.133294000
C	-4.507712000	3.200381000	2.512091000
F	-4.291345000	3.804097000	3.715652000
F	-4.022434000	4.053001000	1.572079000
F	-5.859150000	3.172284000	2.362351000
N	-2.156534000	-0.414860000	-1.590433000
C	-2.710782000	0.672013000	-2.220675000
N	-2.077858000	1.843006000	-2.009239000
O	-0.971626000	1.813480000	-1.208307000
C	-2.441507000	3.184523000	-2.583756000
C	-2.340572000	3.153142000	-4.124602000
H	-1.323692000	2.879433000	-4.426761000
H	-2.559452000	4.148083000	-4.527807000
H	-3.031517000	2.448843000	-4.592501000
C	-3.842133000	3.620134000	-2.098323000
H	-4.642363000	2.949717000	-2.418144000
H	-4.069824000	4.616462000	-2.493279000
H	-3.864286000	3.674791000	-1.005041000
C	-1.429274000	4.224970000	-2.072427000

H	-1.447269000	4.302431000	-0.983638000
H	-1.701155000	5.197987000	-2.496278000
H	-0.411214000	3.981694000	-2.382328000
C	-3.889107000	0.492661000	-3.024415000
H	-4.337825000	1.317041000	-3.556401000
C	-4.466364000	-0.749110000	-3.111634000
H	-5.364483000	-0.880153000	-3.708623000
C	-3.904029000	-1.848406000	-2.420086000
C	-2.747564000	-1.607868000	-1.690445000
H	-2.263817000	-2.405081000	-1.133064000
C	-4.507881000	-3.200588000	-2.511641000
F	-5.859312000	-3.172536000	-2.361843000
F	-4.291544000	-3.804305000	-3.715207000
F	-4.022531000	-4.053188000	-1.571648000
N	2.156481000	0.415271000	-1.590602000
C	2.710718000	-0.671424000	-2.221158000
N	2.077876000	-1.842498000	-2.009917000
O	0.971724000	-1.813212000	-1.208865000
C	2.441451000	-3.183858000	-2.584838000
C	1.429313000	-4.224417000	-2.073558000
H	1.447549000	-4.302158000	-0.984793000
H	1.701081000	-5.197329000	-2.497721000
H	0.411189000	-3.981039000	-2.383170000
C	2.340206000	-3.152111000	-4.125656000
H	2.558991000	-4.146960000	-4.529140000
H	3.031065000	-2.447712000	-4.593529000
H	1.323269000	-2.878319000	-4.427547000

C	3.842173000	-3.619586000	-2.099777000
H	3.864541000	-3.674495000	-1.006513000
H	4.642343000	-2.949102000	-2.419601000
H	4.069782000	-4.615824000	-2.495006000
C	3.888887000	-0.491806000	-3.025068000
H	4.337571000	-1.316031000	-3.557320000
C	4.465987000	0.750043000	-3.112180000
H	5.363952000	0.881298000	-3.709353000
C	3.903627000	1.849170000	-2.420384000
C	2.747348000	1.608369000	-1.690530000
H	2.263571000	2.405444000	-1.132976000
C	4.507252000	3.201454000	-2.511953000
F	4.290758000	3.805144000	-3.715504000
F	4.021806000	4.053981000	-1.571945000
F	5.858696000	3.173631000	-2.362224000

Table 3.4.24. Optimized coordinates of **Ce^{IV}[5-Me-2-(^{t}BuNO)py]$_4$**

Ce	0.000000418	0.000039555	0.000005519
N	-2.079474370	-0.511169008	-1.518845879
C	-2.635936993	0.546581772	-2.182184991
N	-2.006236218	1.728665674	-1.995195099
O	-0.913790343	1.683296948	-1.174223810
C	-2.311674251	3.057861417	-2.629649637
C	-2.188811068	2.951447191	-4.164650752
H	-1.178938208	2.629012153	-4.439837278
H	-2.368004503	3.934403122	-4.612887224
H	-2.900510515	2.252523189	-4.609189275

C	-3.706622692	3.550622614	-2.188302010
H	-4.518809484	2.890614985	-2.500471687
H	-3.896498394	4.535638046	-2.628161665
H	-3.749599912	3.649903415	-1.099120440
C	-1.270882416	4.080070379	-2.140717995
H	-1.304157150	4.205478788	-1.056198799
H	-1.501359788	5.043276019	-2.607593095
H	-0.256948189	3.790431286	-2.424647371
C	-3.802604432	0.347328575	-2.985407299
H	-4.258487844	1.162548376	-3.525121923
C	-4.360771678	-0.905687507	-3.059367355
H	-5.253734986	-1.058798165	-3.657769080
C	-3.784039217	-1.984066030	-2.352099229
C	-2.645642188	-1.721704062	-1.608462850
H	-2.153227851	-2.503162945	-1.039657602
C	-4.364512924	-3.353214825	-2.434716328
F	-5.716097924	-3.338257117	-2.320134827
F	-4.099446606	-3.966067787	-3.618892544
F	-3.888980198	-4.174323324	-1.464712946
N	2.079457770	0.511270900	-1.518868062
C	2.635894050	-0.546472312	-2.182244688
N	2.006158386	-1.728543477	-1.995307755
O	0.913725678	-1.683185864	-1.174322433
C	2.311572512	-3.057718206	-2.629819048
C	1.270911648	-4.079997104	-2.140753381
H	1.304343378	-4.205412688	-1.056239816
H	1.501385654	-5.043184397	-2.607668720

H	0.256920340	-3.790418777	-2.424539789
C	2.188485974	-2.951303418	-4.164802721
H	2.367671275	-3.934247793	-4.613067949
H	2.900079082	-2.252338231	-4.609445768
H	1.178554094	-2.628928019	-4.439843348
C	3.706615558	-3.550384442	-2.188670768
H	3.749747330	-3.649671556	-1.099495293
H	4.518705427	-2.890305691	-2.500946528
H	3.896506739	-4.535380511	-2.628567089
C	3.802581932	-0.347230430	-2.985439627
H	4.258461903	-1.162453527	-3.525153223
C	4.360768900	0.905777065	-3.059377002
H	5.253738727	1.058882897	-3.657770064
C	3.784040556	1.984157620	-2.352107293
C	2.645644887	1.721799568	-1.608466761
H	2.153241208	2.503258826	-1.039652765
C	4.364517417	3.353304399	-2.434736569
F	4.099440838	3.966151900	-3.618912917
F	3.888994629	4.174422756	-1.464737241
F	5.716103904	3.338344907	-2.320167747
N	2.079492680	-0.511157630	1.518830702
C	2.635891547	0.546577793	2.182248419
N	2.006135002	1.728642501	1.995330441
O	0.913701717	1.683271437	1.174342695
C	2.311469910	3.057791915	2.629934604
C	2.188596434	2.951184290	4.164919812
H	1.178736004	2.628667680	4.440057273

H	2.367739872	3.934093432	4.613278921
H	2.900325684	2.252237005	4.609376504
C	3.706393378	3.550699895	2.188670307
H	4.518621663	2.890720238	2.500790770
H	3.896187608	4.535682592	2.628637935
H	3.749387167	3.650098962	1.099501358
C	1.270615213	4.079989372	2.141109851
H	1.303899118	4.205532722	1.056606282
H	1.501020437	5.043153927	2.608105207
H	0.256695964	3.790247688	2.424986595
C	3.802557214	0.347333026	2.985474023
H	4.258390025	1.162542868	3.525247242
C	4.360797306	-0.905655825	3.059347077
H	5.253767747	-1.058756890	3.657740594
C	3.784140967	-1.984013552	2.351984736
C	2.645731794	-1.721665511	1.608363127
H	2.153375058	-2.503110879	1.039488869
C	4.364707910	-3.353129506	2.434487713
F	5.716293667	-3.338067878	2.319931872
F	4.099662743	-3.966107761	3.618603608
F	3.889250851	-4.174180954	1.464398826
N	-2.079490627	0.511103691	1.518882826
C	-2.635867898	-0.546682766	2.182241137
N	-2.006074819	-1.728719989	1.995254795
O	-0.913660631	-1.683283211	1.174247993
C	-2.311384315	-3.057952701	2.629696109
C	-1.270463011	-4.080017398	2.140747000

H	-1.303738185	-4.205426579	1.056227915
H	-1.500799998	-5.043254804	2.607625021
H	-0.256563265	-3.790238317	2.424660516
C	-2.188525625	-2.951566472	4.164700982
H	-2.367589596	-3.934559600	4.612907698
H	-2.900307813	-2.252749068	4.609270594
H	-1.178691304	-2.629012936	4.439890201
C	-3.706265402	-3.550887288	2.188321500
H	-3.749212850	-3.650162194	1.099138104
H	-4.518542874	-2.890989653	2.500483800
H	-3.896022997	-4.535932559	2.628165242
C	-3.802545503	-0.347498804	2.985470462
H	-4.258378256	-1.162743098	3.525187138
C	-4.360795951	0.905479731	3.059429777
H	-5.253767536	1.058532804	3.657833867
C	-3.784143872	1.983893010	2.352150141
C	-2.645740785	1.721600920	1.608500507
H	-2.153392838	2.503088696	1.039677452
C	-4.364707672	3.353003228	2.434766065
F	-4.099658520	3.965884348	3.618931655
F	-3.889248126	4.174134974	1.464746443
F	-5.716294196	3.337954618	2.320211256

Table 3.4.25. Optimized coordinates of **Ce^{III}[2-(^{t}BuNO)py]$_4^-$**

Ce	0.000051000	0.000092000	0.000026000
O	0.998943000	-1.115384000	-1.853730000
O	1.001879000	1.112899000	1.853442000

O	-0.998940000	1.115713000	-1.853490000
O	-1.001606000	-1.112807000	1.853418000
N	1.968785000	-2.084764000	-1.899832000
N	2.030607000	-1.805383000	0.384910000
N	1.974038000	2.079947000	1.899591000
N	2.035245000	1.800587000	-0.385223000
N	-1.968668000	2.085196000	-1.899579000
N	-2.030827000	1.805426000	0.385122000
N	-1.973807000	-2.079798000	1.899722000
N	-2.034938000	-1.800802000	-0.385151000
C	2.528732000	-2.444872000	-0.719803000
C	2.545416000	-2.090553000	1.594051000
C	3.553905000	-3.010830000	1.825023000
C	4.067575000	-3.681283000	0.697264000
C	3.575342000	-3.412828000	-0.562034000
C	2.291220000	-2.634873000	-3.255855000
C	3.752829000	-2.310614000	-3.640785000
C	1.999273000	-4.151792000	-3.312839000
C	1.378649000	-1.954247000	-4.291931000
C	2.534568000	2.439096000	0.719544000
C	2.550687000	2.084878000	-1.594303000
C	3.560926000	3.003254000	-1.825187000
C	4.075704000	3.672804000	-0.697406000
C	3.582868000	3.405230000	0.561841000
C	2.298053000	2.628927000	3.255687000
C	1.384606000	1.949670000	4.291895000
C	2.009049000	4.146383000	3.313335000

C	3.759171000	2.301647000	3.639942000
C	-2.528952000	2.444913000	-0.719596000
C	-2.545914000	2.090342000	1.594206000
C	-3.554721000	3.010297000	1.825096000
C	-4.068434000	3.680681000	0.697316000
C	-3.575903000	3.412503000	-0.561923000
C	-2.291463000	2.635067000	-3.255609000
C	-3.752949000	2.310057000	-3.640335000
C	-2.000396000	4.152151000	-3.312627000
C	-1.378571000	1.955014000	-4.291788000
C	-2.534126000	-2.439305000	0.719683000
C	-2.550300000	-2.085369000	-1.594196000
C	-3.560280000	-3.004046000	-1.825009000
C	-4.074784000	-3.673727000	-0.697179000
C	-3.582018000	-3.405894000	0.562039000
C	-2.297929000	-2.628536000	3.255898000
C	-1.385325000	-1.948328000	4.292221000
C	-2.007934000	-4.145785000	3.314124000
C	-3.759388000	-2.302088000	3.639572000
H	2.108084000	-1.525128000	2.414278000
H	3.926665000	-3.197332000	2.826346000
H	4.862422000	-4.415169000	0.808280000
H	3.991589000	-3.932758000	-1.411356000
H	3.908950000	-1.226206000	-3.628111000
H	3.959220000	-2.672463000	-4.654421000
H	4.488312000	-2.763688000	-2.972652000
H	2.604201000	-4.738821000	-2.619009000

H	2.195546000	-4.528295000	-4.323095000
H	0.944894000	-4.336610000	-3.079360000
H	0.323936000	-2.145711000	-4.084282000
H	1.620417000	-2.363137000	-5.279488000
H	1.531820000	-0.873820000	-4.314634000
H	2.112404000	1.520325000	-2.414621000
H	3.934104000	3.189024000	-2.826490000
H	4.871834000	4.405306000	-0.808349000
H	3.999859000	3.924517000	1.411192000
H	0.330183000	2.143481000	4.084965000
H	1.627782000	2.357500000	5.279554000
H	1.535520000	0.868913000	4.313930000
H	2.614992000	4.732532000	2.619640000
H	2.206200000	4.522094000	4.323715000
H	0.954990000	4.333294000	3.080087000
H	3.912996000	1.216913000	3.627183000
H	3.966756000	2.663055000	4.653489000
H	4.495293000	2.753152000	2.971465000
H	-2.108545000	1.525004000	2.414478000
H	-3.927709000	3.196583000	2.826375000
H	-4.863558000	4.414278000	0.808263000
H	-3.992206000	3.932325000	-1.411290000
H	-3.908541000	1.225574000	-3.627532000
H	-3.959677000	2.671718000	-4.653970000
H	-4.488531000	2.762847000	-2.972099000
H	-2.605598000	4.738868000	-2.618777000
H	-2.196970000	4.528504000	-4.322880000

H	-0.946104000	4.337581000	-3.079242000
H	-0.323961000	2.147222000	-4.084277000
H	-1.620728000	2.363725000	-5.279326000
H	-1.530993000	0.874487000	-4.314434000
H	-2.112129000	-1.520805000	-2.414572000
H	-3.933410000	-3.189996000	-2.826295000
H	-4.870592000	-4.406588000	-0.808070000
H	-3.998691000	-3.925401000	1.411409000
H	-0.330701000	-2.141640000	4.085885000
H	-1.628739000	-2.355852000	5.279949000
H	-1.536854000	-0.867647000	4.313731000
H	-2.613339000	-4.732555000	2.620487000
H	-2.205042000	-4.521318000	4.324581000
H	-0.953703000	-4.332061000	3.081146000
H	-3.913892000	-1.217455000	3.626518000
H	-3.967046000	-2.663383000	4.653142000
H	-4.495027000	-2.754223000	2.970988000

Table 3.4.26. Optimized coordinates of **Ce^{IV}[2-(^{t}BuNO)py]$_4$**

Ce	0.000005068	0.000001711	-0.000002484
O	-0.940485970	-1.119214041	1.706392927
O	-0.940544921	1.119173437	-1.706394715
O	0.940507365	1.119215565	1.706383502
O	0.940541285	-1.119171088	-1.706402706
N	-1.993023196	-1.995149658	1.756194115
N	-2.003264665	-1.640355691	-0.510750962
N	-1.993177340	1.994996985	-1.756203344

N	-2.003251521	1.640366571	0.510769318
N	1.993036680	1.995160258	1.756185193
N	2.003266226	1.640364137	-0.510762044
N	1.993174340	-1.994993212	-1.756215901
N	2.003272666	-1.640362528	0.510754301
C	-2.554797674	-2.290543272	0.553916973
C	-2.500557016	-1.853601248	-1.744261464
C	-3.550218667	-2.711518379	-2.017793957
C	-4.121289810	-3.392363236	-0.926162841
C	-3.640712633	-3.194893782	0.352009938
C	-2.316798751	-2.576511436	3.098666222
C	-3.766623491	-2.222725229	3.497225053
C	-2.070972418	-4.101317364	3.098336942
C	-1.377395853	-1.947542486	4.142666427
C	-2.554858794	2.290486719	-0.553901167
C	-2.500459415	1.853683302	1.744301592
C	-3.550103544	2.711612965	2.017858236
C	-4.121241268	3.392402940	0.926228930
C	-3.640750739	3.194860221	-0.351965235
C	-2.316920557	2.576371225	-3.098680103
C	-1.377587585	1.947271865	-4.142662104
C	-2.070939329	4.101152022	-3.098403824
C	-3.766776465	2.222699865	-3.497236710
C	2.554803262	2.290559788	0.553901331
C	2.500545565	1.853605502	-1.744278652
C	3.550200643	2.711522983	-2.017829740
C	4.121281740	3.392372417	-0.926208398

C	3.640718576	3.194908525	0.351970605
C	2.316790856	2.576502969	3.098676023
C	3.766616823	2.222744358	3.497259714
C	2.070895740	4.101298890	3.098423721
C	1.377402076	1.947462898	4.142642233
C	2.554868621	-2.290482364	-0.553921106
C	2.500493785	-1.853681804	1.744280943
C	3.550139142	-2.711614854	2.017823935
C	4.121263515	-3.392405433	0.926187601
C	3.640759312	-3.194859983	-0.352000909
C	2.316911572	-2.576366700	-3.098689427
C	1.377517664	-1.947314591	-4.142644578
C	2.070998776	-4.101159574	-3.098380276
C	3.766742932	-2.222633861	-3.497280966
H	-2.011504378	-1.289438815	-2.533459485
H	-3.910888073	-2.847171607	-3.031238330
H	-4.947880559	-4.081050457	-1.079779154
H	-4.090460203	-3.724715188	1.177859416
H	-3.896987873	-1.135302183	3.510607935
H	-3.973258830	-2.604974927	4.502750870
H	-4.516933128	-2.643929744	2.824855134
H	-2.702944173	-4.639364788	2.388421987
H	-2.272980292	-4.506802871	4.095714610
H	-1.025516647	-4.312124996	2.848554136
H	-0.330012666	-2.169803503	3.927981990
H	-1.629279847	-2.368306764	5.121837811
H	-1.496762878	-0.862847804	4.190786616

H	-2.011346292	1.289572634	2.533499136
H	-3.910703189	2.847324264	3.031319654
H	-4.947811321	4.081110672	1.079864357
H	-4.090541474	3.724654496	-1.177806350
H	-0.330175543	2.169362069	-3.927941609
H	-1.629375591	2.368088414	-5.121835519
H	-1.497127100	0.862596487	-4.190798178
H	-2.702885096	4.639290184	-2.388534961
H	-2.272863688	4.506620458	-4.095805819
H	-1.025471942	4.311862883	-2.848587336
H	-3.897227447	1.135287107	-3.510609972
H	-3.973374810	2.604954977	-4.502767725
H	-4.517060273	2.643969412	-2.824881889
H	2.011486312	1.289435984	-2.533467555
H	3.910859053	2.847170522	-3.031278780
H	4.947871145	4.081058506	-1.079836808
H	4.090481491	3.724735106	1.177805091
H	3.897012633	1.135324678	3.510597663
H	3.973212818	2.604953697	4.502809450
H	4.516932953	2.644000601	2.824931986
H	2.702858510	4.639419605	2.388559552
H	2.272857312	4.506737332	4.095830277
H	1.025436154	4.312072348	2.848627787
H	0.330015383	2.169717597	3.927969883
H	1.629280234	2.368177433	5.121836779
H	1.496789898	0.862767544	4.190700317
H	2.011391076	-1.289571713	2.533485436

H	3.910749302	-2.847328958	3.031281225
H	4.947832869	-4.081116250	1.079813106
H	4.090537568	-3.724654692	-1.177849605
H	0.330125386	-2.169499888	-3.927924458
H	1.629334855	-2.368080165	-5.121831677
H	1.496964574	-0.862626905	-4.190750023
H	2.702963250	-4.639251660	-2.388491992
H	2.272950510	-4.506641911	-4.095770639
H	1.025539026	-4.311912033	-2.848566434
H	3.897148086	-1.135215641	-3.510664943
H	3.973333322	-2.604886925	-4.502814298
H	4.517061681	-2.643866058	-2.824941146

Table 3.4.27. Optimized coordinates of **Ce^{III}[5-Me-2-(^{t}BuNO)py]$_4^-$**

Ce	-0.000141000	0.000160000	-0.045837000
O	-0.916506000	1.276616000	-1.811642000
N	-2.040044000	2.082622000	-1.920790000
C	-2.647322000	2.349032000	-0.706833000
N	-2.073377000	1.782727000	0.385834000
C	-2.652990000	1.932929000	1.591607000
H	-2.139016000	1.427338000	2.407942000
C	-3.817566000	2.645282000	1.838530000
C	-4.435117000	3.199229000	0.696778000
H	-5.377954000	3.733828000	0.796413000
C	-3.881380000	3.048253000	-0.557998000
H	-4.415036000	3.426632000	-1.414913000
C	-4.397540000	2.788492000	3.223155000

H	-3.812135000	2.221767000	3.955347000
H	-5.432432000	2.425470000	3.271081000
H	-4.413098000	3.836277000	3.551984000
C	-1.853213000	3.072659000	-3.039059000
C	-3.125011000	3.859734000	-3.403628000
H	-3.983887000	3.197153000	-3.556988000
H	-2.941071000	4.386260000	-4.346416000
H	-3.382026000	4.618272000	-2.660707000
C	-0.734981000	4.064222000	-2.659541000
H	-1.033190000	4.670279000	-1.795451000
H	-0.520444000	4.744867000	-3.491939000
H	0.178924000	3.521836000	-2.407445000
C	-1.443863000	2.263632000	-4.285936000
H	-0.536138000	1.690981000	-4.098265000
H	-1.272684000	2.945344000	-5.126396000
H	-2.242002000	1.566511000	-4.568341000
O	-0.929962000	-1.265375000	1.749693000
N	-2.027906000	-2.089973000	1.786665000
C	-2.735924000	-2.214273000	0.635387000
N	-2.246795000	-1.519491000	-0.434443000
C	-2.899265000	-1.574066000	-1.610165000
H	-2.451071000	-0.969130000	-2.397359000
C	-4.053079000	-2.304068000	-1.858130000
C	-4.551051000	-3.033575000	-0.754412000
H	-5.452970000	-3.633080000	-0.865731000
C	-3.922788000	-3.000719000	0.471634000
H	-4.339810000	-3.568146000	1.290165000

C	-4.727863000	-2.313910000	-3.207059000
H	-4.191097000	-1.676024000	-3.917993000
H	-5.762345000	-1.948620000	-3.151980000
H	-4.771566000	-3.323440000	-3.638041000
C	-2.349170000	-2.704372000	3.112932000
C	-3.710994000	-2.191624000	3.634562000
H	-3.685869000	-1.100047000	3.727250000
H	-3.914274000	-2.613341000	4.625525000
H	-4.548544000	-2.453845000	2.984546000
C	-1.273166000	-2.274950000	4.126681000
H	-0.279646000	-2.611448000	3.823076000
H	-1.515693000	-2.727991000	5.094794000
H	-1.244044000	-1.190182000	4.244836000
C	-2.307750000	-4.247169000	3.024782000
H	-3.036527000	-4.663308000	2.326435000
H	-2.509811000	-4.680786000	4.010869000
H	-1.311897000	-4.575169000	2.706553000
O	0.928892000	1.266263000	1.749667000
N	2.027455000	2.090003000	1.787150000
C	2.736023000	2.213848000	0.636161000
N	2.247037000	1.519137000	-0.433780000
C	2.900071000	1.573200000	-1.609211000
H	2.451959000	0.968307000	-2.396482000
C	4.054330000	2.302636000	-1.856777000
C	4.552129000	3.032115000	-0.752964000
H	5.454349000	3.631222000	-0.863989000
C	3.923311000	2.999737000	0.472812000

H	4.340197000	3.567148000	1.291423000
C	4.729731000	2.311931000	-3.205403000
H	5.763986000	1.946075000	-3.149815000
H	4.774187000	3.321381000	-3.636494000
H	4.192931000	1.674250000	-3.916496000
C	2.348288000	2.704568000	3.113440000
C	3.709756000	2.191569000	3.635748000
H	3.684320000	1.100014000	3.728619000
H	3.912709000	2.613413000	4.626724000
H	4.547657000	2.453461000	2.986058000
C	1.271750000	2.275563000	4.126796000
H	0.278447000	2.612289000	3.822741000
H	1.514009000	2.728646000	5.094957000
H	1.242289000	1.190814000	4.245069000
C	2.307297000	4.247360000	3.024995000
H	3.036468000	4.663163000	2.326856000
H	2.509069000	4.681122000	4.011077000
H	1.311658000	4.575554000	2.706297000
O	0.916920000	-1.276251000	-1.811332000
N	2.040578000	-2.082150000	-1.920047000
C	2.647300000	-2.348657000	-0.705826000
N	2.072724000	-1.782670000	0.386676000
C	2.651785000	-1.933030000	1.592698000
H	2.137319000	-1.427751000	2.408918000
C	3.816378000	-2.645212000	1.840033000
C	4.434596000	-3.198791000	0.698464000
H	5.377492000	-3.733221000	0.798441000

C	3.881428000	-3.047656000	-0.556543000
H	4.415566000	-3.425738000	-1.413291000
C	4.395702000	-2.788610000	3.224911000
H	3.809771000	-2.222239000	3.956955000
H	5.430468000	-2.425308000	3.273449000
H	4.411392000	-3.836475000	3.553477000
C	1.854323000	-3.072169000	-3.038450000
C	3.126434000	-3.858886000	-3.402690000
H	3.985178000	-3.196065000	-3.555758000
H	2.942913000	-4.385412000	-4.345560000
H	3.383431000	-4.617393000	-2.659732000
C	1.445139000	-2.263186000	-4.285407000
H	0.537138000	-1.690878000	-4.098026000
H	1.274512000	-2.944892000	-5.125985000
H	2.243129000	-1.565753000	-4.567467000
C	0.736246000	-4.064065000	-2.659347000
H	1.034349000	-4.670111000	-1.795213000
H	0.522141000	-4.744705000	-3.491861000
H	-0.177877000	-3.521937000	-2.407494000

Table 3.4.28. Optimized coordinates of **Ce^{IV}[5-Me-2-(^{t}BuNO)py]$_4$**

Ce	0.000173727	-0.000250437	-0.093810403
O	-0.790319289	1.293645769	-1.721062371
N	-1.815929331	2.226737228	-1.814143172
C	-2.414746830	2.454457561	-0.577339157
N	-1.884233842	1.787168389	0.471523077
C	-2.453710309	1.896122603	1.688377532

H	-1.976381720	1.307404928	2.467573309
C	-3.568267908	2.673164523	1.968725129
C	-4.144764245	3.331886574	0.863822612
H	-5.051227605	3.918429076	0.995903544
C	-3.596624696	3.218477370	-0.399296812
H	-4.094988626	3.675147583	-1.240116061
C	-4.144737564	2.775815828	3.358225890
H	-3.603297897	2.131570468	4.058555201
H	-5.201344856	2.481303331	3.378620111
H	-4.091193753	3.803119406	3.740812183
C	-1.426994599	3.316368197	-2.783400314
C	-2.589031727	4.273616936	-3.097716349
H	-3.494412079	3.730501762	-3.389618404
H	-2.291583005	4.902772246	-3.943209320
H	-2.822289534	4.943741424	-2.266911651
C	-0.239014599	4.116792666	-2.215614695
H	-0.523172970	4.624499903	-1.286198885
H	0.082403542	4.881031708	-2.932526818
H	0.607067917	3.456553315	-2.009575025
C	-1.026798251	2.617943654	-4.096304976
H	-0.185764355	1.940977847	-3.944100883
H	-0.743304198	3.371938227	-4.838339328
H	-1.869349832	2.042416278	-4.496796372
O	-1.004736306	-1.079851075	1.601910731
N	-2.179449346	-1.785192224	1.670191969
C	-2.834766507	-1.922227716	0.483452301
N	-2.264604358	-1.275162211	-0.568609617

C	-2.867362582	-1.310464176	-1.774290527
H	-2.356888711	-0.745492526	-2.550545999
C	-4.043782351	-1.988646096	-2.052730842
C	-4.619706345	-2.679173844	-0.963524739
H	-5.539752410	-3.241890537	-1.106610928
C	-4.041408017	-2.656603677	0.287901730
H	-4.508936497	-3.195229423	1.098253791
C	-4.665051496	-1.989000677	-3.426925480
H	-4.067821651	-1.397033478	-4.128384378
H	-5.678315462	-1.567071066	-3.414318731
H	-4.747264759	-3.004828713	-3.834753056
C	-2.453938856	-2.492589687	2.961761903
C	-3.826368894	-2.059727618	3.522825008
H	-3.844471460	-0.974818271	3.671995597
H	-3.994056379	-2.541211720	4.492532257
H	-4.664921138	-2.324525458	2.875805086
C	-1.382716439	-2.074443768	3.984835588
H	-0.381824418	-2.372786566	3.666689923
H	-1.609524237	-2.570261265	4.934778744
H	-1.383949507	-0.994104686	4.149229622
C	-2.362915924	-4.022738855	2.772257455
H	-3.104873360	-4.412211289	2.071076830
H	-2.518111789	-4.525362657	3.733235481
H	-1.368876718	-4.295448895	2.401156531
O	1.005192103	1.079142332	1.601928813
N	2.180032727	1.784313964	1.670335556
C	2.834709843	1.922359920	0.483309951

N	2.264540344	1.275351831	-0.568765444
C	2.866895022	1.311331577	-1.774626263
H	2.356448626	0.746386375	-2.550920006
C	4.042859783	1.990234490	-2.053238556
C	4.618688817	2.680844149	-0.964040459
H	5.538301353	3.244228252	-1.107282089
C	4.040789028	2.657576231	0.287562226
H	4.508159125	3.196383775	1.097882239
C	4.663706666	1.991307323	-3.427622655
H	5.677121162	1.569727573	-3.415475449
H	4.745437902	3.007315613	-3.835093709
H	4.066471423	1.399385930	-4.129114669
C	2.453682406	2.492715007	2.961558371
C	3.826766761	2.061977431	3.522651395
H	3.846414144	0.977141761	3.672154583
H	3.993796543	2.543990419	4.492209739
H	4.664948354	2.327766648	2.875566951
C	1.383235996	2.073415137	3.984978709
H	0.381871500	2.370273848	3.666960968
H	1.609576536	2.569790366	4.934741469
H	1.386003752	0.993115278	4.149679428
C	2.360524545	4.022644762	2.771396161
H	3.102044897	4.412801301	2.070120776
H	2.514888465	4.525940682	3.732157579
H	1.366150334	4.293789459	2.400038808
O	0.790438740	-1.294228811	-1.721081363
N	1.815914424	-2.227452697	-1.814288728

C	2.415116407	-2.454948960	-0.577629543
N	1.884997270	-1.787383727	0.471257801
C	2.454930296	-1.896040840	1.687927011
H	1.977945492	-1.307072456	2.467139785
C	3.569559635	-2.673059534	1.968058101
C	4.145609034	-3.332110569	0.863120516
H	5.052091455	-3.918664439	0.995020644
C	3.597013234	-3.218992582	-0.399827441
H	4.095041576	-3.675900513	-1.240717609
C	4.146554282	-2.775347136	3.357367856
H	3.605535920	-2.130729187	4.057679947
H	5.203235278	-2.481065683	3.377235868
H	4.092931672	-3.802501618	3.740345432
C	1.426560129	-3.317228158	-2.783203656
C	2.588374452	-4.274714170	-3.097615980
H	3.493746591	-3.731800622	-3.389918993
H	2.290596238	-4.904044976	-3.942861798
H	2.821780317	-4.944654752	-2.266704308
C	1.026117925	-2.619009121	-4.096145519
H	0.185174633	-1.941944008	-3.943875178
H	0.742389642	-3.373111969	-4.837980324
H	1.868625447	-2.043621675	-4.496930074
C	0.238617222	-4.117363505	-2.214931892
H	0.522963160	-4.624948973	-1.285506997
H	-0.083132732	-4.881680744	-2.931612447
H	-0.607304713	-3.456958363	-2.008763685

Table 3.4.29. Optimized coordinates of **Ce^{IV}[5-OMe-2-(^{t}BuNO)py]$_4$ (~S_4 Symmetry)**

Ce	0.012908828	-0.034529224	-0.019515989
O	0.852265783	-0.508367179	1.957890489
N	1.951232180	-1.228960058	2.451412818
C	2.800066762	-1.582852042	1.377262014
N	2.282548897	-1.564930909	0.138690639
C	3.049369504	-1.882368868	-0.921802521
H	2.563105931	-1.824471135	-1.890001313
C	4.380530590	-2.238183803	-0.795076291
H	4.967613573	-2.515741705	-1.664237804
C	4.969510181	-2.169336626	0.474406907
H	6.029209774	-2.365224756	0.587518141
C	4.197260443	-1.796066277	1.571500518
O	4.695556691	-1.564150336	2.813802679
C	6.093395693	-1.748679137	3.025643127
H	6.390868662	-2.789001417	2.847660943
H	6.268898016	-1.494262368	4.071563045
H	6.684384761	-1.084573135	2.383449525
C	1.438526314	-2.332624643	3.363051320
C	2.587525773	-3.041687554	4.095896345
H	3.252333173	-3.575157801	3.411415871
H	2.149892209	-3.783143643	4.773739100
H	3.184289694	-2.342010427	4.684969262
C	0.541182392	-1.657125133	4.414531059
H	1.092744463	-0.867998985	4.938274780
H	0.223523903	-2.400643642	5.154031991
H	-0.347045188	-1.216547893	3.959373139

C	0.637839193	-3.376761546	2.560991429
H	-0.126872788	-2.902881980	1.941968112
H	0.147768737	-4.078619444	3.245926011
H	1.297464979	-3.956265472	1.904566383
O	0.971447777	0.488090600	-1.935031080
N	2.080333680	1.246136839	-2.340876411
C	2.831348287	1.627294581	-1.206242288
N	2.223914401	1.581453543	-0.010026347
C	2.895872080	1.923066583	1.106184120
H	2.340495906	1.839670646	2.034419224
C	4.217907098	2.329906847	1.081125508
H	4.726653094	2.625774377	1.992603479
C	4.903543580	2.288354643	-0.140419017
H	5.960960514	2.523094263	-0.171963610
C	4.231334685	1.891400077	-1.293141209
O	4.831299969	1.680150169	-2.493578994
C	6.231497461	1.927031004	-2.600893685
H	6.468162249	2.978940245	-2.401202803
H	6.495439590	1.684126079	-3.630863697
H	6.802464684	1.287807960	-1.916724748
C	1.607352144	2.322024683	-3.304855369
C	0.634121284	3.289198893	-2.603431773
H	-0.179455240	2.747876820	-2.116411588
H	0.203817961	3.982728748	-3.335207807
H	1.152927680	3.884530326	-1.842903437
C	0.902320834	1.598524076	-4.464829193
H	1.582044306	0.879862451	-4.936474392

H	0.597456095	2.329895422	-5.221646514
H	0.015760181	1.063796292	-4.120894075
C	2.779252443	3.130068092	-3.881433999
H	3.318019468	3.688722308	-3.110969292
H	2.370094240	3.858723399	-4.590251271
H	3.490164669	2.492824657	-4.410660339
O	-0.827387452	-2.002641824	-0.551657609
N	-1.913017237	-2.462886841	-1.312334928
C	-2.728264548	-1.371143365	-1.683551552
N	-2.187821512	-0.142390742	-1.641719090
C	-2.928086645	0.935855960	-1.963499604
H	-2.425483492	1.894064924	-1.883312328
C	-4.253029290	0.838417723	-2.349593442
H	-4.817450533	1.721639312	-2.629775116
C	-4.866675764	-0.420667118	-2.310088514
H	-5.923586259	-0.511323050	-2.531154876
C	-4.124171825	-1.535788568	-1.931377121
O	-4.651718066	-2.770747982	-1.725129833
C	-6.047057811	-2.955390672	-1.952452346
H	-6.646107783	-2.310910098	-1.297870043
H	-6.248191416	-4.000962000	-1.716158363
H	-6.310875901	-2.759763967	-2.998670212
C	-1.393048868	-3.397654157	-2.390854757
C	-0.449279686	-2.648411950	-3.351861512
H	-0.996864938	-1.897217608	-3.932878266
H	0.000798408	-3.355185883	-4.058653882
H	0.351437495	-2.142409923	-2.809045752

C	-0.639264093	-4.528545298	-1.671050988
H	0.222012752	-4.144595675	-1.122552821
H	-0.287758566	-5.261890925	-2.405329089
H	-1.302310946	-5.040948231	-0.964765893
C	-2.534669830	-4.021578867	-3.207587955
H	-3.222402071	-4.587681501	-2.576989166
H	-2.090299490	-4.704841402	-3.939868486
H	-3.106835052	-3.272649467	-3.762807181
O	-0.930527193	1.928803224	0.456375731
N	-2.047694488	2.306566786	1.178009592
C	-2.786322939	1.224699218	1.616972603
N	-2.202877256	0.013001089	1.491692963
C	-2.854699365	-1.102754888	1.880324831
H	-2.315561355	-2.031517338	1.726876182
C	-4.123800100	-1.080047918	2.419732838
H	-4.611324156	-1.992534686	2.745510323
C	-4.791763856	0.156782116	2.478036471
H	-5.818831495	0.196280079	2.821470082
C	-4.156194659	1.307713078	2.042616773
O	-4.767179070	2.522875157	1.937837450
C	-6.144848602	2.620254338	2.292084231
H	-6.760451503	1.953896270	1.676050935
H	-6.425522152	3.656871394	2.102136396
H	-6.301730024	2.386904963	3.351814236
C	-1.898356863	3.644692771	1.877743097
C	-0.416473465	4.066905698	1.843200290
H	-0.051818141	4.201099920	0.824026737

H	0.223484083	3.336143096	2.344963739
H	-0.327379846	5.022802320	2.371462724
C	-2.309341104	3.558901561	3.360807153
H	-2.096741011	4.520225213	3.841547644
H	-1.725917778	2.789540167	3.879245269
H	-3.370382457	3.351416670	3.493072117
C	-2.722263699	4.702759360	1.118995560
H	-2.386223938	4.761025775	0.077406973
H	-2.583725968	5.690131673	1.575639774
H	-3.785114622	4.458135053	1.129075640

Table 3.4.30. Optimized coordinates of **Ce^{III}[5-OMe-2-(^{t}BuNO)py]$_4^-$ (~D_{2d} symmetry)**

Ce	-0.000031000	0.000174000	-0.000044000
O	-1.003817000	1.087961000	-1.860408000
N	-1.978450000	2.058819000	-1.944902000
C	-2.653589000	2.296187000	-0.778977000
N	-2.092152000	1.776361000	0.346343000
C	-2.686404000	1.944146000	1.545168000
H	-2.173801000	1.473309000	2.379027000
C	-3.864437000	2.638150000	1.723547000
H	-4.301734000	2.769330000	2.707724000
C	-4.520904000	3.108162000	0.566536000
H	-5.494860000	3.575375000	0.656500000
C	-3.960048000	2.907896000	-0.680352000
O	-4.610949000	3.192315000	-1.852358000
C	-5.936065000	3.705062000	-1.781861000
H	-5.963962000	4.682722000	-1.284951000

H	-6.267265000	3.815104000	-2.815657000
H	-6.604174000	3.012687000	-1.254393000
C	-1.870782000	2.929922000	-3.168410000
C	-2.851612000	2.433789000	-4.251204000
H	-2.650590000	1.379357000	-4.473845000
H	-2.721271000	3.006129000	-5.177929000
H	-3.886768000	2.529335000	-3.921585000
C	-2.086992000	4.419626000	-2.833541000
H	-3.097542000	4.634471000	-2.491175000
H	-1.906003000	5.016364000	-3.735076000
H	-1.372828000	4.746056000	-2.068540000
C	-0.438820000	2.806401000	-3.729926000
H	0.308247000	3.127825000	-2.999620000
H	-0.361964000	3.454320000	-4.611097000
H	-0.207827000	1.782501000	-4.023589000
O	-1.003426000	-1.087888000	1.860183000
N	-1.977738000	-2.059061000	1.944838000
C	-2.653318000	-2.296250000	0.779130000
N	-2.092576000	-1.775841000	-0.346262000
C	-2.687203000	-1.943595000	-1.544895000
H	-2.175092000	-1.472294000	-2.378799000
C	-3.865001000	-2.638077000	-1.722997000
H	-4.302606000	-2.769219000	-2.707043000
C	-4.520826000	-3.108639000	-0.565853000
H	-5.494618000	-3.576249000	-0.655557000
C	-3.959580000	-2.908426000	0.680872000
O	-4.609939000	-3.193358000	1.853056000

C	-5.934907000	-3.706533000	1.782909000
H	-6.265727000	-3.816872000	2.816795000
H	-6.603421000	-3.014286000	1.255787000
H	-5.962644000	-4.684114000	1.285835000
C	-1.869189000	-2.930510000	3.168015000
C	-0.436978000	-2.806734000	3.728857000
H	0.309813000	-3.127820000	2.998120000
H	-0.359532000	-3.454805000	4.609864000
H	-0.206080000	-1.782831000	4.022578000
C	-2.085129000	-4.420180000	2.832818000
H	-3.095800000	-4.635227000	2.490936000
H	-1.903466000	-5.017125000	3.734080000
H	-1.371280000	-4.746171000	2.067335000
C	-2.849644000	-2.434984000	4.251427000
H	-2.648815000	-1.380559000	4.474278000
H	-2.718726000	-3.007558000	5.177927000
H	-3.884923000	-2.530718000	3.922244000
O	1.003276000	-1.088236000	-1.860127000
N	1.977905000	-2.059062000	-1.944734000
C	2.653771000	-2.295746000	-0.779099000
N	2.093094000	-1.775047000	0.346193000
C	2.687892000	-1.942286000	1.544822000
H	2.175848000	-1.470672000	2.378585000
C	3.865799000	-2.636553000	1.723015000
H	4.303559000	-2.767308000	2.707044000
C	4.521544000	-3.107419000	0.565940000
H	5.495408000	-3.574867000	0.655691000

C	3.960144000	-2.907694000	-0.680789000
O	4.610421000	-3.192935000	-1.852953000
C	5.935484000	-3.705864000	-1.782787000
H	6.266200000	-3.816499000	-2.816675000
H	6.603943000	-3.013327000	-1.255979000
H	5.963446000	-4.683273000	-1.285385000
C	1.869688000	-2.930588000	-3.167886000
C	2.850166000	-2.434929000	-4.251218000
H	2.649146000	-1.380562000	-4.474169000
H	2.719461000	-3.007598000	-5.177689000
H	3.885427000	-2.530433000	-3.921919000
C	2.085876000	-4.420194000	-2.832557000
H	3.096539000	-4.635013000	-2.490511000
H	1.904458000	-5.017244000	-3.733799000
H	1.371983000	-4.746265000	-2.067149000
C	0.437524000	-2.807119000	-3.728909000
H	-0.309315000	-3.128262000	-2.998242000
H	0.360307000	-3.455300000	-4.609855000
H	0.206489000	-1.783289000	-4.022778000
O	1.003828000	1.087735000	1.860493000
N	1.978209000	2.058880000	1.944893000
C	2.653084000	2.296585000	0.778892000
N	2.091517000	1.777053000	-0.346490000
C	2.685572000	1.945311000	-1.545342000
H	2.172819000	1.474856000	-2.379322000
C	3.863554000	2.639426000	-1.723659000
H	4.300667000	2.770985000	-2.707867000

C	4.520209000	3.109036000	-0.566592000
H	5.494162000	3.576260000	-0.656541000
C	3.959525000	2.908329000	0.680303000
O	4.610567000	3.192286000	1.852338000
C	5.935716000	3.704953000	1.781864000
H	5.963624000	4.682810000	1.285340000
H	6.267069000	3.814558000	2.815658000
H	6.603694000	3.012736000	1.254026000
C	1.870333000	2.929985000	3.168370000
C	0.438259000	2.806488000	3.729618000
H	-0.308660000	3.127958000	2.999175000
H	0.361237000	3.454374000	4.610798000
H	0.207178000	1.782579000	4.023179000
C	2.086646000	4.419689000	2.833588000
H	3.097279000	4.634536000	2.491467000
H	1.905468000	5.016394000	3.735107000
H	1.372663000	4.746170000	2.068440000
C	2.850976000	2.433825000	4.251321000
H	2.649947000	1.379375000	4.473865000
H	2.720464000	3.006112000	5.178055000
H	3.886187000	2.529418000	3.921876000

Table 3.4.31. Optimized coordinates of **Ce^{IV}[5-OMe-2-(^{t}BuNO)py]$_4$ (~D_{2d} symmetry)**

Ce	0.000011147	0.000144006	-0.000027275
O	-0.897725162	-1.195492952	1.660576824
N	-1.950959304	-2.084937178	1.737637594
C	-2.674008809	-2.149260710	0.563304863

N	-2.121445296	-1.529963464	-0.503902694
C	-2.761919152	-1.503855510	-1.691555818
H	-2.246939639	-0.967212004	-2.481298965
C	-3.988868807	-2.099405429	-1.893121321
H	-4.470314305	-2.079555715	-2.864845434
C	-4.624262646	-2.687630223	-0.783683338
H	-5.620112262	-3.100539928	-0.892785605
C	-4.002392138	-2.688121003	0.453420691
O	-4.595906805	-3.125421551	1.601614408
C	-5.936011394	-3.606335279	1.530927419
H	-6.008228266	-4.495455781	0.893399906
H	-6.209465484	-3.868871780	2.553587086
H	-6.616257212	-2.832167204	1.156173495
C	-1.742647781	-3.193059722	2.751391139
C	-2.649490646	-2.942365710	3.972288350
H	-2.419632744	-1.965735193	4.413808357
H	-2.473858437	-3.708852994	4.736685633
H	-3.703594369	-2.959766053	3.694539289
C	-1.991900314	-4.580338145	2.127784004
H	-3.029904798	-4.727288027	1.831547124
H	-1.743807118	-5.351189517	2.865941789
H	-1.345275133	-4.731491626	1.255800208
C	-0.276757027	-3.161362402	3.226382141
H	0.421152876	-3.300594625	2.397776089
H	-0.138180631	-3.980168768	3.941414239
H	-0.030969231	-2.222345988	3.724614998
O	-0.897918005	1.195883580	-1.660389733

N	-1.951232317	2.085240767	-1.737371312
C	-2.674166192	2.149532257	-0.562968338
N	-2.121403597	1.530433167	0.504252044
C	-2.761815354	1.504299892	1.691935233
H	-2.246697683	0.967835168	2.481711549
C	-3.988873633	2.099621286	1.893525687
H	-4.470254990	2.079740345	2.865280815
C	-4.624445064	2.687642854	0.784084179
H	-5.620369336	3.100364130	0.893209920
C	-4.002635808	2.688164327	-0.453053482
O	-4.596261301	3.125297152	-1.601253578
C	-5.936457755	3.605960076	-1.530581956
H	-6.209969208	3.868387086	-2.553254133
H	-6.616551805	2.831682240	-1.155780252
H	-6.008840948	4.495102386	-0.893104440
C	-1.743140609	3.193315373	-2.751188221
C	-0.277191018	3.161975464	-3.226041430
H	0.420594152	3.301574084	-2.397389726
H	-0.138797900	3.980696157	-3.941204865
H	-0.031064935	2.222944948	-3.724083392
C	-1.992829475	4.580578492	-2.127711004
H	-3.030890814	4.727246132	-1.831530016
H	-1.744935811	5.351440982	-2.865922617
H	-1.346286528	4.731993159	-1.255712068
C	-2.649814449	2.942268151	-3.972137122
H	-2.419692806	1.965636136	-4.413517076
H	-2.474288854	3.708705607	-4.736607542

H	-3.703947706	2.959462019	-3.694481286
O	0.898027497	1.195824439	1.660362322
N	1.951406491	2.085100800	1.737336386
C	2.674324754	2.149349136	0.562924570
N	2.121526583	1.530227540	-0.504263939
C	2.761894466	1.504068133	-1.691972116
H	2.246750040	0.967582899	-2.481716698
C	3.988941924	2.099388908	-1.893621367
H	4.470288508	2.079497739	-2.865393487
C	4.624553148	2.687437126	-0.784213885
H	5.620468239	3.100168662	-0.893389010
C	4.002796144	2.687970897	0.452948108
O	4.596483375	3.125090720	1.601121320
C	5.936686466	3.605723164	1.530372688
H	6.210274437	3.868118391	2.553032847
H	6.616738287	2.831439474	1.155506562
H	6.009046903	4.494879597	0.892912174
C	1.743387211	3.193188249	2.751157190
C	2.650224287	2.942232056	3.972007553
H	2.420177723	1.965623912	4.413476123
H	2.474770966	3.708715741	4.736447223
H	3.704322755	2.959435894	3.694223407
C	1.992926262	4.580448897	2.127616905
H	3.030936890	4.727153664	1.831274550
H	1.745114720	5.351316096	2.865852009
H	1.346248120	4.731833686	1.255712682
C	0.277495562	3.161770752	3.226185239

H	-0.420397422	3.301328736	2.397620437
H	0.139141665	3.980472066	3.941378388
H	0.031482633	2.222718397	3.724244701
O	0.897559435	-1.195765346	-1.660524933
N	1.950758984	-2.085257796	-1.737543755
C	2.673903635	-2.149445795	-0.563264572
N	2.121450689	-1.530039946	0.503935505
C	2.762047959	-1.503866660	1.691523358
H	2.247183177	-0.967117191	2.481268500
C	3.988988200	-2.099459029	1.893019957
H	4.470510138	-2.079576544	2.864705631
C	4.624282527	-2.687755416	0.783560420
H	5.620129831	-3.100681752	0.892605933
C	4.002306232	-2.688274359	-0.453491443
O	4.595694102	-3.125591777	-1.601750475
C	5.935824965	-3.606460953	-1.531238998
H	6.008157198	-4.495593859	-0.893742395
H	6.209164117	-3.868966307	-2.553937634
H	6.616089198	-2.832275918	-1.156554121
C	1.742266768	-3.193547761	-2.751058869
C	0.276266560	-3.161933204	-3.225707937
H	-0.421442868	-3.300842295	-2.396873556
H	0.137472535	-3.980984442	-3.940415401
H	0.030403689	-2.223074597	-3.724198594
C	1.991667397	-4.580726615	-2.127293456
H	3.029758100	-4.727673474	-1.831359732
H	1.743318508	-5.351680752	-2.865257070

H	1.345304793	-4.731726697	-1.255088290
C	2.648847537	-2.943026737	-3.972192913
H	2.418868237	-1.966474051	-4.413822105
H	2.473078435	-3.709645331	-4.736424595
H	3.703011671	-2.960349825	-3.694660354

Table 3.4.32. Optimized coordinates of **Ce^{III}[5-NMe_2-2-(^{t}BuNO)py]$_4^-$**

Ce	0.014752000	-0.007304000	-0.008135000
O	1.003198000	0.669936000	2.029651000
O	-0.962718000	-1.683115000	1.338182000
O	-0.934233000	1.711245000	-1.313861000
O	0.953247000	-0.700872000	-2.048621000
N	2.292406000	1.582681000	0.032581000
N	2.173528000	1.351519000	2.360087000
N	-2.255801000	-1.368330000	-0.845344000
N	-2.122460000	-2.458205000	1.237489000
N	-2.227035000	1.395626000	0.868409000
N	-2.077560000	2.509971000	-1.201932000
N	2.244412000	-1.685279000	-0.075769000
N	2.085710000	-1.436194000	-2.413433000
N	4.935931000	2.721860000	-2.342939000
N	-4.851426000	-1.062665000	-3.479105000
N	-4.809590000	1.132429000	3.517883000
N	4.822905000	-3.000766000	2.244202000
C	2.952561000	1.895300000	-1.102124000
H	2.418190000	1.640874000	-2.010707000
C	4.230026000	2.450735000	-1.143342000

C	4.850175000	2.636788000	0.115780000
H	5.875888000	2.991254000	0.168808000
C	4.193934000	2.309422000	1.283050000
H	4.723464000	2.387127000	2.221031000
C	2.865868000	1.800586000	1.233297000
C	1.930194000	2.219987000	3.566237000
C	1.375457000	1.300260000	4.670454000
H	0.457803000	0.811956000	4.342946000
H	1.169573000	1.886247000	5.573340000
H	2.108783000	0.525380000	4.924888000
C	0.903327000	3.319801000	3.227194000
H	1.303117000	4.000905000	2.466014000
H	0.663204000	3.913678000	4.117205000
H	-0.018070000	2.873944000	2.846079000
C	3.209120000	2.878151000	4.112383000
H	4.000990000	2.140787000	4.286153000
H	2.972119000	3.343372000	5.075592000
H	3.592415000	3.666191000	3.459189000
C	-2.930112000	-0.986921000	-1.945741000
H	-2.403693000	-0.264726000	-2.558517000
C	-4.217316000	-1.427591000	-2.281273000
C	-4.835249000	-2.255781000	-1.312170000
H	-5.860238000	-2.586638000	-1.436706000
C	-4.162153000	-2.619776000	-0.161092000
H	-4.688000000	-3.187164000	0.593769000
C	-2.825783000	-2.198829000	0.050406000
C	-1.825107000	-3.869648000	1.674196000

C	-1.234201000	-3.779466000	3.093620000
H	-0.327154000	-3.174633000	3.097884000
H	-0.998091000	-4.783732000	3.463624000
H	-1.957832000	-3.323108000	3.779982000
C	-0.808599000	-4.527472000	0.719534000
H	-1.232578000	-4.628659000	-0.286935000
H	-0.537491000	-5.529611000	1.072852000
H	0.098664000	-3.922598000	0.654891000
C	-3.085519000	-4.748710000	1.750084000
H	-3.865867000	-4.282314000	2.362159000
H	-2.816959000	-5.700631000	2.221743000
H	-3.498488000	-4.980968000	0.764957000
C	-2.902001000	1.021064000	1.970298000
H	-2.387456000	0.282133000	2.573161000
C	-4.177405000	1.488247000	2.317212000
C	-4.785185000	2.332485000	1.355785000
H	-5.803253000	2.681400000	1.487390000
C	-4.110726000	2.689969000	0.203077000
H	-4.628448000	3.271573000	-0.546732000
C	-2.783749000	2.246161000	-0.015972000
C	-1.744851000	3.925985000	-1.598729000
C	-0.732402000	4.542558000	-0.612509000
H	-1.170051000	4.627487000	0.389602000
H	-0.438311000	5.547822000	-0.937340000
H	0.163677000	3.921102000	-0.548973000
C	-2.989140000	4.828280000	-1.673327000
H	-3.769356000	4.385636000	-2.303081000

H	-2.699714000	5.784453000	-2.123661000
H	-3.410561000	5.048758000	-0.689118000
C	-1.133382000	3.859593000	-3.010553000
H	-0.232360000	3.245991000	-3.015315000
H	-0.881805000	4.869129000	-3.355171000
H	-1.851446000	3.425642000	-3.716922000
C	2.922068000	-2.007082000	1.041325000
H	2.417287000	-1.734996000	1.961084000
C	4.188956000	-2.607088000	1.056724000
C	4.787418000	-2.770537000	-0.216836000
H	5.799278000	-3.148379000	-0.310562000
C	4.111331000	-2.406182000	-1.366274000
H	4.622095000	-2.470829000	-2.316858000
C	2.792035000	-1.896926000	-1.288405000
C	1.731912000	-2.377900000	-3.536724000
C	2.965607000	-3.085046000	-4.124645000
H	3.744813000	-2.366071000	-4.402716000
H	2.662460000	-3.617268000	-5.033080000
H	3.393254000	-3.825080000	-3.443316000
C	0.719461000	-3.437111000	-3.057484000
H	1.168574000	-4.086449000	-2.296296000
H	0.396372000	-4.070924000	-3.892158000
H	-0.160147000	-2.953329000	-2.626300000
C	1.108929000	-1.521881000	-4.655389000
H	0.199935000	-1.029595000	-4.308926000
H	0.867044000	-2.154822000	-5.516934000
H	1.815908000	-0.750773000	-4.984800000

C	5.490300000	4.071566000	-2.462348000
H	4.712028000	4.832557000	-2.650921000
H	6.201893000	4.096325000	-3.294350000
H	6.026093000	4.351306000	-1.553146000
C	4.303511000	2.281865000	-3.578503000
H	4.044505000	1.220758000	-3.512423000
H	5.012575000	2.412570000	-4.402082000
H	3.386412000	2.846303000	-3.828313000
C	-4.243335000	0.012950000	-4.250643000
H	-4.182281000	0.965307000	-3.695950000
H	-4.831325000	0.175969000	-5.156656000
H	-3.228639000	-0.262645000	-4.557397000
C	-6.307906000	-1.117265000	-3.519576000
H	-6.664758000	-2.135156000	-3.334351000
H	-6.643409000	-0.832469000	-4.519527000
H	-6.789263000	-0.446372000	-2.787663000
C	-4.224188000	0.037112000	4.279066000
H	-4.192179000	-0.913143000	3.718688000
H	-4.809477000	-0.115589000	5.188570000
H	-3.200320000	0.284217000	4.579638000
C	-6.262270000	1.236983000	3.578605000
H	-6.585620000	2.268619000	3.407637000
H	-6.594380000	0.954251000	4.580223000
H	-6.776562000	0.590655000	2.847029000
C	6.273883000	-3.141667000	2.225552000
H	6.581816000	-3.906601000	1.505712000
H	6.608440000	-3.470246000	3.212167000

H	6.798711000	-2.204061000	1.975328000
C	4.251725000	-2.522763000	3.495867000
H	4.238442000	-1.421945000	3.575643000
H	4.835127000	-2.923535000	4.327764000
H	3.222585000	-2.880276000	3.608726000

Table 3.4.33. Optimized coordinates of **Ce^{IV}[5-NMe_2-2-(^{t}BuNO)py]$_4$**

Ce	0.005855000	-0.010143000	-0.009978000
O	0.933236000	0.473463000	1.957112000
O	-0.931930000	-1.723874000	1.051555000
O	-0.901705000	1.735535000	-1.043464000
O	0.896418000	-0.512092000	-1.981922000
N	2.173847000	1.554022000	0.066882000
N	2.085676000	1.140179000	2.364775000
N	-2.144718000	-1.180234000	-1.078847000
N	-2.080741000	-2.494267000	0.863333000
N	-2.097241000	1.212203000	1.103110000
N	-2.023030000	2.539804000	-0.830720000
N	2.117652000	-1.655954000	-0.109804000
N	2.030291000	-1.203771000	-2.411071000
N	4.696387000	3.032842000	-2.234227000
N	-4.557821000	-0.682736000	-3.836153000
N	-4.497462000	0.748147000	3.877399000
N	4.532512000	-3.312871000	2.149502000
C	2.791764000	1.997253000	-1.048880000
H	2.247918000	1.802845000	-1.964788000
C	4.040172000	2.620784000	-1.055859000

C	4.672499000	2.724901000	0.206886000
H	5.678461000	3.125974000	0.281384000
C	4.055297000	2.263861000	1.350662000
H	4.593967000	2.289083000	2.285889000
C	2.756360000	1.700826000	1.271163000
C	1.807857000	1.893195000	3.642513000
C	1.253497000	0.867925000	4.649137000
H	0.328429000	0.417524000	4.287401000
H	1.053431000	1.364985000	5.604555000
H	1.983759000	0.069278000	4.824299000
C	0.773815000	3.006859000	3.388966000
H	1.171864000	3.756067000	2.694627000
H	0.524658000	3.515623000	4.327407000
H	-0.143096000	2.590569000	2.964746000
C	3.081537000	2.504862000	4.250125000
H	3.880611000	1.761509000	4.345837000
H	2.841716000	2.867776000	5.255180000
H	3.451751000	3.359909000	3.679468000
C	-2.751951000	-0.700370000	-2.179799000
H	-2.206234000	0.090008000	-2.679321000
C	-4.000169000	-1.142077000	-2.643538000
C	-4.657418000	-2.072381000	-1.800658000
H	-5.663001000	-2.408523000	-2.024991000
C	-4.049363000	-2.540108000	-0.650256000
H	-4.603189000	-3.194198000	0.007480000
C	-2.743567000	-2.115564000	-0.318473000
C	-1.774960000	-3.938625000	1.178688000

C	-1.192751000	-3.967536000	2.603866000
H	-0.267236000	-3.393583000	2.664708000
H	-0.984441000	-5.003140000	2.894306000
H	-1.909665000	-3.548352000	3.319511000
C	-0.755740000	-4.509382000	0.174431000
H	-1.169211000	-4.512214000	-0.840856000
H	-0.500929000	-5.542817000	0.436795000
H	0.161626000	-3.915362000	0.175029000
C	-3.044635000	-4.806696000	1.171644000
H	-3.832272000	-4.372303000	1.797334000
H	-2.792806000	-5.789126000	1.584825000
H	-3.437084000	-4.971206000	0.165080000
C	-2.705252000	0.738854000	2.206280000
H	-2.173602000	-0.067538000	2.695027000
C	-3.939733000	1.204717000	2.683734000
C	-4.583474000	2.155581000	1.853720000
H	-5.579339000	2.512349000	2.089283000
C	-3.974579000	2.617946000	0.701467000
H	-4.518091000	3.289671000	0.052681000
C	-2.682108000	2.166063000	0.355487000
C	-1.671427000	3.978794000	-1.122184000
C	-0.624583000	4.494869000	-0.116872000
H	-1.031424000	4.500238000	0.901068000
H	-0.329616000	5.520741000	-0.366562000
H	0.267611000	3.863650000	-0.131818000
C	-2.912295000	4.886631000	-1.086328000
H	-3.717558000	4.490437000	-1.715015000

H	-2.632985000	5.869666000	-1.479994000
H	-3.292745000	5.040529000	-0.073477000
C	-1.101197000	4.014963000	-2.551882000
H	-0.192386000	3.416973000	-2.630523000
H	-0.866794000	5.048988000	-2.827642000
H	-1.835686000	3.627191000	-3.267407000
C	2.731636000	-2.114576000	0.996743000
H	2.201358000	-1.909181000	1.917873000
C	3.968350000	-2.776925000	0.992214000
C	4.608373000	-2.842233000	-0.270356000
H	5.605924000	-3.254857000	-0.364960000
C	3.993725000	-2.341562000	-1.403119000
H	4.534763000	-2.342739000	-2.338230000
C	2.698090000	-1.785514000	-1.317121000
C	1.691292000	-1.996373000	-3.650714000
C	2.936582000	-2.652682000	-4.270496000
H	3.742658000	-1.925868000	-4.420531000
H	2.662546000	-3.054532000	-5.251789000
H	3.313488000	-3.486866000	-3.673660000
C	0.645215000	-3.080642000	-3.329049000
H	1.046281000	-3.808860000	-2.614364000
H	0.365975000	-3.622464000	-4.240267000
H	-0.255205000	-2.632825000	-2.901410000
C	1.126011000	-0.995987000	-4.675341000
H	0.220781000	-0.515443000	-4.301859000
H	0.887394000	-1.520605000	-5.606952000
H	1.865242000	-0.218136000	-4.899533000

C	5.282554000	4.374452000	-2.224300000
H	4.518067000	5.167555000	-2.293335000
H	5.959552000	4.474370000	-3.078398000
H	5.864390000	4.539595000	-1.315947000
C	4.034809000	2.724092000	-3.494290000
H	3.804207000	1.655766000	-3.547249000
H	4.714704000	2.968502000	-4.315625000
H	3.098235000	3.289677000	-3.647062000
C	-3.942830000	0.473478000	-4.473570000
H	-3.962913000	1.376662000	-3.840913000
H	-4.473189000	0.689907000	-5.402936000
H	-2.898445000	0.262070000	-4.728101000
C	-5.989490000	-0.858949000	-4.045332000
H	-6.257881000	-1.920401000	-4.029139000
H	-6.250739000	-0.471406000	-5.032110000
H	-6.604420000	-0.337146000	-3.293669000
C	-3.901770000	-0.425685000	4.500913000
H	-3.944699000	-1.322788000	3.860809000
H	-4.430105000	-0.639049000	5.432122000
H	-2.851545000	-0.237760000	4.749715000
C	-5.923915000	0.950833000	4.098258000
H	-6.171667000	2.017373000	4.091687000
H	-6.185689000	0.561202000	5.084080000
H	-6.554128000	0.446604000	3.347259000
C	5.959028000	-3.612255000	2.149702000
H	6.202446000	-4.347363000	1.375725000
H	6.225673000	-4.052031000	3.112870000

H	6.588599000	-2.721636000	1.988634000
C	3.946235000	-2.936876000	3.428849000
H	3.991802000	-1.851863000	3.621414000
H	4.479911000	-3.453449000	4.228996000
H	2.896087000	-3.245202000	3.476384000

Table 3.4.34. Optimized coordinates of **Ce^{III}[4-NMe_2-2-(^{t}BuNO)py]$_4^-$**

Ce	0.000000000	0.000000000	0.016193000
O	-1.539183000	-0.068769000	1.835100000
N	-2.918111000	-0.066412000	1.836153000
C	-3.525590000	0.288495000	0.670608000
N	-2.676707000	0.441553000	-0.392901000
C	-3.212069000	0.793726000	-1.573431000
C	-4.553415000	1.003810000	-1.821423000
C	-5.460961000	0.856039000	-0.731921000
N	-6.813787000	1.087671000	-0.897168000
C	-7.732887000	0.777902000	0.187240000
H	-7.716464000	-0.288124000	0.462755000
H	-8.747643000	1.038060000	-0.117750000
H	-7.493565000	1.361693000	1.084396000
C	-7.359851000	1.260909000	-2.237090000
H	-6.893635000	2.111479000	-2.746674000
H	-8.428481000	1.468060000	-2.160063000
H	-7.226412000	0.369642000	-2.868743000
C	-4.927832000	0.491914000	0.511674000
H	-5.586422000	0.385249000	1.355340000
H	-4.880672000	1.279346000	-2.814987000

H	-2.486935000	0.923538000	-2.374977000
C	-3.565145000	-0.259898000	3.169663000
C	-4.594442000	-1.412485000	3.117382000
H	-5.415200000	-1.239967000	2.419357000
H	-5.031096000	-1.561678000	4.111512000
H	-4.095239000	-2.342451000	2.822857000
C	-4.196904000	1.059174000	3.670964000
H	-3.428055000	1.837940000	3.730177000
H	-4.618836000	0.919659000	4.673043000
H	-4.995322000	1.424830000	3.021017000
C	-2.484801000	-0.676654000	4.185052000
H	-1.984126000	-1.598096000	3.878305000
H	-2.971837000	-0.849691000	5.151687000
H	-1.727103000	0.098415000	4.307698000
O	1.539183000	0.068769000	1.835100000
N	2.918111000	0.066412000	1.836153000
C	3.525590000	-0.288495000	0.670608000
N	2.676707000	-0.441553000	-0.392901000
C	3.212069000	-0.793726000	-1.573431000
C	4.553415000	-1.003810000	-1.821423000
C	5.460961000	-0.856039000	-0.731921000
N	6.813787000	-1.087671000	-0.897168000
C	7.732887000	-0.777902000	0.187240000
H	7.716464000	0.288124000	0.462755000
H	8.747643000	-1.038060000	-0.117750000
H	7.493565000	-1.361693000	1.084396000
C	7.359851000	-1.260909000	-2.237090000

H	6.893635000	-2.111479000	-2.746674000
H	8.428481000	-1.468060000	-2.160063000
H	7.226412000	-0.369642000	-2.868743000
C	4.927832000	-0.491914000	0.511674000
H	5.586422000	-0.385249000	1.355340000
H	4.880672000	-1.279346000	-2.814987000
H	2.486935000	-0.923538000	-2.374977000
C	3.565145000	0.259898000	3.169663000
C	4.594442000	1.412485000	3.117382000
H	5.415200000	1.239967000	2.419357000
H	5.031096000	1.561678000	4.111512000
H	4.095239000	2.342451000	2.822857000
C	4.196904000	-1.059174000	3.670964000
H	3.428055000	-1.837940000	3.730177000
H	4.618836000	-0.919659000	4.673043000
H	4.995322000	-1.424830000	3.021017000
C	2.484801000	0.676654000	4.185052000
H	1.984126000	1.598096000	3.878305000
H	2.971837000	0.849691000	5.151687000
H	1.727103000	-0.098415000	4.307698000
O	-0.211661000	-1.511283000	-1.820415000
N	-0.383331000	-2.879351000	-1.833836000
C	-0.166121000	-3.532571000	-0.659642000
N	0.042119000	-2.716473000	0.420042000
C	0.262949000	-3.299936000	1.609198000
C	0.282227000	-4.658366000	1.852234000
C	0.061941000	-5.533210000	0.748235000

N	0.052866000	-6.905816000	0.919599000
C	0.000000000	-7.773431000	-0.247135000
H	0.872895000	-7.650519000	-0.907519000
H	-0.038153000	-8.813264000	0.081699000
H	-0.901769000	-7.577161000	-0.838882000
C	0.515823000	-7.479313000	2.177101000
H	-0.076833000	-7.108975000	3.020476000
H	0.392205000	-8.562914000	2.138277000
H	1.575051000	-7.260362000	2.381332000
C	-0.142237000	-4.950569000	-0.509388000
H	-0.263088000	-5.583501000	-1.370606000
H	0.475440000	-5.023698000	2.851843000
H	0.450508000	-2.604207000	2.425397000
C	-0.612312000	-3.490464000	-3.178777000
C	0.634128000	-4.277970000	-3.644270000
H	0.880600000	-5.116007000	-2.987705000
H	0.474109000	-4.678190000	-4.652215000
H	1.502179000	-3.609787000	-3.677053000
C	-1.884623000	-4.369299000	-3.170754000
H	-2.754763000	-3.759542000	-2.902858000
H	-2.054208000	-4.782321000	-4.171637000
H	-1.835991000	-5.205363000	-2.471926000
C	-0.859063000	-2.361157000	-4.196915000
H	0.009350000	-1.707930000	-4.291018000
H	-1.064400000	-2.817797000	-5.172049000
H	-1.717445000	-1.747898000	-3.912409000
O	0.211661000	1.511283000	-1.820415000

N	0.383331000	2.879351000	-1.833836000
C	0.166121000	3.532571000	-0.659642000
N	-0.042119000	2.716473000	0.420042000
C	-0.262949000	3.299936000	1.609198000
C	-0.282227000	4.658366000	1.852234000
C	-0.061941000	5.533210000	0.748235000
N	-0.052866000	6.905816000	0.919599000
C	0.000000000	7.773431000	-0.247135000
H	-0.872895000	7.650519000	-0.907519000
H	0.038153000	8.813264000	0.081699000
H	0.901769000	7.577161000	-0.838882000
C	-0.515823000	7.479313000	2.177101000
H	0.076833000	7.108975000	3.020476000
H	-0.392205000	8.562914000	2.138277000
H	-1.575051000	7.260362000	2.381332000
C	0.142237000	4.950569000	-0.509388000
H	0.263088000	5.583501000	-1.370606000
H	-0.475440000	5.023698000	2.851843000
H	-0.450508000	2.604207000	2.425397000
C	0.612312000	3.490464000	-3.178777000
C	-0.634128000	4.277970000	-3.644270000
H	-0.880600000	5.116007000	-2.987705000
H	-0.474109000	4.678190000	-4.652215000
H	-1.502179000	3.609787000	-3.677053000
C	1.884623000	4.369299000	-3.170754000
H	2.754763000	3.759542000	-2.902858000
H	2.054208000	4.782321000	-4.171637000

H	1.835991000	5.205363000	-2.471926000
C	0.859063000	2.361157000	-4.196915000
H	-0.009350000	1.707930000	-4.291018000
H	1.064400000	2.817797000	-5.172049000
H	1.717445000	1.747898000	-3.912409000

Table 3.4.35. Optimized coordinates of **Ce^{IV}[4-NMe_2-2-(^{t}BuNO)py]$_4$**

Ce	0.000000000	0.000000000	0.000528000
O	0.941936000	1.110529000	1.715655000
N	1.876747000	2.121985000	1.747987000
C	2.502598000	2.358300000	0.554482000
N	1.953943000	1.691742000	-0.502002000
C	2.488286000	1.897736000	-1.720913000
C	3.549399000	2.732653000	-1.991683000
C	4.149862000	3.432308000	-0.903394000
N	5.215169000	4.276062000	-1.105059000
C	5.867415000	4.909040000	0.032238000
H	5.159273000	5.522758000	0.602915000
H	6.662033000	5.562814000	-0.328771000
H	6.311181000	4.173421000	0.719021000
C	5.836047000	4.370084000	-2.421241000
H	6.258121000	3.410588000	-2.751669000
H	6.644024000	5.101329000	-2.380290000
H	5.117717000	4.706495000	-3.178192000
C	3.613467000	3.219668000	0.377314000
H	4.061248000	3.703537000	1.227251000
H	3.909065000	2.830036000	-3.007085000

H	2.018566000	1.333554000	-2.522075000
C	2.293792000	2.574769000	3.111070000
C	2.244262000	4.116730000	3.200203000
H	2.924806000	4.620583000	2.512447000
H	2.509459000	4.430859000	4.215660000
H	1.229421000	4.470028000	2.987722000
C	3.688590000	2.016735000	3.470514000
H	3.677046000	0.922299000	3.418644000
H	3.957784000	2.308054000	4.492035000
H	4.474274000	2.377935000	2.802210000
C	1.280575000	2.034766000	4.137231000
H	0.265282000	2.371432000	3.910843000
H	1.559928000	2.416616000	5.125230000
H	1.281284000	0.944191000	4.172441000
O	-0.941936000	-1.110529000	1.715655000
N	-1.876747000	-2.121985000	1.747987000
C	-2.502598000	-2.358300000	0.554482000
N	-1.953943000	-1.691742000	-0.502002000
C	-2.488286000	-1.897736000	-1.720913000
C	-3.549399000	-2.732653000	-1.991683000
C	-4.149862000	-3.432308000	-0.903394000
N	-5.215169000	-4.276062000	-1.105059000
C	-5.867415000	-4.909040000	0.032238000
H	-5.159273000	-5.522758000	0.602915000
H	-6.662033000	-5.562814000	-0.328771000
H	-6.311181000	-4.173421000	0.719021000
C	-5.836047000	-4.370084000	-2.421241000

H	-6.258121000	-3.410588000	-2.751669000
H	-6.644024000	-5.101329000	-2.380290000
H	-5.117717000	-4.706495000	-3.178192000
C	-3.613467000	-3.219668000	0.377314000
H	-4.061248000	-3.703537000	1.227251000
H	-3.909065000	-2.830036000	-3.007085000
H	-2.018566000	-1.333554000	-2.522075000
C	-2.293792000	-2.574769000	3.111070000
C	-2.244262000	-4.116730000	3.200203000
H	-2.924806000	-4.620583000	2.512447000
H	-2.509459000	-4.430859000	4.215660000
H	-1.229421000	-4.470028000	2.987722000
C	-3.688590000	-2.016735000	3.470514000
H	-3.677046000	-0.922299000	3.418644000
H	-3.957784000	-2.308054000	4.492035000
H	-4.474274000	-2.377935000	2.802210000
C	-1.280575000	-2.034766000	4.137231000
H	-0.265282000	-2.371432000	3.910843000
H	-1.559928000	-2.416616000	5.125230000
H	-1.281284000	-0.944191000	4.172441000
O	-0.943639000	1.107683000	-1.715349000
N	-1.876460000	2.121002000	-1.747544000
C	-2.502901000	2.357067000	-0.554305000
N	-1.954866000	1.690269000	0.502431000
C	-2.489246000	1.897392000	1.721111000
C	-3.549643000	2.733330000	1.991423000
C	-4.149935000	3.432558000	0.902777000

N	-5.214855000	4.276788000	1.104141000
C	-5.867415000	4.909072000	-0.033277000
H	-6.312297000	4.173092000	-0.718984000
H	-6.661377000	5.563646000	0.327724000
H	-5.159315000	5.521746000	-0.605087000
C	-5.834932000	4.372382000	2.420480000
H	-5.116184000	4.709641000	3.176655000
H	-6.642897000	5.103632000	2.379125000
H	-6.256875000	3.413238000	2.752128000
C	-3.613467000	3.218659000	-0.377822000
H	-4.060877000	3.702097000	-1.228195000
H	-3.909211000	2.831516000	3.006777000
H	-2.019987000	1.333684000	2.522722000
C	-2.293935000	2.572807000	-3.110708000
C	-3.688201000	2.013190000	-3.470424000
H	-4.474472000	2.373363000	-2.802086000
H	-3.957654000	2.304485000	-4.491883000
H	-3.675408000	0.918806000	-3.418687000
C	-2.246052000	4.114719000	-3.200559000
H	-1.231470000	4.469298000	-2.989015000
H	-2.512281000	4.427953000	-4.216004000
H	-2.926727000	4.618065000	-2.512609000
C	-1.279881000	2.033335000	-4.136523000
H	-1.279147000	0.942744000	-4.171076000
H	-1.559733000	2.414121000	-5.124813000
H	-0.265042000	2.371646000	-3.910427000
O	0.943639000	-1.107683000	-1.715349000

N	1.876460000	-2.121002000	-1.747544000
C	2.502901000	-2.357067000	-0.554305000
N	1.954866000	-1.690269000	0.502431000
C	2.489246000	-1.897392000	1.721111000
C	3.549643000	-2.733330000	1.991423000
C	4.149935000	-3.432558000	0.902777000
N	5.214855000	-4.276788000	1.104141000
C	5.867415000	-4.909072000	-0.033277000
H	6.312297000	-4.173092000	-0.718984000
H	6.661377000	-5.563646000	0.327724000
H	5.159315000	-5.521746000	-0.605087000
C	5.834932000	-4.372382000	2.420480000
H	5.116184000	-4.709641000	3.176655000
H	6.642897000	-5.103632000	2.379125000
H	6.256875000	-3.413238000	2.752128000
C	3.613467000	-3.218659000	-0.377822000
H	4.060877000	-3.702097000	-1.228195000
H	3.909211000	-2.831516000	3.006777000
H	2.019987000	-1.333684000	2.522722000
C	2.293935000	-2.572807000	-3.110708000
C	3.688201000	-2.013190000	-3.470424000
H	4.474472000	-2.373363000	-2.802086000
H	3.957654000	-2.304485000	-4.491883000
H	3.675408000	-0.918806000	-3.418687000
C	2.246052000	-4.114719000	-3.200559000
H	1.231470000	-4.469298000	-2.989015000
H	2.512281000	-4.427953000	-4.216004000

H	2.926727000	-4.618065000	-2.512609000
C	1.279881000	-2.033335000	-4.136523000
H	1.279147000	-0.942744000	-4.171076000
H	1.559733000	-2.414121000	-5.124813000
H	0.265042000	-2.371646000	-3.910427000

Table 3.4.36. Optimized coordinates of **$[Ce^{III}(NO_3)_6]^{3-}$ + 2 $[NEt_4]^+$**

Ce	-0.008996000	0.229165000	0.087774000
O	0.756537000	-1.436512000	-1.852034000
O	2.109157000	-1.380493000	-0.155303000
O	2.615755000	-2.584497000	-1.908975000
N	1.841820000	-1.817488000	-1.319973000
O	-2.104363000	-0.592784000	-1.327386000
O	-0.942782000	0.952545000	-2.312266000
O	-2.790562000	0.232408000	-3.232583000
N	-1.961848000	0.198711000	-2.312014000
O	-1.918753000	-0.828234000	1.592616000
O	-0.690722000	-2.302551000	0.580010000
O	-2.528454000	-2.928900000	1.587403000
N	-1.729135000	-2.043047000	1.262462000
O	-0.815845000	1.879456000	1.997534000
O	-2.119537000	1.822819000	0.263721000
O	2.052877000	1.089018000	1.523169000
O	0.983159000	-0.569792000	2.423389000
O	1.938069000	1.234901000	-1.413581000
O	0.660144000	2.728714000	-0.493622000
N	-1.882389000	2.275222000	1.429641000

N	1.999019000	0.191409000	2.422072000
N	1.684594000	2.464391000	-1.198511000
O	-2.655093000	3.062709000	1.983178000
O	2.904285000	0.062533000	3.256819000
O	2.403545000	3.357817000	-1.654089000
N	-6.073614000	-0.444993000	-0.307990000
C	-5.662041000	0.568119000	-1.384076000
C	-5.423932000	2.007527000	-0.940900000
H	-6.461552000	0.524615000	-2.127885000
H	-4.751637000	0.180252000	-1.838952000
H	-5.279111000	2.589127000	-1.858198000
H	-6.271913000	2.450118000	-0.411774000
H	-4.515211000	2.114001000	-0.344743000
C	-7.438830000	-0.039370000	0.240623000
C	-8.100392000	-1.025909000	1.199218000
H	-8.072816000	0.120195000	-0.634965000
H	-7.296328000	0.923123000	0.728359000
H	-8.969585000	-0.521705000	1.633772000
H	-8.463327000	-1.925186000	0.696630000
H	-7.447519000	-1.323910000	2.024027000
C	-6.220248000	-1.806609000	-0.998927000
C	-4.943554000	-2.424553000	-1.559908000
H	-6.963339000	-1.657492000	-1.786688000
H	-6.646631000	-2.475520000	-0.252422000
H	-5.238633000	-3.364507000	-2.038744000
H	-4.446783000	-1.806195000	-2.309273000
H	-4.220604000	-2.663957000	-0.776276000

C	-5.008368000	-0.567033000	0.792580000
C	-5.078336000	0.420750000	1.952861000
H	-4.047464000	-0.482326000	0.286678000
H	-5.088675000	-1.583964000	1.179917000
H	-4.221080000	0.180550000	2.588634000
H	-4.972232000	1.462497000	1.649512000
H	-5.983175000	0.312430000	2.556096000
N	6.018681000	-0.338262000	-0.090438000
C	6.296534000	-0.039334000	-1.564816000
C	5.084724000	-0.057472000	-2.490616000
H	7.026743000	-0.781595000	-1.888643000
H	6.782798000	0.937497000	-1.585772000
H	5.453023000	0.176125000	-3.495455000
H	4.600905000	-1.036302000	-2.536591000
H	4.329530000	0.688092000	-2.229672000
C	5.515374000	-1.779304000	0.033543000
C	5.307154000	-2.289351000	1.455547000
H	6.243458000	-2.397406000	-0.494865000
H	4.571578000	-1.823435000	-0.508287000
H	4.955255000	-3.322899000	1.371150000
H	6.226518000	-2.306405000	2.047155000
H	4.542781000	-1.729327000	1.999849000
C	4.943203000	0.601781000	0.462357000
C	5.215065000	2.093446000	0.311645000
H	4.832221000	0.350579000	1.516764000
H	4.013581000	0.331531000	-0.035469000
H	4.361518000	2.602124000	0.769063000

H	6.116293000	2.424993000	0.834487000
H	5.265653000	2.418855000	-0.730513000
C	7.307921000	-0.135039000	0.703107000
C	8.451608000	-1.092987000	0.387167000
H	7.028070000	-0.205854000	1.755270000
H	7.618988000	0.892040000	0.511345000
H	9.294502000	-0.805428000	1.023847000
H	8.211230000	-2.134675000	0.614257000
H	8.790245000	-1.025063000	-0.649691000

Table 3.4.37. Optimized coordinates of **$[Ce^{IV}(NO_3)_6]^{2-}$ + 2 $[NEt_4]^+$**

Ce	-0.011337494	0.216100790	0.102211775
O	0.663328000	-1.346405905	-1.806324785
O	2.011880428	-1.323787853	-0.121022217
O	2.546394567	-2.456278258	-1.913929216
N	1.757617967	-1.736584944	-1.307188161
O	-2.011789012	-0.549801324	-1.260778798
O	-0.830488335	0.991742147	-2.200260702
O	-2.687573691	0.325665267	-3.147846188
N	-1.861550808	0.262570817	-2.240644065
O	-1.855294387	-0.771790756	1.513976665
O	-0.618691052	-2.223687680	0.507869572
O	-2.473028586	-2.871098769	1.477230560
N	-1.669461572	-1.996179321	1.180593389
O	-0.710549677	1.761092830	1.961571176
O	-2.034466612	1.710903305	0.259270195
O	1.957035963	1.004947570	1.470140156

O	0.852148481	-0.633139337	2.333019240
O	1.869888879	1.135917690	-1.301794898
O	0.594522479	2.619521190	-0.393813387
N	-1.795809673	2.165827874	1.436293635
N	1.891634275	0.092770274	2.366663869
N	1.635414006	2.380077332	-1.082527352
O	-2.569225670	2.919512698	2.002408287
O	2.791629242	-0.071831434	3.182654870
O	2.375976204	3.254432948	-1.499620277
N	-5.885136981	-0.416601181	-0.334454937
C	-5.477699234	0.629195115	-1.384095597
C	-5.258423068	2.059861125	-0.905145873
H	-6.273430789	0.590732528	-2.134998658
H	-4.560923474	0.264173392	-1.844655469
H	-5.093260900	2.660178158	-1.806690282
H	-6.119436135	2.489577647	-0.384086814
H	-4.360618349	2.162026630	-0.292290672
C	-7.254151069	-0.043538866	0.212035030
C	-7.912416557	-1.064573283	1.138466769
H	-7.887323078	0.137127528	-0.661822009
H	-7.124340556	0.905797973	0.729064837
H	-8.777029686	-0.581986477	1.606302511
H	-8.281636330	-1.944201467	0.605440507
H	-7.248664983	-1.396547212	1.941104225
C	-6.002572579	-1.764245203	-1.056123667
C	-4.716351140	-2.354310322	-1.626757926
H	-6.746585048	-1.607753520	-1.844186539

H	-6.422956224	-2.455720289	-0.325337724
H	-4.998861754	-3.287484883	-2.127536433
H	-4.222091895	-1.715604527	-2.360152962
H	-3.992368188	-2.604362347	-0.848262727
C	-4.825166948	-0.544613275	0.777991100
C	-4.930382016	0.405767126	1.965226156
H	-3.865485316	-0.416184998	0.281853270
H	-4.875040755	-1.576535206	1.129186762
H	-4.070652400	0.167500815	2.598105540
H	-4.842174461	1.458982814	1.697570785
H	-5.834740469	0.257535161	2.562885524
N	5.834349089	-0.311053132	-0.107078585
C	6.125651587	0.053251865	-1.562898250
C	4.923108539	0.094405768	-2.501146843
H	6.853576698	-0.681208359	-1.913832821
H	6.620236519	1.026958867	-1.531622144
H	5.304640599	0.361489518	-3.493217540
H	4.419121323	-0.871017343	-2.592797109
H	4.177180341	0.841506774	-2.220228285
C	5.319954195	-1.754558227	-0.053919910
C	5.081289614	-2.327240619	1.338567885
H	6.054854762	-2.350562974	-0.600667704
H	4.385337287	-1.774690103	-0.612149950
H	4.694673844	-3.341789131	1.196632815
H	5.991602205	-2.404901715	1.942211570
H	4.322706694	-1.778285963	1.900962341
C	4.759094580	0.617066314	0.478651331

C	5.043002688	2.111152905	0.393840134
H	4.631450672	0.318267398	1.518762735
H	3.836178570	0.376687138	-0.043424923
H	4.191431609	2.601974842	0.873521526
H	5.944628358	2.418466131	0.933458078
H	5.086273443	2.485433787	-0.632034383
C	7.108482119	-0.154834802	0.709565989
C	8.259658276	-1.094779790	0.362132029
H	6.813298160	-0.284407536	1.752421557
H	7.422329737	0.882423928	0.583300159
H	9.095628680	-0.849261851	1.025718354
H	8.012665588	-2.146997059	0.525606429
H	8.615934426	-0.972327491	-0.664334130

Table 3.4.38. Optimized coordinates of **$[Ce^{III}(acac)_4]^-$**

Ce	0.000011000	0.000196000	0.000003000
O	1.848719000	-1.519346000	0.693818000
C	2.694405000	-2.297001000	0.149464000
C	3.700829000	-2.951806000	1.082506000
H	4.263503000	-2.176086000	1.615840000
H	4.404741000	-3.604825000	0.559673000
H	3.168504000	-3.538340000	1.841177000
C	2.756192000	-2.589342000	-1.227346000
C	1.870990000	-2.060723000	-2.189499000
O	0.925815000	-1.249272000	-1.943457000
C	2.035038000	-2.480207000	-3.642106000
H	2.198178000	-1.591237000	-4.263316000

H	1.108325000	-2.949564000	-3.993918000
H	2.864454000	-3.176099000	-3.793921000
H	3.524244000	-3.275499000	-1.566734000
O	-0.925786000	-1.249442000	1.943367000
C	-1.870960000	-2.060912000	2.189354000
C	-2.035000000	-2.480506000	3.641931000
H	-2.198086000	-1.591582000	4.263219000
H	-1.108302000	-2.949935000	3.993684000
H	-2.864444000	-3.176374000	3.793704000
C	-2.756194000	-2.589423000	1.227173000
C	-2.694425000	-2.296970000	-0.149615000
O	-1.848733000	-1.519296000	-0.693928000
C	-3.700902000	-2.951659000	-1.082685000
H	-4.404802000	-3.604723000	-0.559893000
H	-3.168621000	-3.538115000	-1.841446000
H	-4.263589000	-2.175870000	-1.615906000
H	-3.524261000	-3.275586000	1.566516000
O	-1.848019000	1.519938000	0.695247000
C	-2.694419000	2.297175000	0.151395000
C	-3.700161000	2.952027000	1.085142000
H	-3.167296000	3.538954000	1.843130000
H	-4.262144000	2.176338000	1.619249000
H	-4.404721000	3.604687000	0.562734000
C	-2.757570000	2.589045000	-1.225449000
C	-1.873096000	2.060440000	-2.188288000
O	-0.927443000	1.249344000	-1.942930000
C	-2.038615000	2.479536000	-3.640841000

H	-2.202150000	1.590379000	-4.261680000
H	-1.112337000	2.949008000	-3.993644000
H	-2.868328000	3.175207000	-3.792040000
H	-3.526125000	3.274895000	-1.564319000
O	0.927459000	1.249197000	1.943025000
C	1.873103000	2.060289000	2.188425000
C	2.038697000	2.479210000	3.641022000
H	2.868397000	3.174888000	3.792258000
H	1.112423000	2.948605000	3.993936000
H	2.202299000	1.589981000	4.261741000
C	2.757555000	2.588983000	1.225612000
C	2.694371000	2.297232000	-0.151253000
O	1.847984000	1.519999000	-0.695136000
C	3.700083000	2.952160000	-1.084975000
H	3.167192000	3.539143000	-1.842900000
H	4.262058000	2.176518000	-1.619159000
H	4.404652000	3.604783000	-0.562533000
H	3.526119000	3.274799000	1.564529000

Table 3.4.39. Optimized coordinates of **$Ce^{IV}(acac)_4$**

Ce	-0.000011000	0.000000000	-0.000001000
O	1.854846000	1.269654000	-0.744626000
C	2.824215000	1.908384000	-0.214434000
C	3.935600000	2.326938000	-1.152223000
H	4.342344000	1.439498000	-1.650567000
H	4.742927000	2.852571000	-0.637200000
H	3.526614000	2.976740000	-1.934922000

C	2.896586000	2.241968000	1.149759000
C	1.874489000	1.951605000	2.067181000
O	0.803120000	1.319658000	1.770195000
C	1.996863000	2.409300000	3.503646000
H	1.932390000	1.540923000	4.169643000
H	1.154611000	3.066487000	3.750016000
H	2.932373000	2.939693000	3.695531000
H	3.759536000	2.795725000	1.499107000
O	-0.803117000	1.319680000	-1.770183000
C	-1.874474000	1.951654000	-2.067163000
C	-1.996863000	2.409315000	-3.503636000
H	-1.932322000	1.540937000	-4.169626000
H	-1.154650000	3.066556000	-3.749999000
H	-2.932404000	2.939648000	-3.695539000
C	-2.896581000	2.241995000	-1.149747000
C	-2.824225000	1.908387000	0.214441000
O	-1.854844000	1.269679000	0.744640000
C	-3.935592000	2.326975000	1.152236000
H	-4.742896000	2.852652000	0.637221000
H	-3.526584000	2.976745000	1.934952000
H	-4.342373000	1.439540000	1.650557000
H	-3.759532000	2.795752000	-1.499094000
O	-1.854848000	-1.269675000	-0.744639000
C	-2.824219000	-1.908397000	-0.214437000
C	-3.935585000	-2.326996000	-1.152228000
H	-3.526572000	-2.976762000	-1.934944000
H	-4.342376000	-1.439565000	-1.650550000

H	-4.742883000	-2.852679000	-0.637211000
C	-2.896569000	-2.242004000	1.149752000
C	-1.874466000	-1.951649000	2.067168000
O	-0.803114000	-1.319668000	1.770185000
C	-1.996848000	-2.409312000	3.503640000
H	-1.932346000	-1.540929000	4.169628000
H	-1.154613000	-3.066519000	3.750012000
H	-2.932372000	-2.939678000	3.695538000
H	-3.759513000	-2.795771000	1.499099000
O	0.803120000	-1.319648000	-1.770193000
C	1.874492000	-1.951589000	-2.067186000
C	1.996852000	-2.409297000	-3.503647000
H	2.932374000	-2.939666000	-3.695543000
H	1.154615000	-3.066515000	-3.749992000
H	1.932337000	-1.540931000	-4.169654000
C	2.896587000	-2.241958000	-1.149766000
C	2.824225000	-1.908367000	0.214427000
O	1.854852000	-1.269650000	0.744627000
C	3.935592000	-2.326964000	1.152219000
H	3.526581000	-2.976747000	1.934922000
H	4.342369000	-1.439536000	1.650558000
H	4.742899000	-2.852630000	0.637199000
H	3.759529000	-2.795731000	-1.499112000

Table 3.4.40. Optimized coordinates of **[Ce^{III}(BrSALEN)$_2$]$^-$**

Ce	-0.001406000	-0.000282000	0.000112000
N	-0.784513000	1.234834000	-2.290853000

C	-1.193637000	2.440880000	-2.490538000
H	-1.393822000	2.764247000	-3.522653000
C	-1.450031000	3.466260000	-1.493918000
C	-1.389432000	3.233007000	-0.075175000
O	-1.066273000	2.089688000	0.438186000
C	-1.715240000	4.334655000	0.772476000
H	-1.677293000	4.167619000	1.845448000
C	-2.064350000	5.576680000	0.272445000
H	-2.301160000	6.392525000	0.948144000
C	-2.112812000	5.775082000	-1.116274000
C	-1.817835000	4.739614000	-1.982418000
H	-1.866097000	4.897409000	-3.056183000
C	-0.669872000	0.372752000	-3.466738000
H	-0.771527000	0.941802000	-4.403042000
H	-1.482413000	-0.364916000	-3.430896000
C	0.666847000	-0.373718000	-3.467096000
N	0.782397000	-1.235436000	-2.291009000
C	1.193141000	-2.440960000	-2.490549000
H	1.393991000	-2.764088000	-3.522614000
C	1.451369000	-3.465775000	-1.493832000
C	1.389718000	-3.232707000	-0.075099000
O	1.063788000	-2.090170000	0.438203000
C	1.717612000	-4.333692000	0.772630000
H	1.679022000	-4.166745000	1.845594000
C	2.069587000	-5.574940000	0.272695000
H	2.308009000	-6.390266000	0.948455000
C	2.118933000	-5.773204000	-1.116015000

C	1.822056000	-4.738340000	-1.982224000
H	1.871049000	-4.895994000	-3.055978000
H	0.767745000	-0.943091000	-4.403295000
H	1.479447000	0.363937000	-3.432199000
N	1.233666000	0.782851000	2.291281000
C	2.439324000	1.193041000	2.491091000
H	2.762002000	1.394556000	3.523163000
C	3.464461000	1.450629000	1.494574000
C	3.231660000	1.388829000	0.075777000
O	2.088668000	1.064825000	-0.437740000
C	4.333463000	1.714458000	-0.771762000
H	4.166837000	1.675528000	-1.844763000
C	5.575010000	2.065068000	-0.271597000
H	6.390909000	2.301935000	-0.947213000
C	5.772818000	2.115160000	1.117147000
C	4.737272000	1.820154000	1.983184000
H	4.894642000	1.869525000	3.056962000
C	0.371496000	0.667913000	3.467083000
H	-0.365826000	1.480800000	3.431928000
H	0.940655000	0.768645000	4.403437000
C	-0.375374000	-0.668590000	3.466708000
N	-1.237302000	-0.783455000	2.290726000
C	-2.443104000	-1.193358000	2.490252000
H	-2.766480000	-1.393795000	3.522316000
C	-3.467972000	-1.450752000	1.493372000
C	-3.234345000	-1.389893000	0.074687000
O	-2.091327000	-1.065144000	-0.438310000

C	-4.335288000	-1.717225000	-0.773295000
H	-4.167947000	-1.679200000	-1.846217000
C	-5.577035000	-2.067859000	-0.273637000
H	-6.392346000	-2.305814000	-0.949580000
C	-5.775844000	-2.116411000	1.115018000
C	-4.741029000	-1.820084000	1.981481000
H	-4.899102000	-1.868489000	3.055200000
H	0.362082000	-1.481337000	3.431096000
H	-0.944569000	-0.769982000	4.402962000
Br	2.610567000	-7.497937000	-1.809703000
Br	-2.600808000	7.500793000	-1.810097000
Br	7.497923000	2.605092000	1.811128000
Br	-7.501230000	-2.606337000	1.808299000

Table 3.4.41. Optimized coordinates of **Ce^{IV}(BrSALEN)$_2$**

Ce	0.000097000	0.000065000	0.000001000
N	-0.706602000	-1.253163000	-2.219574000
C	-1.586461000	-2.179401000	-2.380912000
H	-1.806696000	-2.526758000	-3.398381000
C	-2.340415000	-2.856940000	-1.338949000
C	-2.083532000	-2.671044000	0.052584000
O	-1.155330000	-1.848150000	0.482025000
C	-2.851426000	-3.417649000	0.977964000
H	-2.653264000	-3.279714000	2.036490000
C	-3.832892000	-4.303190000	0.557152000
H	-4.411858000	-4.861576000	1.285146000
C	-4.070440000	-4.474299000	-0.813130000

C	-3.334097000	-3.769362000	-1.749064000
H	-3.517023000	-3.912302000	-2.809536000
C	-0.019246000	-0.764310000	-3.416005000
H	-0.500158000	-1.123924000	-4.335847000
H	1.008959000	-1.146124000	-3.396820000
C	0.018941000	0.763495000	-3.416218000
N	0.706462000	1.252685000	-2.220019000
C	1.586244000	2.178931000	-2.381733000
H	1.806394000	2.525943000	-3.399339000
C	2.340362000	2.856751000	-1.340073000
C	2.083722000	2.671213000	0.051554000
O	1.155628000	1.848398000	0.481374000
C	2.851752000	3.418085000	0.976605000
H	2.653775000	3.280425000	2.035202000
C	3.833120000	4.303545000	0.555392000
H	4.412190000	4.862143000	1.283140000
C	4.070433000	4.474296000	-0.814974000
C	3.333955000	3.769087000	-1.750597000
H	3.516695000	3.911753000	-2.811138000
H	0.499722000	1.122854000	-4.336227000
H	-1.009262000	1.145313000	-3.396994000
N	-1.252664000	0.706885000	2.219801000
C	-2.178934000	1.586686000	2.381283000
H	-2.526049000	1.806996000	3.398819000
C	-2.856757000	2.340529000	1.339426000
C	-2.671117000	2.083612000	-0.052135000
O	-1.848201000	1.155492000	-0.481706000

C	-3.417994000	2.851386000	-0.977393000
H	-3.280254000	2.653197000	-2.035940000
C	-4.303556000	3.832773000	-0.556440000
H	-4.862156000	4.411646000	-1.284343000
C	-4.474407000	4.070361000	0.813867000
C	-3.769198000	3.334134000	1.749687000
H	-3.911937000	3.517089000	2.810181000
C	-0.763551000	0.019599000	3.416166000
H	-1.145375000	-1.008605000	3.397123000
H	-1.122964000	0.500565000	4.336057000
C	0.764253000	-0.018595000	3.416061000
N	1.253185000	-0.706178000	2.219791000
C	2.179374000	-1.586046000	2.381367000
H	2.526697000	-1.806047000	3.398898000
C	2.856936000	-2.340248000	1.339599000
C	2.671154000	-2.083628000	-0.051999000
O	1.848351000	-1.155458000	-0.481683000
C	3.417773000	-2.851755000	-0.977174000
H	3.279925000	-2.653795000	-2.035749000
C	4.303219000	-3.833196000	-0.556106000
H	4.861618000	-4.412343000	-1.283946000
C	4.474221000	-4.070481000	0.814235000
C	3.769267000	-3.333907000	1.749974000
H	3.912123000	-3.516630000	2.810492000
H	1.146073000	1.009605000	3.396712000
H	1.123801000	-0.499336000	4.336016000
Br	5.423054000	5.704558000	-1.394590000

Br	-5.423201000	-5.704667000	-1.392192000
Br	-5.704804000	5.423011000	1.393127000
Br	5.704464000	-5.423205000	1.393648000

Table 3.4.42. Optimized coordinates of **[Ce^{III}(SALEN)$_2$]$^-$**

Ce	-0.000722000	-0.001405000	-0.000637000
N	-1.380306000	-0.500088000	-2.289117000
C	-2.647323000	-0.638998000	-2.487863000
H	-3.004261000	-0.767850000	-3.521346000
C	-3.705839000	-0.669056000	-1.495863000
C	-3.468054000	-0.648858000	-0.075832000
O	-2.279888000	-0.574582000	0.441041000
C	-4.615523000	-0.721568000	0.768882000
H	-4.443139000	-0.709812000	1.842373000
C	-5.900704000	-0.800634000	0.257377000
H	-6.745931000	-0.850113000	0.940976000
C	-6.125447000	-0.820220000	-1.132101000
H	-7.133548000	-0.885098000	-1.530439000
C	-5.030887000	-0.760113000	-1.980281000
H	-5.182882000	-0.781014000	-3.058473000
C	-0.512105000	-0.572674000	-3.462118000
H	-1.087711000	-0.549164000	-4.400539000
H	0.034272000	-1.524848000	-3.427197000
C	0.507061000	0.571092000	-3.462753000
N	1.375965000	0.499726000	-2.290134000
C	2.642486000	0.642252000	-2.489858000
H	2.998543000	0.768489000	-3.523969000

C	3.702072000	0.673920000	-1.499017000
C	3.466052000	0.650355000	-0.078801000
O	2.278765000	0.569375000	0.439131000
C	4.614080000	0.726537000	0.764792000
H	4.442954000	0.712301000	1.838450000
C	5.898380000	0.811567000	0.252005000
H	6.744147000	0.863472000	0.934754000
C	6.121496000	0.833906000	-1.137677000
H	7.128890000	0.903365000	-1.537032000
C	5.026240000	0.770649000	-1.984744000
H	5.176956000	0.793833000	-3.063066000
H	1.082225000	0.547005000	-4.401429000
H	-0.039448000	1.523221000	-3.428252000
N	-0.498909000	1.375906000	2.291604000
C	-0.641519000	2.642590000	2.490188000
H	-0.759342000	3.000307000	3.524707000
C	-0.670820000	3.701729000	1.498717000
C	-0.650304000	3.465214000	0.078411000
O	-0.574569000	2.277665000	-0.439712000
C	-0.723437000	4.613368000	-0.765302000
H	-0.711424000	4.441964000	-1.838945000
C	-0.802874000	5.898091000	-0.252707000
H	-0.852560000	6.743884000	-0.935589000
C	-0.822350000	6.121646000	1.136942000
H	-0.887493000	7.129393000	1.536131000
C	-0.761931000	5.026383000	1.984192000
H	-0.783009000	5.177477000	3.062507000

C	-0.567346000	0.507703000	3.464957000
H	-1.519162000	-0.039478000	3.432699000
H	-0.541689000	1.083307000	4.403311000
C	0.577065000	-0.510750000	3.462260000
N	0.502853000	-1.379120000	2.289416000
C	0.644500000	-2.645946000	2.487832000
H	0.774532000	-3.002591000	3.521261000
C	0.674247000	-3.704873000	1.496145000
C	0.649816000	-3.468209000	0.075945000
O	0.570356000	-2.280732000	-0.441737000
C	0.723708000	-4.616051000	-0.768143000
H	0.708855000	-4.444476000	-1.841723000
C	0.807453000	-5.900656000	-0.255954000
H	0.857628000	-6.746216000	-0.939088000
C	0.830787000	-6.124369000	1.133619000
H	0.899235000	-7.132018000	1.532503000
C	0.769776000	-5.029384000	1.981181000
H	0.793636000	-5.180606000	3.059421000
H	1.528743000	0.036376000	3.425362000
H	0.555806000	-1.086256000	4.400794000

Table 3.4.43. Optimized coordinates of **$Ce^{IV}(SALEN)_2$**

Ce	0.000051000	0.000141000	-0.000002000
N	-1.102943000	-0.920311000	2.221665000
C	-1.856008000	-1.954545000	2.380220000
H	-2.155476000	-2.234170000	3.399094000
C	-2.389873000	-2.818690000	1.343655000

C	-2.252930000	-2.535930000	-0.049487000
O	-1.605032000	-1.475179000	-0.480343000
C	-2.852130000	-3.423804000	-0.973583000
H	-2.749863000	-3.201656000	-2.031976000
C	-3.549176000	-4.544975000	-0.542039000
H	-3.995269000	-5.210746000	-1.276819000
C	-3.686035000	-4.825124000	0.827679000
H	-4.234154000	-5.701224000	1.159868000
C	-3.113948000	-3.960248000	1.749338000
H	-3.217031000	-4.156687000	2.814494000
C	-0.747851000	-0.158920000	3.419623000
H	-1.013151000	-0.699846000	4.338717000
H	-1.310597000	0.783002000	3.405121000
C	0.747127000	0.158558000	3.419847000
N	1.102550000	0.920149000	2.222110000
C	1.855819000	1.954186000	2.381020000
H	2.154385000	2.234090000	3.400083000
C	2.389876000	2.818577000	1.344761000
C	2.253182000	2.536153000	-0.048473000
O	1.605214000	1.475599000	-0.479698000
C	2.852634000	3.424197000	-0.972243000
H	2.750554000	3.202311000	-2.030709000
C	3.549666000	4.545224000	-0.540301000
H	3.995950000	5.211135000	-1.274838000
C	3.686252000	4.825060000	0.829508000
H	4.234358000	5.701050000	1.162009000
C	3.113918000	3.960013000	1.750853000

H	3.216803000	4.156196000	2.816075000
H	1.012194000	0.699322000	4.339101000
H	1.309866000	-0.783369000	3.405335000
N	0.920582000	-1.102350000	-2.221918000
C	1.954685000	-1.855575000	-2.380604000
H	2.234583000	-2.154458000	-3.399575000
C	2.818661000	-2.389900000	-1.344135000
C	2.535924000	-2.253167000	0.049030000
O	1.475362000	-1.605039000	0.479997000
C	3.423624000	-2.852791000	0.973016000
H	3.201491000	-2.750684000	2.031427000
C	4.544623000	-3.550035000	0.541343000
H	5.210268000	-3.996454000	1.276039000
C	4.824768000	-3.686662000	-0.828398000
H	5.700741000	-4.234924000	-1.160688000
C	3.960055000	-3.114158000	-1.749951000
H	4.156495000	-3.217051000	-2.815126000
C	0.159213000	-0.746987000	-3.419812000
H	-0.782699000	-1.309759000	-3.405502000
H	0.700181000	-1.012040000	-4.338951000
C	-0.158305000	0.747984000	-3.419664000
N	-0.919912000	1.103114000	-2.221856000
C	-1.954206000	1.856038000	-2.380649000
H	-2.233373000	2.155829000	-3.399553000
C	-2.818670000	2.389763000	-1.344282000
C	-2.536178000	2.252911000	0.048927000
O	-1.475405000	1.605214000	0.480032000

C	-3.424347000	2.851998000	0.972814000
H	-3.202411000	2.749802000	2.031257000
C	-4.545533000	3.548859000	0.541009000
H	-5.211530000	3.994870000	1.275634000
C	-4.825403000	3.685649000	-0.828773000
H	-5.701509000	4.233635000	-1.161166000
C	-3.960243000	3.113667000	-1.750230000
H	-4.156459000	3.216704000	-2.815431000
H	0.783601000	1.310749000	-3.404983000
H	-0.699057000	1.013261000	-4.338867000

Table 3.4.44. Optimized coordinates of **[Ce^{III}(OMeSALEN)$_2$]$^-$**

Ce	-0.000124000	-0.000550000	0.000000000
N	-1.375978000	-0.510732000	-2.299927000
C	-2.640482000	-0.663321000	-2.501227000
H	-2.996270000	-0.793568000	-3.534732000
C	-3.698654000	-0.703773000	-1.506621000
C	-3.459901000	-0.679551000	-0.088421000
O	-2.270250000	-0.587633000	0.433095000
C	-4.608822000	-0.770404000	0.743609000
H	-4.448572000	-0.758777000	1.818748000
C	-5.899836000	-0.869163000	0.238636000
H	-6.732930000	-0.931384000	0.931133000
C	-6.116874000	-0.889489000	-1.151285000
C	-5.017649000	-0.812288000	-1.997024000
H	-5.188307000	-0.836147000	-3.071205000
C	-0.505286000	-0.576070000	-3.471493000

H	-1.079045000	-0.557683000	-4.411147000
H	0.048445000	-1.523853000	-3.434670000
C	0.504786000	0.575937000	-3.471482000
N	1.375544000	0.510593000	-2.299949000
C	2.639947000	0.664001000	-2.501281000
H	2.995584000	0.794802000	-3.534767000
C	3.698175000	0.704833000	-1.506756000
C	3.459582000	0.679693000	-0.088550000
O	2.270079000	0.586258000	0.433023000
C	4.608488000	0.771276000	0.743421000
H	4.448347000	0.759016000	1.818569000
C	5.899365000	0.871446000	0.238377000
H	6.732461000	0.934165000	0.930828000
C	6.116257000	0.892542000	-1.151555000
C	5.017029000	0.814720000	-1.997231000
H	5.187567000	0.839227000	-3.071416000
H	1.078508000	0.557604000	-4.411158000
H	-0.048962000	1.523711000	-3.434605000
N	-0.510594000	1.375048000	2.300064000
C	-0.663449000	2.639506000	2.501469000
H	-0.793825000	2.995169000	3.535000000
C	-0.704085000	3.697770000	1.506974000
C	-0.679648000	3.459181000	0.088751000
O	-0.587279000	2.269625000	-0.432892000
C	-0.770773000	4.608168000	-0.743160000
H	-0.758995000	4.448040000	-1.818315000
C	-0.869950000	5.899098000	-0.238054000

H	-0.932351000	6.732249000	-0.930466000
C	-0.890457000	6.115978000	1.151890000
C	-0.813019000	5.016681000	1.997513000
H	-0.837026000	5.187214000	3.071711000
C	-0.575866000	0.504261000	3.471570000
H	-1.523651000	-0.049468000	3.434763000
H	-0.557429000	1.077950000	4.411265000
C	0.576137000	-0.505815000	3.471427000
N	0.510721000	-1.376461000	2.299823000
C	0.663860000	-2.640914000	2.501034000
H	0.794533000	-2.996685000	3.534490000
C	0.704511000	-3.699047000	1.506395000
C	0.679593000	-3.460295000	0.088211000
O	0.586602000	-2.270702000	-0.433243000
C	0.770911000	-4.609137000	-0.743875000
H	0.758805000	-4.448876000	-1.819006000
C	0.870660000	-5.900098000	-0.238960000
H	0.933201000	-6.733139000	-0.931493000
C	0.891571000	-6.117145000	1.150950000
C	0.813983000	-5.017985000	1.996737000
H	0.838336000	-5.188646000	3.070907000
H	1.523914000	0.047925000	3.434549000
H	0.557842000	-1.079620000	4.411053000
O	-7.353562000	-0.985767000	-1.753216000
O	7.352796000	0.990215000	-1.753560000
O	-0.987126000	7.352574000	1.753950000
O	0.988837000	-7.353777000	1.752829000

C	-1.076063000	8.492068000	0.912247000
H	-1.144228000	9.355183000	1.577518000
H	-0.187622000	8.597939000	0.275311000
H	-1.969362000	8.457982000	0.274189000
C	-8.492983000	-1.074470000	-0.911388000
H	-8.598551000	-0.186049000	-0.274375000
H	-9.356190000	-1.142362000	-1.576567000
H	-8.459055000	-1.967825000	-0.273401000
C	1.077677000	-8.493149000	0.910950000
H	1.146171000	-9.356334000	1.576095000
H	0.189047000	-8.599057000	0.274289000
H	1.970769000	-8.458865000	0.272611000
C	8.492238000	1.079243000	-0.911797000
H	8.598425000	0.190574000	-0.275237000
H	9.355335000	1.148005000	-1.577031000
H	8.457818000	1.972263000	-0.273365000

Table 3.4.45. Optimized coordinates of **Ce^{IV}(OMeSALEN)$_2$**

Ce	-0.000007000	0.000016000	0.000001000
N	1.265868000	-0.681772000	-2.235270000
C	2.203751000	-1.549922000	-2.395481000
H	2.552874000	-1.767632000	-3.413659000
C	2.891592000	-2.294935000	-1.353401000
C	2.707628000	-2.033913000	0.037904000
O	1.877042000	-1.104039000	0.471566000
C	3.464451000	-2.796723000	0.950567000
H	3.334445000	-2.600828000	2.011031000

C	4.358799000	-3.777127000	0.528720000
H	4.913347000	-4.337280000	1.273459000
C	4.537387000	-4.029279000	-0.842204000
C	3.807946000	-3.281263000	-1.762997000
H	3.955032000	-3.473694000	-2.822708000
C	0.764533000	-0.005426000	-3.431312000
H	1.132402000	-0.479519000	-4.352125000
H	1.126019000	1.030422000	-3.414245000
C	-0.764545000	0.005463000	-3.431317000
N	-1.265889000	0.681799000	-2.235272000
C	-2.203787000	1.549934000	-2.395482000
H	-2.552912000	1.767638000	-3.413660000
C	-2.891641000	2.294936000	-1.353404000
C	-2.707661000	2.033934000	0.037903000
O	-1.877048000	1.104084000	0.471565000
C	-3.464490000	2.796739000	0.950566000
H	-3.334469000	2.600860000	2.011030000
C	-4.358863000	3.777119000	0.528716000
H	-4.913417000	4.337274000	1.273451000
C	-4.537466000	4.029250000	-0.842209000
C	-3.808014000	3.281246000	-1.763002000
H	-3.955113000	3.473665000	-2.822714000
H	-1.132407000	0.479565000	-4.352128000
H	-1.126032000	-1.030386000	-3.414265000
N	-0.681793000	-1.265855000	2.235281000
C	-1.549932000	-2.203749000	2.395491000
H	-1.767647000	-2.552863000	3.413671000

C	-2.294923000	-2.891615000	1.353413000
C	-2.033910000	-2.707646000	-0.037893000
O	-1.104061000	-1.877033000	-0.471555000
C	-2.796706000	-3.464486000	-0.950556000
H	-2.600819000	-3.334471000	-2.011020000
C	-3.777086000	-4.358858000	-0.528707000
H	-4.337235000	-4.913420000	-1.273441000
C	-4.029228000	-4.537450000	0.842218000
C	-3.281235000	-3.807987000	1.763011000
H	-3.473662000	-3.955076000	2.822723000
C	-0.005468000	-0.764501000	3.431328000
H	1.030379000	-1.125993000	3.414292000
H	-0.479582000	-1.132350000	4.352138000
C	0.005427000	0.764577000	3.431307000
N	0.681785000	1.265898000	2.235265000
C	1.549939000	2.203778000	2.395475000
H	1.767642000	2.552908000	3.413651000
C	2.294962000	2.891605000	1.353394000
C	2.033942000	2.707636000	-0.037912000
O	1.104060000	1.877058000	-0.471571000
C	2.796759000	3.464450000	-0.950576000
H	2.600865000	3.334444000	-2.011040000
C	3.777171000	4.358791000	-0.528731000
H	4.337329000	4.913333000	-1.273470000
C	4.029324000	4.537381000	0.842193000
C	3.281298000	3.807951000	1.762988000
H	3.473728000	3.955041000	2.822699000

H	-1.030420000	1.126067000	3.414227000
H	0.479514000	1.132454000	4.352120000
O	5.392219000	-4.968093000	-1.361014000
O	-5.392326000	4.968038000	-1.361008000
O	4.968137000	5.392213000	1.361000000
O	-4.968020000	-5.392306000	1.361015000
C	5.746046000	6.160311000	0.450814000
H	6.415435000	6.765243000	1.064884000
H	6.342603000	5.519623000	-0.211125000
H	5.117417000	6.821842000	-0.158918000
C	-6.160378000	5.745958000	-0.450796000
H	-5.519643000	6.342489000	0.211123000
H	-6.765314000	6.415369000	-1.064840000
H	-6.821902000	5.117346000	0.158961000
C	-5.745931000	-6.160363000	0.450800000
H	-6.415347000	-6.765296000	1.064840000
H	-6.342454000	-5.519630000	-0.211127000
H	-5.117313000	-6.821889000	-0.158949000
C	6.160362000	-5.745965000	-0.450835000
H	5.519711000	-6.342543000	0.211121000
H	6.765309000	-6.415336000	-1.064910000
H	6.821879000	-5.117304000	0.158880000

Table 3.4.46. Optimized coordinates of **$[Ce^{III}(OQ)_4]^-$**

Ce	-0.000027000	-0.000016000	0.000002000
O	0.935957000	1.300769000	1.775036000
C	1.953277000	2.118296000	1.715249000

C	2.421099000	2.854071000	2.814258000
H	1.908572000	2.736492000	3.765690000
C	3.523873000	3.726444000	2.706057000
H	3.844172000	4.273245000	3.590580000
C	4.204522000	3.902549000	1.515105000
H	5.054235000	4.575843000	1.443690000
C	3.780696000	3.184143000	0.366674000
C	4.410831000	3.285248000	-0.901869000
H	5.266326000	3.946627000	-1.018729000
C	3.940195000	2.548608000	-1.967159000
H	4.407559000	2.607011000	-2.945179000
C	2.825509000	1.702519000	-1.771858000
H	2.434069000	1.103087000	-2.590360000
N	2.206110000	1.582572000	-0.607624000
C	2.660815000	2.298815000	0.461407000
O	-0.936016000	1.301294000	-1.774660000
C	-1.953300000	2.118847000	-1.714593000
C	-2.421098000	2.855010000	-2.813352000
H	-1.908582000	2.737728000	-3.764827000
C	-3.523834000	3.727395000	-2.704854000
H	-3.844116000	4.274504000	-3.589192000
C	-4.204468000	3.903133000	-1.513839000
H	-5.054153000	4.576438000	-1.442194000
C	-3.780662000	3.184331000	-0.365649000
C	-4.410781000	3.285045000	0.902934000
H	-5.266249000	3.946419000	1.020019000
C	-3.940165000	2.548036000	1.967978000

H	-4.407518000	2.606136000	2.946021000
C	-2.825512000	1.701972000	1.772389000
H	-2.434085000	1.102254000	2.590689000
N	-2.206129000	1.582383000	0.608111000
C	-2.660817000	2.298988000	-0.460684000
N	-2.206123000	-1.582381000	-0.608204000
C	-2.825467000	-1.701944000	-1.772506000
H	-2.433998000	-1.102224000	-2.590784000
C	-3.940128000	-2.547985000	-1.968144000
H	-4.407448000	-2.606065000	-2.946205000
C	-4.410797000	-3.284997000	-0.903125000
H	-5.266273000	-3.946353000	-1.020248000
C	-3.780722000	-3.184309000	0.365482000
C	-4.204583000	-3.903116000	1.513648000
H	-5.054278000	-4.576404000	1.441965000
C	-3.523989000	-3.727403000	2.704689000
H	-3.844313000	-4.274516000	3.589010000
C	-2.421241000	-2.855040000	2.813238000
H	-1.908758000	-2.737777000	3.764733000
C	-1.953389000	-2.118873000	1.714504000
O	-0.936094000	-1.301338000	1.774617000
C	-2.660864000	-2.298989000	0.460566000
N	2.206117000	-1.582563000	0.607718000
C	2.825482000	-1.702486000	1.771972000
H	2.434008000	-1.103048000	2.590454000
C	3.940175000	-2.548555000	1.967318000
H	4.407510000	-2.606939000	2.945353000

C	4.410855000	-3.285202000	0.902053000
H	5.266357000	-3.946565000	1.018947000
C	3.780757000	-3.184122000	-0.366512000
C	4.204630000	-3.902536000	-1.514920000
H	5.054351000	-4.575816000	-1.443470000
C	3.524015000	-3.726456000	-2.705895000
H	3.844351000	-4.273263000	-3.590402000
C	2.421231000	-2.854101000	-2.814141000
H	1.908732000	-2.736542000	-3.765592000
C	1.953363000	-2.118321000	-1.715157000
O	0.936034000	-1.300808000	-1.774986000
C	2.660865000	-2.298813000	-0.461290000

Table 3.4.47. Optimized coordinates of **$Ce^{IV}(OQ)_4$**

Ce	-0.000454000	0.000094000	0.000095000
O	0.899280000	-1.281156000	-1.606664000
C	2.384533000	-2.882600000	-2.593617000
H	1.873072000	-2.811857000	-3.549115000
C	3.492839000	-3.747114000	-2.437581000
H	3.818246000	-4.335117000	-3.291901000
C	4.165323000	-3.860453000	-1.236528000
H	5.015168000	-4.528284000	-1.129818000
C	3.738181000	-3.089655000	-0.122302000
C	4.353514000	-3.122256000	1.156020000
H	5.209378000	-3.772110000	1.319857000
C	3.864489000	-2.331625000	2.174376000
H	4.318151000	-2.336569000	3.159924000

C	2.751571000	-1.498387000	1.924273000
C	2.620231000	-2.217394000	-0.272609000
H	2.349183000	-0.858225000	2.704376000
O	-0.900183000	-1.281163000	1.607215000
C	-2.384327000	-2.884407000	2.592963000
H	-1.873054000	-2.813733000	3.548558000
C	-3.491890000	-3.749756000	2.436385000
H	-3.816861000	-4.338467000	3.290386000
C	-4.164182000	-3.862964000	1.235208000
H	-5.013477000	-4.531416000	1.127988000
C	-3.737521000	-3.091196000	0.121475000
C	-4.352738000	-3.123581000	-1.156897000
H	-5.208092000	-3.774009000	-1.321106000
C	-3.864247000	-2.332074000	-2.174836000
H	-4.317855000	-2.336863000	-3.160411000
C	-2.751945000	-1.498174000	-1.924251000
C	-2.620263000	-2.218103000	0.272338000
H	-2.349855000	-0.857393000	-2.703994000
N	-2.148269000	1.442912000	0.746971000
C	-2.752351000	1.498469000	1.924462000
H	-2.350156000	0.857922000	2.704345000
C	-3.864959000	2.332042000	2.174792000
H	-4.318714000	2.336779000	3.160299000
C	-4.353597000	3.123251000	1.156688000
H	-5.209219000	3.773375000	1.320694000
C	-3.738172000	3.090927000	-0.121585000
C	-4.164846000	3.862491000	-1.235462000

H	-5.014406000	4.530645000	-1.128468000
C	-3.492268000	3.749456000	-2.436492000
H	-3.817250000	4.338035000	-3.290577000
C	-2.384374000	2.884462000	-2.592788000
O	-0.900044000	1.281635000	-1.606673000
C	-2.620585000	2.218214000	-0.272159000
H	-1.872827000	2.813931000	-3.548236000
N	2.147496000	1.442857000	-0.746950000
C	2.751387000	1.498595000	-1.924537000
H	2.348749000	0.858578000	-2.704623000
C	3.864422000	2.331632000	-2.174731000
H	4.317973000	2.336558000	-3.160331000
C	4.353760000	3.122060000	-1.156358000
H	5.209734000	3.771751000	-1.320251000
C	3.738608000	3.089470000	0.122038000
C	4.166194000	3.859980000	1.236316000
H	5.016120000	4.527689000	1.129487000
C	3.493980000	3.746549000	2.437493000
H	3.819696000	4.334294000	3.291875000
C	2.385492000	2.882252000	2.593615000
O	0.899467000	1.281505000	1.606726000
C	2.620498000	2.217436000	0.272427000
H	1.874301000	2.811438000	3.549249000
C	1.929939000	-2.110249000	-1.528211000
C	-1.930207000	-2.111042000	1.528072000
N	2.147518000	-1.442632000	0.746780000
N	-2.148066000	-1.442549000	-0.746658000

C	1.930403000	2.110276000	1.528162000
C	-1.930319000	2.111286000	-1.527749000

Table 3.4.48. Optimized coordinates of **$[Ce^{III}(HA)_4]^-$**

Ce	-0.038911000	-0.000018000	-0.000159000
O	-1.104987000	2.142534000	0.469928000
N	-2.059197000	2.278033000	1.446654000
C	-2.651516000	3.581364000	1.429765000
C	-1.932134000	4.665210000	1.945164000
H	-0.965145000	4.489168000	2.406275000
C	-2.468041000	5.950370000	1.871959000
H	-1.914112000	6.789287000	2.283942000
C	-3.715284000	6.159394000	1.273033000
H	-4.131936000	7.161224000	1.219402000
C	-4.419669000	5.078730000	0.737381000
H	-5.382815000	5.236915000	0.260292000
C	-3.884765000	3.789233000	0.804785000
H	-4.416450000	2.946160000	0.374067000
C	-2.362873000	1.194815000	2.178137000
O	-1.775258000	0.111423000	1.885094000
C	-3.382685000	1.173449000	3.343231000
C	-3.612096000	2.512416000	4.073679000
H	-4.153304000	3.243079000	3.470551000
H	-2.666895000	2.963747000	4.394576000
H	-4.211126000	2.319804000	4.971679000
C	-4.725524000	0.645672000	2.783011000
H	-5.437685000	0.490514000	3.602178000

H	-4.582742000	-0.310227000	2.267636000
H	-5.172815000	1.354131000	2.077509000
C	-2.847629000	0.163057000	4.385346000
H	-1.898610000	0.506009000	4.814308000
H	-2.682299000	-0.818874000	3.938719000
H	-3.572025000	0.063763000	5.201667000
O	-1.105333000	-2.142361000	-0.470671000
N	-2.059731000	-2.277455000	-1.447270000
C	-2.652626000	-3.580526000	-1.430269000
C	-3.885649000	-3.787886000	-0.804671000
H	-4.416709000	-2.944605000	-0.373587000
C	-4.421125000	-5.077136000	-0.737134000
H	-5.384098000	-5.234921000	-0.259564000
C	-3.717529000	-6.158068000	-1.273288000
H	-4.134628000	-7.159708000	-1.219562000
C	-2.470505000	-5.949561000	-1.872845000
H	-1.917190000	-6.788690000	-2.285222000
C	-1.934027000	-4.664645000	-1.946178000
H	-0.967202000	-4.489005000	-2.407786000
C	-2.363046000	-1.194125000	-2.178726000
O	-1.774875000	-0.110995000	-1.885836000
C	-3.383180000	-1.172340000	-3.343532000
C	-2.848180000	-0.161967000	-4.385687000
H	-1.899369000	-0.505102000	-4.814962000
H	-2.682477000	0.819875000	-3.939004000
H	-3.572787000	-0.062405000	-5.201789000
C	-4.725722000	-0.644288000	-2.782849000

H	-5.438075000	-0.488807000	-3.601788000
H	-4.582535000	0.311493000	-2.267367000
H	-5.173003000	-1.352736000	-2.077330000
C	-3.613146000	-2.511171000	-4.074050000
H	-2.668150000	-2.962679000	-4.395303000
H	-4.212428000	-2.318329000	-4.971834000
H	-4.154318000	-3.241776000	-3.470820000
O	1.034928000	1.591240000	-1.502450000
N	2.032542000	1.208768000	-2.363464000
C	2.638010000	2.336688000	-3.004892000
C	1.956412000	2.979748000	-4.044194000
H	1.010789000	2.573571000	-4.389904000
C	2.503152000	4.121195000	-4.629456000
H	1.979342000	4.611996000	-5.444998000
C	3.722774000	4.631528000	-4.170966000
H	4.148003000	5.519397000	-4.630345000
C	4.388276000	4.001813000	-3.116848000
H	5.329138000	4.401096000	-2.748544000
C	3.842411000	2.859593000	-2.524491000
H	4.342610000	2.375333000	-1.691410000
C	2.361559000	-0.091836000	-2.401959000
O	1.753493000	-0.870059000	-1.608527000
C	3.435193000	-0.698599000	-3.339325000
C	4.767552000	-0.772958000	-2.555294000
H	5.168738000	0.224272000	-2.346769000
H	5.515508000	-1.321115000	-3.140632000
H	4.629813000	-1.295497000	-1.602356000

C	3.654802000	0.039142000	-4.676201000
H	2.710013000	0.197405000	-5.208057000
H	4.297080000	-0.579054000	-5.314571000
H	4.145836000	1.005887000	-4.556256000
C	2.977327000	-2.137881000	-3.672115000
H	2.832399000	-2.729024000	-2.766168000
H	3.735904000	-2.625393000	-4.294891000
H	2.032970000	-2.133200000	-4.229065000
O	1.034047000	-1.591696000	1.502406000
N	2.031438000	-1.209455000	2.363770000
C	2.636649000	-2.337559000	3.005138000
C	3.841100000	-2.860509000	2.524910000
H	4.341548000	-2.376147000	1.692037000
C	4.386690000	-4.002909000	3.117167000
H	5.327591000	-4.402232000	2.749004000
C	3.720869000	-4.632762000	4.171004000
H	4.145891000	-5.520771000	4.630301000
C	2.501201000	-4.122377000	4.629313000
H	1.977139000	-4.613281000	5.444631000
C	1.954735000	-2.980746000	4.044152000
H	1.009081000	-2.574526000	4.389726000
C	2.360617000	0.091098000	2.402555000
O	1.752872000	0.869534000	1.609076000
C	3.434091000	0.697570000	3.340286000
C	3.653241000	-0.040419000	4.677103000
H	4.295422000	0.577584000	5.315760000
H	4.144183000	-1.007205000	4.557126000

H	2.708286000	-0.198655000	5.208669000
C	4.766663000	0.771896000	2.556616000
H	4.629240000	1.294620000	1.603733000
H	5.167784000	-0.225341000	2.348014000
H	5.514529000	1.319863000	3.142246000
C	2.976319000	2.136856000	3.673180000
H	3.734841000	2.624206000	4.296149000
H	2.031865000	2.132204000	4.229968000
H	2.831604000	2.728139000	2.767289000

Table 3.4.49. Optimized coordinates of **$[Ce^{III}(C_8H_8)_2]^-$**

Ce	-0.000176000	0.000008000	0.000000000
C	-1.708410000	-2.122343000	0.707727000
H	-2.712919000	-2.048230000	1.123700000
C	-0.707635000	-2.122190000	1.708502000
H	-1.123615000	-2.047950000	2.712998000
C	0.707819000	-2.121991000	1.708502000
H	1.123781000	-2.047627000	2.712996000
C	1.708594000	-2.121864000	0.707727000
H	2.713081000	-2.047449000	1.123698000
C	-1.708405000	2.122301000	0.707727000
H	-2.712912000	2.048135000	1.123694000
C	-0.707635000	2.122171000	1.708507000
H	-1.123619000	2.047934000	2.713001000
C	0.707819000	2.121998000	1.708505000
H	1.123784000	2.047677000	2.713002000
C	1.708592000	2.121878000	0.707728000

H	2.713081000	2.047505000	1.123699000
C	-1.708410000	-2.122343000	-0.707727000
C	-0.707635000	-2.122190000	-1.708502000
H	-2.712919000	-2.048230000	-1.123700000
H	-1.123615000	-2.047950000	-2.712998000
C	0.707819000	-2.121991000	-1.708502000
C	1.708594000	-2.121864000	-0.707727000
C	-1.708405000	2.122301000	-0.707727000
H	-2.712912000	2.048135000	-1.123694000
C	-0.707635000	2.122171000	-1.708507000
H	-1.123619000	2.047934000	-2.713001000
C	0.707819000	2.121998000	-1.708505000
H	1.123784000	2.047677000	-2.713002000
C	1.708592000	2.121878000	-0.707728000
H	2.713081000	2.047505000	-1.123699000
H	1.123781000	-2.047627000	-2.712996000
H	2.713081000	-2.047449000	-1.123698000

Table 3.4.50. Optimized coordinates of **$Ce^{IV}(C_8H_8)_2$**

C	2.295536000	-0.875859000	1.219103000
C	1.566818000	-0.223706000	2.239276000
C	0.237240000	-0.288502000	2.713278000
C	-0.914055000	-1.030389000	2.364811000
C	-1.213432000	-2.017397000	1.398824000
C	-0.483305000	-2.672739000	0.382140000
C	0.846279000	-2.608244000	-0.092281000
C	1.996751000	-1.863946000	0.253761000

H	3.298377000	-0.471307000	1.101893000
H	2.141155000	0.564219000	2.721468000
H	0.031329000	0.462106000	3.473261000
H	-1.794466000	-0.712933000	2.919250000
H	-2.269072000	-2.279832000	1.387374000
H	-1.110171000	-3.320256000	-0.227045000
H	0.999495000	-3.219567000	-0.978832000
H	2.824230000	-2.038867000	-0.430171000
Ce	0.000000000	0.000000000	0.000000000
C	-2.295536000	0.875859000	-1.219103000
C	-1.566818000	0.223706000	-2.239276000
C	-0.237240000	0.288502000	-2.713278000
C	0.914055000	1.030389000	-2.364811000
C	1.213432000	2.017397000	-1.398824000
C	0.483305000	2.672739000	-0.382140000
C	-0.846279000	2.608244000	0.092281000
C	-1.996751000	1.863946000	-0.253761000
H	-3.298377000	0.471307000	-1.101893000
H	-2.141155000	-0.564219000	-2.721468000
H	-0.031329000	-0.462106000	-3.473261000
H	1.794466000	0.712933000	-2.919250000
H	2.269072000	2.279832000	-1.387374000
H	1.110171000	3.320256000	0.227045000
H	-0.999495000	3.219567000	0.978832000
H	-2.824230000	2.038867000	0.430171000

Table 3.4.51. Optimized coordinates of **[Ce^{III}(omtaa)$_2$]$^-$**

Ce	0.000016000	0.000021000	0.000102000
N	1.988316000	0.094826000	1.685070000
N	0.096357000	1.993431000	1.671644000
N	-1.988423000	-0.094825000	1.684908000
N	-0.096436000	-1.993450000	1.671574000
N	-1.988146000	0.094694000	-1.685383000
N	-0.096338000	1.993531000	-1.670998000
N	1.988275000	-0.094573000	-1.685225000
N	0.096436000	-1.993446000	-1.671047000
C	2.425837000	1.412284000	1.455724000
C	3.739960000	1.779523000	1.112908000
C	4.101898000	3.090378000	0.790432000
C	3.105298000	4.090697000	0.784136000
C	1.791182000	3.734959000	1.100175000
C	1.417580000	2.424456000	1.448355000
C	-0.743377000	2.561140000	2.529417000
C	-2.010804000	2.018273000	2.849505000
C	-2.556954000	0.749759000	2.535899000
C	-2.425906000	-1.412299000	1.455575000
C	-4.101986000	-3.090394000	0.790338000
C	-3.105395000	-4.090722000	0.784091000
C	-1.791273000	-3.734984000	1.100112000
C	-1.417653000	-2.424476000	1.448240000
C	0.743293000	-2.561242000	2.529299000
C	2.010713000	-2.018397000	2.849442000
C	2.556891000	-0.749873000	2.535928000

C	-0.368292000	3.822019000	3.303905000
C	-3.819836000	0.382851000	3.311015000
C	0.368198000	-3.822195000	3.303656000
C	3.819830000	-0.383111000	3.311020000
C	5.534889000	3.416088000	0.434463000
C	3.438449000	5.520236000	0.421584000
C	-5.534983000	-3.416099000	0.434395000
C	-3.438550000	-5.520267000	0.421544000
C	-2.425854000	1.412017000	-1.455931000
C	-3.740196000	1.778838000	-1.113530000
C	-4.102539000	3.089522000	-0.790847000
C	-3.106101000	4.090009000	-0.783821000
C	-1.417737000	2.424303000	-1.447823000
C	0.743223000	2.561632000	-2.528720000
C	2.010399000	2.018709000	-2.849507000
C	2.556396000	0.749932000	-2.536522000
C	2.425951000	-1.411948000	-1.455858000
C	3.740274000	-1.778760000	-1.113423000
C	4.102609000	-3.089458000	-0.790768000
C	3.106178000	-4.089939000	-0.783832000
C	1.791866000	-3.734555000	-1.099479000
C	1.417826000	-2.424226000	-1.447845000
C	-0.743114000	-2.561548000	-2.528779000
C	-2.010319000	-2.018658000	-2.849527000
C	-2.556352000	-0.749902000	-2.536546000
C	0.368079000	3.823080000	-3.302207000
C	3.818538000	0.382740000	-3.312745000

C	-0.367951000	-3.822950000	-3.302335000
C	-3.818601000	-0.382845000	-3.312651000
C	-5.535686000	3.414934000	-0.435318000
C	5.535747000	-3.414865000	-0.435195000
H	4.501594000	1.006376000	1.076196000
H	1.020343000	4.498497000	1.054163000
H	-2.586945000	2.597576000	3.563665000
H	-1.020457000	-4.498545000	1.054134000
H	2.586880000	-2.597783000	3.563512000
H	-0.976743000	3.916231000	4.207076000
H	0.687145000	3.812581000	3.593367000
H	-0.526588000	4.726162000	2.703150000
H	-3.905120000	0.986728000	4.218217000
H	-3.821512000	-0.674367000	3.593602000
H	-4.723615000	0.555788000	2.713634000
H	0.976793000	-3.916621000	4.206707000
H	-0.687190000	-3.812652000	3.593309000
H	0.526253000	-4.726276000	2.702749000
H	3.905146000	-0.987120000	4.218131000
H	3.821555000	0.674066000	3.593761000
H	4.723572000	-0.555994000	2.713568000
H	6.166327000	2.523420000	0.486641000
H	5.963860000	4.167559000	1.111074000
H	5.621203000	3.826690000	-0.580626000
H	2.547863000	6.155293000	0.464687000
H	4.187558000	5.950489000	1.099989000
H	3.855230000	5.598933000	-0.591606000

H	-6.166375000	-2.523387000	0.486376000
H	-5.964015000	-4.167405000	1.111153000
H	-5.621293000	-3.826910000	-0.580608000
H	-2.547974000	-6.155336000	0.464686000
H	-4.187690000	-5.950495000	1.099927000
H	-3.855296000	-5.598979000	-0.591662000
H	-4.501635000	1.005468000	-1.077398000
H	2.586342000	2.598112000	-3.563743000
H	4.501703000	-1.005381000	-1.077236000
H	1.021257000	-4.498299000	-1.053035000
H	-2.586253000	-2.598077000	-3.563760000
H	-0.687467000	3.814055000	-3.591267000
H	0.526751000	4.726753000	-2.700837000
H	0.976214000	3.917851000	-4.205534000
H	3.819451000	-0.674372000	-3.595769000
H	4.722900000	0.554979000	-2.716057000
H	3.903369000	0.986926000	-4.219780000
H	0.687619000	-3.813975000	-3.591298000
H	-0.526751000	-4.726657000	-2.701046000
H	-0.976012000	-3.917610000	-4.205724000
H	-3.819707000	0.674276000	-3.595632000
H	-4.722888000	-0.555265000	-2.715899000
H	-3.903413000	-0.987009000	-4.219704000
H	-5.964418000	4.166686000	-1.111763000
H	-5.622414000	3.825083000	0.579918000
H	-6.167051000	2.522252000	-0.488122000
H	5.964535000	-4.166531000	-1.111698000

H	5.622433000	-3.825117000	0.580003000
H	6.167087000	-2.522159000	-0.487873000
C	-1.791782000	3.734622000	-1.099412000
H	-1.021169000	4.498360000	-1.052932000
C	-3.740028000	-1.779531000	1.112768000
H	-4.501649000	-1.006369000	1.076040000
C	3.439683000	-5.519392000	-0.421131000
H	4.188686000	-5.949642000	-1.099659000
H	3.856722000	-5.597887000	0.591969000
H	2.549178000	-6.154581000	-0.463947000
C	-3.439631000	5.519440000	-0.421083000
H	-4.188475000	5.949773000	-1.099738000
H	-3.856886000	5.597875000	0.591932000
H	-2.549095000	6.154603000	-0.463662000

Table 3.4.52. Optimized coordinates of **$Ce^{IV}(omtaa)_2$**

Ce	0.000003000	0.000006000	0.000000000
N	0.081227000	1.955250000	-1.565541000
N	1.955950000	0.084329000	-1.564654000
N	-0.081166000	-1.955583000	-1.565105000
N	-1.955912000	-0.084640000	-1.564726000
C	1.394323000	2.401777000	-1.313204000
C	1.755258000	3.717613000	-0.972653000
H	0.982361000	4.478082000	-0.934746000
C	3.068893000	4.076825000	-0.670178000
C	4.070901000	3.076932000	-0.669750000
C	3.714626000	1.762370000	-0.971733000

H	4.476783000	0.991154000	-0.933103000
C	2.399695000	1.398447000	-1.312658000
C	2.526296000	-0.727474000	-2.451606000
C	1.981630000	-1.978068000	-2.804103000
H	2.543798000	-2.539260000	-3.541571000
C	0.731744000	-2.524623000	-2.451913000
C	-1.394294000	-2.402046000	-1.312818000
C	-1.755285000	-3.717837000	-0.972157000
H	-0.982397000	-4.478306000	-0.934056000
C	-3.068977000	-4.077016000	-0.669884000
C	-4.070990000	-3.077129000	-0.669781000
C	-3.714664000	-1.762604000	-0.971862000
H	-4.476840000	-0.991390000	-0.933525000
C	-2.399667000	-1.398720000	-1.312569000
C	-2.526183000	0.726952000	-2.451912000
C	-1.981471000	1.977444000	-2.804709000
H	-2.543581000	2.538452000	-3.542362000
C	-0.731616000	2.524084000	-2.452546000
C	3.779802000	-0.323965000	-3.216496000
H	3.766674000	0.738272000	-3.477001000
H	3.868931000	-0.908366000	-4.135309000
H	4.684501000	-0.500785000	-2.622866000
C	0.330458000	-3.778805000	-3.216871000
H	0.508543000	-4.683206000	-2.623160000
H	0.915291000	-3.867015000	-4.135493000
H	-0.731713000	-3.767406000	-3.477725000
C	-3.779639000	0.323236000	-3.216772000

H	-3.766498000	-0.739078000	-3.476967000
H	-3.868706000	0.907370000	-4.135760000
H	-4.684374000	0.500228000	-2.623247000
C	-0.330284000	3.778091000	-3.217766000
H	-0.508469000	4.682634000	-2.624302000
H	-0.915018000	3.866057000	-4.136476000
H	0.731916000	3.766664000	-3.478499000
C	3.402973000	5.510015000	-0.326912000
H	2.511982000	6.143785000	-0.370832000
H	4.147003000	5.930028000	-1.016536000
H	3.827387000	5.598041000	0.681864000
C	5.503310000	3.414129000	-0.326137000
H	6.138893000	2.524415000	-0.369676000
H	5.590188000	3.838969000	0.682565000
H	5.922015000	4.158840000	-1.015826000
C	-3.403122000	-5.510170000	-0.326534000
H	-2.512117000	-6.143939000	-0.370190000
H	-4.146998000	-5.930265000	-1.016275000
H	-3.827758000	-5.598088000	0.682158000
C	-5.503472000	-3.414291000	-0.326432000
H	-6.139059000	-2.524594000	-0.370261000
H	-5.590570000	-3.838967000	0.682320000
H	-5.922011000	-4.159123000	-1.016094000
N	0.084502000	-1.955764000	1.564879000
N	1.955410000	-0.081033000	1.565316000
N	-0.084480000	1.956106000	1.564492000
N	-1.955414000	0.081346000	1.565341000

C	1.398590000	-2.399534000	1.312777000
C	1.762475000	-3.714504000	0.971961000
H	0.991258000	-4.476668000	0.933520000
C	3.077002000	-4.070809000	0.669861000
C	4.076891000	-3.068797000	0.670051000
C	3.717711000	-1.755128000	0.972423000
H	4.478175000	-0.982233000	0.934346000
C	2.401915000	-1.394158000	1.313084000
C	2.524372000	0.731934000	2.452122000
C	1.977788000	1.981847000	2.804168000
H	2.538903000	2.544064000	3.541658000
C	0.727236000	2.526500000	2.451492000
C	-1.398598000	2.399817000	1.312431000
C	-1.762536000	3.714757000	0.971558000
H	-0.991330000	4.476926000	0.932967000
C	-3.077109000	4.071033000	0.669625000
C	-4.077000000	3.069022000	0.670055000
C	-3.717767000	1.755375000	0.972459000
H	-4.478240000	0.982479000	0.934593000
C	-2.401919000	1.394438000	1.312956000
C	-2.524323000	-0.731438000	2.452346000
C	-1.977709000	-1.981267000	2.804646000
H	-2.538790000	-2.543332000	3.542277000
C	-0.727177000	-2.525991000	2.452021000
C	3.778490000	0.330704000	3.217213000
H	3.767084000	-0.731454000	3.478118000
H	3.866610000	0.915584000	4.135814000

H	4.682942000	0.508772000	2.623576000
C	0.323632000	3.780045000	3.216266000
H	0.500525000	4.684713000	2.622612000
H	0.907912000	3.869223000	4.135151000
H	-0.738640000	3.766929000	3.476633000
C	-3.778408000	-0.330045000	3.217404000
H	-3.767005000	0.732177000	3.478056000
H	-3.866474000	-0.914707000	4.136149000
H	-4.682887000	-0.508268000	2.623853000
C	-0.323562000	-3.779394000	3.217023000
H	-0.500452000	-4.684170000	2.623532000
H	-0.907842000	-3.868406000	4.135924000
H	0.738709000	-3.766225000	3.477388000
C	3.414163000	-5.503259000	0.326386000
H	2.524460000	-6.138843000	0.370127000
H	4.158970000	-5.921871000	1.016031000
H	3.838870000	-5.590266000	-0.682361000
C	5.510043000	-3.402913000	0.326664000
H	6.143818000	-2.511917000	0.370413000
H	5.597957000	-3.827442000	-0.682073000
H	5.930133000	-4.146866000	1.016326000
C	-3.414328000	5.503457000	0.326089000
H	-2.524612000	6.139039000	0.369603000
H	-4.158999000	5.922135000	1.015839000
H	-3.839227000	5.590375000	-0.682584000
C	-5.510207000	3.403110000	0.326875000
H	-6.143975000	2.512117000	0.370809000

H	-5.598289000	3.827548000	-0.681886000
H	-5.930183000	4.147125000	1.016539000

Table 3.4.53. Optimized coordinates of **Pr[2-(^{t}BuNO)py]$_4$**

O	-0.986669000	-1.111531000	-1.840049000
N	-1.965847000	-2.037615000	-1.844827000
C	-2.518491000	-2.360022000	-0.638261000
N	-1.968340000	-1.722001000	0.433046000
C	-2.442253000	-1.970409000	1.664063000
H	-1.950652000	-1.411194000	2.456388000
C	-3.474464000	-2.854521000	1.933356000
H	-3.818117000	-3.020373000	2.948530000
C	-4.052927000	-3.514380000	0.835368000
H	-4.872460000	-4.213438000	0.983332000
C	-3.592632000	-3.279522000	-0.444310000
H	-4.056156000	-3.786871000	-1.276582000
C	-2.314088000	-2.615747000	-3.183635000
C	-2.078351000	-4.142561000	-3.190387000
H	-1.033409000	-4.358134000	-2.944338000
H	-2.284110000	-4.540922000	-4.190442000
H	-2.707271000	-4.684844000	-2.481839000
C	-3.764252000	-2.244814000	-3.566650000
H	-4.512393000	-2.660173000	-2.887874000
H	-3.986940000	-2.615219000	-4.573846000
H	-3.881708000	-1.156064000	-3.568110000
C	-1.374024000	-1.996193000	-4.232879000
H	-1.479643000	-0.911085000	-4.277322000

H	-1.629580000	-2.418492000	-5.211464000
H	-0.328918000	-2.222777000	-4.013196000
O	0.983930000	-1.113433000	1.839722000
N	1.961322000	-2.041299000	1.844761000
C	2.513091000	-2.365507000	0.638241000
N	1.964333000	-1.726618000	-0.433239000
C	2.437430000	-1.976687000	-1.664230000
H	1.947120000	-1.416565000	-2.456716000
C	3.467428000	-2.863447000	-1.933308000
H	3.810520000	-3.030556000	-2.948465000
C	4.044454000	-3.524244000	-0.835137000
H	4.862219000	-4.225402000	-0.982939000
C	3.584963000	-3.287684000	0.444524000
H	4.047367000	-3.795834000	1.276926000
C	2.308840000	-2.619331000	3.183821000
C	1.370670000	-1.996901000	4.233055000
H	1.478900000	-0.912017000	4.276783000
H	1.625635000	-2.419186000	5.211799000
H	0.324935000	-2.221111000	4.013946000
C	3.760014000	-2.251423000	3.565895000
H	4.506860000	-2.668850000	2.886972000
H	3.982375000	-2.621753000	4.573190000
H	3.879894000	-1.162938000	3.566666000
C	2.069602000	-4.145611000	3.191737000
H	1.024122000	-4.358962000	2.946047000
H	2.274629000	-4.543674000	4.192056000
H	2.697136000	-4.689909000	2.483498000

O	0.985887000	1.111823000	-1.840355000
N	1.965034000	2.037849000	-1.845365000
C	2.518205000	2.360046000	-0.638947000
N	1.968506000	1.721832000	0.432457000
C	2.442992000	1.969948000	1.663305000
H	1.951749000	1.410550000	2.455721000
C	3.475359000	2.853977000	1.932308000
H	3.819497000	3.019581000	2.947358000
C	4.053336000	3.514058000	0.834208000
H	4.872956000	4.213061000	0.981947000
C	3.592443000	3.279479000	-0.445312000
H	4.055594000	3.786993000	-1.277691000
C	2.312839000	2.616126000	-3.184241000
C	2.077254000	4.142963000	-3.190710000
H	1.032431000	4.358617000	-2.944231000
H	2.282660000	4.541404000	-4.190804000
H	2.706512000	4.685110000	-2.482359000
C	3.762826000	2.245081000	-3.567810000
H	4.511253000	2.660263000	-2.889241000
H	3.985196000	2.615595000	-4.575036000
H	3.880160000	1.156318000	-3.569456000
C	1.372316000	1.996799000	-4.233208000
H	1.477787000	0.911685000	-4.277815000
H	1.627559000	2.419188000	-5.211835000
H	0.327316000	2.223484000	-4.013117000
O	-0.983233000	1.113513000	1.840128000
N	-1.960564000	2.041348000	1.845501000

C	-2.512808000	2.365526000	0.639149000
N	-1.964454000	1.726593000	-0.432493000
C	-2.438043000	1.976569000	-1.663305000
H	-1.948057000	1.416376000	-2.455939000
C	-3.468162000	2.863311000	-1.932019000
H	-3.811671000	3.030342000	-2.947048000
C	-4.044769000	3.524156000	-0.833667000
H	-4.862612000	4.225283000	-0.981181000
C	-3.584763000	3.287663000	0.445829000
H	-4.046865000	3.795824000	1.278393000
C	-2.307628000	2.619407000	3.184688000
C	-1.369057000	1.997044000	4.233602000
H	-1.477284000	0.912167000	4.277456000
H	-1.623636000	2.419414000	5.212411000
H	-0.323404000	2.221226000	4.014072000
C	-3.758650000	2.251438000	3.567274000
H	-4.505762000	2.668863000	2.888644000
H	-3.980645000	2.621736000	4.574661000
H	-3.878494000	1.162950000	3.568060000
C	-2.068468000	4.145696000	3.192467000
H	-1.023095000	4.359107000	2.946380000
H	-2.273137000	4.543760000	4.192858000
H	-2.696311000	4.689944000	2.484464000
Pr	-0.000012000	-0.000132000	-0.000566000

3.5 References

[1] L. J. Nugent, R. D. Baybarz, J. L. Burnett, J. L. Ryan, *J. Inorg. Nucl. Chem.* **1971**, *33*, 2503-2530.

[2] E. Mamontov, T. Egami, *J. Phys. Chem. Solids* **2000**, *61*, 1345-1356.

[3] C. K. Kim, T. Kim, I.-Y. Choi, M. Soh, D. Kim, Y.-J. Kim, H. Jang, H.-S. Yang, J. Y. Kim, H.-K. Park, S. P. Park, S. Park, T. Yu, B.-W. Yoon, S.-H. Lee, T. Hyeon, *Angew. Chem. Int. Ed.*, *51*, 11039-11043.

[4] a) J. Paier, C. Penschke, J. Sauer, *Chem. Rev.* **2013**, *113*, 3949-3985; b) H.-F. Wang, H.-Y. Li, X.-Q. Gong, Y.-L. Guo, G.-Z. Lu, P. Hu, *Phys. Chem. Chem. Phys.* **2012**, *14*, 16521-16535; c) N. V. Skorodumova, S. I. Simak, B. I. Lundqvist, I. A. Abrikosov, B. Johansson, *Phys. Rev. Lett.* **2002**, *89*, 166601.

[5] a) R. J. Gorte, *AIChE J.* **2010**, *56*, 1126-1135; b) J. Stubenrauch, J. M. Vohs, *J. Catal.* **1996**, *159*, 50-57; c) H. Cordatos, T. Bunluesin, J. Stubenrauch, J. M. Vohs, R. J. Gorte, *J. Phys. Chem.* **1996**, *100*, 785-789.

[6] V. Nair, A. Deepthi, *Chem. Rev.* **2007**, *107*, 1862-1891.

[7] a) D. Hong, M. Murakami, Y. Yamada, S. Fukuzumi, *Energy Environ. Sci.* **2012**, *5*, 5708-5716; b) D. J. Wasylenko, C. Ganesamoorthy, M. A. Henderson, C. P. Berlinguette, *Inorg. Chem.* **2011**, *50*, 3662-3672.

[8] H. B. Lee, J. A. Bogart, P. J. Carroll, E. J. Schelter, *Chem. Commun.* **2014**, *50*, 5361-5363.

[9] a) S. Cotton, in *Lanthanide and Actinide Chemistry*, John Wiley & Sons Inc., Hoboken, NJ, **2006**; b) C. K. Gupta, N. Krishnamurthy, *Int. Mater. Rev.* **1992**, *37*, 197-248.

[10] N. A. Piro, J. R. Robinson, P. J. Walsh, E. J. Schelter, *Coord. Chem. Rev.* **2014**, *260*, 21-36.

[11] D. A. Atwood, in *The Rare Earth Elements: Fundementals and Applications*, John Wiley & Sons, **2012**, pp. 84-85.

[12] P. G. Eller, R. A. Penneman, *J. Less-Common Met.* **1987**, *127*, 19-33.

[13] a) S. J. Konezny, M. D. Doherty, O. R. Luca, R. H. Crabtree, G. L. Soloveichik, V. S. Batista, *J. Phys. Chem. C* **2012**, *116*, 6349-6356; b) L. E. Roy, E. R. Batista, P. J. Hay, *Inorg. Chem.* **2008**, *47*, 9228-9237; c) L. E. Roy, E. Jakubikova, M. G. Guthrie, E. R. Batista, *J. Phys. Chem. A* **2009**, *113*, 6745-6750.

[14] a) A. Elkechai, Y. Mani, A. Boucekkine, M. Ephritikhine, *Inorg. Chem.* **2012**, *51*, 6943-6952; b) A. Elkechai, A. Boucekkine, L. Belkhiri, M. Amarouche, C. Clappe, D. Hauchard, M. Ephritikhine, *Dalton Trans.* **2009**, 2843-2849.

[15] K. Koide, T. Ishida, *Inorg. Chem. Commun.* **2011**, *14*, 194-196.

[16] W. J. Evans, J. M. Perotti, R. J. Doedens, J. W. Ziller, *Chem. Commun.* **2001**, 2326-2327.

[17] G. Parkin, *J. Chem. Educ.* **2006**, *83*, 791.

[18] R. Shannon, *Acta Crystallogr. Sect. A* **1976**, *32*, 751-767.

[19] C. Hansch, A. Leo, R. W. Taft, *Chem. Rev.* **1991**, *91*, 165-195.

[20] a) E. L. Muetterties, L. J. Guggenberger, *J. Am. Chem. Soc.* **1974**, *96*, 1748-1756; b) J. L. Hoard, J. V. Silverton, *Inorg. Chem.* **1963**, *2*, 235-242.

[21] a) W. J. Evans, M. A. Hozbor, *J. Organomet. Chem.* **1987**, *326*, 299-306; b) S. D. Stults, R. A. Andersen, A. Zalkin, *Organometallics* **1990**, *9*, 115-122; c) M. D. Walter, R. Fandos, R. A. Andersen, *New J. Chem.* **2006**, *30*, 1065-1070.

[22] A. Kotani, T. Jo, J. C. Parlebas, *Adv. Phys.* **1988**, *37*, 37-85.

[23] a) H. Isago, M. Shimoda, *Chem. Lett.* **1992**, *21*, 147-150; b) C. H. Booth, M. D. Walter, M. Daniel, W. W. Lukens, R. A. Andersen, *Phys. Rev. Lett.* **2005**, *95*, 267202.

[24] W. W. Lukens, N. Magnani, C. H. Booth, *Inorg. Chem.* **2012**, *51*, 10105-10110.

[25] M. D. Walter, C. H. Booth, W. W. Lukens, R. A. Andersen, *Organometallics* **2009**, *28*, 698-707.

[26] A. Streitwieser, S. A. Kinsley, J. T. Rigsbee, I. L. Fragala, E. Ciliberto, *J. Am. Chem. Soc.* **1985**, *107*, 7786-7788.

[27] a) A. Greco, S. Cesca, W. Bertolini, *J. Organomet. Chem.* **1976**, *113*, 321-330; b) A. Streitwieser, S. A. Kinsley, C. H. Jenson, J. T. Rigsbee, *Organometallics* **2004**, *23*, 5169-5175; c) J. P. Clark, J. C. Green, *J. Chem. Soc., Dalton Trans.* **1977**, 505-508.

[28] U. J. Williams, D. Schneider, W. L. Dorfner, C. Maichle-Mossmer, P. J. Carroll, R. Anwander, E. J. Schelter, *Dalton Trans.* **2014**, *43*, 16197-16206.

[29] M. R. MacDonald, J. E. Bates, J. W. Ziller, F. Furche, W. J. Evans, *J. Am. Chem. Soc.* **2013**, *135*, 9857-9868.

[30] N. G. Connelly, W. E. Geiger, *Chem. Rev.* **1996**, *96*, 877-910.

[31] G. F. Smith, C. A. Getz, *Ind. Eng. Chem. Anal. Ed.* **1938**, *10*, 191-195.

[32] H. Zheng, S. J. Yoo, E. Münck, L. Que, *J. Am. Chem. Soc.* **2000**, *122*, 3789-3790.

[33] S. R. Sofen, S. R. Cooper, K. N. Raymond, *Inorg. Chem.* **1979**, *18*, 1611-1616.

[34] U. J. Williams, B. D. Mahoney, A. J. Lewis, P. T. DeGregorio, P. J. Carroll, E. J. Schelter, *Inorg. Chem.* **2013**, *52*, 4142-4144.

[35] L. Maron, O. Eisenstein, *J. Phys. Chem. A* **2000**, *104*, 7140-7143.

[36] a) L. M. A. Saleh, K. H. Birjkumar, A. V. Protchenko, A. D. Schwarz, S. Aldridge, C. Jones, N. Kaltsoyannis, P. Mountford, *J. Am. Chem. Soc.* **2011**, *133*, 3836-3839; b) S. G. Minasian, J. L. Krinsky, J. Arnold, *Chem. Eur. J.* **2011**, *17*, 12234-12245; c) J. L. Krinsky, S. G. Minasian, J. Arnold, *Inorg. Chem.* **2011**, *50*, 345-357; d) R. G. Denning, J. Harmer, J. C. Green, M. Irwin, *J. Am. Chem. Soc.* **2011**, *133*, 20644-20660; e) M. W. Löble, J. M. Keith, A. B. Altman, S. C. E. Stieber, E. R. Batista, K. S. Boland, S. D. Conradson, D. L. Clark, J. Lezama Pacheco, S. A. Kozimor, R. L. Martin, S. G. Minasian, A. C. Olson, B. L. Scott, D. K. Shuh, T. Tyliszczak, M. P. Wilkerson, R. A. Zehnder, *J. Am. Chem. Soc.* **2015**, *137*, 2506-2523.

[37] F. Ferraro, C. A. Barboza, R. Arratia-Pérez, *J. Phys. Chem. A* **2012**, *116*, 4170-4175.

[38] D. L. Clark, J. C. Gordon, P. J. Hay, R. Poli, *Organometallics* **2005**, *24*, 5747-5758.

[39] P. L. Arnold, Z. R. Turner, N. Kaltsoyannis, P. Pelekanaki, R. M. Bellabarba, R. P. Tooze, *Chem. Eur. J.* **2010**, *16*, 9623-9629.

[40] A. V. Marenich, J. Ho, M. L. Coote, C. J. Cramer, D. G. Truhlar, *Phys. Chem. Chem. Phys.* **2014**, *16*, 15068-15106.

[41] a) J. Cui, G. A. Hope, A. N. Buckley, *Miner. Eng.* **2012**, *36–38*, 91-99; b) Pradip, D. W. Fuerstenau, in *Adv. Sci. Technol. Miner. Benefic. India, Proc. Symp.*, **1983**, pp. 217-228.

[42] a) D. W. Wester, G. J. Palenik, R. C. Palenik, *Inorg. Chem.* **1985**, *24*, 4435-4437; b) T. Behrsing, A. M. Bond, G. B. Deacon, C. M. Forsyth, M. Forsyth, K. J. Kamble, B. W. Skelton, A. H. White, *Inorg. Chim. Acta* **2003**, *352*, 229-237; c) L. Li, F. Yuan, T. Li, Y. Zhou, M. Zhang, *Inorg. Chim. Acta* **2013**, *397*, 69-74.

[43] R. Murakami, T. Ishida, S. Yoshii, H. Nojiri, *Dalton Trans.* **2013**, *42*, 13968-13973.

[44] T. Ishida, R. Murakami, T. Kanetomo, H. Nojiri, *Polyhedron* **2013**, *66*, 183-187.

[45] T. Kanetomo, T. Ishida, *Inorg. Chem.* **2014**, *53*, 10794-10796.

[46] D. N. Woodruff, R. E. P. Winpenny, R. A. Layfield, *Chem. Rev.* **2013**, *113*, 5110-5148.

[47] M. Shibasaki, K.-I. Yamada, N. Yoshikawa, in *Lewis Acids in Organic Synthesis*, Wiley-VCH Verlag GmbH, **2008**, pp. 911-944.

[48] D. J. Procter, R. A. Flowers, T. Skrydstrup, *Organic Synthesis using Samarium Diiodide: A Practical Guide*, Royal Society of Chemistry, UK, **2010**.

[49] a) B. Siriwardena-Mahanama, M. Allen, *Molecules* **2013**, *18*, 9352-9381; b) C.-H. Huang, J. R. Morrow, *Inorg. Chem.* **2009**, *48*, 7237-7243.

[50] R. K. Thomson, B. L. Scott, D. E. Morris, J. L. Kiplinger, *C. R. Chimie* **2010**, *13*, 790-802.

[51] Bruker (2009) SAINT. Bruker AXS Inc., Madison, Wisconsin, USA.

[52] Bruker (2009) SHELXTL. Bruker AXS Inc., Madison, Wisconsin, USA.

[53] Sheldrick, G.M. (2008) TWINABS. University of Göttingen: Göttingen, Germany.

[54] Sheldrick, G.M. (2007) SADABS. University of Göttingen: Göttingen, Germany.

[55] G. Sheldrick, *Acta Crystallogr. Sect. A* **2008**, *64*, 112-122.

[56] G. A. Bain, J. F. Berry, *J. Chem. Educ.* **2008**, *85*, 532.

[57] C. H. Booth, M. D. Walter, D. Kazhdan, Y.-J. Hu, W. W. Lukens, E. D. Bauer, L. Maron, O. Eisenstein, R. A. Andersen, *J. Am. Chem. Soc.* **2009**, *131*, 6480-6491.

[58] Gaussian 09, Revision D.01, Frisch, M. J.; Trucks, G. W.; Schlegel, H. B.; Scuseria, G. E.; Robb, M. A.; Cheeseman, J. R.; Scalmani, G.; Barone, V.; Mennucci, B.; Petersson, G. A.; Nakatsuji, H.; Caricato, M.; Li, X.; Hratchian, H. P.; Izmaylov, A. F.; Bloino, J.; Zheng, G.; Sonnenberg, J. L.; Hada, M.; Ehara, M.; Toyota, K.; Fukuda, R.; Hasegawa, J.; Ishida, M.; Nakajima, T.; Honda, Y.; Kitao, O.; Nakai, H.; Vreven, T.; Montgomery, Jr., J. A.; Peralta, J. E.; Ogliaro, F.; Bearpark, M.; Heyd, J. J.; Brothers, E.; Kudin, K. N.; Staroverov, V. N.; Kobayashi, R.; Normand, J.; Raghavachari, K.; Rendell, A.; Burant, J. C.; Iyengar, S. S.; Tomasi, J.; Cossi, M.; Rega, N.; Millam, N. J.; Klene, M.; Knox, J. E.; Cross, J. B.; Bakken, V.; Adamo, C.; Jaramillo, J.; Gomperts, R.; Stratmann, R. E.; Yazyev, O.; Austin, A. J.; Cammi, R.; Pomelli, C.; Ochterski, J. W.; Martin, R. L.; Morokuma, K.; Zakrzewski, V. G.; Voth, G. A.; Salvador, P.; Dannenberg, J. J.; Dapprich, S.; Daniels, A. D.; Farkas, Ö.; Foresman, J. B.; Ortiz, J. V.; Cioslowski, J.; Fox, D. J. Gaussian, Inc., Wallingford CT, **2009**.

[59] a) X. Cao, M. Dolg, *J. Molec. Struct. (Theochem)* **2002**, *581*, 139-147; b) Institute for Theoretical Chemistry, University of Cologne, http://www.tc.uni-koeln.de/PP/clickpse.en.html; c) M. Dolg, H. Stoll, H. Preuss, *J. Chem. Phys.* **1989**, *90*, 1730-1734.

[60] Chemcraft. www.chemcraftprog.com.

[61] S. I. Gorelsky, A. B. P. Lever, *J. Organomet. Chem.* **2001**, *635*, 187-196.

[62] S. I. Gorelsky, *AOMix: Program for Molecular Orbital Analysis,* http://www.sg-chem.net/, University of Ottawa, version 6.5, **2011**.

Chapter 4

Coordination Chemistry of the Rare Earth Metals within a Tripodal Nitroxide Ligand Framework: Towards Targeted Separations of Rare Earth Elements

Abstract

Rare earth metals are critical components of electronic materials and permanent magnets. Recycling of consumer materials is a promising new source of rare earths. To incentivize recycling there is a clear need for the development of simple methods for targeted separations of mixtures of rare earth metal salts. Metal complexes of a tripodal nitroxide ligand, $TriNOx^{3-}$, featured a size-sensitive aperture formed of its three η^2-(*N*,*O*) ligand arms. Exposure of cations in the aperture induced a self-associative equilibrium comprising RE(TriNOx)THF/$[RE(TriNOx)]_2$ species. Differences in the equilibrium constants $K_{dimerization}$ for early and late metals enabled simple separations through leaching. As proof of concept, a complete recycling process of Nd/Dy was performed and a separations factor of $S_{Nd/Dy}$ = 359 was achieved. This separations technique was extended to other early/late rare earth combinations with particular emphasis on Eu/Y, key components of phosphors in compact fluorescent light bulbs.

Adapted with permission from *Angew. Chem. Int. Ed.* **2015**, *54,* 8222–8225. © 2015 John Wiley & Sons and work to be submitted to *J. Am. Chem. Soc.*, **2015.** This chapter also contains work adapted from International Patent Application No. PCT/US15/42703.

4.1 Introduction

The rare earth elements, La–Lu, Y and Sc (RE), comprise vital materials with diverse applications in electric motors for automobiles and wind turbines, phosphors in fluorescent light bulbs, NiMH batteries and catalysts, among others.[1] Their broad, and in many cases irreplaceable, uses result from unique magnetic and electronic properties due to their 4f valence electron shell. A chief application of rare earth materials is in permanent magnets. Neodymium (Nd), typically mixed with praseodymium (Pr), is a key component of sintered neo magnets ($Nd_2Fe_{14}B$), which have the highest energy product (52 MGOe) among the commercialized permanent magnets.[2] Terbium (Tb) and Dysprosium (Dy) are also key components of this material. The Tb or Dy dopants increase the intrinsic coercivity of the material, H_{cJ}, without significant losses in residual induction, B_r.[3] In this context, high performance neo magnets comprise 9% Dy by total magnet weight. Devices such as computer hard drives or generators include $Nd_2Fe_{14}B$ with Dy content ranging from 0 – 9%.[3b, 4] The demand for Nd and especially Dy is expected to grow significantly in the next 20 y with the concomitant growth of renewable energy and energy efficient technologies, particularly wind power and electric vehicles.[5] On the basis of the projected growth of demand for neo magnets, the U.S. Department of Energy (DOE) has categorized dysprosium and neodymium as "critical materials" due to their supply risk and importance to clean energy.[6]

Neodymium and dysprosium are obtained industrially through mining, beneficiation, and separation of the rare earths from light- and heavy rare earth element containing ores, respectively.[7] Currently, suppliers in the People's Republic of China (PRC) comprise 90% of global rare earth element production.[1] A "rare earths crisis" in 2011 illustrated the need for a more diverse supply chain for these elements to improve their economic stability. A potential new supply stream of neodymium and dysprosium is end-of-life magnet recycling, namely, urban mining of rare earth elements from electronic waste. In 2007, global in-use stocks for rare earth metals in neo magnets were estimated to be 62.6 Gg Nd, 15.7 Gg Pr and Dy, and 3.1 Gg Tb.[8] In 2011, however, less than 1% of rare earth metals were recycled.[4a] A recent life cycle

assessment suggested that end-of-life product recycling is a viable and important alternative to rare earth metals mining, especially in the context of growth of demand for Dy.[9] Recycling processes have been reported recently for the separations of RE from dismantled magnetic material.[4a, 10] But the varying blends of Dy, Tb, Nd and Pr in magnetic materials necessitate separations of the RE for re-blending into new sintered magnets in the highest value recycling schemes.

Another important use of rare earth elements is in phosphors for fluorescent light bulbs, which represent 32% of the rare earth market value compared to 38% for hard magnetic materials.[4a] Lamp phosphor waste consists of the non-rare earth containing halophosphate, $(Sr, Ca)_{10}(PO_4)_6(Cl,F)_2:Sb^{3+},Mn^{2+}$ (HALO, 40–50%) and rare-earth containing components, $Y_2O_3:Eu^{2+}$ (YOX, 20%), $LaPO_4:Ce^{3+},Tb^{3+}$ (LAP, 6–7%), $BaMgAl_{10}O_{17}:Eu^{2+}$ (BAM, 5%), and small quantities of other phosphors such as $(Ce,Tb)MgAl_{11}O_{19}$ (CAT) and $(Gd,Mg)B_5O_{10}:Ce^{3+},Tb^{3+}$.[11] Of these, YOX has the highest intrinsic value since it contains 80 wt% of the total rare earth content of the phosphor waste and is comprised exclusively of the two critical rare earth elements, Y and Eu.[4a] Recent developments in the recycling of phosphor materials have focused mostly on the recovery of Y and Eu from YOX.[12] Dupont and Binnemans recently reported on the selective dissolution of YOX and recovery of yttrium and europium using the functionalized ionic liquid betainium bis(trifluoromethylsulfonyl)imide, $[Hbet][Tf_2N]$.[11] Currently, however, only one industrially applied recycling process exists for lamp phosphor waste, which was implemented by Solvay in 2012.[11] The main drawbacks of this process are that it involves costly acidic and basic washes at relatively high temperatures to fully solubilize the phosphors followed by inefficient liquid-liquid extraction steps to separate the individual rare earth ions.[11]

Rare earth metals are separated commercially using a Rhône-Poulenc liquid-liquid extractions (LLE) process that exploits differences in binding constants of the metals to organic extractants.[7] Due to the chemical similarities between ions of the 4f-block, the extractants have only small separations factors between neighboring RE.[13] Using unpurified Cyanex 302 (bis(2,4,4‐trimethylpentyl) monothiophosphinic acid), a key commercial extractant, average separations

factors of 3.26 between neighboring rare earths were reported at low metal loadings. The LLE separations factors for $S_{Nd/Dy}$ and $S_{Eu/Y}$ under these conditions were determined to be 246 and 116, respectively.[14] Synergistic effects of using mixtures of extractants have been observed with enhancements to selectivity.[15] In part because of the inherent inefficiency of the LLE process, the PRC's rare earth metal production is associated with extensive pollution.[16] The environmental damage underscores the need to develop more efficient separations methods, which could also contribute to diversifying the supply chain. Recent fundamental studies have worked to enhance the selectivity for one type of rare earth metal cation over another, based on ionic size, through molecular self assembly of helical Ln_2L_3 dimers,[17] or with the use of lanthanide based metal organic frameworks for fractional crystallization.[18] It was of interest, therefore, to develop simple and direct chemical methods for efficient separations of early and late rare earth metals, namely dysprosium and neodymium or europium and yttrium, to enable recycling from their primary consumer use in magnetic materials or phosphors.

Herein, we report rare earth metal coordination compounds of $[((2\text{-}^{t}BuNO)C_6H_4CH_2)_3N]^{3-}$ ($TriNOx^{3-}$) of the form RE(TriNOx)THF, RE = La–Lu and Y (**4.1-RE**), that underwent a self-association (dimerization) equilibrium to form $[RE(TriNOx)]_2$ complexes, (**4.2-RE**), based on the size of the cations and solvent polarity. This allowed for the development of a coordination chemistry-based separations method that was an improvement on current systems based on performance, smaller quantities of solvent required, and overall greater ease in separations. Complete recycling cycles were performed on Nd/Dy mixtures to show proof of concept that the method could be used for urban mining of permanent magnetic materials. This method was extended to other early/late rare earth combinations, with focus on europium and yttrium, in order to optimize the separations of these materials for potential recycling of other end-of-use products such as fluorescent light bulbs. Furthermore, the ligand framework allowed for the successful isolation of $[RE(TriNOx)]_2[BAr^{F}_4]_2$, RE = Pr or Tb (**4.3-RE**), oxidized forms of **4.1-Pr** and **4.1-Tb**, which we expect could also have applications in redox-based separations techniques.

4.2 Results/Discussion

4.2.1 Ligand and Complex Syntheses

Tris(2-*tert*-butylhydroxylaminato)benzylamine, $((2\text{-}^{t}BuNOH)C_6H_4CH_2)_3N$ ($H_3TriNOx$), was synthesized in 70% yield by a lithium halogen exchange reaction between the known *tris*-2-bromobenzylamine precursor[19] and $^{n}BuLi$ at –78 °C, followed by the addition of 2-methyl-2-nitrosopropane dimer (Scheme 4.2.1.1). X-ray quality crystals of $H_3TriNOx$ were obtained by slow evaporation of a saturated methylene chloride solution (Figure 4.2.1.1). The crystal structure of $H_3TriNOx$ included a single interstitial CH_2Cl_2 molecule in close contact with the hydroxylamine oxygen atoms, revealing the coordination pocket provided by the tripodal framework. Unlike the 2-pyridylhydroxylamines discussed in Chapter 2, $H_3TriNOx$ was stable to air in both the solid and solution states. We attributed this stability to the presence of an intramolecular hydrogen-bonding network, as evident in the crystal structure.

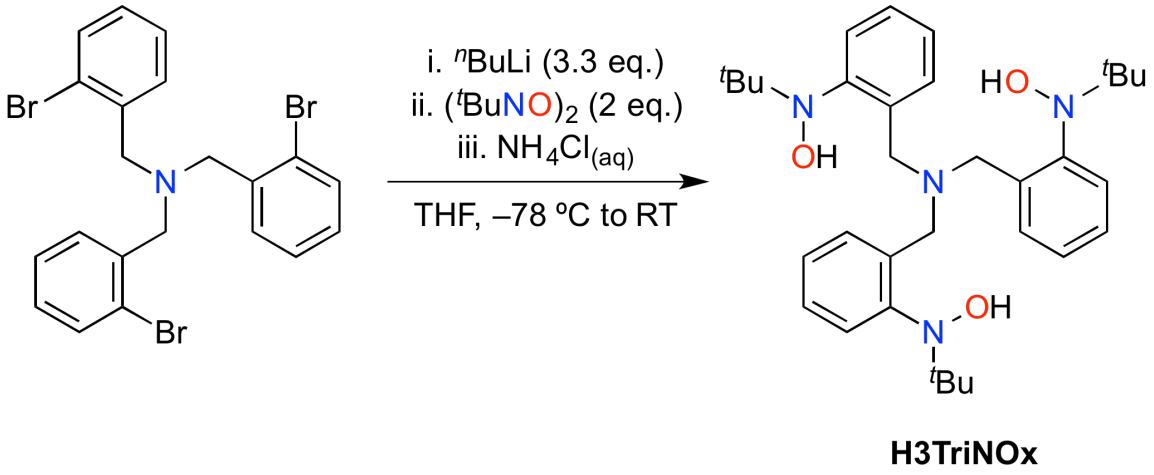

Scheme 4.2.1.1. Schematic of the synthesis of $H_3TriNOx$ from the known 2-bromobenzylamine precursor and 2-methyl-2-nitrosopropane dimer by a lithium halogen exchange reaction. Scheme reprinted with permission of John Wiley & Sons © 2015.

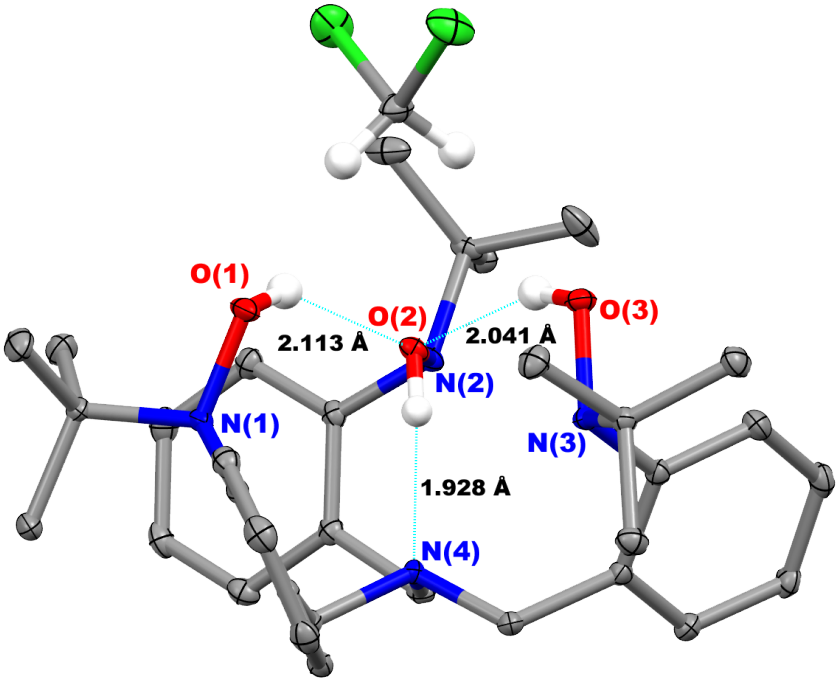

Figure 4.2.1.1. Thermal ellipsoid plot of H_3TriNOx at 30% probability. Hydrogen atoms (except for hydrogen-bonded hydrogens) omitted for clarity. Figure reprinted with permission of John Wiley & Sons © 2015.

Rare earth metal cation complexes of TriNOx^{3-} formed isostructural RE(TriNOx)THF, RE = La–Lu and Y (**4.1-RE**), compounds through a simple protonolysis route between H_3TriNOx and their respective RE^{III}[N(SiMe$_3$)$_2$]$_3$ reagents (Scheme 4.2.1.2, Method A). These compounds exhibited only low solubility in THF (*vide infra*). The compounds could also be synthesized through an alternative, one pot synthetic route starting from the RE(OTf)$_3$ salts, 1 equiv. of H_3TriNOx, and 3 equiv. of K[N(SiMe$_3$)$_2$] in THF (Scheme 4.2.1.2, Method B). Figure 4.2.1.2 shows the thermal ellipsoid plot of **4.1-Nd**, which serves as a representative example of the series of **4.1-RE** complexes. As shown, the structure revealed that each arm of the nitroxide ligand was coordinated η^2-(*N*,*O*) to the rare earth cations. This coordination mode provided a C_3-symmetric environment with an open site in the apical position that was occupied by a THF molecule. The

complexes were characterized in solution by ^{1}H NMR spectroscopy in d_5-pyr, where their C_3-symmetric structures were maintained.

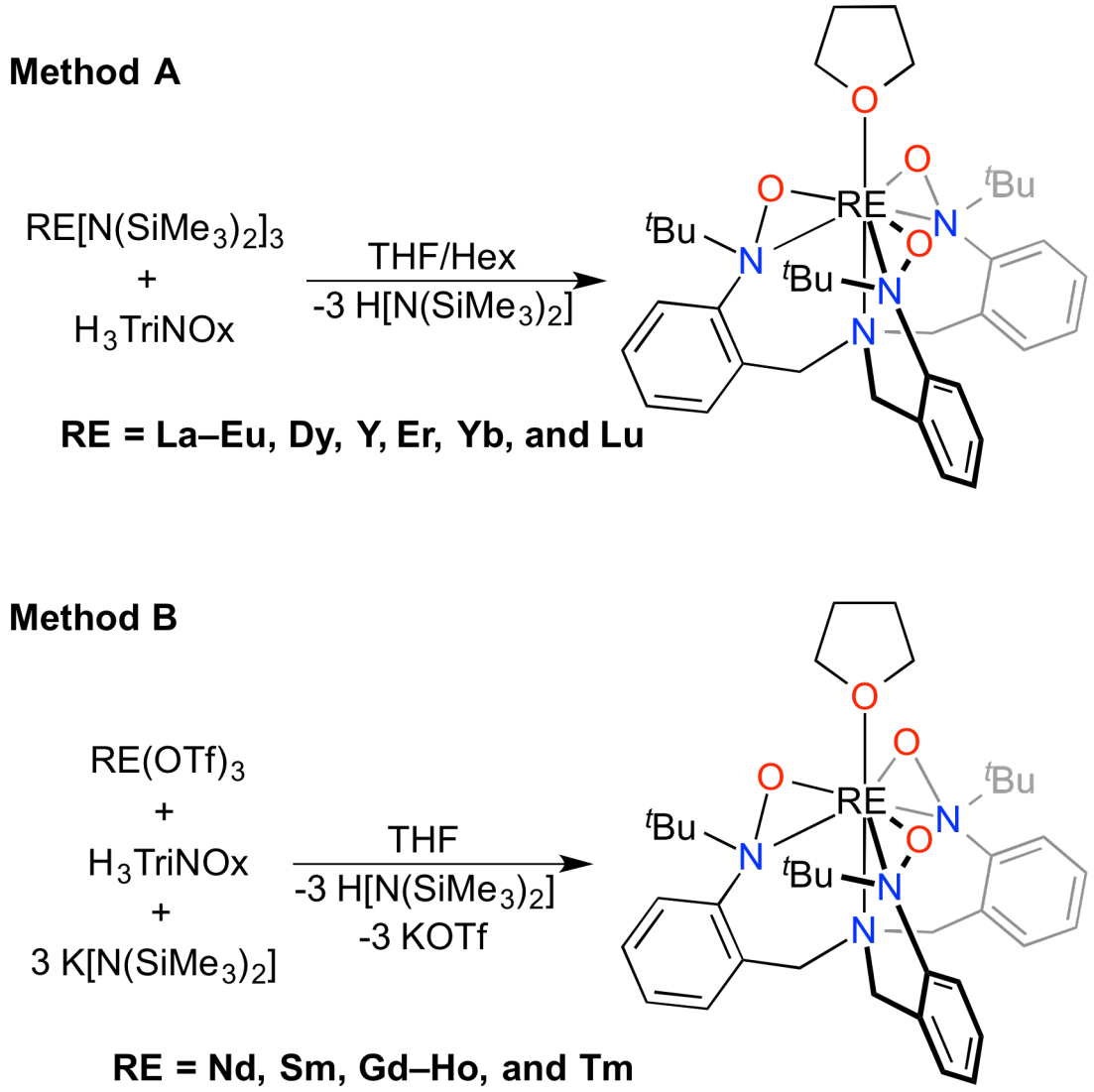

Scheme 4.2.1.2. Schematic of the synthesis of **4.1-RE**, where RE = La–Lu and Y, from the $RE[N(SiMe_3)_2]_3$ reagents (Method A, top) or the $RE(OTf)_3$ reagents (Method B, bottom). Scheme adapted with permission of John Wiley & Sons © 2015.

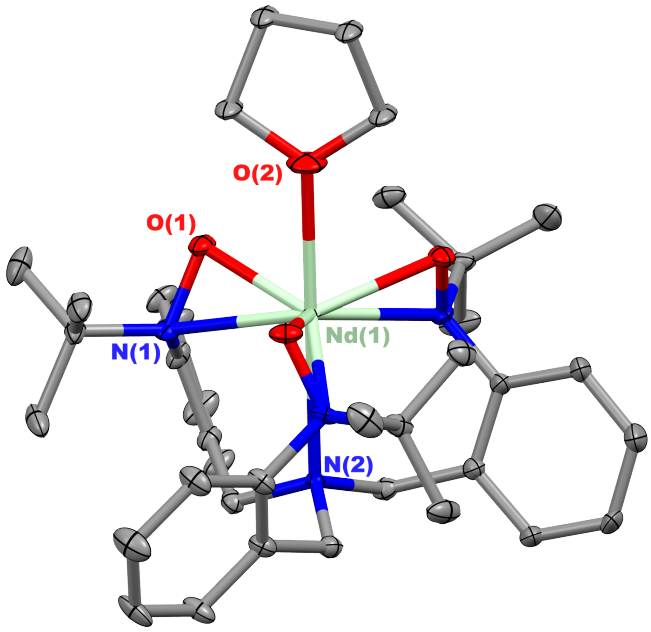

Figure 4.2.1.2. Thermal ellipsoid plot of **4.1-Nd** at 30% probability as a representative example of the solid state structures of the series of **4.1-RE** complexes. Hydrogen atoms excluded for clarity. Figure reprinted with permission of John Wiley & Sons © 2015.

It was noteworthy that these complexes showed resistance to decomposition by moisture in the air with only 20% decomposition being observed for **4.1-Y** when stirred in pyridine overnight. Only 3% decomposition was observed for **4.1-La** under the same conditions. These results seemed promising for the development of bench-top syntheses of these complexes.

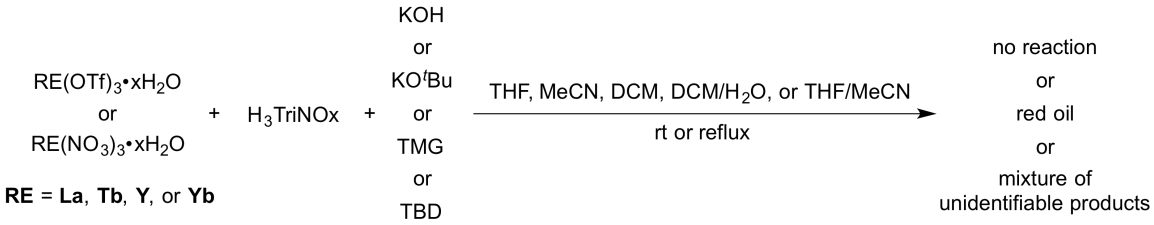

TMG = 1,1,3,3-tetramethylguanidine
TBD = 1,5,7-triazabicyclo[4.4.0]dec-5-ene

Scheme 4.2.1.3. Attempted bench-top syntheses of RE(TriNOx) complexes.

However, attempts to isolate these complexes under aerobic conditions have, as yet, failed. These included the reaction of hydrated salts of either $RE(NO_3)_3$ or $RE(OTf)_3$ (RE = La, Tb, Y, or Yb), 1 equiv. of H_3TriNOx, and either KOH, KO^{t}Bu, 1,1,3,3-tetramethylguanidine (TMG), or 1,5,7-triazabicyclo[4.4.0]dec-5-ene (TBD) as bases. The choice of solvent was also altered and included THF, MeCN, DCM as well as mixtures of solvents such as DCM/H_2O or THF/MeCN. Reaction conditions of hot refluxing DCM or MeCN were also examined. In each case, no reaction occurred, an NMR silent red-orange oil was formed, or a mixture of unidentifiable products was produced. In one particular example, $Yb(OTf)_3$•xH_2O, H_3TriNOx, and 20 equiv. of KO^{t}Bu were suspended in wet THF and an immediate orange-pink solution formed. Analysis by ^{1}H NMR spectroscopy confirmed that no complex formation had occurred. A similar reaction using dry $Tb(OTf)_3$, H_3TriNOx, and 3 equiv. of KO^{t}Bu was performed in dry THF under an N_2 atmosphere and **4.1-Tb** precipitated. These results indicated that KO^{t}Bu was a strong enough base to deprotonate H_3TriNOx and induce complex formation and suggested that the lack of complex formation under aerobic conditions was rather the result of ligand oxidation by O_2 occurring at a faster rate than complex formation. To test this hypothesis, $Yb(OTf)_3$•xH_2O, H_3TriNOx, and 20 equiv. of KO^{t}Bu were reacted in deaerated THF. In contrast to the reaction performed under O_2, an orange-pink solution did not form. Analysis by ^{1}H NMR spectroscopy, however, indicated that no complex formation had occurred and that the major species in solution was unreacted H_3TriNOx.

4.2.2 Detection of Dimeric [RE(TriNOx)]$_2$ Species

Analysis of the solution structures of **4.1-RE**, RE = La–Eu, in C_6D_6, using ^{1}H NMR spectroscopy revealed two species in each case, consistent with the **4.1-RE** complexes and C_2-symmetric dimeric compounds, [RE(TriNOx)]$_2$ (**4.2-RE**), having each arm of the TriNOx^{3-} ligand in chemically inequivalent environments. The minimal amount of dimer in the Eu case prevented its isolation. However, the identities of the dimeric compounds for **4.2-RE**, RE = La–Sm, were confirmed by X-ray crystallography. Figure 4.2.2.1 shows the thermal ellipsoid plot of **4.2-Nd**, which serves as a representative example of the series of **4.2-RE**, RE = La–Sm, complexes.

These dimeric compounds could be isolated in good yields by dissolving **4.1-RE**, RE = La–Sm, in toluene and stripping the solvent under reduced pressure. It was noteworthy that the **4.2-RE** compounds could be converted back into the respective **4.1-RE** congeners by addition of THF to their benzene, toluene, or methylene chloride solutions. It was also noteworthy that **4.2-Sm** and **4.2-Eu** were not observed by ^{1}H NMR spectroscopy in solutions of CD_2Cl_2 and only minimal amounts of **4.2-Nd** were present in $CDCl_3$ solutions, indicating that solvent polarity significantly affected the ratios of monomeric/dimeric species in solution. In the cases of RE = Gd–Lu, dimeric species were not observed.

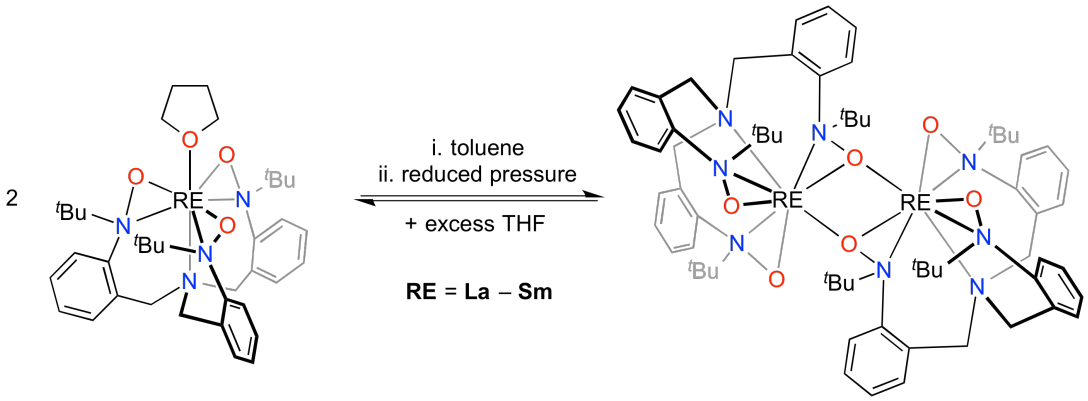

Scheme 4.2.2.1. Schematic of the synthesis of **4.2-RE** by removal of THF and regeneration of **4.1-RE** through the addition of THF.

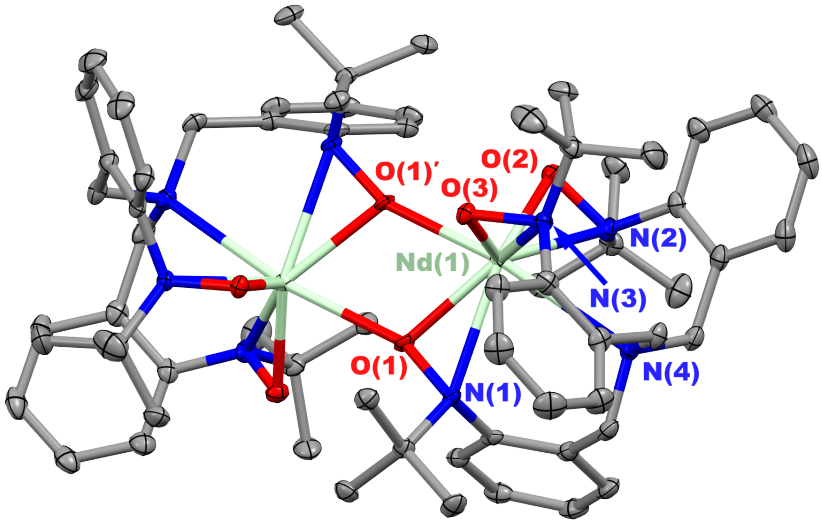

Figure 4.2.2.1. Thermal ellipsoid plot of **4.2-Nd** at 30% probability as a representative example of the solid state structures of the series of **4.2-RE** complexes. Hydrogen atoms excluded for clarity. Figure reprinted with permission of John Wiley & Sons © 2015.

We also observed a visible color change from light purple to light blue when dissolving **4.1-Nd** in toluene; addition of pyridine reestablished the purple color. This result suggested that there was a change in the energies of the optical transitions upon dimerization of **4.1-Nd** to **4.2-Nd**. The UV-Vis spectra of these Nd complexes were recorded at a spectral resolution of 0.1 nm in benzene for **4.2-Nd** and pyridine for **4.1-Nd** to insure uniform speciation of the Nd cations in each case (Figure 4.2.2.3). The most intense absorptive features of each spectrum occurred in the 560 nm – 620 nm region and were assigned to the hypersensitive $^4I_{9/2} \rightarrow {}^2G_{7/2}$, $^4G_{5/2}$ 4f-4f transition.[20] Rare earth 4f-4f transitions are typically sharp and insensitive to ligand field environment due to the core-like nature of the 4f-orbitals. However, certain hypersensitive 4f-4f excitations are known to shift with varying ligand fields.[21] With the Nd-TriNOx system, there was a noticeable color change and shift in the $^4I_{9/2} \rightarrow {}^2G_{7/2}$, $^4G_{5/2}$ transition maximum from 593.3 nm in **4.2-Nd** to 595.8 nm in **4.1-Nd**. This shift served as another spectroscopic handle for the presence of dimer in solution.

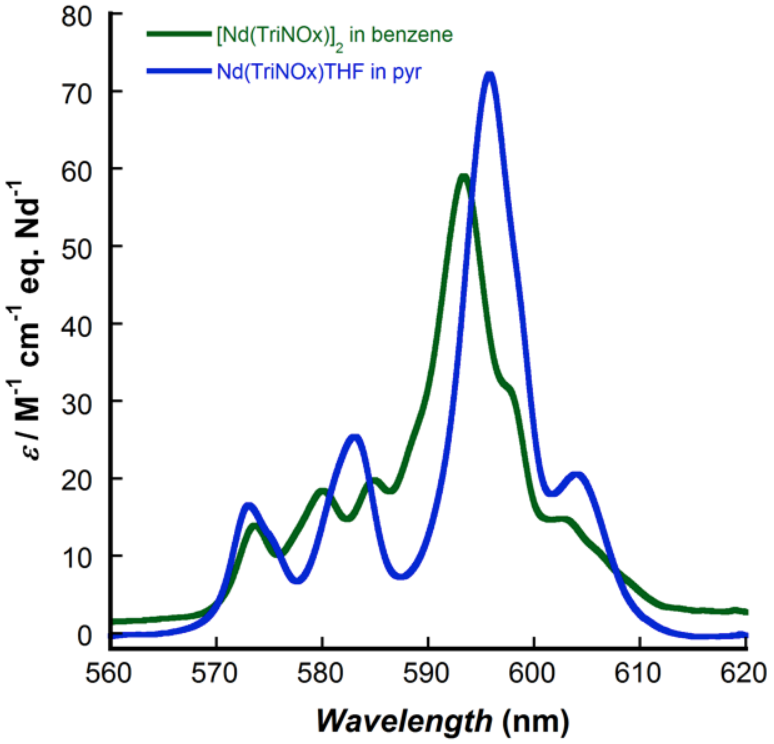

Figure 4.2.2.2. UV-Vis spectra of **4.2-Nd** in benzene and **4.1-Nd** in pyridine. Figure reprinted with permission of John Wiley & Sons © 2015.

4.2.3 Determination of $K_{dimerization}$ for the RE(TriNOx)THF Complexes

The observation of an isosbestic point at 594.1 nm in the overlay of the UV-Vis spectra of **4.1-Nd** and **4.2-Nd** suggested the presence of a self-association equilibrium between these two species in solution. Scheme 4.2.3.1 shows a schematic of this equilibrium process. It was of interest to determine the value of the equilibrium constant in benzene for this process. A spectrophotometric titration of **4.2-Nd** with THF was performed (Figure 4.2.3.1). Again, there was a clear isosbestic point observed at 594.1 nm concomitant with a decrease in the absorbance of the peak at 593.2 nm and an increase in the absorbance of the peak at 595.3 nm. Plots of absorbance at 593.2 nm and 595.3 nm versus concentration of THF added indicated that the endpoint of the titration had been reached and allowed for the determination of the molar absorptivity of monomer, ε_m, at 593.2 nm and 595.3 nm respectively. With these values, the equilibrium concentrations of **4.1-Nd** and **4.2-Nd** were determined at each titration point by solving the following linear system:

$$A_{593.2\ nm} = \varepsilon_{m\ 593.2\ nm}[M] + \varepsilon_{d\ 593.2\ nm}[D]$$

$$A_{595.3\ nm} = \varepsilon_{m\ 595.3\ nm}[M] + \varepsilon_{d\ 595.3\ nm}[D]$$

The concentration of unbound THF was taken as the difference between the known amount of added THF and the determined concentration of monomer. This yielded an equilibrium constant of $K_{eq} = 2.9 \pm 0.4$ for the dimerization of **4.1-Nd**.

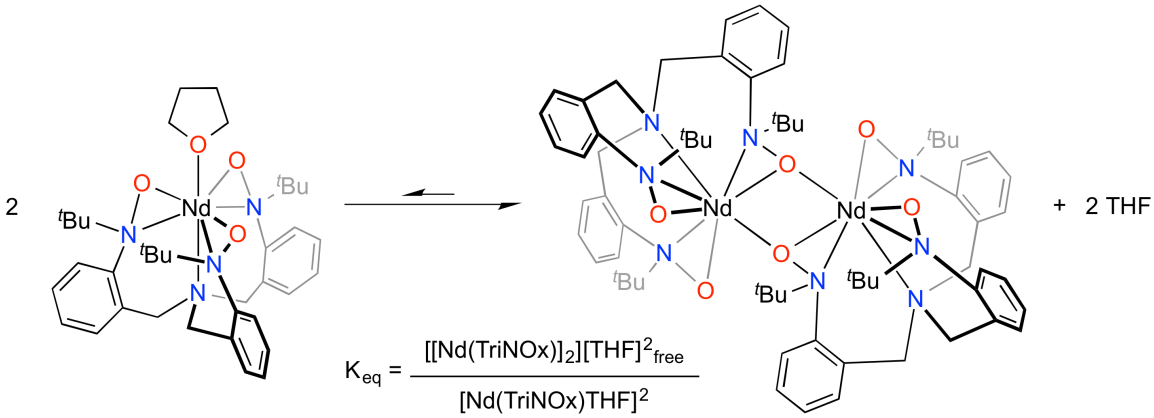

Scheme 4.2.3.1. Schematic of the self association equilibrium between **4.1-Nd** and **4.2-Nd**. Figure reprinted with permission of John Wiley & Sons © 2015.

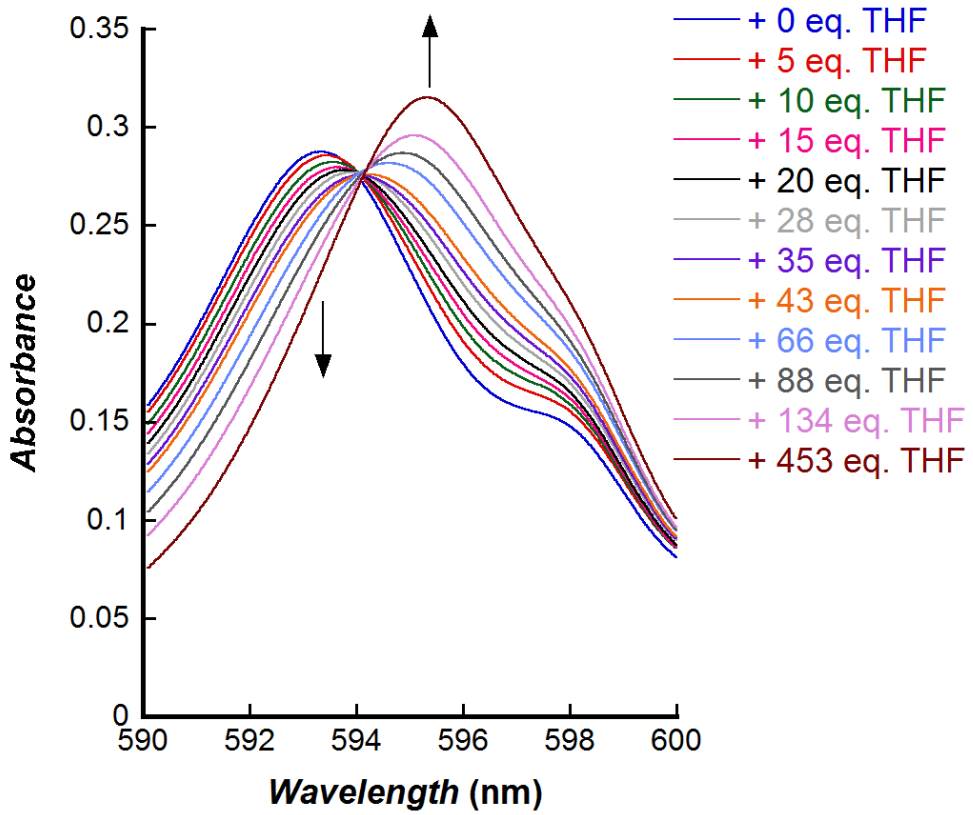

Figure 4.2.3.1. Spectrophotometric titration of **4.2-Nd** with THF in benzene. Figure reprinted with permission of John Wiley & Sons © 2015.

The equilibrium constant for this process was alternatively determined by performing a similar titration of **4.2-Nd** with THF in C_6D_6 and using ^{1}H NMR spectroscopy for analysis (Figure 4.2.3.2). The equilibrium concentrations of **4.1-Nd** and **4.2-Nd** at each titration point were determined through integration of the peaks at 18 ppm and 38 ppm, respectively, relative to an internal ferrocene reference. This yielded a value of 2.4 ± 0.2 for the equilibrium constant, which was in good agreement with the UV-Vis spectrophotometric results.

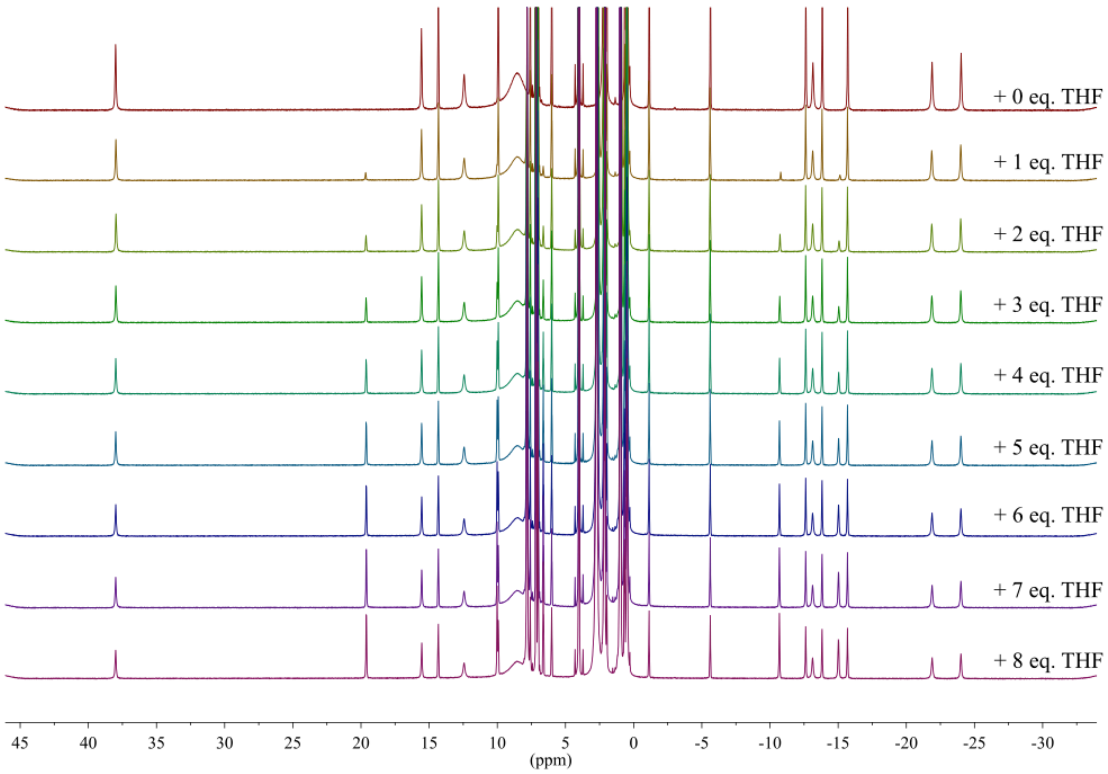

Figure 4.2.3.2. ^{1}H NMR titration experiments of **4.2-Nd** with THF in C_6D_6. Figure reprinted with permission of John Wiley & Sons © 2015.

These results established the use of ^{1}H NMR spectroscopy as a viable method for the determination of the equilibrium constant for this dimerization processes and allowed us to determine the values of K_{eq} for **4.1-RE**, RE = La–Sm. Interestingly, we noticed that as the series was traversed from left to right, there was an order of magnitude decrease in K_{eq} between adjacent rare earth metals. In fact, a linear correlation could be formed between the log of the equilibrium constant, Log(K_{eq}), and the ionic radius of the trivalent rare earth metal (CN = 8), $r_{RE(III)}$ (Figure 4.2.3.3).

The linear correlation of logK_{eq} to metal cation radius allowed for the estimation of the self-association equilibrium constants for the **4.1-RE**, RE = Eu–Lu, species. According to these predictions, there was a 10^{11}-fold decrease in the self-association equilibrium constants across the series as a result of the ~0.18 Å decrease in ionic radii.

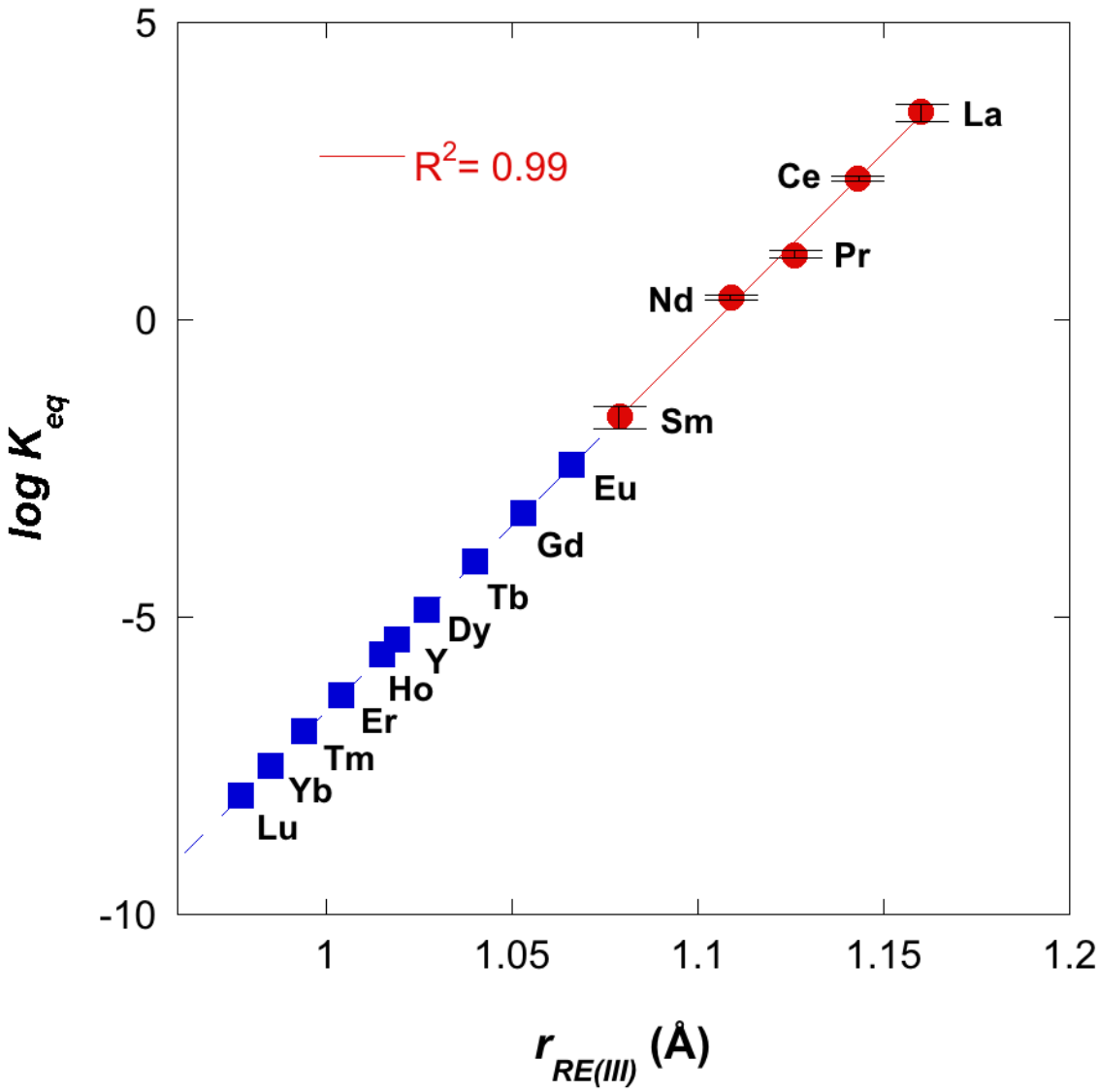

Figure 4.2.3.3. Correlation of log K_{eq} of dimerization for the series of **4.1-RE** complexes, RE = La – Sm, to the ionic radius of the rare earth metal, $r_{RE(III)}$. Extrapolation of the experimental data (red circles) allowed for the prediction of the value of log(K_{eq}) for the **4.1-RE**, RE = Eu–Lu, species (blue squares).

4.2.4 Determination of Percent Buried Volumes

We hypothesized that the high sensitivity of the dimerization equilibrium constant to slight decreases in metal ionic radius was a result of an effective closing of the $(N,O)_3$ aperture formed by the three η^2-(N,O) arms of the TriNOx^{3-} ligand. To quantify the increase in sterics imposed by the TriNOx^{3-} ligand as the metal ionic radius decreased, we calculated the percent buried volume

(%V_{bur}) across the series of **4.1-RE** complexes. %V_{bur} has previously been established as a useful metric to quantify the sterics imposed by N-heterocyclic carbene (NHC) and phosphine ligands in transition metal chemistry. In the case of the **4.1-RE** complexes, a systematic increase in %V_{bur} was observed as the rare earth metal ionic radius decreased. In fact, a similar linear correlation could be established between metal ionic radius and the relative buried volumes, ($V_{bur\ Ln}/V_{bur\ La}$), for the series of complexes (Figure 4.2.4.1). We contended that this small, but significant, increase in %V_{bur} and change in size of the $(N,O)_3$ molecular aperture was responsible for shifting the thermodynamic preference from dimer to monomer as the series of **4.1-RE** complexes was traversed.

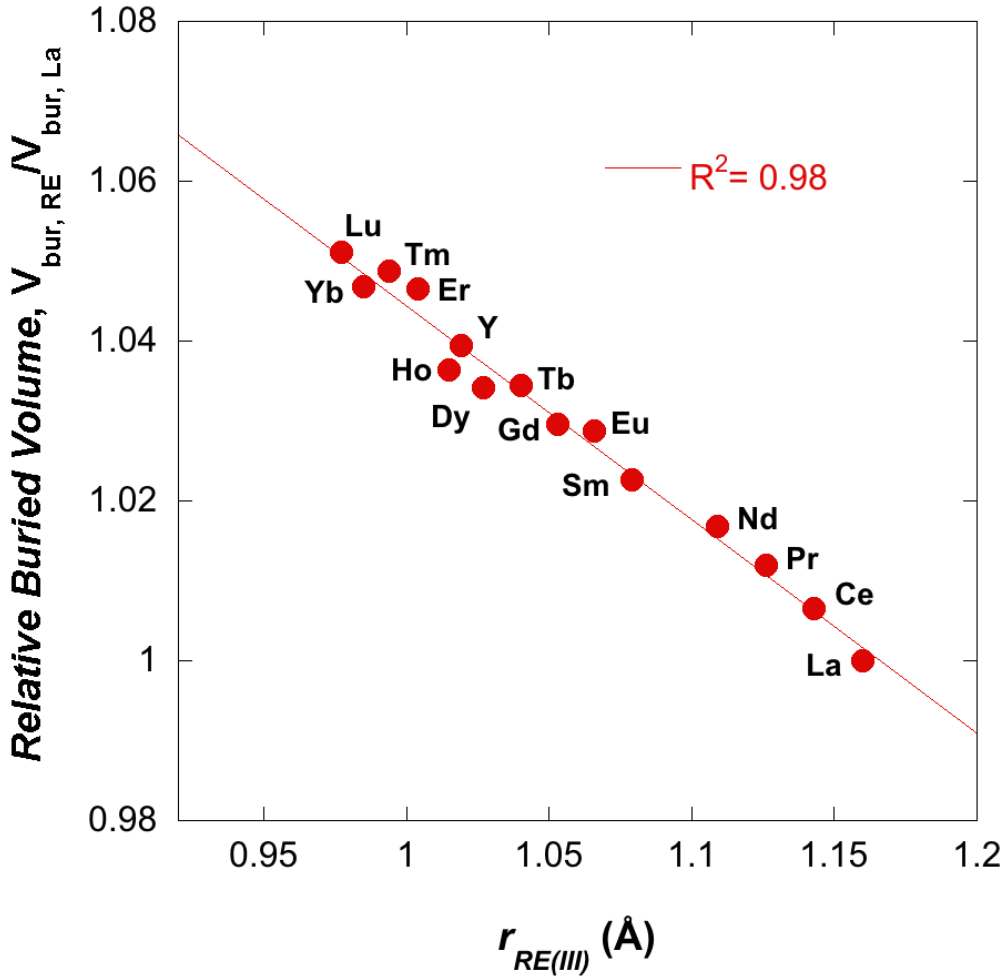

Figure 4.2.4.1. Correlation of relative buried volume ($V_{bur,RE}/V_{bur,La}$) for the series of **4.1-RE**, RE = La – Lu, and Y, to the ionic radius of the rare earth metal, $r_{RE(III)}$.

4.2.5 Nd/Dy Separations

The preferential formation of dimeric structures from the larger cations within the TriNOx^{3-} ligand framework and monomeric ones from the smaller cations was promising for targeted separations of Nd and Dy. To test for the formation of mixed metal dimers between Nd and Dy, which would interfere with a clean separation, ^{1}H EXSY NMR spectroscopy experiments were performed on mixtures of **4.1-Nd** and **4.1-Dy** in CD_2Cl_2. No exchange was observed between Nd and Dy during these experiments. ^{1}H EXSY NMR spectroscopy experiments were also performed on mixtures of **4.1-Nd** and **4.1-Y**, a diamagnetic analog of **4.1-Dy**, to allow for longer delay times; no exchange was observed in the Nd/Y experiments.

The absence of mixed-metal dimer formation prompted us to search for conditions where the dimerization of **4.1-Nd** could be exploited for solubility differences between the Nd and Dy species. Significantly different solubilities were observed for **4.1-Nd** and **4.1-Dy** complexes in benzene. These solubilities were quantified by ^{1}H NMR spectroscopy, where saturated C_6D_6 solutions of the complexes were prepared and measured against a ferrocene internal standard. The values of 60 mmol/L and 1.2 mmol/L determined for the Nd and Dy species, respectively, suggested that benzene could be used to effectively separate these ions. A schematic of this separations process is shown in Scheme 4.2.5.1.

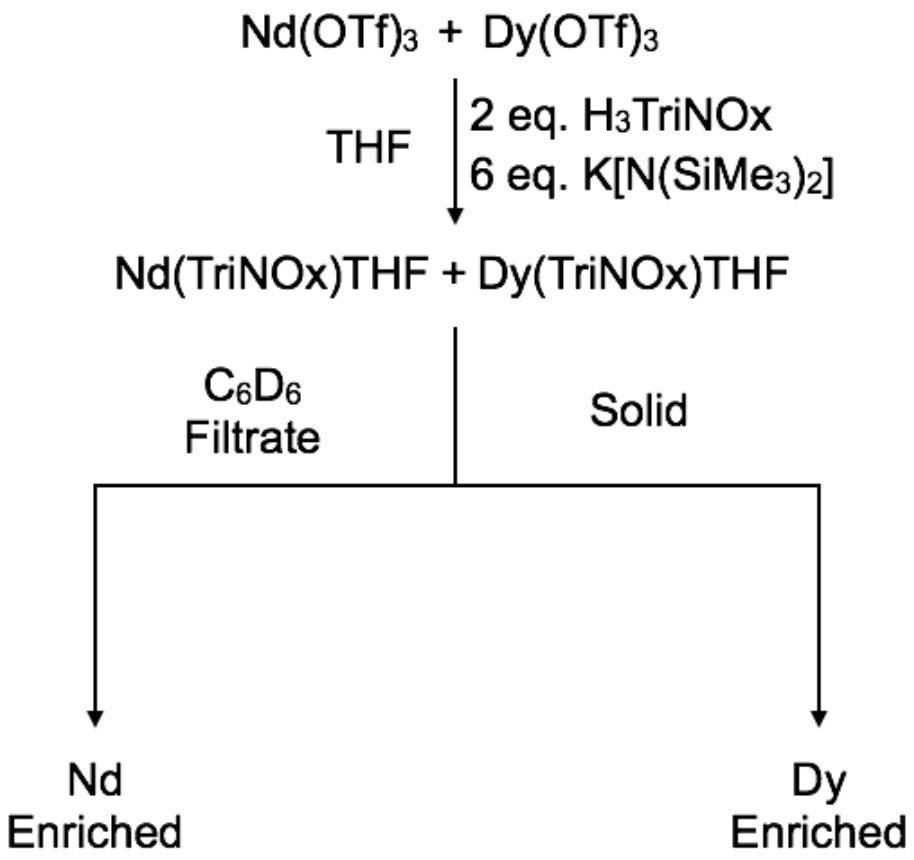

Scheme 4.2.5.1. Schematic of the $TriNOx^{3-}$-based separations process of Nd and Dy starting from simple mixtures of $RE(OTf)_3$ salts. Figure reprinted with permission of John Wiley & Sons © 2015.

To test the feasibility of a separations method based on the self association equilibrium between **4.1-Nd** and **4.2-Nd**, 50:50 mixtures of **4.1-Nd** and **4.1-Dy** were prepared in 90% isolated yield by reacting equimolar mixtures of $Nd(OTf)_3$ and $Dy(OTf)_3$ with 2 equivalents $H_3TriNOx$ and 6 equivalents $K[N(SiMe_3)_2]$ in THF. The ratio of rare earth elements in the prepared mixture was confirmed by ^1H NMR spectroscopy. **4.1-Nd** was selectively leached into minimal benzene leaving a solid residue enriched with **4.1-Dy**. The ratios of Nd:Dy in the final filtrate and solid phases were determined by ^1H NMR spectroscopy and inductively coupled plasma optical emission spectroscopy (ICP-OES).[22] Good agreement between the two methods was obtained. The ICP-OES data showed the filtrate was enriched to 95.37% Nd while the solid was enriched to

94.56% Dy. From these data, a separations factor, $S_{Nd/Dy}$, could be determined from the ratios (by mole) of Nd and Dy in the solid and filtrate fractions using the following equation:

$$S_{Nd/Dy} = (n_{Nd\ filtrate}/n_{Nd\ solid})/(n_{Dy\ filtrate}/n_{Dy\ solid}) = (n_{Nd\ filtrate}/n_{Dy\ filtrate})/(n_{Nd\ solid}/n_{Dy\ solid})$$

This provided a separations factor, $S_{Nd/Dy}$ = 359. Subsequent extractions with benzene to the isolated fractions improved upon the purities of both the filtrate and solid phases to 97.90% Nd and 95.28% Dy. The more benign solvent toluene was also used to achieve comparable separations of Nd and Dy, albeit with larger solvent volumes. The $S_{Nd/Dy}$ = 359 achieved for the RE-TriNOx system compared favorably to that of 41.5 determined for the RE(III)-HCl-HDEHP extraction used industrially, indicating an ~10-fold improvement in the separations of Nd and Dy.[13] It was also an ~1.5-fold improvement in the separations based on the RE(III)-HNO_3-Cyanex 302 system.[14]

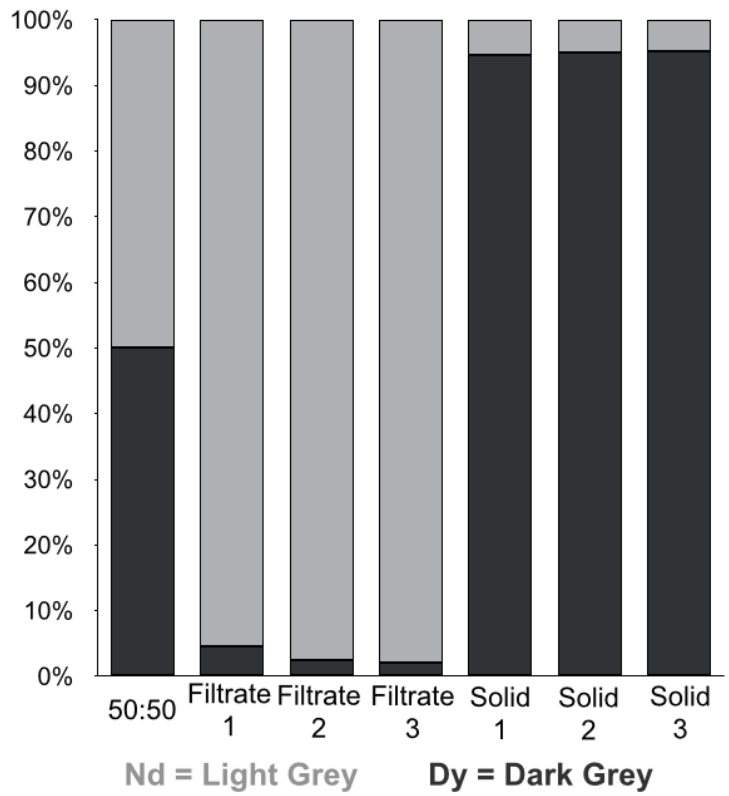

Figure 4.2.5.1. Bar graph showing the enrichment in RE at each separations cycle. %RE in each sample was determined using ICP-OES. Figure reprinted with permission of John Wiley & Sons © 2015.

A separation was also performed on a 75:25 mole ratio mixture of **4.1-Nd** to **4.1-Dy**, a ratio that is used in $Nd_2Fe_{14}B$ high performance magnets. The filtrate phase was enriched to 97.6% Nd and the solid phase was enriched to 95.2% Dy as indicated by ^{1}H NMR spectroscopic analysis. These results were comparable to those obtained from the 50:50 mixtures.

Aqueous oxalic acid solutions (1.5 equivalents) were added to pure samples of **4.1-Nd** and **4.1-Dy** in an effort to reclaim the H_3TriNOx compound. In both cases, pure H_3TriNOx was extracted using 3 × 50 mL of chloroform in 87% and 77% recoveries, respectively. Based on these results, a complete synthetic cycle was performed, starting from the addition of THF solutions of H_3TriNOx to mixtures of Nd/Dy$(OTf)_3$ salts and ending with the isolation of $RE_2(C_2O_4)_3$ RE = Nd, Dy and recovery of H_3TriNOx.

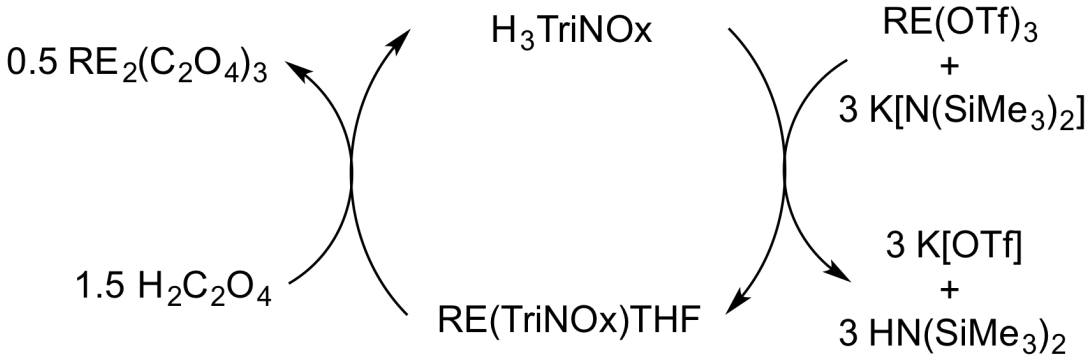

Scheme 4.2.5.2. Schematic of the recyclability of the **H_3TriNOx** ligand. Figure reprinted with permission of John Wiley & Sons © 2015.

4.2.6 Extension to Early/Late RE Separations

We next examined whether the method used for separating neodymium and dysprosium based on the TriNOx^{3-} ligand system could be extended to the other RE1/RE2 combinations. While no mixed dimer formation was observed in the neodymium and dysprosium mixtures, we expected mixed dimer formation in the early/early RE combinations. Indeed, in C_6D_6 solutions of **4.1-La** and **4.1-Ce** mixtures, resonances corresponding to **4.2-La**, **4.2-Ce**, and a new species, postulated to be the mixed La/Ce dimer, were observed in the ^{1}H NMR spectrum (Figure 4.2.6.1). Therefore, early/late RE combinations were explored for targeted separations where the formation of mixed dimers would be unfavorable. Separations were performed on mixtures of

RE1/RE2(TriNOx)THF combinations, RE1 = La–Eu, RE2 = Gd–Lu, and Y. These mixtures were formed by reacting 50:50 mixtures of RE1/RE2$(OTf)_3$ salts with 2 equiv of H_3TriNOx and 6 equiv. of K[N$(SiMe_3)_2$] in THF. Leaching with 4 mL of benzene followed by a wash of 1 mL of benzene led to filtrates enriched with the larger RE1 and solids enriched with the smaller RE2. The molar ratios of the two rare earth metals in the filtrate and solid fractions were determined by ^{1}H NMR and, in select cases, ICP-OES spectroscopies. From these data, the separations factors, $S_{RE1/RE2,}$ were calculated as described previously and are tabulated in Table 4.2.6.3. The enrichment factors for the solid and filtrate fractions, which express the ratio by mole of the more enriched metal to the less enriched metal and indicate the purity of each fraction, were also determined and tabulated (Tables 4.2.6.1 and 4.2.6.2).

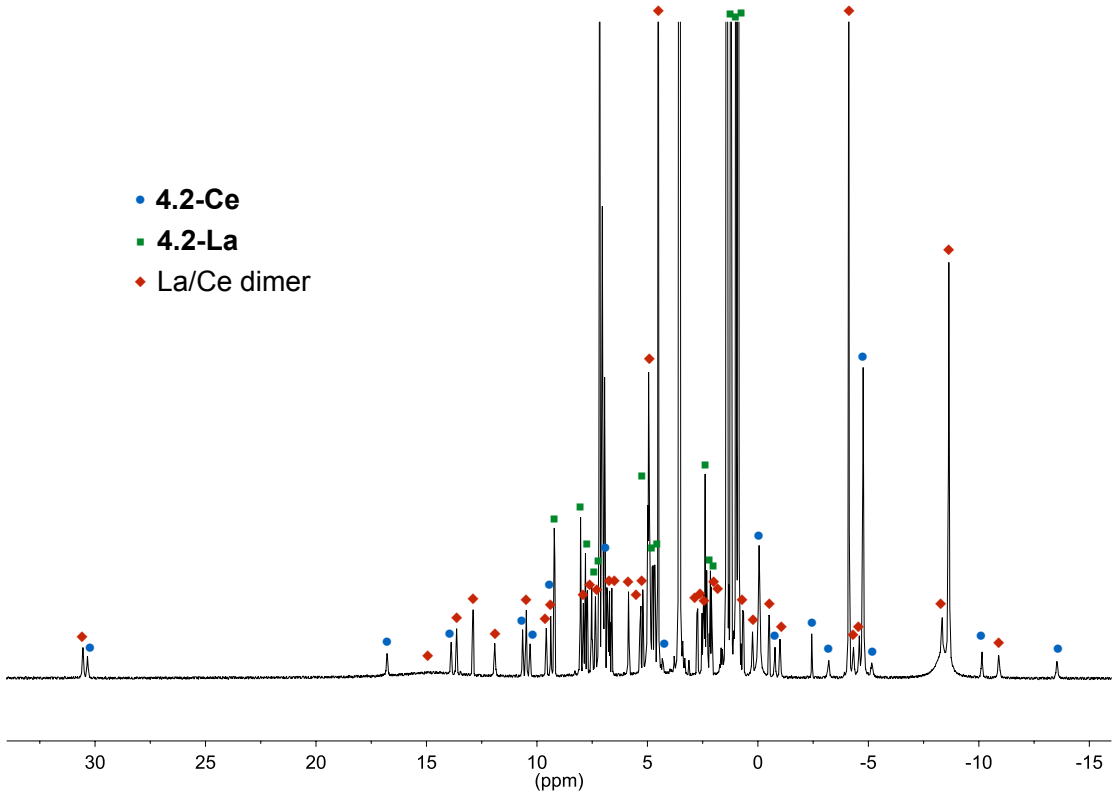

Figure 4.2.6.1. ^{1}H NMR of **4.1-La** + **4.1-Ce** in C_6D_6 showing resonances for **4.2-Ce** (blue circles), **4.2-La** (green squares) and mixed La/Ce dimer (red diamonds).

Table 4.2.6.1. Solid enrichment factors (RE2/RE1). Values in parentheses are from ICP-OES.

RE1	RE2								
	Gd	Tb	Dy	Y	Ho	Er	Tm	Yb	Lu
La	(5.40)	12.2	43.6 (12.2)	30.7	41.8	18.5	29.5	18.7	5.40
Ce	(29.1)	17.7	71.8 (37.6)	17.9	26.7	14.1	142	27.1	17.8
Pr	(10.4)	65.4	46.1 (38.0)	33.1	36.8	24.2	30.1	10.8	10.5
Nd	(37.7)	20.2 (26.2)	12.0 (15.4)	15.8 (19.4)	11.8 (24.7)	13.2 (17.9)	12.0 (18.7)	7.26 (10.1)	2.08 (27.3)
Sm	(1.42)	3.05	2.94	2.79	3.32	2.98	2.98	1.50	1.85
Eu	(1.12)	1.51	1.78	1.55 (1.78)	1.61	1.24	1.23	1.48	0.150

Table 4.2.6.2. Filtrate enrichment factors (RE1/RE2). Values in parentheses are from ICP-OES.

RE1	RE2								
	Gd	Tb	Dy	Y	Ho	Er	Tm	Yb	Lu
La	(1.36)	7.46	4.18 (4.45)	11.1	20.0	9.52	40.5	12.8	16.8
Ce	(2.01)	3.40	6.90 (7.35)	6.85	12.6	18.5	13.7	5.10	29.2
Pr	(1.95)	6.99	7.69 (5.89)	14.7	25.0	9.35	8.62	26.5	58.1
Nd	(1.70)	6.58 (6.84)	25.1 (23.2)	20.2 (23.2)	45.0 (44.2)	92.6 (68.0)	2.45 (2.05)	24.9 (17.2)	19.0 (24.2)
Sm	(1.92)	11.8	18.9	22.1	35.8	15.6	12.3	38.2	57.5
Eu	(2.84)	9.01	21.5	18.3 (22.0)	48.1	17.7	58.8	18.1	70.9

Table 4.2.6.3. Separations factors ($S_{RE1/RE2}$) of the rare earth elements in the $TriNOx^{3-}$ based separations system. Values in parentheses are from ICP-OES.

RE1	RE2								
	Gd	Tb	Dy	Y	Ho	Er	Tm	Yb	Lu
La	(7.32)	91.0	182 (54.4)	341	834	176	1194	239	90.0
Ce	(58.4)	60.2	495 (276)	122	337	260	1942	138	520
Pr	(20.2)	457	355 (224)	485	920	226	259	286	610
Nd	(64.0)	133 (179)	302 (359)	319 (450)	532 (1089)	1222 (1220)	29.4 (38.5)	181 (175)	39.6 (660)
Sm	(2.72)	35.8	55.6	61.6	119	46.4	36.6	57.3	106
Eu	(3.17)	13.6	38.2	28.2 (39.2)	77.4	22.0	72.4	26.9	10.7

In general, the separations factors, $S_{RE2/RE1}$, increased from larger to smaller RE2 ions across each row for a given RE1 ion. Furthermore, down each column for a given RE2 ion, the separations factors decreased from larger to smaller RE1 ions. These trends were expected due to the greater tendency of the larger RE ions to form higher concentrations of dimeric species and be extracted into the benzene solutions. Surprisingly, the trends were not systematic, however, and breaks in the separation factors were observed, in particular for the very late RE2 ions in each row and the very early RE1 ions in each column. These NMR data were corroborated by performing ICP-OES spectroscopy on the Nd/late RE and early RE/Dy separations, which showed good agreement with the ^{1}H NMR results. The discrepancy in the values for $S_{Nd/Lu}$ could be explained by the insolubility of **4.1-Lu** in d_5-pyr, which caused a low measurement for the enrichment factor of the solid fraction. Therefore, the ^{1}H NMR values for the RE1/Lu combinations provide a lower limit for the $S_{RE1/Lu}$ separations factors. Similarly, the discrepancy in the values for $S_{Nd/Ho}$ could be explained by error in the integration of **4.1-Ho** in the solid fraction due to the paramagnetism of the Ho metal center. The enrichment factor of the filtrate fraction in this case, however, was accurately determined by ^{1}H NMR spectroscopy and matched the ICP-OES value.

The results from the separations based on the TriNOx^{3-}-system were compared to the RE-HCl-HDEHP and RE-HNO_3-Cyanex 302 based separations used industrially.[13-14] Unlike with the TriNOx^{3-}-system, the separations factors for both the HDEHP- and the Cyanex 302-systems increased linearly as the difference in ionic radii between the two RE ions increased with no breaks to the trend. On average, the separations factors for the TriNOx^{3-}-system were approximately five times larger than those for the HDEHP-system. In contrast, the separations factors for the TriNOx^{3-}-system were comparable to those of the Cyanex 302-system for RE1 = Pr, Nd, Sm, Eu and RE2 = Tb, Dy, Ho. The separations factors for the TriNOx^3 system, however, deviated precipitously from those of the Cyanex 302 system for RE1 = La, Ce and/or RE2 = Y, Er–Lu. As such, the data showed separations factors for the TriNOx^{3-}-system that were approximately 0.4 times smaller than those for the Cyanex 302-system on average.

We hypothesized that the decreases in separations factors of the very early RE1 ions for a given RE2 ion and the very late RE2 ions for a given RE1 ion were results of increased mixed dimer formation in the former and increased free THF concentrations in solutions of the latter due to dissociation of the weakly bound THF molecules. To test this hypothesis, the strength of the RE–O_{THF} bond was quantified by TGA analysis on **4.1-RE**, RE = La, Sm, Dy, Ho, Er, Tm, and Lu (Figures 4.4.85–4.4.91). In the case of **4.1-La**, two small decreases in weight percent of 3.1% and 8.8% were observed at 50.0 ºC and 118 ºC, respectively, before onset of decomposition was observed as indicated by the large decrease in weight percent at 215 ºC. These small decreases in weight percent were assigned as the loss of interstitial and bound THF, respectively. The TGA of **4.1-Sm** was similar to that of **4.1-La** except there was a much sharper decrease of 6.8% for the bound THF at 130 ºC in the former compared to the broad decrease in the latter. In contrast, only one small decrease in weight percent of 12.6% at 58.3 ºC was observed before complex decomposition in the case of **4.1-Dy**. The TGA of **4.1-Ho**, **4.1-Er** and **4.1-Tm** were similar to that of **4.1-Dy** with decreases of 12.0%, 9.5%, and 15.4% at 52.1 ºC, 48.7 ºC, and 46.2 ºC, respectively. These peaks corresponded to the dissociation of both interstitial and bound THF, processes that were not resolved at unique temperatures. Finally, no decrease in weight percent was observed prior to complex decomposition in the case of **4.1-Lu**. This result indicated that the Lu metal cation was desolvated through simple drying at room temperature under reduced pressure prior to TGA analysis. Taken together, these results indicated that there was a systematic decrease in Ln–O_{THF} bond strength across the series, which supported the hypothesis that secondary equilibria involving the dissociation of bound THF were complicating the separations processes.

The moderate separations factor of 39.2 for the Eu/Y mixtures had potential implications in the recycling of rare earth containing phosphor materials. Furthermore, the high enrichment factor of 22.0 for europium in the filtrate fraction suggested that the small separations factor was a result of limited solubility of **4.1-Eu** in benzene solution but that pure samples of europium could be formed with this method.

4.2.7 Solution Electrochemistry

As a possible secondary perturbation to the separations system, we looked into whether the series of **4.1-RE** complexes showed variable redox chemistries. Indeed, differences in the redox properties of the early and late rare earths were observed in solution electrochemistry experiments. Figure 4.2.7.1 shows the cyclic voltammograms of **4.1-RE**, RE = La–Lu and Y, measured in 0.10 M [^{n}Pr$_4$N][BAr$^F_4$] dichloromethane solutions. The CVs of **4.1-La**, **4.1-Pr**, and **4.1-Nd** exhibited two overlapping quasi-reversible ligand oxidation features with E_{pa} between –0.2 V and –0.5 V versus Fc/Fc$^+$ followed by an irreversible ligand oxidation feature with E_{pa} around 0.3 V versus Fc/Fc$^+$. The two overlapping quasi-reversible oxidation features were assigned as successive oxidations of one half and both halves of the [RE(TriNOx)]$_2$ species present in solutions of these early RE cations. In contrast, the CVs of **4.1-RE**, RE = Eu–Lu, which do not contain dimeric species in dichloromethane solutions, exhibited only one quasi-reversible ligand oxidation feature with E_{pa} ranging from –0.05 V to 0.33 V versus Fc/Fc$^+$. The position of this oxidation gradually shifted towards more positive potentials due to the slight increase in Lewis acidity of the central metal cation across the series. Indeed, the E_{pa} values of **4.1-RE**, RE = Eu–Lu, could be correlated to the radius of the central metal cation (Figure 4.2.7.2). Upon sweeping back to negative potentials, however, two overlapping return reductions were observed, suggesting dimer formation upon ligand oxidation (*vide infra*).

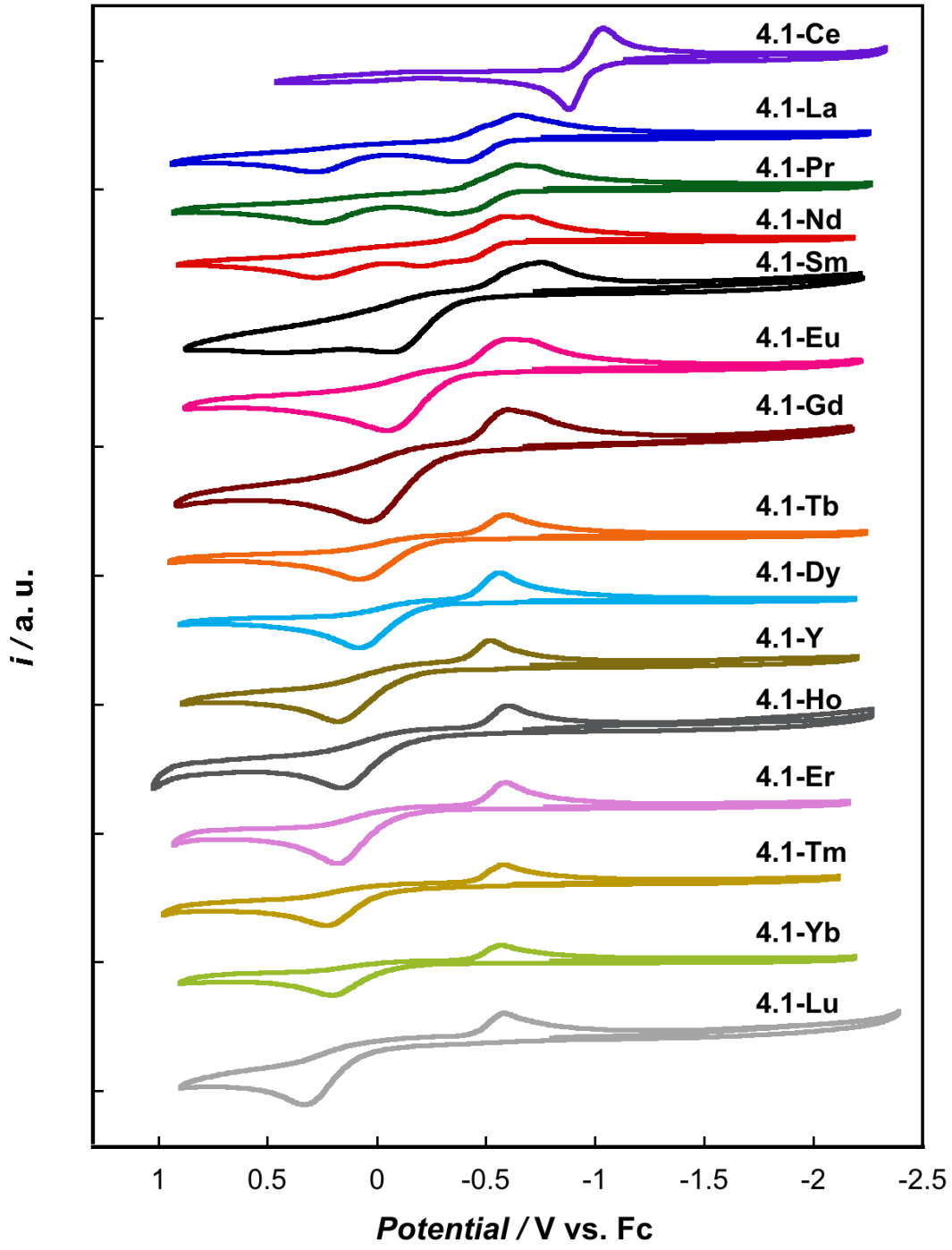

Figure 4.2.7.1. Cyclic voltammograms of **4.1-RE**, RE = La–Lu, complexes in 0.10 M [^{n}Pr$_4$N][BAr$^F{}_4$] solutions in dichloromethane.

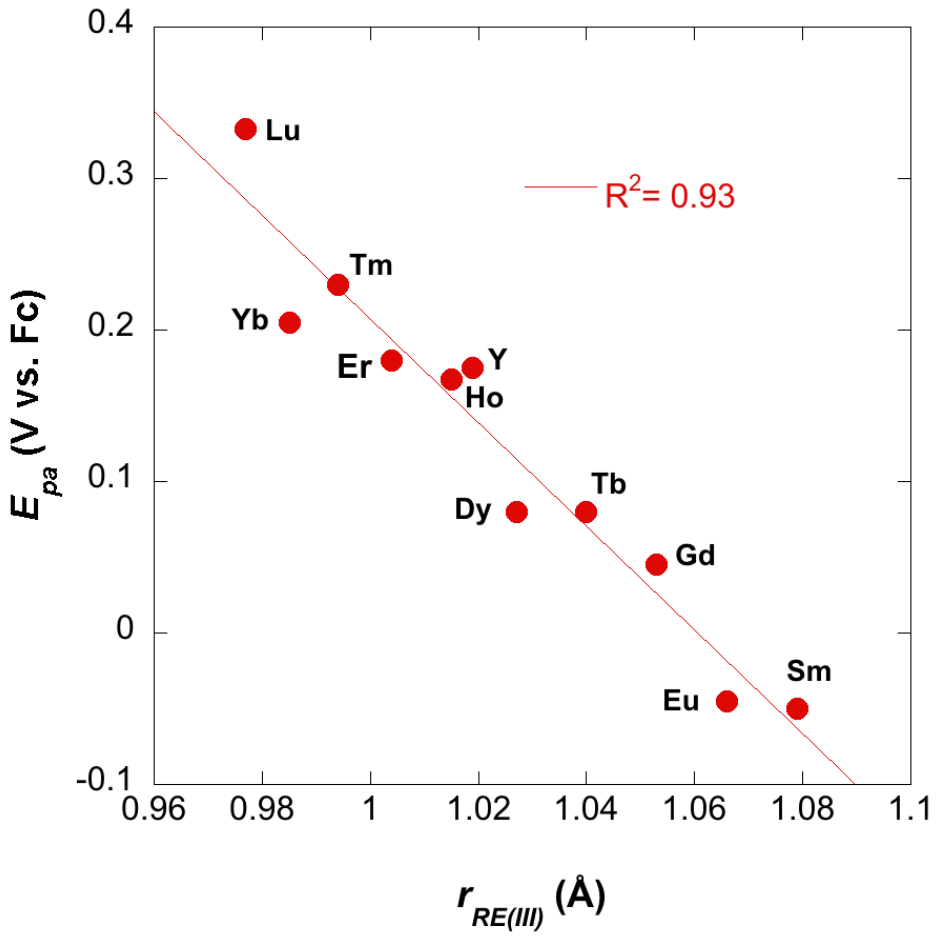

Figure 4.2.7.2. Correlation between the E_{pa} of the first oxidation feature versus ionic radius of the central metal cation for **4.1-RE**, RE = Sm–Lu.

The CV of **4.1-Sm** exhibited features similar to those in the CVs of the early rare earths and others similar to those in the CVs of the late rare earths. The main ligand oxidation feature occurred with an E_{pa} = –0.05 V versus Fc/Fc$^+$. Two overlapping return reductions were observed with E_{pc} = –0.60 V and –0.76 V versus Fc/Fc$^+$. This region of the CV resembled that of the **4.1-RE**, RE = Eu–Lu, species. In fact, the value of E_{pa} for the oxidation of **4.1-Sm** also fit the correlation between E_{pa} and ionic radius. Unlike in the CVs of **4.1-RE**, RE = Eu–Lu, however, a small irreversible oxidation feature was observed in that of **4.1-Sm** with an E_{pa} = 0.46 V versus Fc/Fc$^+$. This feature resembled the irreversible oxidation feature present in the CVs of **4.1-La**, **4.1-Pr**, and **4.1-Nd**.

Despite **4.1-Ce** having a similar solution chemistry as **4.1-La**, **4.1-Pr**, and **4.1-Nd**, the CV of this complex contained a single reversible oxidation feature with $E_{1/2}$ = –0.96 V versus Fc/Fc^+. These differences in the electrochemistry of **4.1-Ce** were consistent with the oxidation of the central cerium cation occurring at a more favorable thermodynamic potential than the nitroxide moieties of the coordinated $TriNOx^{3-}$ ligand.

4.2.8 Redox Chemistry of 4.1-Pr and 4.1-Tb

The presence of two overlapping return reductions in the CVs of **4.1-RE**, RE = Gd–Lu and Y, suggested that chemical oxidation could induce dimer formation in the late RE complexes and be exploited for late RE/late RE separations. This compelled us to perform controlled redox chemistry on **4.1-Tb** in attempts to isolate such a dimeric complex. Based on the E_{pa} value of 0.08 V versus Fc/Fc^+ for the ligand oxidation of **4.1-Tb**, silver(I) salts were chosen as oxidants. Reaction of **4.1-Tb** with AgOTf in DCM led to the deposition of silver metal and the formation of an orange terbium containing product. The ^{1}H NMR spectrum of this compound indicated full conversion to a new terbium containing compound. Furthermore, reaction of **4.1-Tb** with FcOTf led to the formation of the same product, albeit in less than full conversion based on ^{1}H NMR spectroscopy.

Attempts to crystallize this oxidation product failed, however, and only produced microcrystalline solid. To assist in the formation of X-ray quality crystals, the $[OTf]^-$ ion was exchanged for the bigger $[BAr^F{}_4]^-$ ion through the use of $Ag[BAr^F{}_4]$ as oxidant. Again, reaction of **4.1-Tb** with $Ag[BAr^F{}_4]$ led to the deposition of Ag^0 and the formation of a crude orange terbium containing compound. Cooling a saturated DCM solution of this complex to –25 ºC led to the formation of X-ray quality crystals, which confirmed the formation of the dimeric $[Tb(TriNOx)]_2[BAr^F{}_4]_2$ species (**4.3-Tb**). Reacting **4.1-Pr** with $Ag[BAr^F{}_4]$ in a similar fashion led to the formation of the analogous $[Pr(TriNOx)]_2[BAr^F{}_4]_2$ complex (**4.3-Pr**) (Scheme 4.2.8.1).

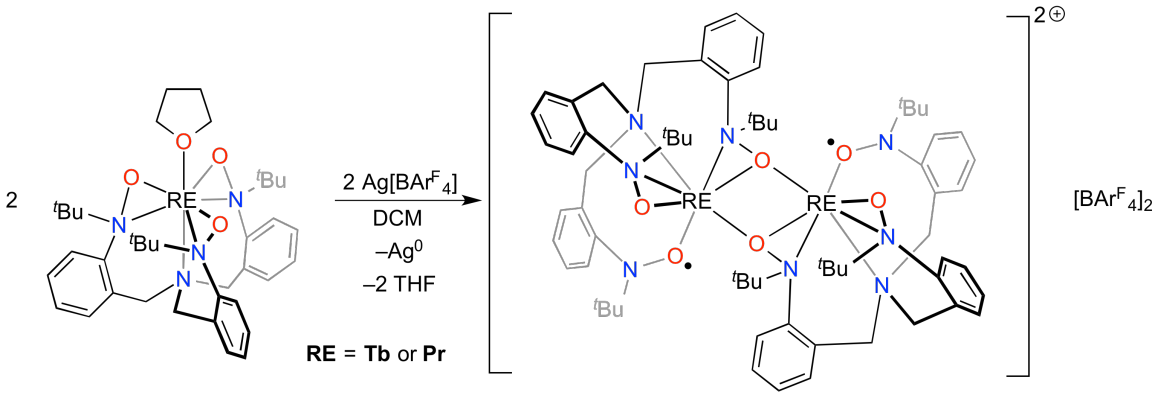

Scheme 4.2.8.1. Schematic of the syntheses of $[Pr(TriNOx)]_2[BAr^F{}_4]_2$ (**4.3-Pr**) and $[Tb(TriNOx)]_2[BAr^F{}_4]_2$ (**4.3-Tb**).

The solid-state structures of **4.3-Pr** and **4.3-Tb** revealed coordination environments with retention of the η^2-(N,O) bonding in two of the three arms of the TriNOx ligand. The third arm of TriNOx, however, switched hapticity from η^2-(N,O) bound to κ^1-O bound as a result of the oxidation (Figure 4.2.8.1). The hapticity change suggested the presence of a localized ligand radical. Indeed, structural metrics indicated that the lengths of the two η^2-(N,O) bound N–O bonds remained essential unchanged between **4.3-RE** and **4.1-RE**, RE = Pr and Tb. The length of the κ^1-O bound nitroxide, however, was significantly reduced from 1.424(3) Å and 1.444(2) Å in **4.1-Pr** and **4.1-Tb**, respectively, to 1.272(6) A in **4.3-Pr** and 1.275(5) Å in **4.3-Tb**. This ~0.15 Å reduction in bond length was consistent with the removal of a π* electron from the nitroxide anion upon oxidation. DFT calculations performed on **4.3-Tb** corroborated the proposed electronic structure of a localized ligand radical bound to a trivalent Tb^{III} cation (Figure 4.2.8.2).

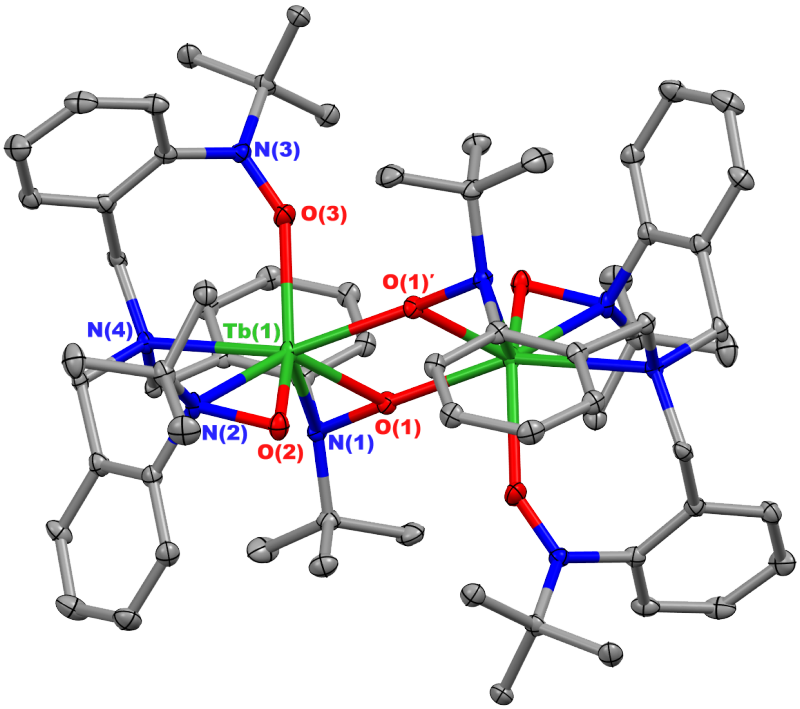

Figure 4.2.8.1. Thermal ellipsoid plot of **4.3-Tb** at 30% probability. Hydrogen atoms and $[BAr^{F}_{4}]^{-}$ counter-ions omitted for clarity.

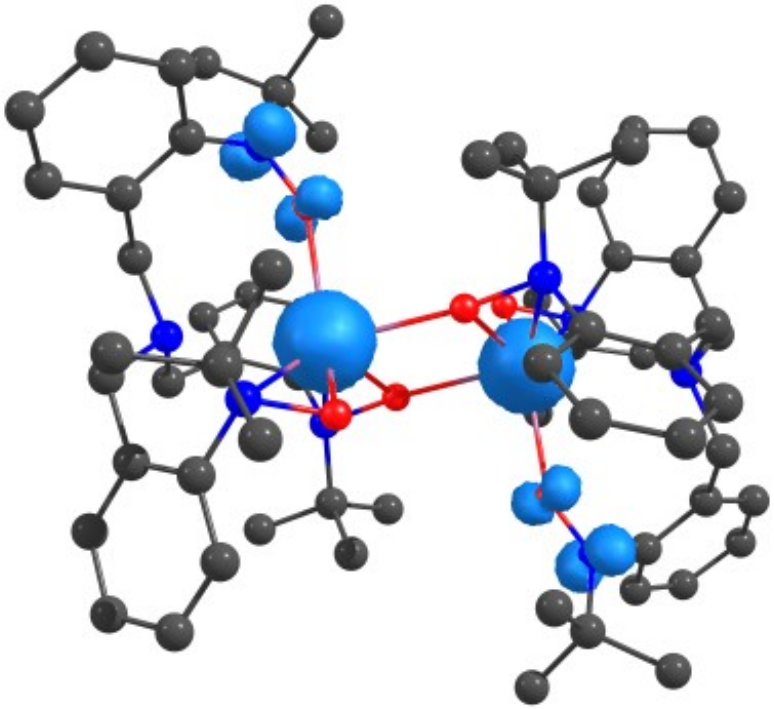

Figure 4.2.8.2. Spin density plot of **4.3-Tb**.

The formation of a dimer in **4.3-Tb** was noteworthy considering the lack of dimer formation in the fully reduced **4.1-Tb** complex. Dimer formation in **4.3-Tb** was attributed to opening up of the structure as a result of the η^2-(N,O) to κ^1-O hapticity change (Figure 4.2.8.3). This reduction in sterics shifted the thermodynamics of the self-association equilibrium from heavily favoring monomer in **4.1-Tb** towards favoring dimer in **4.3-Tb**.

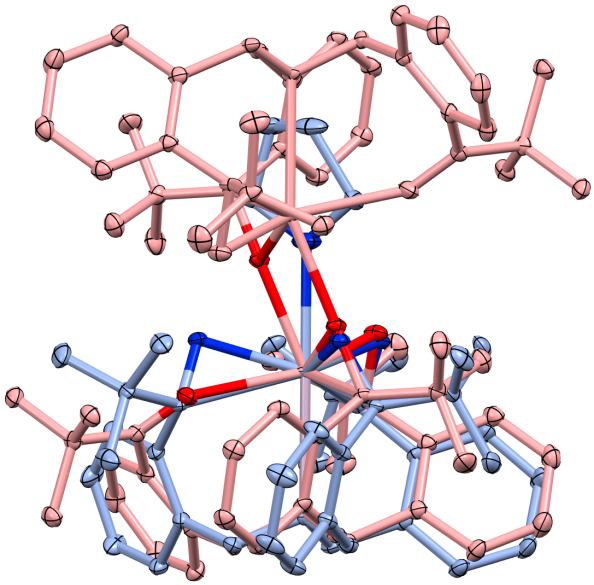

Figure 4.2.8.3. Overlay of the thermal ellipsoid plots of **4.1-Tb** and **4.3-Tb** highlighting the hapticity change of the N–O bond from η^2-(N,O) to κ^1-O.

4.3 Conclusions

Our results suggest that the use of coordination chemistry toward the realization of size-sensitive molecular apertures of *N,O* ligands could contribute to new methods for rare earth element separations. Such methods are advantageous for targeted separations because they are expected to eliminate the capital cost associated with mixer-settlers used in liquid-liquid extraction, making recycling of these critical materials more economically feasible. We showed proof of concept that differences in self-association equilibria between Nd and Dy could be exploited for separation of these ions.

This method was extended to other early/late RE combinations, with particular focus on Eu and Y which are critical components of phosphor materials in fluorescent light bulbs. In general, the separations factors increased as the difference in ionic radii of the pair of RE ions increased. In the extreme cases with the very large early RE ions and the very small late RE ions, decreases in the separations factors were observed, however. We attributed these observations to increased amounts of mixed dimer formation with the early RE ions and increased amounts of dissociated THF in solutions of the late RE ions.

We are currently examining methods to improve upon this separations technique using smaller volumes of more benign solvents and modified TriNOx^{3-}-type ligand systems. Lastly, the systematic increase in ligand oxidation potential observed for the **4.1-RE**, RE = Eu–Lu, complexes and the isolation of the dimeric **4.3-Tb** complex suggest the possibility of redox based late/late RE separations through selective oxidation. These studies are also ongoing.

4.4 Experimental Section

General Methods Unless otherwise noted, all reactions and manipulations were performed under an inert atmosphere (N_2) using standard Schlenk techniques or in a drybox equipped with a molecular sieves 13X / Q5 Cu–0226S catalyst purifier system. Glassware was oven-dried for at least 3 h at 150 °C prior to use. ^{1}H and ^{19}F{^{1}H} NMR spectra were obtained on a Bruker DMX-300 Fourier transform NMR spectrometer at 300 MHz and 282.2 MHz, respectively. ^{13}C(^{1}H} NMR spectra were obtained on a Bruker DRX-500 Fourier transform NMR spectrometer or a Bruker AVIII 500 Fourier transform NMR spectrometer equipped with a cryogenic probe at 125.7 MHz. Chemical shifts were recorded in units of parts per million downfield from residual proteo solvent for ^{1}H–NMR, characteristic solvent peaks for ^{13}C–NMR, or relative to an external $CFCl_3$ reference (0 ppm). Elemental analyses were preformed either at the University of California, Berkeley, Microanalytical Facility using a Perkin-Elmer Series II 2400 CHNS analyzer or at Complete Analysis Laboratories, Inc. using a Carlo Erba EA 1108 analyzer. Inductively Coupled Plasma Optical Emission spectroscopy (ICP-OES) measurements were performed at Galbraith Laboratories, Inc. using a Perkin-Elmer ICP-OES Optima 5300.

Materials. Tetrahydrofuran, dimethoxyethane, diethyl ether, dichloromethane, toluene, hexanes, and pentane were purchased from Fisher Scientific. All solvents were sparged for 20 min with dry N_2 and dried using a commercial two-column solvent purification system comprising columns packed with Q5 reactant and neutral alumina respectively (for hexanes and pentane), or two columns of neutral alumina (for THF, Et_2O, and CH_2Cl_2). Deuterated solvents were purchased from Cambridge Isotope Laboratories, Inc. and stored over 4A molecular sieves prior to use. Potassium bis(trimethylsilyl)amide and silver triflate were used as received. $RE(OTf)_3$ were dried at 150 ºC for 24 h. prior to use. Tris-2-bromobenzylamine, $Ag[BAr^F{}_4]$, Fc[OTf], $RE[N(SiMe_3)_2]_3$, and $[^nPr_4N][B(3,5\text{-}(CF_3)_2\text{-}C_6H_3)_4]$ were synthesized according to literature procedures.

Synthetic Details and Characterization

Synthesis of tris(2-tert-butylhydroxylaminato)benzylamine ($((2\text{-}^tBuNOH)C_6H_4CH_2)_3N$, $H_3TriNOx$). Solid tris-2-bromobenzylamine (3.0 g, 5.76 mmol, 1 equiv) was dissolved in THF (10 mL) and added to a 50 mL Schlenk flask equipped with a magnetic stir bar. The flask was placed under an N_2 atmosphere and cooled to –78 ºC. A 1.6 M solution of *n*-butyllithium complex in hexanes (11.8 mL, 19.0 mmol, 3.3 equiv) was added dropwise and the reaction stirred for 3 h. A THF solution of 2-methyl-2-nitrosopropane dimer (1.99 g, 11.4 mmol, 2 equiv) was then added and the reaction was gradually warmed to room temperature overnight. The reaction was then quenched with a saturated aqueous ammonium chloride solution. The layers were separated and the aqueous layer was extracted by 3 × 50 mL dichloromethane. The extracts were collected and dried over magnesium sulfate. The drying agent was removed by filtration and volatiles were removed under reduced pressure, yielding crude $H_3TriNOx$. The crude mixture was purified by recrystallization from a boiling mixture of 90% petroleum ether and 10% dichloromethane, yielding pure $H_3TriNOx$ (2.46 g, 78%). Mp = 140.0 – 140.7 ºC. ^1H NMR (500 MHz, $CDCl_3$): δ = 8.00 (s, 3H), 7.51 (dd, J = 8.0, 0.6 Hz, 3H), 7.31 (dd, J = 7.5, 1.6 Hz, 3H), 7.25 (ddd, J = 8.0, 7.7, 1.6 Hz, 3H), 7.12 (ddd, J = 7.7, 7.5, 0.6 Hz, 3H), 3.71 (s, 6H), 0.90 (s, 27H). ^{13}C NMR (125.8 MHz, $CDCl_3$): δ = 149.6, 135.3, 132.1, 127.8, 126.8, 125.5, 59.3, 56.2, 26.5. IR: v = 3371, 3067,

2975, 2933, 2875, 2806, 1917, 1812, 1734, 1596, 1580, 1484, 1449, 1385, 1363, 1355, 1250, 1216, 1189, 1075, 1045, 986, 942, 884, 825, 736, 704, 677, 629, 590, 568, 548, 517, 490, 434 cm^{-1}. HRMS: (ESI) m/z calc. for $C_{33}H_{49}N_4O_3$ (M+H) 549.3805, found 549.3805

Synthesis of La(TriNOx)THF (**4.1-La**). To a THF solution of H_3TriNOx (0.27 g, 0.49 mmol, 1 equiv) was layered a hexanes solution of $La[N(SiMe_3)_2]_3$ (0.30 g, 0.49 mmol, 1 equiv). The reaction was allowed to sit, unperturbed, at room temperature for 48 h. The resulting crystals of **4.1-La** were collected, washed with THF, and dried under reduced pressure. Yield: 0.35 g (95%). Anal. Calc. for $C_{37}H_{53}N_4O_4La$: C, 58.72; H, 7.06; N, 7.40. Found: C, 58.66; H, 7.15; N, 7.35. ^{1}H NMR (500 MHz, d_5-pyr): δ = 8.10 (d, J = 7.8 Hz, 3H), 7.45 (dd, J = 7.8, 7.4 Hz, 3H), 7.41 (d, J = 7.3 Hz, 3H), 7.27 (dd, J = 7.4, 7.3 Hz, 3H), 4.81 (d, J = 11.8 Hz, 3H), 3.67 (m, 4H), 2.81 (d, J = 11.8 Hz, 3H), 1.63 (m, 4H) 0.99 (s, 27H). ^{13}C NMR (125.8 MHz, d_5-pyr): δ = 152.7, 133.3, 132.9, 131.6, 129.4, 126.0, 68.3, 61.6, 60.9, 26.8, 26.3.

Synthesis of Ce(TriNOx)THF (**4.1-Ce**). To a THF solution of H_3TriNOx (0.26 g, 0.47 mmol, 1 equiv) was layered a hexanes solution of $Ce[N(SiMe_3)_2]_3$ (0.30 g, 0.47 mmol, 1 equiv). The reaction was allowed to sit, unperturbed, at room temperature for 48 h. The resulting red-orange crystals of **4.1-Ce** were collected, washed with THF, and dried under reduced pressure. Yield: 0.30 g (84%). Anal. Calcd. for $C_{37}H_{53}N_4O_4Ce$: C, 58.63; H, 7.05; N, 7.39. Found: C, 58.88; H, 7.05; N, 7.56. ^{1}H NMR (500 MHz, d_5-pyr): δ 13.04 (d, J = 6.5 Hz, 3H) 8.39 (dd, J = 6.7, 6.5 Hz, 3H), 7.15 (dd, J = 7.2, 6.7 Hz, 3H), 4.58 (d, J = 7.2 Hz, 3H), 3.66 (m, 4H), 2.95 (s, 27H), –3.28 (s, 3H), –3.58 (s, 3H).

Synthesis of Pr(TriNOx)THF (**4.1-Pr**). To a THF solution of H_3TriNOx (0.13 g, 0.24 mmol, 1 equiv) was layered a hexanes solution of $Pr[N(SiMe_3)_2]_3$ (0.15 g, 0.24 mmol, 1 equiv). The reaction was allowed to sit, unperturbed, at room temperature for 48 h. The resulting crystals of **4.1-Pr** were collected, washed with THF, and dried under reduced pressure. Yield: 0.15 g (83%). Anal. Calcd. for $C_{37}H_{53}N_4O_4Pr$•THF: C, 59.27.63; H, 7.40; N, 6.74. Found: C, 59.25; H, 7.6; N, 6.83. ^{1}H NMR (300 MHz, d_5-pyr): δ = 25.67 (d, J = 7.9 Hz, 3H), 12.10–11.40 (overlap, 30H), 6.59

(at., J = 7.4 Hz, 3H), 3.72 (m, 4H), 1.68 (m, 4H), –2.55 (d, J = 7.4 Hz, 3H), –20.28 (d, J = 9.9 Hz, 3H), –26.28 (d, J = 9.9 Hz, 3H).

Synthesis of Nd(TriNOx)THF (**4.1-Nd**). To a THF solution of H_3TriNOx (0.26 g, 0.48 mmol, 1 equiv) was layered a hexanes solution of $Nd[N(SiMe_3)_2]_3$ (0.30 g, 0.48 mmol, 1 equiv). The reaction was allowed to sit, unperturbed, at room temperature for 48 h. The resulting crystals of **4.1-Nd** were collected, washed with THF, and dried under reduced pressure. Yield: 0.35 g (95%). Anal. Calc. for $C_{37}H_{53}N_4O_4Nd$: C, 58.31; H, 7.01; N, 7.35. Found: C, 58.28; H, 6.95; N, 7.20. ^{1}H NMR (300 MHz, d_5-pyr): δ = 17.86 (d, J = 6.5 Hz, 3H), 9.80 (dd, J = 6.9, 6.5 Hz, 3H), 6.99 (dd, J = 7.0, 6.9 Hz, 3H), 6.51 (s, 27H), 3.68 (m, 4H) 2.02 (d, J = 7.0 Hz, 3H), 1.65 (m, 4H), –7.71 (s, 3H), –11.74 (s, 3H).

Synthesis of Sm(TriNOx)THF (**4.1-Sm**). To a THF suspension of $Sm(OTf)_3$ (0.50 g, 0.84 mmol, 1 equiv) was added a THF solution of H_3TriNOx (0.46 g, 0.84 mmol, 1 equiv). Solid $K[N(SiMe_3)_2]$ (0.50 g, 2.51 mmol, 3 equiv) was added to the suspension and a crude white powder precipitated. The crude powder was collected on a medium porosity fritted filter, washed with THF, and recrystallized from layering THF onto a saturated DCM solution. Crystalline yield: 0.22 g (35%). Anal. Calcd. for $C_{37}H_{53}N_4O_4Sm$: C, 57.85; H, 6.95; N, 7.29. Found: C, 58.01; H, 7.19; N, 6.96. ^{1}H NMR (300 MHz, d_5-pyr): δ = 9.28 (d, J = 7.7 Hz, 3H), 7.63 (dd, J = 7.7, 7.3 Hz, 3H), 7.15 (dd, J = 7.3, 7.1 Hz, 3H), 6.77 (d, J = 7.1 Hz, 3H), 3.67 (m, 4H), 2.69 (d, J = 11.7 Hz, 3H), 1.63 (m, 4H), 1.59 (s, 27H), 0.51 (d, J = 11.7 Hz, 3H).

Synthesis of Eu(TriNOx)THF (**4.1-Eu**). To a THF solution H_3TriNOx (0.087 g, 0.16 mmol, 1 equiv) was layered a hexanes solution of $Eu[N(SiMe_3)_2]_3$ (0.10 g, 0.16 mmol, 1 equiv). The reaction was allowed to sit, unperturbed, at room temperature for 48 h. The resulting crystals of **4.1-Eu** were collected, washed with THF, and dried under reduced pressure. Yield: 0.083 g (68%). Anal. Calcd. for $C_{37}H_{53}N_4O_4Eu$: C, 57.73; H, 6.94; N, 7.28. Found: C, 57.58; H, 7.13; N, 7.09. ^{1}H NMR (300 MHz, d_5-pyr): δ = 30.01 (br s, 3H), 15.83 (br s, 3H), 15.36 (d, J = 6.4 Hz, 3H), 7.49 (br m, 3H), 3.66 (br m, 4H), 3.12 (br m, 3H), 1.62 (br m, 4H), –6.06 (d, J = 5.6 Hz, 3H), –8.60 (s, 27H).

Synthesis of Gd(TriNOx)THF (**4.1-Gd**). To a THF suspension of $Gd(OTf)_3$ (0.10 g, 0.17 mmol, 1 equiv) was added a THF solution of H_3TriNOx (0.091 g, 0.17 mmol, 1 equiv). Solid $K[N(SiMe_3)_2]$ (0.099 g, 0.50 mmol, 3 equiv) was added to the suspension and a crude white powder precipitated. The crude powder was collected on a medium porosity fritted filter, washed with THF, and recrystallized from layering THF onto a saturated DCM solution. Crystalline yield: 0.058 g (45%). Anal. Calcd. for $C_{37}H_{53}N_4O_4Gd$: C, 57.34; H, 6.89; N, 7.23. Found: C, 57.27; H, 6.77; N, 7.02.

Synthesis of Tb(TriNOx)THF (**4.1-Tb**). To a THF suspension of $Tb(OTf)_3$ (0.20 g, 0.33 mmol, 1 equiv) was added a THF solution of H_3TriNOx (0.18 g, 0.33 mmol, 1 equiv). Solid $K[N(SiMe_3)_2]$ (0.20 g, 1.00 mmol, 3 equiv) was added to the suspension and a crude white powder precipitated. The crude powder was collected on a medium porosity fritted filter, washed with THF, extracted with DCM, and dried under reduced pressure. Yield: 0.11 g (43%). Anal. Calcd. for $C_{37}H_{53}N_4O_4Tb$: C, 57.21; H, 6.88; N, 7.21. Found: C, 57.26; H, 6.84; N, 7.07. ^{1}H NMR (300 MHz, d_5-pyr): δ = 129.81 (br s, 3H), 72.0 (br s, 27H), 41.85 (br s, 3H), 2.40 (br s, 3H), 0.56 (br s, 4H), –0.13 (br s, 4H), –62.05 (br s, 3H), –220.05 (br s, 3H), –221.66 (br s, 3H).

Synthesis of Dy(TriNOx)THF (**4.1-Dy**).To a THF solution H_3TriNOx (0.088 g, 0.16 mmol, 1 equiv) was layered a hexanes solution of $Dy[N(SiMe_3)_2]_3$ (0.10 g, 0.16 mmol, 1 equiv). The reaction was allowed to sit, unperturbed, at room temperature for 48 h. The resulting crystals of **4.1-Dy** were collected, washed with THF, and dried under reduced pressure. Yield: 0.11 g (89%). Anal. Calcd. for $C_{37}H_{53}N_4O_4Dy$: C, 56.95; H, 6.85; N, 7.18. Found: C, 56.86; H, 6.94; N, 7.10. ^{1}H NMR (300 MHz, d_5-pyr): δ = 208.64 (s, 3H), 129.70 (s, 27H), 57.81 (s, 3H), –3.69 (s, 3H), –101.55 (s, 3H), –298.61 (s, 3H), –350.91 (s, 3H).

Synthesis of Y(TriNOx)THF (**4.1-Y**).To a THF solution H_3TriNOx (0.096 g, 0.18 mmol, 1 equiv) was layered a hexanes solution of $Y[N(SiMe_3)_2]_3$ (0.10 g, 0.18 mmol, 1 equiv). The reaction was allowed to sit, unperturbed, at room temperature for 48 h. The resulting crystals of **4.1-Y** were collected, washed with THF, and dried under reduced pressure. Yield: 0.094 g (76%). Anal. Calcd. for $C_{33}H_{45}N_4O_3Y$ (M–THF): C, 62.45; H, 7.15; N, 8.83. Found: C, 62.05; H, 7.05; N, 8.81.

^{1}H NMR (500 MHz, d_5-pyr): δ = 8.10 (d, J = 7.8 Hz, 3H), 7.44 (dd, J = 7.8, 7.4 Hz, 3H), 7.36 (d, J = 7.3 Hz, 3H), 7.26 (dd, J = 7.4, 7.3 Hz, 3H), 4.66 (d, J = 11.7 Hz, 3H), 2.69 (d, J = 11.7 Hz, 3H), 1.00 (s, 27H). ^{13}C NMR (125.8 MHz, d_5-pyr): δ = 152.54, 133.13, 132.54, 130.89, 128.86, 126.03, 62.09, 62.04, 26.90.

Synthesis of Ho(TriNOx)THF (**4.1-Ho**). To a THF suspension of $Ho(OTf)_3$ (0.10 g, 0.16 mmol, 1 equiv) was added a THF solution of H_3TriNOx (0.090 g, 0.16 mmol, 1 equiv). Solid $K[N(SiMe_3)_2]$ (0.098 g, 0.49 mmol, 3 equiv) was added to the suspension and a crude white powder precipitated. The crude powder was collected on a medium porosity fritted filter, washed with THF, and dried under reduced pressure. Yield: 0.098 g (77%). Anal. Calcd. for $C_{37}H_{53}N_4O_4Ho$: C, 56.77; H, 6.82; N, 7.16. Found: C, 56.70; H, 6.67; N, 7.01. ^{1}H NMR (300 MHz, d_5-pyr): δ = 107.77 (br s, 3H), 66.49 (br s, 27H), 33.5 (br s, 3H), 3.93 (br m, 4H), 2.13 (br s, 3H), 1.91 (br m, 4H), –45.71 (br s, 3H), –149.73 (br s, 3H).

Synthesis of Er(TriNOx)THF (**4.1-Er**). To a THF solution H_3TriNOx (0.085 g, 0.15 mmol, 1 equiv) was layered a hexanes solution of $Er[N(SiMe_3)_2]_3$ (0.10 g, 0.15 mmol, 1 equiv). The reaction was allowed to sit, unperturbed, at room temperature for 48 h. The resulting crystals of **4.1-Er** were collected, washed with THF, and dried under reduced pressure. Yield: 0.075 g (62%). Anal. Calcd. for $C_{37}H_{53}N_4O_4Er$: C, 56.60; H, 6.80; N, 7.14. Found: C, 56.49; H, 6.84; N, 7.24. ^{1}H NMR (300 MHz, d_5-pyr): δ = 92.44 (br s, 3H), 69.15 (br s, 3H), 34.82 (br s, 3H), –4.71 (br s, 3H), –31.51 (br s, 27H), –43.23 (br s, 3H).

Synthesis of Tm(TriNOx)THF (**4.1-Tm**). To a THF suspension of $Tm(OTf)_3$ (0.10 g, 0.16 mmol, 1 equiv) was added a THF solution of H_3TriNOx (0.089 g, 0.16 mmol, 1 equiv). Solid $K[N(SiMe_3)_2]$ (0.097 g, 0.49 mmol, 3 equiv) was added to the suspension and a crude white powder precipitated. The crude powder was collected on a medium porosity fritted filter and washed with THF. Yield: 0.086 g (67%). Anal. Calcd. for $C_{37}H_{53}N_4O_4Tm$: C, 56.48; H, 6.79; N, 7.12. Found: C, 56.35; H, 6.56; N, 7.24. ^{1}H NMR (300 MHz, d_5-pyr): δ = 159.36 (br s, 3H), 125.23 (br s, 3H), 54.35 (br s, 3H) 10.41 (br s, 3H), –14.48 (br s, 3H), –54.58 (br s, 27H) –82.15 (br s, 3H).

Synthesis of Yb(TriNOx)THF (**4.1-Yb**). To a THF solution H_3TriNOx (0.084 g, 0.15 mmol, 1 equiv) was layered a hexanes solution of $Yb[N(SiMe_3)_2]_3$ (0.10 g, 0.15 mmol, 1 equiv). The reaction was allowed to sit, unperturbed, at room temperature for 48 h. The resulting crystals of **4.1-Yb** were collected, washed with THF, and dried under reduced pressure. Yield: 0.068 g (56%). Anal. Calcd. for $C_{37}H_{53}N_4O_4Yb$: C, 56.19; H, 6.75; N, 7.08. Found: C, 55.98; H, 6.56; N, 7.26. ^{1}H NMR (300 MHz, *d*$_5$-pyr): δ = 85.11 (br s, 3H), 67.28 (br s, 3H), 31.89 (br s, 3H), 8.89 (br s, 3H) –3.86 (br s, 3H), –32.31 (br s, 27H), –39.05 (br s, 3H).

Synthesis of Lu(TriNOx)THF (**4.1-Lu**). To a THF solution H_3TriNOx (0.084 g, 0.15 mmol, 1 equiv) was layered a hexanes solution of $Lu[N(SiMe_3)_2]_3$ (0.10 g, 0.15 mmol, 1 equiv). The reaction was allowed to sit, unperturbed, at room temperature for 48 h. The resulting crystals of **4.1-Lu** were collected, washed with THF, and dried under reduced pressure. Yield: 0.063 g (52%). Anal. Calcd. for $C_{37}H_{53}N_4O_4Lu$: C, 58.63; H, 7.05; N, 7.39. Found: C, 55.96; H, 6.45; N, 7.21. ^{1}H NMR (300 MHz, *d*$_5$-pyr): δ = 8.06 (d, J = 7.8 Hz, 3H), 7.40 (ddd, J = 7.8, 7.8, 1.7 Hz, 3H), 7.32 (dd, J = 7.5, 1.7 Hz, 3H), 7.24 (dd, J = 7.8, 7.5 Hz, 3H), 4.60 (d, J = 11.7 Hz, 3H), 2.68 (d, J = 11.7 Hz, 3H), 0.98 (s, 27H). ^{13}C{^{1}H} NMR (500 MHz, *d*$_5$-pyr): δ = 152.4, 133.2, 132.4, 130.8, 128.8, 126.1, 62.2, 62.0, 27.0.

Synthesis of [La(TriNOx)]$_2$ (**4.2-La**). Isolated **4.1-La** (0.046 g, 0.061 mmol, 1 equiv) was dissolved in toluene and solvent was removed under reduced pressure. Yield: 0.041 g (87%). Anal. Calc. for $C_{66}H_{90}N_8O_6La_2$•2tol: C, 61.85; H, 6.88; N, 7.21. Found: C, 61.94; H, 7.38; N, 7.33. ^{1}H NMR (500 MHz, C_6D_6): δ = 9.21 (d, J = 8.0 Hz, 2H), 8.02 (d, J = 7.6 Hz, 2H), 7.82 (d, J = 8.0 Hz, 2H), 7.52 (ddd, J = 8.3, 6.8, 1.6 Hz, 2H), 7.20 (ddd, J = 8.4, 7.1, 1.4 Hz, 2H), 7.15 – 6.89 (overlapping, 14H), 4.97 (d, J = 11.6 Hz, 2H), 4.77 (d, J = 11.9 Hz, 2H), 4.68 (d, J = 11.8 Hz, 2H), 2.40 (d, J = 11.6 Hz, 2H), 2.36 (d, J = 11.8 Hz, 2H), 2.29 (d, J = 11.9 Hz, 2H), 1.22 (s, 18H), 0.99 (s, 18H), 0.89 (s, 18H). ^{13}C NMR (125.8 MHz, C_6D_6): δ = 152.63, 152.45, 151.46, 133.60, 132.48, 132.33, 132.27, 132.24, 132.00, 131.97, 131.82, 129.66, 129.60, 128.97, 128.91, 125.66, 125.42, 124.99, 62.43, 61.64, 61.59, 61.23, 59.75, 27.74, 26.83, 26.58.

Synthesis of [Ce(TriNOx)]$_2$ (4.2-Ce). Isolated **4.1-Ce** (0.088 g, 0.12 mmol, 1 equiv) was dissolved in toluene and solvent was removed under reduced pressure. Yield: 0.083 g (92%). Anal. Calcd. for $C_{66}H_{90}N_8O_6Ce_2$•Et_2O: C, 58.15; H, 6.97; N, 7.75. Found: C, 58.13; H, 6.89; N, 7.77. ^{1}H NMR (500 MHz, C_6D_6): δ 30.31 (as., 2H), 16.76 (as., 2H), 13.87 (as., 2H), 10.65 (at., J = 7.2 Hz, 2H), 10.29 (as., 2H), 9.22 (d, J = 7.2 Hz, 2H), 6.76 (at., J = 7.2 Hz, 2H), 4.71 (br s, 18H), 2.06 (s, 2H), 1.38 (d, J = 5.5 Hz, 2H), 1.18 (s, 2H), 1.03 (s, 2H), 0.94 (at, J = 6.8 Hz, 2H), –0.08 (s, 18H), –0.79 (s, 2H), –2.46 (d, J = 7.2 Hz, 2H), –3.21 (as., 2H), –4.79 (s, 18H), –5.18 (s, 2H), –10.15 (as., 2H), –13.56 (as., 2H).

Synthesis of [Pr(TriNOx)]$_2$ (**4.2-Pr**). Isolated **4.1-Pr** (0.11 g, 0.15 mmol, 1 equiv) was dissolved in toluene and solvent was removed under reduced pressure. X-ray quality crystals of **4.2-Pr** were formed from slow evaporation of a saturated Et_2O solution. Yield: 0.11 g (97%). Anal. Calcd. for $C_{66}H_{90}N_8O_6Pr_2$•2tol: C, 61.69; H, 6.86; N, 7.19. Found: C, 61.92; H, 7.16; N, 7.46. ^{1}H NMR (300 MHz, C_6D_6): δ = 71.79 (s, 2H), 23.27 (br m, 2H), 21.40 (br s, 18H), 14.98 (d, J = 4.5 Hz, 2H), 11.50 (br s, 2H), 11.07 (br m, 2H), 10.15 (at., J = 6.9 Hz, 2H), 5.07 (at., J = 7.5 Hz, 2H), 2.52 (d, J = 8.1 Hz, 2H), –1.50—2.80 (overlap, 20H), –4.95 (br s, 18H), –5.34 (at., J = 7.2 Hz, 2H), 7.50 (d, J = 7.5 Hz, 2H), –17.71 (d, J = 6.9 Hz, 2H), –23.57 (br s, 2H), –27.50 (br s, 2H), –29.93 (d, J = 5.7 Hz, 2H), –32.10 (br s, 2H), –45.70 (br s, 2H), –46.60 (br m, 2H).

Synthesis of [Nd(TriNOx)]$_2$ (**4.2-Nd**). Isolated **4.1-Nd** (0.038 g, 0.050 mmol, 1 equiv) was dissolved in toluene and solvent was removed under reduced pressure. Yield: 0.040 g (quantitative). Anal. Calc. for $C_{66}H_{90}N_8O_6Nd_2$•2tol: C, 61.43; H, 6.83; N, 7.16. Found: C, 60.95; H, 7.04; N, 7.30. ^{1}H NMR (300 MHz, C_6D_6): δ = 38.04 (s, 2H), 15.58 (d, J = 3.6 Hz, 2H), 14.34 (d, J = 6.3 Hz, 2H), 12.45 (s, 2H), 9.94 (d, J = 3.6 Hz, 2H), 8.58 (s, 18H), 7.58 (dd, J = 6.5, 6.3 Hz, 2H), 7.15-6.95 (overlapping, 2H), 6.01 (dd, J = 7.2, 7.0 Hz, 2H), 2.19 (s, 18H), 1.97 (dd, J = 6.5, 6.3 Hz, 2H), 0.63 (d, J = 6.5 Hz, 2H), 0.52 (s, 18H), –1.14 (d, J = 7.0 Hz, 2H), –5.62 (d, J = 7.2 Hz, 2H), –12.64 (s, 2H), –13.16 (s, 2H), –13.85 (s, 2H), –15.71 (s, 2H), –21.91 (s, 2H), –24.03 (s, 2H).

Synthesis of [Sm(TriNOx)]$_2$ (**4.2-Sm**). Isolated **4.1-Sm** (0.059 g, 0.077 mmol, 1 equiv) was dissolved in toluene and the volatiles were removed under reduced pressure. X-ray quality crystals of **4.2-Sm** were grown from layering hexanes onto a saturated THF solution. Yield: 0.065 g (quantitative). Anal. Calcd. for $C_{66}H_{90}N_8O_6Sm_2$•2.2tol: C, 61.30; H, 6.80; N, 7.03. Found: C, 61.73; H, 7.12; N, 7.44. ^{1}H NMR (300 MHz, C_6D_6): δ = 11.93 (br s, 2H), 10.03 (br s, 2H), 8.35 (br s, 2H), 7.80–7.50 (overlap, 4H), 7.40–7.20 (overlap, 4H), 6.90–6.50 (overlap, 4H), 6.20–5.55 (overlap, 4H), 4.98 (br s, 2H), 3.31 (br s, 2H), 3.17 (br s, 2H), 1.58 (s, 18H), 1.00 (br s, 18H), 0.77–0.30 (overlap, 20H), 0.15—0.40 (overlap, 4H), –1.31 (br s, 2H).

Synthesis of [Pr(TriNOx)]$_2$[BAr$^F{}_4$]$_2$ (**4.3-Pr**). To a DCM solution of **4.1-Pr** (0.020 g, 0.026 mmol, 1 equiv) was added Ag[BAr$^F{}_4$] (0.026 g, 0.026 mmol, 1 equiv) and the reaction was stirred in the dark for 4 h. The solution was filtered through celite and volatiles were removed under reduced pressure. X-ray quality crystals were formed by cooling a saturated DCM solution to –25 ºC. ^{1}H NMR (300 MHz, CD_2Cl_2): δ = 85.63 (br s, 2H), 62.54 (br s, 2H), 48.20 (br s, 2H), 47.70 (br s, 2H), 44.96 (br s, 2H), 34.57 (br s, 2H), 25.95 (br s, 18H), 19.99 (br s, 2H), 19.05 (br s, 2H), 14.98 (br s, 2H), 7.45 (br s, 16H), 7.32 (br s, 8H), 7.13 (br s, 2H), 6.81 (br s, 18H), 5.51 (br s, 2H), –1.52 (br s, 2H), –2.29 (br s, 2H), –6.64 (br s, 2H), –31.52 (br s, 2H), –61.77 (br s, 18H), –63.54 (br s, 2H), –95.54 (br s, 2H).

Synthesis of [Tb(TriNOx)]$_2$[BAr$^F{}_4$]$_2$ (**4.3-Tb**). To a DCM solution of **4.1-Tb** (0.060 g, 0.077 mmol, 1 equiv) was added Ag[BAr$^F{}_4$] (0.075 g, 0.077 mmol, 1 equiv) and the reaction was stirred in the dark for 4 h. The solution was filtered through celite and volatiles were removed under reduced pressure. X-ray quality crystals were formed by cooling a saturated DCM solution to –25 ºC. Yield: 0.071 g (59%). Anal. Calcd. for $C_{130}H_{114}N_8O_6F_{48}B_2Tb_2$: C, 49.79; H, 3.66; N, 3.57. Found: C, 49.71; H, 3.52; N, 3.53. ^{1}H NMR (300 MHz, CD_2Cl_2): δ = 158.68 (br s, 18H), 151.61 (br s, 2H), 127.00 (br s, 2H), 104.78 (br s, 2H), 102.46 (br s, 2H), 93.57 (br s, 18H), 51.60 (br s, 18H), 43.77 (br s, 2H), 6.17 (br s, 16H), 6.12 (br s, 8H), 3.45 (br s, 2H), 1.16 (br s, 2H), –32.38 (br s, 2H), –41.30 (br s, 2H), –57.74 (br s, 2H), –66.99 (br s, 2H), –83.24 (br s, 2H).

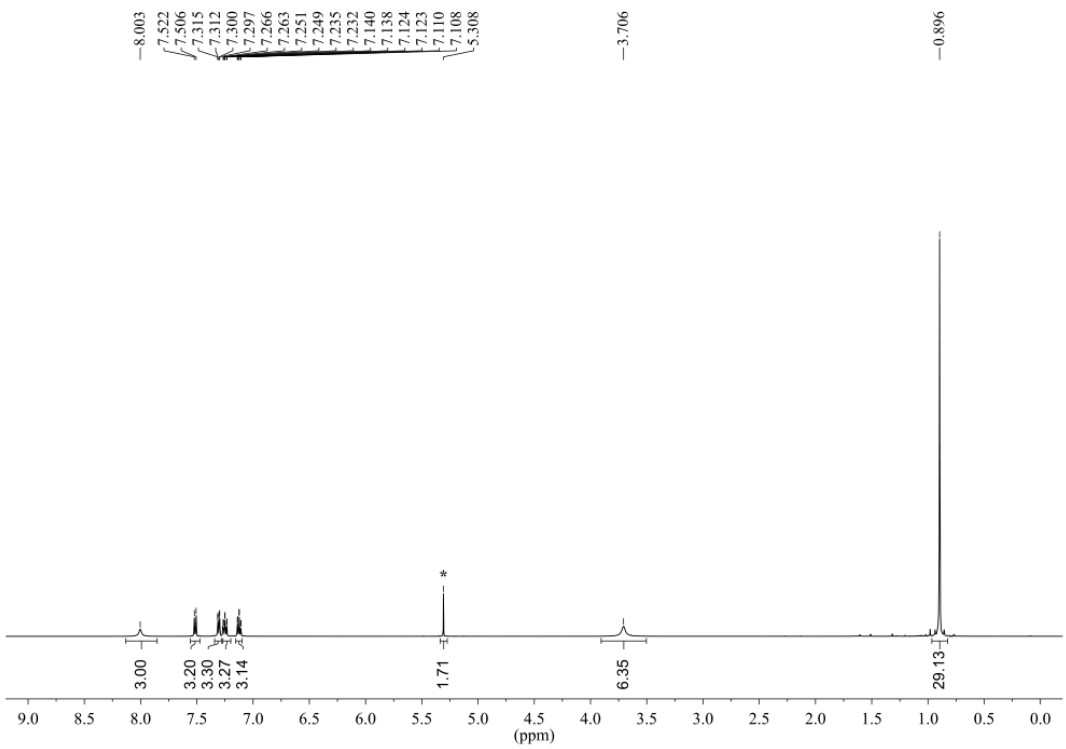

Figure 4.4.1. ^{1}H NMR spectrum of H_3TriNOx in $CDCl_3$. * indicates CH_2Cl_2 solvent impurity.

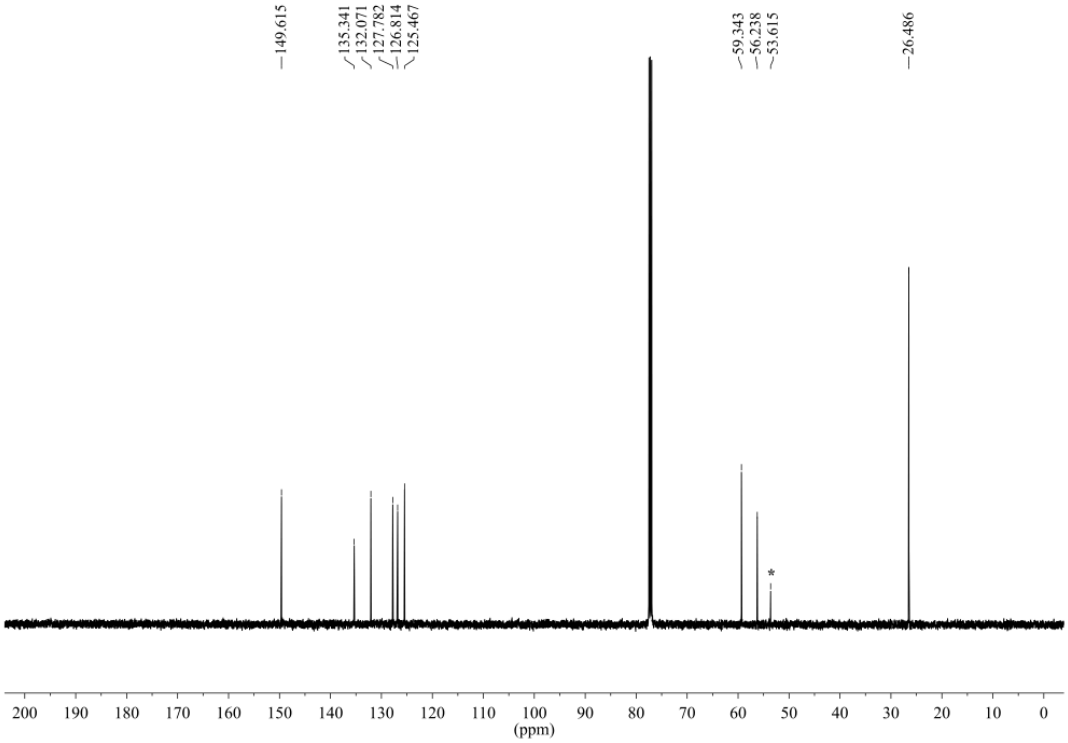

Figure 4.4.2. ^{13}C{^{1}H} NMR spectrum of H_3TriNOx in $CDCl_3$. * indicates CH_2Cl_2 solvent impurity.

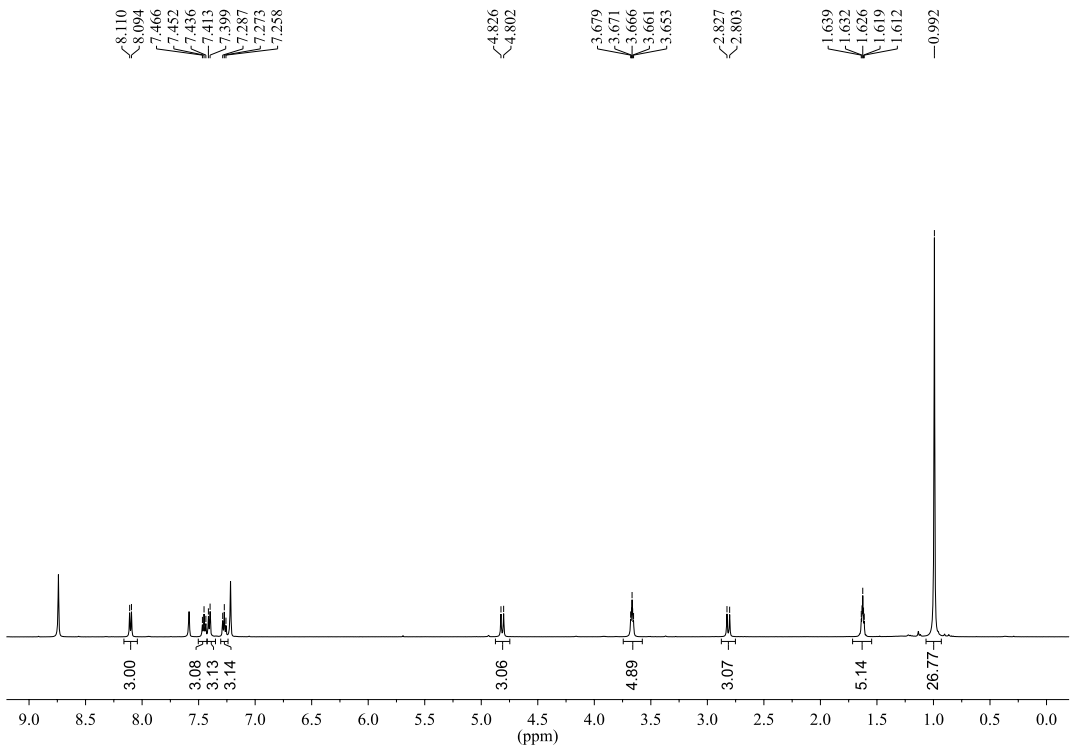

Figure 4.4.3. ^{1}H NMR spectrum of **4.1-La** in d_5-pyr. * indicates CH_2Cl_2 solvent impurity.

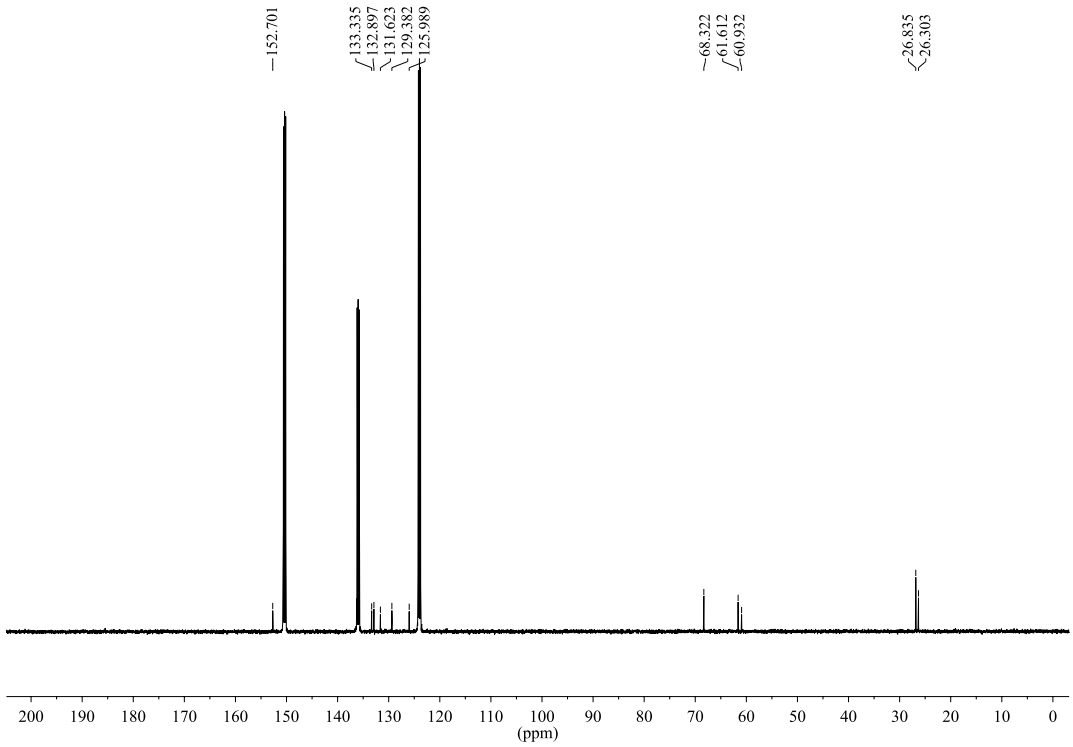

Figure 4.4.4. ^{13}C{^{1}H} NMR spectrum of **4.1-La** in d_5-pyr.

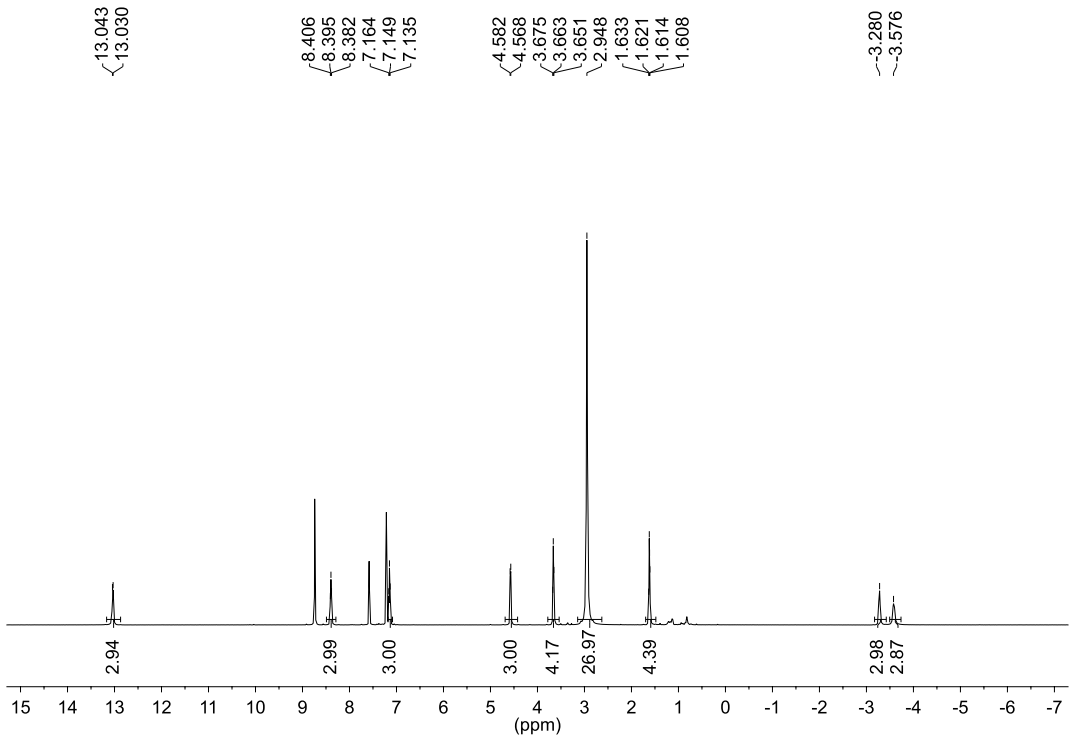

Figure 4.4.5. ^{1}H NMR spectrum of **4.1-Ce** in d_5-pyr.

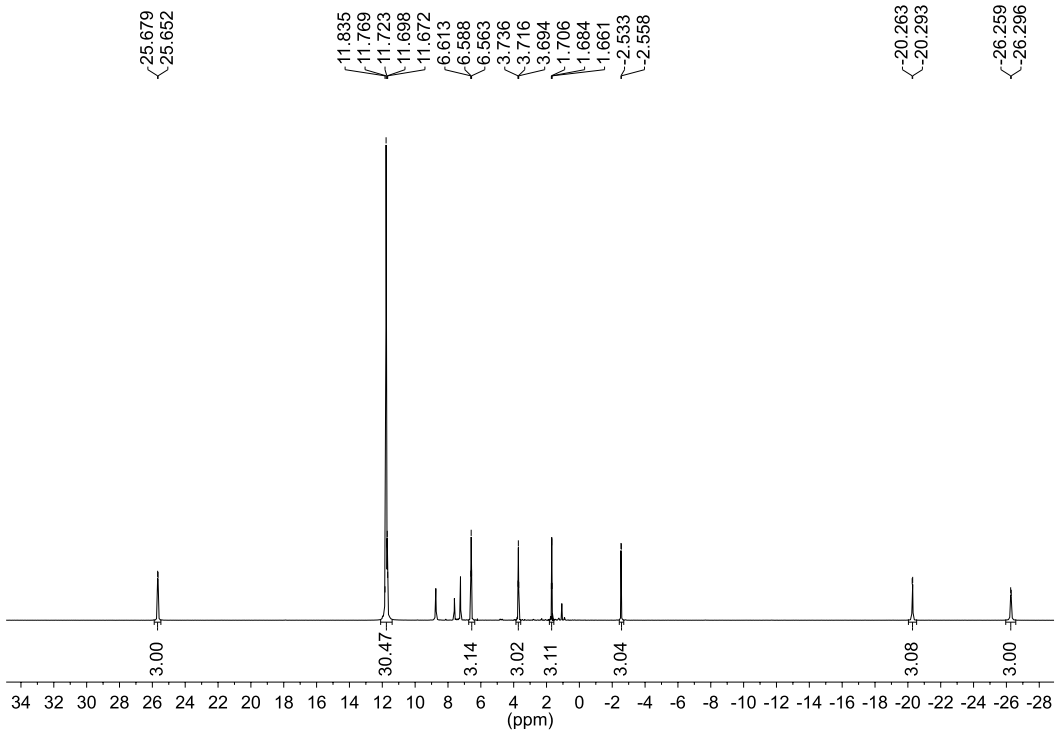

Figure 4.4.6. ^{1}H NMR spectrum of **4.1-Pr** in d_5-pyr.

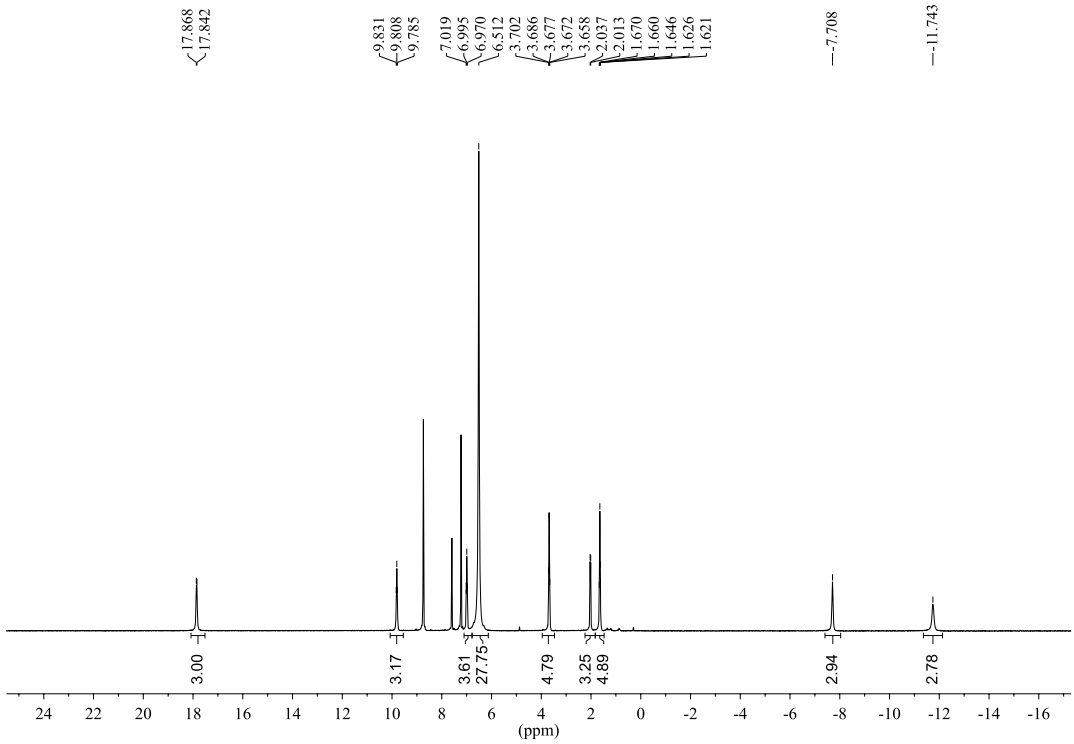

Figure 4.4.7. ^{1}H NMR spectrum of **4.1-Nd** in d_5-pyr.

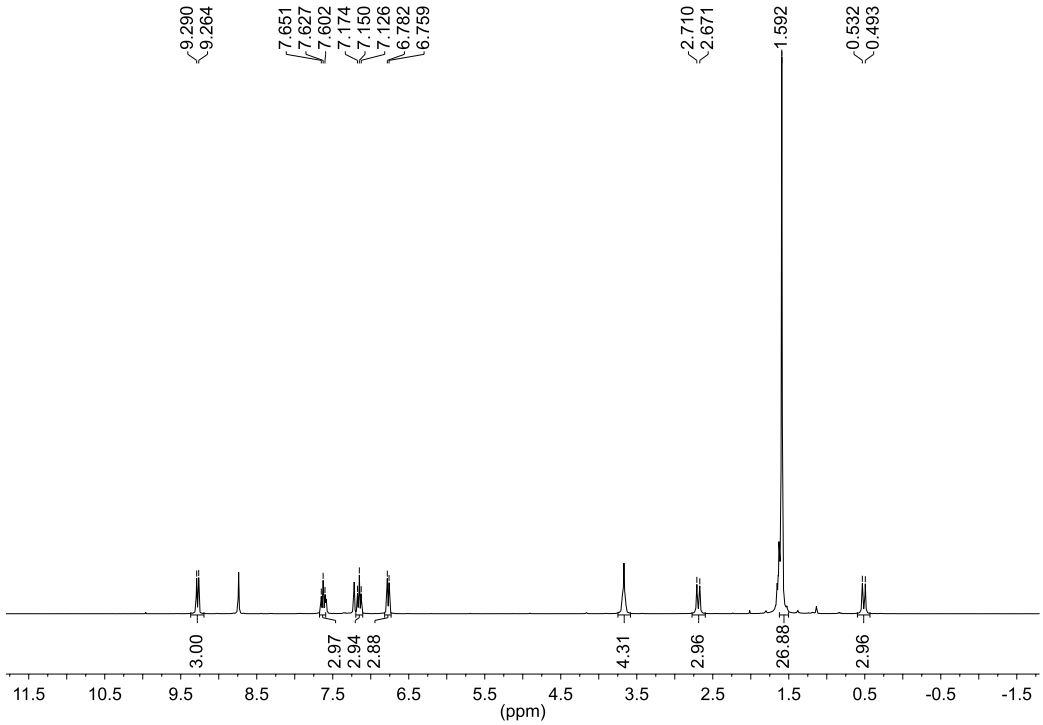

Figure 4.4.8. ^{1}H NMR spectrum of **4.1-Sm** in d_5-pyr.

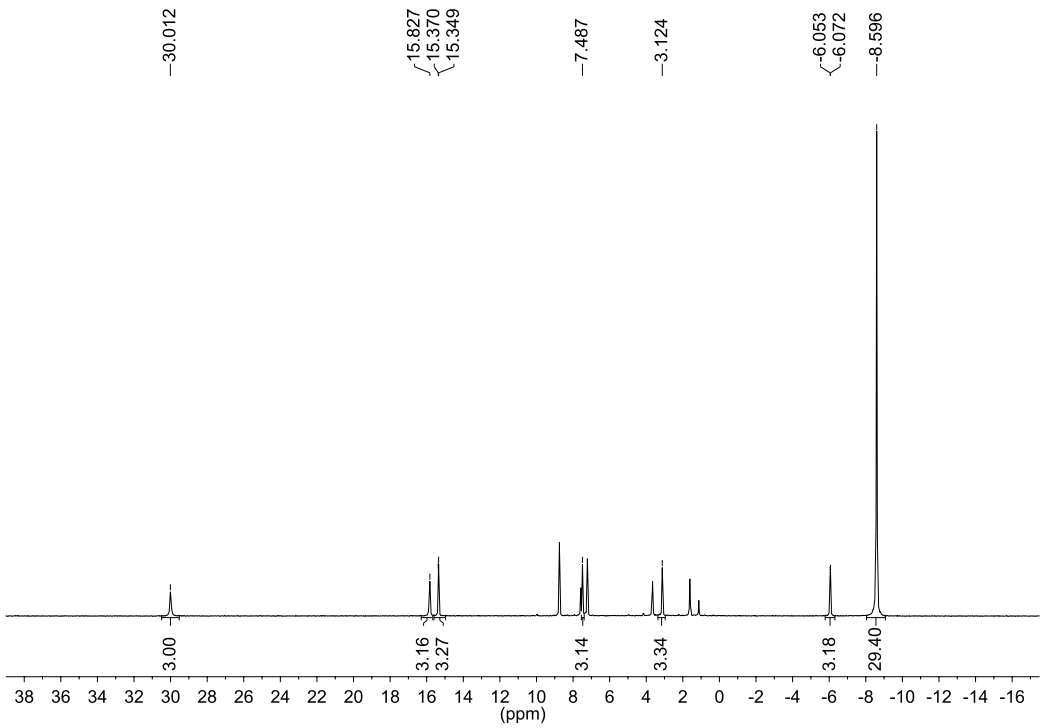

Figure 4.4.9. ^{1}H NMR spectrum of **4.1-Eu** in d_5-pyr.

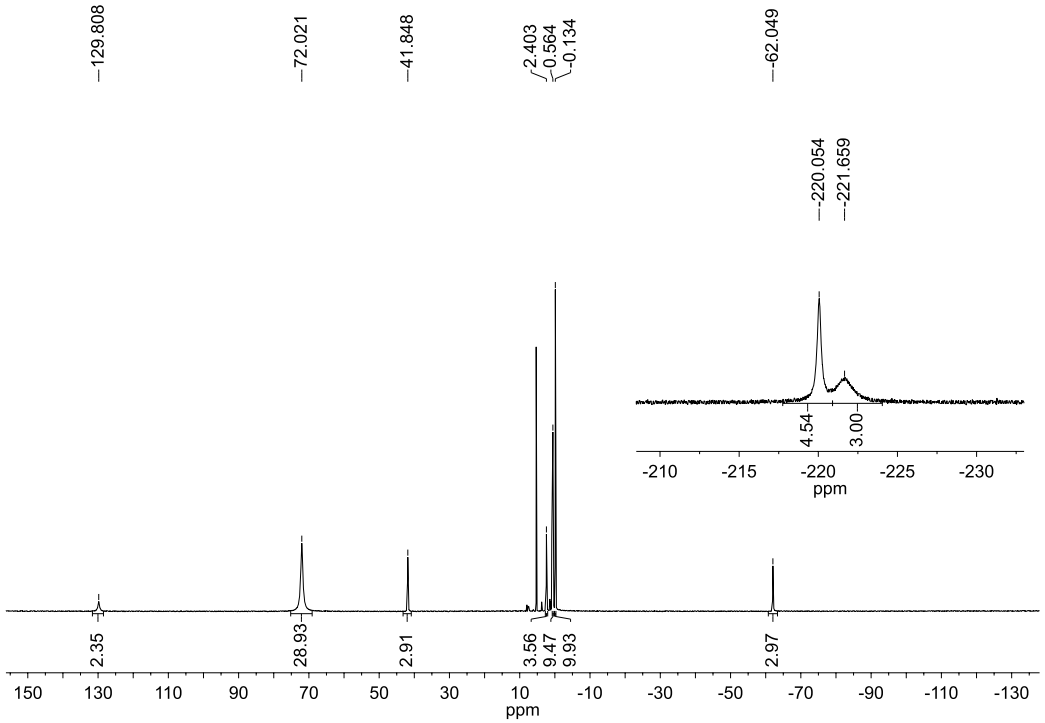

Figure 4.4.10. ^{1}H NMR spectrum of **4.1-Tb** in d_5-pyr.

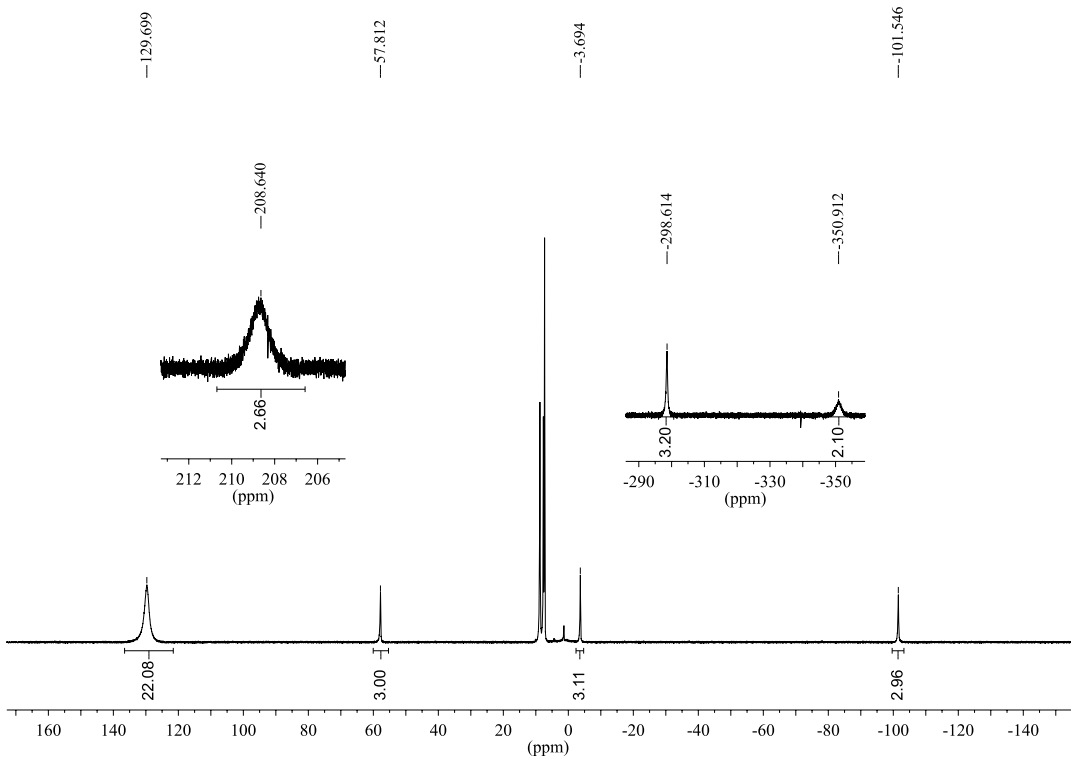

Figure 4.4.11. ^{1}H NMR spectrum of **4.1-Dy** in d_5-pyr.

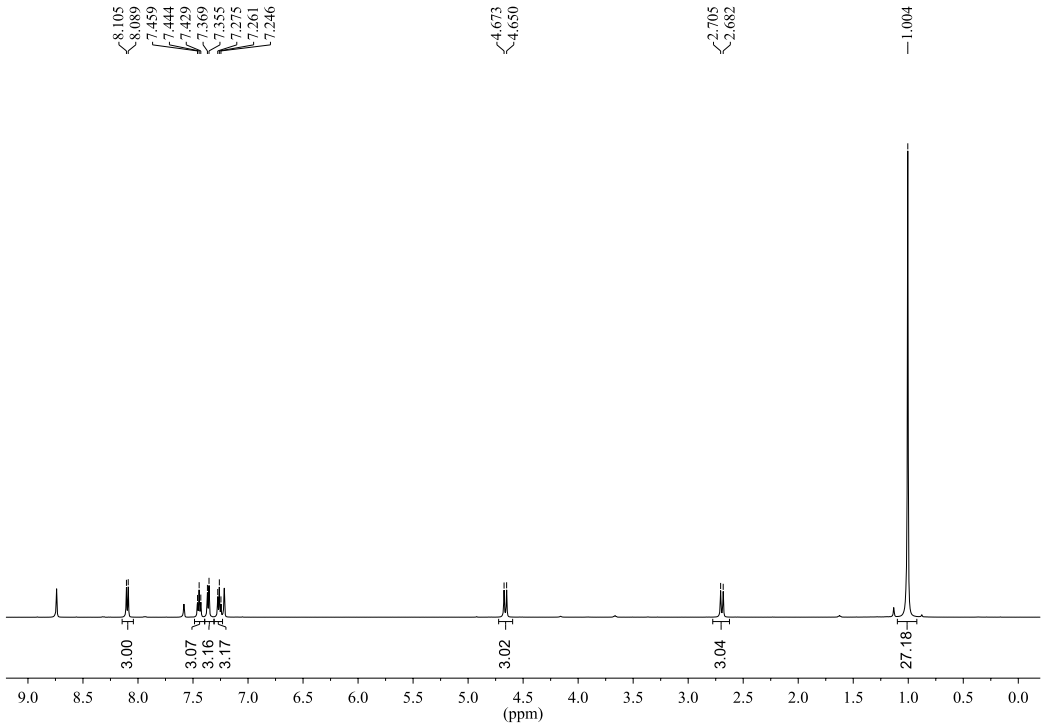

Figure 4.4.12. ^{1}H NMR spectrum of **4.1-Y** in d_5-pyr.

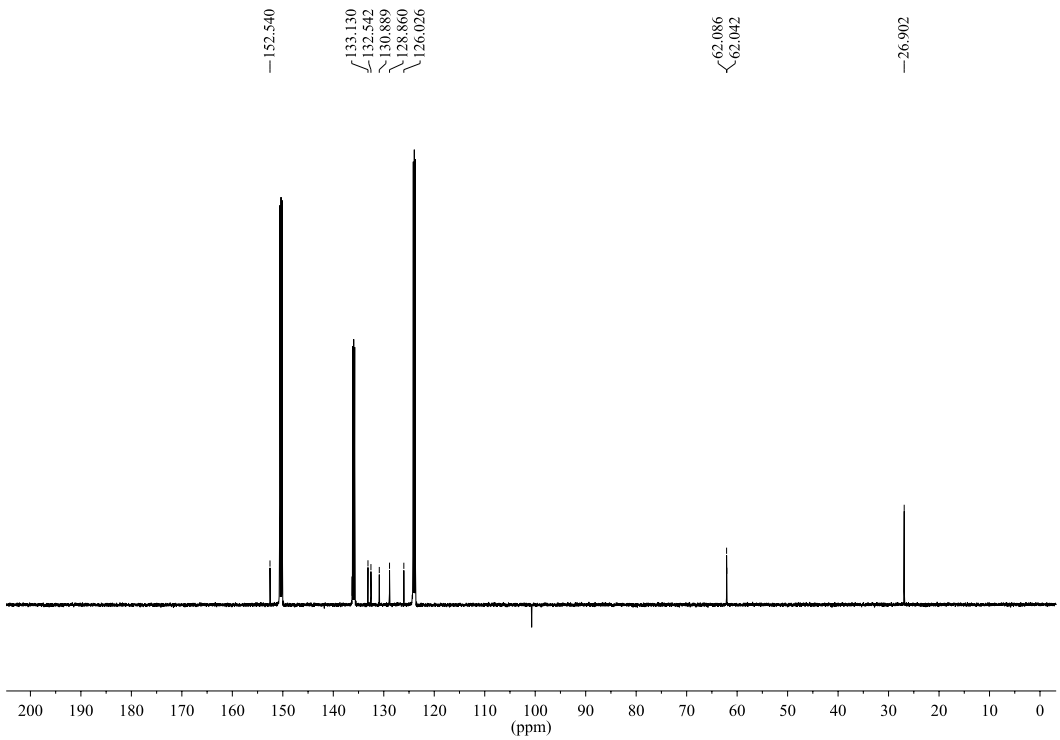

Figure 4.4.13. $^{13}C\{^{1}H\}$ NMR spectrum of **4.1-Y** in d_5-pyr.

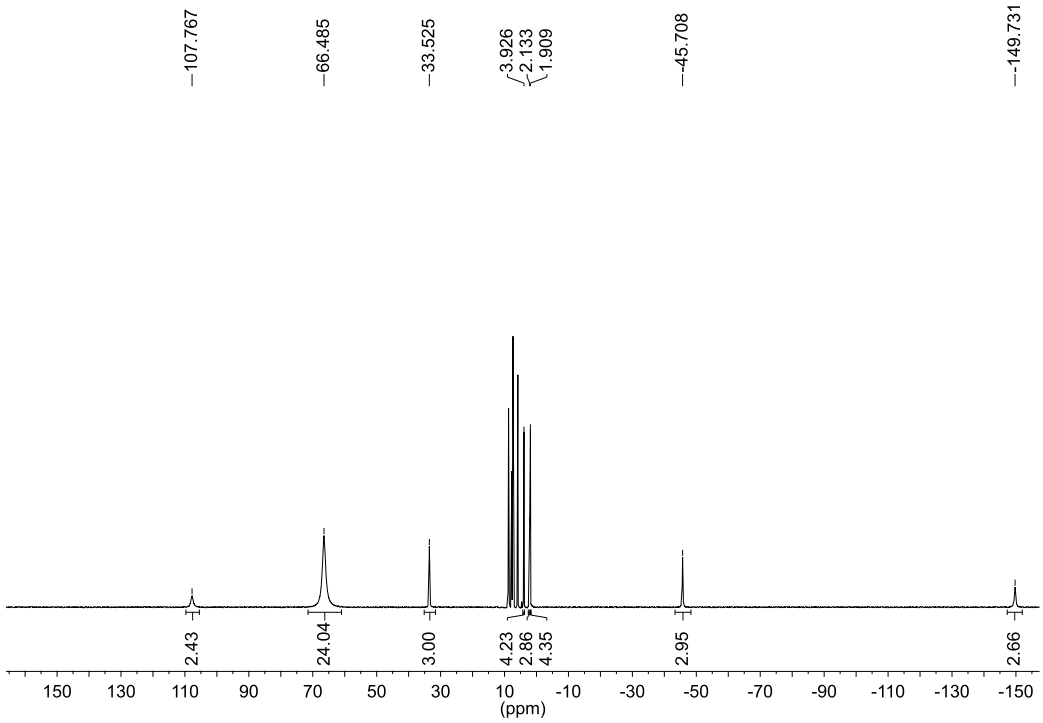

Figure 4.4.14. ^{1}H NMR spectrum of **4.1-Ho** in d_5-pyr.

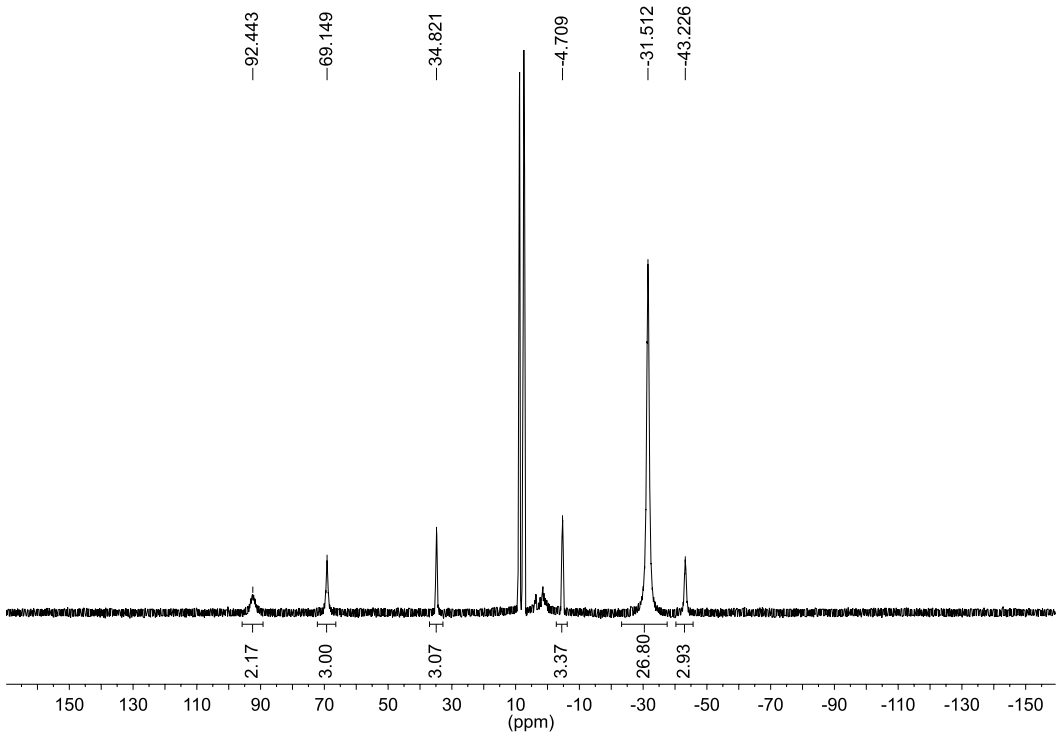

Figure 4.4.15. ^{1}H NMR spectrum of **4.1-Er** in d_5-pyr.

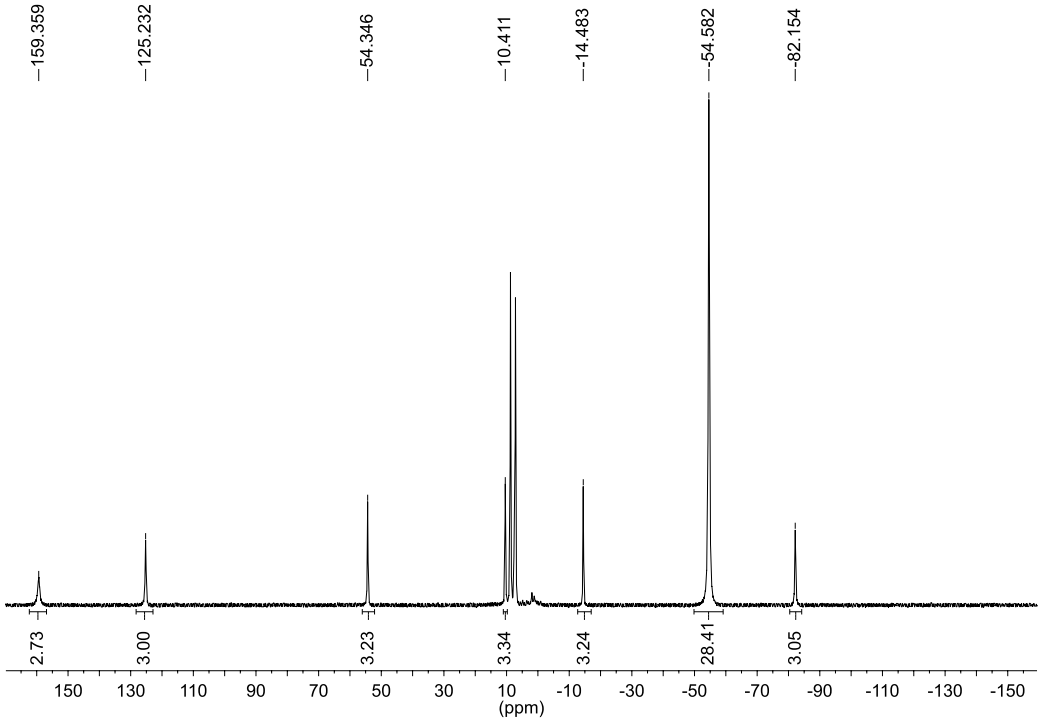

Figure 4.4.16. ^{1}H NMR spectrum of **4.1-Tm** in d_5-pyr.

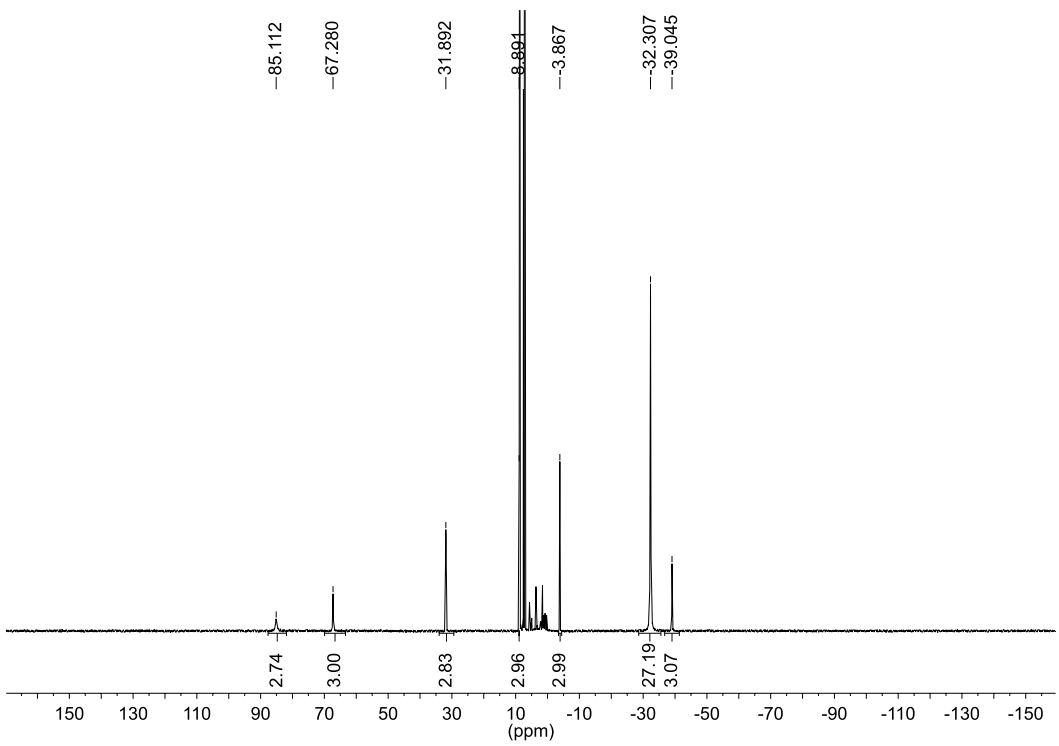

Figure 4.4.17. ^{1}H NMR spectrum of **4.1-Yb** in d_5-pyr.

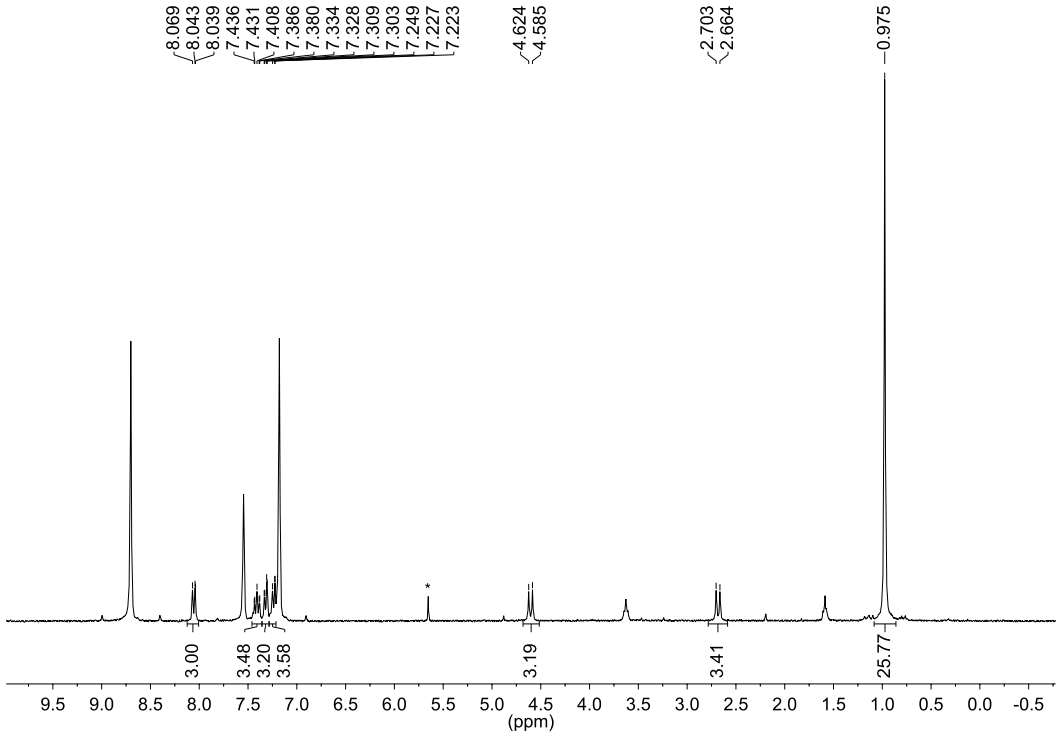

Figure 4.4.18. ^{1}H NMR spectrum of **4.1-Lu** in d_5-pyr. * indicates CH_2Cl_2 solvent impurity.

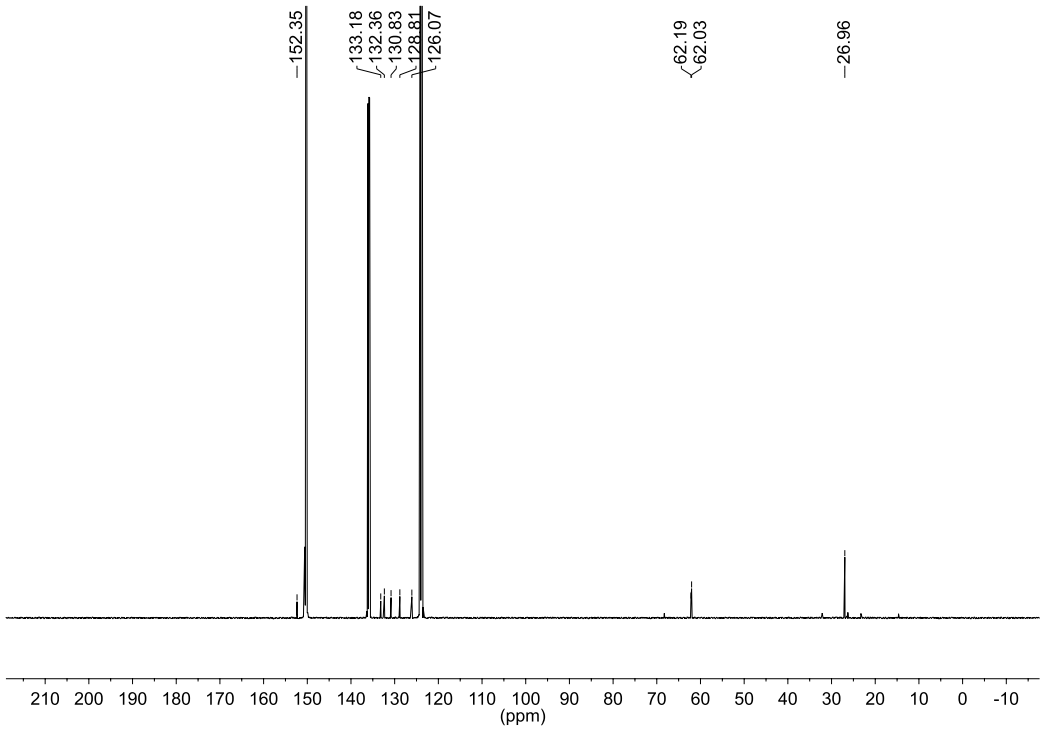

Figure 4.4.19. $^{13}C\{^{1}H\}$ NMR spectrum of **4.1-Lu** in d_5-pyr.

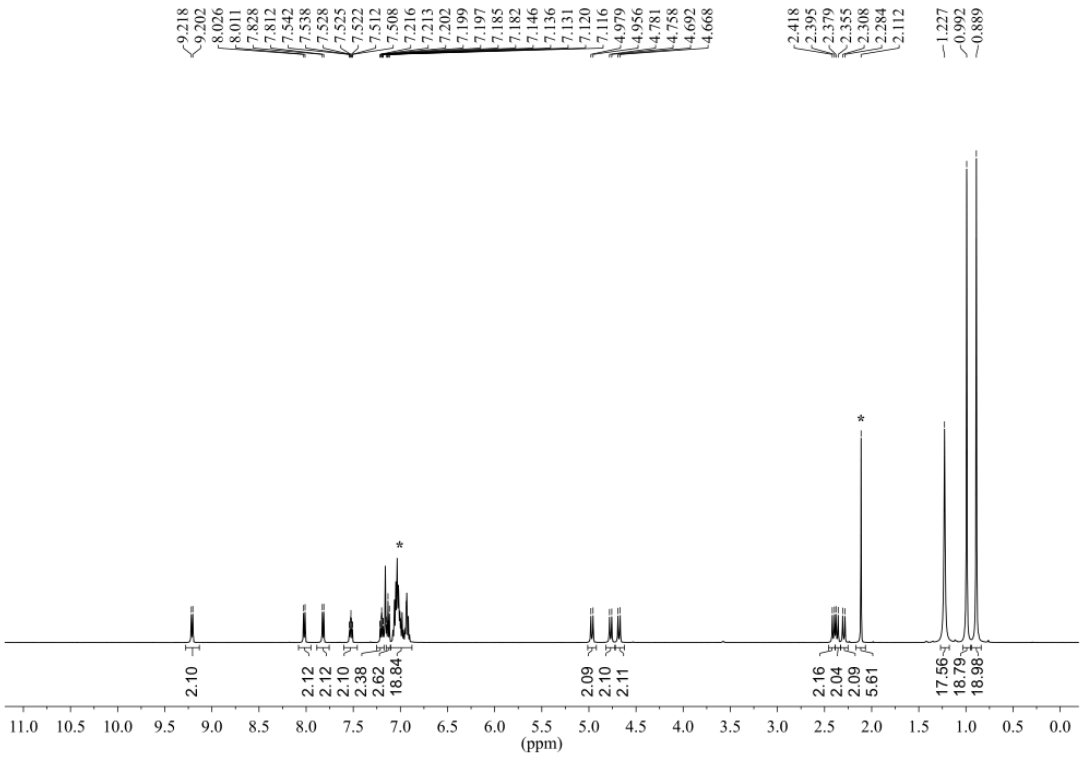

Figure 4.4.20. ^{1}H NMR spectrum of **4.2-La** in C_6D_6. * indicates toluene solvent impurity.

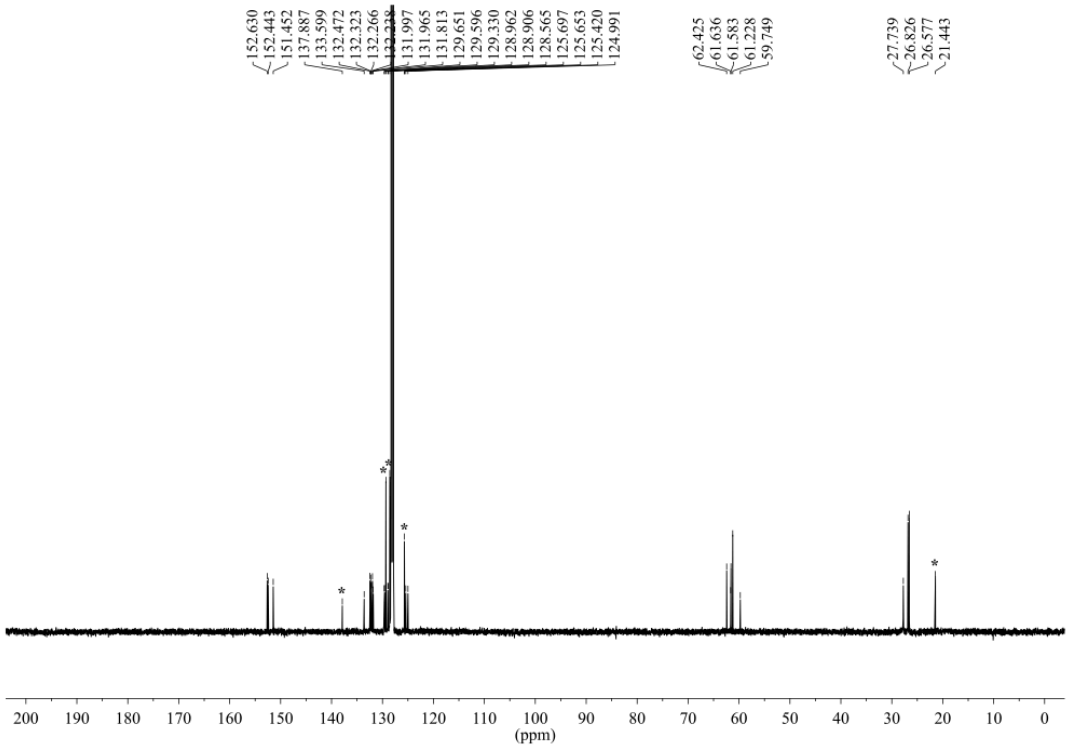

Figure 4.4.21. $^{13}C\{^{1}H\}$ NMR spectrum of **4.2-La** in C_6D_6. * indicates toluene solvent impurity.

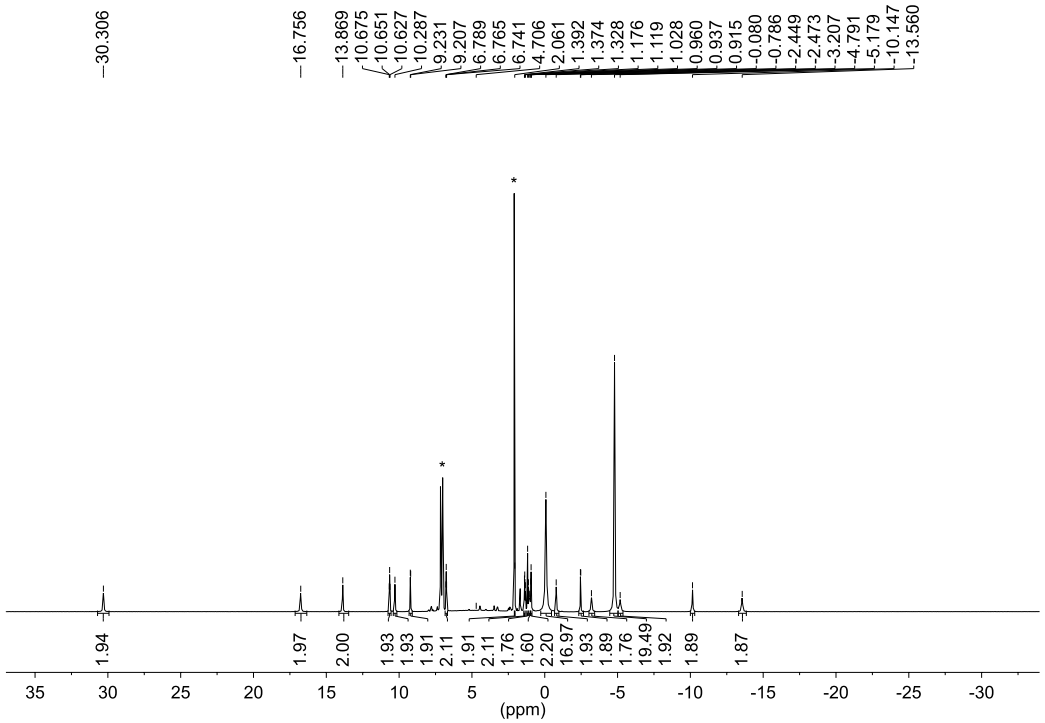

Figure 4.4.22. ^{1}H NMR spectrum of **4.2-Ce** in C_6D_6. * indicates toluene solvent impurity.

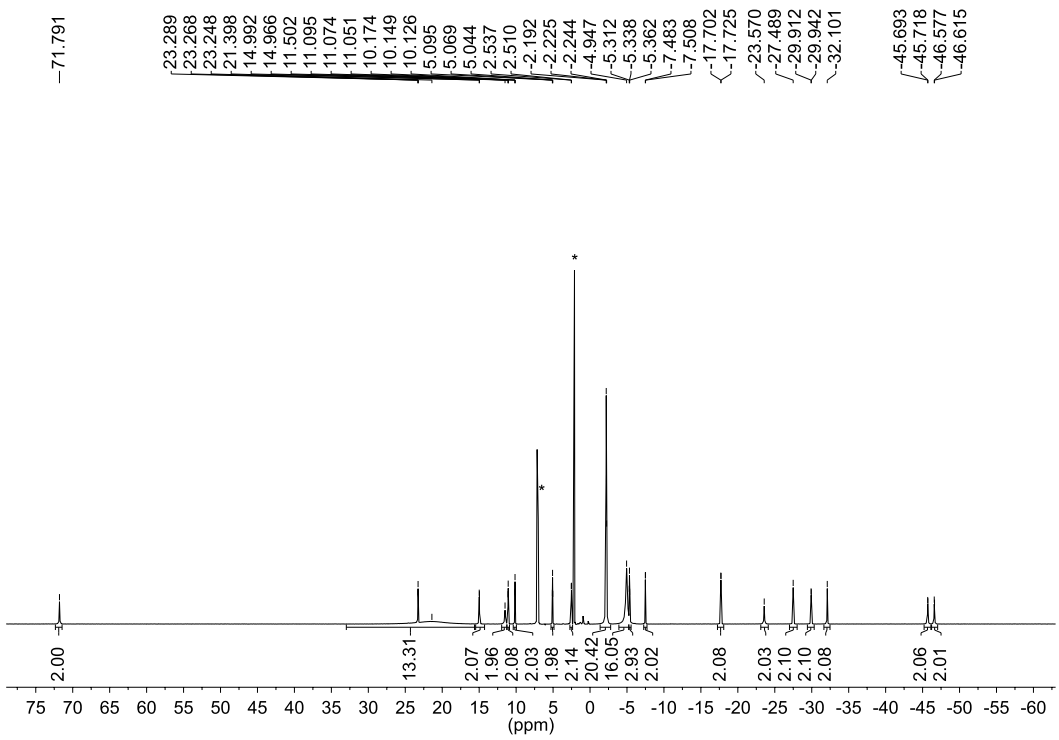

Figure 4.4.23. ^{1}H NMR spectrum of **4.2-Pr** in C_6D_6. * indicates toluene solvent impurity.

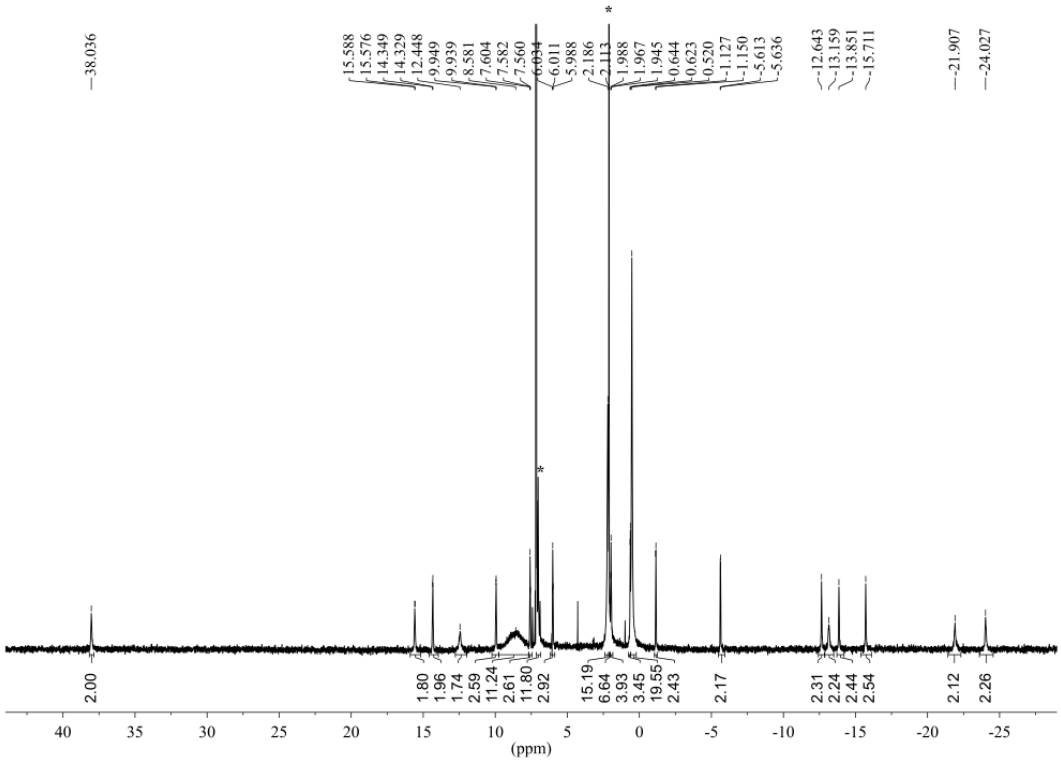

Figure 4.4.24. ^{1}H NMR spectrum of **4.2-Nd** in C_6D_6. * indicates toluene solvent impurity.

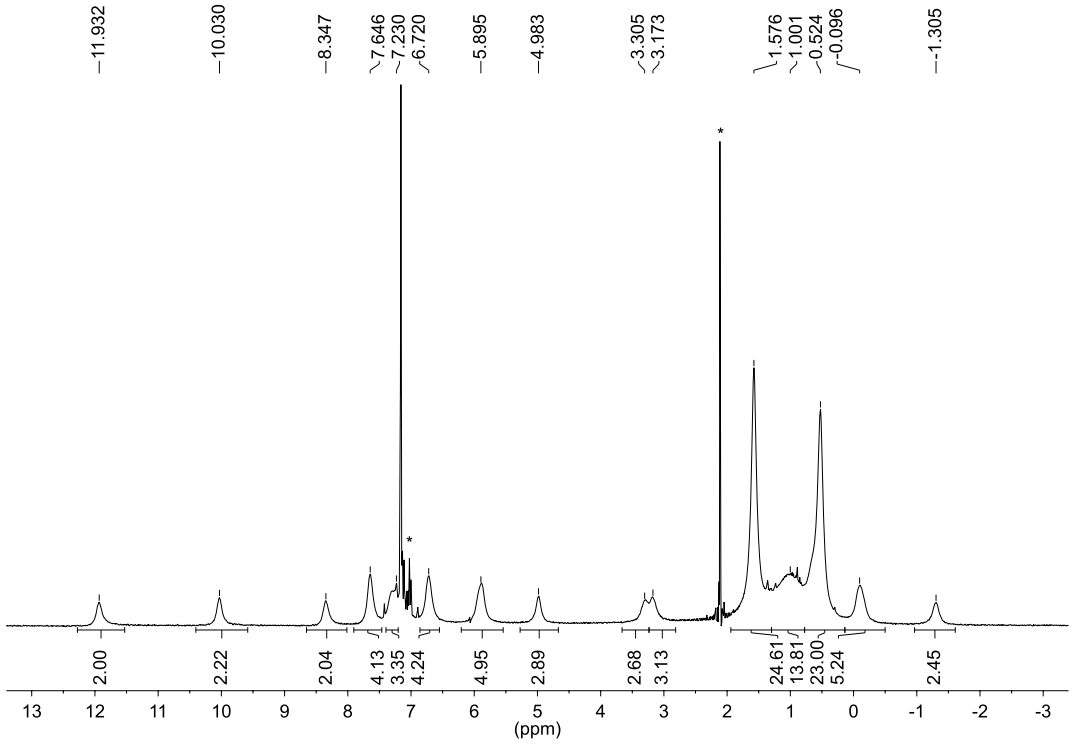

Figure 4.4.25. ^{1}H NMR spectrum of **4.2-Sm** in C_6D_6. * indicates toluene solvent impurity.

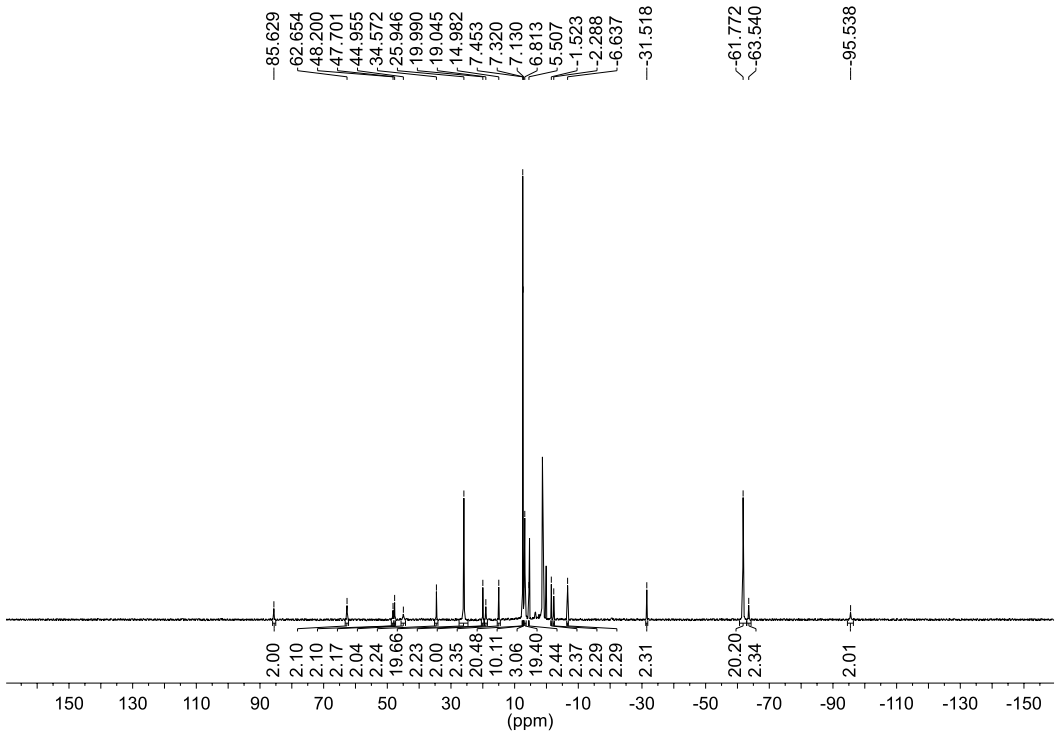

Figure 4.4.26. ^{1}H NMR spectrum of **4.3-Pr** in CD_2Cl_2.

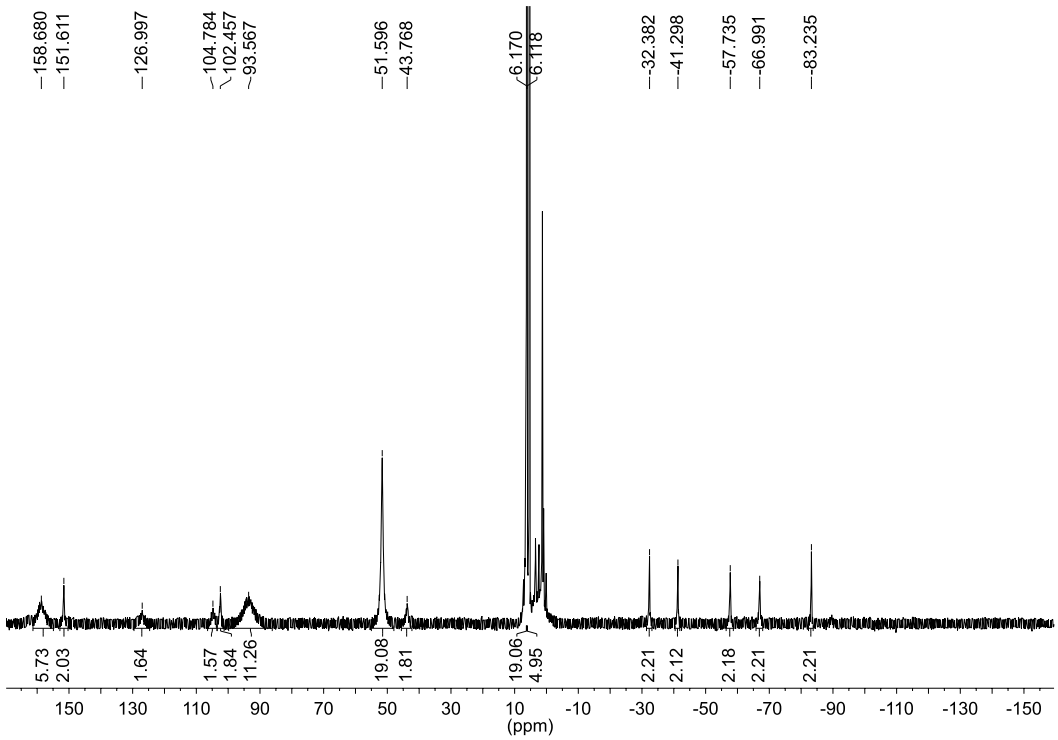

Figure 4.4.27. ^{1}H NMR spectrum of **4.3-Tb** in CD_2Cl_2.

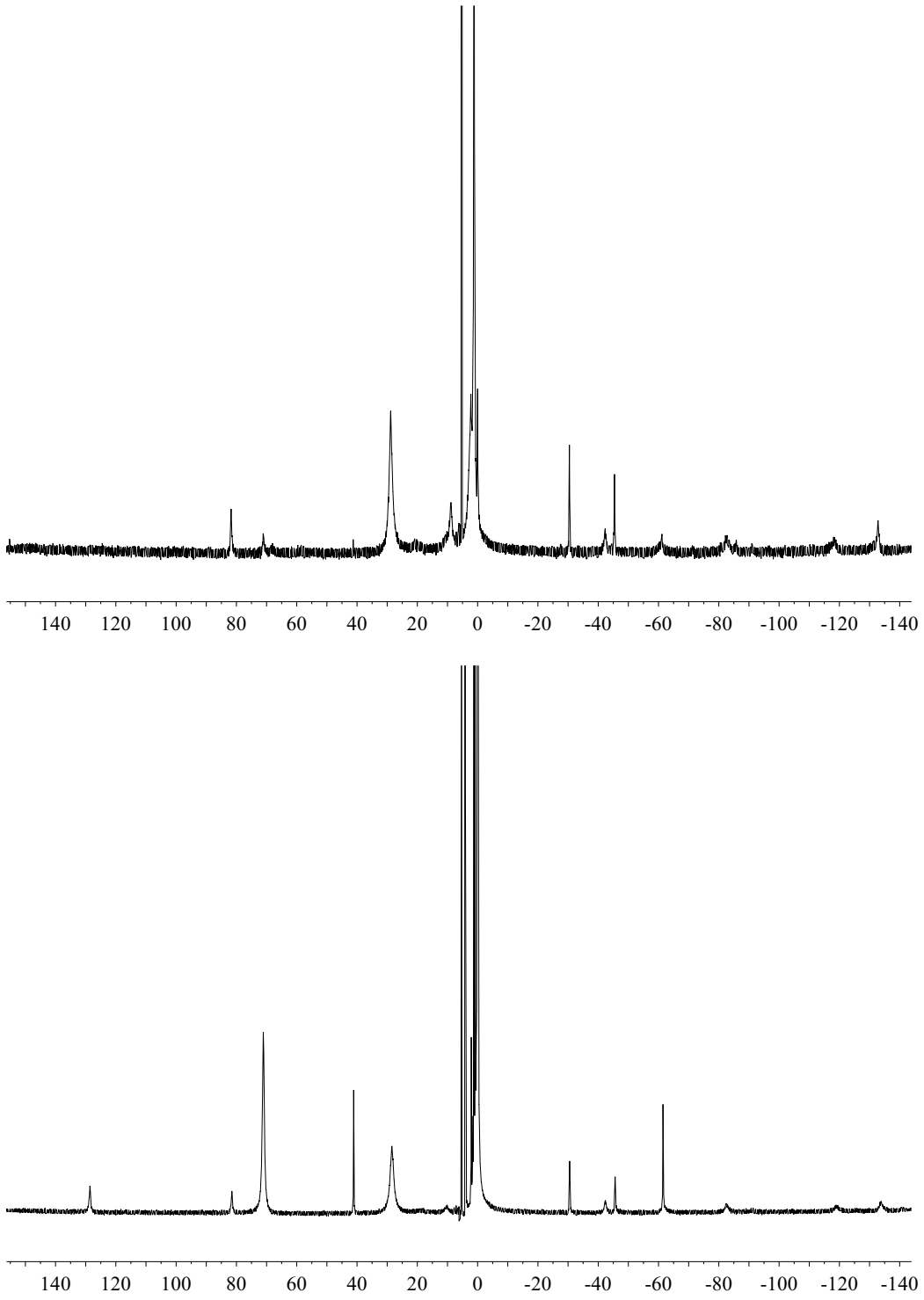

Figure 4.4.28. ^{1}H NMR spectra of the crude product mixtures of the oxidations of **4.1-Tb** with AgOTf (top) and FcOTf (bottom)

X-ray Crystallography. X-ray intensity data were collected on a Bruker APEXII CCD area detector employing graphite-monochromated Mo-Kα radiation (λ=0.71073 Å) at a temperature of 143(1) K. In all cases, rotation frames were integrated using SAINT,[23] producing a listing of unaveraged F^2 and $\sigma(F^2)$ values that were then passed to the SHELXTL[24] program package for further processing and structure solution on a Dell Pentium 4 computer. The intensity data were corrected for Lorentz and polarization effects and for absorption using TWINABS[25] or SADABS.[26] The structures were solved by direct methods (SHELXS-97).[27] Refinement was by full-matrix least squares based on F^2 using SHELXL-97.[27] All reflections were used during refinements. Non-hydrogen atoms were refined anisotropically and hydrogen atoms were refined using a riding model.

Crystallographic data and structure refinement information for **H_3TriNOx** (Penn4438), **4.1-RE,** RE = La (Penn4666), Ce (Penn4443), Pr (Penn4454), Nd (Penn4667), Sm (Penn4626), Eu (Penn4761), Gd (Penn4757), Tb (Penn4568), Dy (Penn4621), Y (Penn4663), Ho (Penn4756), Er (Penn4760), Tm (Penn4785), Yb (Penn4787), Lu (Penn4784), **4.2-RE,** RE = La (Penn4665), Ce (Penn4522), Pr (Penn4474), Nd (Penn4614), Sm (Penn4685), and **4.3-RE**, RE = Pr (Penn4786) and Tb (Penn4758), are summarized in Tables 4.4.2 – 4.4.24.

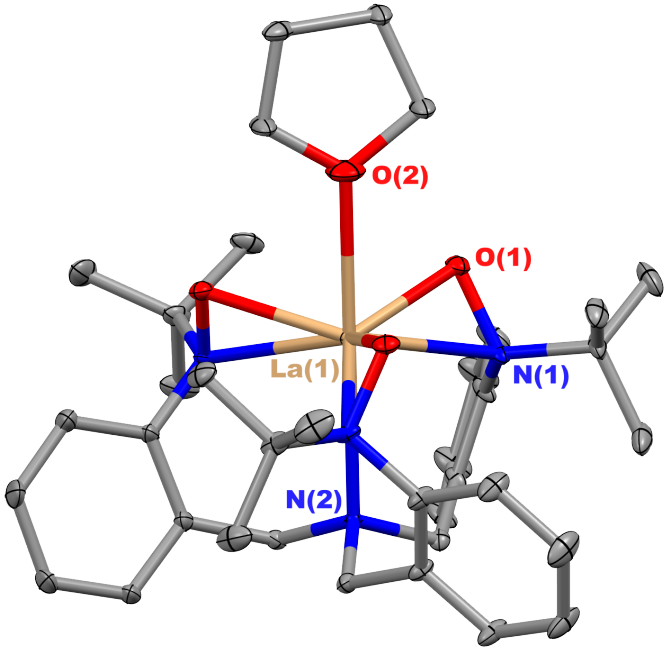

Figure 4.4.29. Thermal ellipsoid plot of **4.1-La** at 30% probability. Hydrogen atoms excluded for clarity.

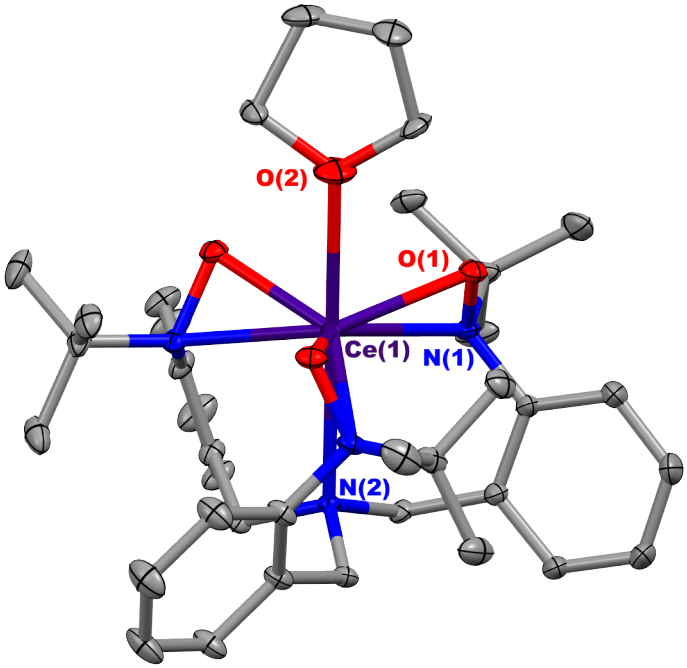

Figure 4.4.30. Thermal ellipsoid plot of **4.1-Ce** at 30% probability. Hydrogen atoms excluded for clarity.

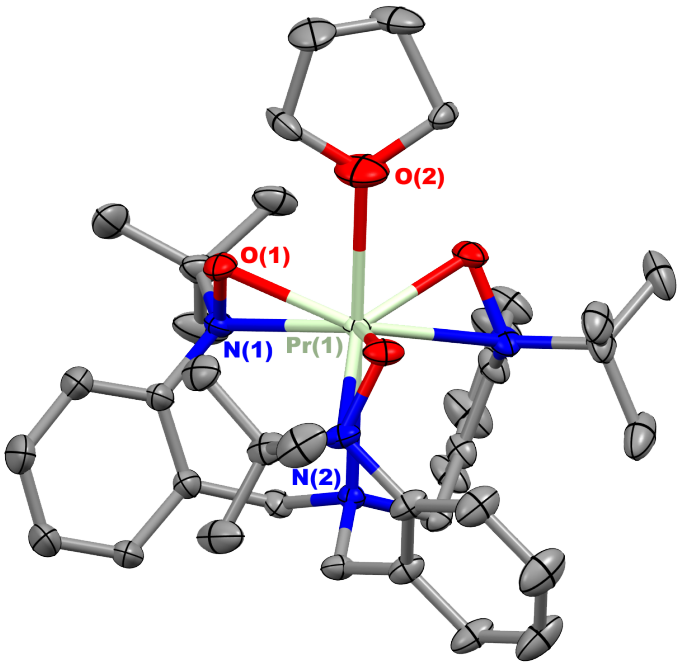

Figure 4.4.31. Thermal ellipsoid plot of **4.1-Pr** at 30% probability. Hydrogen atoms excluded for clarity.

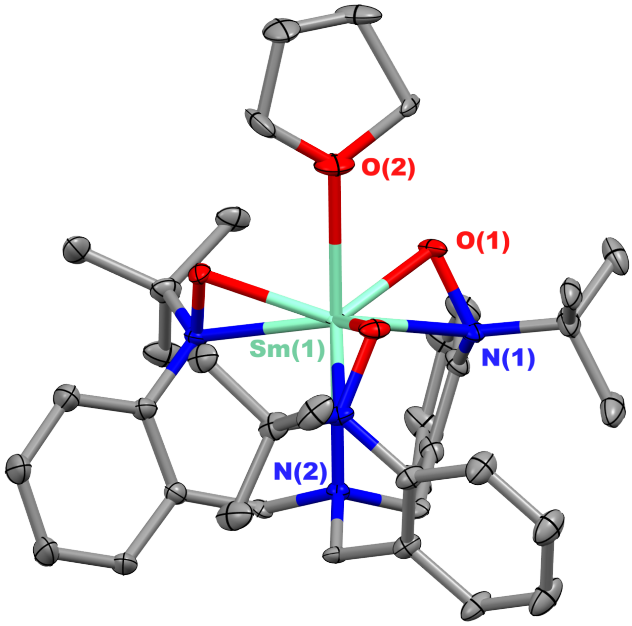

Figure 4.4.32. Thermal ellipsoid plot of **4.1-Sm** at 30% probability. Hydrogen atoms excluded for clarity.

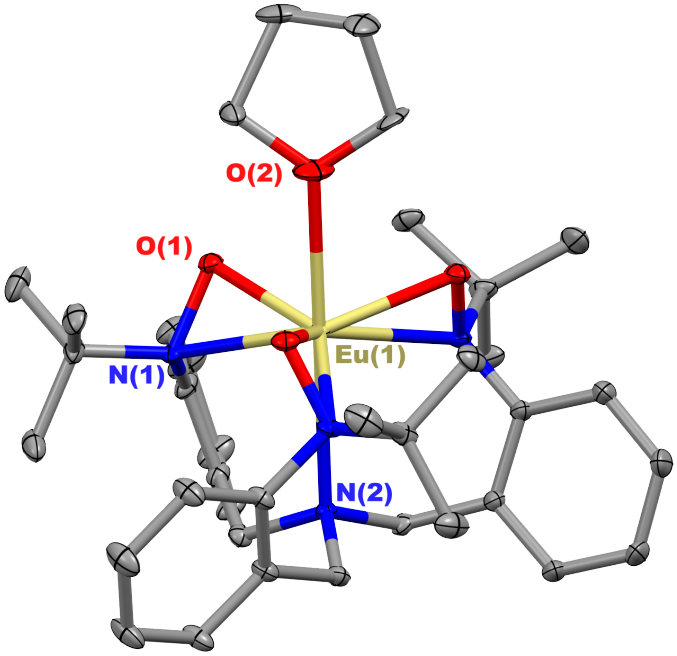

Figure 4.4.33. Thermal ellipsoid plot of **4.1-Eu** at 30% probability. Hydrogen atoms excluded for clarity.

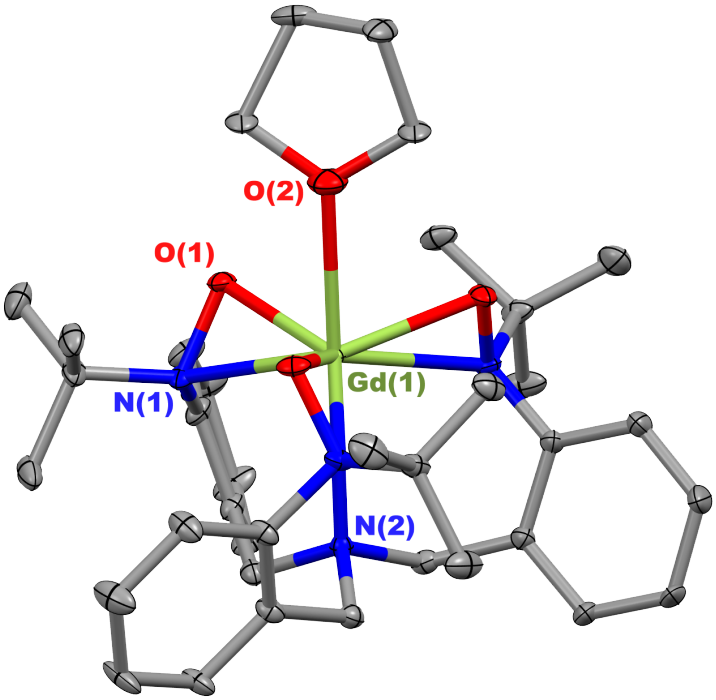

Figure 4.4.34. Thermal ellipsoid plot of **4.1-Gd** at 30% probability. Hydrogen atoms excluded for clarity.

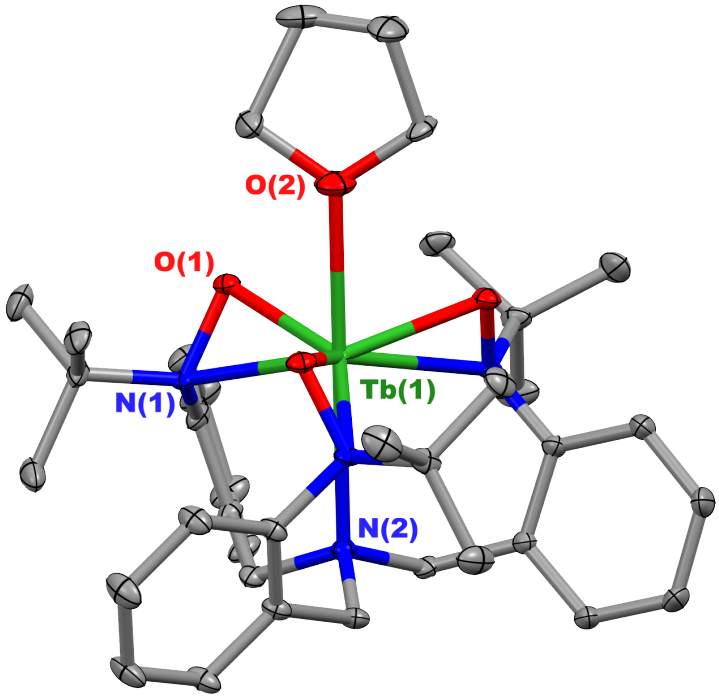

Figure 4.4.35. Thermal ellipsoid plot of **4.1-Tb** at 30% probability. Hydrogen atoms excluded for clarity.

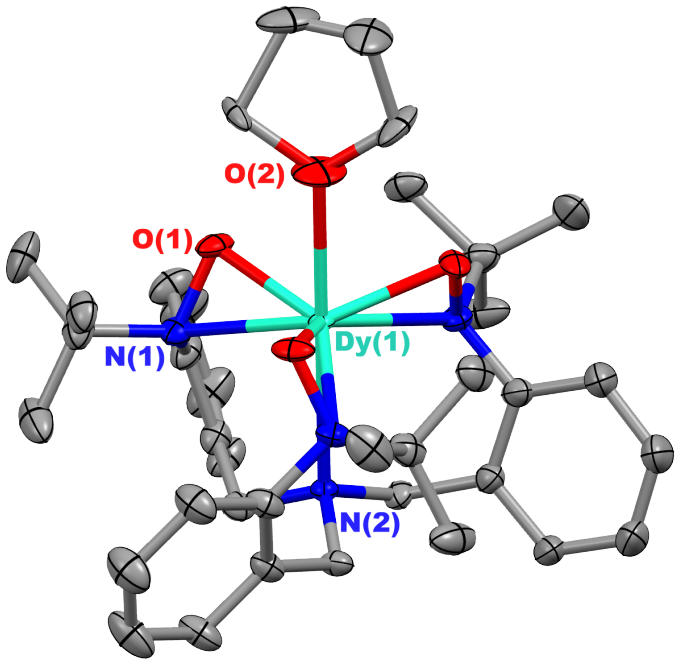

Figure 4.4.36. Thermal ellipsoid plot of **4.1-Dy** at 30% probability. Hydrogen atoms excluded for clarity.

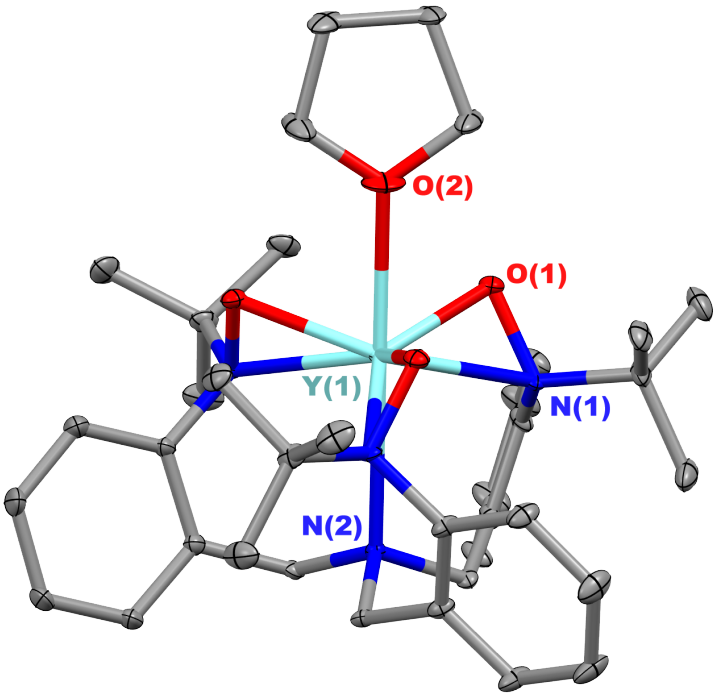

Figure 4.4.37. Thermal ellipsoid plot of **4.1-Y** at 30% probability. Hydrogen atoms excluded for clarity.

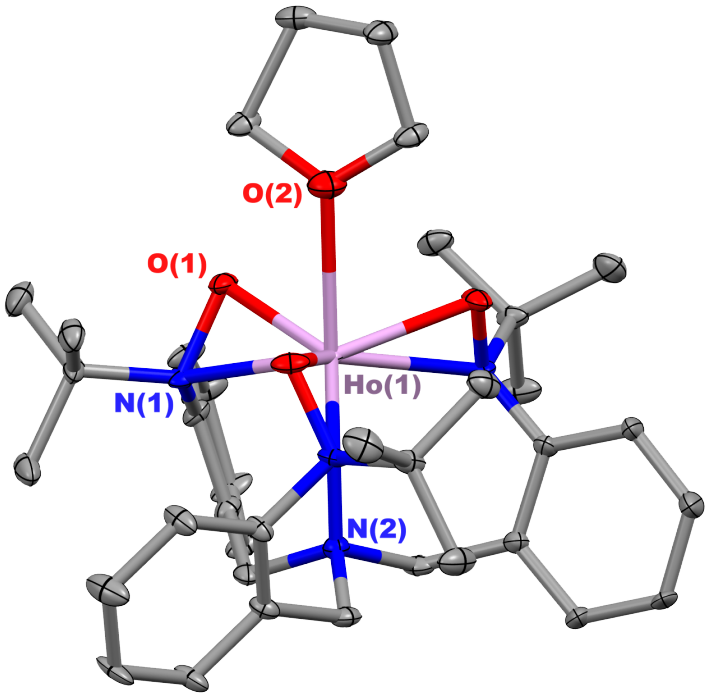

Figure 4.4.38. Thermal ellipsoid plot of **4.1-Ho** at 30% probability. Hydrogen atoms excluded for clarity.

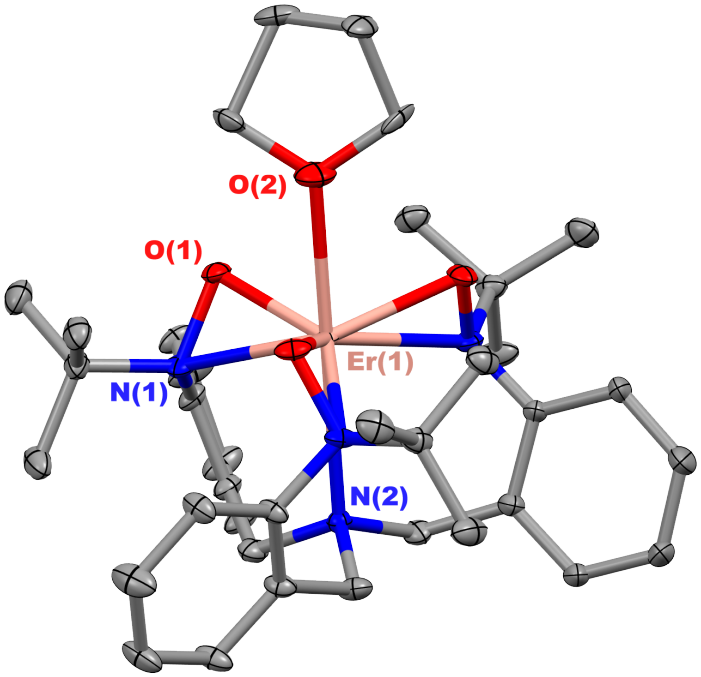

Figure 4.4.39. Thermal ellipsoid plot of **4.1-Er** at 30% probability. Hydrogen atoms excluded for clarity.

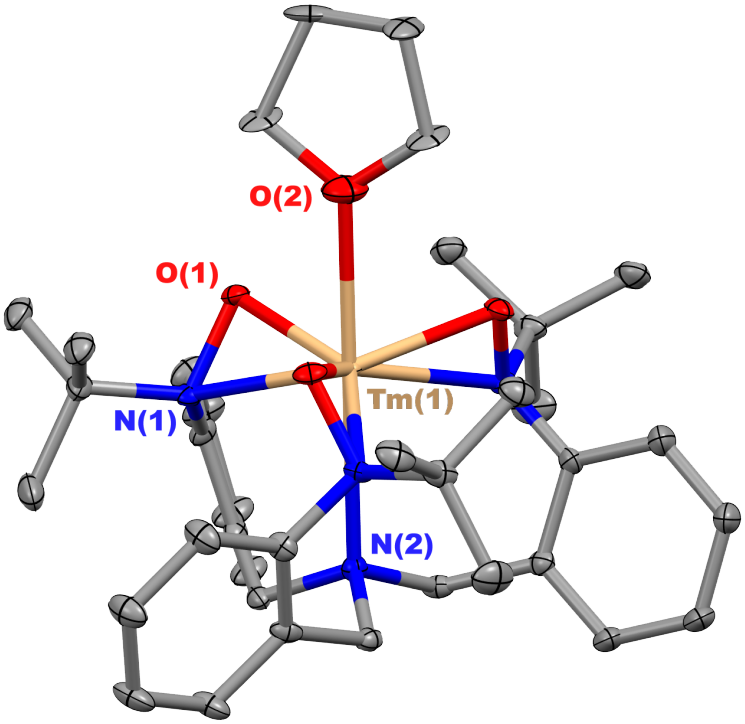

Figure 4.4.40. Thermal ellipsoid plot of **4.1-Tm** at 30% probability. Hydrogen atoms excluded for clarity.

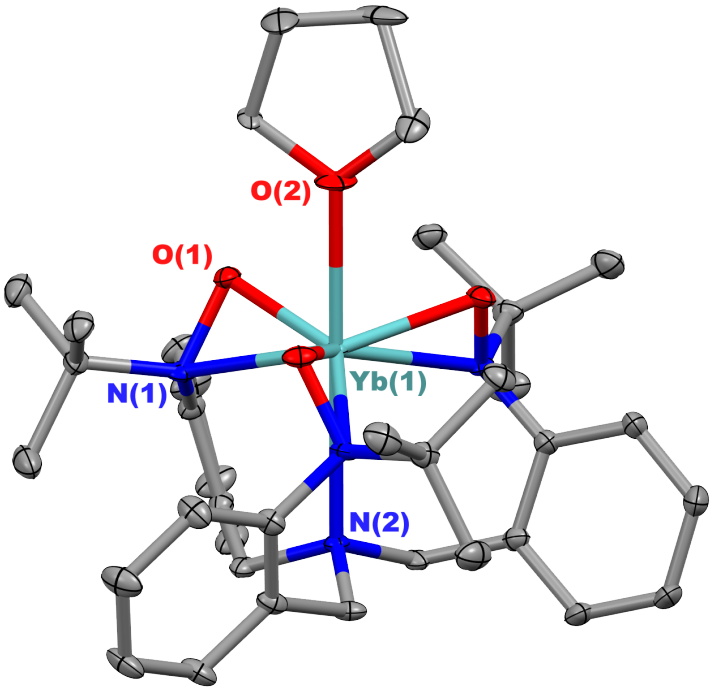

Figure 4.4.41. Thermal ellipsoid plot of **4.1-Yb** at 30% probability. Hydrogen atoms excluded for clarity.

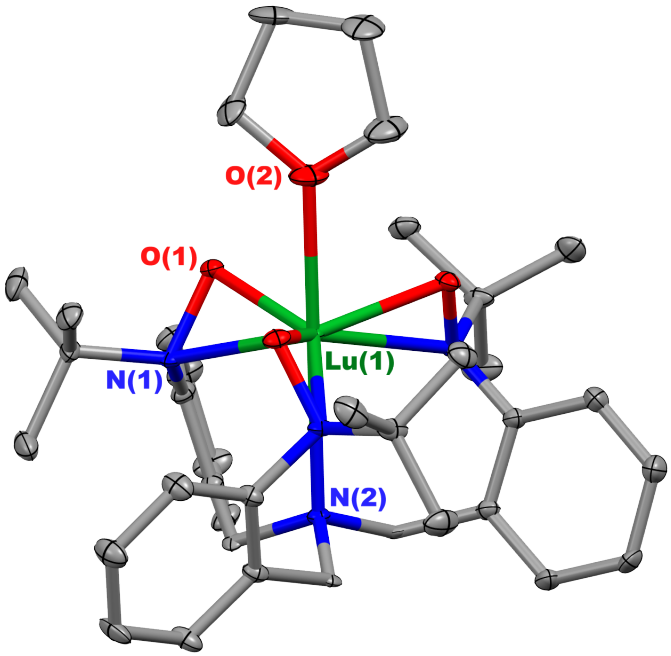

Figure 4.4.42. Thermal ellipsoid plot of **4.1-Lu** at 30% probability. Hydrogen atoms excluded for clarity.

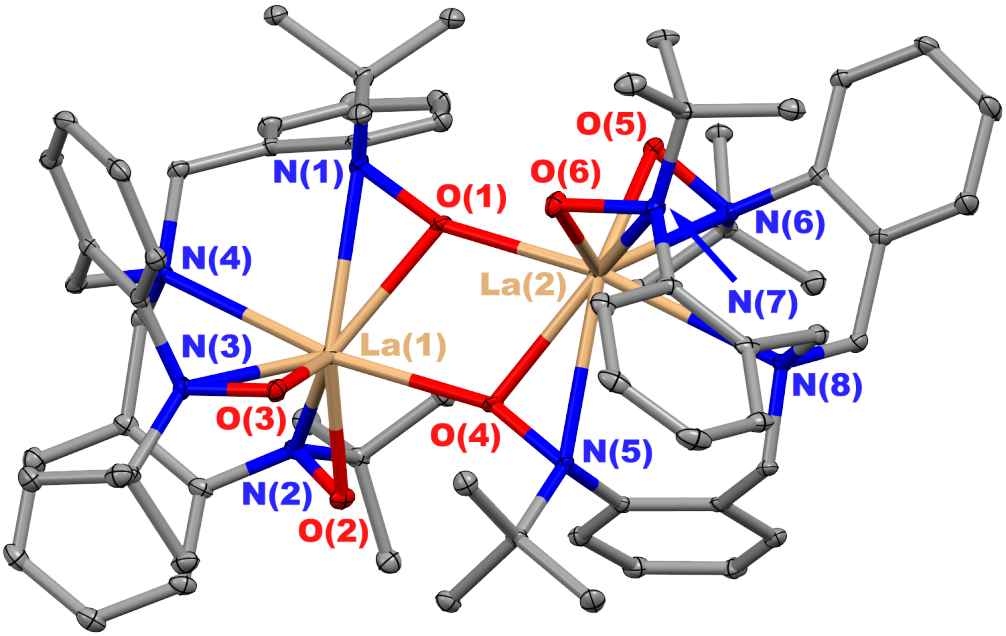

Figure 4.4.43. Thermal ellipsoid plot of **4.2-La** at 30% probability. Hydrogen atoms excluded for clarity.

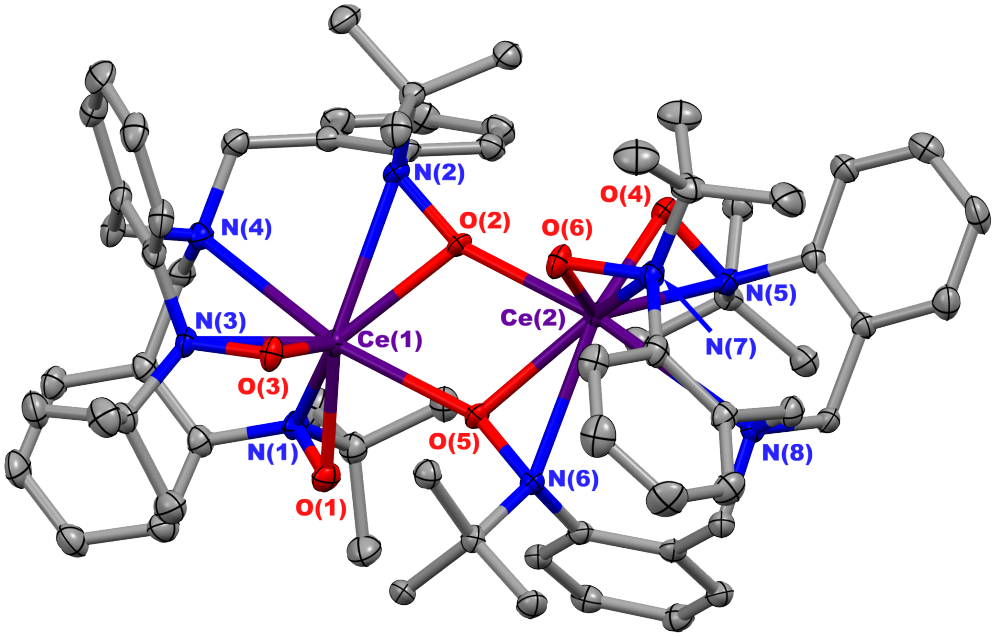

Figure 4.4.44. Thermal ellipsoid plot of **4.2-Ce** at 30% probability. Hydrogen atoms excluded for clarity.

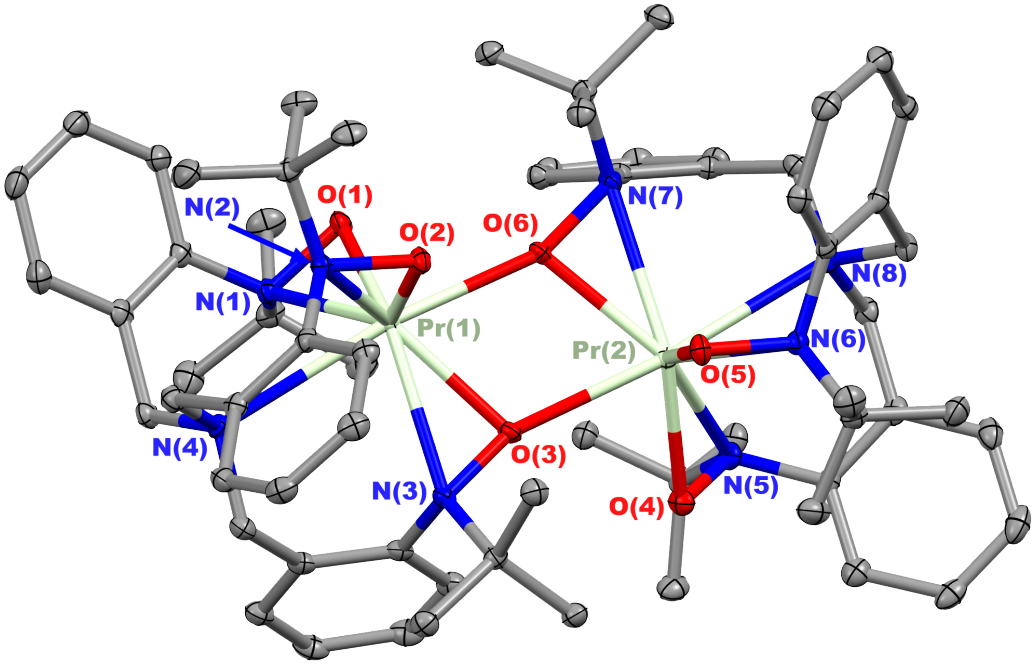

Figure 4.4.45. Thermal ellipsoid plot of **4.2-Pr** at 30% probability. Hydrogen atoms excluded for clarity.

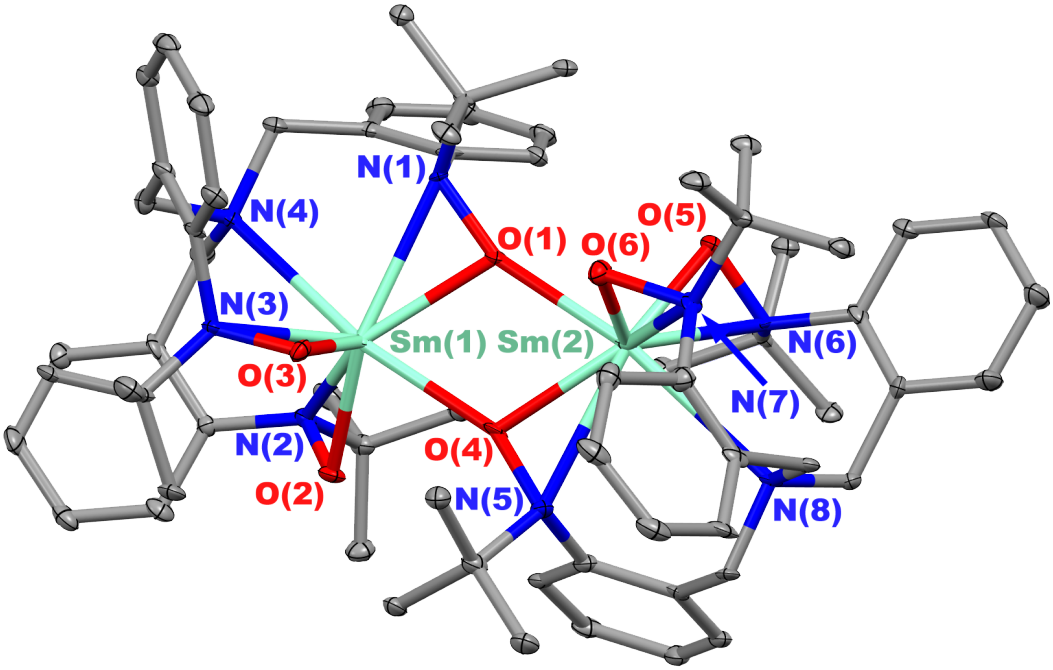

Figure 4.4.46. Thermal ellipsoid plot of **4.2-Sm** at 30% probability. Hydrogen atoms excluded for clarity.

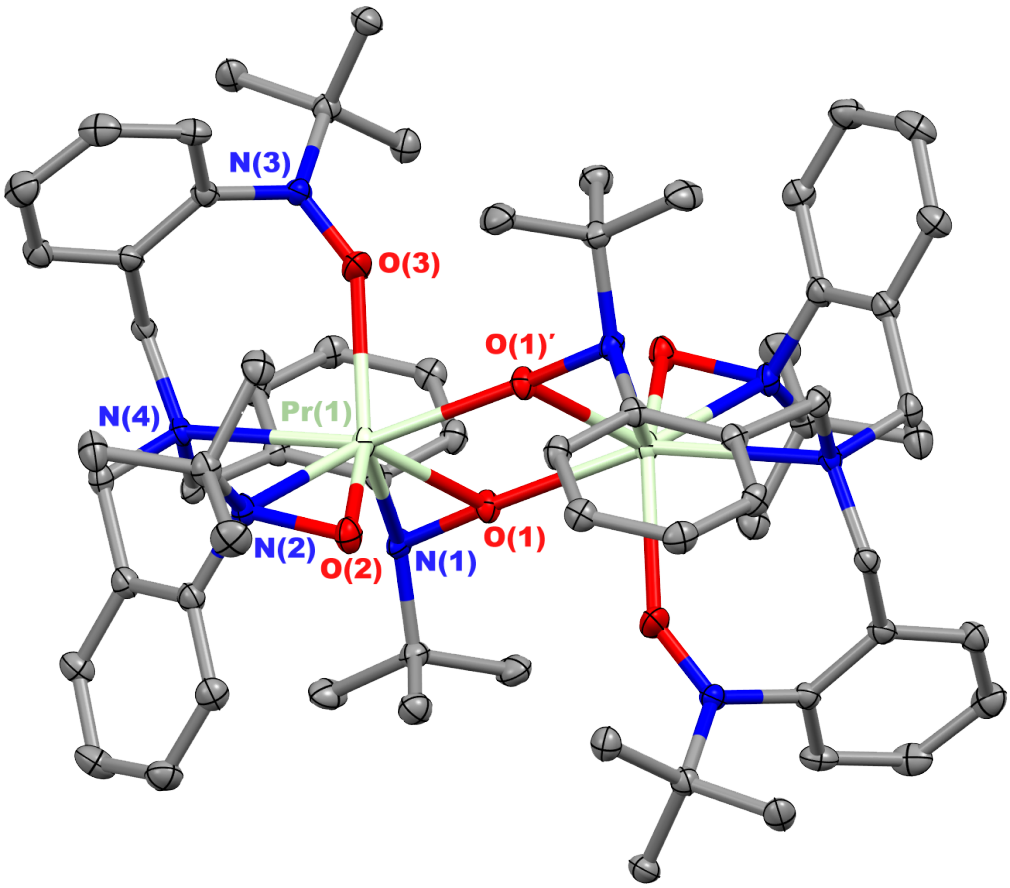

Figure 4.4.47. Thermal ellipsoid plot of **4.3-Pr** at 30% probability. Hydrogen atoms excluded for clarity.

Table 4.4.1. Structural metrics for the series of **4.1-RE** complexes.

	N–O	RE–$O_{nitroxide}$	RE–$N_{nitroxide}$	RE–O_{THF}
4.1-La	1.441(2)	2.3219(16)	2.6022(17)	2.595(6)
4.1-Ce	1.433(2)	2.2921(18)	2.581(2)	2.577(6)
4.1-Pr	1.424(3)	2.270(2)	2.569(3)	2.573(8)
4.1-Nd	1.420(4)	2.260(3)	2.554(4)	2.546(9)
4.1-Sm	1.429(3)	2.236(3)	2.547(3)	2.545(10)
4.1-Eu	1.438(2)	2.2270(16)	2.5266(19)	2.506(5)
4.1-Gd	1.437(4)	2.220(3)	2.529(4)	2.530(10)
4.1-Tb	1.444(2)	2.2054(18)	2.514(2)	2.501(6)
4.1-Dy	1.424(4)	2.180(3)	2.508(3)	2.487(10)
4.1-Y	1.4429(17)	2.1784(13)	2.4966(15)	2.469(3)
4.1-Ho	1.433(5)	2.189(4)	2.506(5)	2.509(10)
4.1-Er	1.439(4)	2.162(3)	2.487(4)	2.484(10)
4.1-Tm	1.446(5)	2.151(4)	2.483(6)	2.477(11)
4.1-Yb	1.441(5)	2.151(4)	2.474(5)	2.447(7)
4.1-Lu	1.452(4)	2.134(4)	2.480(5)	2.428(8)

Table 4.4.2. Crystallographic parameters for H_3TriNOx.

	H_3TriNOx (Penn4438)
Empirical formula	$C_{34}H_{50}N_4O_3Cl_2$
Formula weight	633.68
Temperature	100(1) K
Wavelength	0.71073 Å
Crystal system	triclinic
Space group	$P\bar{1}$
Cell constants:	
a	9.9758(9) Å
b	12.0528(11) Å
c	14.9731(14) Å
α	86.976(5)°
β	88.293(5)°
γ	70.262(4)°
Volume	1692.0(3) $Å^3$
Z	2
Density (calculated)	1.244 Mg/m^3
Absorption coefficient	0.231 mm^{-1}
F(000)	680
Crystal size	0.25 x 0.20 x 0.18 mm^3
Theta range for data collection	1.80 to 27.62°
Index ranges	$-12 \leq h \leq 12$, $-15 \leq k \leq 15$, $-19 \leq l \leq 19$
Reflections collected	55592
Independent reflections	7769 [R(int) = 0.0253]
Completeness to theta = 27.62°	98.9 %
Absorption correction	Semi-empirical from equivalents
Max. and min. transmission	0.7456 and 0.6815
Refinement method	Full-matrix least-squares on F^2
Data / restraints / parameters	7769 / 0 / 383
Goodness-of-fit on F^2	1.044
Final R indices [I>2sigma(I)]	R1 = 0.0503, wR2 = 0.1341
R indices (all data)	R1 = 0.0545, wR2 = 0.1381
Largest diff. peak and hole	0.758 and -0.286 $e.Å^{-3}$

Table 4.4.3. Crystallographic parameters for **4.1-La**.

	4.1-La (Penn4666)
Empirical formula	$C_{37}H_{53}N_4O_4La$
Formula weight	756.74
Temperature	100(1) K
Wavelength	0.71073 Å
Crystal system	trigonal
Space group	P31c
Cell constants:	
a	13.5415(9) Å
c	12.1291(9) Å
Volume	1926.2(2) $Å^3$
Z	2
Density (calculated)	1.219 Mg/m^3
Absorption coefficient	1.554 mm^{-1}
F(000)	748
Crystal size	0.25 x 0.08 x 0.05 mm^3
Theta range for data collection	1.74 to 27.52°
Index ranges	$-17 \leq h \leq 17$, $-17 \leq k \leq 17$, $-15 \leq l \leq 15$
Reflections collected	59659
Independent reflections	2919 [R(int) = 0.0261]
Completeness to theta = 27.53°	98.6 %
Absorption correction	Semi-empirical from equivalents
Max. and min. transmission	0.7456 and 0.6203
Refinement method	Full-matrix least-squares on F^2
Data / restraints / parameters	2919 / 11 / 166
Goodness-of-fit on F^2	1.062
Final R indices [I>2sigma(I)]	R1 = 0.0217, wR2 = 0.0570
R indices (all data)	R1 = 0.0223, wR2 = 0.0574
Absolute structure parameter	0.000(4)
Largest diff. peak and hole	0.538 and -0.230 $e.Å^{-3}$

Table 4.4.4. Crystallographic parameters for **4.1-Ce**.

	4.1-Ce (Penn4443)
Empirical formula	$C_{37}H_{53}N_4O_4Ce$
Formula weight	757.95
Temperature	100(1) K
Wavelength	0.71073 Å
Crystal system	trigonal
Space group	P31c
Cell constants:	
a	13.5691(6) Å
c	12.1861(6) Å
Volume	1943.11(15) $Å^3$
Z	2
Density (calculated)	1.295 Mg/m^3
Absorption coefficient	1.211 mm^{-1}
F(000)	786
Crystal size	0.48 x 0.15 x 0.12 mm^3
Theta range for data collection	1.73 to 27.52°
Index ranges	$-17 \leq h \leq 17$, $-17 \leq k \leq 17$, $-15 \leq l \leq 15$
Reflections collected	76575
Independent reflections	2997 [R(int) = 0.0189]
Completeness to theta = 27.52°	99.9 %
Absorption correction	Semi-empirical from equivalents
Max. and min. transmission	0.7456 and 0.6616
Refinement method	Full-matrix least-squares on F^2
Data / restraints / parameters	2997 / 25 / 158
Goodness-of-fit on F^2	1.104
Final R indices [I>2sigma(I)]	R1 = 0.0160, wR2 = 0.0398
R indices (all data)	R1 = 0.0162, wR2 = 0.0399
Absolute structure parameter	0.007(11)
Largest diff. peak and hole	0.577 and -0.316 $e.Å^{-3}$

Table 4.4.5. Crystallographic parameters for **4.1-Pr**.

	4.1-Pr (Penn4454)
Empirical formula	$C_{37}H_{53}N_4O_4Pr$
Formula weight	758.74
Temperature	100(1) K
Wavelength	0.71073 Å
Crystal system	trigonal
Space group	P31c
Cell constants:	
a	13.5633(9) Å
c	12.1677(8) Å
Volume	1938.5(2) $Å^3$
Z	2
Density (calculated)	1.300 Mg/m^3
Absorption coefficient	1.297 mm^{-1}
F(000)	788
Crystal size	0.50 x 0.12 x 0.12 mm^3
Theta range for data collection	1.73 to 27.54°
Index ranges	$-17 \leq h \leq 17$, $-17 \leq k \leq 17$, $-15 \leq l \leq 15$
Reflections collected	91489
Independent reflections	2992 [R(int) = 0.0189]
Completeness to theta = 27.54°	100.0 %
Absorption correction	Semi-empirical from equivalents
Max. and min. transmission	0.7456 and 0.6683
Refinement method	Full-matrix least-squares on F^2
Data / restraints / parameters	2992 / 25 / 158
Goodness-of-fit on F^2	1.080
Final R indices [I>2sigma(I)]	R1 = 0.0200, wR2 = 0.0512
R indices (all data)	R1 = 0.0203, wR2 = 0.0515
Absolute structure parameter	-0.002(15)
Largest diff. peak and hole	0.448 and -0.257 $e.Å^{-3}$

Table 4.4.6. Crystallographic parameters for **4.1-Nd**.

	4.1-Nd (Penn4667)
Empirical formula	$C_{37}H_{53}N_4O_4Nd$
Formula weight	762.07
Temperature	100(1) K
Wavelength	0.71073 Å
Crystal system	trigonal
Space group	P31c
Cell constants:	
a	13.5638(4) Å
c	12.1731(4) Å
Volume	1939.52(10) $Å^3$
Z	2
Density (calculated)	1.305 Mg/m^3
Absorption coefficient	1.378 mm^{-1}
F(000)	790
Crystal size	0.40 x 0.22 x 0.12 mm^3
Theta range for data collection	1.73 to 27.56°
Index ranges	$-17 \leq h \leq 17$, $-17 \leq k \leq 17$, $-15 \leq l \leq 15$
Reflections collected	62102
Independent reflections	2995 [R(int) = 0.0202]
Completeness to theta = 27.56°	99.9 %
Absorption correction	Semi-empirical from equivalents
Max. and min. transmission	0.7456 and 0.6681
Refinement method	Full-matrix least-squares on F^2
Data / restraints / parameters	2995 / 32 / 167
Goodness-of-fit on F^2	0.423
Final R indices [I>2sigma(I)]	R1 = 0.0213, wR2 = 0.0558
R indices (all data)	R1 = 0.0215, wR2 = 0.0562
Absolute structure parameter	0.14(2)
Largest diff. peak and hole	0.577 and -0.448 $e.Å^{-3}$

Table 4.4.7. Crystallographic parameters for **4.1-Sm**.

	4.1-Sm (Penn4626)
Empirical formula	$C_{37}H_{53}N_4O_4Sm$
Formula weight	768.18
Temperature	100(1) K
Wavelength	0.71073 Å
Crystal system	trigonal
Space group	P31c
Cell constants:	
a	13.5786(7) Å
c	12.1673(7) Å
Volume	1942.83(18) $Å^3$
Z	2
Density (calculated)	1.313 Mg/m^3
Absorption coefficient	1.551 mm^{-1}
F(000)	794
Crystal size	0.38 x 0.12 x 0.12 mm^3
Theta range for data collection	1.73 to 25.30°
Index ranges	$-16 \leq h \leq 16$, $-16 \leq k \leq 16$, $-14 \leq l \leq 14$
Reflections collected	27031
Independent reflections	2367 [R(int) = 0.0165]
Completeness to theta = 25.30°	100.0 %
Absorption correction	Semi-empirical from equivalents
Max. and min. transmission	0.7452 and 0.6373
Refinement method	Full-matrix least-squares on F^2
Data / restraints / parameters	2367 / 48 / 158
Goodness-of-fit on F^2	1.075
Final R indices [I>2sigma(I)]	R1 = 0.0186, wR2 = 0.0518
R indices (all data)	R1 = 0.0187, wR2 = 0.0519
Absolute structure parameter	0.048(15)
Largest diff. peak and hole	0.332 and -0.219 $e.Å^{-3}$

Table 4.4.8. Crystallographic parameters for **4.1-Eu**.

	4.1-Eu (Penn4761)
Empirical formula	$C_{37}H_{53}N_4O_4Ho$
Formula weight	769.79
Temperature	100(1) K
Wavelength	0.71073 Å
Crystal system	trigonal
Space group	P31c
Cell constants:	
a	13.5447(7) Å
c	12.1381(6) Å
Volume	1928.50(17) $Å^3$
Z	2
Density (calculated)	1.326 Mg/m^3
Absorption coefficient	1.666 mm^{-1}
F(000)	796
Crystal size	0.25 x 0.25 x 0.12 mm^3
Theta range for data collection	2.41 to 27.61°
Index ranges	$-17 \leq h \leq 17$, $-17 \leq k \leq 17$, $-15 \leq l \leq 15$
Reflections collected	28355
Independent reflections	2984 [R(int) = 0.0205]
Completeness to theta = 27.61°	99.7 %
Absorption correction	Semi-empirical from equivalents
Max. and min. transmission	0.7456 and 0.6740
Refinement method	Full-matrix least-squares on F^2
Data / restraints / parameters	2984 / 51 / 158
Goodness-of-fit on F^2	1.112
Final R indices [I>2sigma(I)]	R1 = 0.0140, wR2 = 0.0364
R indices (all data)	R1 = 0.0142, wR2 = 0.0366
Absolute structure parameter	-0.011(9)
Largest diff. peak and hole	0.495 and -0.195 $e.Å^{-3}$

Table 4.4.9. Crystallographic parameters for **4.1-Gd**.

	4.1-Gd (Penn4757)
Empirical formula	$C_{37}H_{53}N_4O_4Gd$
Formula weight	775.08
Temperature	100(1) K
Wavelength	0.71073 Å
Crystal system	trigonal
Space group	P31c
Cell constants:	
a	13.5075(2) Å
c	12.1309(2) Å
Volume	1916.79(5) $Å^3$
Z	2
Density (calculated)	1.343 Mg/m^3
Absorption coefficient	1.770 mm^{-1}
F(000)	798
Crystal size	0.32 x 0.15 x 0.12 mm^3
Theta range for data collection	1.74 to 27.53°
Index ranges	$-17 \leq h \leq 17$, $-17 \leq k \leq 16$, $-15 \leq l \leq 15$
Reflections collected	51286
Independent reflections	2960 [R(int) = 0.0191]
Completeness to theta = 27.53°	100.0 %
Absorption correction	Semi-empirical from equivalents
Max. and min. transmission	0.7456 and 0.6591
Refinement method	Full-matrix least-squares on F^2
Data / restraints / parameters	2960 / 51 / 153
Goodness-of-fit on F^2	1.109
Final R indices [I>2sigma(I)]	R1 = 0.0213, wR2 = 0.0558
R indices (all data)	R1 = 0.0214, wR2 = 0.0560
Absolute structure parameter	-0.021(19)
Largest diff. peak and hole	0.682 and -0.580 $e.Å^{-3}$

Table 4.4.10. Crystallographic parameters for **4.1-Tb**.

	4.1-Tb (Penn4568)
Empirical formula	$C_{37}H_{53}N_4O_4Tb$
Formula weight	776.75
Temperature	100(1) K
Wavelength	0.71073 Å
Crystal system	trigonal
Space group	P31c
Cell constants:	
a	13.5633(3) Å
c	12.1442(3) Å
Volume	1934.77(8) $Å^3$
Z	2
Density (calculated)	1.333 Mg/m^3
Absorption coefficient	1.868 mm^{-1}
F(000)	800
Crystal size	0.42 x 0.10 x 0.10 mm^3
Theta range for data collection	1.73 to 27.49°
Index ranges	$-17 \leq h \leq 17$, $-17 \leq k \leq 17$, $-15 \leq l \leq 15$
Reflections collected	21447
Independent reflections	2974 [R(int) = 0.0161]
Completeness to theta = 27.49°	99.9 %
Absorption correction	Semi-empirical from equivalents
Max. and min. transmission	0.7456 and 0.6085
Refinement method	Full-matrix least-squares on F^2
Data / restraints / parameters	2974 / 48 / 158
Goodness-of-fit on F^2	1.101
Final R indices [I>2sigma(I)]	R1 = 0.0146, wR2 = 0.0372
R indices (all data)	R1 = 0.0154, wR2 = 0.0375
Absolute structure parameter	-0.023(9)
Largest diff. peak and hole	0.678 and -0.221 $e.Å^{-3}$

Table 4.4.11. Crystallographic parameters for **4.1-Dy**.

	4.1-Dy (Penn4621)
Empirical formula	$C_{37}H_{53}N_4O_4Dy$
Formula weight	780.33
Temperature	100(1) K
Wavelength	0.71073 Å
Crystal system	trigonal
Space group	P31c
Cell constants:	
a	13.5645(4) Å
c	12.1276(4) Å
Volume	1932.47(10) $Å^3$
Z	2
Density (calculated)	1.341 Mg/m^3
Absorption coefficient	1.973 mm^{-1}
F(000)	802
Crystal size	0.38 x 0.08 x 0.06 mm^3
Theta range for data collection	1.73 to 27.50°
Index ranges	$-17 \leq h \leq 17$, $-17 \leq k \leq 17$, $-15 \leq l \leq 15$
Reflections collected	31171
Independent reflections	2985 [R(int) = 0.0218]
Completeness to theta = 27.50°	100.0 %
Absorption correction	Semi-empirical from equivalents
Max. and min. transmission	0.7456 and 0.6063
Refinement method	Full-matrix least-squares on F^2
Data / restraints / parameters	2985 / 48 / 158
Goodness-of-fit on F^2	0.678
Final R indices [I>2sigma(I)]	R1 = 0.0226, wR2 = 0.0685
R indices (all data)	R1 = 0.0230, wR2 = 0.0690
Absolute structure parameter	0.024(16)
Largest diff. peak and hole	0.532 and -0.375 $e.Å^{-3}$

Table 4.4.12. Crystallographic parameters for **4.1-Y**.

	4.1-Y (Penn4663)
Empirical formula	$C_{37}H_{53}N_4O_4Y$
Formula weight	706.74
Temperature	100(1) K
Wavelength	0.71073 Å
Crystal system	trigonal
Space group	P31c
Cell constants:	
a	13.5415(9) Å
c	12.1291(9) Å
Volume	1926.2(2) $Å^3$
Z	2
Density (calculated)	1.219 Mg/m^3
Absorption coefficient	1.554 mm^{-1}
F(000)	748
Crystal size	0.25 x 0.08 x 0.05 mm^3
Theta range for data collection	1.74 to 27.52°
Index ranges	$-17 \leq h \leq 17$, $-17 \leq k \leq 17$, $-15 \leq l \leq 15$
Reflections collected	59659
Independent reflections	2919 [R(int) = 0.0261]
Completeness to theta = 27.52°	99.9 %
Absorption correction	Semi-empirical from equivalents
Max. and min. transmission	0.7456 and 0.6203
Refinement method	Full-matrix least-squares on F^2
Data / restraints / parameters	2919 / 11 / 166
Goodness-of-fit on F^2	1.085
Final R indices [I>2sigma(I)]	R1 = 0.0217, wR2 = 0.0570
R indices (all data)	R1 = 0.0223, wR2 = 0.0574
Absolute structure parameter	0.000(4)
Largest diff. peak and hole	0.329 and -0.205 $e.Å^{-3}$

Table 4.4.13. Crystallographic parameters for **4.1-Ho**.

	4.1-Ho (Penn4756)
Empirical formula	$C_{37}H_{53}N_4O_4Ho$
Formula weight	782.76
Temperature	100(1) K
Wavelength	0.71073 Å
Crystal system	trigonal
Space group	P31c
Cell constants:	
a	13.5786(5) Å
c	12.1673(5) Å
Volume	1942.83(13) $Å^3$
Z	2
Density (calculated)	1.338 Mg/m^3
Absorption coefficient	2.076 mm^{-1}
F(000)	804
Crystal size	0.45 x 0.20 x 0.12 mm^3
Theta range for data collection	1.73 to 27.37°
Index ranges	$-17 \leq h \leq 17$, $-17 \leq k \leq 17$, $-15 \leq l \leq 15$
Reflections collected	50421
Independent reflections	2944 [R(int) = 0.0157]
Completeness to theta = 27.37°	99.9 %
Absorption correction	Semi-empirical from equivalents
Max. and min. transmission	0.7456 and 0.6192
Refinement method	Full-matrix least-squares on F^2
Data / restraints / parameters	2944 / 51 / 153
Goodness-of-fit on F^2	1.137
Final R indices [I>2sigma(I)]	R1 = 0.0210, wR2 = 0.0540
R indices (all data)	R1 = 0.0211, wR2 = 0.0541
Absolute structure parameter	-0.042(18)
Largest diff. peak and hole	0.821 and -0.599 $e.Å^{-3}$

Table 4.4.14. Crystallographic parameters for **4.1-Er**.

	4.1-Er (Penn4760)
Empirical formula	$C_{37}H_{53}N_4O_4Er$
Formula weight	785.09
Temperature	100(1) K
Wavelength	0.71073 Å
Crystal system	trigonal
Space group	P31c
Cell constants:	
a	13.5144(3) Å
c	12.1058(3) Å
Volume	1914.77(8) $Å^3$
Z	2
Density (calculated)	1.362 Mg/m^3
Absorption coefficient	2.232 mm^{-1}
F(000)	806
Crystal size	0.38 x 0.18 x 0.18 mm^3
Theta range for data collection	1.74 to 27.52°
Index ranges	$-17 \leq h \leq 17$, $-17 \leq k \leq 17$, $-15 \leq l \leq 15$
Reflections collected	33208
Independent reflections	2937 [R(int) = 0.0181]
Completeness to theta = 27.52°	99.7 %
Absorption correction	Semi-empirical from equivalents
Max. and min. transmission	0.7456 and 0.5747
Refinement method	Full-matrix least-squares on F^2
Data / restraints / parameters	2937 / 51 / 159
Goodness-of-fit on F^2	0.677
Final R indices [I>2sigma(I)]	R1 = 0.0192, wR2 = 0.0597
R indices (all data)	R1 = 0.0194, wR2 = 0.0606
Absolute structure parameter	-0.019(18)
Largest diff. peak and hole	0.688 and -0.413 $e.Å^{-3}$

Table 4.4.15. Crystallographic parameters for **4.1-Tm**.

	4.1-Tm (Penn4785)
Empirical formula	$C_{37}H_{53}N_4O_4Tm$
Formula weight	786.76
Temperature	100(1) K
Wavelength	0.71073 Å
Crystal system	trigonal
Space group	P31c
Cell constants:	
a	13.5226(3) Å
c	12.0726(3) Å
Volume	1911.84(8) $Å^3$
Z	2
Density (calculated)	1.367 Mg/m^3
Absorption coefficient	2.361 mm^{-1}
F(000)	808
Crystal size	0.18 x 0.02 x 0.02 mm^3
Theta range for data collection	2.42 to 27.51°
Index ranges	$-17 \leq h \leq 17$, $-17 \leq k \leq 17$, $-15 \leq l \leq 15$
Reflections collected	29411
Independent reflections	2937 [R(int) = 0.0435]
Completeness to theta = 27.51°	99.9 %
Absorption correction	Semi-empirical from equivalents
Max. and min. transmission	0.7456 and 0.6572
Refinement method	Full-matrix least-squares on F^2
Data / restraints / parameters	2937 / 11 / 153
Goodness-of-fit on F^2	1.071
Final R indices [I>2sigma(I)]	R1 = 0.0217, wR2 = 0.0548
R indices (all data)	R1 = 0.0246, wR2 = 0.0556
Absolute structure parameter	0.146(17)
Largest diff. peak and hole	0.848 and -0.483 $e.Å^{-3}$

Table 4.4.16. Crystallographic parameters for **4.1-Yb**.

	4.1-Yb (Penn4787)
Empirical formula	$C_{37}H_{53}N_4O_4Yb$
Formula weight	790.87
Temperature	100(1) K
Wavelength	0.71073 Å
Crystal system	trigonal
Space group	P31c
Cell constants:	
a	13.5366(6) Å
c	12.0766(6) Å
Volume	1916.44(15) $Å^3$
Z	2
Density (calculated)	1.371 Mg/m^3
Absorption coefficient	2.480 mm^{-1}
F(000)	810
Crystal size	0.25 x 0.02 x 0.01 mm^3
Theta range for data collection	2.42 to 27.52°
Index ranges	$-17 \leq h \leq 17$, $-16 \leq k \leq 17$, $-15 \leq l \leq 15$
Reflections collected	39936
Independent reflections	2952 [R(int) = 0.0343]
Completeness to theta = 27.52°	99.9 %
Absorption correction	Semi-empirical from equivalents
Max. and min. transmission	0.7456 and 0.6445
Refinement method	Full-matrix least-squares on F^2
Data / restraints / parameters	2952 / 18 / 159
Goodness-of-fit on F^2	1.092
Final R indices [I>2sigma(I)]	R1 = 0.0197, wR2 = 0.0517
R indices (all data)	R1 = 0.0215, wR2 = 0.0524
Absolute structure parameter	-0.018(16)
Largest diff. peak and hole	0.824 and -0.445 $e.Å^{-3}$

Table 4.4.17. Crystallographic parameters for **4.1-Lu**.

	4.1-Lu (Penn4784)
Empirical formula	$C_{37}H_{53}N_4O_4Lu$
Formula weight	792.80
Temperature	100(1) K
Wavelength	0.71073 Å
Crystal system	trigonal
Space group	P31c
Cell constants:	
a	13.5458(4) Å
c	12.0507(4) Å
Volume	1914.93(10) $Å^3$
Z	2
Density (calculated)	1.375 Mg/m^3
Absorption coefficient	2.618 mm^{-1}
F(000)	812
Crystal size	0.28 x 0.03 x 0.02 mm^3
Theta range for data collection	2.42 to 27.53°
Index ranges	$-17 \leq h \leq 17$, $-17 \leq k \leq 17$, $-15 \leq l \leq 15$
Reflections collected	26436
Independent reflections	2955 [R(int) = 0.0493]
Completeness to theta = 27.53°	99.9 %
Absorption correction	Semi-empirical from equivalents
Max. and min. transmission	0.7456 and 0.6234
Refinement method	Full-matrix least-squares on F^2
Data / restraints / parameters	2955 / 28 / 159
Goodness-of-fit on F^2	1.054
Final R indices [I>2sigma(I)]	R1 = 0.0228, wR2 = 0.0539
R indices (all data)	R1 = 0.0272, wR2 = 0.0550
Absolute structure parameter	0.008(14)
Largest diff. peak and hole	0.748 and -0.346 $e.Å^{-3}$

Table 4.4.18. Crystallographic parameters for **4.2-La**.

	4.2-La (Penn4665)
Empirical formula	$C_{80}H_{106}N_8O_6La_2$
Formula weight	1553.55
Temperature	100(1) K
Wavelength	0.71073 Å
Crystal system	monoclinic
Space group	$P2_1/c$
Cell constants:	
a	18.0557(7) Å
b	14.3002(6) Å
c	28.5121(11) Å
β	94.636(2)°
Volume	7337.7(5) $Å^3$
Z	4
Density (calculated)	1.406 Mg/m^3
Absorption coefficient	1.207 mm^{-1}
F(000)	3216
Crystal size	0.18 x 0.08 x 0.02 mm^3
Theta range for data collection	1.43 to 27.56°
Index ranges	$-23 \leq h \leq 23$, $-18 \leq k \leq 18$, $-37 \leq l \leq 37$
Reflections collected	204284
Independent reflections	16935 [R(int) = 0.0860]
Completeness to theta = 27.56°	99.9 %
Absorption correction	Semi-empirical from equivalents
Max. and min. transmission	0.7456 and 0.5602
Refinement method	Full-matrix least-squares on F^2
Data / restraints / parameters	16935 / 0 / 886
Goodness-of-fit on F^2	1.189
Final R indices [I>2sigma(I)]	R1 = 0.0397, wR2 = 0.0819
R indices (all data)	R1 = 0.0580, wR2 = 0.0878
Largest diff. peak and hole	1.995 and -1.141 $e.Å^{-3}$

Table 4.4.19. Crystallographic parameters for **4.2-Ce**.

	4.2-Ce (Penn4522)
Empirical formula	$C_{74}H_{110}N_8O_8Ce_2$
Formula weight	1519.94
Temperature	100(1) K
Wavelength	0.71073 Å
Crystal system	orthorhombic
Space group	Pbca
Cell constants:	
a	17.6437(7) Å
b	30.2224(12) Å
c	30.4738(11) Å
Volume	16249.7(11) $Å^3$
Z	8
Density (calculated)	1.243 Mg/m^3
Absorption coefficient	1.159 mm^{-1}
F(000)	6320
Crystal size	0.28 x 0.08 x 0.03 mm^3
Theta range for data collection	1.35 to 27.56°
Index ranges	$-22 \leq h \leq 22$, $-39 \leq k \leq 39$, $-39 \leq l \leq 39$
Reflections collected	654133
Independent reflections	18732 [R(int) = 0.0846]
Completeness to theta = 27.56°	99.7 %
Absorption correction	Semi-empirical from equivalents
Max. and min. transmission	0.7456 and 0.6706
Refinement method	Full-matrix least-squares on F^2
Data / restraints / parameters	18732 / 31 / 848
Goodness-of-fit on F^2	1.106
Final R indices [I>2sigma(I)]	R1 = 0.0420, wR2 = 0.1117
R indices (all data)	R1 = 0.0615, wR2 = 0.1242
Largest diff. peak and hole	3.435 and -0.938 $e.Å^{-3}$

Table 4.4.20. Crystallographic parameters for **4.2-Pr**.

	4.2-Pr (Penn4474)
Empirical formula	$C_{136}H_{190}N_{16}O_{13}Pr_4$
Formula weight	2820.68
Temperature	100(1) K
Wavelength	0.71073 Å
Crystal system	triclinic
Space group	$P\bar{1}$
Cell constants:	
a	17.5928(11) Å
b	18.8257(12) Å
c	20.2448(14) Å
α	96.772(3)°
β	98.616(3)°
γ	94.047(3)°
Volume	6556.4(7) $Å^3$
Z	2
Density (calculated)	1.429 Mg/m^3
Absorption coefficient	1.526 mm^{-1}
F(000)	2916
Crystal size	0.30 x 0.25 x 0.12 mm^3
Theta range for data collection	1.53 to 27.55°
Index ranges	$-22 \leq h \leq 22$, $-24 \leq k \leq 24$, $-26 \leq l \leq 26$
Reflections collected	351879
Independent reflections	30003 [R(int) = 0.0226]
Completeness to theta = 27.55°	99.0 %
Absorption correction	Semi-empirical from equivalents
Max. and min. transmission	0.7456 and 0.6858
Refinement method	Full-matrix least-squares on F^2
Data / restraints / parameters	30003 / 0 / 1561
Goodness-of-fit on F^2	1.205
Final R indices [I>2sigma(I)]	R1 = 0.0204, wR2 = 0.0515
R indices (all data)	R1 = 0.0256, wR2 = 0.0596
Largest diff. peak and hole	0.707 and -0.688 $e.Å^{-3}$

Table 4.4.21. Crystallographic parameters for **4.2-Nd**.

	4.2-Nd (Penn4614)
Empirical formula	$C_{67}H_{92}N_8O_6Cl_2Nd_2$
Formula weight	1464.87
Temperature	100(1) K
Wavelength	0.71073 Å
Crystal system	monoclinic
Space group	C2/c
Cell constants:	
a	21.5250(11) Å
b	12.2392(7) Å
c	26.2466(19) Å
β	108.591(2)°
Volume	6553.8(7) $Å^3$
Z	4
Density (calculated)	1.485 Mg/m^3
Absorption coefficient	1.705 mm^{-1}
F(000)	3008
Crystal size	0.25 x 0.10 x 0.10 mm^3
Theta range for data collection	1.64 to 27.54°
Index ranges	$-27 \leq h \leq 27$, $-15 \leq k \leq 15$, $-34 \leq l \leq 34$
Reflections collected	101806
Independent reflections	7556 [R(int) = 0.0452]
Completeness to theta = 27.54°	99.9 %
Absorption correction	Semi-empirical from equivalents
Max. and min. transmission	0.7456 and 0.6147
Refinement method	Full-matrix least-squares on F^2
Data / restraints / parameters	7556 / 0 / 394
Goodness-of-fit on F^2	1.086
Final R indices [I>2sigma(I)]	R1 = 0.0273, wR2 = 0.0673
R indices (all data)	R1 = 0.0344, wR2 = 0.0740
Largest diff. peak and hole	1.736 and -1.697 $e.Å^{-3}$

Table 4.4.22. Crystallographic parameters for **4.2-Sm**.

	4.2-Sm (Penn4685)
Empirical formula	$C_{80}H_{106}N_8O_6Sm_2$
Formula weight	1576.43
Temperature	100(1) K
Wavelength	0.71073 Å
Crystal system	triclinic
Space group	$P\bar{1}$
Cell constants:	
a	14.1980(17) Å
b	18.021(2) Å
c	28.592(3) Å
α	83.972(6)°
β	83.821(6)°
γ	87.628(6)°
Volume	7229.5(14) $Å^3$
Z	4
Density (calculated)	1.448 Mg/m^3
Absorption coefficient	1.667 mm^{-1}
F(000)	3256
Crystal size	0.30 x 0.08 x 0.02 mm^3
Theta range for data collection	1.14 to 27.77°
Index ranges	$-18 \leq h \leq 18$, $-23 \leq k \leq 23$, $-37 \leq l \leq 37$
Reflections collected	162678
Independent reflections	32612 [R(int) = 0.1128]
Completeness to theta = 27.77°	95.4 %
Absorption correction	Semi-empirical from equivalents
Max. and min. transmission	0.7456 and 0.4790
Refinement method	Full-matrix least-squares on F^2
Data / restraints / parameters	32612 / 300 / 1670
Goodness-of-fit on F^2	1.076
Final R indices [I>2sigma(I)]	R1 = 0.0972, wR2 = 0.2300
R indices (all data)	R1 = 0.1425, wR2 = 0.2590
Largest diff. peak and hole	7.040 and -2.614 $e.Å^{-3}$

Table 4.4.23. Crystallographic parameters for **4.3-Pr**.

	4.3-Pr (Penn4786)
Empirical formula	$C_{66}BH_{59}N_4O_3F_{24}Cl_2Pr$
Formula weight	1634.79
Temperature	100(1) K
Wavelength	0.71073 Å
Crystal system	monoclinic
Space group	$P2_1/c$
Cell constants:	
a	14.6291(4) Å
b	15.1931(4) Å
c	30.9203(8) Å
β	100.474(2)°
Volume	6757.9(3) $Å^3$
Z	4
Density (calculated)	1.607 Mg/m^3
Absorption coefficient	0.916 mm^{-1}
F(000)	3284
Crystal size	0.38 x 0.08 x 0.08 mm^3
Theta range for data collection	1.42 to 27.54°
Index ranges	$-19 \leq h \leq 18$, $-19 \leq k \leq 19$, $-39 \leq l \leq 39$
Reflections collected	98028
Independent reflections	15183 [R(int) = 0.0769]
Completeness to theta = 27.54°	97.4 %
Absorption correction	Semi-empirical from equivalents
Max. and min. transmission	0.7456 and 0.5581
Refinement method	Full-matrix least-squares on F^2
Data / restraints / parameters	15183 / 48 / 942
Goodness-of-fit on F^2	1.064
Final R indices [I>2sigma(I)]	R1 = 0.0687, wR2 = 0.1659
R indices (all data)	R1 = 0.0908, wR2 = 0.1796
Largest diff. peak and hole	7.754 and -0.916 e.$Å^{-3}$

Table 4.4.24. Crystallographic parameters for **4.3-Tb**.

	4.3-Tb (Penn4758)
Empirical formula	$C_{132}B_2H_{118}N_6O_6F_{48}Cl_4Tb_2$
Formula weight	3305.60
Temperature	100(1) K
Wavelength	0.71073 Å
Crystal system	monoclinic
Space group	$P2_1/c$
Cell constants:	
a	14.6276(4) Å
b	15.1459(4) Å
c	30.7706(9) Å
β	100.851(2)°
Volume	6695.3(3) $Å^3$
Z	2
Density (calculated)	1.640 Mg/m^3
Absorption coefficient	1.253 mm^{-1}
F(000)	3308
Crystal size	0.35 x 0.05 x 0.04 mm^3
Theta range for data collection	1.35 to 27.58°
Index ranges	$-19 \leq h \leq 19$, $-19 \leq k \leq 19$, $-40 \leq l \leq 39$
Reflections collected	162493
Independent reflections	15472 [R(int) = 0.0827]
Completeness to theta = 27.58°	99.7 %
Absorption correction	Semi-empirical from equivalents
Max. and min. transmission	0.7456 and 0.6502
Refinement method	Full-matrix least-squares on F^2
Data / restraints / parameters	15472 / 48 / 947
Goodness-of-fit on F^2	1.051
Final R indices [I>2sigma(I)]	R1 = 0.0558, wR2 = 0.1299
R indices (all data)	R1 = 0.0814, wR2 = 0.1448
Largest diff. peak and hole	6.552 and -1.034 $e.Å^{-3}$

Electrochemistry. Cyclic voltammetry experiments were performed using a CH Instruments 620D Electrochemical Analyzer/Workstation and the data were processed using CHI software v 9.24. All experiments were performed in an N_2 atmosphere drybox using electrochemical cells that consisted of a 4 mL vial, glassy carbon (3 mm diameter) working electrode, a platinum wire counter electrode, and a silver wire plated with AgCl as a quasi-reference electrode. The working electrode surfaces were polished prior to each set of experiments, and were periodically replaced on scanning > 0 V versus ferrocene (Fc) to prevent the buildup of oxidized product on the electrode surfaces. Potentials were reported versus Fc, which was added as an internal standard for calibration at the end of each run. Solutions employed during CV studies were ~3 mM in analyte and 100 mM in [$^{n}Pr_4N$][B(3,5-$(CF_3)_2$-$C_6H_3)_4$] ([$^{n}Pr_4N$][BAr^{F}_4]). All complexes were measured in DCM. The THF was necessary to dissolve the complexes in solution. All data were collected in a positive-feedback IR compensation mode. The solution cell resistances were measured prior to each run to ensure resistances ≤ ~500 Ω.[28] Scan rate dependences of 50–1000 mV/s were performed to determine electrochemical reversibility.

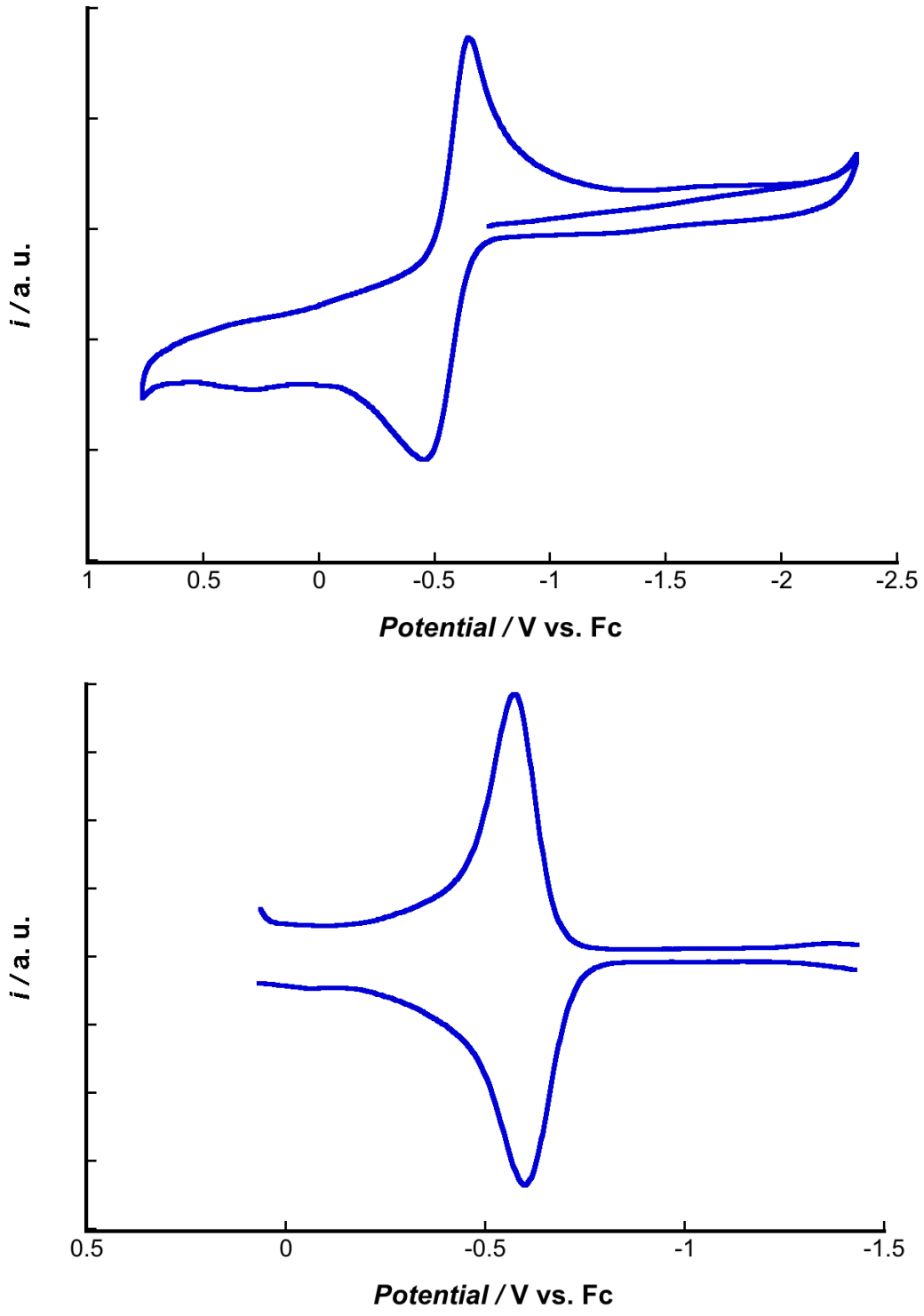

Figure 4.4.48. Cyclic voltammogram (top) and differential pulse voltammogram (bottom) of H_3TriNOx.

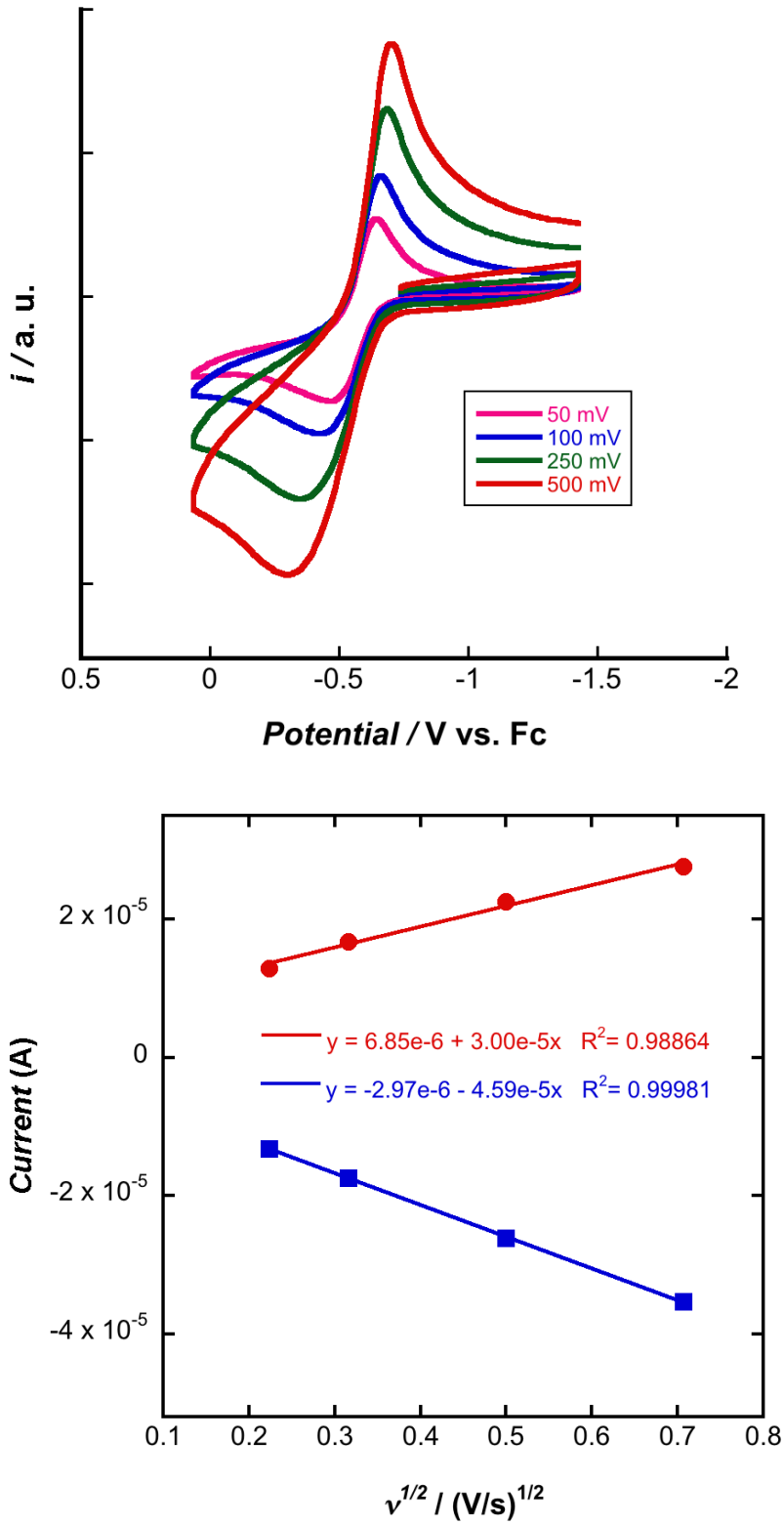

Figure 4.4.49. Scan rate dependence of the oxidation feature of H_3TriNOx.

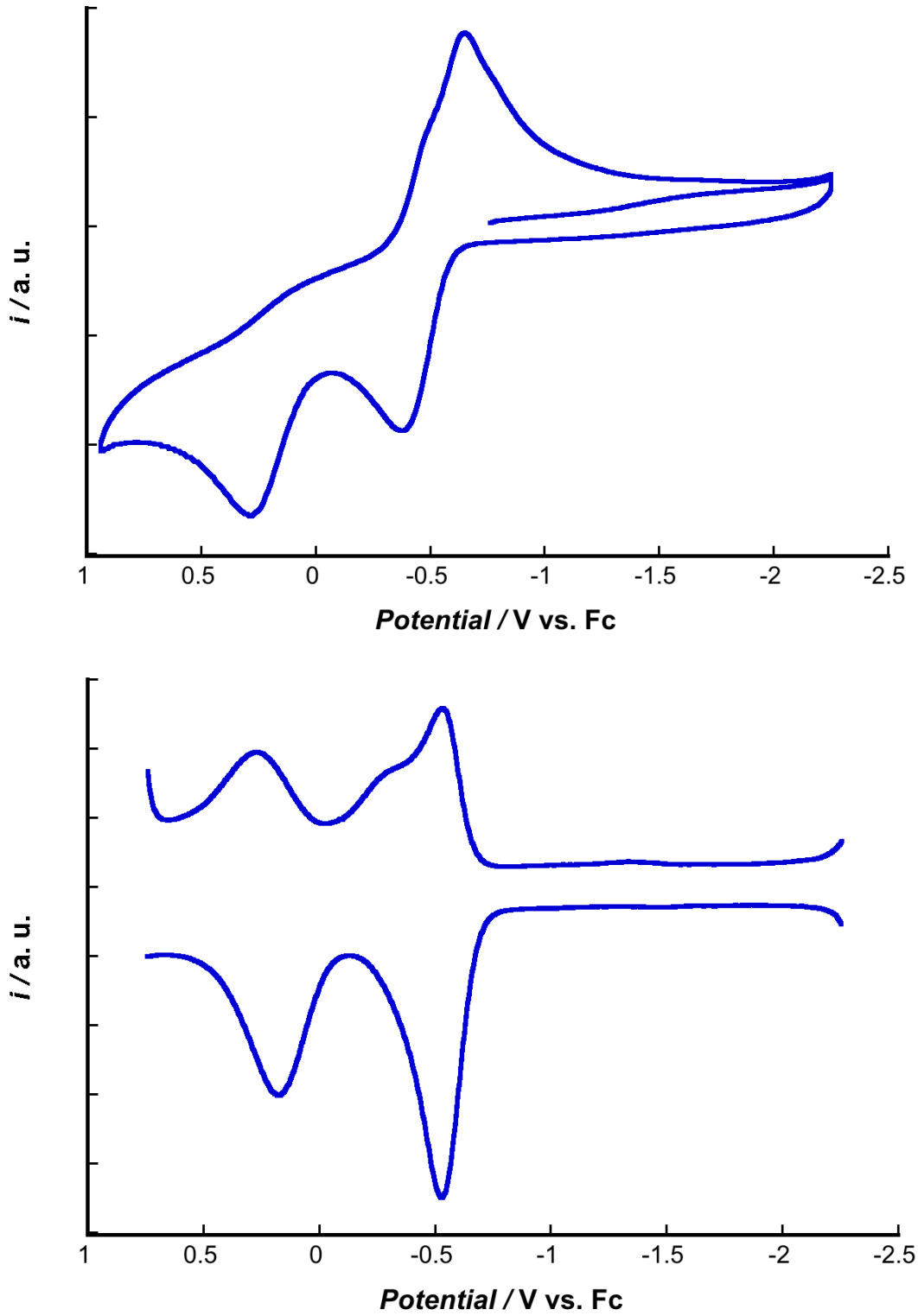

Figure 4.4.50. Cyclic voltammogram (top) and differential pulse voltammogram (bottom) of **4.1-La**.

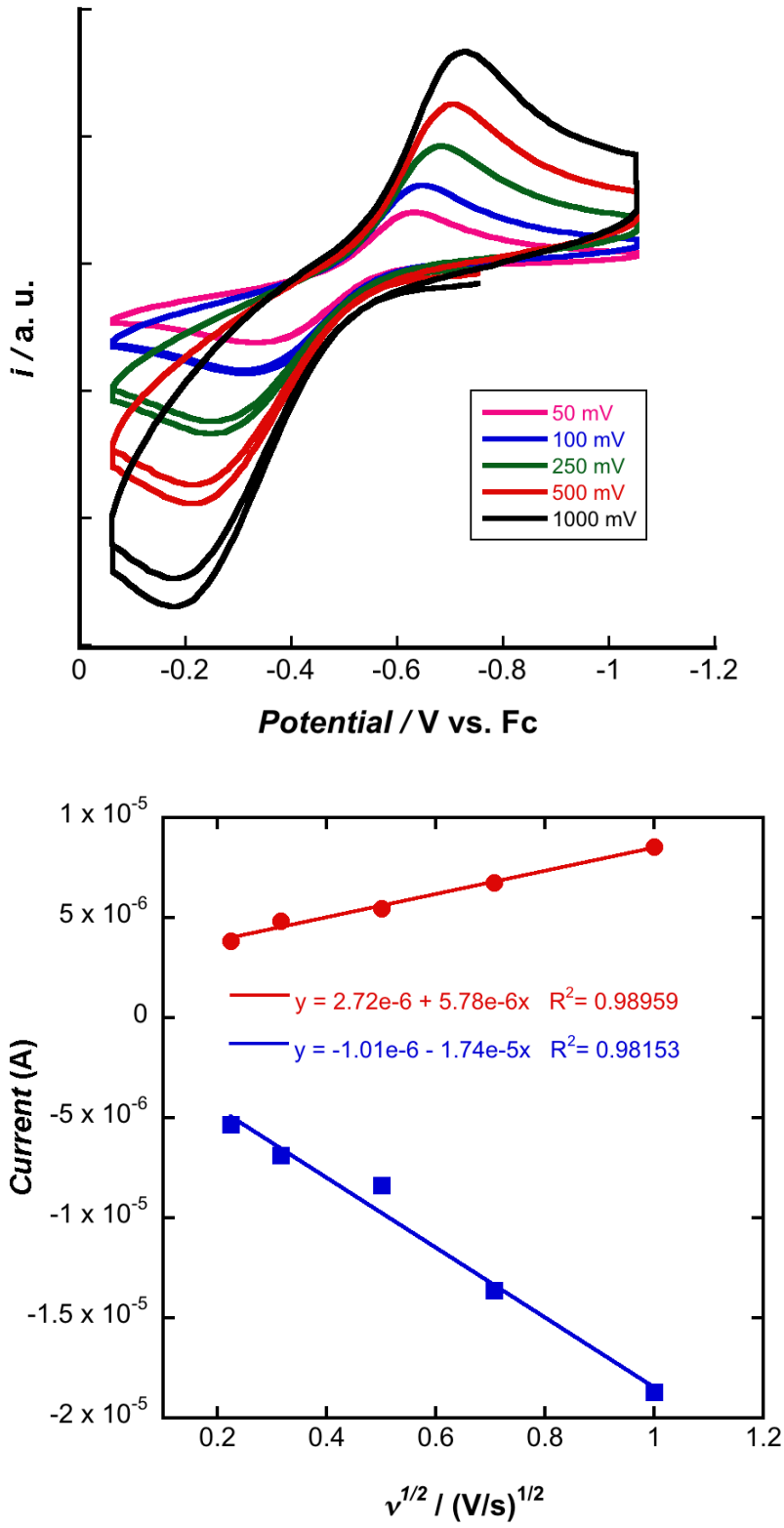

Figure 4.4.51. Scan rate dependence of the first oxidation feature of **4.1-La**.

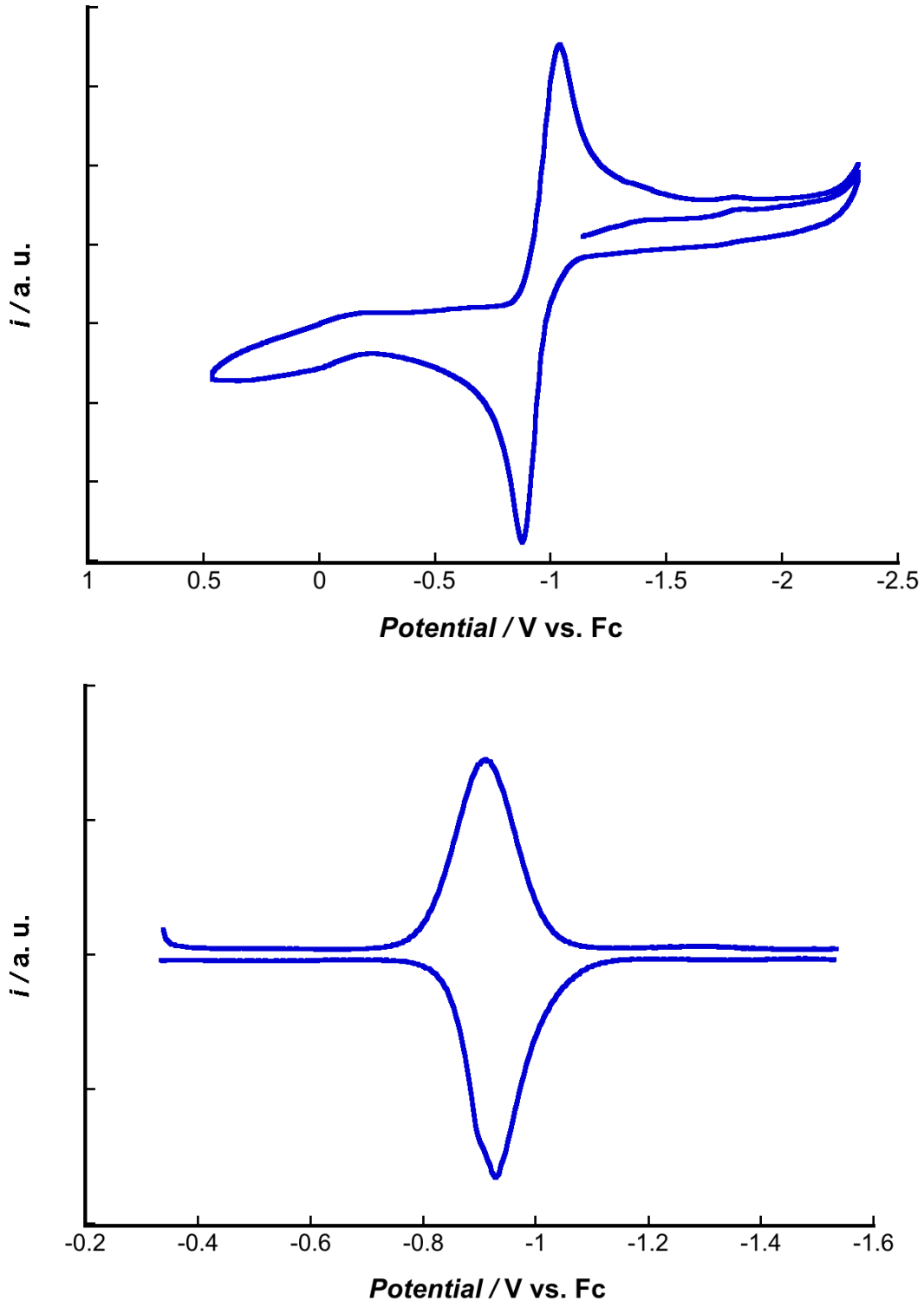

Figure 4.4.52. Cyclic voltammogram (top) and differential pulse voltammogram (bottom) of **4.1-Ce**.

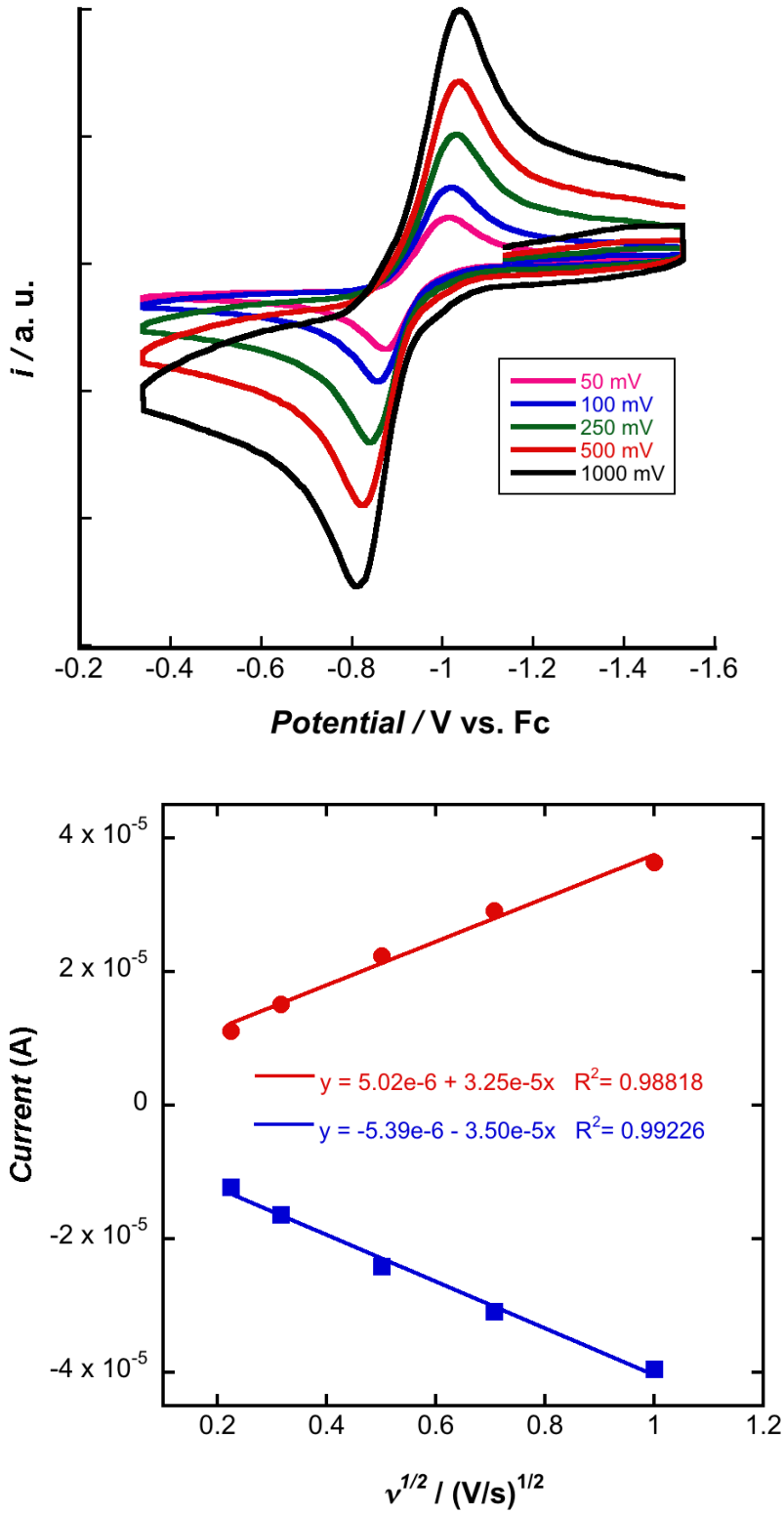

Figure 4.4.53. Scan rate dependence of the $Ce^{IV/III}$ couple of **4.1-Ce**.

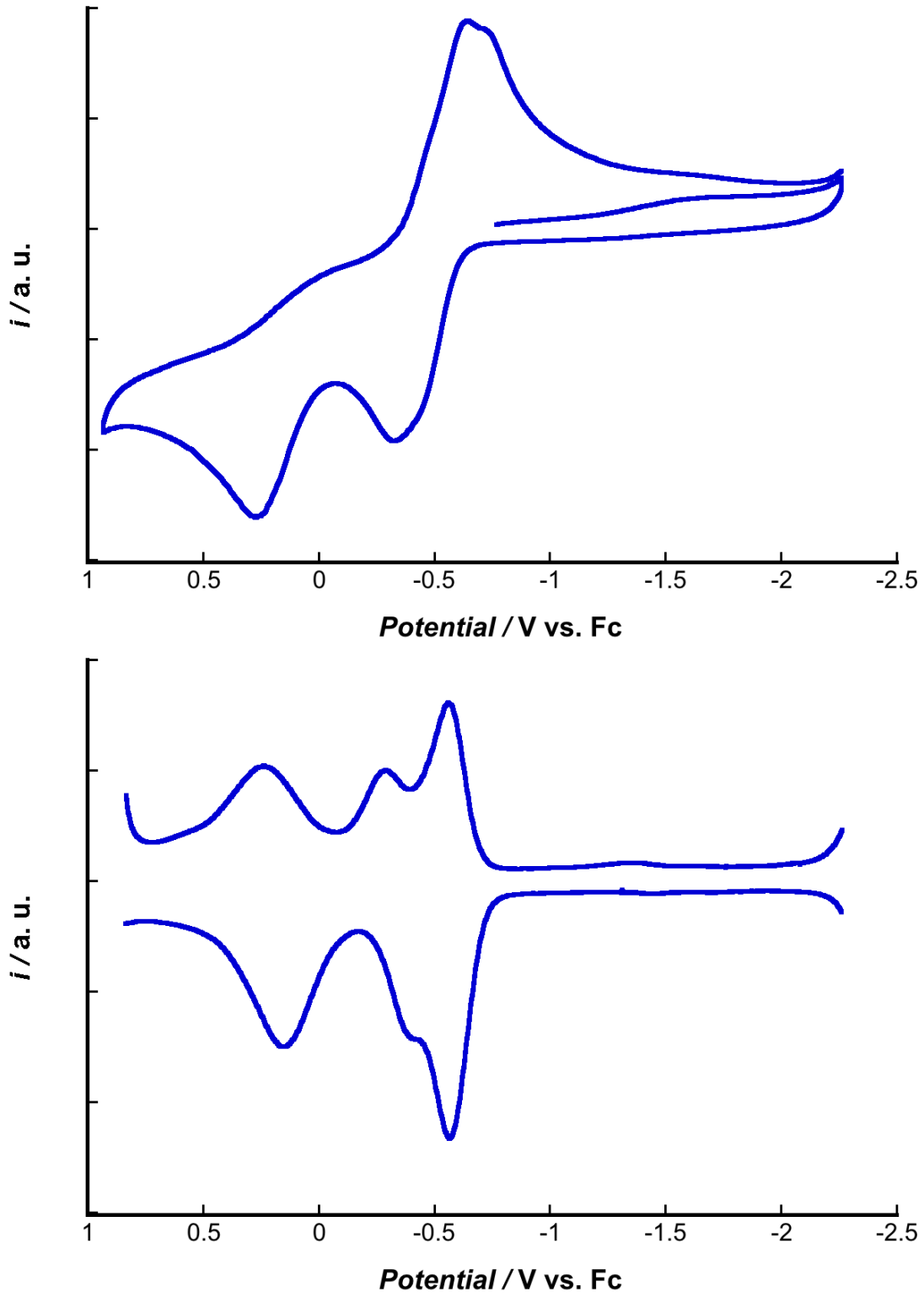

Figure 4.4.54. Cyclic voltammogram (top) and differential pulse voltammogram (bottom) of **4.1-Pr**.

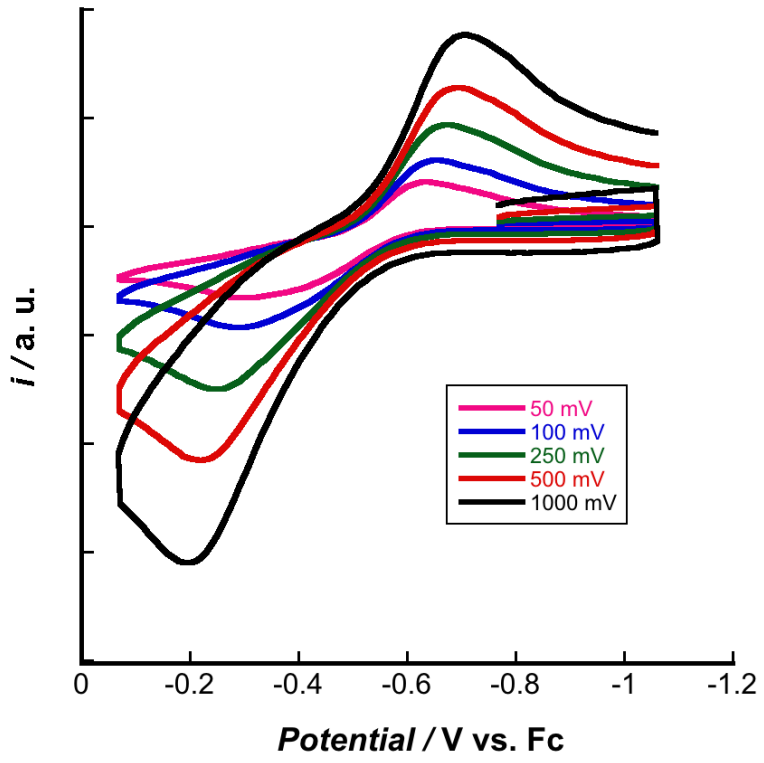

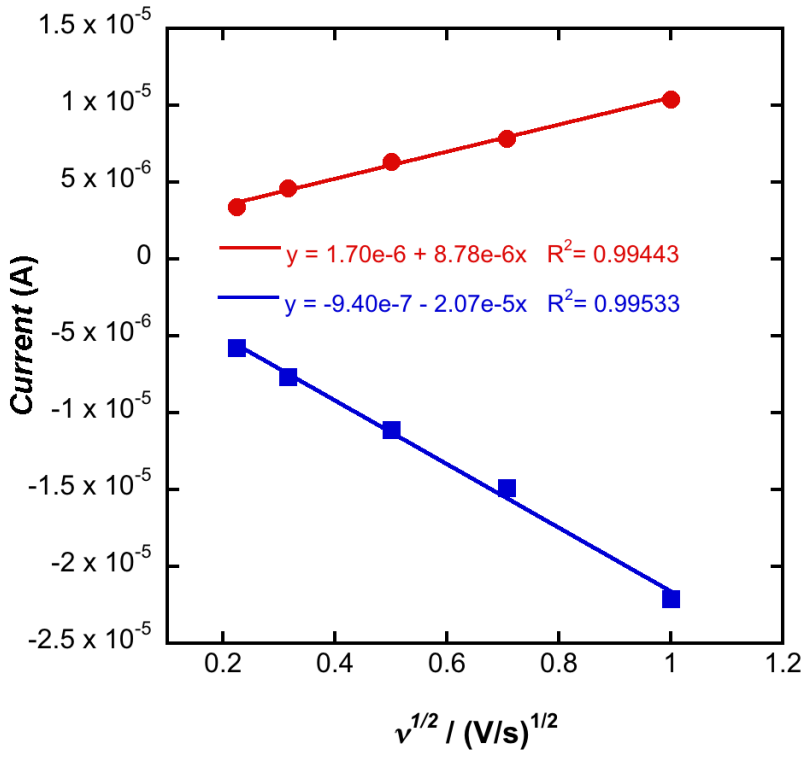

Figure 4.4.55. Scan rate dependence of the first oxidation feature of **4.1-Pr**.

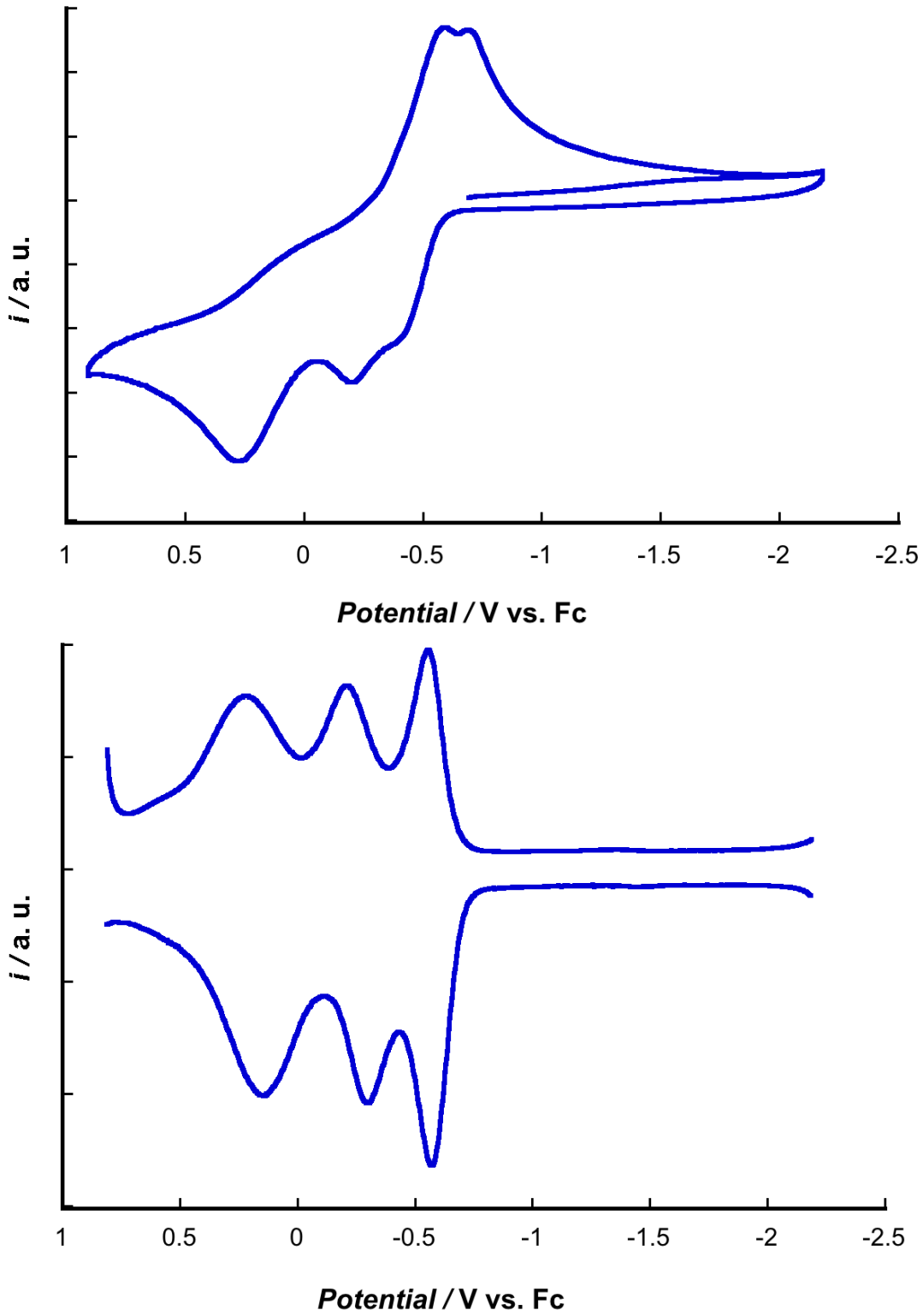

Figure 4.4.56. Cyclic voltammogram (top) and differential pulse voltammogram (bottom) of **4.1-Nd**.

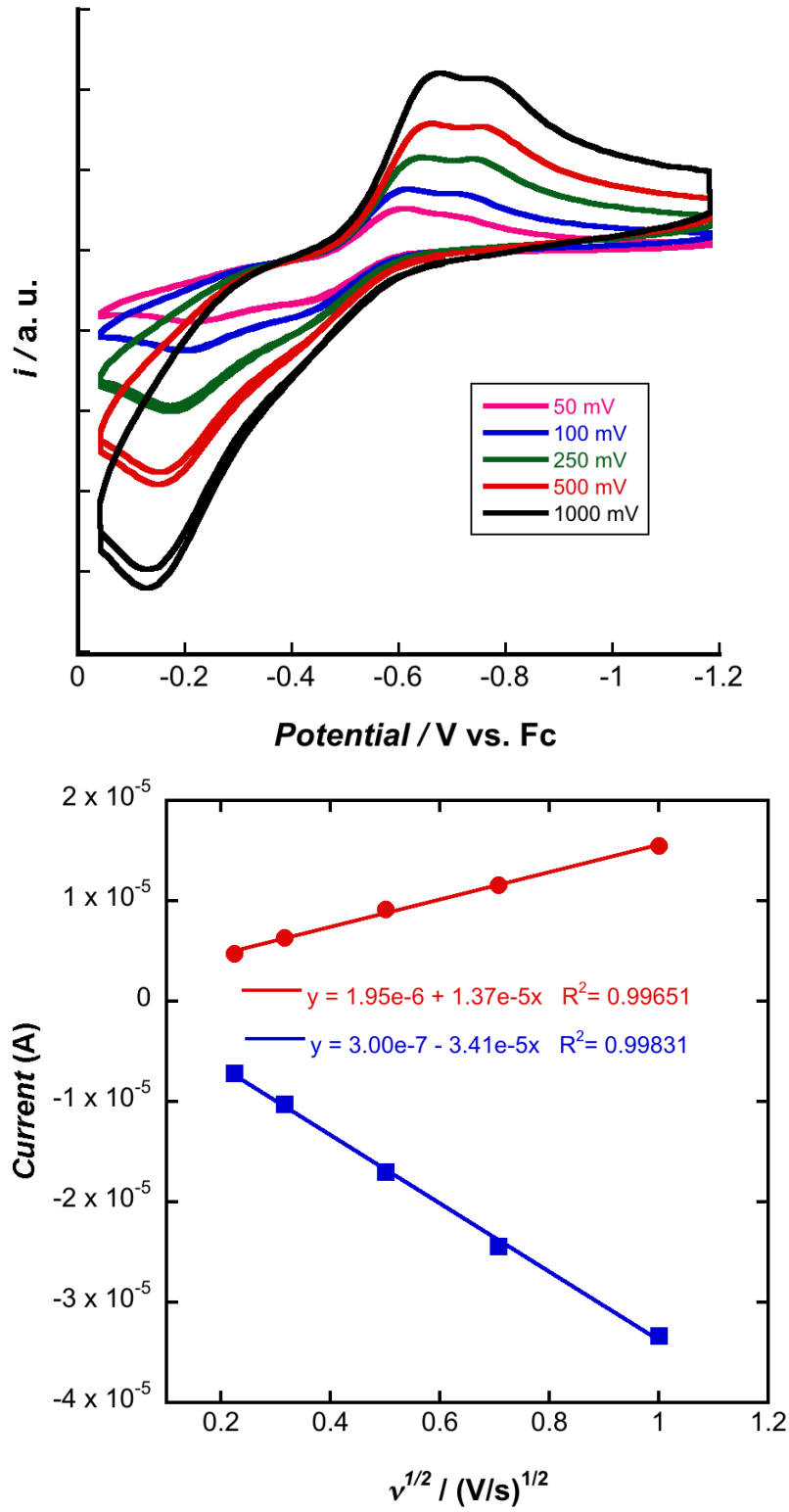

Figure 4.4.57. Scan rate dependence of the first oxidation feature of **4.1-Nd**.

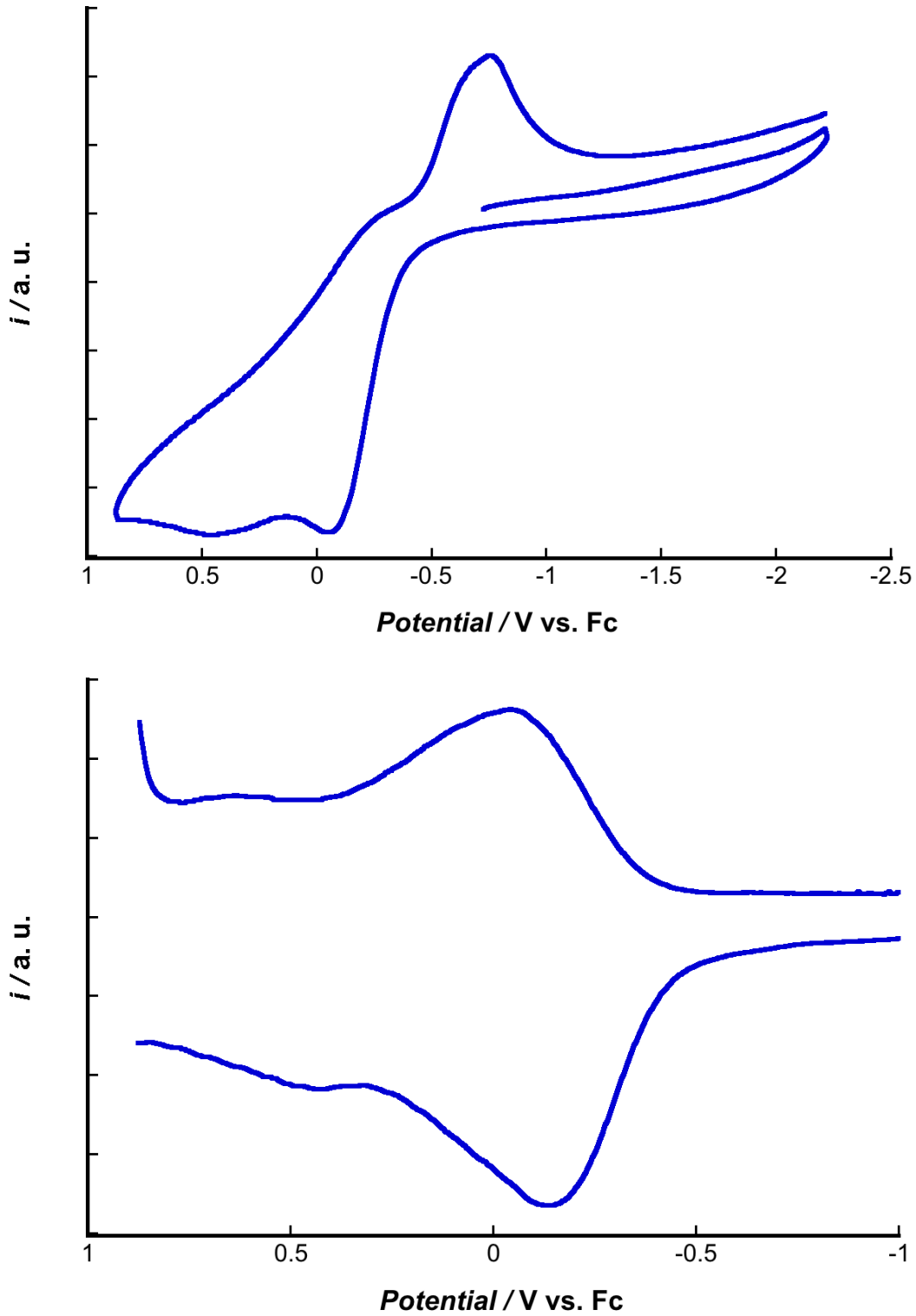

Figure 4.4.58. Cyclic voltammogram (top) and differential pulse voltammogram (bottom) of **4.1-Sm**.

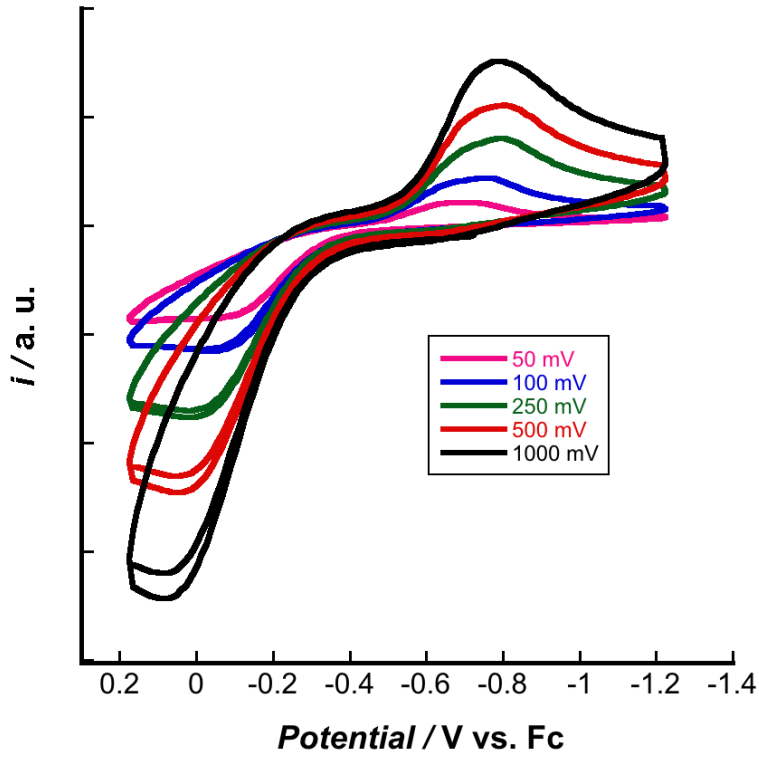

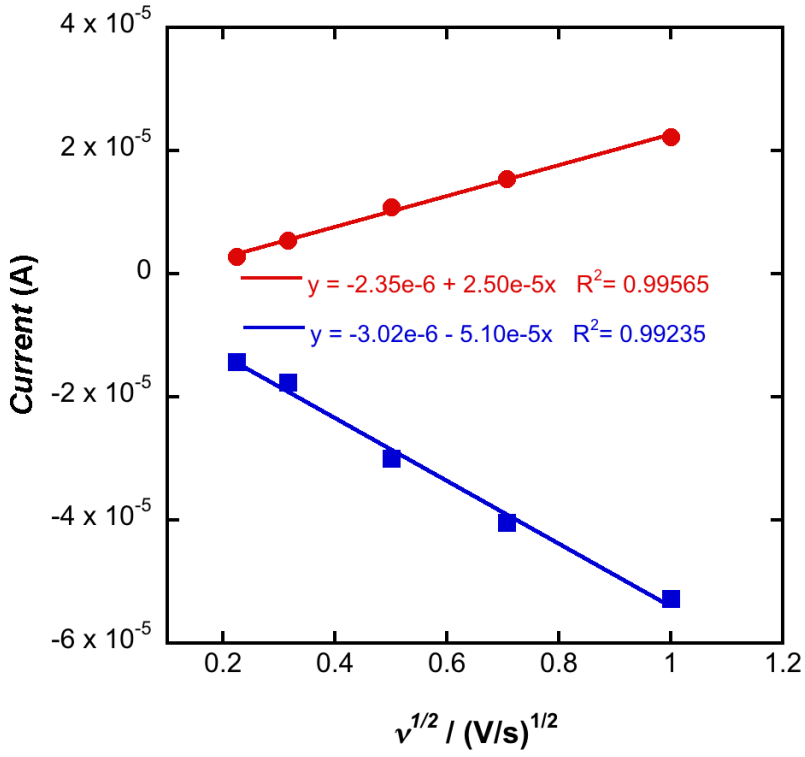

Figure 4.4.59. Scan rate dependence of the first oxidation feature of **4.1-Sm**.

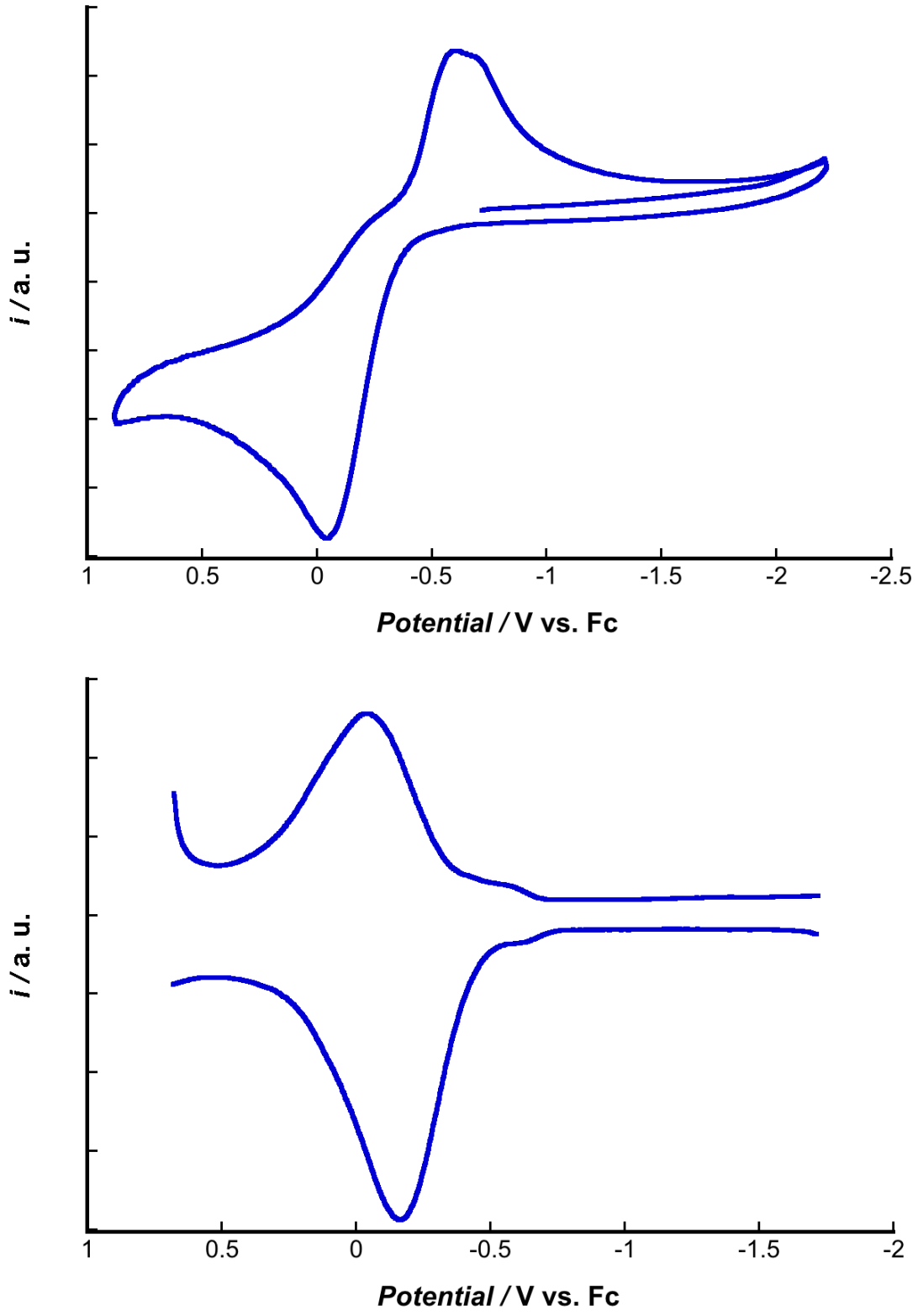

Figure 4.4.60. Cyclic voltammogram (top) and differential pulse voltammogram (bottom) of **4.1-Eu**.

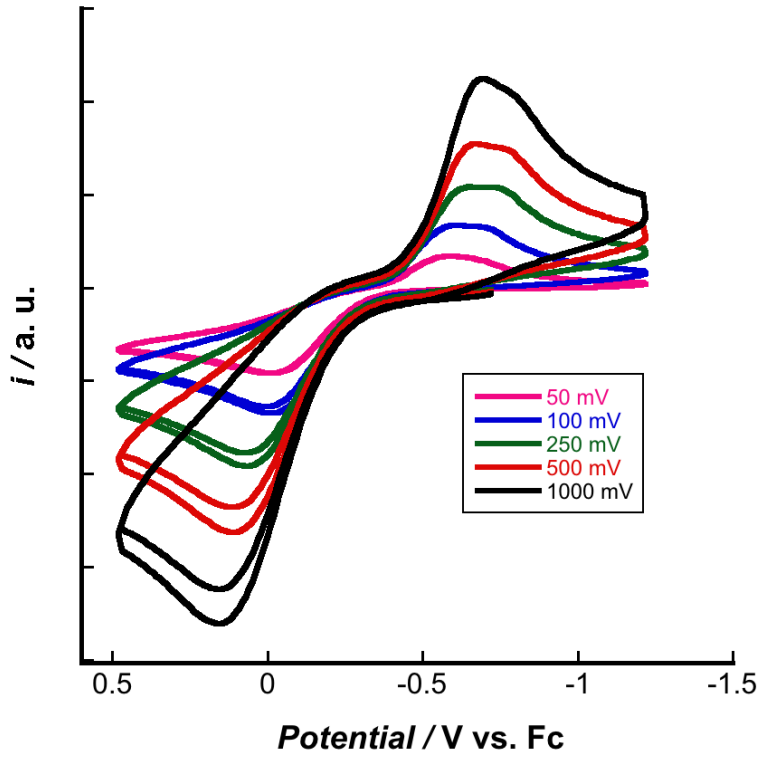

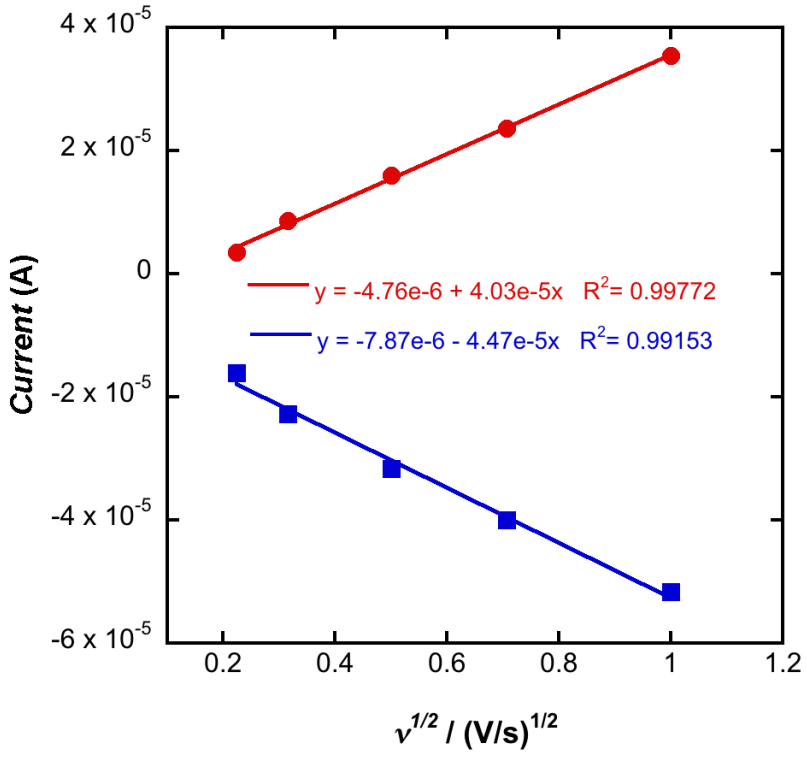

Figure 4.4.61. Scan rate dependence of the first oxidation feature of **4.1-Eu**.

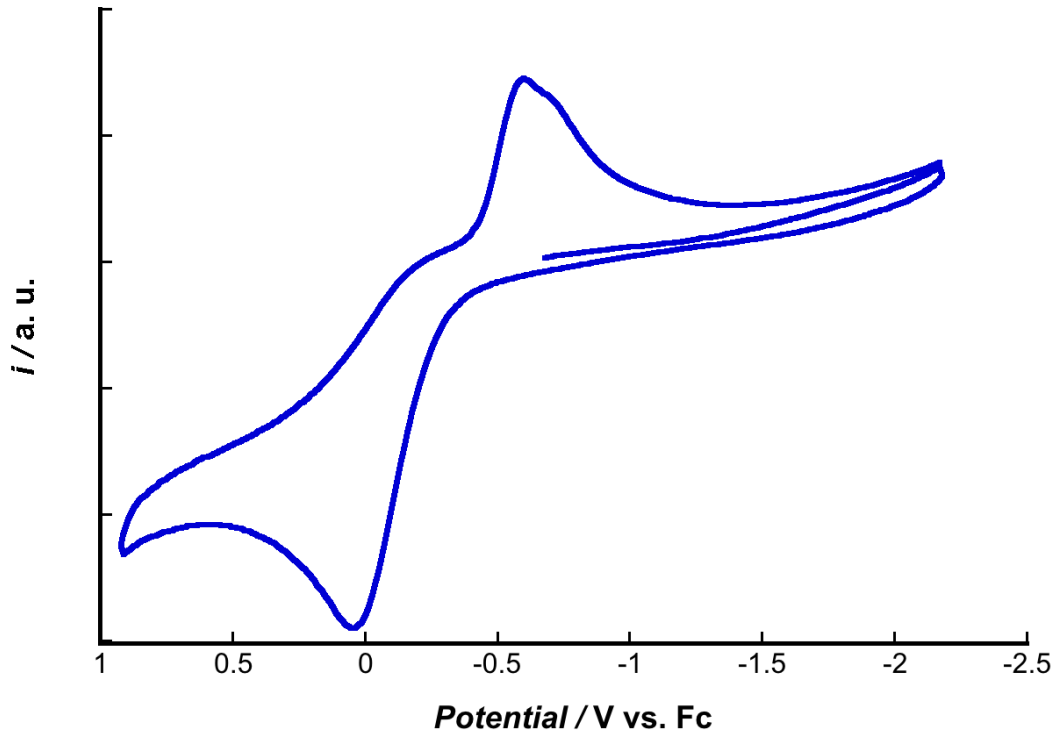

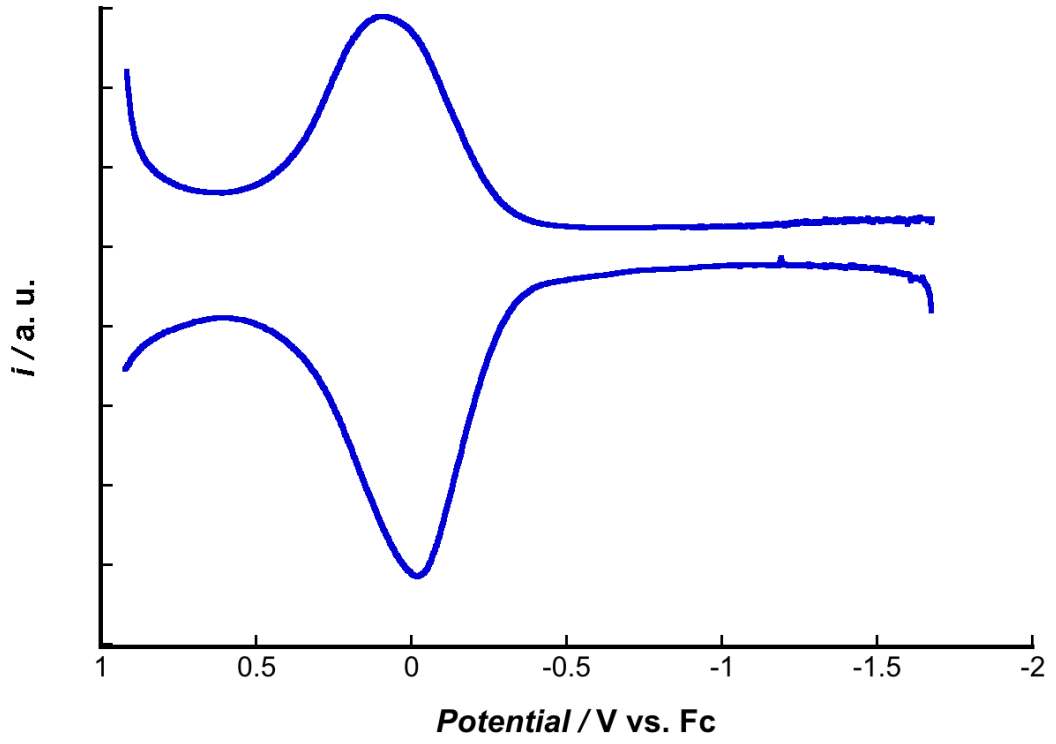

Figure 4.4.62. Cyclic voltammogram (top) and differential pulse voltammogram (bottom) of **4.1-Gd**.

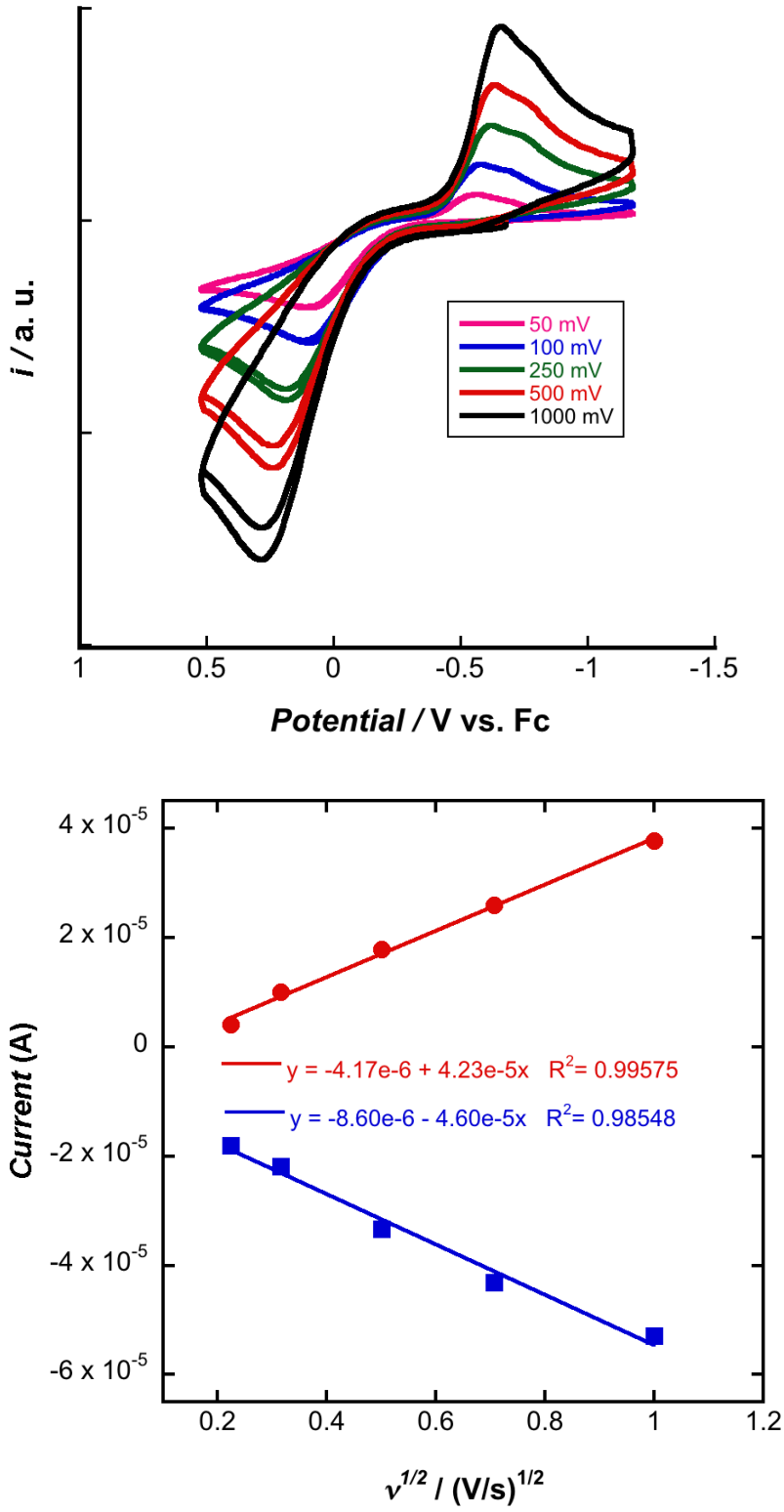

Figure 4.4.63. Scan rate dependence of the first oxidation feature of **4.1-Gd**.

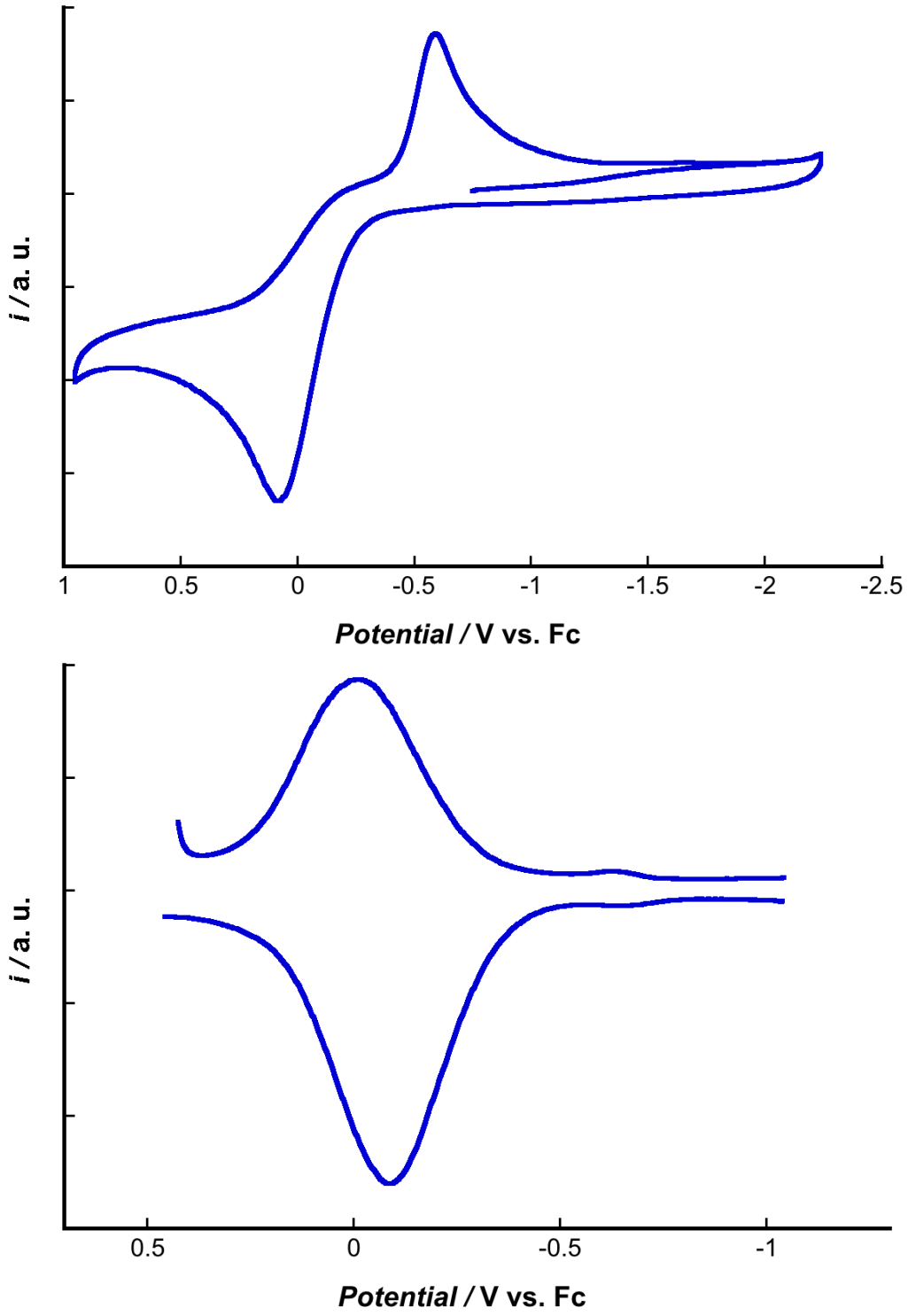

Figure 4.4.64. Cyclic voltammogram (top) and differential pulse voltammogram (bottom) of **4.1-Tb**.

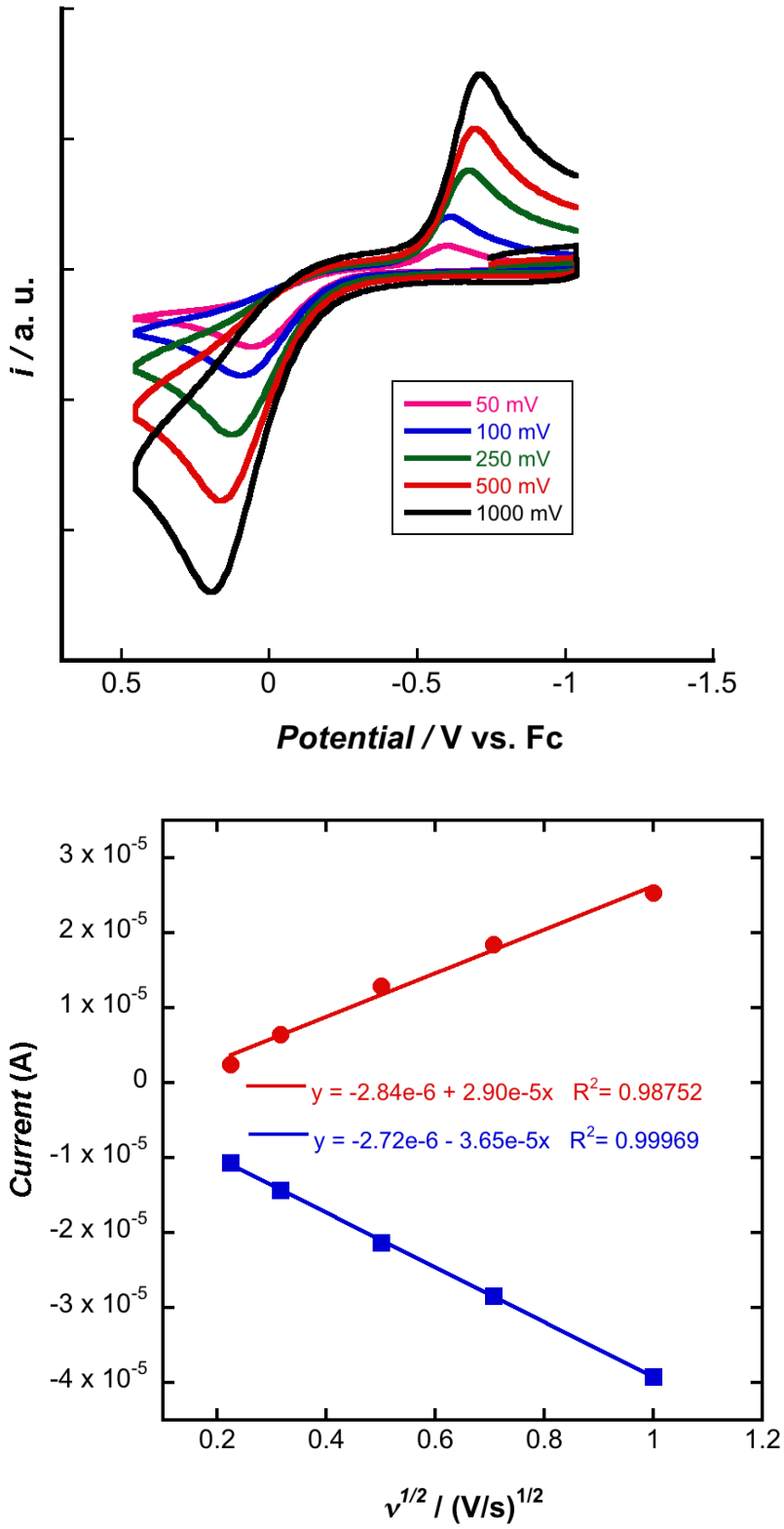

Figure 4.4.65. Scan rate dependence of the first oxidation feature of **4.1-Tb**.

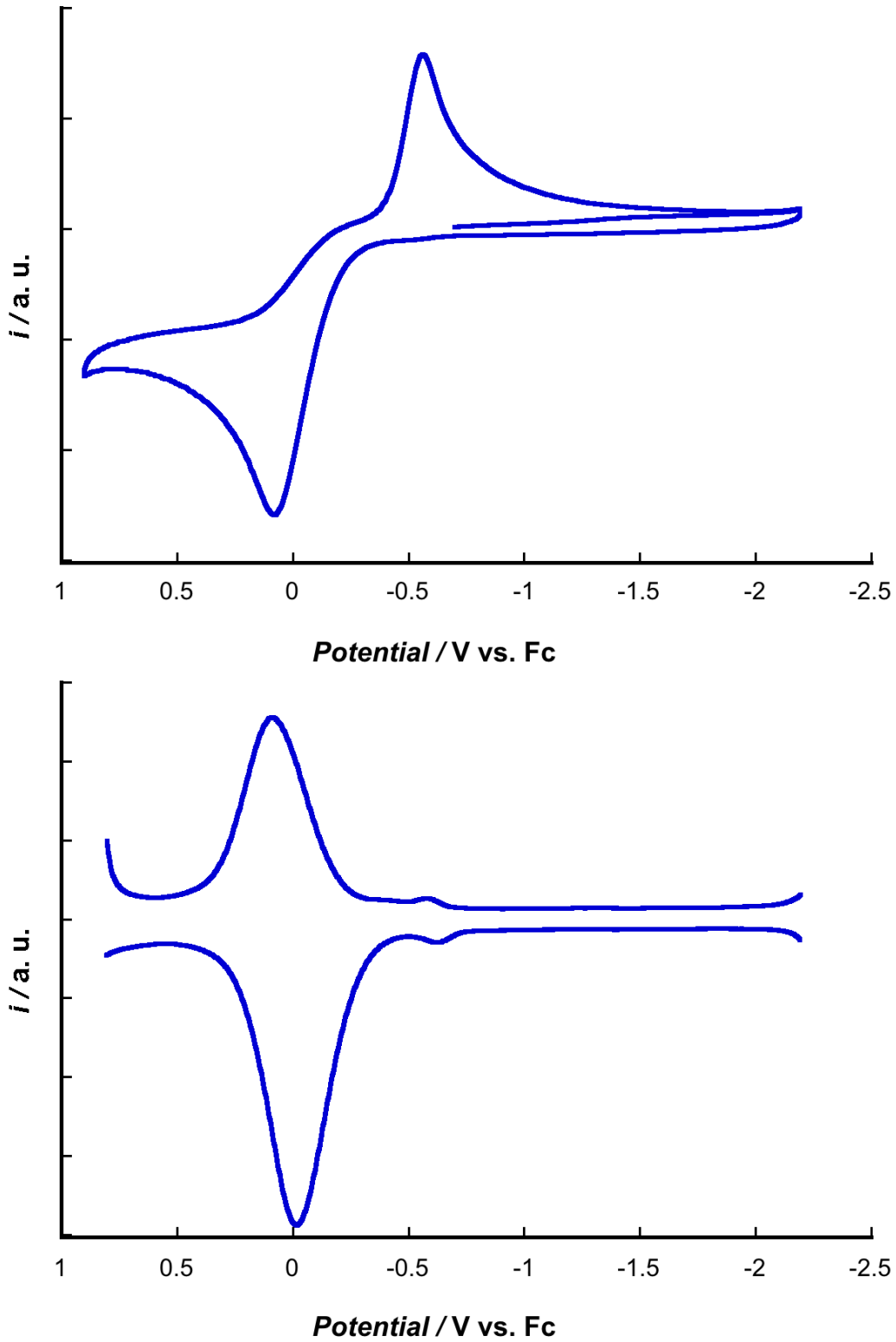

Figure 4.4.66. Cyclic voltammogram (top) and differential pulse voltammogram (bottom) of **4.1-Dy**.

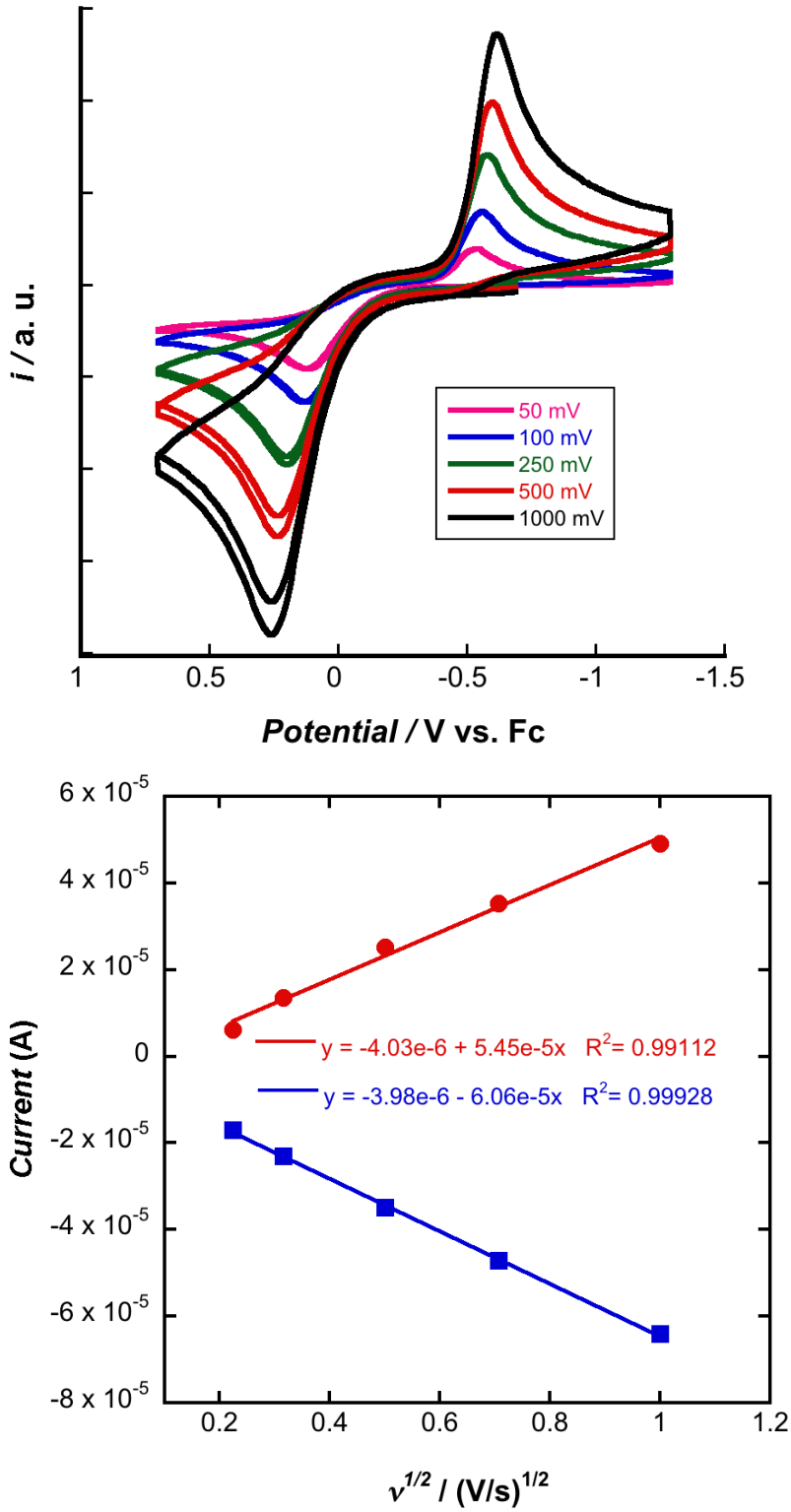

Figure 4.4.67. Scan rate dependence of the first oxidation feature of **4.1-Dy**.

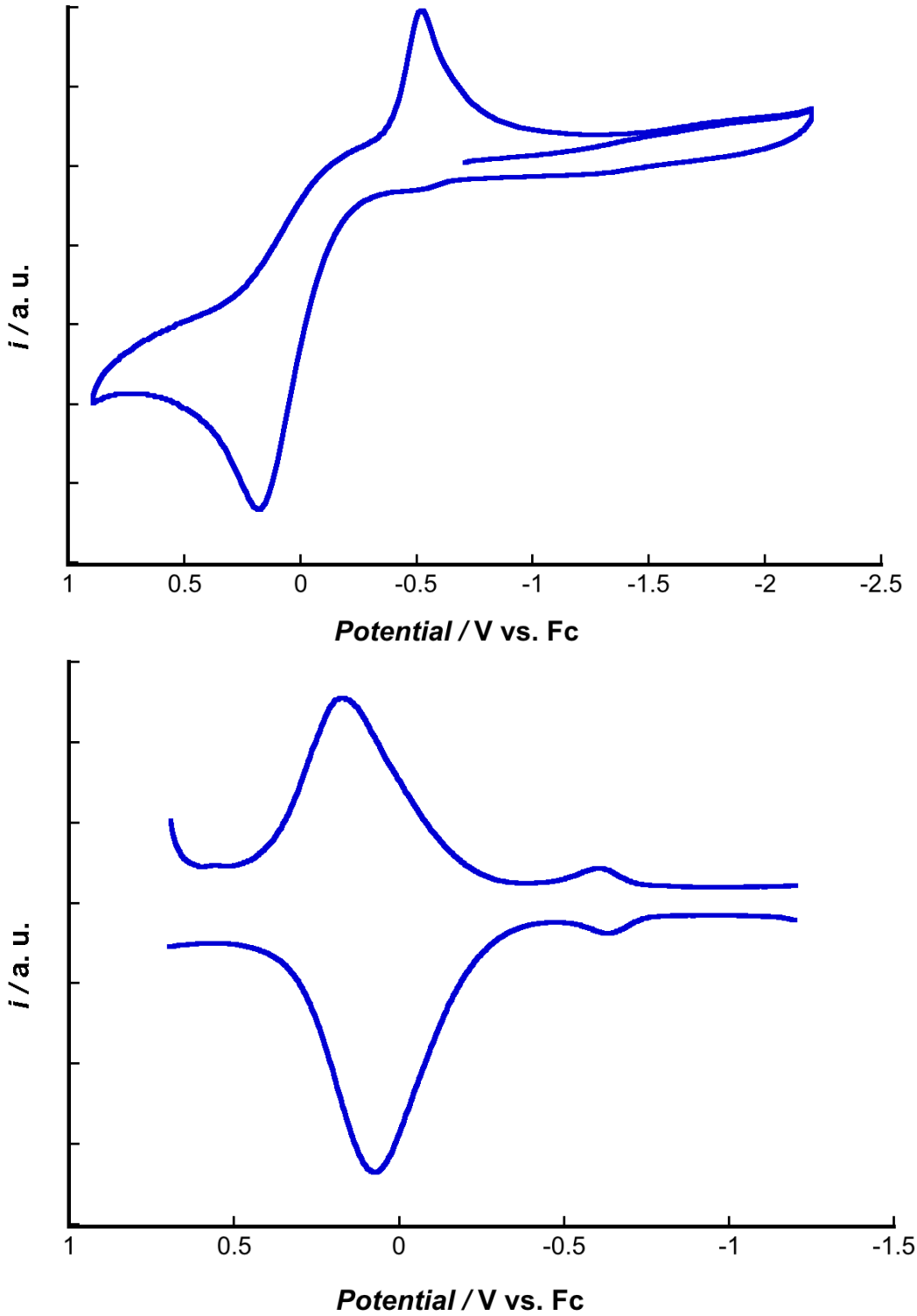

Figure 4.4.68. Cyclic voltammogram (top) and differential pulse voltammogram (bottom) of **4.1-Y**.

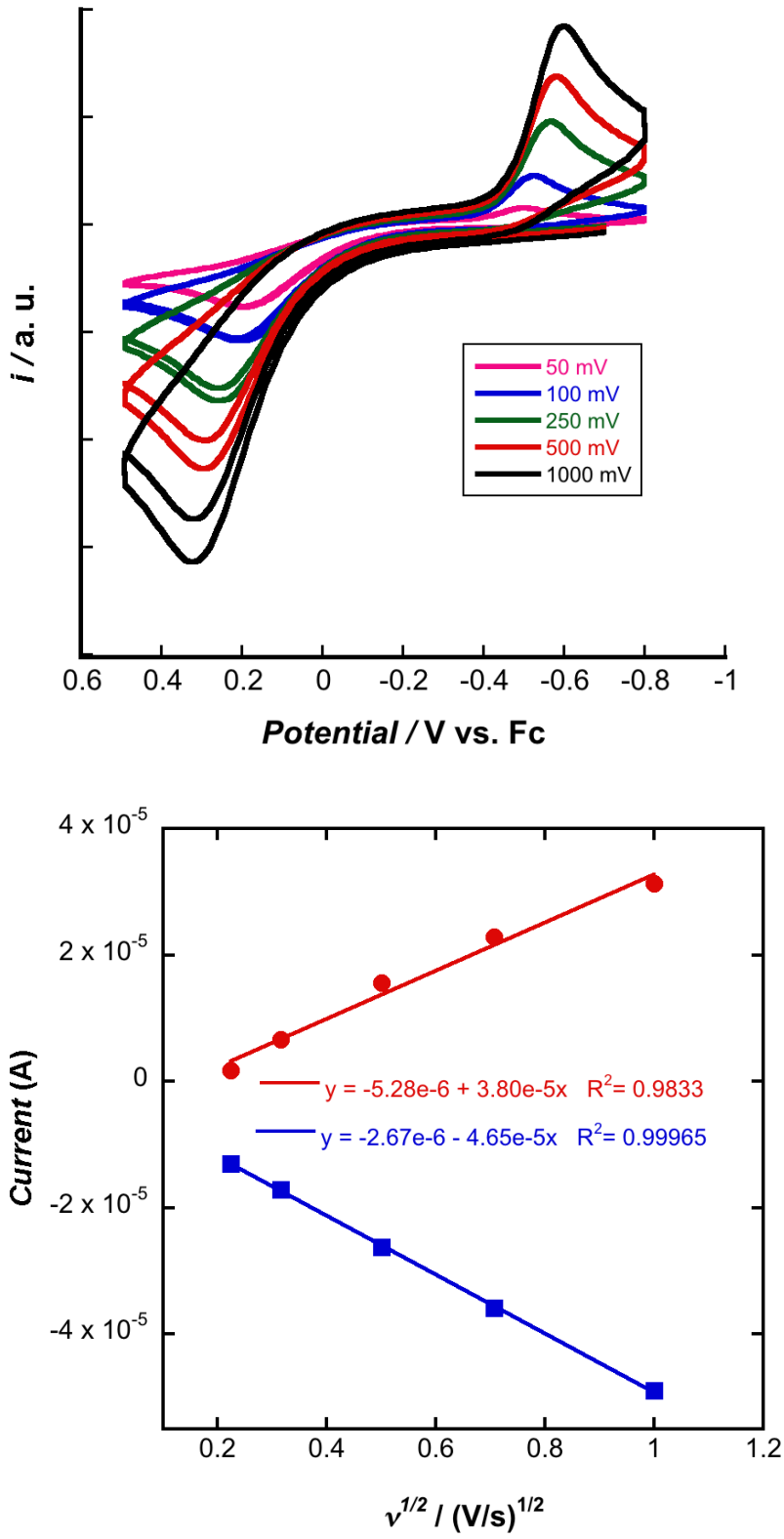

Figure 4.4.69. Scan rate dependence of the first oxidation feature of **4.1-Y**.

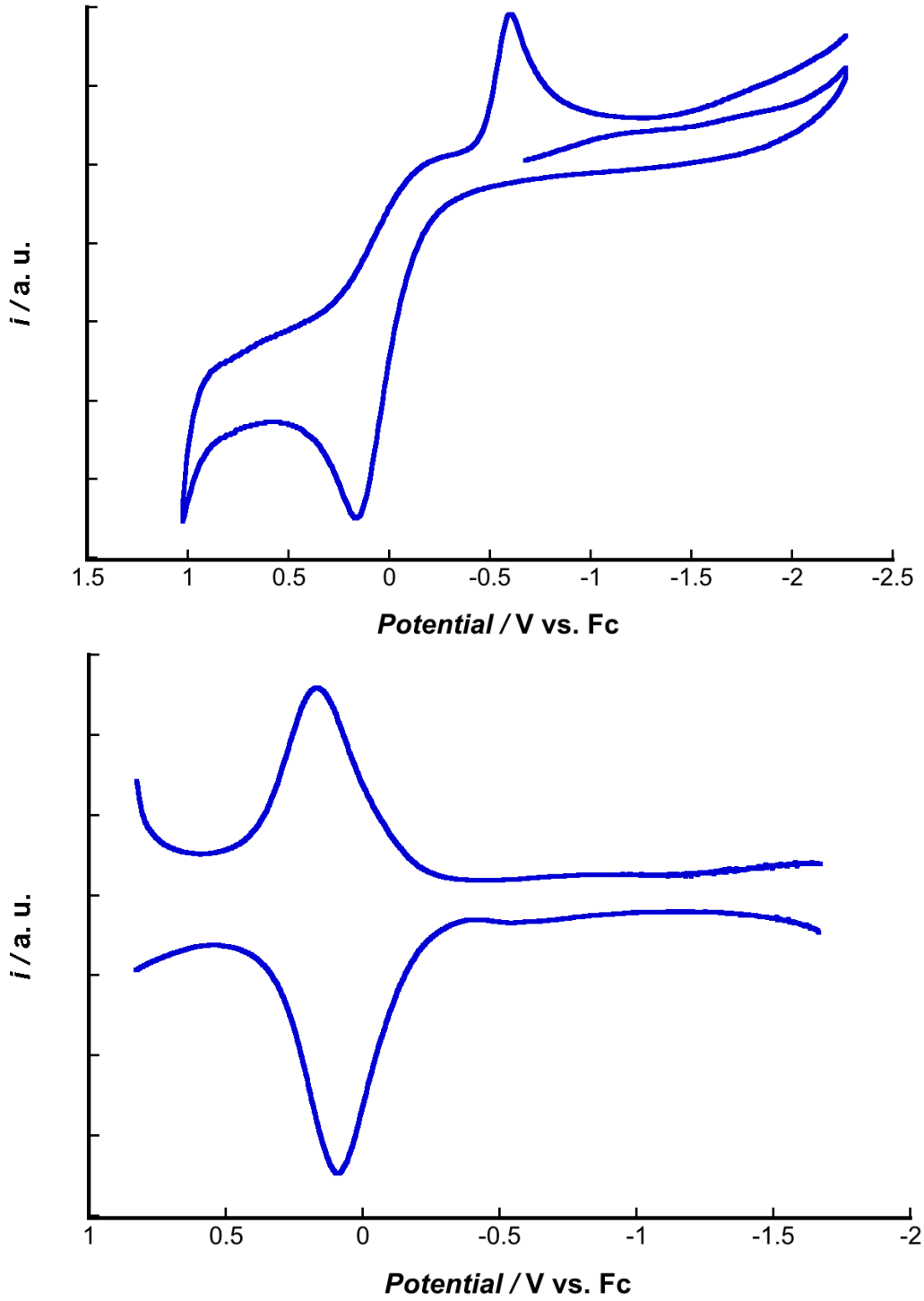

Figure 4.4.70. Cyclic voltammogram (top) and differential pulse voltammogram (bottom) of **4.1-Ho**.

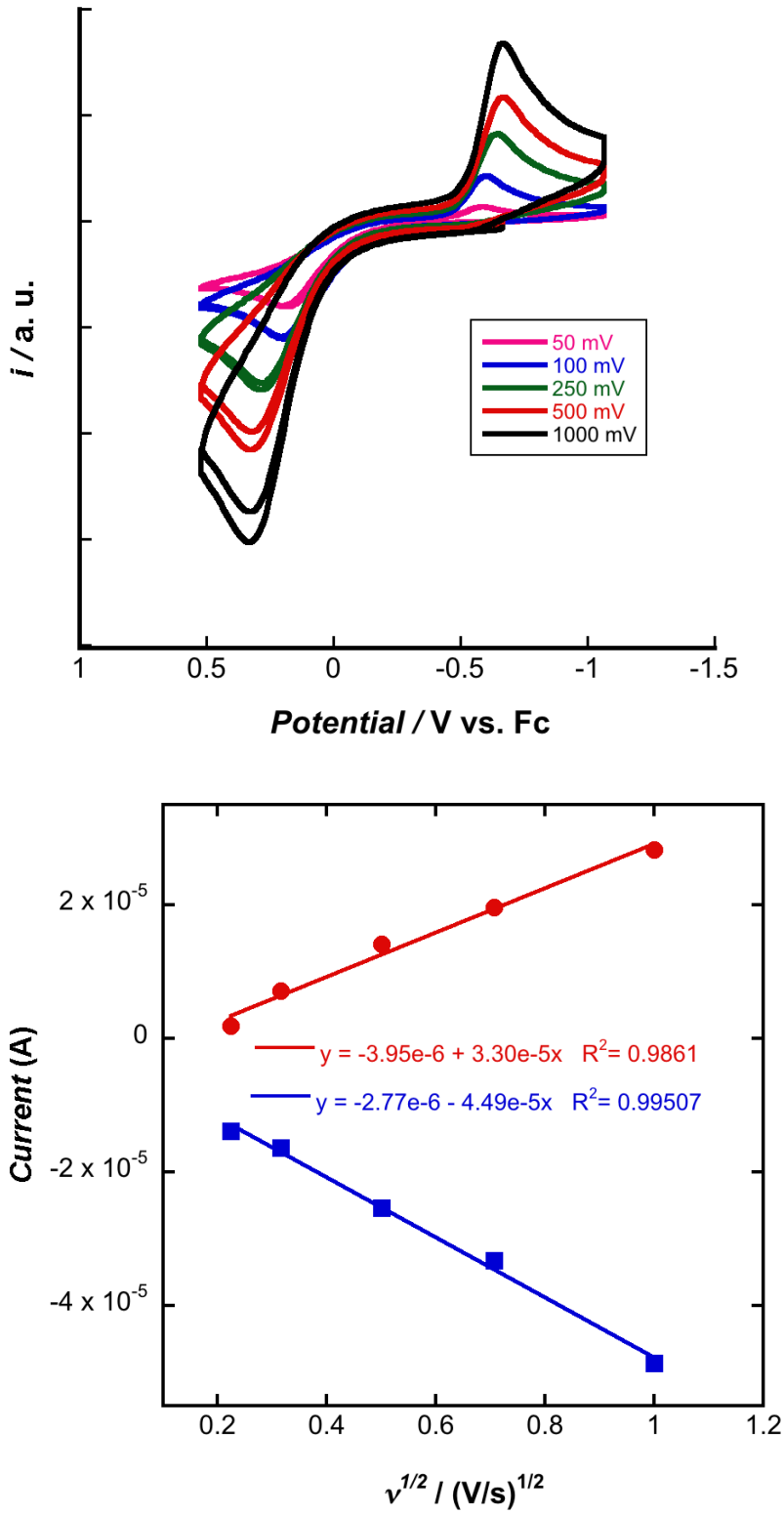

Figure 4.4.71. Scan rate dependence of the first oxidation feature of **4.1-Ho**.

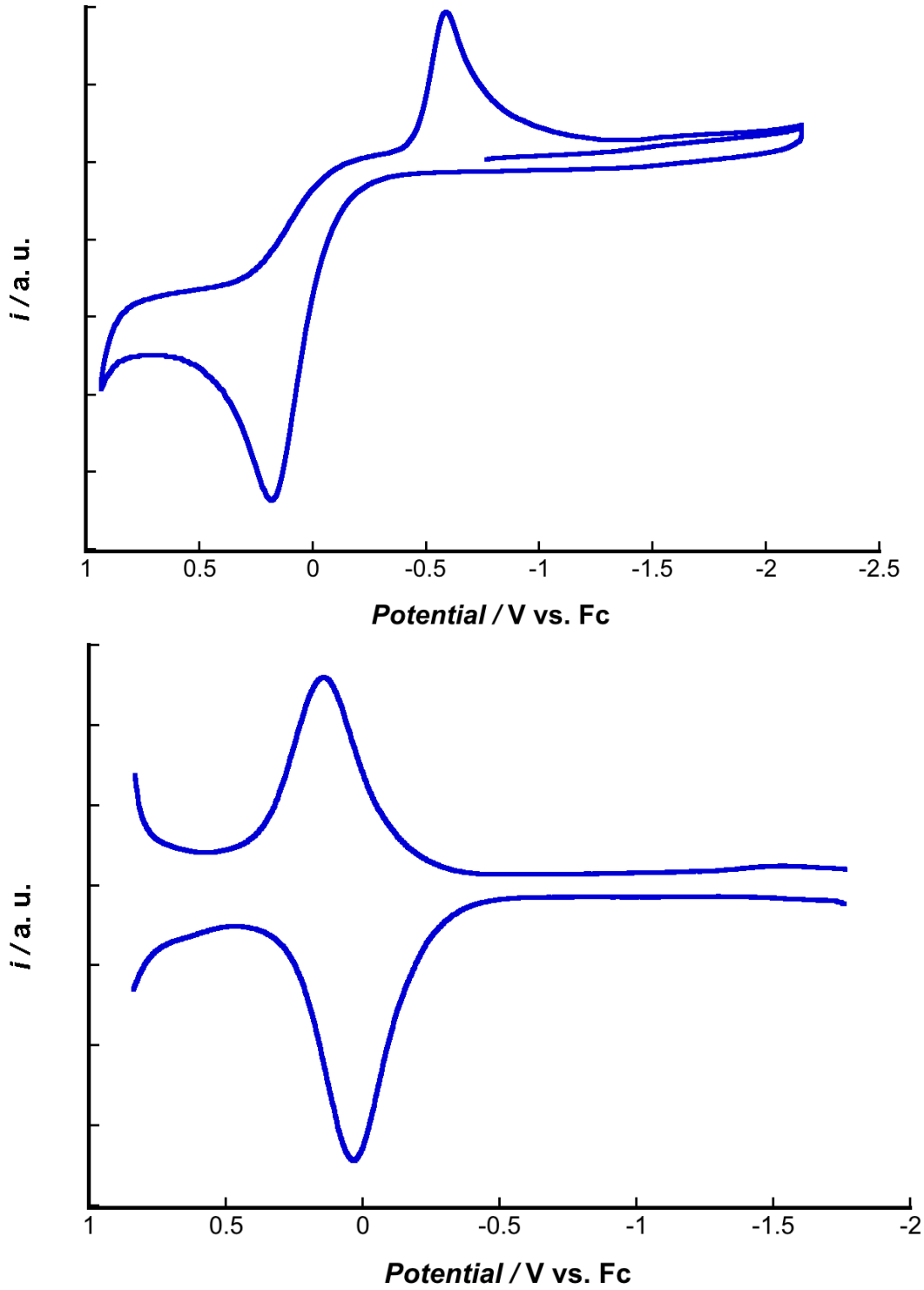

Figure 4.4.72. Cyclic voltammogram (top) and differential pulse voltammogram (bottom) of **4.1-Er**.

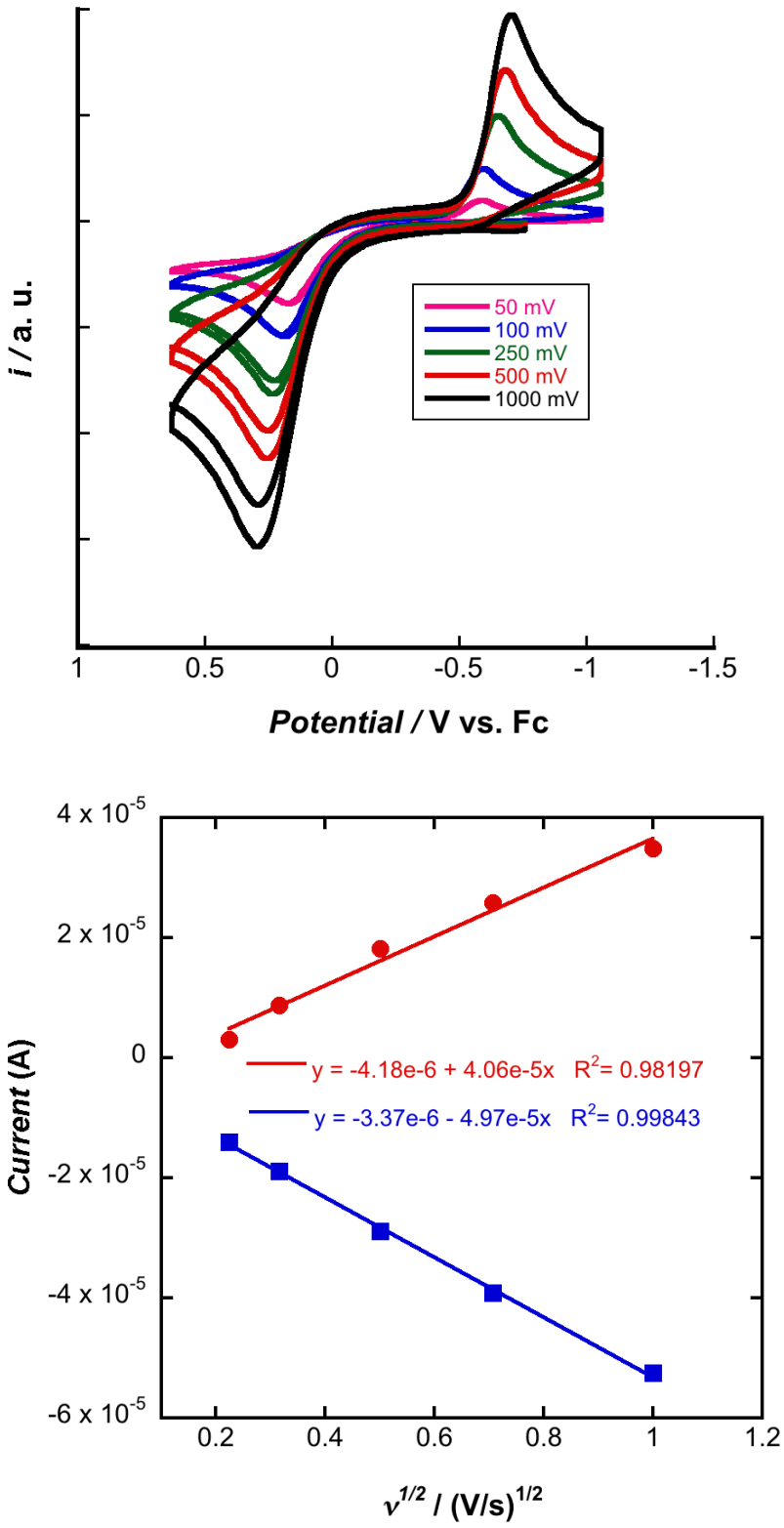

Figure 4.4.73. Scan rate dependence of the first oxidation feature of **4.1-Er**.

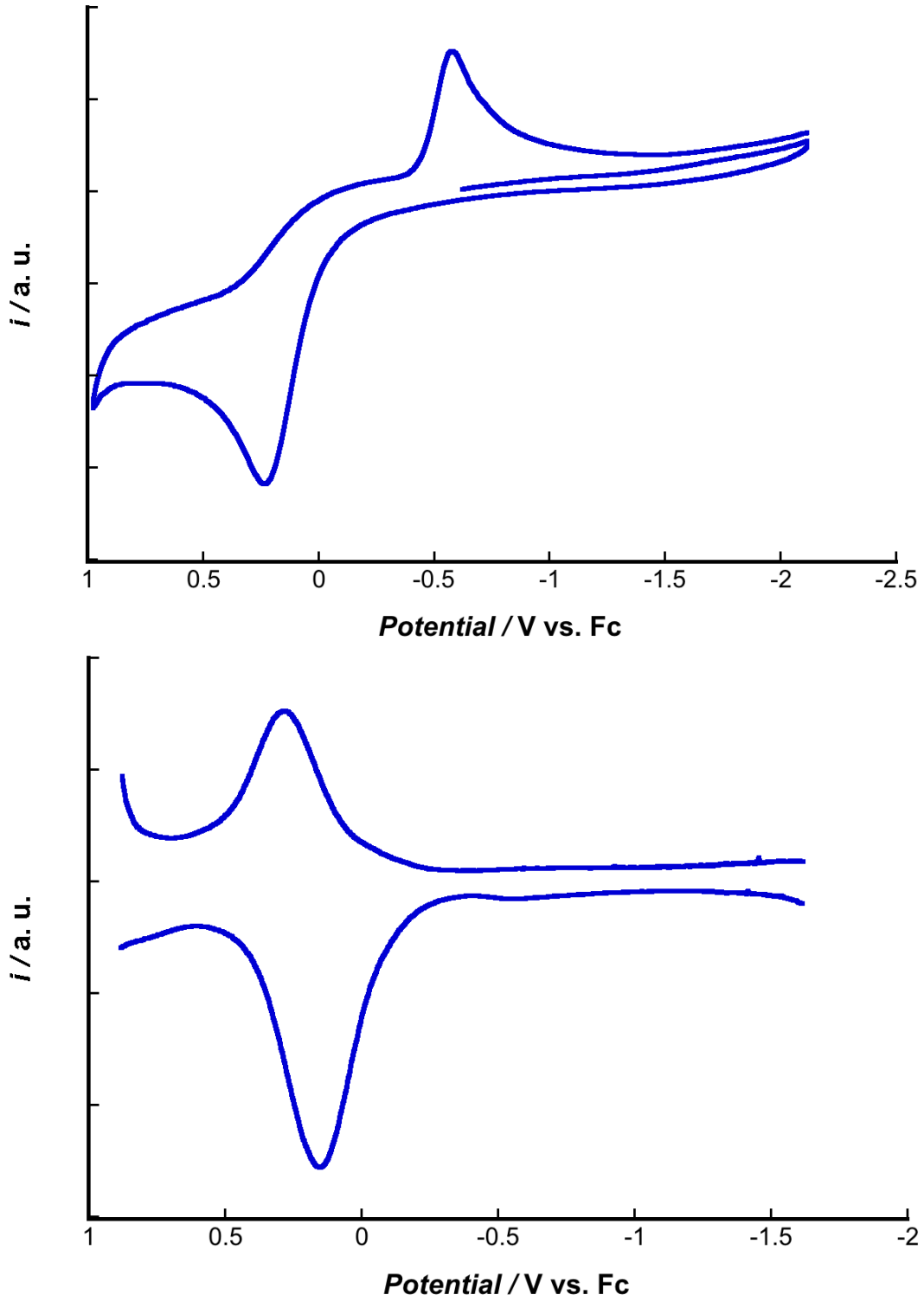

Figure 4.4.74. Cyclic voltammogram (top) and differential pulse voltammogram (bottom) of **4.1-Tm**.

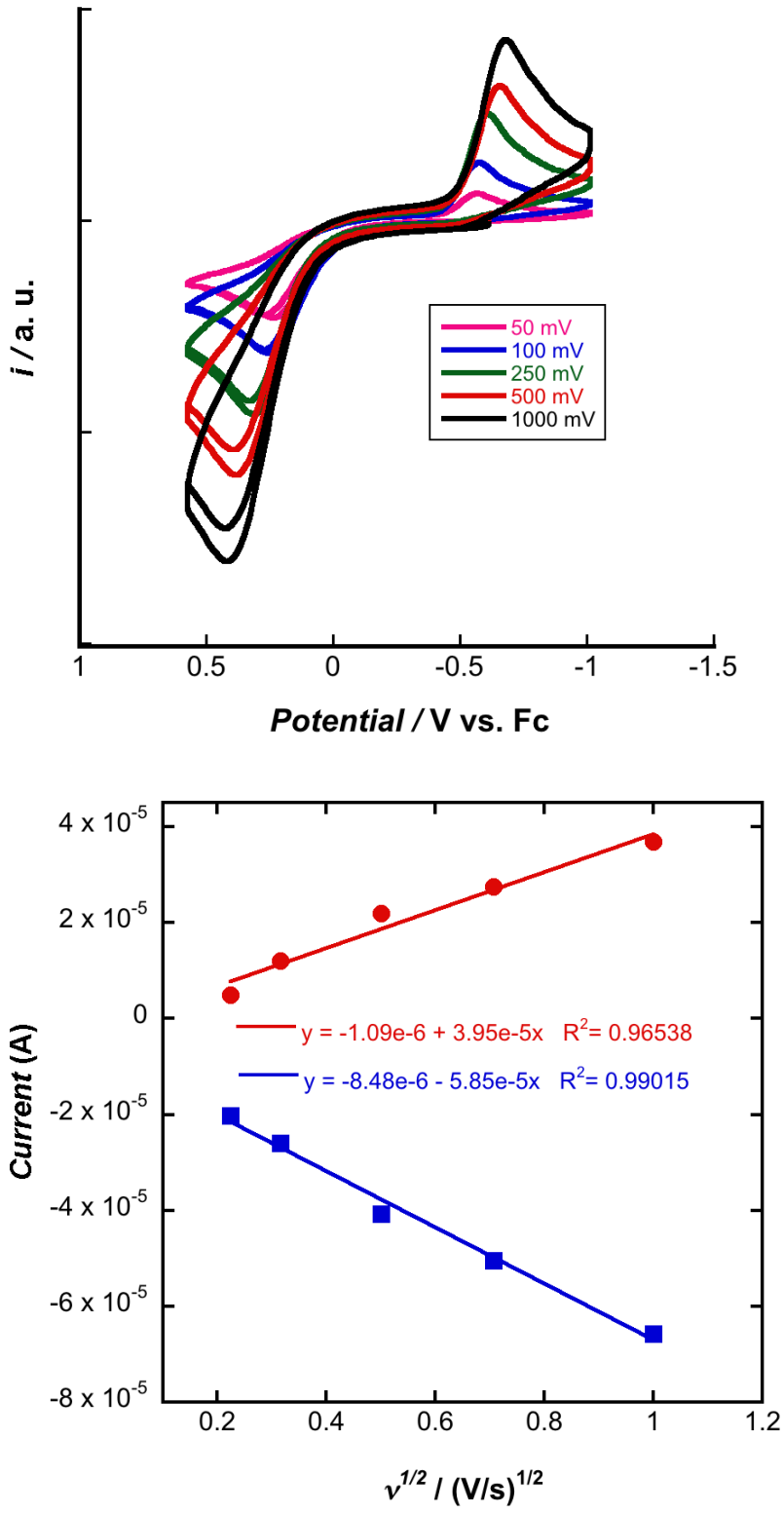

Figure 4.4.75. Scan rate dependence of the first oxidation feature of **4.1-Tm**.

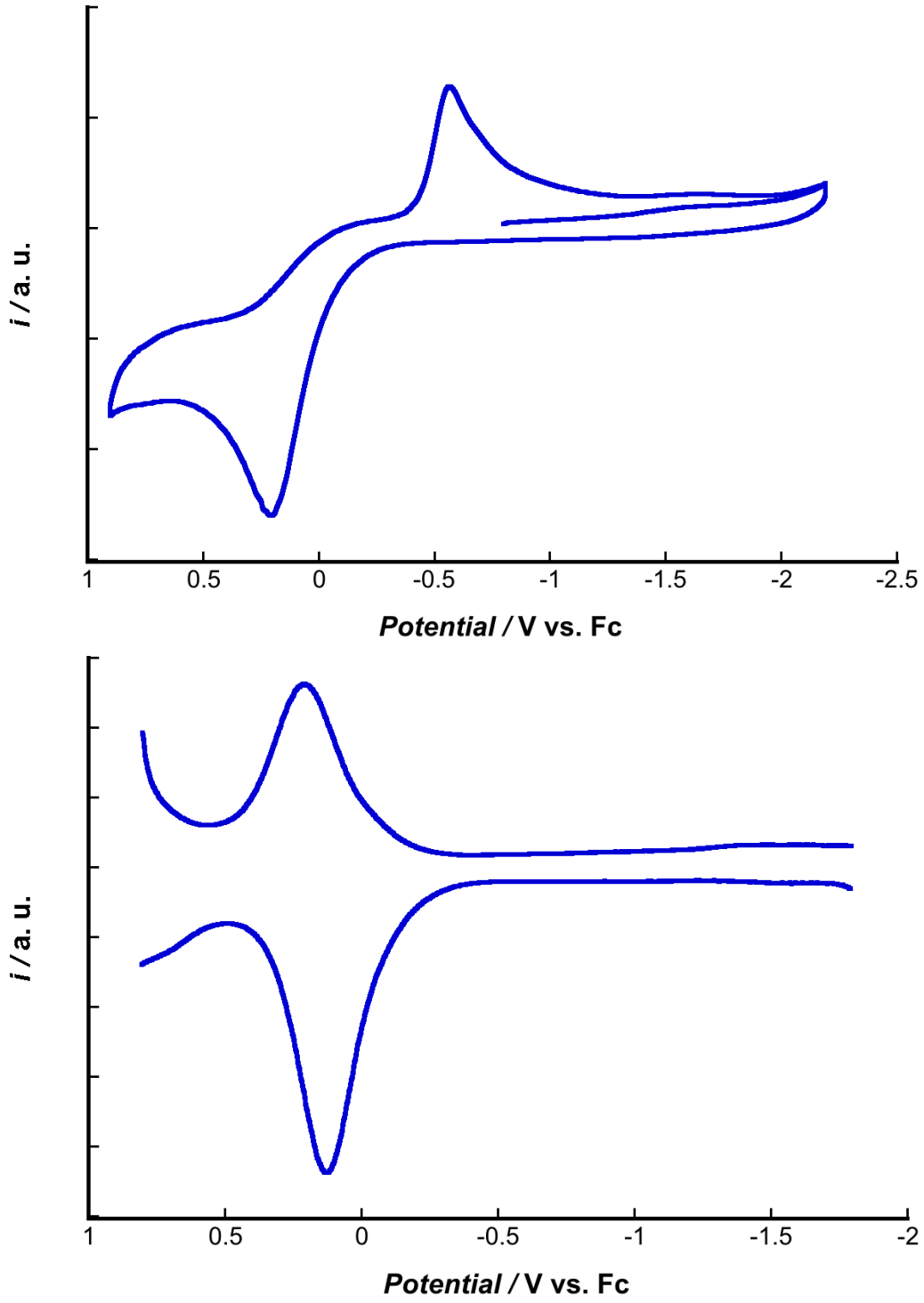

Figure 4.4.76. Cyclic voltammogram (top) and differential pulse voltammogram (bottom) of **4.1-Yb**.

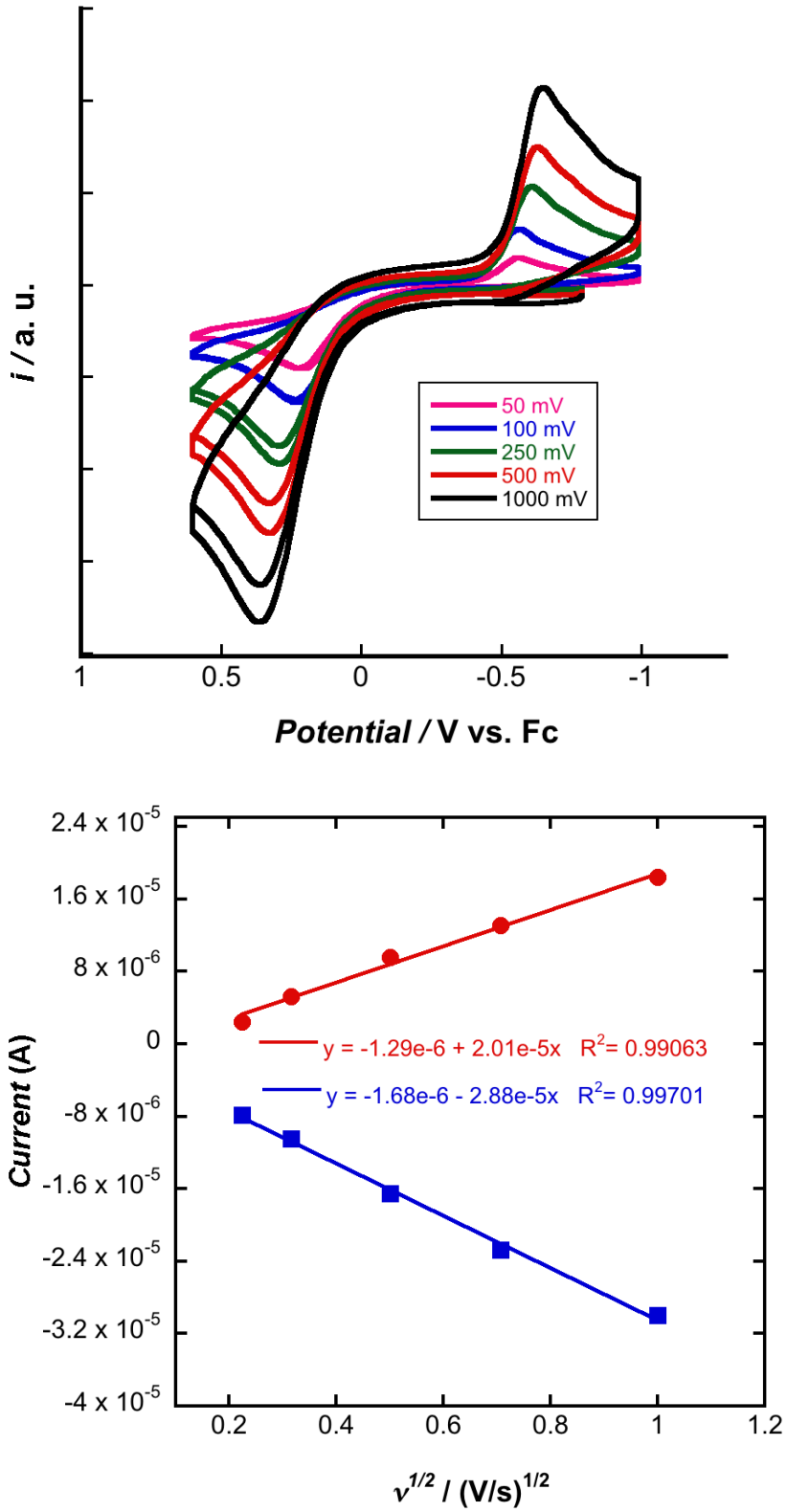

Figure 4.4.77. Scan rate dependence of the first oxidation feature of **4.1-Yb**.

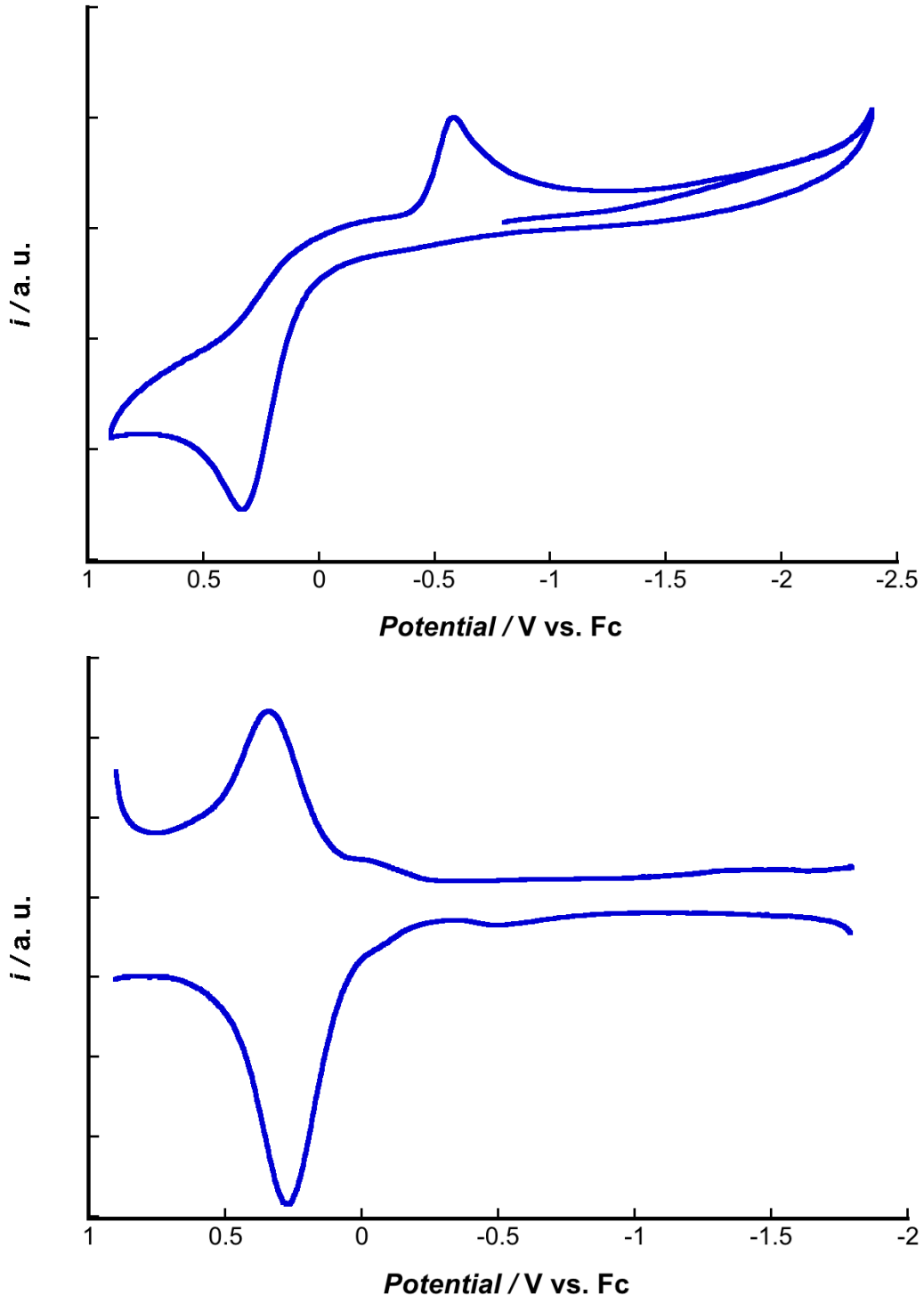

Figure 4.4.78. Cyclic voltammogram (top) and differential pulse voltammogram (bottom) of **4.1-Lu**.

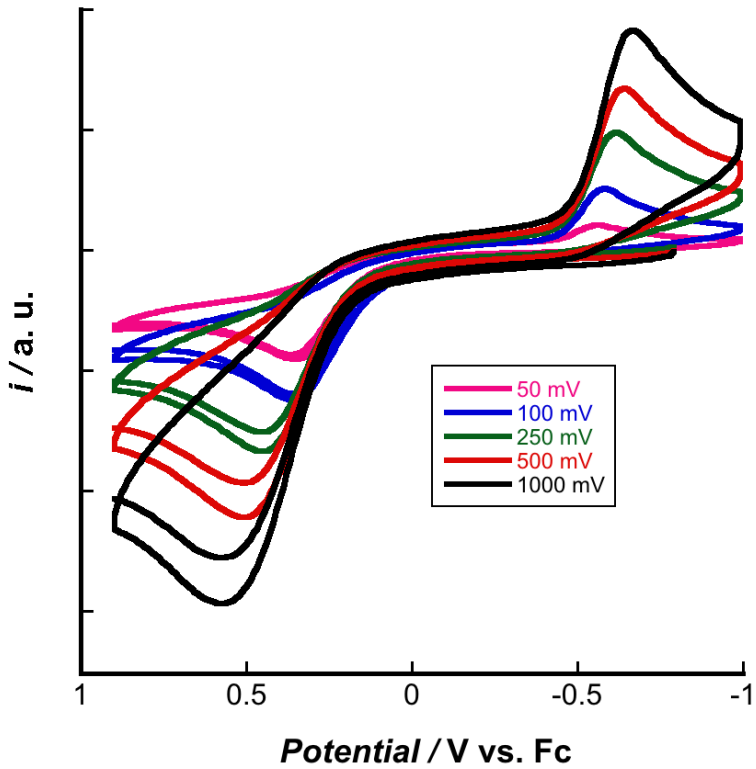

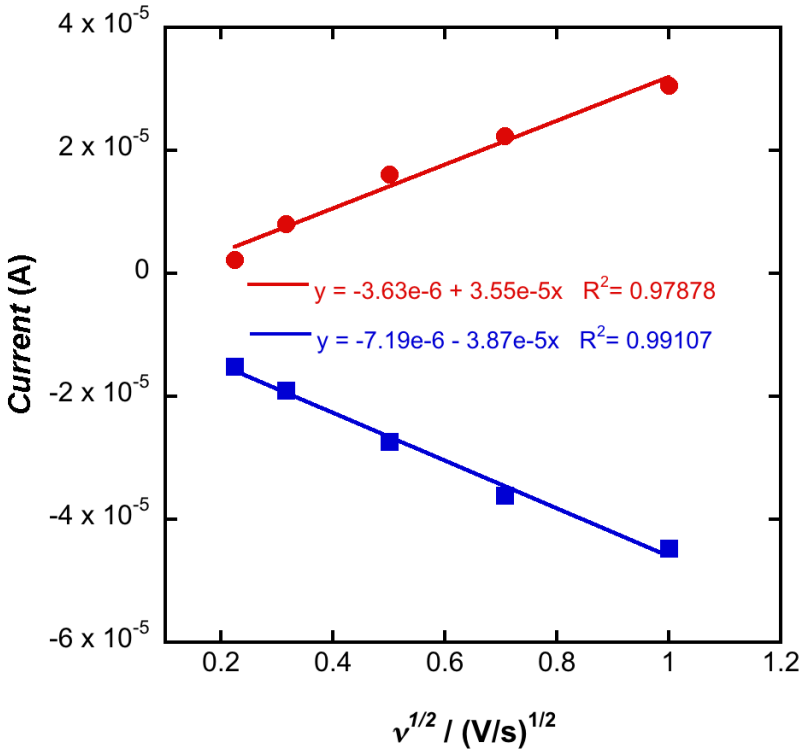

Figure 4.4.79. Scan rate dependence of the first oxidation feature of **4.1-Lu**.

2D Exchange Spectroscopy (EXSY) NMR Experiments

All 2D ^{1}H EXSY experiments were performed on a Bruker UNI-400 Fourier transform NMR spectrometer at 400 MHz using $CDCl_3$ as a solvent and a conventional NOESY sequence. Relevant parameters are listed in Table 4.4.25.

Table 4.4.25. Parameters used for the 2D ^{1}H-NMR EXSY experiments.

Mixture	SW	O1	TD (t_2/t_1)	NS	t_{mix}
4.1-Dy / 4.1-Nd	69.4286	6001.27	2048 / 512	8	0.010
4.1-Y / 4.1-Nd	49.9894	0	2048 / 512	8	0.080

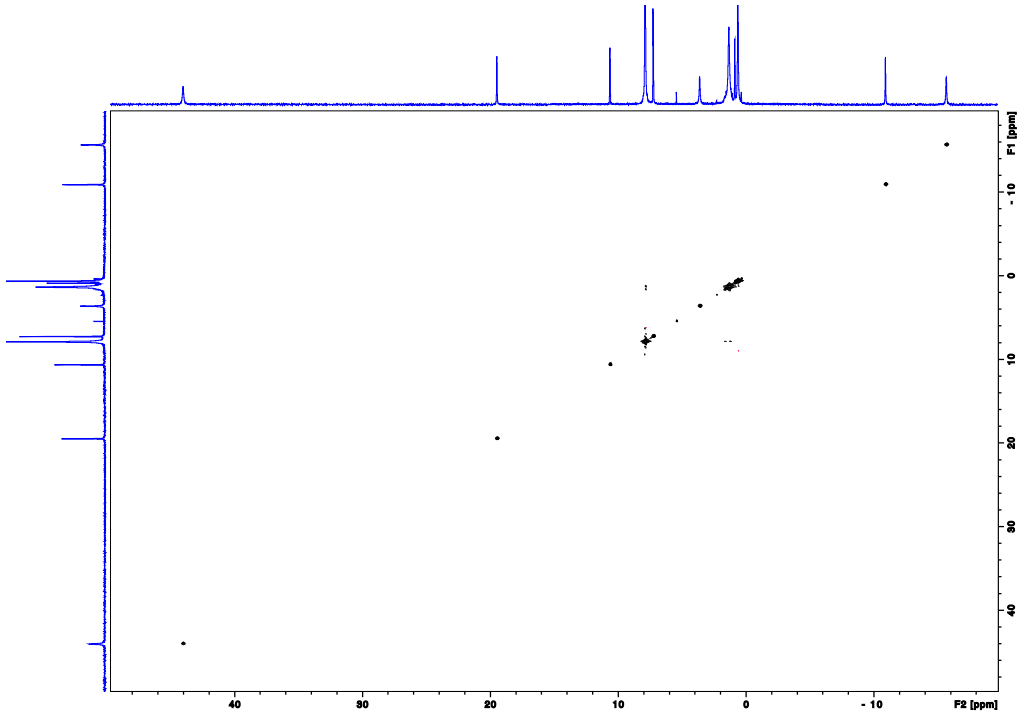

Figure 4.4.80. 2D ^{1}H-NMR EXSY experiment of a 50:50 mixture of **4.1-Nd** and **4.1-Dy** in $CDCl_3$.

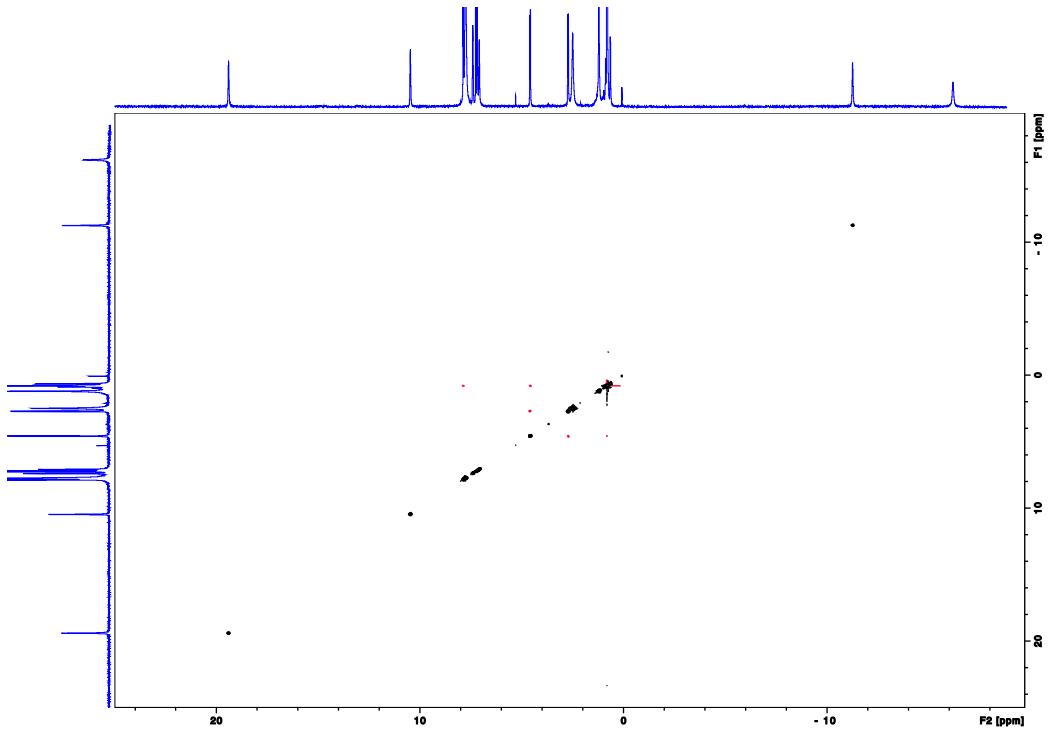

Figure 4.4.81. 2D ^{1}H-NMR EXSY experiment of a 50:50 mixture of **4.1-Nd** and **4.1-Y** in $CDCl_3$.

Determination of K_{eq} for Dimerization of 4.1-RE in Benzene

The equilibrium constant, K_{eq}, for the dimerization of **4.1-RE** in benzene was determined by solving the following equilibrium expression:

$$K_{eq} = \frac{[\text{Dimer}][\text{THF}]^2_{\text{free}}}{[\text{Monomer}]^2}$$

Data were obtained from titration experiments of benzene solutions of **4.2-RE** with varying amounts of THF using UV-Vis spectroscopy for **4.2-Nd** and ^{1}H NMR Spectroscopy for **4.2-RE**, RE = La–Sm.

UV-Vis Spectroscopy

A solution of **4.2-Nd** (0.00242 M) in 4.0 mL of benzene was added to an air-tight cuvette with a 1 cm path length. This solution was titrated with THF from 5 equivalents to 450 equivalents. UV-Vis spectra were obtained in the range of 590 – 600 nm at a resolution of 0.01 nm.

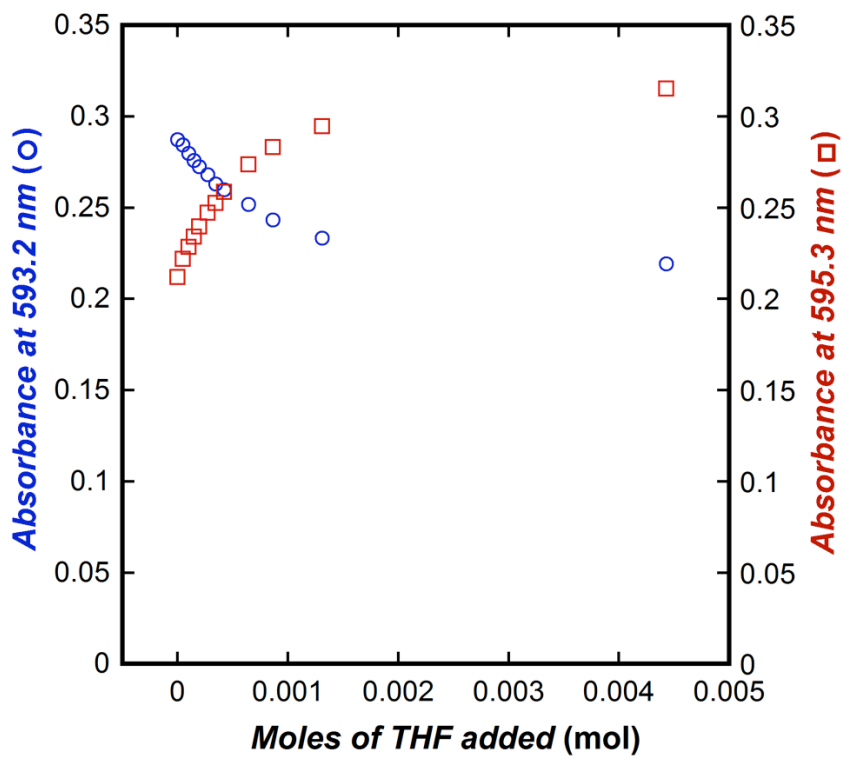

Figure 4.4.82. Plot of absorbance at 593.2 nm (blue circles) and 595.3 nm (red squares) versus number of moles of THF added for the titration of **4.2-Nd** in benzene.

Table 4.4.26. Data from UV-Vis titration experiment of **4.2-Nd**.

$[THF]_0$ M	[Dimer] M	$[THF]_{free}$ M	[Monomer] M	K_{eq}
0	0.00242	0	0	N/A
0.01220	0.00224	0.01181	0.00039	2.08
0.02441	0.00208	0.02371	0.00070	2.42
0.03656	0.00194	0.03560	0.00096	2.68
0.04843	0.00181	0.04722	0.00121	2.77
0.06644	0.00164	0.06490	0.00154	2.90
0.08439	0.00149	0.08257	0.00182	3.09
0.10230	0.00137	0.10023	0.00207	3.20
0.15577	0.00105	0.15306	0.00272	3.33
0.20860	0.00079	0.20542	0.00319	3.29
0.31310	0.00049	0.30934	0.00373	3.37
0.9922	0	0.98782	0.00438	N/A

^{1}H NMR Spectroscopy

A solution of **4.2-RE**, RE = La–Sm, with an internal ferrocene reference in 0.5 mL of C_6D_6 was added to a J-young tube. This solution was titrated with THF. At each titration point, the equilibrium concentrations of dimer and monomer were determined by integration of the compound peaks compared to that of ferrocene at 4 ppm. The concentration of free THF at equilibrium was determined as the difference between the known concentration of added THF and the equilibrium concentration of monomer.

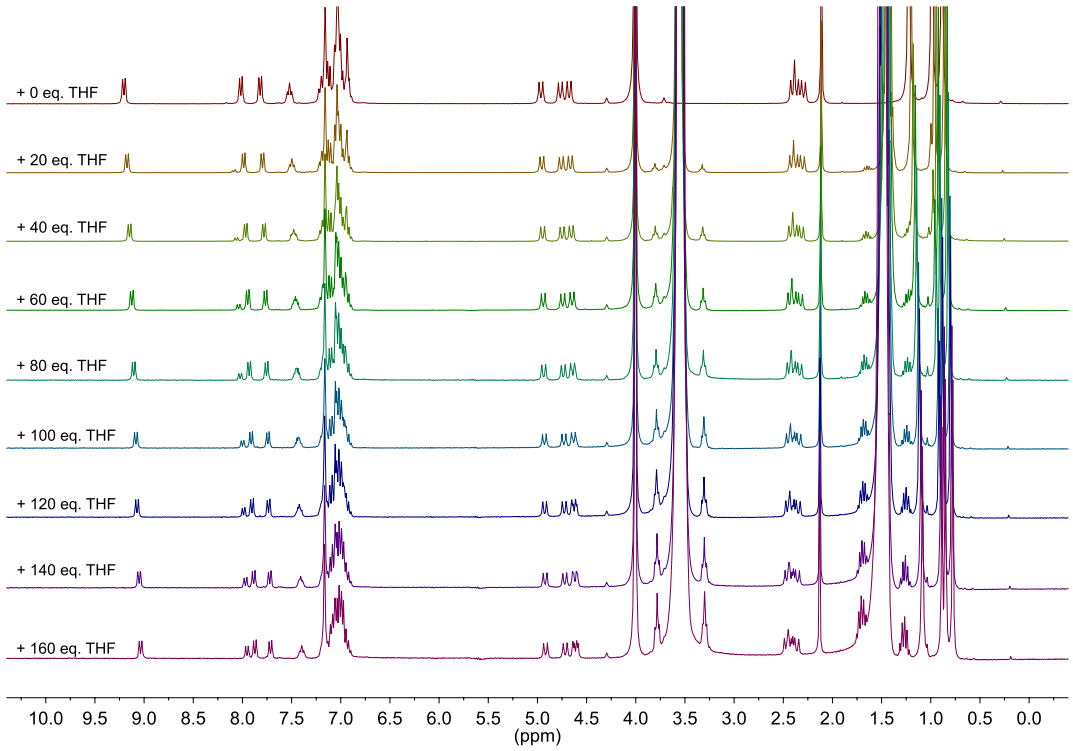

Figure 4.4.83. Titration of **4.2-La** with THF in C_6D_6.

Table 4.4.27. Data from ^{1}H NMR titration experiment of **4.2-La**.

$[THF]_0$ M	[Dimer] M	$[THF]_{free}$ M	[Monomer] M	K_{eq}
0	0.03055	0	0	N/A
0.57280	0.02570	0.57023	0.00257	1265
1.09462	0.02309	1.09139	0.00323	2631
1.57209	0.02107	1.56767	0.00442	2645
2.01064	0.02047	2.00600	0.00464	3827
2.41484	0.01810	2.40947	0.00537	3646
2.78857	0.01676	2.78276	0.00581	3842
3.13515	0.01545	3.12902	0.00613	4028
3.45744	0.01514	3.45058	0.00687	3824

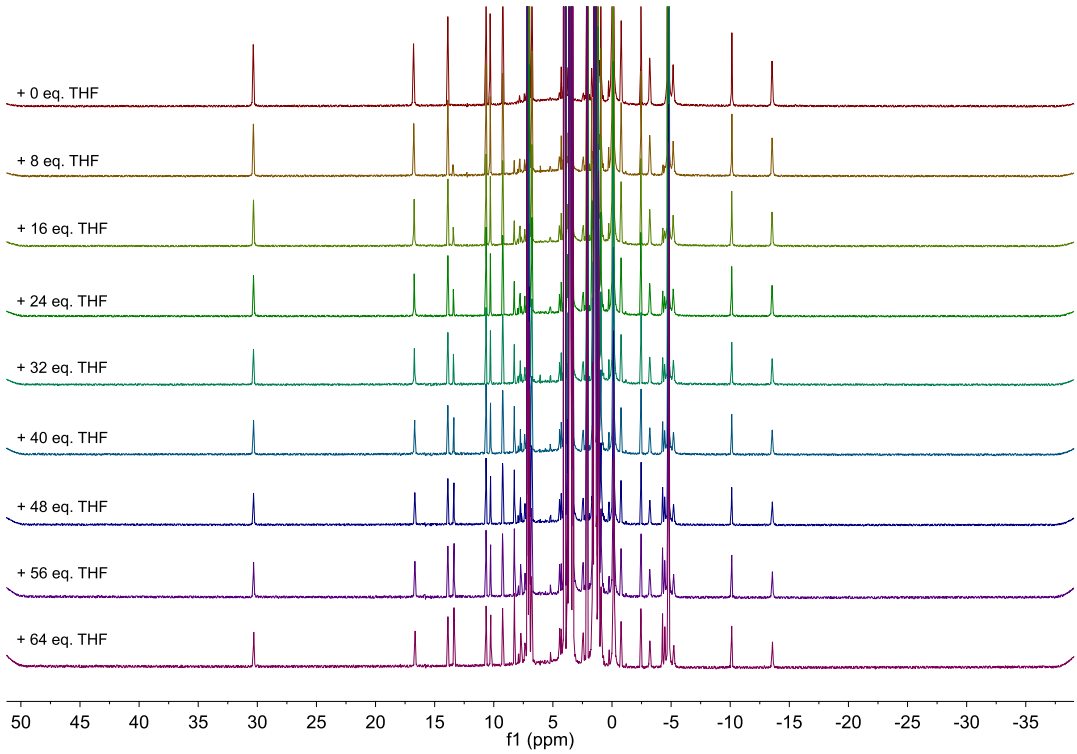

Figure 4.4.84. Titration of **4.2-Ce** with THF in C_6D_6.

Table 4.4.28. Data from ^{1}H NMR titration experiment of **4.2-Ce**.

$[THF]_0$ M	[Dimer] M	$[THF]_{free}$ M	[Monomer] M	K_{eq}
0	0.02844	0	0	N/A
0.21976	0.02577	0.21745	0.00231	228
0.43183	0.02407	0.42763	0.00420	249
0.63660	0.02238	0.63055	0.00605	244
0.83444	0.02033	0.82734	0.00710	276
1.02570	0.01794	1.01685	0.00885	237
1.21070	0.01667	1.20084	0.00986	247
1.38974	0.01485	1.37868	0.01106	231
1.56311	0.01320	1.55104	0.01206	218

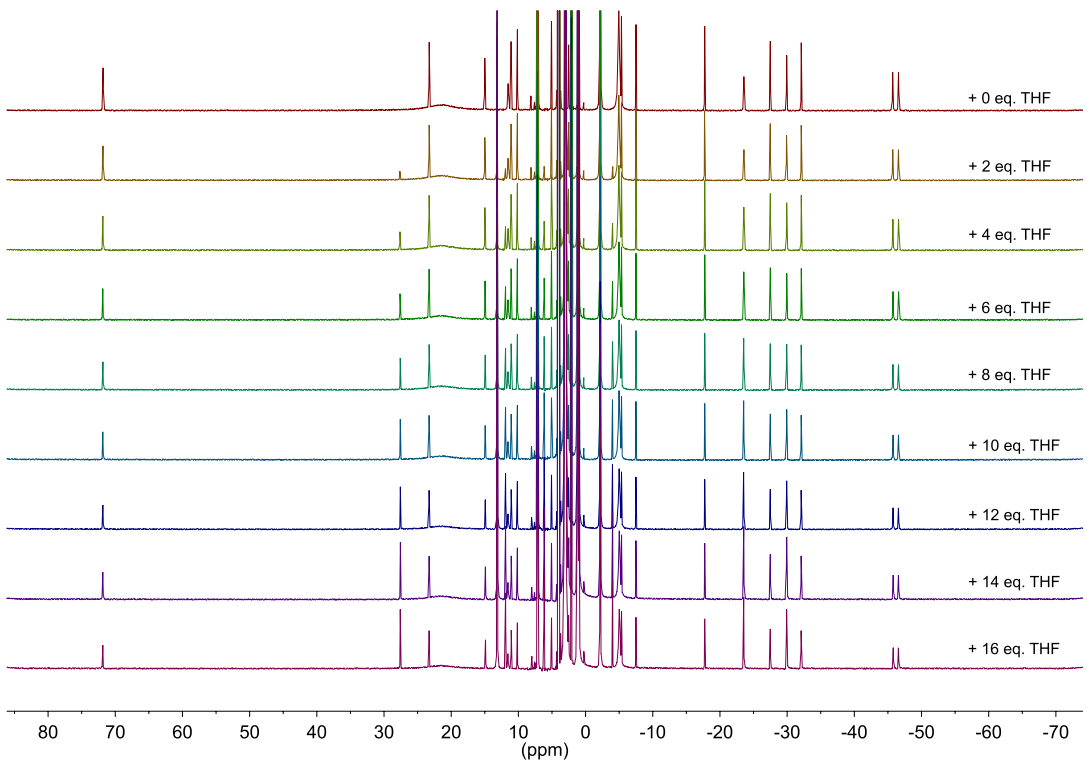

Figure 4.4.85. Titration of **4.2-Pr** with THF in C_6D_6.

Table 4.4.29. Data from ^{1}H NMR titration experiment of **4.2-Pr**.

$[THF]_0$ M	[Dimer] M	$[THF]_{free}$ M	[Monomer] M	K_{eq}
0	0.03786	0	0	N/A
0.07441	0.03453	0.07084	0.00357	13.6
0.14777	0.03291	0.14075	0.00702	13.2
0.22026	0.03066	0.20943	0.01083	11.5
0.29189	0.03097	0.27808	0.01381	12.6
0.36269	0.02838	0.34642	0.01627	12.9
0.43265	0.02791	0.41367	0.01898	13.3
0.50180	0.02222	0.48002	0.02178	10.8
0.57015	0.02178	0.54540	0.02475	10.6

Table 4.4.30. Data from ^{1}H NMR titration experiment of **4.2-Nd**.

$[THF]_0$ M	**[Dimer] M**	**$[THF]_{free}$ M**	**[Monomer] M**	**K_{eq}**
0	0.02708	0	0	N/A
0.02432	0.02566	0.02221	0.00211	2.83
0.04836	0.02463	0.04400	0.00436	2.51
0.07211	0.02358	0.06567	0.00645	2.45
0.09559	0.02263	0.08714	0.00845	2.41
0.11880	0.02171	0.10829	0.01051	2.31
0.14174	0.02106	0.12950	0.01224	2.36
0.16442	0.01960	0.15037	0.01405	2.25
0.18684	0.01912	0.17108	0.01576	2.25

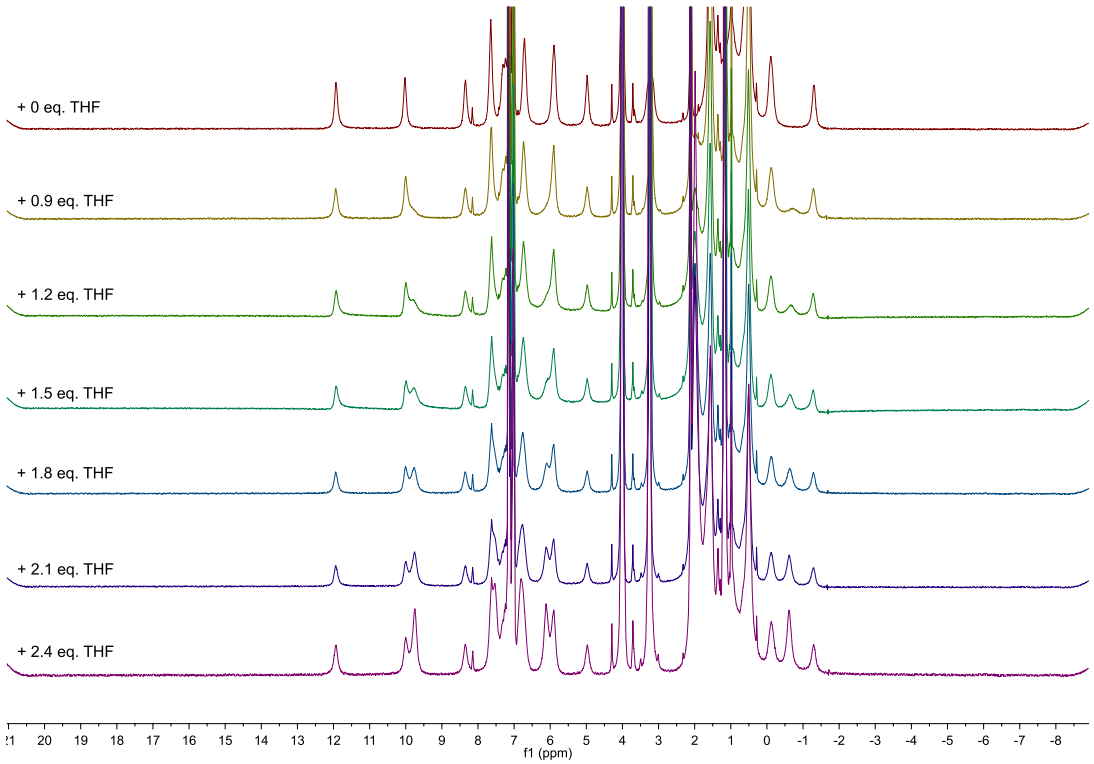

Figure 4.4.86. Titration of **4.2-Sm** with THF in C_6D_6.

Table 4.4.31. Data from ^{1}H NMR titration experiment of **4.2-Sm**.

$[THF]_0$ M	[Dimer] M	$[THF]_{free}$ M	[Monomer] M	K_{eq}
0	0.02710	0	0	N/A
0.02345	0.01929	0.01136	0.01209	0.017
0.03109	0.01881	0.01448	0.01661	0.014
0.03865	0.01700	0.02136	0.01728	0.026
0.04612	0.01551	0.02590	0.02022	0.026
0.05350	0.01418	0.03370	0.01980	0.041
0.06081	0.01317	0.03447	0.02633	0.023

Thermal Gravimetric Analysis (TGA). TGA of complexes (5–10 mg) were performed with a TA Instruments SDT Q600 thermogravimetric analyzer from 18 to 450 ºC at a heating rate of 5 ºC/min in an argon atmosphere with a flow rate of 300 mL/min. The amounts of KOTf byproduct in the TGA samples were determined by ^{19}F NMR spectroscopy using an internal fluorobenzene standard. Determined ratios (by mole) of complex:KOTf were 1:0.2 for **4.1-La**, 1:2.1 for **4.1-Sm**, 1:0.6 for **4.1-Dy**, 1:0.4 for **4.1-Ho**, 1:0.5 for **4.1-Er**, 1:0.3 for **4.1-Tm**, and 1:2.9 for **4.1-Lu**.

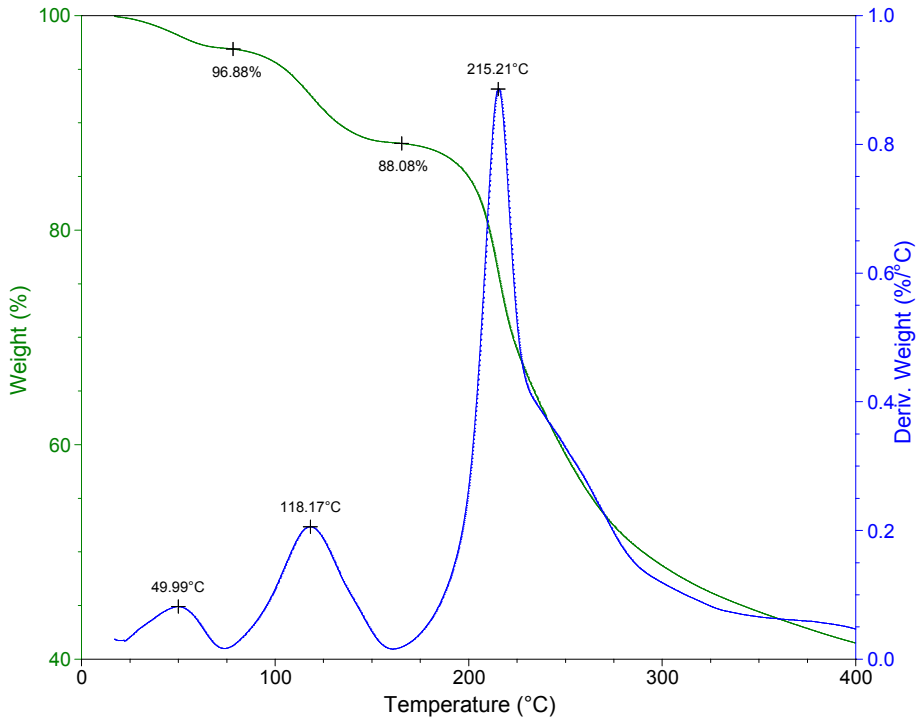

Figure 4.4.87. TGA of **4.1-La**.

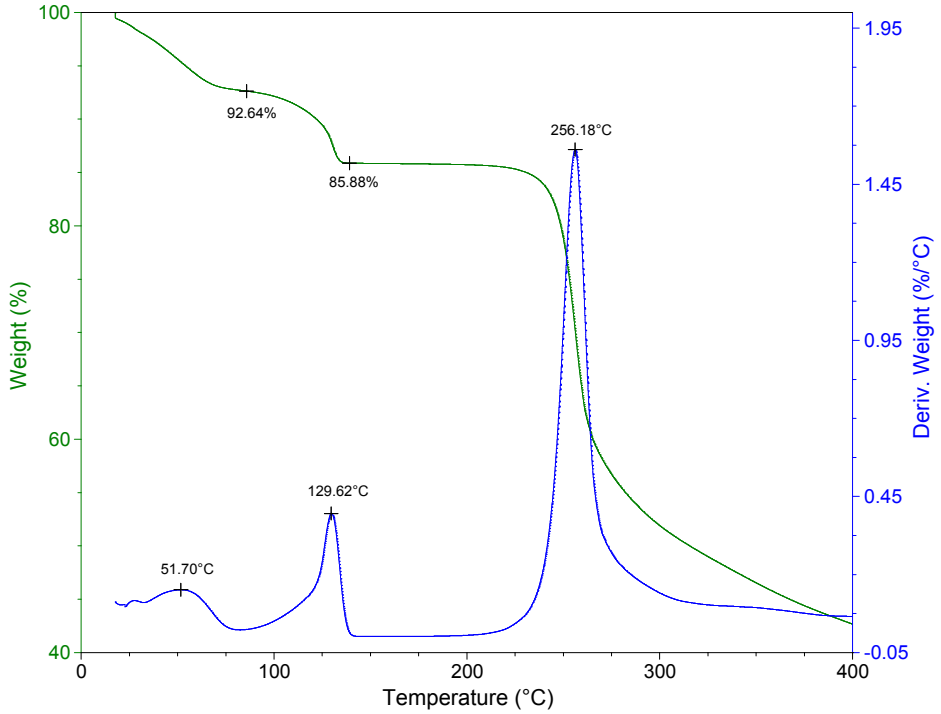

Figure 4.4.88. TGA of **4.1-Sm**.

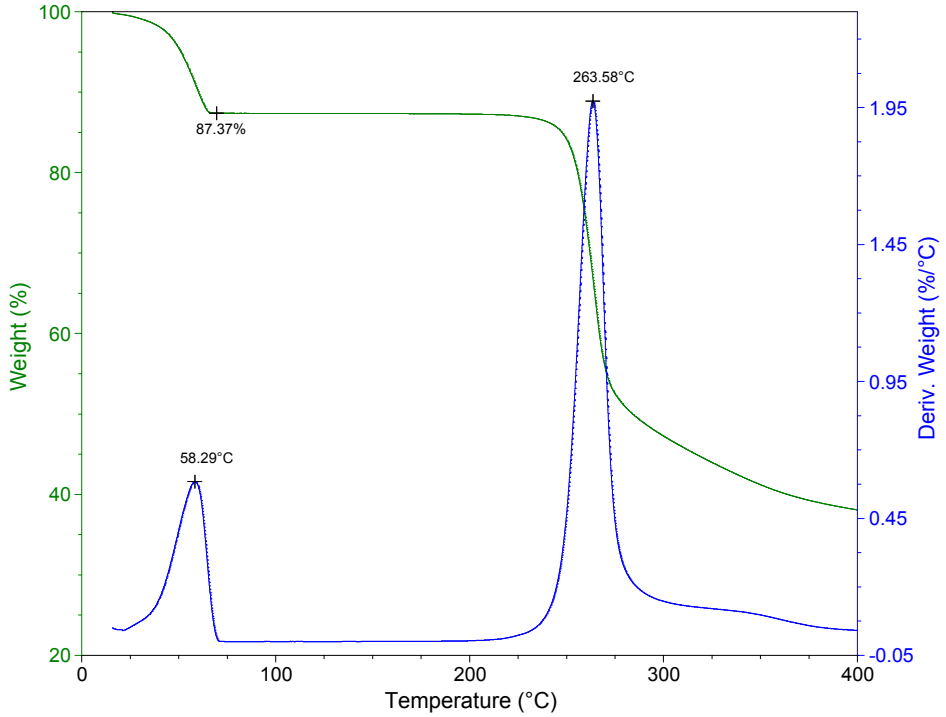

Figure 4.4.89. TGA of **4.1-Dy**.

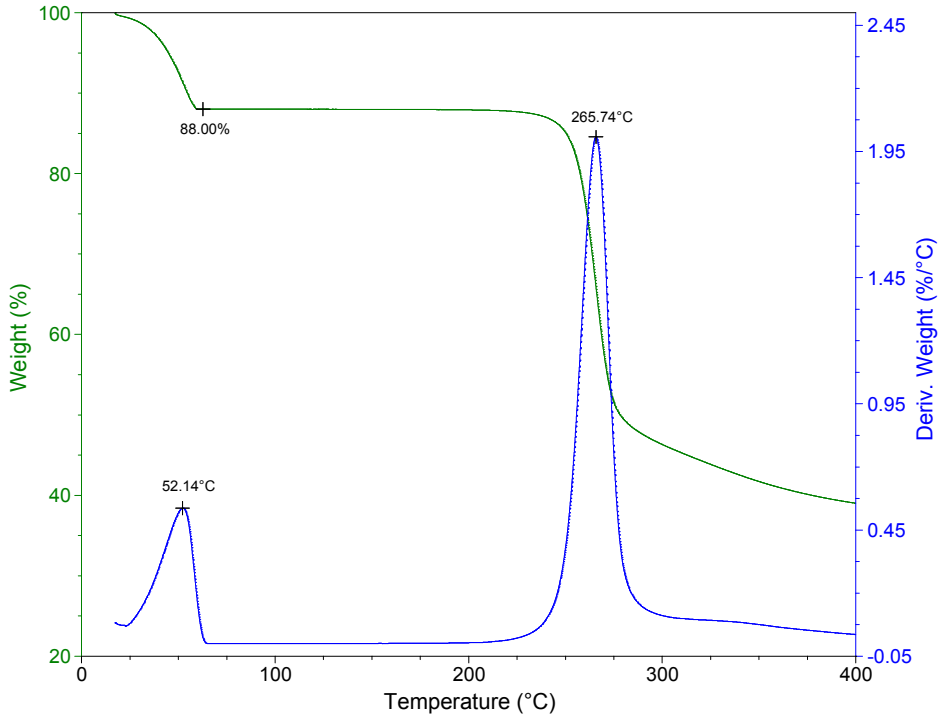

Figure 4.4.90. TGA of **4.1-Ho**.

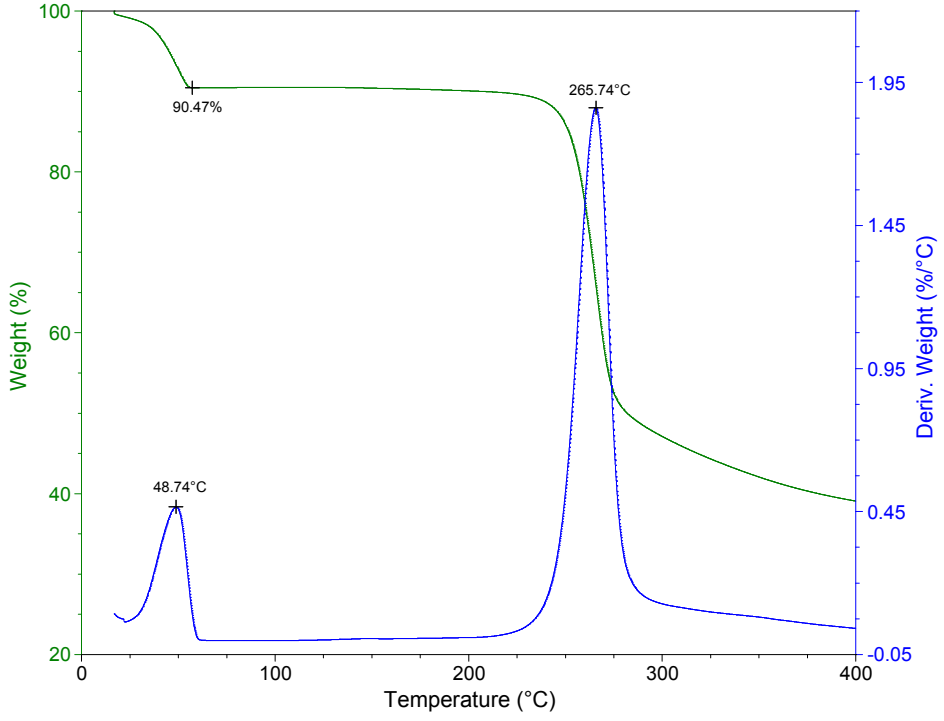

Figure 4.4.91. TGA of **4.1-Er**.

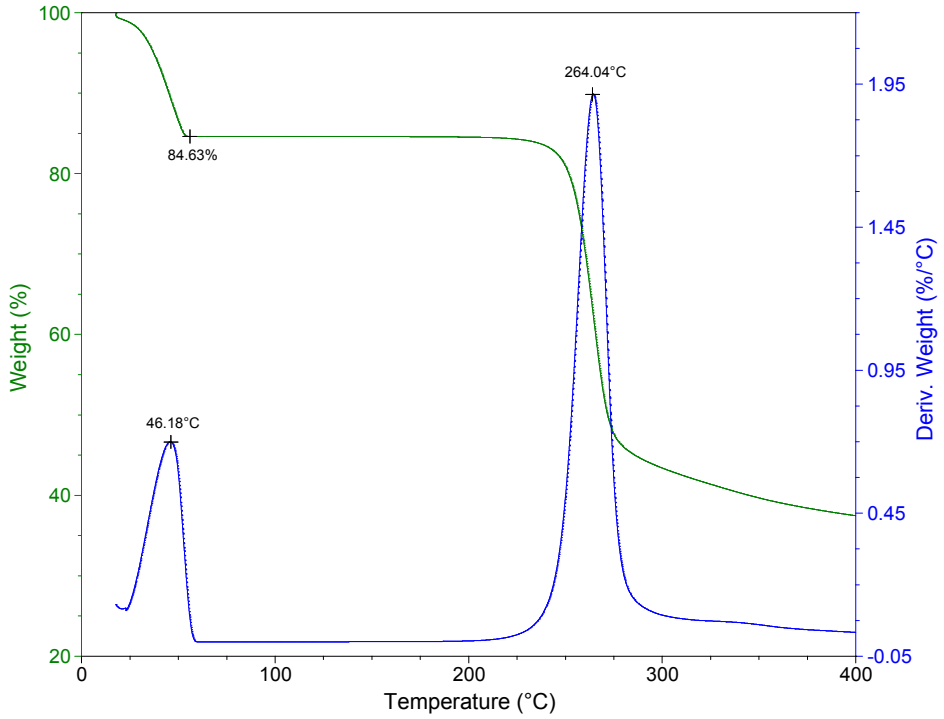

Figure 4.4.92. TGA of **4.1-Tm**.

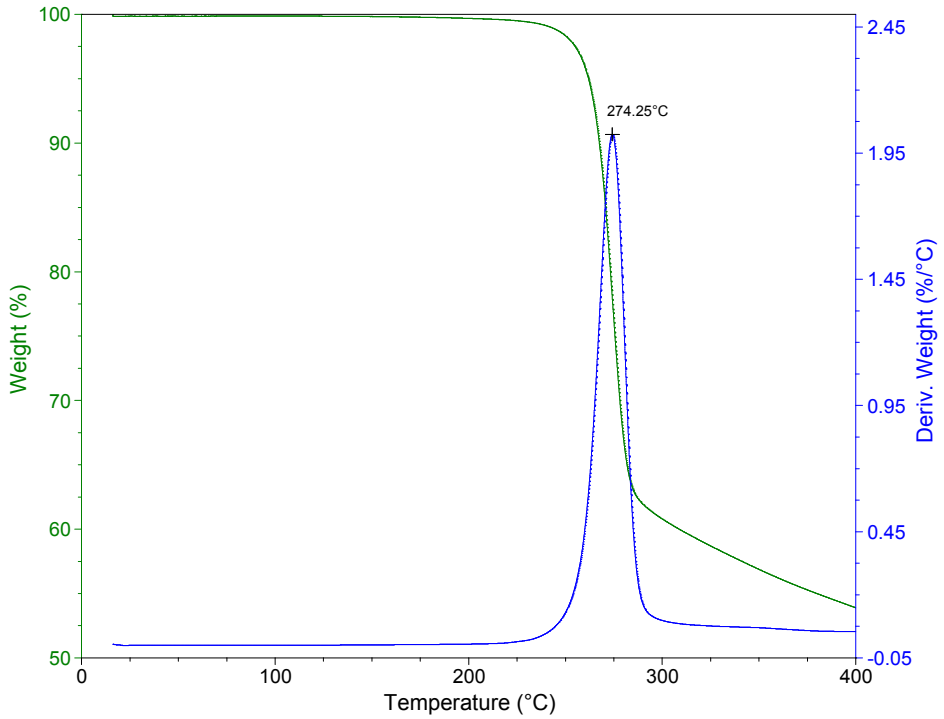

Figure 4.4.93. TGA of **4.1-Lu**.

Computational Details. Gaussian 09 Rev. D.01 was used in electronic structure calculations.[29] The B3LYP hybrid DFT method was employed, with a 28-electron small core pseudopotential on terbium with published segmented natural orbital basis set incorporating quasi-relativistic effects,[30] and the 6-31G* basis set on all other atoms.[31] No restraints were imposed other than spin. Molecular orbitals were rendered with the Chemcraft v1.6 program.[32]

Table 4.4.32. Optimized coordinates of **4.3-Tb**.

Tb	-1.882881969	0.339555268	0.079984729
O	-0.054500433	0.457322166	-1.222236390
O	-1.909188381	1.984975463	1.413361628
O	-2.656369082	-1.914599530	0.232741422
N	-0.989616707	0.932659015	-2.211301520
N	-3.337544558	2.037743886	1.207575053
N	-3.642567077	-2.755784876	0.234222921
N	-4.237036612	0.378784169	-1.458902199
C	-3.813679477	0.674162888	-2.868349418
H	-3.456102313	1.699007956	-2.867130797
H	-4.701078799	0.644393112	-3.520327137
C	-2.765798450	-0.268597503	-3.420213554
C	-3.151251306	-1.280175261	-4.312919603
H	-4.192407237	-1.340060959	-4.620301431
C	-2.232068663	-2.201852128	-4.813478618
H	-2.555769783	-2.970144298	-5.509168717
C	-0.901288494	-2.135806627	-4.398702230
H	-0.178614462	-2.863194914	-4.756891684
C	-0.487987153	-1.125790084	-3.530480054
H	0.535220691	-1.100180043	-3.179371388

C	-1.400938679	-0.168646503	-3.072552870
C	-0.410295822	2.160419878	-2.924610967
C	-0.235682724	3.254779279	-1.867624482
H	0.104927509	4.175557566	-2.353367031
H	0.500102042	2.965564322	-1.116391552
H	-1.182811700	3.476497571	-1.368256983
C	-1.378755643	2.667894452	-4.007584113
H	-2.285479983	3.102920273	-3.579215352
H	-1.650413588	1.894151804	-4.730508711
H	-0.876669184	3.467321744	-4.561409041
C	0.937000597	1.831169593	-3.587971553
H	0.829944256	1.088528306	-4.383907884
H	1.667582871	1.469580128	-2.861140791
H	1.342613244	2.741643281	-4.041609808
C	-5.134631861	1.493274828	-1.005100259
H	-5.576804819	1.171628947	-0.066631869
H	-5.955426960	1.599406220	-1.732553931
C	-4.475386448	2.842575015	-0.819729722
C	-4.755747465	3.879748643	-1.723440012
H	-5.430075980	3.687303266	-2.554440802
C	-4.199975482	5.148793793	-1.568590937
H	-4.438963210	5.937043660	-2.275982844
C	-3.333535035	5.394363131	-0.501164278
H	-2.886132806	6.376033707	-0.374923729
C	-3.044081356	4.379597264	0.409565145
H	-2.349818633	4.553449305	1.222100677
C	-3.629871527	3.113927927	0.274169065

C	-4.034298468	2.112536005	2.564775533
C	-5.551300751	2.264728440	2.368157800
H	-5.805785001	3.136005329	1.757898801
H	-6.016969481	2.406662626	3.348664747
H	-6.000688813	1.370989422	1.924837978
C	-3.510880059	3.290231747	3.407196826
H	-2.418995451	3.280738116	3.453143418
H	-3.900641609	3.207132799	4.427155440
H	-3.841378530	4.254199698	3.009971347
C	-3.756964726	0.791049707	3.295116164
H	-4.063171976	-0.068556515	2.685968993
H	-4.333215783	0.755130791	4.225438608
H	-2.701905340	0.686240681	3.555945582
C	-5.048015600	-0.884037781	-1.492473738
H	-4.409214537	-1.655177226	-1.926053318
H	-5.887547172	-0.734950246	-2.190169228
C	-5.618002485	-1.361652073	-0.172488341
C	-6.910982904	-0.989222729	0.222881724
H	-7.490976779	-0.336175349	-0.423437956
C	-7.478265042	-1.454540783	1.410004147
H	-8.483355151	-1.149252915	1.683965426
C	-6.756768482	-2.318245135	2.234848161
H	-7.185784279	-2.679191963	3.164291710
C	-5.482011182	-2.734568107	1.852380769
H	-4.916469497	-3.412870431	2.480815318
C	-4.929228791	-2.268010821	0.655195265
C	-3.403017405	-4.174926692	-0.251588456

C	-2.231660688	-4.153745970	-1.243692072
H	-2.432853153	-3.492138008	-2.090966031
H	-2.097934824	-5.168244364	-1.631536984
H	-1.296566277	-3.841694846	-0.776236787
C	-3.071868586	-5.068931759	0.961200508
H	-2.239653180	-4.659937083	1.538598330
H	-2.782651290	-6.061363642	0.600715705
H	-3.935011195	-5.198683015	1.619890211
C	-4.677157203	-4.679336165	-0.950588520
H	-5.539015743	-4.706035877	-0.279295958
H	-4.496465229	-5.700558899	-1.299356311
H	-4.929600861	-4.069420411	-1.823865868
Tb	1.882876201	-0.338922970	-0.079381660
O	0.054347516	-0.456833769	1.222631145
O	1.907921239	-1.984308213	-1.412781031
O	2.657759887	1.914639769	-0.233546879
N	0.989320992	-0.931855947	2.212006013
N	3.336249445	-2.037963172	-1.207149292
N	3.644530853	2.755157960	-0.235568111
N	4.236804991	-0.379139593	1.459108943
C	3.813356324	-0.673765603	2.868701882
H	3.455346669	-1.698459083	2.867878736
H	4.700763171	-0.644085310	3.520667245
C	2.765822295	0.269667588	3.420096177
C	3.151616285	1.281690756	4.312149899
H	4.192793393	1.341446535	4.619482990
C	2.232718445	2.203956693	4.812145150

H	2.556663209	2.972594521	5.507339087
C	0.901894434	2.138035347	4.397474375
H	0.179455221	2.865860634	4.755247652
C	0.488237383	1.127576857	3.529936017
H	-0.535043428	1.102007028	3.179002557
C	1.400914099	0.169895421	3.072552256
C	0.409727188	-2.159024374	2.926021097
C	0.235368390	-3.254161898	1.869795622
H	-0.105564534	-4.174513224	2.356124384
H	-0.500065478	-2.965392112	1.118046046
H	1.182666769	-3.476369003	1.370970668
C	1.377846379	-2.665726444	4.009673956
H	2.284661219	-3.101143338	3.581893185
H	1.649359891	-1.891446565	4.732079309
H	0.875549006	-3.464687790	4.563978260
C	-0.937758469	-1.829239652	3.588704876
H	-0.830963245	-1.085943884	4.384065489
H	-1.668113991	-1.468251078	2.861346366
H	-1.343524493	-2.739343366	4.042943710
C	5.133693836	-1.494319688	1.005579508
H	5.576178009	-1.173105521	0.067108411
H	5.954346222	-1.600874586	1.733128607
C	4.473606793	-2.843231216	0.820300842
C	4.753356282	-3.880496122	1.724101647
H	5.427728762	-3.688352593	2.555138184
C	4.196960939	-5.149272714	1.569278503
H	4.435499904	-5.937602418	2.276733583

C	3.330493848	-5.394471400	0.501786689
H	2.882627631	-6.375931523	0.375553639
C	3.041604928	-4.379603604	-0.409007665
H	2.347310857	-4.553146230	-1.221583374
C	3.628012078	-3.114217964	-0.273643621
C	4.032817819	-2.113274419	-2.564400855
C	5.549711949	-2.266771069	-2.367968259
H	5.803523668	-3.138363057	-1.757879465
H	6.015157313	-2.408927388	-3.348549143
H	5.999912775	-1.373489112	-1.924552381
C	3.508308459	-3.290513571	-3.406784893
H	2.416427788	-3.280092631	-3.452600064
H	3.898043745	-3.207741914	-4.426778951
H	3.838022726	-4.254769384	-3.009600130
C	3.756525799	-0.791516362	-3.294664855
H	4.063716611	0.067788582	-2.685602204
H	4.332523985	-0.756149393	-4.225164102
H	2.701488544	-0.685682759	-3.555189864
C	5.048545481	0.883216540	1.492169228
H	4.410191610	1.654953231	1.925353513
H	5.887925110	0.733906158	2.189993817
C	5.618964529	1.359865576	0.172020196
C	6.911780374	0.986461556	-0.222982758
H	7.491253539	0.333320923	0.423711370
C	7.479556129	1.450929006	-1.410199561
H	8.484506377	1.144911222	-1.683857834
C	6.758733370	2.314741527	-2.235525275

H	7.188127740	2.675034757	-3.165047232
C	5.484174300	2.732013652	-1.853446728
H	4.919164274	3.410406730	-2.482261364
C	4.930884269	2.266293318	-0.656163792
C	3.405899654	4.174774538	0.249298221
C	2.235481512	4.154809733	1.242561236
H	2.437194592	3.493670749	2.090082030
H	2.102594828	5.169624681	1.629861958
H	1.299796529	3.842901354	0.776214911
C	3.073882449	5.067860768	-0.963926766
H	2.241146577	4.658490465	-1.540304530
H	2.785084135	6.060624064	-0.604020449
H	3.936498442	5.196953537	-1.623436926
C	4.680822476	4.679329418	0.946750191
H	5.542098200	4.705271359	0.274685597
H	4.500738933	5.700866139	1.294908905
H	4.933860304	4.069982281	1.820254979

4.5 References

[1] M. Humphries, Rare Earth Elements: The Global Supply Chain, **2013**, pp. 1-26.

[2] a) D. Goll, H. Kronmüller, *Naturwissenschaften* **2000**, *87*, 423-438; b) O. Gutfleisch, M. A. Willard, E. Brück, C. H. Chen, S. G. Sankar, J. P. Liu, *Adv. Mater.* **2011**, *23*, 821-842.

[3] a) M. Sagawa, S. Fujimura, H. Yamamoto, Y. Matsuura, K. Hiraga, *IEEE Trans. Magn.* **1984**, *20*, 1584-1589; b) S. Constantinides, The Important Role of Dysprosium in Modern Permanent Magnets, Rochester, NY., **2012**, pp. 1-8.

[4] a) K. Binnemans, P. T. Jones, B. Blanpain, T. Van Gerven, Y. Yang, A. Walton, M. Buchert, *J. Clean Prod.* **2013**, *51*, 1-22; b) S. Hoenderdaal, L. Tercero Espinoza, F. Marscheider-Weidemann, W. Graus, *Energy* **2013**, *49*, 344-355.

[5] E. Alonso, A. M. Sherman, T. J. Wallington, M. P. Everson, F. R. Field, R. Roth, R. E. Kirchain, *Environ. Sci. Technol.* **2012**, *46*, 3406-3414.

[6] U. S. D. o. Energy, Critical Materials Strategy, Washington, D. C., **2011**, pp. 1-191.

[7] F. Xie, T. A. Zhang, D. Dreisinger, F. Doyle, *Miner. Eng.* **2014**, *56*, 10-28.

[8] X. Du, T. E. Graedel, *J. Ind. Ecol.* **2011**, *15*, 836-843.

[9] B. Sprecher, Y. Xiao, A. Walton, J. Speight, R. Harris, R. Kleijn, G. Visser, G. J. Kramer, *Environ. Sci. Technol.* **2014**, *48*, 3951-3958.

[10] a) C. Sonich-Mullin, Rare Earth Elements: A Review of Production, Processing, Recycling and Associated Issues, Cincinatti, **2012**; b) D. Schüler, M. Buchert, R. Liu, S. Dittrich, C. Merz, Study on Rare Earths and Their Recycling, Darmstadt, **2011**; c) T. Elwert, D. Goldmann, F. Römer, *World Metall. - Erzmet.* **2013**, *66*, 209-219; d) T. Elwert, D. Goldmann, F. Römer, *World Metall. - Erzmet.* **2014**, *67*, 287-296.

[11] D. Dupont, K. Binnemans, *Green Chem.* **2015**, *17*, 856-868.

[12] a) V. Innocenzi, I. De Michelis, B. Kopacek, F. Vegliò, *Waste Manage.* **2014**, *34*, 1237-1250; b) H. Liu, S. Zhang, D. Pan, J. Tian, M. Yang, M. Wu, A. A. Volinsky, *J. Hazard. Mater.* **2014**, *272*, 96-101; c) F. Yang, F. Kubota, Y. Baba, N. Kamiya, M. Goto, *J. Hazard. Mater.* **2013**, *254–255*, 79-88.

[13] C. K. Gupta, N. Krishnamurthy, *Extractive Metallurgy of Rare Earths*, CRC Press, New York, **2005**.

[14] M. Yuan, A. Luo, D. Li, *Acta Metall. Sin. (Engl. Lett.)* **1995**, *8*, 10-14.

[15] X. Wang, W. Li, S. Meng, D. Li, *J. Chem. Technol. Biotechnol.* **2006**, *81*, 761-766.

[16] B. Wei, Y. Li, H. Li, J. Yu, B. Ye, T. Liang, *Ecotoxicol. Environ. Saf.* **2013**, *96*, 118-123.

[17] A. M. Johnson, M. C. Young, X. Zhang, R. R. Julian, R. J. Hooley, *J. Am. Chem. Soc.* **2013**, *135*, 17723-17726.

[18] X. Zhao, M. Wong, C. Mao, T. X. Trieu, J. Zhang, P. Feng, X. Bu, *J. Am. Chem. Soc.* **2014**, *136*, 12572-12575.

[19] Q. Chen, C. Buss, V. Young, Jr., S. Fox, *J. Chem. Crystallogr.* **2005**, *35*, 177-181.

[20] G. R. Choppin, D. E. Henrie, K. Buijs, *Inorg. Chem.* **1966**, *5*, 1743-1748.

[21] S. Cotton, in *Lanthanide and Actinide Chemistry*, John Wiley & Sons Inc., Hoboken, NJ, **2006**.

[22] G. L. B. Scheffler, F. R. S.; Pozebon, D.;, *Br. J. Anal. Chem.* **2012**, *8*, 358-365.

[23] Bruker (2009) SAINT. Bruker AXS Inc., Madison, Wisconsin, USA.

[24] Bruker (2009) SHELXTL. Bruker AXS Inc., Madison, Wisconsin, USA.

[25] Sheldrick, G.M. (2008) TWINABS. University of Göttingen: Göttingen, Germany.

[26] Sheldrick, G.M. (2007) SADABS. University of Göttingen: Göttingen, Germany.

[27] G. Sheldrick, *Acta Crystallogr. Sect. A* **2008**, *64*, 112-122.

[28] R. K. Thomson, B. L. Scott, D. E. Morris, J. L. Kiplinger, *C. R. Chimie* **2010**, *13*, 790-802.

[29] Gaussian 09, Revision D.01, Frisch, M. J.; Trucks, G. W.; Schlegel, H. B.; Scuseria, G. E.; Robb, M. A.; Cheeseman, J. R.; Scalmani, G.; Barone, V.; Mennucci, B.; Petersson, G. A.; Nakatsuji, H.; Caricato, M.; Li, X.; Hratchian, H. P.; Izmaylov, A. F.; Bloino, J.; Zheng, G.; Sonnenberg, J. L.; Hada, M.; Ehara, M.; Toyota, K.; Fukuda, R.; Hasegawa, J.; Ishida, M.; Nakajima, T.; Honda, Y.; Kitao, O.; Nakai, H.; Vreven, T.; Montgomery, Jr., J. A.; Peralta, J. E.; Ogliaro, F.; Bearpark, M.; Heyd, J. J.; Brothers, E.; Kudin, K. N.; Staroverov, V. N.; Kobayashi, R.; Normand, J.; Raghavachari, K.; Rendell, A.; Burant, J. C.; Iyengar, S. S.;

Tomasi, J.; Cossi, M.; Rega, N.; Millam, N. J.; Klene, M.; Knox, J. E.; Cross, J. B.; Bakken, V.; Adamo, C.; Jaramillo, J.; Gomperts, R.; Stratmann, R. E.; Yazyev, O.; Austin, A. J.; Cammi, R.; Pomelli, C.; Ochterski, J. W.; Martin, R. L.; Morokuma, K.; Zakrzewski, V. G.; Voth, G. A.; Salvador, P.; Dannenberg, J. J.; Dapprich, S.; Daniels, A. D.; Farkas, Ö.; Foresman, J. B.; Ortiz, J. V.; Cioslowski, J.; Fox, D. J. Gaussian, Inc., Wallingford CT, 2009.

[30] a) X. Cao, M. Dolg, *J. Molec. Struct. (Theochem)* **2002**, *581*, 139-147; b) M. Dolg, H. Stoll, H. Preuss, *J. Chem. Phys.* **1989**, *90*, 1730-1734.

[31] W. J. Hehre, R. Ditchfield, J. A. Pople, *J. Chem. Phys.* **1972**, *56*, 2257-2261.

[32] Chemcraft. www.chemcraftprog.com.

Chapter 5

Controlled Redox Chemistry of Cerium within a Tripodal Nitroxide Ligand Framework

Abstract

Ligand reorganization has a profound effect on the outcome of cerium redox chemistry. Through the use of the tethered, tripodal, trianionic nitroxide ligand, $[((2\text{-}^{t}BuNOH)C_6H_4CH_2)_3N]^{3-}$ ($TriNOx^{3-}$), controlled redox chemistry on cerium was performed and typically reactive complexes of tetravalent cerium were isolated. These included the cationic complexes $[Ce(TriNOx)thf][BAr^{F}_4]$, where Ar^{F} = 3,5-$(CF_3)_2$-C_6H_3, and [Ce(TriNOx)py][OTf]. A rare complete Ce^{IV}–halide series, Ce(TriNOx)X where X = F, Cl, Br, I, was also synthesized. The solution chemistries of these complexes were explored through electrochemistry and ^{1}H NMR experiments, which showed a unique shift in the ratio of species with inner and outer sphere anions with size of the anionic X ligand. DFT calculations on the series of complexes corroborated these experimental findings.

Adapted from work submitted to *Chem. Eur. J.*, **2015.**

5.1 Introduction

A recent survey of the literature by our group showed that the redox properties of cerium(III) are highly sensitive to ligand field.[1] For example, exchanging the weakly coordinating nitrate ligands in ceric ammonium nitrate ($E_{1/2}$ = 1.21 V vs Fc/Fc^+) with catecholate ligands in $[Ce(O_2C_6H_4)_4]^{4-}$ ($E_{1/2}$ = –0.85 V vs Fc/Fc^+) changed the cerium cation from a potent oxidant to a potent reductant.[2] Understanding the characteristics that underlie the tuning of the redox potential of cerium has broad applications in energy science,[3] separations chemistry,[4] and organic synthesis.[2b] This has motivated renewed interest by us and others in studying the coordination chemistry of cerium in the 4+ oxidation state.[5]

Few studies have explored the coordination chemistry of Ce^{IV} in tripodal, trianionic ligand environments.[6] In a seminal study by Scott and coworkers, use of the silyl substituted tris(2-aminoethyl)amine ligand, $[N(CH_2CH_2N(SiMe_2{}^tBu))_3]^{3-}$ (NN'_3), afforded isolation of the Ce^{IV} oxidation state, in particular of the $CeI(NN'_3)$ complex. In the cases of Cl and Br, however, the stability of the 4+ oxidation state was not sufficient to inhibit trapping of the mixed valent $Ce^{IV/III}$ dimers, $[Ce(NN'_3)]_2(\mu\text{-}X)$, X = Cl, Br, which served as thermodynamic sinks to the reactions.[6a] In contrast, extensive studies have been performed on the coordination chemistry of tripodal trianionic ligands to various transition metals as well as uranium in the f-block.[7]

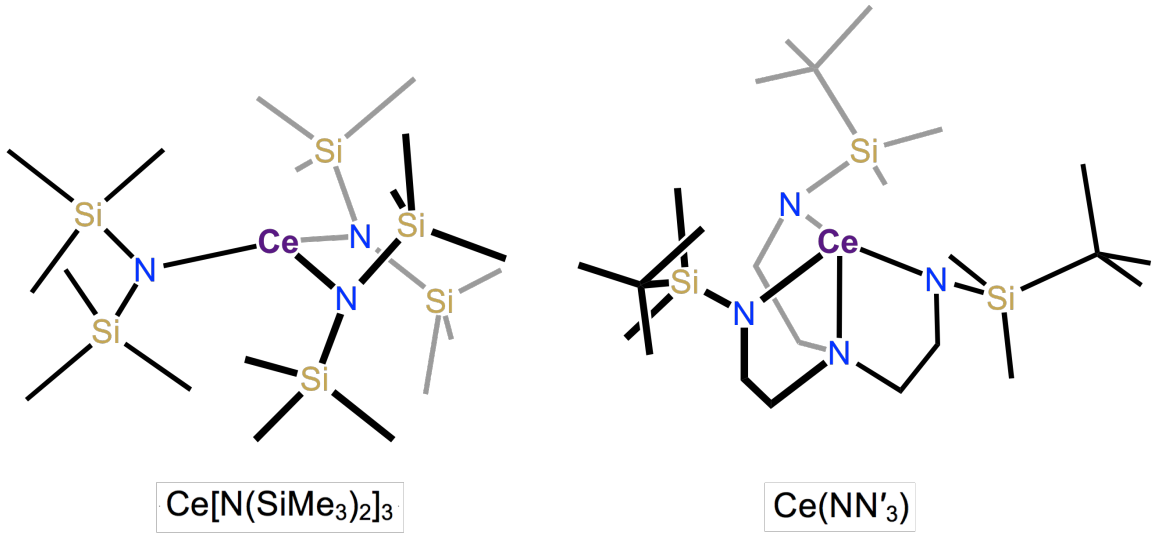

Figure 5.1.1. Select published *tris*(silylamide) complexes of cerium.

The coordination and redox chemistries of cerium within the related, untethered $Ce[N(SiMe_3)_2]_3$ system have also been studied. Unlike the $Ce(NN'_3)$ system, no reaction occurred upon addition of molecular halogens to $Ce^{III}[N(SiMe_3)_2]_3$ ($Ce^{IV/III}$ $E_{1/2}$ = 0.35 V vs. Fc/Fc^+).[6a, 8] Therefore, while $CeI(NN'_3)$ could be formed through oxidation with molecular I_2, an analogous reaction in the formation of $CeI[N(SiMe_3)_2]_3$ did not occur. In fact, $CeI[N(SiMe_3)_2]_3$ was formed through a halide transfer reaction from a cerium(IV) precursor, $CeF[N(SiMe_3)_2]_3$, using $Me_3Si–I$ rather than through oxidation of $Ce^{III}[N(SiMe_3)_2]_3$.[5e] Scott and coworkers postulated that the increased stability of the Ce^{IV} state in their tethered $Ce(NN'_3)$ systems compared to $Ce[N(SiMe_3)_2]_3$ system was a result of reduced ligand reorganization involved in accommodating the X^- ligand in the former. Indeed, ligand reorganization has been shown to have profound effects on the redox chemistry at cerium.[5b] As shown by Anwander and coworkers, oxidation of $Ce[N(SiHMe_2)_2]_3(thf)_2$ with chlorinating agents in THF led to the clean formation of $Ce[N(SiHMe_2)_2]_4$ through ligand redistribution pathways. Performing the same reaction in non-coordinating solvents, however, led to the formation of the $Ce_5[N(SiHMe_2)_2]_8Cl_7$ cluster and other intractable products.[5j] In this context, there is a clear need to expand the coordination chemistry of cerium using strongly donating, tethered tripodal systems where reduced ligand reorganization effects would confer stability to the Ce^{IV} oxidation state and allow for rational syntheses of Ce^{IV} complexes.

In Chapter 4, we reported on the synthesis of the tripodal trianionic nitroxide, $[((2\text{-}^tBuNOH)C_6H_4CH_2)_3N]^{3-}$ ($TriNOx^{3-}$), and its coordination chemistry with the rare earth elements La–Lu, and Y. The η^2-(N,O) binding mode of the three ligand arms provided a single coordination site for substrate binding. Furthermore, in Chapter 3, we showed that nitroxide ligand fields provided significant stabilization to the Ce^{IV} state through increased electron donation into the empty metal 4f orbitals from the well energy-matched N–O π* orbitals. We hypothesized that the environment of $TriNOx^{3-}$ would impart an improved stabilization to the Ce^{IV} state compared to the NN'_3 framework while providing a single coordination site to elucidate controlled redox chemistry.

Herein we report on the redox chemistry of **4.1-Ce** from which the Ce^{IV} complexes, [Ce(TriNOx)thf][$BAr^F{}_4$] (**5.1-BAr$^F{}_4$**) and [Ce(TriNOx)pyr][OTf] (**5.1-OTf**), rare examples of crystallographically characterized cationic Ce^{IV} complexes, were accessed. The complete halide series, Ce(TriNOx)X, where X = F (**5.1-F**), Cl (**5.1-Cl**), Br (**5.1-Br**), and I (**5.1-I**), were also synthesized. Detailed characterization of the cerium complexes were carried out to understand their coordination chemistries in solution. These included solution phase electrochemistry and ^{1}H NMR spectroscopy experiments. DFT calculations corroborated the experimental findings and provided evidence for 4f orbital mixing in the Ce^{IV} complexes.

5.2 Results/Discussion

The shortage of tridentate frameworks that stabilize the Ce^{IV} oxidation state in the literature prompted us to study the redox chemistry of cerium using the $TriNOx^{3-}$ framework. As mentioned in Chapter 4, the cyclic voltammogram of **4.1-Ce** showed only one wave centered at –0.96 V versus Fc/Fc^+ (E_{pa} = –0.88 V, E_{pc} = –1.04 V). Based on the open circuit potential of –1.14 V, this wave was assigned as the metal based $Ce^{IV/III}$ redox couple. This was confirmed chemically through the isolation of a series of Ce^{IV} complexes (*vide infra)*. The measured potential was compared to that of the $Ce^{IV/III}$ redox couple for $Ce[N(SiMe_3)_2]_3$, which showed a quasi-reversible $Ce^{IV/III}$ wave at $E_{1/2}$ = 0.35 V versus Fc/Fc^+.[8] This 1.31 V shift in $Ce^{IV/III}$ redox potential between **4.1-Ce** and $Ce[N(SiMe_3)_2]_3$ indicated the stability to the 4+ oxidation state imposed by the $TriNOx^{3-}$ framework relative to the $[N(SiMe_3)_2]^-$ framework. Furthermore, the peak separation, ΔE, of 0.16 V in **4.1-Ce** compared to ~0.5 V in $Ce[N(SiMe_3)_2]_3$ was suggestive of a relatively small ligand reorganization involved in the oxidation of **4.1-Ce** compared to that in the oxidation of $Ce[N(SiMe_3)_2]_3$. These results are summarized in Table 5.2.1 and compared to the redox potentials of the $Ce^{IV/III}$ couple for cerium in other salient ligand frameworks.

Table 5.2.1. Redox potentials of the $Ce^{IV/III}$ couple (in V versus Fc/Fc^{+}) for cerium in salient ligand frameworks.

	$E_{1/2\ Ce}^{IV/III}$	$\Delta E_{1/2\ Ce}^{IV/III}$	I_{pa}/i_{pc}	ref
$[^{n}Bu_4N]_2[Ce(NO_3)_6]$	0.62	0.075	–	[9]
$Ce[N(SiMe_3)_2]_3$	0.35	~0.5	~2	[10]
CeLiB[a]	–0.76	0.64	1.94	[5b]
3.2-H	–1.80	0.19	0.90	Chapter 3
4.1-Ce	–0.96	0.16	1.08	Chapter 4

[a] CeLiB = $[M_3(THF)_4][(binolate)_3Ce(THF)]$, M = Li, Na, K; B = (*S*)-binolate

The absence of a second oxidation feature to 1.0 V suggested that formation of the doubly oxidized $[Ce^{IV}(TriNOx^{2-})]^{2+}$ complex, where both the metal center and one of the nitroxide arms of the ligand were oxidized, was chemically unfeasible. This result was surprising given the ease at which free $H_3TriNOx$ was oxidized ($E_{1/2}$ = –0.55 V versus Fc/Fc^{+}) and indicated that coordination to the highly Lewis acidic Ce^{IV} center stabilized the potential of the $TriNOx^{3-/2-}$ redox couple by over 1.0 V.

5.2.1 Controlled Redox Chemistry of 4.1-Ce

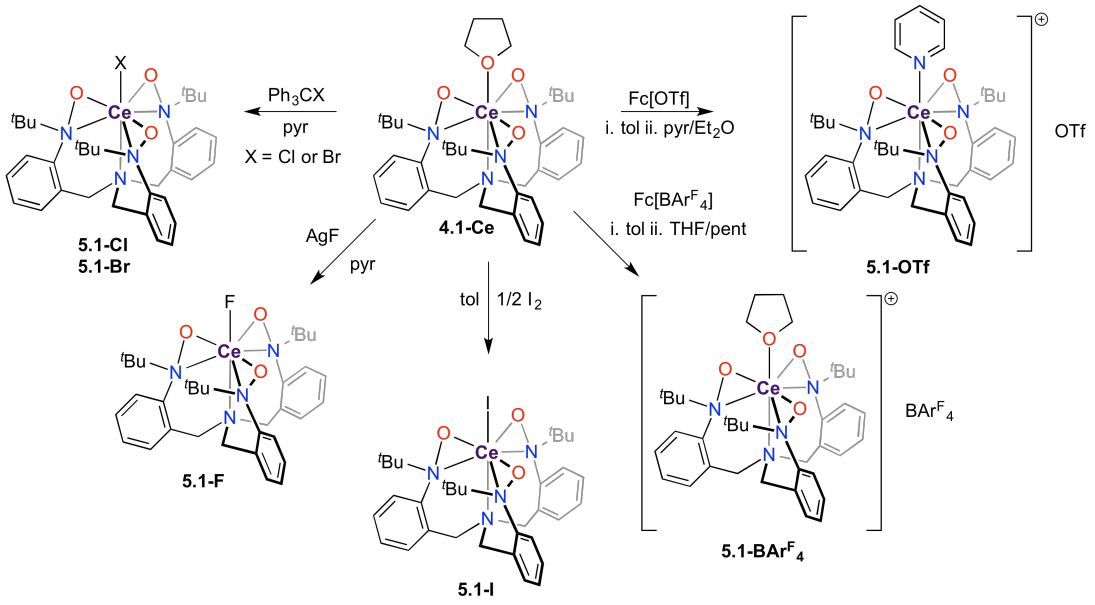

Scheme 5.2.1.1. Schematic of the redox chemistry performed on **4.1-Ce** to form the series of **5.1-X** complexes, where **X** = **BAr^F_4**, **OTf**, **F**, **Cl**, **Br**, and **I**.

Based on the measured redox potential of cerium within the $TriNOx^{3-}$ ligand framework, ferrocenium salts were selected as oxidants for controlled oxidation chemistry at the cerium cation. The quasi-reversibility of the $Ce^{IV/III}$ redox wave in the CV of **4.1-Ce** suggested that a cationic $[Ce(TriNOx)thf]^{+}$ complex could be isolable. In fact, reaction of **4.1-Ce** with $Fc[BAr^{F}_{4}]$ in toluene led to the immediate formation of a sparingly soluble dark red-brown solid. Crystallization of this complex through vapor diffusion of pentane into a saturated THF solution induced formation of X-ray quality crystals of $[Ce(TriNOx)thf][BAr^{F}_{4}]$ (**5.1-BAr$^{F}_{4}$**), where Ar^{F} = 3,5-$(CF_3)_2$-C_6H_3. Similarly, reaction of **4.1-Ce** with Fc[OTf] in toluene led to the formation of an insoluble dark red-brown solid. Crystallization of this complex by vapor diffusion of Et_2O into a saturated pyridine solution afforded X-ray quality crystals of [Ce(TriNOx)pyr][OTf] (**5.1-OTf**) (Scheme 5.2.1.1).

Complexes **5.1-BAr$^{F}_{4}$** and **5.1-OTf** are rare examples of structurally characterized cationic cerium complexes. To date, only one other crystallographically characterized cationic Ce^{IV} complex, $[(TRENDSAL)Ce][BPh_4]$, has been reported.[11] Like with $TriNOx^{3-}$, the Schiff base framework in $[(TRENDSAL)Ce][BPh_4]$ was sufficiently bulky and electron rich to mitigate the strong Lewis acidity of the Ce^{IV} cation and prevent unwanted reactivity. The structural metrics of **5.1-BAr$^{F}_{4}$** and **5.1-OTf** were consistent with the central cerium cation being in the 4+ oxidation state. The N–O bond lengths ranged from 1.418(8) Å to 1.436(7) Å in **5.1-BAr$^{F}_{4}$** and 1.431(4) Å to 1.435(4) Å in **5.1-OTf**, which fell in the range of typical anionic nitroxide bond lengths and were similar to that of 1.433(2) Å for the N–O bonds found in **4.1-Ce**.[12] The average $Ce–O_{nitroxide}$ and $Ce–N_{nitroxide}$ bond lengths of 2.156(5) Å and 2.493(6) Å, respectively, in **5.1-BAr$^{F}_{4}$** and 2.177(3) Å and 2.489(3) Å in **5.1-OTf** were ~0.10 – 0.14 Å shorter than those in **4.1-Ce** consistent with the smaller ionic radius of Ce^{IV} compared to Ce^{III}.[13] Lastly, the $Ce–O_{thf}$ bond distance of 2.507(4) Å in **5.1-BAr$^{F}_{4}$** and the $Ce–N_{pyr}$ bond distance of 2.645(3) Å in **5.1-OTf** were typical of neutral oxygen and nitrogen donors bound to a Ce^{IV} cation.[5a, 5f]

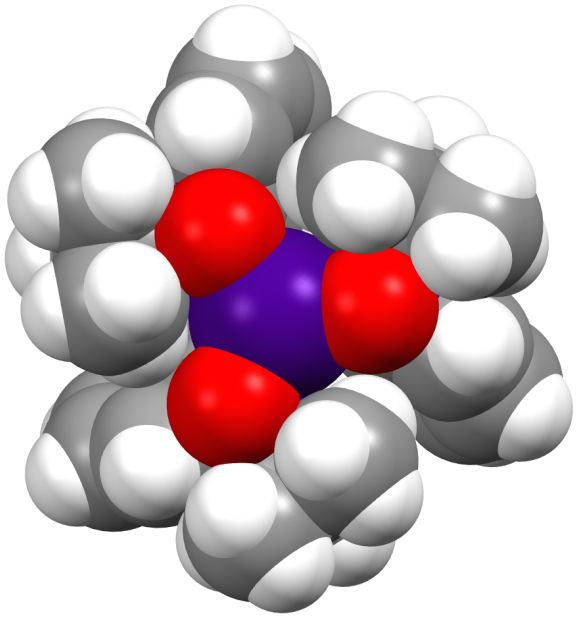

Figure 5.2.1.1. Spacefill of **4.1-Ce** with the THF molecule removed.

A spacefill diagram of **4.1-Ce** with the THF molecule removed indicated that the TriNOx^{3-} framework limited the central cerium cation to one open coordination site that we postulated would allow for the formation of stable 1:1 adducts with anionic ligands upon oxidation (Figure 5.2.1.1). To test this hypothesis, we sought to synthesize the halide series, Ce(TriNOx)X, where X = F (**5.1-F**), Cl (**5.1-Cl**), Br (**5.1-Br**), and I (**5.1-I**), using AgF, Ph_3CCl, Ph_3CBr, and I_2 as oxidants, respectively. Indeed, these reactions proceeded cleanly and in good yields to dark red-brown products in pyridine solution for **5.1-F**, **5.1-Cl**, and **5.1-Br**, and toluene solution for **5.1-I** (Scheme 5.2.1.1). To the best of our knowledge, this is only the second complete halide series reported for Ce^{IV} within a conserved ligand framework. The other reported halide series for Ce^{IV} is the $CeX[N(SiMe)_3]$ system completed by us with the isolation of $CeF[N(SiMe)_3]$.[10] The low solubility of these complexes in solution made growing diffraction quality crystals difficult.[14] X-ray quality crystals of **5.1-Cl** could be isolated, however, by layering Et_2O onto a saturated pyridine solution of the complex.

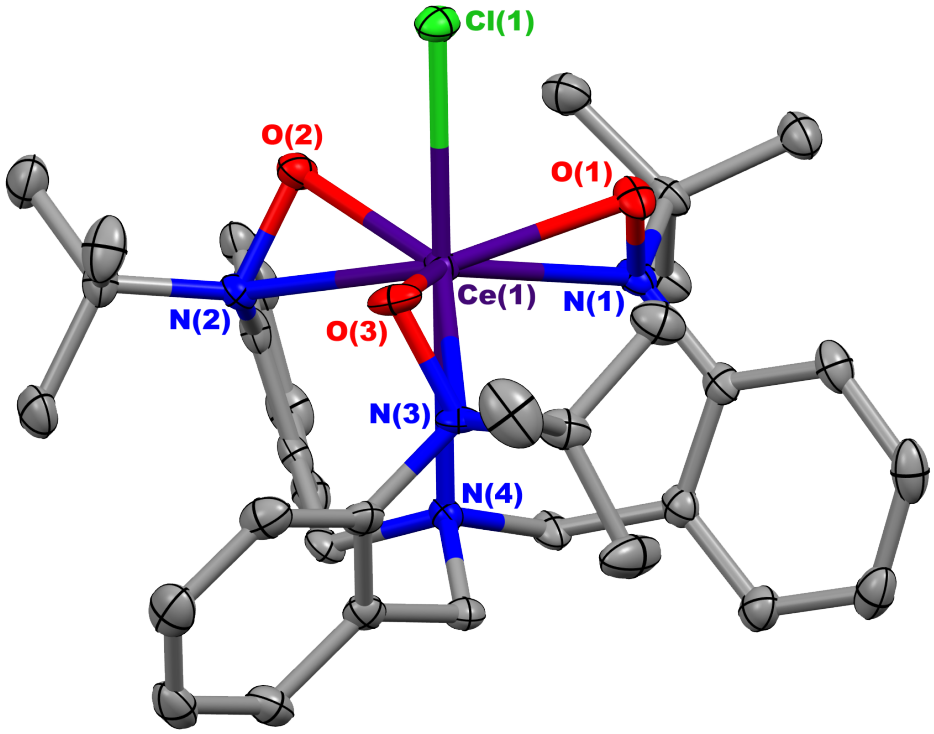

Figure 5.2.1.2. Thermal ellipsoid plot of **5.1-Cl**. Hydrogen atoms omitted for clarity. Selected bond distances (Å): Ce(1)–O(1): 2.163(2), Ce(1)–O(2): 2.171(2), Ce(1)–O(3): 2.174(2), Ce(1)–N(1): 2.548(3), Ce(1)–N(2): 2.527(3), Ce(1)–N(3): 2.519(3), Ce(1)–Cl(1): .2.7436(8).

Figure 5.2.1.2 shows the thermal ellipsoid plot of **5.1-Cl.** Here, again, the structural metrics were consistent with a central Ce^{IV} cation (Table 5.2.1.1). The Ce–Cl bond length of 2.7436(8) Å was significantly longer than that of 2.597(2) Å found in $CeCl[N(SiMe_3)_2]_3$ indicative of the larger steric demand of the $TriNOx^{3-}$ ligand.[15] However, the Ce–Cl bond length in **5.1-Cl** was significantly shorter than that of 3.0080(3) Å in the known $[\{Ce(NN'_3)\}_2(\mu\text{-Cl})]$, where NN'_3 = $[N(CH_2CH_2N(SiMe_2{}^tBu]^{3-}$, due to the bridging nature of the chloride moiety between the $Ce^{IV/III}$ sites in the latter.[6a]

Table 5.2.1.1. Bond metrics for **4.1-Ce**, **5.1-BAr$^F_4$**, **5.1-OTf**, and **5.1-Cl**.

	4.1-Ce	**5.1-BAr$^F_4$**	**5.1-OTf**	**5.1-Cl**
N–O	1.433(2)	1.418(8)–1.436(7)	1.431(4)–1.435(4)	1.425(3)–1.436(3)
(Ce–O$_{nitroxide}$)$_{avg}$	2.2921(18)	2.156(5)	2.177(3)	2.169(2)
(Ce–N$_{nitroxide}$)$_{avg}$	2.581(2)	2.493(6)	2.489(3)	2.531(3)
Ce–X[a]	2.577(6)	2.507(4)	2.645(3)	2.7436(8)

[a] X = O_{thf} for **4.1-Ce** and **5.1-BAr$^F_4$**, N_{pyr} for **5.1-OTf**, and Cl^- for **5.1-Cl**.

The 4+ oxidation state of cerium in **5.1-Cl** was confirmed by Ce L_{III}-edge X-ray absorption spectroscopy. Figure 5.2.1.3 shows the near edge regions of the XAS spectra of **4.1-Ce** and **5.1-Cl**. The spectrum of **5.1-Cl** showed the two features indicative of the core-hole excitation from a central Ce^{IV} cation to final states $\underline{2p}4f^1\underline{L}5d^1$ and $\underline{2p}4f^0 5d^1$, where $\underline{L}$ indicates a ligand hole. The data were compared to the spectrum of **4.1-Ce**, which showed only one feature indicative of the core-hole excitation from a central Ce^{III} cation to final state $\underline{2p}4f^1 5d^1$.[16]

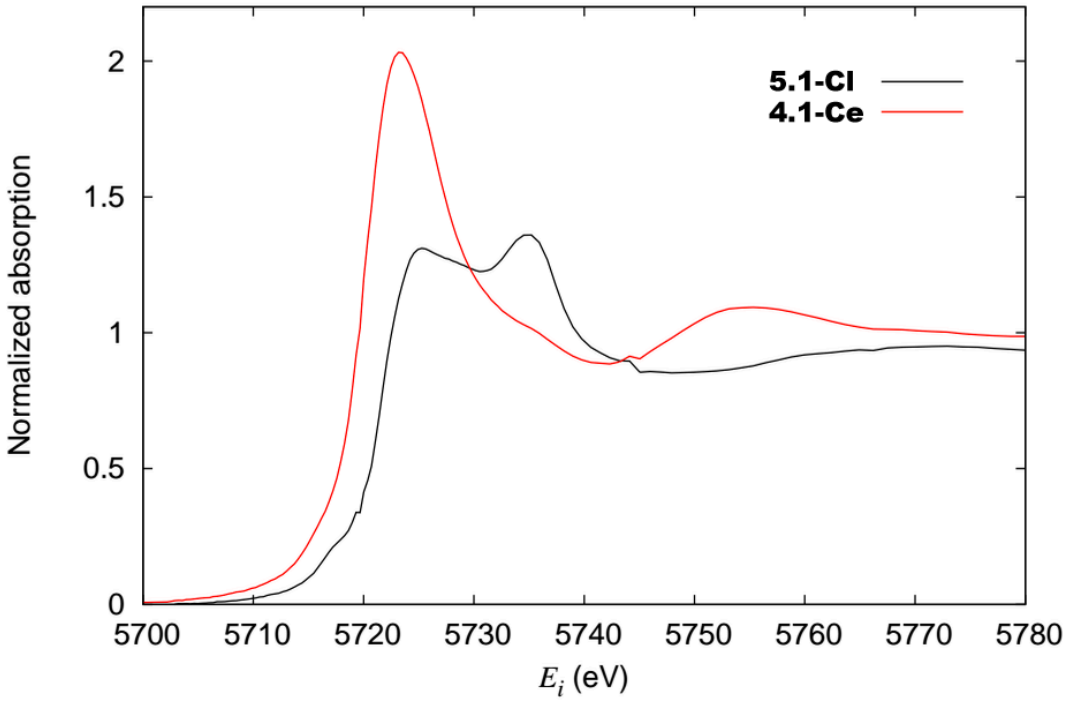

Figure 5.2.1.3. Overlay of the Ce L_{III}-edge XAS spectra of **4.1-Ce** and **5.1-Cl**.

Interestingly, the ^{1}H NMR spectrum of **5.1-Br** in d^5-pyr showed two Ce^{IV} species in solution in a 4:1 ratio by integration. To gain insight into the identities of these two species, **5.1-Br** was synthesized by an alternative route starting from the reported Ce^{IV} complex, CeBr[N(SiMe$_3$)$_2$]$_3$,[5e] and protonated H$_3$TriNOx. The ^{1}H NMR of the isolated dark red-brown powder from this protonolysis reaction was identical to that of **5.1-Br** synthesized using Ph$_3$CBr, with the same two Ce^{IV} species in solution again in a 4:1 ratio by integration. These data indicated that the presence of two Ce^{IV} species was characteristic of the solution chemistry of the **5.1-Br** product and not due to an unwanted side reaction occurring during the oxidation process. Based on these results, the two Ce^{IV} species were assigned as Ce(TriNOx)Br and [Ce(TriNOx)]Br, with inner and outer sphere bromide ions, respectively. This assignment was supported by electrochemistry experiments and corroborated by more detailed analysis of the ^{1}H NMR spectroscopic data (*vide infra*).

An analogous route to the formation of **5.1-F** from **4.1-Ce** was not readily available. However, a titanium fluoride complex supported by the TriNOx^{3-} ligand framework was recently reported by us through reaction of [Ti(TriNOx)]Cl with AgF.[17] Reduction of Ag$^+$ by **4.1-Ce** to Ag^0 ($E_{1/2}$ = 0.65 V vs Fc/Fc$^+$ in DCM) would also be thermodynamically favorable.[18] Therefore, AgF was expected to act as both an oxidant and fluoride transfer reagent toward **4.1-Ce**. Indeed, reaction of **4.1-Ce** with AgF in pyridine led to the clean formation of Ag^0 and **5.1-F**.

The final complex of the series, **5.1-I**, was synthesized from **4.1-Ce** in an analogous manner as **5.1-F** using AgI as the oxidant. Our preferred method, however, was the synthesis of **5.1-I** in toluene using 0.5 equivalents of I$_2$ as the oxidant. This led to the precipitation of **5.1-I**, which was easily isolated as an analytically pure, dark-brown powder.

5.2.2 Solution Electrochemistry

Solution electrochemistry experiments were performed on the series of **5.1-X,** where **X** = **BAr$^F_4$**, **OTf**, **F**, **Cl**, **Br**, and **I**, in 0.10 M [^{n}Pr$_4$N][BAr$^F_4$] dichloromethane solutions. Figure 5.2.2.1 shows the metal-based Ce$^{IV/III}$ redox couples for the series of complexes.

The cyclic voltammograms of **5.1-BAr$^F_4$** and **5.1-OTf** exhibited metal based features with E_{pa} = –0.86 V and E_{pc} = –1.04 V versus Fc/Fc$^+$, which were at similar potentials to the Ce$^{IV/III}$ feature in **4.1-Ce**, consistent with their solid state structures of having non-coordinating outer sphere anions.

It was noteworthy that the cyclic voltammogram of **5.1-Br** exhibited two separate reduction features consistent with the ^{1}H NMR spectrum of the complex, which showed two Ce^{IV} species in solution. The first reduction feature occurred with an E_{pc}, ≈ –1.04 V, which was similar to those observed in **4.1-Ce**, **5.1-BAr$^F_4$**, and **5.1-OTf**, supporting the assignment of this feature to the reduction of the [Ce(TriNOx)]Br species with an outer sphere bromide ion. The second reduction feature occurred with an E_{pc} = –1.16 V, which was assigned as the reduction of the Ce(TriNOx)Br species, with an inner sphere bromide ion. Despite the presence of two species in solutions of **5.1-Br**, only one return metal-based oxidation feature with E_{pa} = –0.85 V was observed in the cyclic voltammogram. Given the similarity of this feature to the return oxidation waves for **4.1-Ce**, **5.1-BAr$^F_4$**, and **5.1-OTf**, it was proposed that the bromide ion dissociated from the [Ce^{III}(TriNOx)Br]$^-$ species upon reduction.

The cyclic voltammogram of **5.1-Cl** was similar to that of **5.1-Br** except that only one reduction feature with E_{pc} = –1.26 V was observed. This observation was consistent with effectively all of the chloride ligand being bound to the cerium cation in solution. The shift of 100 mV towards more negative potentials between the E_{pc} of **5.1-Cl** and that of **5.1-Br** was a result of increased stabilization of the 4+ oxidation state of the central metal cation by Cl$^-$ compared to Br$^-$ (Figure 5.2.2.1). The return oxidation feature, however, occurred with E_{pa} = –0.87 V, which indicated that upon reduction of the metal center, the chloride ion also dissociated from the central Ce^{III} cation as was in the case of the [Ce^{III}(TriNOx)Br]$^-$ species in solutions of **5.1-Br**.

Unlike in the cyclic voltammograms of **5.1-Cl** and **5.1-Br**, the metal-based feature in the cyclic voltammogram of **5.1-F** was more reversible (E_{pa} = –1.31 V, E_{pc} = –1.40 V versus Fc/Fc$^+$). The 140 mV shift towards more negative potentials between the E_{pc} of **5.1-F** and that of **5.1-Cl** indicated that F$^-$ more effectively stabilized the 4+ oxidation state of Ce than Cl$^-$. The large shift in

potential of 440 mV towards more negative potentials between the E_{pa} of **5.1-F** and that of **5.1-Cl**, however, indicated that the fluoride ion remained bound to the reduced $[Ce^{III}(TriNOx)F]^{-}$ species.

Based on the similarity of the metal-based wave in the CV of **5.1-I** to that of **4.1-Ce**, **5.1-BAr$^{F}_{4}$**, and **5.1-OTf**, the solution structure of **5.1-I** was assigned as [Ce(TriNOx)]I with completely outer sphere iodide. These results were corroborated through analysis of the ^{1}H NMR spectroscopic data for **5.1-F**, **5.1-Cl**, **5.1-Br**, and **5.1-I** (*vide infra*).

A similar trend in the potential of the $Ce^{IV/III}$ redox couple was observed in the electrochemistry of the related $CeX[N(SiMe_3)_2]_3$ halide series. There, the addition of a Br^{-} ligand to the central cerium cation shifted the measured reduction potential by 0.66 V to more negative potentials; although replacing the Br^{-} with a Cl^{-} had no effect on the position of the of the measured redox potential. This potential was shifted by a further 0.25 V through the coordination of an F^{-} ligand. The peak separations of the $CeBr[N(SiMe_3)_2]_3$ and $CeCl[N(SiMe_3)_2]_3$ complexes, however, were significantly smaller than the related **5.1-Br** and **5.1-Cl** complexes due to the dissociation of halide ligands upon reduction of the latter. The peak separation of the **5.1-F** complex where fluoride coordination was conserved during the redox cycling was significantly smaller than that of the $CeF[N(SiMe_3)_2]_3$ complex suggesting fast ET kinetics in the redox cycling of **5.1-F** due to the conformationally restricted $TriNOx^{3-}$ framework.

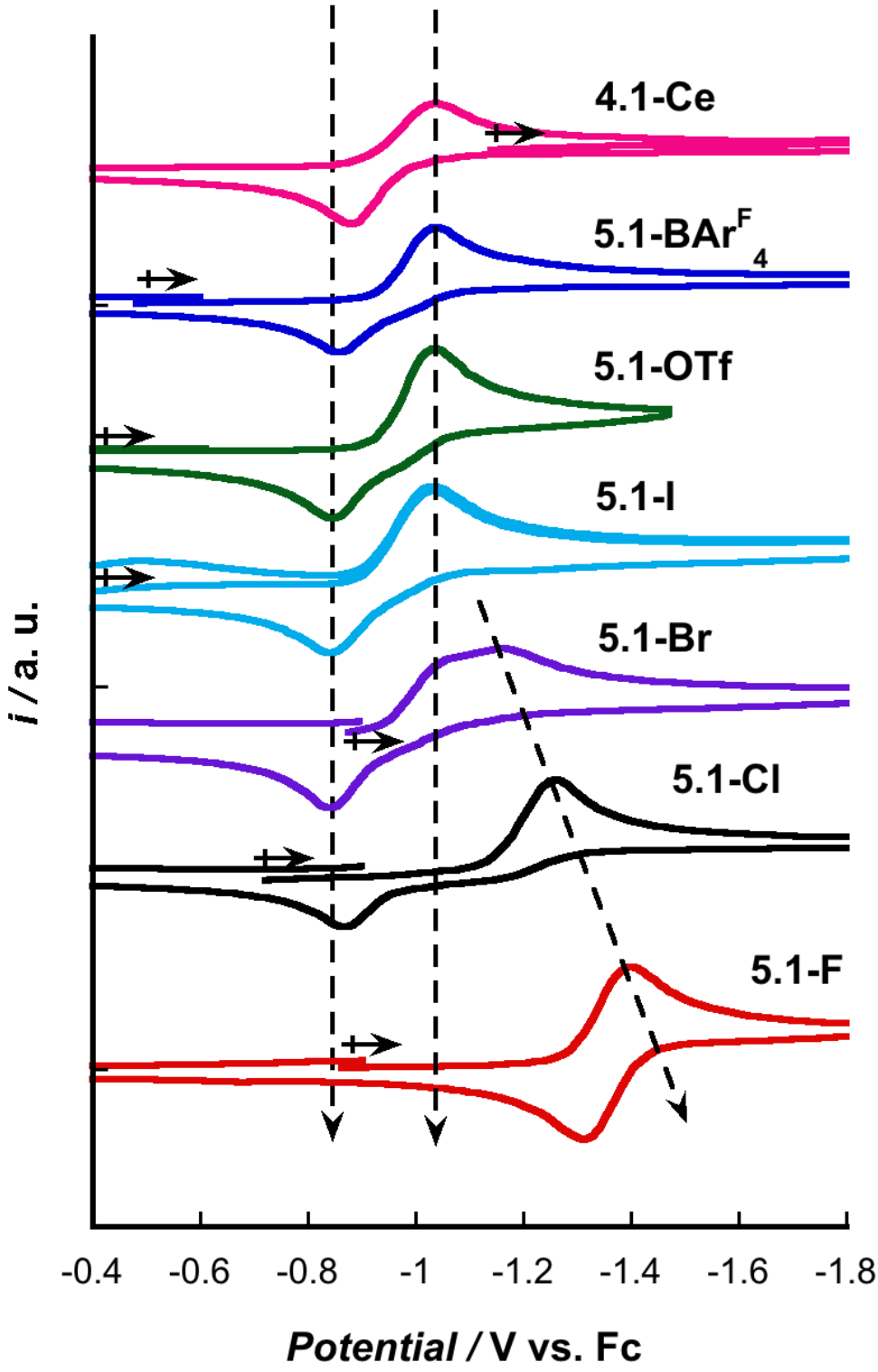

Figure 5.2.2.1. Metal-based $Ce^{IV/III}$ redox regions of the cyclic voltammograms for **4.1-Ce** and **5.1-X**.

5.2.3 ^{1}H NMR Spectroscopy

The solution structures of **5.1-F**, **5.1-Cl**, **5.1-Br**, and **5.1-I** were studied in d^5-pyr using ^{1}H NMR spectroscopy. As shown in Figure 5.2.3.1, all the complexes displayed characteristic diamagnetic ^{1}H NMR spectra with resonances appearing in the 0 – 10 ppm range. The presence of diastereotopic benzylic resonances between 2.5 – 5.0 ppm was indicative of coordination of TriNOx^{3-} to the central Ce cation.

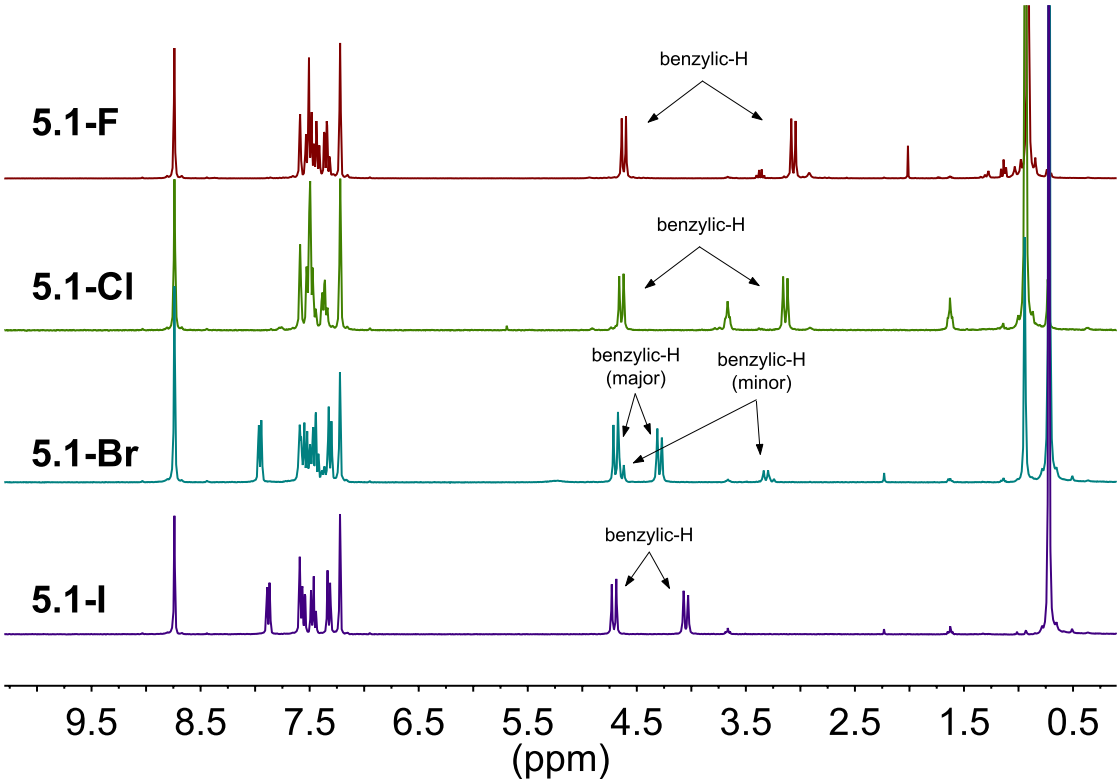

Figure 5.2.3.1. ^{1}H NMR (in d_5-pyr) spectral overlay of **5.1-F**, **5.1-Cl**, **5.1-Br**, and **5.1-I**.

Subtle differences in the ^{1}H NMR spectra were observed, however. Both **5.1-F** and **5.1-Cl** had aromatic resonances between 7.5 and 7.3 ppm, diastereotopic benzylic proton resonances at ~4.5 ppm and 3 ppm for both species ($\Delta\delta_{benzylH}$ > 1 ppm), and *tert*-butyl resonances at around 0.90 ppm. Based on solid state structural determination of **5.1-Cl** and the solution electrochemical data across the series, these spectral signatures were attributed to species with coordinated halides.

In contrast, the aromatic resonances of **5.1-I** were more diffuse and appeared as far up field as 7.9 ppm. Furthermore, the diastereotopic benzylic proton resonances were closer together at 4.7 ppm and 4.0 ppm ($\Delta\delta_{benzylH}$ = 0.7 ppm), and the *tert*-butyl resonance was shifted upfield by 0.2 ppm to 0.7 ppm. These spectral signatures were assigned to the species with outer sphere halides.

These NMR characteristics are similar to what was observed in the case of Ti(TriNOx)F where coordinated fluoride compared to outer sphere chloride resulted in the appearance of an aromatic resonance downfield at 7.89 ppm as well as diastereotopic benzylic resonances with a smaller shift: $\Delta\delta_{benzylH}$ ($\Delta\delta_{benzylH}$ = 1.56 for Ti(TriNOx)F; $\Delta\delta_{benzylH}$ = 0.48 for [Ti(TriNOx)]Cl)[17] As mentioned previously, **5.1-Br** was unique in that both species were present in solution as indicated by the presence of two sets of diastereotopic benzylic proton resonances in a 4:1 ratio by integration. The major species had an aromatic resonance at 7.95 ppm, diastereotopic benzylic proton resonances with a $\Delta\delta_{benzylH}$ of 0.4 ppm and a *tert*-butyl resonance at 0.72 ppm. The minor species exhibited aromatic resonances between 7 – 7.5 ppm, diastereotopic benzylic proton resonances with a $\Delta\delta_{benzylH}$ of 1.3 ppm, and a *tert*-butyl resonance at 0.94 ppm. These spectral characteristics supported the assignment of the major species as [Ce(TriNOx)]Br with an outer sphere bromide and the minor species as Ce(TriNOx)Br with an inner sphere bromide.

5.2.4 DFT Calculations

In Chapter 3, we showed there was strong stability of the 4+ oxidation state of Ce in the Ce pyridyl nitroxide systems due to symmetry allowed donation from the N–O π* orbitals into the Ce $4f_{z(x^2-y^2)}$ as a result of the D_{2d} complex symmetry, and Kozimor and coworkers recently described metal-ligand covalency for a Ce^{IV} chloride complex using chlorine K-edge XAS spectroscopy.[19] We hypothesized that symmetry allowed donation from $TriNOx^{3-}$ into the $4f_{y(3x^2-y^2)}$ orbital of Ce as a result of the C_3 complex symmetry was similarly lending structural stability to these complexes.

The frontier molecular orbitals of $[Ce(TriNOx)thf]^+$ (**[4.1-Ce]$^+$**), the cationic portion of **5.1-BAr$^F_4$**, were compared with those of **4.1-Ce**. Indeed, the in-phase interaction between the oxygen 2p orbitals of $TriNOx^{3-}$ and the Ce $4f_{y(3x^2-y^2)}$ orbital was observed in the HOMO–12 of **[4.1-Ce]$^+$**. The

corresponding out-of-phase interaction was observed in the LUMO+6. The main interaction between the orbitals of TriNOx^{3-} and those of the central cerium cation in **[4.1-Ce]$^{+}$**, however, was observed in the HOMO with head-on overlap of the N–O π* orbitals with a linear combination of the Ce $4f_{z^3}$ and Ce $4f_{x(x^2-3y^2)}$ orbitals. The corresponding antibonding interaction of these orbitals was observed in the LUMO+3 (Figure 5.2.4.1). In contrast, the occupied frontier MOs of **4.1-Ce** contained significantly less Ce 4f character than the occupied frontier MOs of **[4.1-Ce]$^{+}$** while the frontier unoccupied MOs of **4.1-Ce** contained significantly less ligand character than the frontier unoccupied MOs of **[4.1-Ce]$^{+}$**.

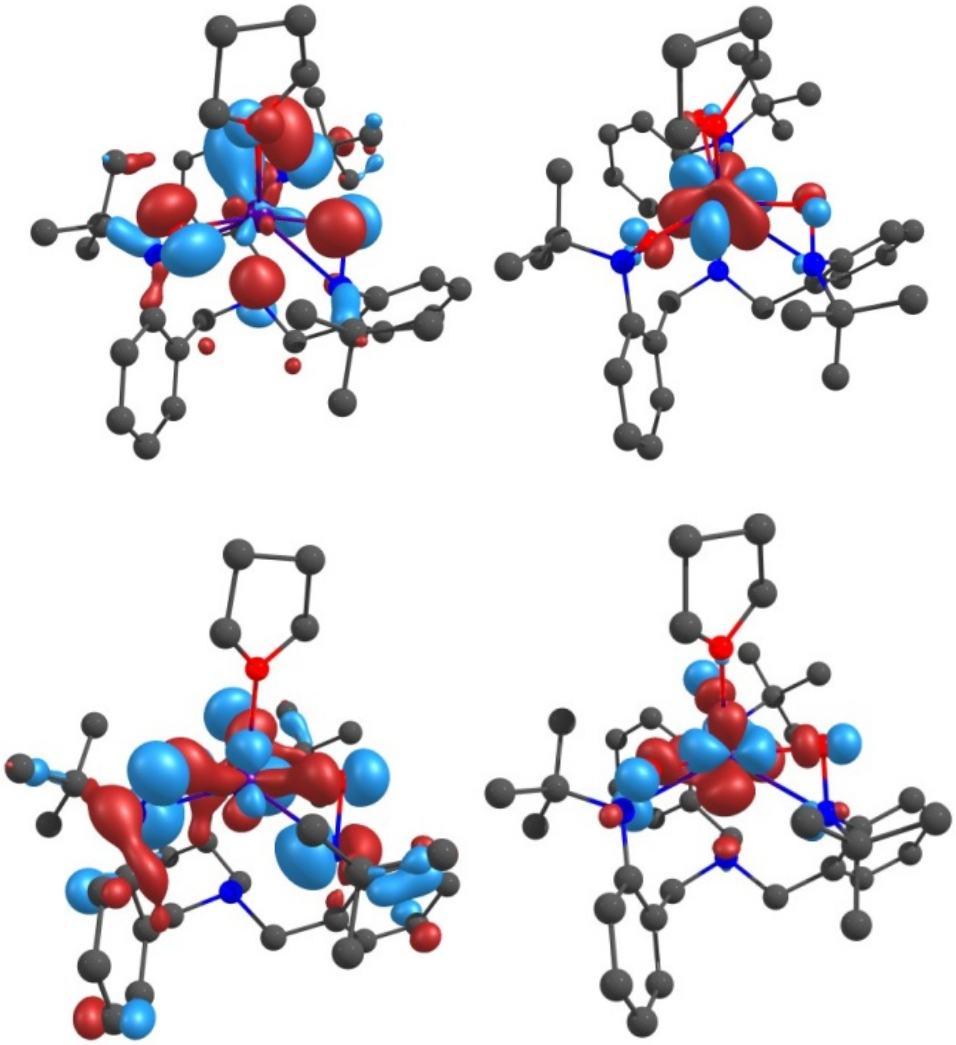

Figure 5.2.4.1. HOMO–12 (top left), LUMO+6 (top right), HOMO (bottom left), and LUMO+3 (bottom right) of [Ce(TriNOx)thf]$^{+}$ ([**4.1-Ce**]$^{+}$), the cationic portion of **5.1-BAr$^{F}_{4}$**.

To corroborate these findings, population analyses on **4.1-Ce** and **[4.1-Ce]$^+$** were performed. Upon oxidation of the central metal cation from Ce^{III} to Ce^{IV}, there was a marginal increase in the natural charge on cerium, q_{ce}, from 1.78 to 1.90 as expected for an increase in formal oxidation state. The natural charge to formal charge ratio, however, decreased significantly from 0.593 in **4.1-Ce** to 0.475 in **[4.1-Ce]$^+$**. As shown in Table 5.2.4.1, this decrease was a result of increased donation of the ligand electron density into the unfilled 4f, 5d, and 6s orbitals on cerium.

Population and Mayer Bond Order (MBO) analyses were also performed on geometry-optimized structures of **5.1-F**, **5.1-Cl**, **5.1-Br**, and **5.1-I** in order to probe the iconicity and strength of the metal-halide bond.

Table 5.2.4.1. Natural charges (q_{Ce} and q_X), natural populations (6s, 5d, and 4f), Mayer Bond Orders (MBOs), and theoretical formal shortness ratios (FSR) for **4.1-Ce**, **[4.1-Ce]$^+$**, **5.1-F**, **5.1-Cl**, **5.1-Br**, and **5.1-I**.

			Ce			**MBO Ce–X**	**FSR[a]**
	q_{Ce}	**q_X**	**6s**	**5d**	**4f**		
4.1-Ce	1.78	–0.60	0.11	0.83	0.17	0.202	
[4.1-Ce]$^+$	1.90	–0.61	0.13	1.01	0.87	0.255	
5.1-F	1.89	–0.53	0.12	1.04	0.85	1.044	0.892
5.1-Cl	1.71	–0.48	0.15	1.17	0.88	0.973	0.946
5.1-Br	1.66	–0.44	0.17	1.20	0.88	0.940	0.948
5.1-I	1.68	–0.49	0.18	1.18	0.88	0.870	0.988

[a] FSR = (calculated bond distance$_{Ce–X}$)/(ionic radius$_{Ce}^{IV}$ + ionic radius$_X^-$)

The metrics suggested that the iconicity of the Ce–halide bond generally decreased upon traversing the series towards the heavier halides as indicated by the smaller positive natural charge on cerium and the smaller negative natural charge on the X ligand. The metal-iodide bond, however, was calculated to be more ionic than the metal-bromide bond and comparable to that of the metal-chloride bond.

Similarly, there was a general decrease in the strength of the Ce–X bond across the series as indicated by the decrease in MBO from 1.044 for **5.1-F** to 0.870 for **5.1-I**. This calculated decrease in bond strength was consistent with the solution chemistry of these species in coordinating solvents such as pyridine where solvent molecules competed with the heavier halides for metal ligation.

Another useful metric for determining the strength of the metal-halide interaction is the theoretical formal shortness ratio (FSR) of the metal-halide bond. These were calculated for the series of Ce-halide complexes using the determined Ce–X bond length from the gas-phase optimized structures and the tabulated Shannon radii for Ce^{4+} and X^{-} ions. Values significantly less than 1 indicate stronger interactions between metal and halide ligand. As shown in Table 5.2.4.1, the theoretical FSR of the Ce–X bond increased significantly from 0.892 in **5.1-F** to 0.988 in **5.1-I**. This trend was consistent with experiment and with our findings from the MBO analyses.

These results were contrasted with those obtained from calculations on the $CeX[N(SiMe_3)_2]_3$ system. Like in the **5.1-X** halide series, the ionicity of the metal halide bonds in the $CeX[N(SiMe_3)_2]_3$ series generally decreased with coordination of the heavier halides. Unlike in the **5.1-X** halide series, however, the calculated MBO of the Ce–X bond in the $CeX[N(SiMe_3)_2]_3$ system trended upward with coordination of the heavier halides.

5.2.5 Oxidation with O_2

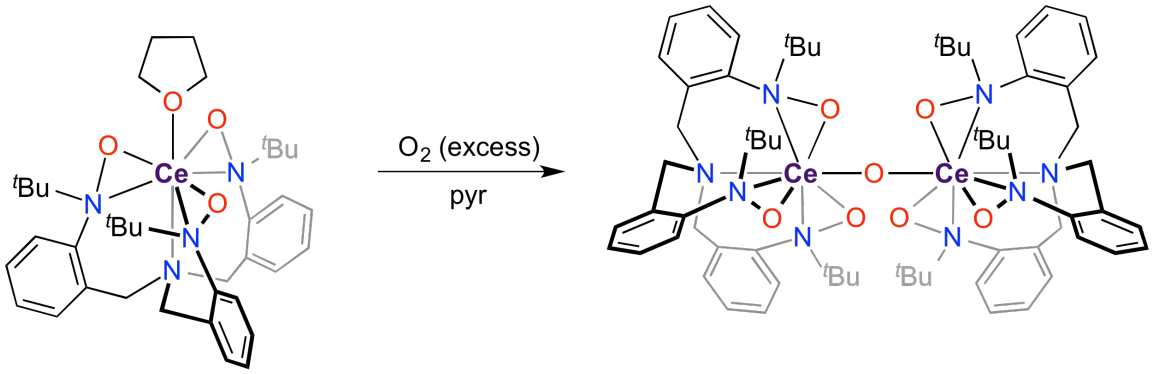

Scheme 5.2.5.1. Schematic of the reactivity of **4.1-Ce** with O_2.

We observed oxidation of **4.1-Ce** to a putative Ce^{IV} containing product upon exposure to air. It was of interest to characterize this oxidation product. Slowly diffusing O_2 into a saturated pyridine solution (~0.6 mL) of **4.1-Ce** led to the deposition of X-ray quality crystals of the bridging oxide complex, (TriNOx)Ce(μ-O)Ce(TriNOx) (**5.1-μO)** (Scheme 5.2.5.1). We postulated that this product was the result of an inner sphere electron transfer from two Ce^{III} cations to a bridging μ-O_2 moiety followed by two outer sphere electron transfer events from Ce^{III} cations to break the O–O single bond. Formation of a Lewis acid/base adduct between the electrophilic cationic Ce^{IV} and nucleophilic Ce^{IV}–O^{2-} intermediates would lead to the observed product. Overall, the stoichiometry is postulated to involve the reaction of one equivalent of **4.1-Ce** with 0.25 equivalents of O_2. Attempts to reproduce this result on a larger scale failed, however. Here, reaction of a saturated pyridine solution (~6 mL) of **4.1-Ce** led to a similar dark brown solution but no precipitate. After letting this solution stand for 14 h, the dark brown color disappeared and a light orange solution reformed, possibly suggesting re-reduction to a Ce^{III} product had occurred.

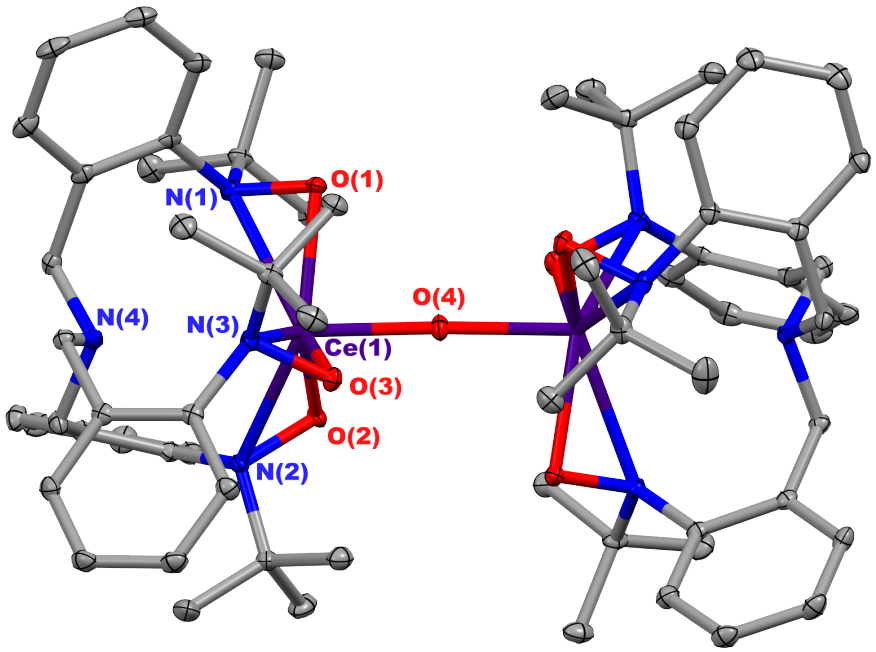

Figure 5.2.5.1. Thermal ellipsoid plot of **5.1-μO** at 30% probability. Hydrogen atoms excluded for clarity.

Figure 5.2.5.1 shows a thermal ellipsoid plot of **5.1-μO**. The complex sits on a 2-fold rotation axis symmetry element passing through the bridging oxo ligand, indicating that the two halves of the dimeric structure are crystallographically equivalent. The symmetry of the complex supported the electronic structure assignment of two Ce^{IV} cations bridged by an O^{2-} ligand, though a mixed valent $Ce^{IV/III}$ dimer, with each cerium cation having a valence of 3.5, could not be ruled out. The average $Ce–O_{nitroxide}$ bond distance of 2.209(3) Å in **5.1-μO** was slightly longer than the average $Ce^{IV}–O_{nitroxide}$ bond distances in **5.1-BAr$^F_4$**, **5.1-OTf**, and **5.1-Cl**, which ranged from 2.156(5) Å – 2.177(3) Å, though slightly longer Ce^{IV}-$O_{nitroxide}$ bond distances were expected as a result of the increased donation from the μ-oxo ligand. Furthermore, the average $Ce–O_{nitroxide}$ bond distance for **5.1-μO** was closer to those in **5.1-BAr$^F_4$**, **5.1-OTf**, and **5.1-Cl** than it was to the Ce^{III}-$O_{nitroxide}$ bond distance of 2.2921(18) Å in **4.1**. The Ce–(μ-O) bond distance of 2.0520(3) Å was shorter than bond distances of typical monoanionic oxygen donors to Ce^{IV},[5f, 5g, 20] supporting the assignment of an O^{2-} ligand. The nearly linear Ce–(μ-O)–Ce bond angle of 178.0(3)º led further support to this assignment. However, these structural metrics did not rule out the possibility of a mixed valent Ce dimer since the presence of a disordered H^+ cation over multiple oxygen atom sites was possible.

5.3 Conclusions

The electron rich and sterically protected environment imposed by the $TriNOx^{3-}$ framework allowed for the isolation and characterization of the stable cationic Ce^{IV} complexes, **5.1-BAr$^F_4$** and **5.1-OTf**. Due to the high Lewis acidity of the Ce^{IV} cation, these types of complexes are quite rare. The $TriNOx^{3-}$ framework, however, was sufficiently bulky and electron rich to mitigate the high Lewis acidity of Ce^{IV}.

The complete halide series, **5.1-X**, where **X = F**, **Cl**, **Br**, and **I**, was also synthesized. Here, the bulky $TriNOx^{3-}$ framework caused diverse solution behaviors within the series. As the size of the X^- ligand increased, we observed increased concentrations of [Ce(TriNOx)]X species, with outer sphere halides in solution. We are interested in exploring the use of Ce^{IV} supported by $TriNOx^{3-}$-type frameworks in Lewis acid catalysis, which would require binding and activation of substrate

through polarization of the Ce–substrate bond. Further modification of the nitrogen R-groups is, therefore, warranted to accommodate larger anionic ligands in the cleft and to prevent the formation of outer sphere anions.

5.4 Experimental Section

General Methods. Unless otherwise noted, all reactions and manipulations were performed under an inert atmosphere (N_2) using standard Schlenk techniques or in a drybox equipped with a molecular sieves 13X / Q5 Cu–0226S catalyst purifier system. Glassware was oven-dried for at least 3 h at 150 °C prior to use. ^{1}H and $^{19}F\{^{1}H\}$ NMR spectra were obtained on a Bruker DMX-300 Fourier transform NMR spectrometer at 300 MHz and 282.2 MHz, respectively. $^{13}C(^{1}H\}$ NMR spectra were obtained on a Bruker DRX-500 Fourier transform NMR spectrometer or a Bruker AVIII 500 Fourier transform NMR spectrometer equipped with a cryogenic probe at 125.7 MHz. Chemical shifts were recorded in units of parts per million downfield from residual proteo solvent for ^{1}H–NMR, characteristic solvent peaks for ^{13}C–NMR, or relative to an external $CFCl_3$ reference (0 ppm). Elemental analyses were preformed either at the University of California, Berkeley, Microanalytical Facility using a Perkin-Elmer Series II 2400 CHNS analyzer or at Complete Analysis Laboratories, Inc. using a Carlo Erba EA 1108 analyzer.

Materials. Tetrahydrofuran, dimethoxyethane, diethyl ether, dichloromethane, toluene, hexanes, and pentane were purchased from Fisher Scientific. All solvents were sparged for 20 min with dry N_2 and dried using a commercial two-column solvent purification system comprising columns packed with Q5 reactant and neutral alumina respectively (for hexanes and pentane), or two columns of neutral alumina (for THF, Et_2O, and CH_2Cl_2). Deuterated solvents were purchased from Cambridge Isotope Laboratories, Inc. and stored over 4A molecular sieves prior to use. Cerium chloride (Strem), potassium bis(trimethylsilyl)amide (Sigma), silver triflate, trityl chloride, and trityl bromide were used as received. Iodine was sublimed prior to use. $Fc[BAr^{F}_{4}]$,[21] Fc[OTf],[22] $Ce[N(SiMe_3)_2]_3$,[23] and $[^{n}Pr_4N][B(3,5\text{-}(CF_3)_2\text{-}C_6H_3)_4]$[24] were synthesized according to literature procedures.

X-Ray Absorption Spectroscopy. Ce L_{III}-edge XANES data were collected at the Stanford Synchrotron Radiation Lightsource, beamline 11-2, using a Si 220 (phi=0) double monochromator that was detuned to 20% in order to reduce harmonic contamination. The resulting data have an energy resolution limited by the broadening due to the $2p_{3/2}$ corehole lifetime of 3.2 eV. Data were collected in transmission, using a CeO_2 reference to calibrate the energy scale, setting the first inflection point of the CeO_2 absorption to 5723 eV. A linear pre-edge background was subtracted and the data were subsequently normalized at 5800 eV.

The samples were prepared for these experiments using procedures outlined previously.[25] In particular, each sample was ground into a powder, mixed with dry boron nitride as a diluent, and then packed into the slots of a machined aluminum sample holder in an N_2 atmosphere drybox. Aluminized mylar was affixed to the holder with an indium-wire seal. After packaging, the samples were transported in dry, nitrogen-filled containers to the beamline. Sample holders were quickly transferred to the vacuum chamber, exposing the sealed holders to air for less than thirty seconds before pumping out the chamber and collecting the data under vacuum. Compound **1** shows extreme air sensitivity and has easily identifiable spectral changes upon exposure. This sample served as a "canary" sample and was monitored to check for sample holder integrity. Following measurement, no significant changes in the sample were observed.

Synthetic Details and Characterization.

Ce(TriNOx)F (**5.1-F**). To a pyridine solution of **4.1-Ce** (0.10 g, 0.13 mmol, 1 equiv) was added solid AgF (0.018 g, 0.15 mmol, 1.1 equiv) and the reaction was stirred in the dark for 6 h. The Ag^0 byproduct was removed by filtration through a coarse porosity fritted filter and the pyridine filtrate was collected. Volatiles were removed under reduced pressure and the resulting dark red-brown powder was washed with minimal diethyl either and dried. Isolated Yield: 0.026 g (28%). ^{1}H NMR (300 MHz, d_5-pyr): δ 7.56–7.47 (overlap 6H), 7.43 (ddd, J = 7.7, 7.5, 1.8 Hz, 3H), 7.34 (ddd, J = 7.6, 7.5, 1.5 Hz, 3H), 4.62 (d, J = 11.9 Hz, 3H), 3.06 (d, J = 11.9 Hz, 3H), 0.091 (s, 27H). ^{13}C NMR (125.7 MHz, d_5-pyr): δ 149.6, 133.3, 133.0, 130.1, 129.6, 127.9, 65.2, 62.1, 26.5. ^{19}F NMR

(282.2 MHz, d_5-pyr): δ 219.1. Anal. Calcd. for $C_{33}H_{45}N_4O_3CeF$: C, 56.23; H, 6.44; N, 7.95. Found: C, 55.99; H, 6.54; N, 8.09.

Ce(TriNOx)Cl (**5.1-Cl**). To a pyridine solution of **4.1-Ce** (0.10 g, 0.13 mmol, 1 equiv) was added solid Ph_3CCl (0.056 g, 0.20 mmol, 1.5 equiv) and the reaction was stirred for 3 h. Volatiles were removed under reduced pressure and the resulting dark red-brown solid was washed with Et_2O and dried. X-ray quality crystals were obtained by vapour diffusion of diethyl ether into a saturated pyridine solution of **5.1-Cl**. Yield: 0.079 g (84%). ^{1}H NMR (300 MHz, d_5-pyr): δ 7.56–7.42 (overlap, 9H), 7.36 (a.td., J = 7.1, 2.1 Hz, 3H), 4.64 (d, J = 12.0 Hz, 3H), 3.14 (d, J = 12.0 Hz, 3H), 0.94 (s, 27H). ^{13}C NMR (125.7 MHz, d_5-pyr): δ 133.1, 133.0, 130.3, 129.9, 128.4, 66.3, 62.0, 26.8. Anal. Calcd. for $C_{33}H_{45}N_4O_3CeCl$: C, 54.95; H, 6.29; N, 7.77. Found: C, 54.57; H, 6.57; N, 7.76.

Ce(TriNOx)Br (**3-Br**). *Method A:* Ce(TriNOx)Br was synthesized in a similar manner to Ce(TriNOx)Cl except Ph_3CBr was used as the oxidant. To a pyridine solution of **4.1-Ce** (0.074 g, 0.098 mmol, 1 equiv) was added solid Ph_3CBr (0.047 g, 0.15 mmol, 1.5 equiv) and the reaction was stirred for 3 h. The reaction mixture was filtered and volatiles were removed under reduced pressure. The resulting dark red-brown solid was washed with Et_2O and dried. Yield: 0.059 g (79%). *Method B:* To a THF solution of H_3TriNOx (0.060 g, 0.11 mmol, 1 equiv) was then added a THF solution of freshly prepared $CeBr[N(SiMe_3)_2]_3$ (0.077 g, 0.11 mmol, 1 equiv) and the reaction was allowed to react for 3h, after which a dark red-brown solid crashed out. This solid was isolated on a medium porosity fritted filter, washed with Et_2O, and dried under reduced pressure. Yield: 0.030 g (36%) ^{1}H NMR (300 MHz, d_5-pyr): δ (major species, 80%) 7.95 (d, J = 7.6 Hz, 3H), 7.59–7.27 (overlap, 9H), 4.69 (d, J = 12.4 Hz, 3H), 4.29 (d, J = 12.4 Hz, 3H), 0.72 (s, 27H); (minor species, 20%) 7.59–7.27 (overlap, 12H), 4.64 (d, J = 12.1 Hz, 3H), 3.32 (d, J = 12.1 Hz, 3H), 0.94 (s, 27H). ^{13}C NMR (125.7 MHz, d_5-pyr): δ (major species) 146.9, 134.4, 132.9, 130.7, 130.5, 129.6, 66.9, 59.7, 26.9; (minor species) 148.7, 133.3, 133.1, 130.3, 130.0, 128.5, 66.6, 61.6, 26.9 (overlap). Anal. Calcd. for $C_{33}H_{45}N_4O_3CeBr$: C, 51.76; H, 5.92; N, 7.32. Found: C, 51.55; H, 5.82; N, 7.15.

Ce(TriNOx)I (**5.1-I**). To a toluene solution of **4.1-Ce** (0.20 g, 0.26 mmol, 1 equiv.) was added solid I_2 (0.040 g, 0.13 mmol, 0.6 equiv.) causing the immediate precipitation of a dark red-brown powder. The reaction was stirred for 6 h. The dark red-brown powder was isolated on a medium porosity fritted filter, washed with Et_2O, and dried under reduced pressure. Yield: 0.17 g (79%). ^{1}H NMR (300 MHz, d_5-pyr): δ 7.88 (dd, J = 7.5, 1.7 Hz, 3H), 7.56 (ddd, J = 8.0, 7.7, 1.7 Hz, 3H), 7.46 (ddd, J = 7.7, 7.5, 1.4 Hz, 3H), 7.32 (dd, J = 8.0, 1.4 Hz), 4.71 (d, J = 12.5 Hz, 3H), 4.05 (d, J = 12.5 Hz), 0.72 (s, 27H). ^{13}C NMR (125.7 MHz, d_5-pyr): δ 146.9, 134.2, 132.6, 130.9, 130.6, 129.7, 67.0, 60.0, 26.9. Anal. Calcd. for $C_{33}H_{45}N_4O_3CeI$: C, 48.77; H, 5.58; N, 6.89. Found: C, 48.63; H, 5.37; N, 6.79.

[Ce(TriNOx)THF][BAr$^F_4$] (**5.1-BAr$^F_4$**). To a toluene solution of **4.1-Ce** (0.30 g, 0.39 mmol, 1 equiv.) was added Fc[BAr$^F_4$] (0.41 g, 0.39 mmol, 1 equiv) and the reaction was stirred for 14 h. Volatiles were removed under reduced pressure and the resulting dark red-brown powder was rinsed with hexanes and recrystallized from vapour diffusion of pentane into a saturated THF solution. Yield: 0.39 g (61%). ^{1}H NMR (300 MHz, d_5-pyr): δ 8.43 (m, 8H), 7.84 (br s, 4H), 7.69–7.57 (overlap, 6H), 7.49 (a.td., J = 7.4, 1.2 Hz, 3H), 7.37 (dd, J = 8.0, 0.8 Hz, 3H), 4.75 (d, J = 12.5 Hz, 3H), 3.67 (m, 4H), 3.40 (d, J = 12.5 Hz, 3H), 1.63 (m, 4H), 0.74 (s, 27H). ^{13}C NMR (125.7 MHz, d_5-pyr): δ 163.1 (q, $^1J(^{11}B,^{13}C)$ = 49 Hz), 146.9, 133.9, 132.1, 131.1, 130.8, 130.3 (qq, $^2J(^{19}F,^{13}C)$ = 31, $^4J(^{19}F,^{13}C)$ = 3 Hz), 129.8, 125.5 (q, $^1J(^{19}F,^{13}C)$ = 273 Hz), 118.7 (sept, $^3J(^{19}F,^{13}C)$ = 4 Hz), 68.3, 67.1, 60.9, 26.8, 26.3. ^{19}F NMR (282.2 MHz, d_5-pyr): δ –62.1; Anal. Calcd. for $C_{69}H_{65}N_4O_4F_{24}BCe$: C, 51.12; H, 4.04; N, 3.46. Found: C, 50.87; H, 4.14; N, 3.24.

[Ce(TriNOx)pyr][OTf] (**5.1-OTf**). To a toluene solution of **4.1-Ce** (0.057 g, 0.075 mmol, 1 equiv.) was added solid FcOTf (0.025, 0.075 mmol, 1 equiv.) and the reaction was stirred for 5 h. The resulting dark red-brown powder was isolated on a medium porosity fritted filter and rinsed with Et_2O. X-ray quality crystals of **5.1-OTf** were grown from vapour diffusion of Et_2O into a saturated pyridine solution. Yield: 0.040 g (58%). ^{1}H NMR (300 MHz, d_5-pyr): δ 7.79 (dd, J = 7.4, 1.7 Hz, 3H), 7.57 (ddd, J = 8.1, 7.4, 1.7 Hz, 3H), 7.48 (ddd, J = 7.4, 7.4, 1.4 Hz, 3H), 7.33 (dd, J = 8.1, 1.4 Hz, 3H), 4.73 (d, J = 12.5 Hz, 3H), 3.69 (d, J = 12.5 Hz, 3H), 0.72 (s, 27H). ^{13}C NMR

(125.7 MHz, d_5-pyr): δ 146.8, 134.1, 132.4, 130.9, 130.7, 129.8, 67.0, 60.4, 26.9; ^{19}F NMR (282.2 MHz, d_5-pyr): δ –77.2; Anal. Calcd. for $C_{39}H_{50}N_5O_6F_3SCe$•0.5pyr: C, 52.27; H, 5.55; N, 8.08. Found: C, 52.22; H, 5.62; N, 7.96.

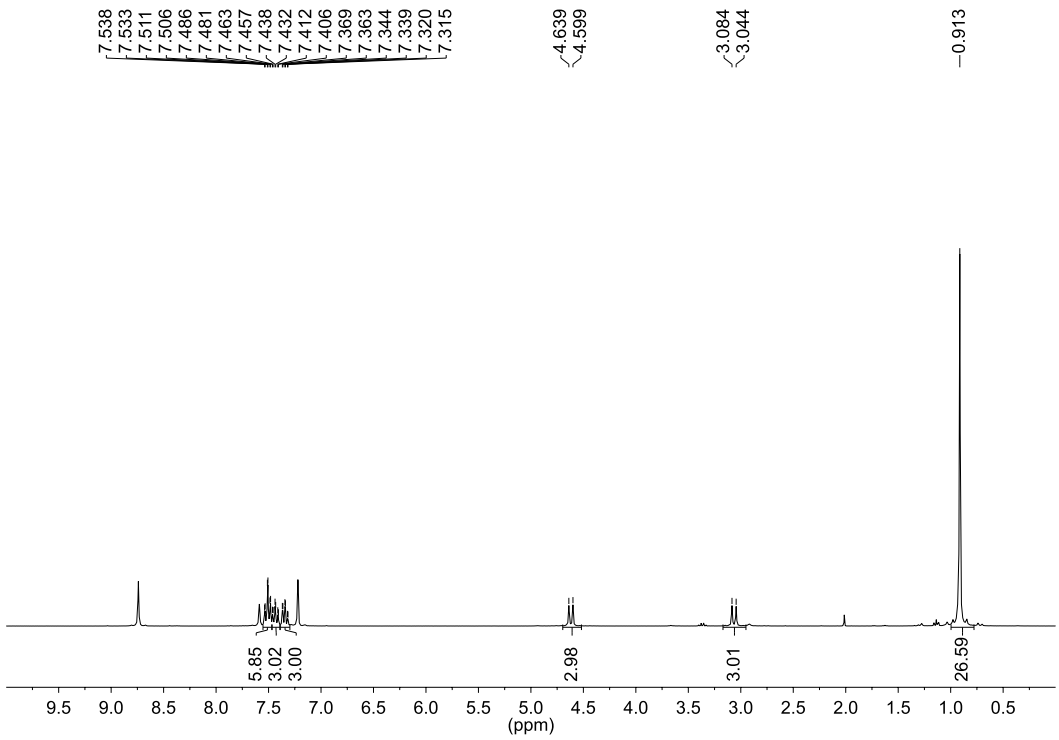

Figure 5.4.1. ^{1}H NMR spectrum of **5.1-F** in d_5-pyr.

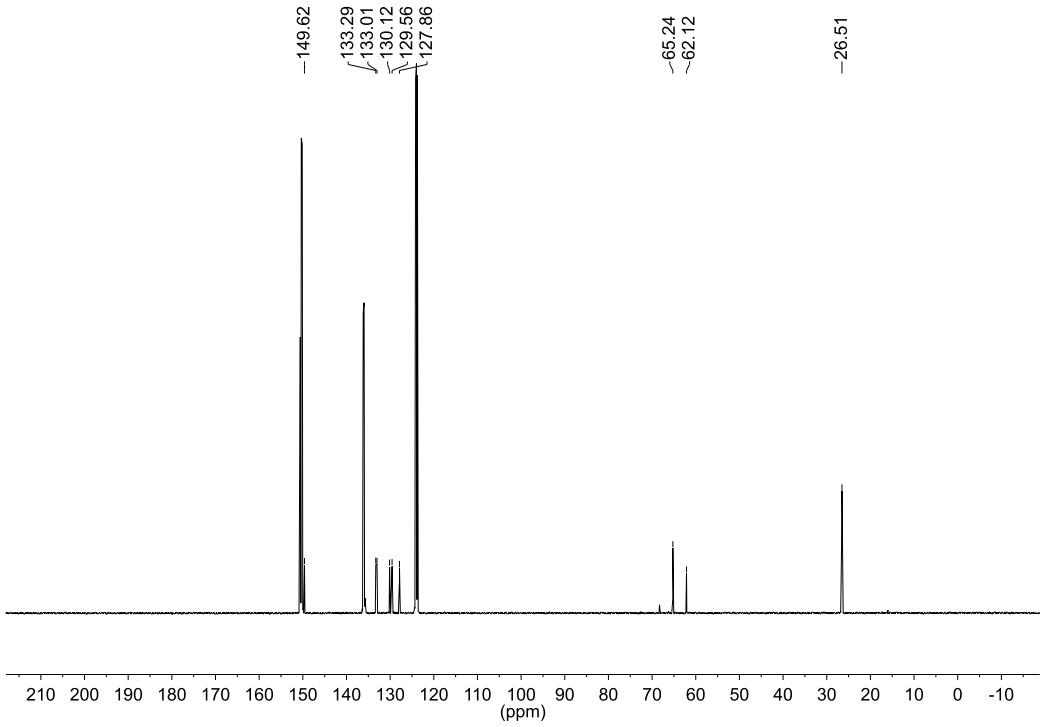

Figure 5.4.2. ^{13}C{^{1}H} NMR spectrum of **5.1-F** in d_5-pyr.

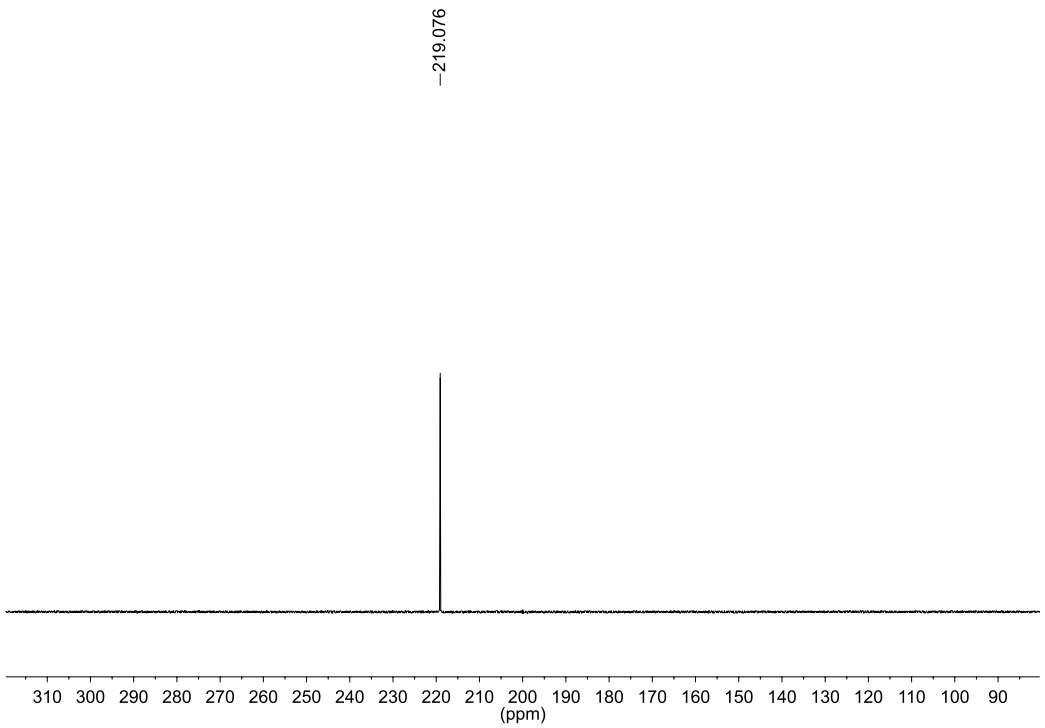

Figure 5.4.3. $^{19}F\{^{1}H\}$ NMR spectrum of **5.1-F** in d_5-pyr.

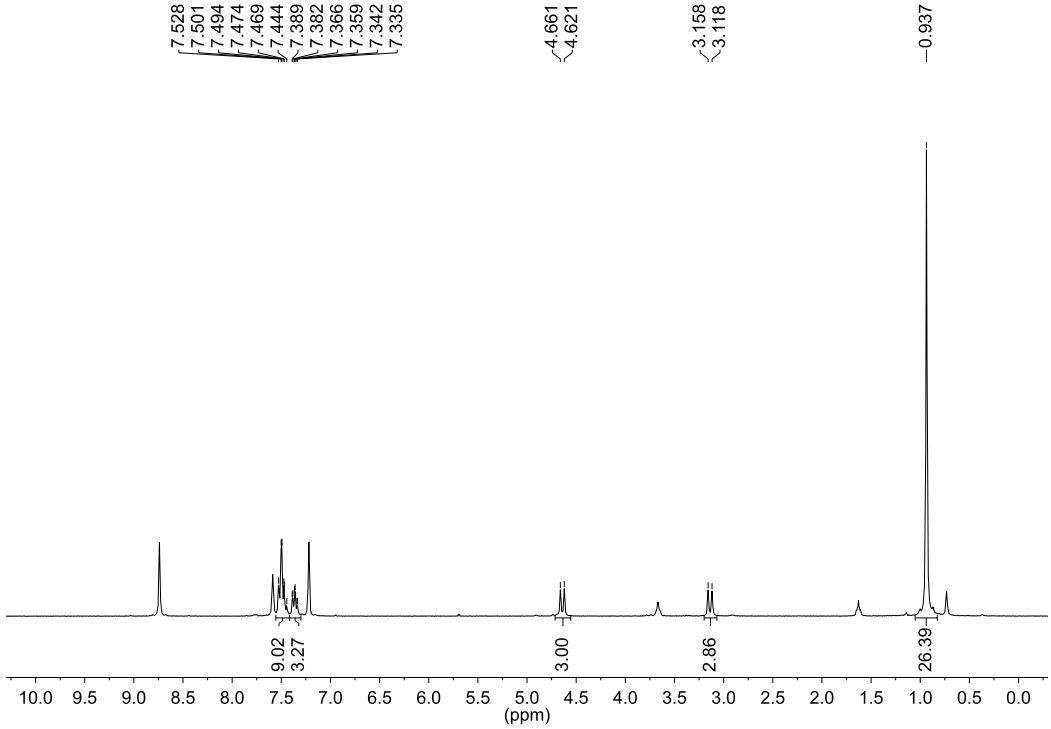

Figure 5.4.4. ^{1}H NMR spectrum of **5.1-Cl** in d_5-pyr.

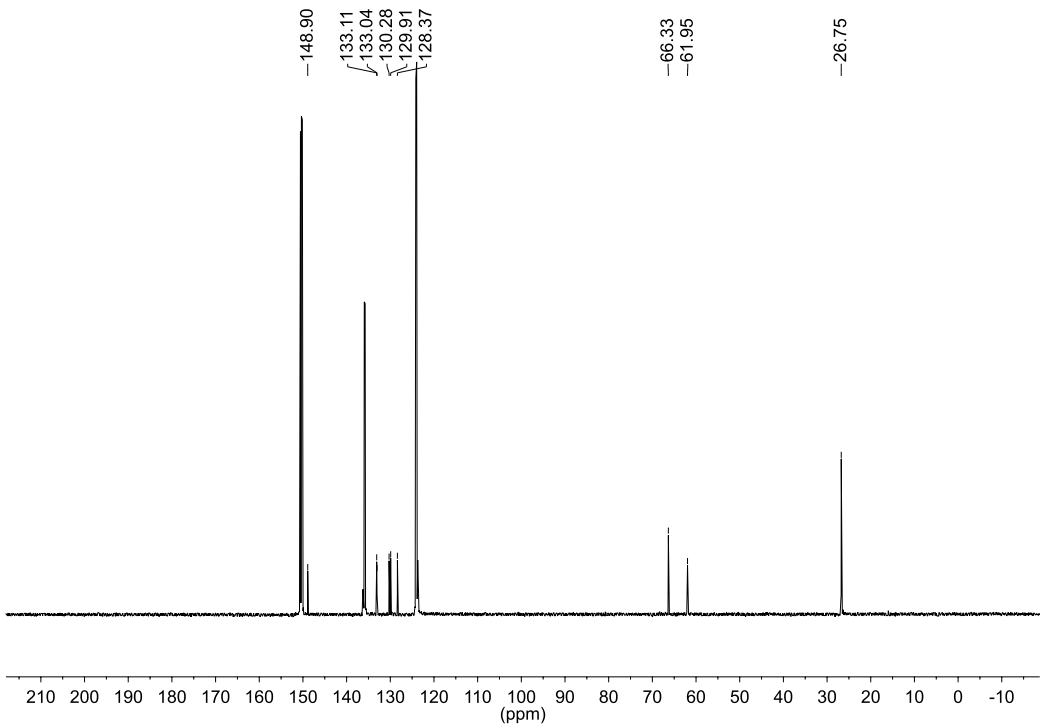

Figure 5.4.5. $^{13}C\{^{1}H\}$ NMR spectrum of **5.1-Cl** in d_5-pyr.

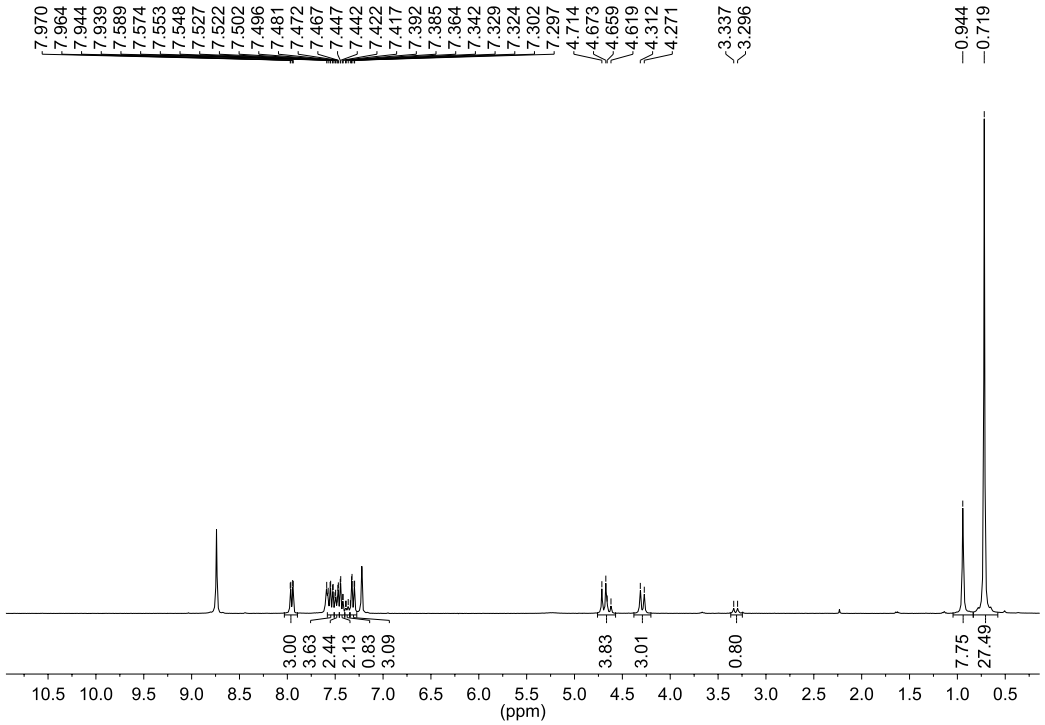

Figure 5.4.6. ^{1}H NMR spectrum of **5.1-Br** in d_5-pyr.

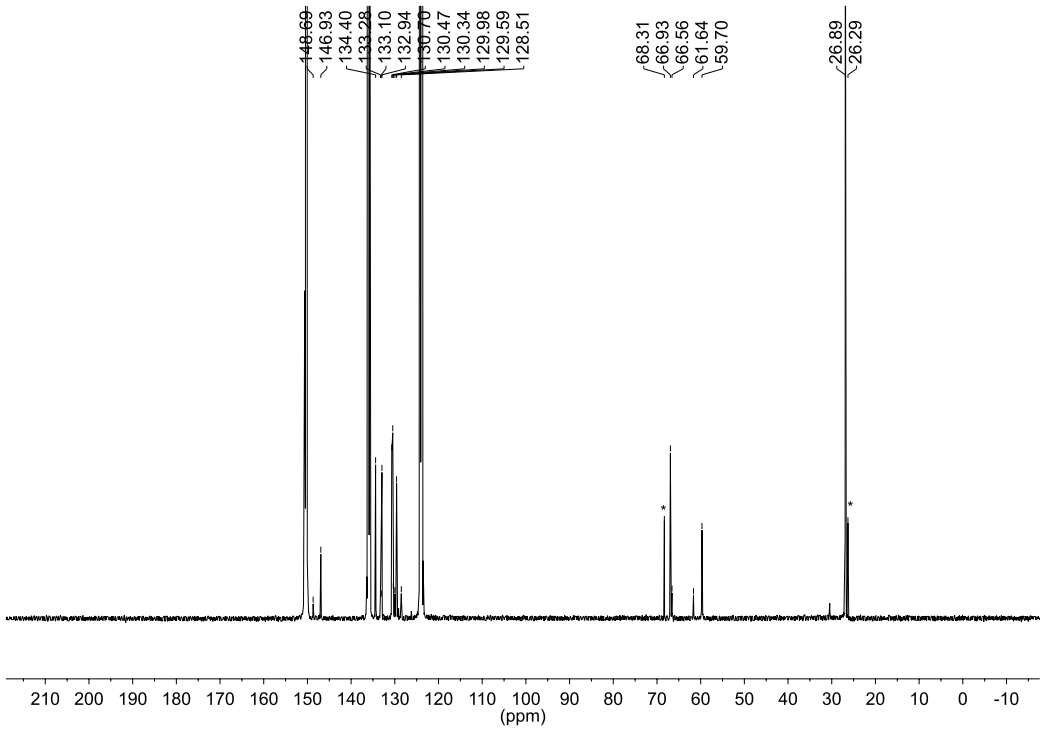

Figure 5.4.7. $^{13}C\{^{1}H\}$ NMR spectrum of **5.1-Br** in d_5-pyr. * indicates THF solvent impurity

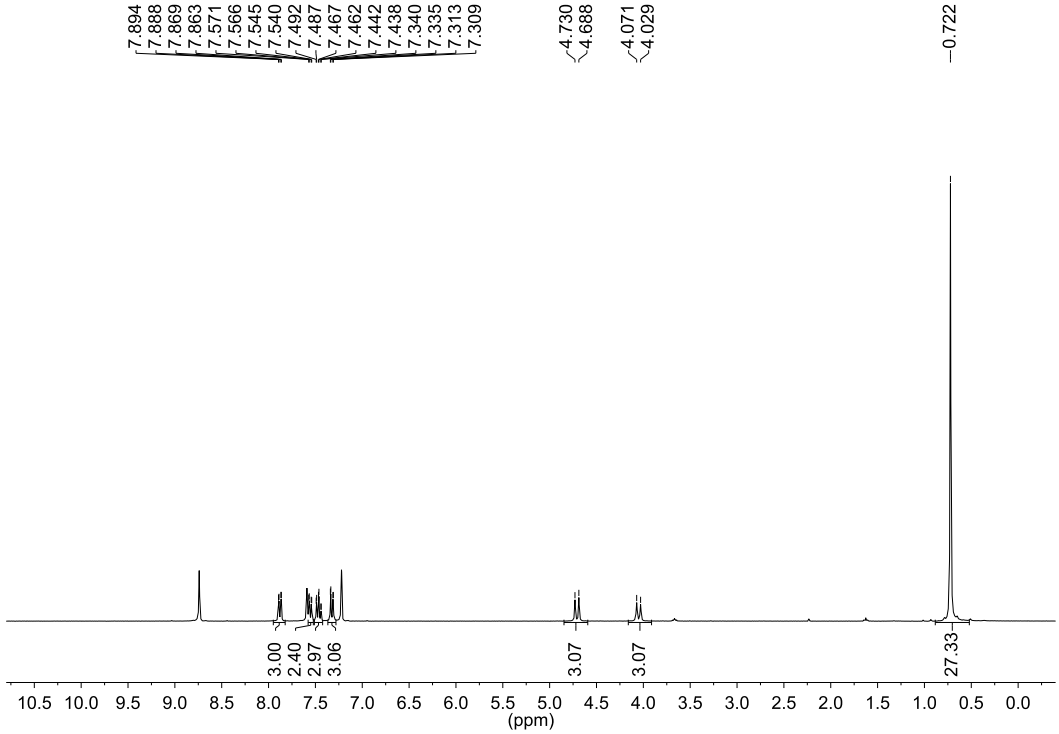

Figure 5.4.8. ^{1}H NMR spectrum of **5.1-I** in d_5-pyr.

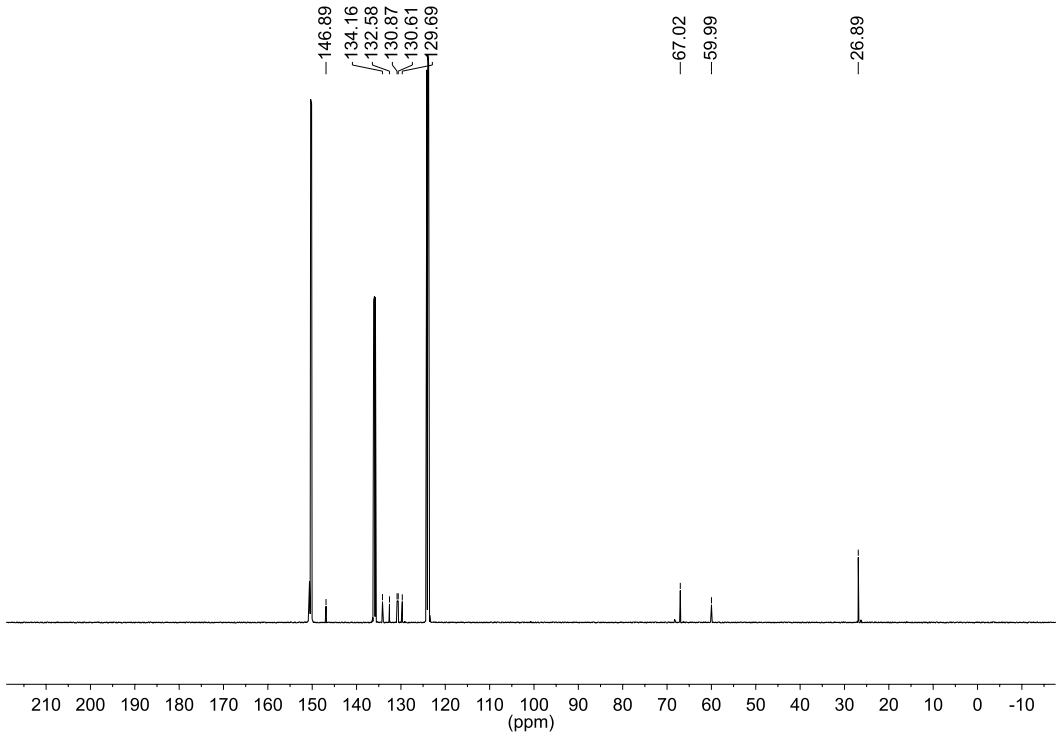

Figure 5.4.9. $^{13}C\{^{1}H\}$ NMR spectrum of **5.1-I** in d_5-pyr.

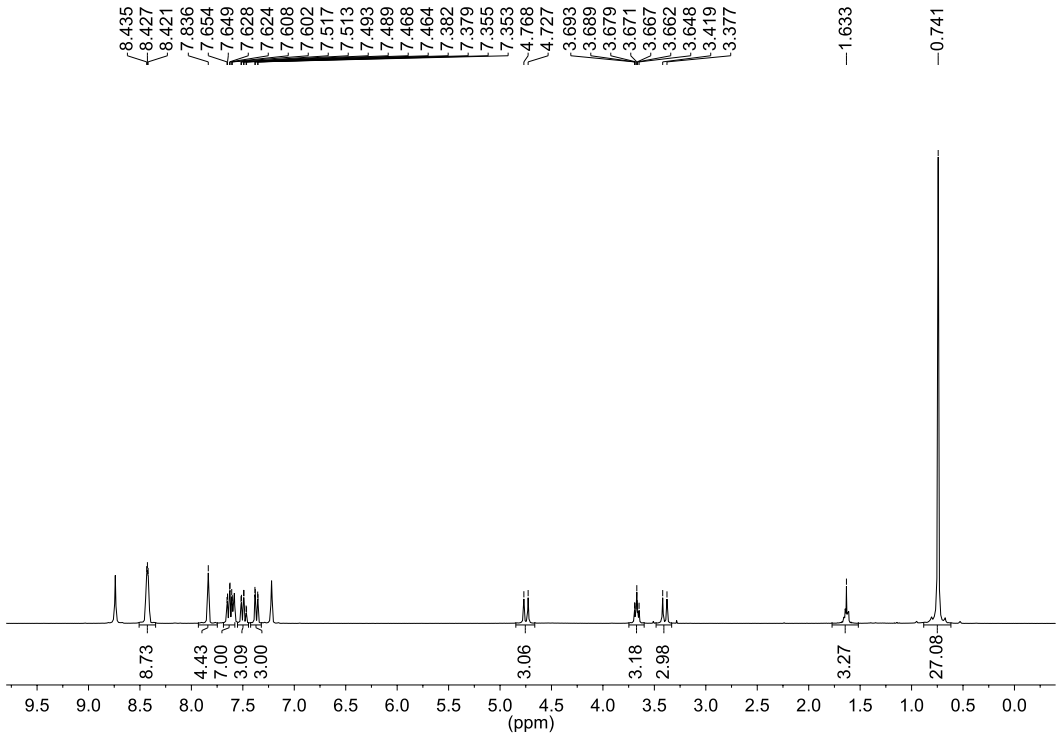

Figure 5.4.10. ^{1}H NMR spectrum of **5.1-BAr$^{F}_{4}$** in d_5-pyr.

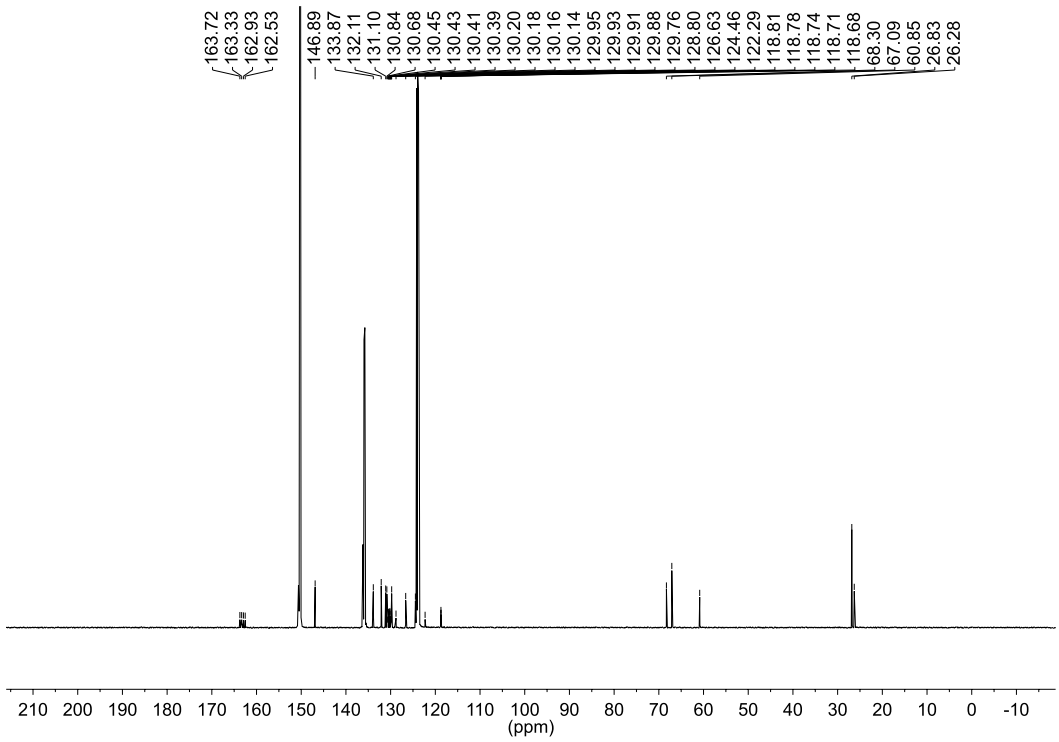

Figure 5.4.11. $^{13}C\{^{1}H\}$ NMR spectrum of **5.1-BAr$^{F}_{4}$** in d_5-pyr.

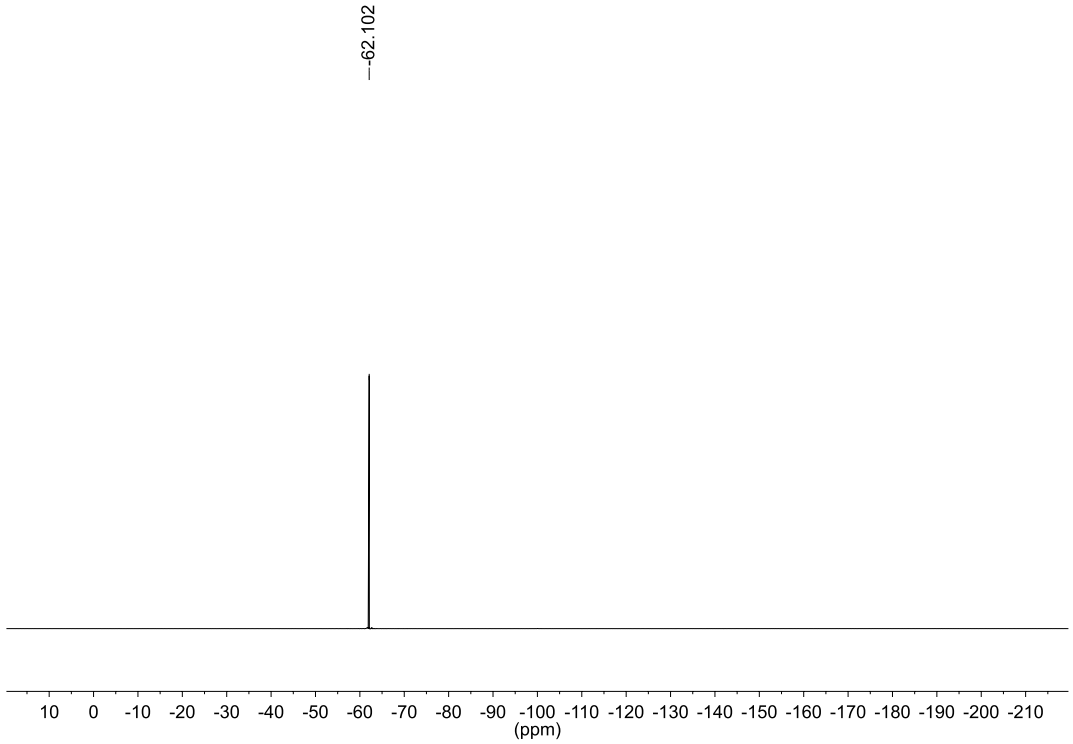

Figure 5.4.12. $^{19}F\{^{1}H\}$ NMR spectrum of **5.1-BAr$^{F}_{4}$** in d_5-pyr.

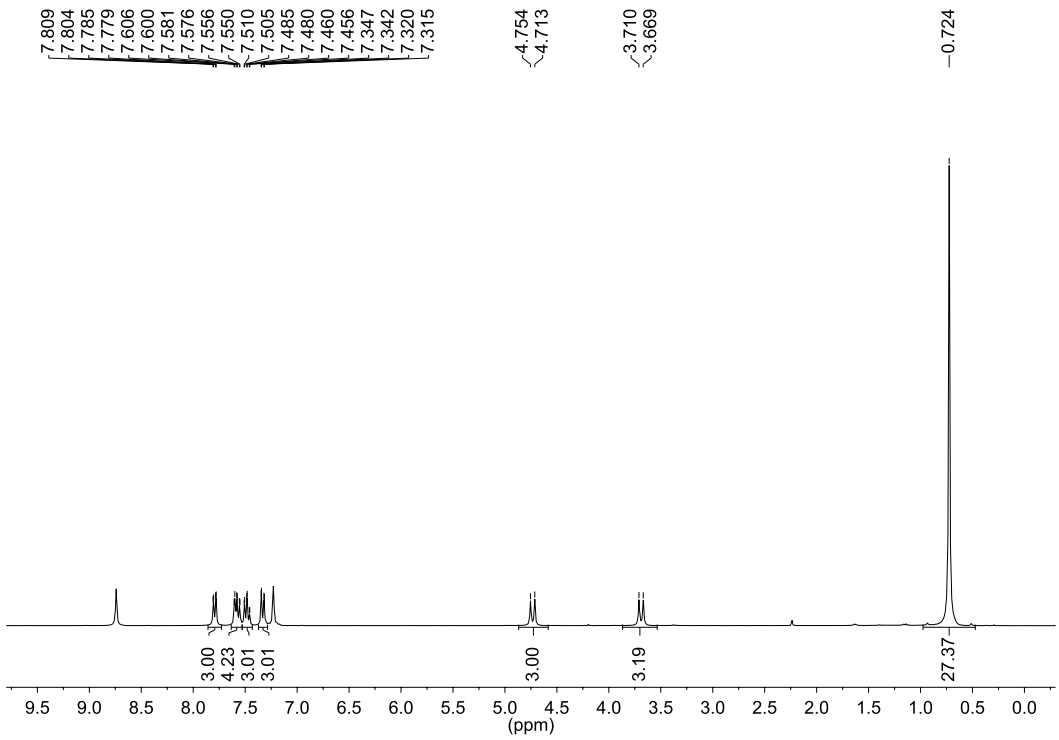

Figure 5.4.13. ^{1}H NMR spectrum of **5.1-OTf** in d_5-pyr.

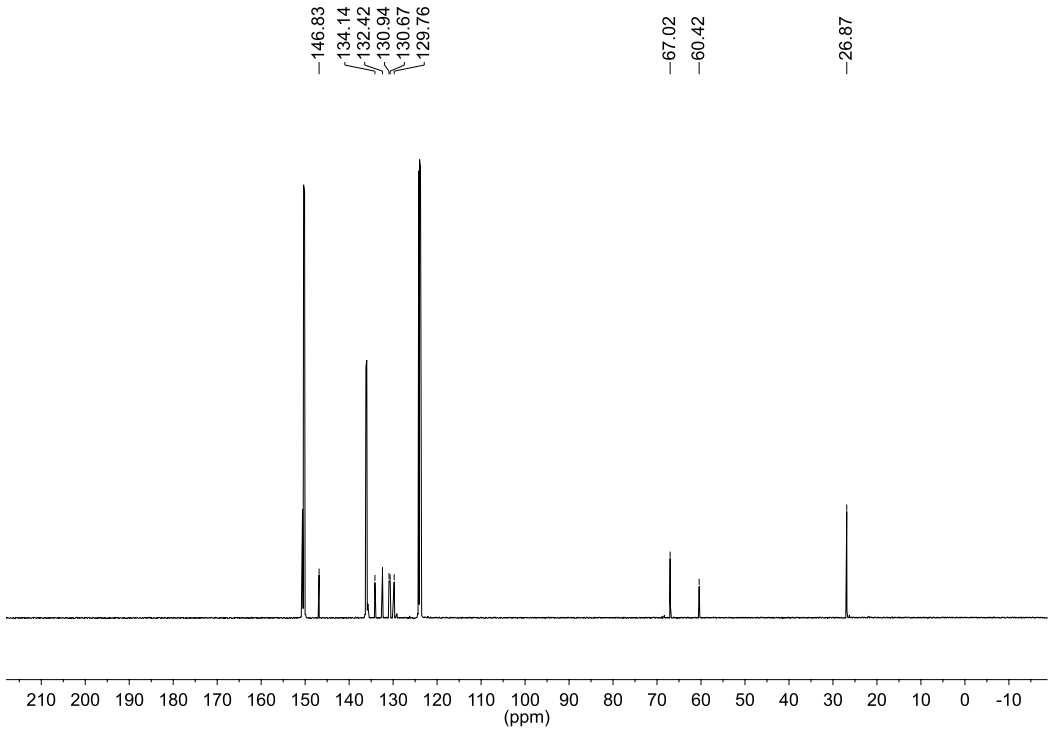

Figure 5.4.14. ^{13}C{^{1}H} NMR spectrum of **5.1-OTf** in d_5-pyr.

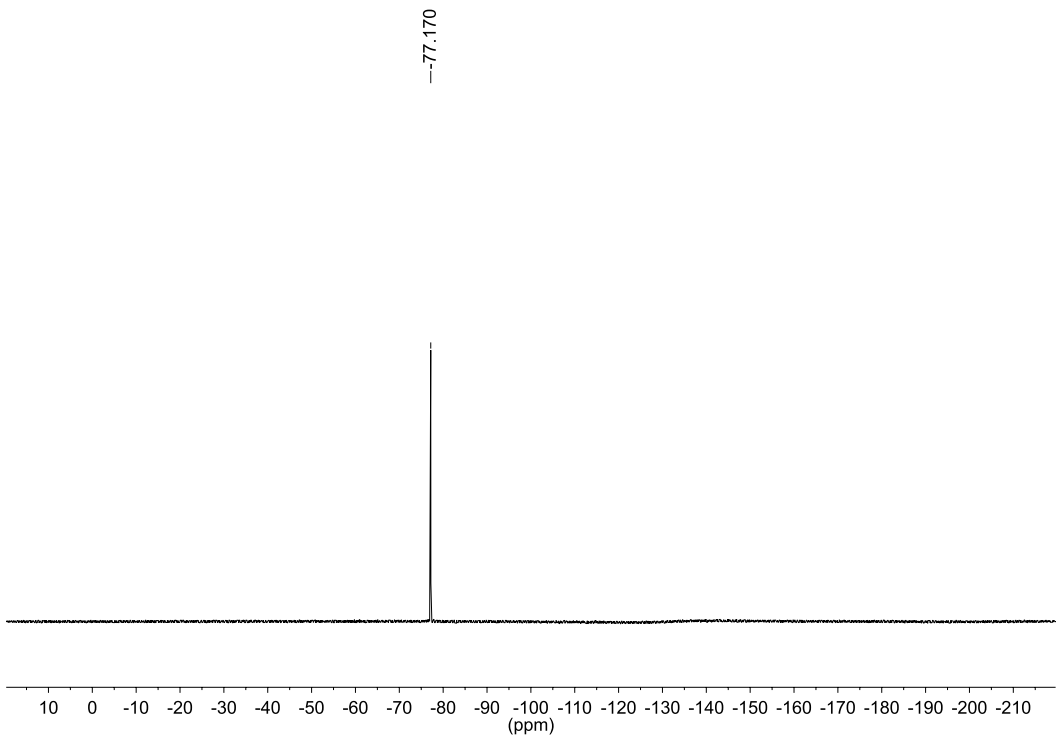

Figure 5.4.15. $^{19}F\{^{1}H\}$ NMR spectrum of **5.1-OTf** in d_5-pyr.

X-ray Crystallography. X-ray intensity data were collected on a Bruker APEXII CCD area detector employing graphite-monochromated Mo-Kα radiation (λ=0.71073 Å) at a temperature of 143(1) K. In all cases, rotation frames were integrated using SAINT,[26] producing a listing of unaveraged F^2 and $\sigma(F^2)$ values that were then passed to the SHELXTL[27] program package for further processing and structure solution on a Dell Pentium 4 computer. The intensity data were corrected for Lorentz and polarization effects and for absorption using TWINABS[28] or SADABS.[29] The structures were solved by direct methods (SHELXS-97).[30] Refinement was by full-matrix least squares based on F^2 using SHELXL-97.[30] All reflections were used during refinements. Non-hydrogen atoms were refined anisotropically and hydrogen atoms were refined using a riding model.

Crystallographic data and structure refinement information for **5.1-X**, **X = BAr$^F_4$** (Penn4524), **OTf** (Penn4539), **Cl** (Penn4449), **μO** (Penn4766) are summarized in Tables 5.4.1 – 5.4.4.

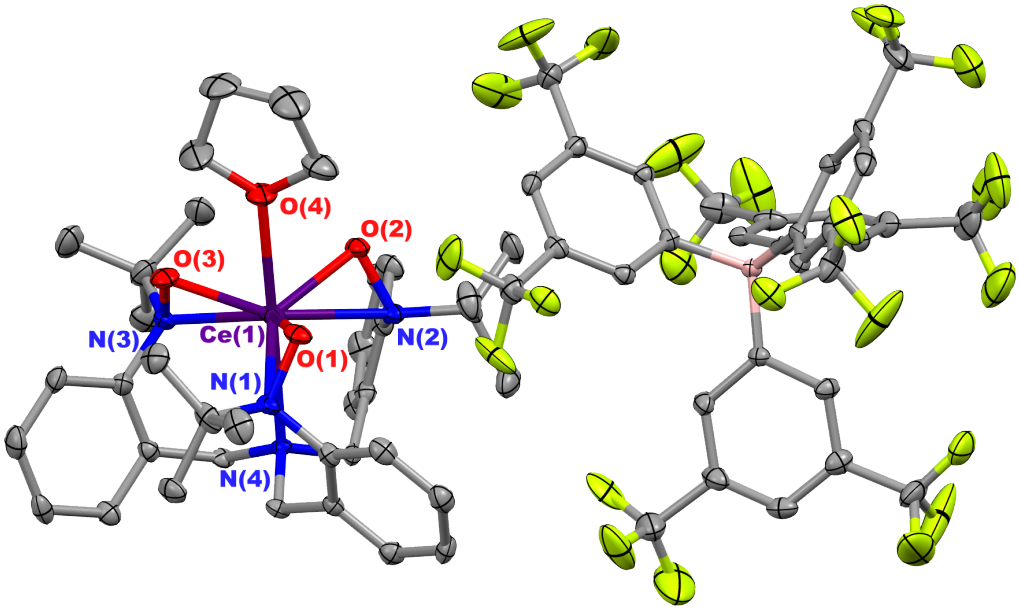

Figure 5.4.16. Thermal ellipsoid plot of **5.1-BAr$^F_4$** at 30% probability. Hydrogen atoms excluded for clarity.

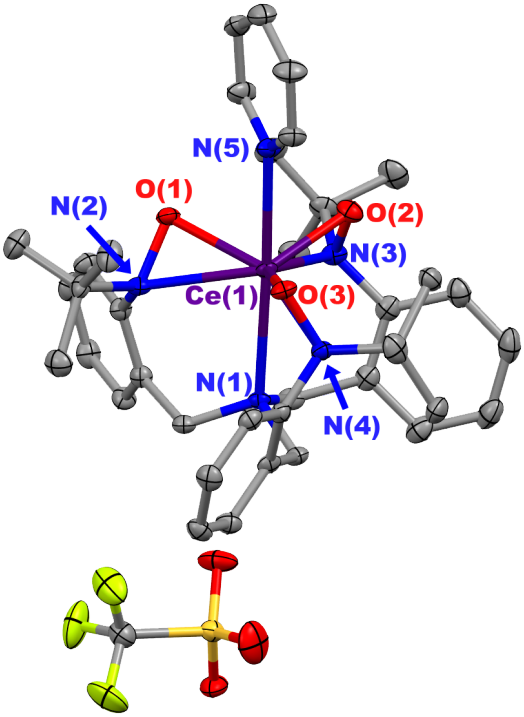

Figure 5.4.17. Thermal ellipsoid plot of **5.1-OTf** at 30% probability. Hydrogen atoms excluded for clarity.

Table 5.4.1. Crystallographic parameters for **5.1-BAr$^F_4$**.

	5.1-BAr$^F_4$ (Penn4524)
Empirical formula	$C_{69}BH_{65}N_4O_4F_{24}Ce$
Formula weight	1621.18
Temperature	100(1) K
Wavelength	0.71073 Å
Crystal system	monoclinic
Space group	C2/c
Cell constants:	
a	40.674(2) Å
b	19.3146(10) Å
c	18.6876(9) Å
β	110.450(3)°
Volume	13755.8(12) Å^3
Z	8
Density (calculated)	1.566 Mg/m^3
Absorption coefficient	0.778 mm^{-1}
F(000)	6544
Crystal size	0.28 x 0.10 x 0.02 mm^3
Theta range for data collection	1.52 to 27.59°
Index ranges	$-52 \leq h \leq 52$, $-25 \leq k \leq 25$, $-24 \leq l \leq 24$
Reflections collected	205840
Independent reflections	15924 [R(int) = 0.0491]
Completeness to theta = 27.59°	99.8 %
Absorption correction	Semi-empirical from equivalents
Max. and min. transmission	0.7456 and 0.6901
Refinement method	Full-matrix least-squares on F^2
Data / restraints / parameters	15924 / 1257 / 1238
Goodness-of-fit on F^2	1.128
Final R indices [I>2sigma(I)]	R1 = 0.0845, wR2 = 0.2066
R indices (all data)	R1 = 0.0969, wR2 = 0.2153
Largest diff. peak and hole	12.543 and -3.185 e.Å^{-3}

Table 5.4.2. Crystallographic parameters for **5.1-OTf**.

	5.1-OTf (Penn4539)
Empirical formula	$C_{83}H_{105}N_{11}S_2O_{12}F_6Ce_2$
Formula weight	1907.14
Temperature	100(1) K
Wavelength	0.71073 Å
Crystal system	triclinic
Space group	$P\bar{1}$
Cell constants:	
a	10.1667(4) Å
b	13.3652(5) Å
c	16.7847(7) Å
α	100.249(2)°
β	107.294(2)°
γ	94.680(2)°
Volume	2120.79(15) $Å^3$
Z	1
Density (calculated)	1.493 Mg/m^3
Absorption coefficient	1.188 mm^{-1}
F(000)	978
Crystal size	0.25 x 0.12 x 0.05 mm^3
Theta range for data collection	1.30 to 27.60°
Index ranges	$-13 \leq h \leq 12$, $-17 \leq k \leq 17$, $-21 \leq l \leq 21$
Reflections collected	52105
Independent reflections	9667 [R(int) = 0.0678]
Completeness to theta = 27.60°	98.3 %
Absorption correction	Semi-empirical from equivalents
Max. and min. transmission	0.7456 and 0.4680
Refinement method	Full-matrix least-squares on F^2
Data / restraints / parameters	9667 / 0 / 518
Goodness-of-fit on F^2	1.197
Final R indices [I>2sigma(I)]	R1 = 0.0455, wR2 = 0.1246
R indices (all data)	R1 = 0.0484, wR2 = 0.1270
Largest diff. peak and hole	2.892 and -2.766 $e.Å^{-3}$

Table 5.4.3. Crystallographic parameters for **5.1-Cl**.

	5.1-Cl (Penn4449)
Empirical formula	$C_{43}H_{55}N_6O_3ClCe$
Formula weight	879.50
Temperature	100(1) K
Wavelength	0.71073 Å
Crystal system	monoclinic
Space group	$P2_1/c$
Cell constants:	
a	12.6321(8) Å
b	18.8187(11) Å
c	17.7801(12) Å
β	102.886(4)°
Volume	4120.2(5) $Å^3$
Z	4
Density (calculated)	1.418 Mg/m^3
Absorption coefficient	1.216 mm^{-1}
F(000)	1816
Crystal size	0.38 x 0.07 x 0.02 mm^3
Theta range for data collection	1.60 to 27.57°
Index ranges	$-16 \leq h \leq 16$, $-24 \leq k \leq 24$, $-23 \leq l \leq 23$
Reflections collected	138198
Independent reflections	9516 [R(int) = 0.0406]
Completeness to theta = 27.57°	99.8 %
Absorption correction	Semi-empirical from equivalents
Max. and min. transmission	0.7456 and 0.6629
Refinement method	Full-matrix least-squares on F^2
Data / restraints / parameters	9516 / 0 / 497
Goodness-of-fit on F^2	1.184
Final R indices [I>2sigma(I)]	R1 = 0.0323, wR2 = 0.0761
R indices (all data)	R1 = 0.0414, wR2 = 0.0801
Largest diff. peak and hole	1.595 and -0.793 $e.Å^{-3}$

Table 5.4.4. Crystallographic parameters for **5.1-μO**.

	5.1-μO (Penn4766)
Empirical formula	$C_{81}H_{105}N_{11}O_7Ce_2$
Formula weight	1625.00
Temperature	100(1) K
Wavelength	0.71073 Å
Crystal system	monoclinic
Space group	C2/c
Cell constants:	
a	11.7973(7) Å
b	21.0910(13) Å
c	30.400(2) Å
β	92.804(3)°
Volume	7555.0(8) $Å^3$
Z	4
Density (calculated)	1.429 Mg/m^3
Absorption coefficient	1.252 mm^{-1}
F(000)	3360
Crystal size	0.25 x 0.25 x 0.10 mm^3
Theta range for data collection	1.34 to 27.58°
Index ranges	$-15 \leq h \leq 15$, $-27 \leq k \leq 27$, $-39 \leq l \leq 39$
Reflections collected	94083
Independent reflections	8640 [R(int) = 0.0465]
Completeness to theta = 27.58°	98.7 %
Absorption correction	Semi-empirical from equivalents
Max. and min. transmission	0.7456 and 0.5977
Refinement method	Full-matrix least-squares on F^2
Data / restraints / parameters	8640 / 0 / 467
Goodness-of-fit on F^2	1.143
Final R indices [I>2sigma(I)]	R1 = 0.0440, wR2 = 0.1344
R indices (all data)	R1 = 0.0464, wR2 = 0.1358
Largest diff. peak and hole	2.299 and -2.089 $e.Å^{-3}$

Electrochemistry. Cyclic voltammetry experiments were performed using a CH Instruments 620D Electrochemical Analyzer/Workstation and the data were processed using CHI software v 9.24. All experiments were performed in an N_2 atmosphere drybox using electrochemical cells that consisted of a 4 mL vial, glassy carbon (3 mm diameter) working electrode, a platinum wire counter electrode, and a silver wire plated with AgCl as a quasi-reference electrode. The working electrode surfaces were polished prior to each set of experiments, and were periodically replaced on scanning > 0 V versus ferrocene (Fc) to prevent the buildup of oxidized product on the electrode surfaces. Potentials were reported versus Fc, which was added as an internal standard for calibration at the end of each run. Solutions employed during CV studies were ~3 mM in analyte and 100 mM in [$^{n}Pr_4N$][B(3,5-$(CF_3)_2$-$C_6H_3)_4$] ([$^{n}Pr_4N$][BAr^{F}_4]). All complexes were measured in DCM. The THF was necessary to dissolve the complexes in solution. All data were collected in a positive-feedback IR compensation mode. The solution cell resistances were measured prior to each run to ensure resistances ≤ ~500 Ω.[24] Scan rate dependences of 50–1000 mV/s were performed to determine electrochemical reversibility.

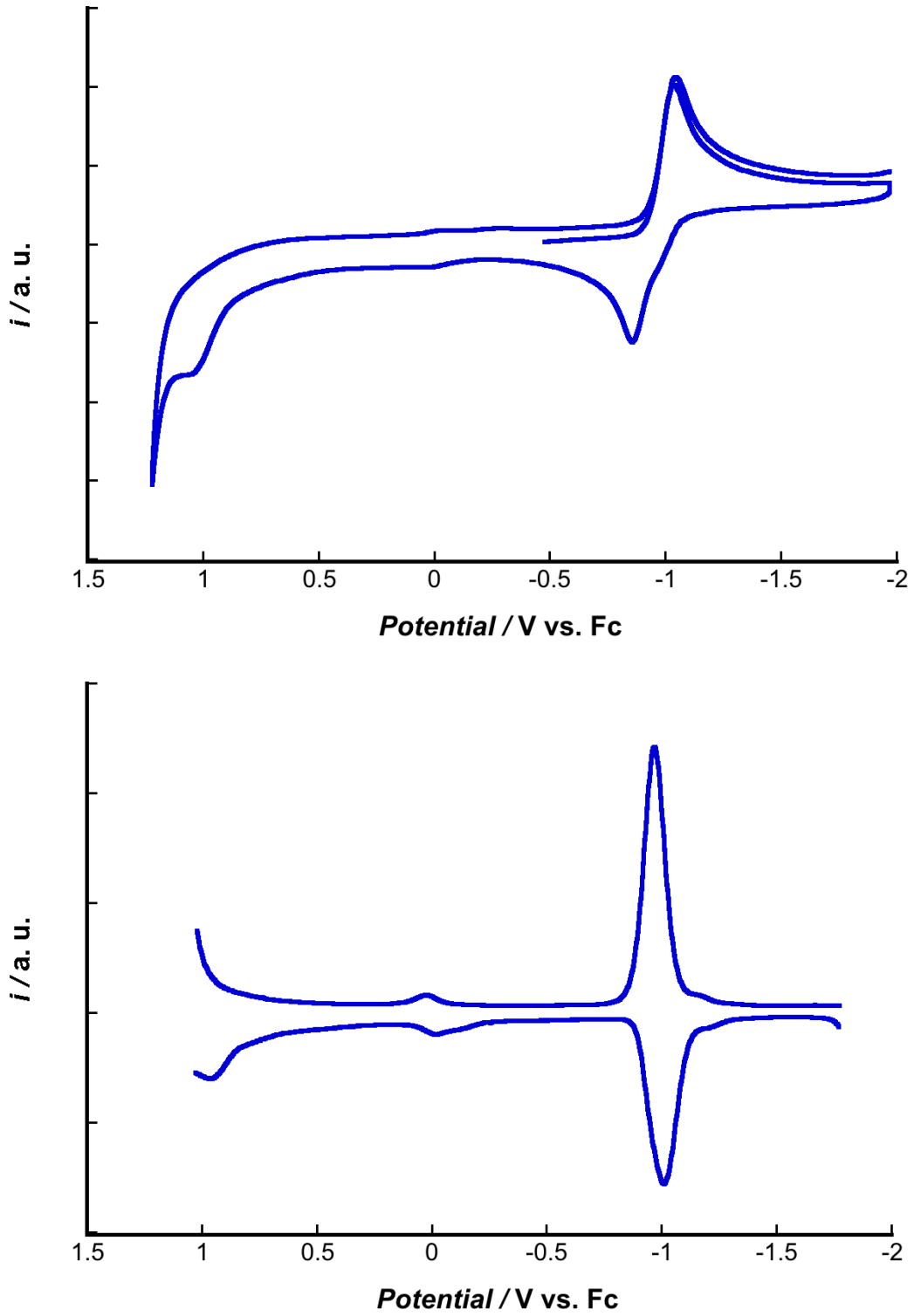

Figure 5.4.18. Cyclic voltammogram (top) and differential pulse voltammogram (bottom) of **5.1-BAr$^{F}_{4}$**.

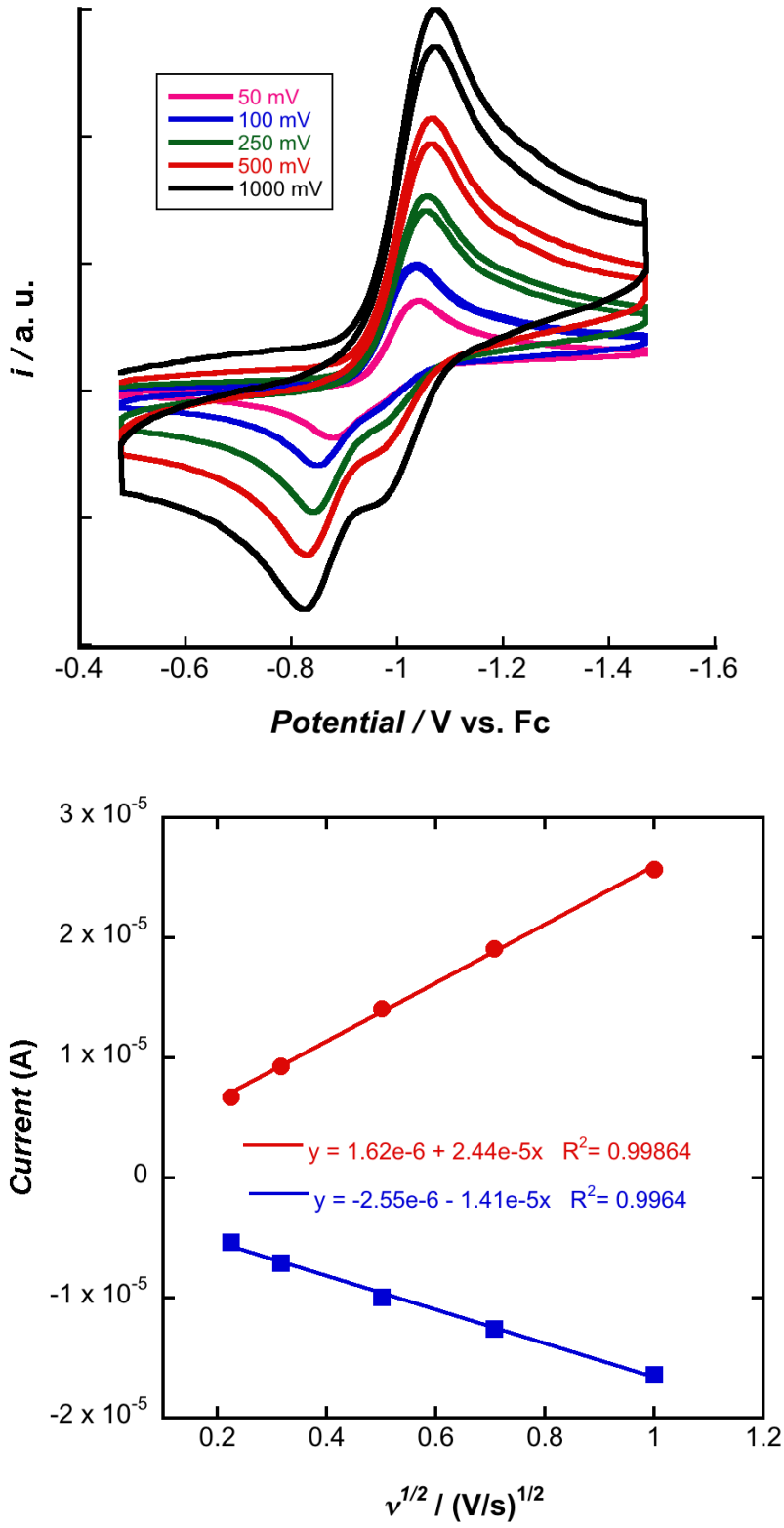

Figure 5.4.19. Scan rate dependence of the $Ce^{IV/III}$ couple of **5.1-BAr$^{F}_{4}$**.

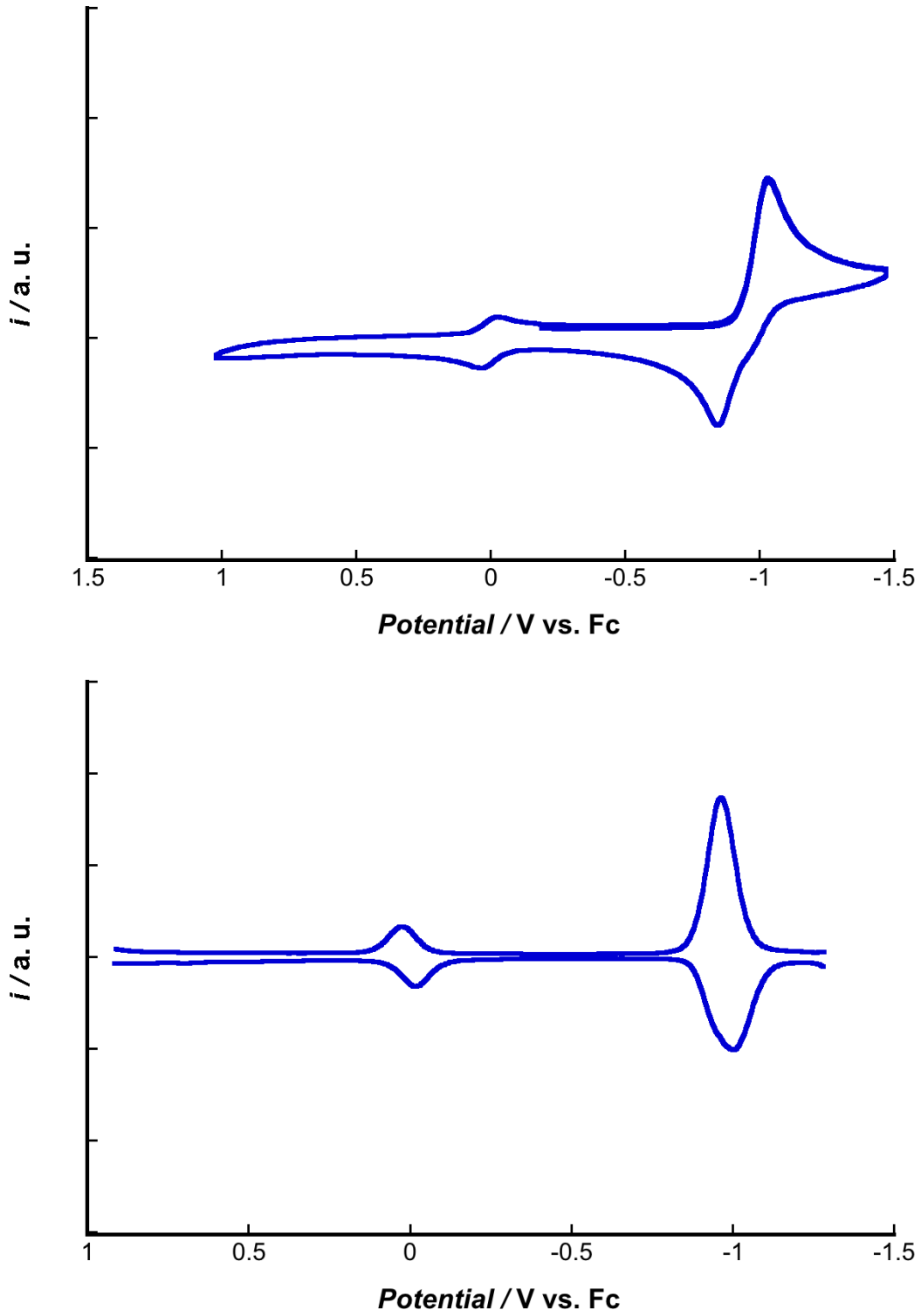

Figure 5.4.20. Cyclic voltammogram (top) and differential pulse voltammogram (bottom) of **5.1-OTf**. Wave at 0 V is due to a slight ferrocene impurity.

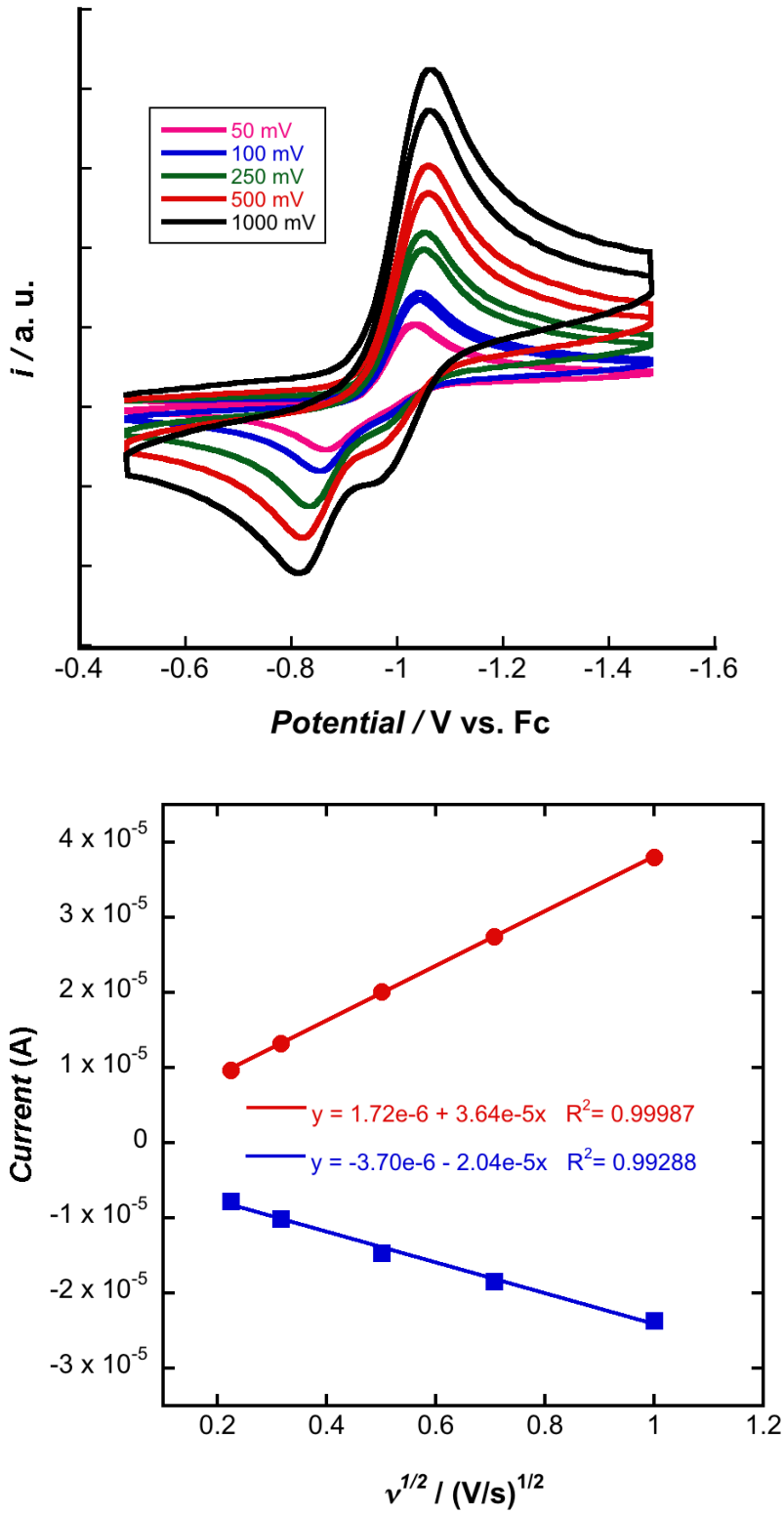

Figure 5.4.21. Scan rate dependence of the $Ce^{IV/III}$ couple of **5.1-OTf**.

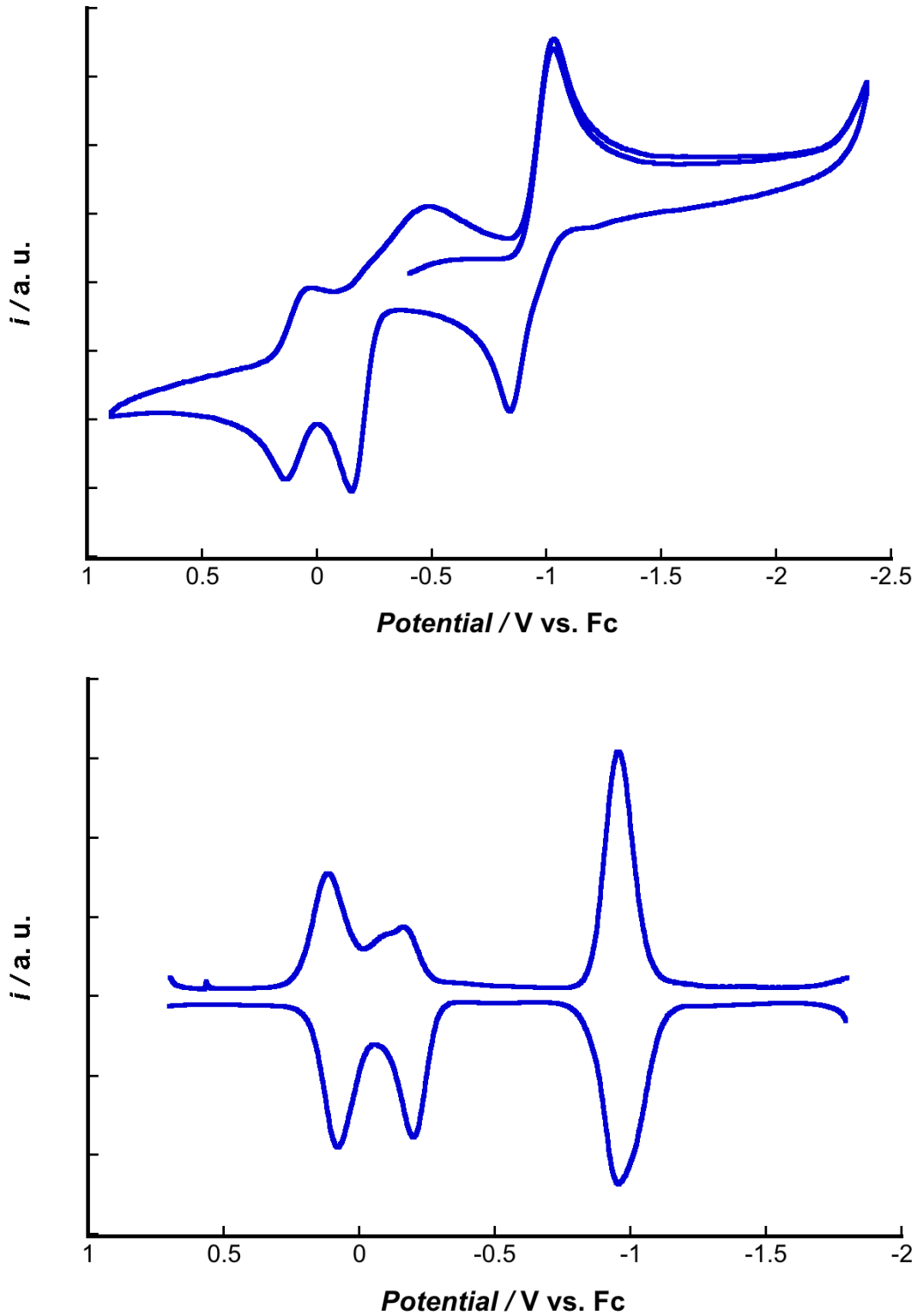

Figure 5.4.22. Cyclic voltammogram (top) and differential pulse voltammogram (bottom) of **5.1-l**.

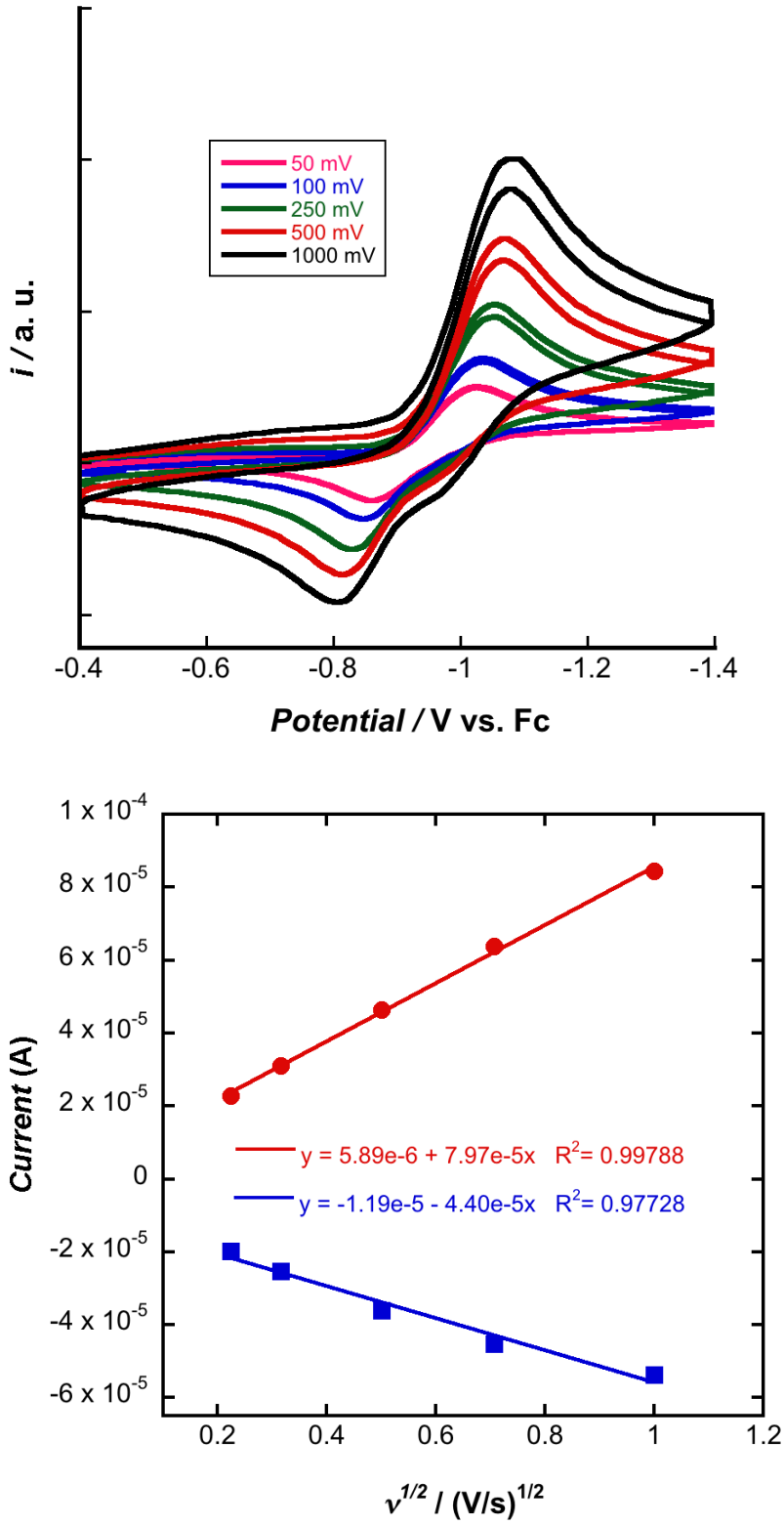

Figure 5.4.23. Scan rate dependence of the $Ce^{IV/III}$ couple of **5.1-I**.

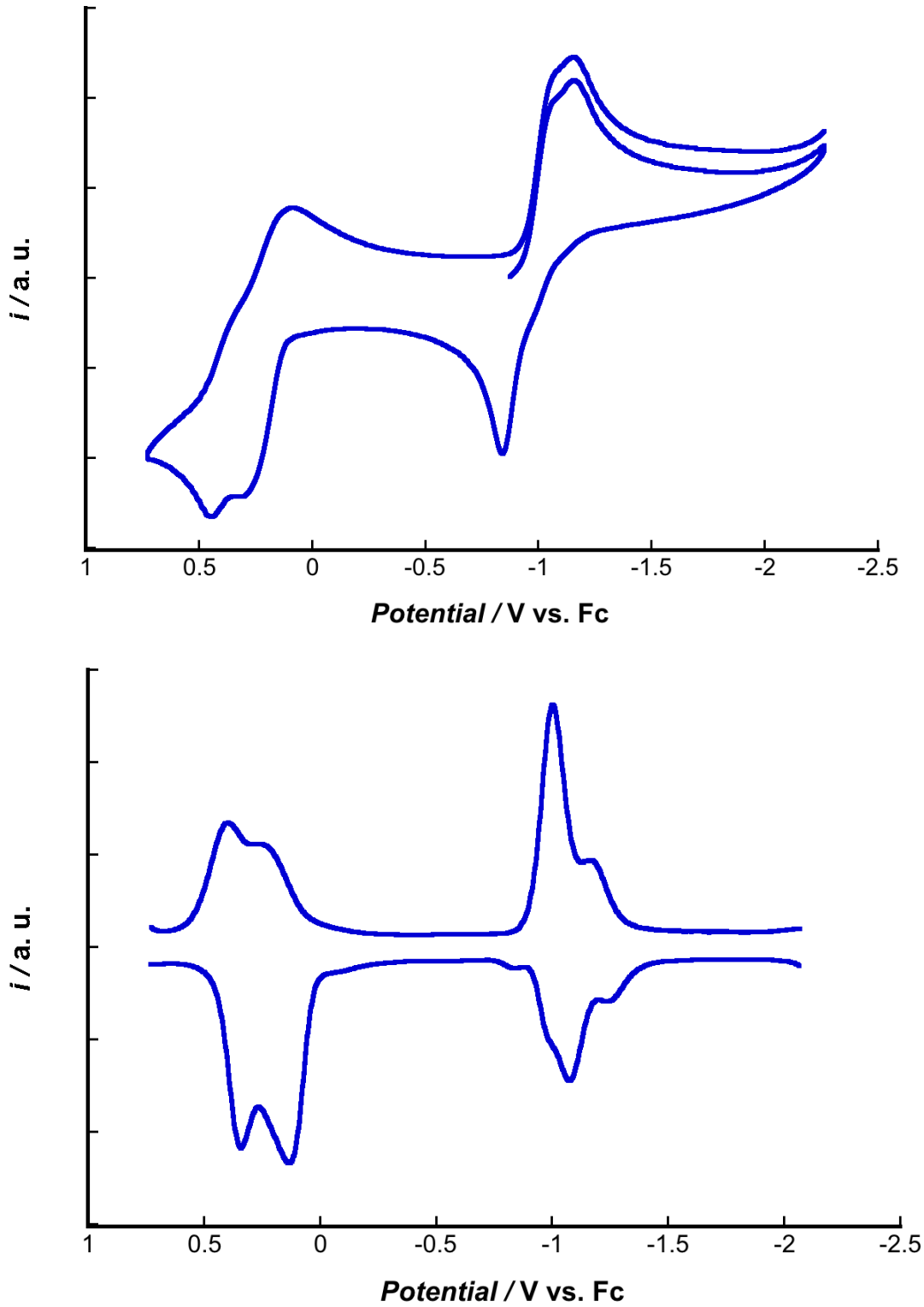

Figure 5.4.24. Cyclic voltammogram (top) and differential pulse voltammogram (bottom) of **5.1-Br**.

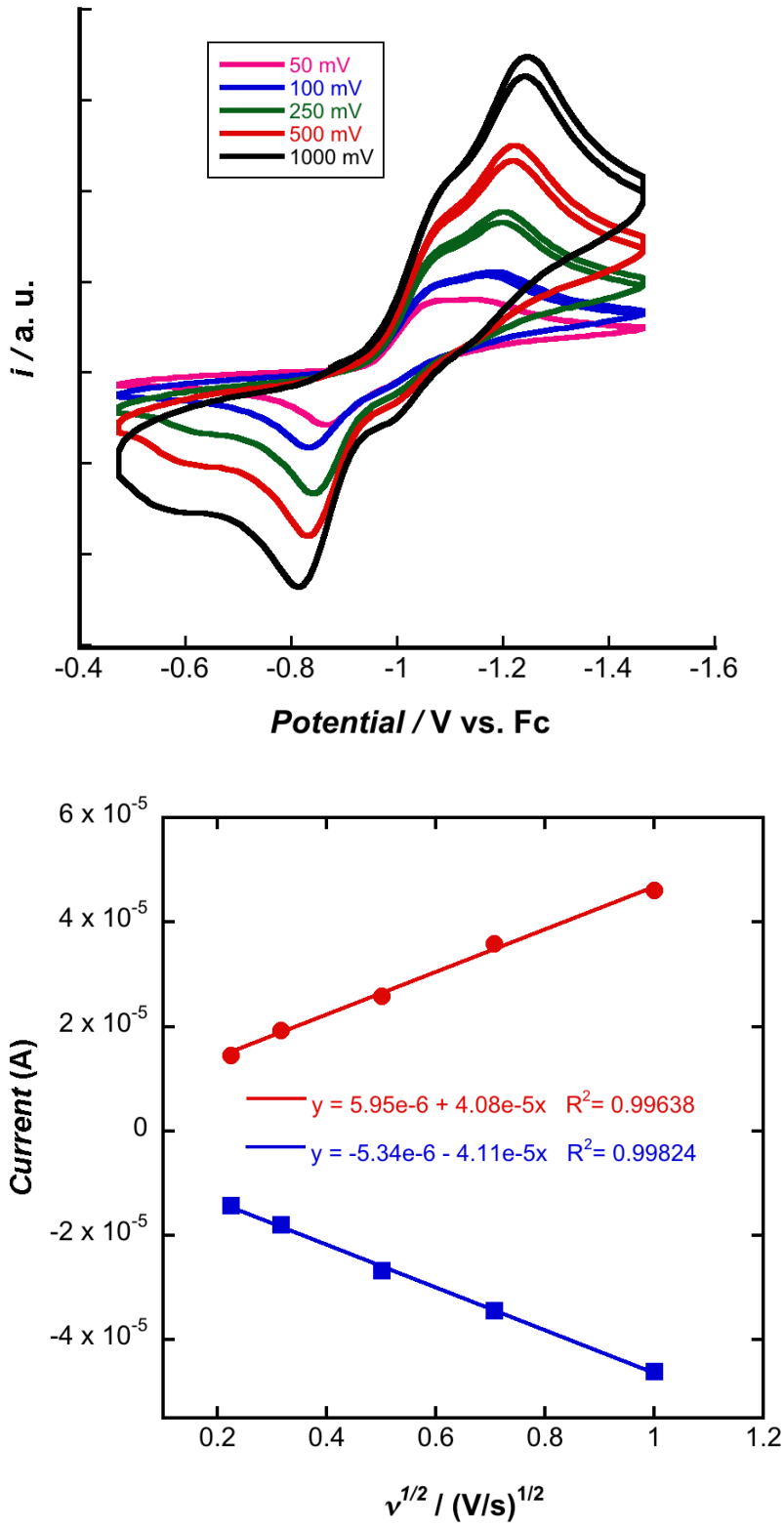

Figure 5.4.25. Scan rate dependence of the $Ce^{IV/III}$ couple of **5.1-Br**.

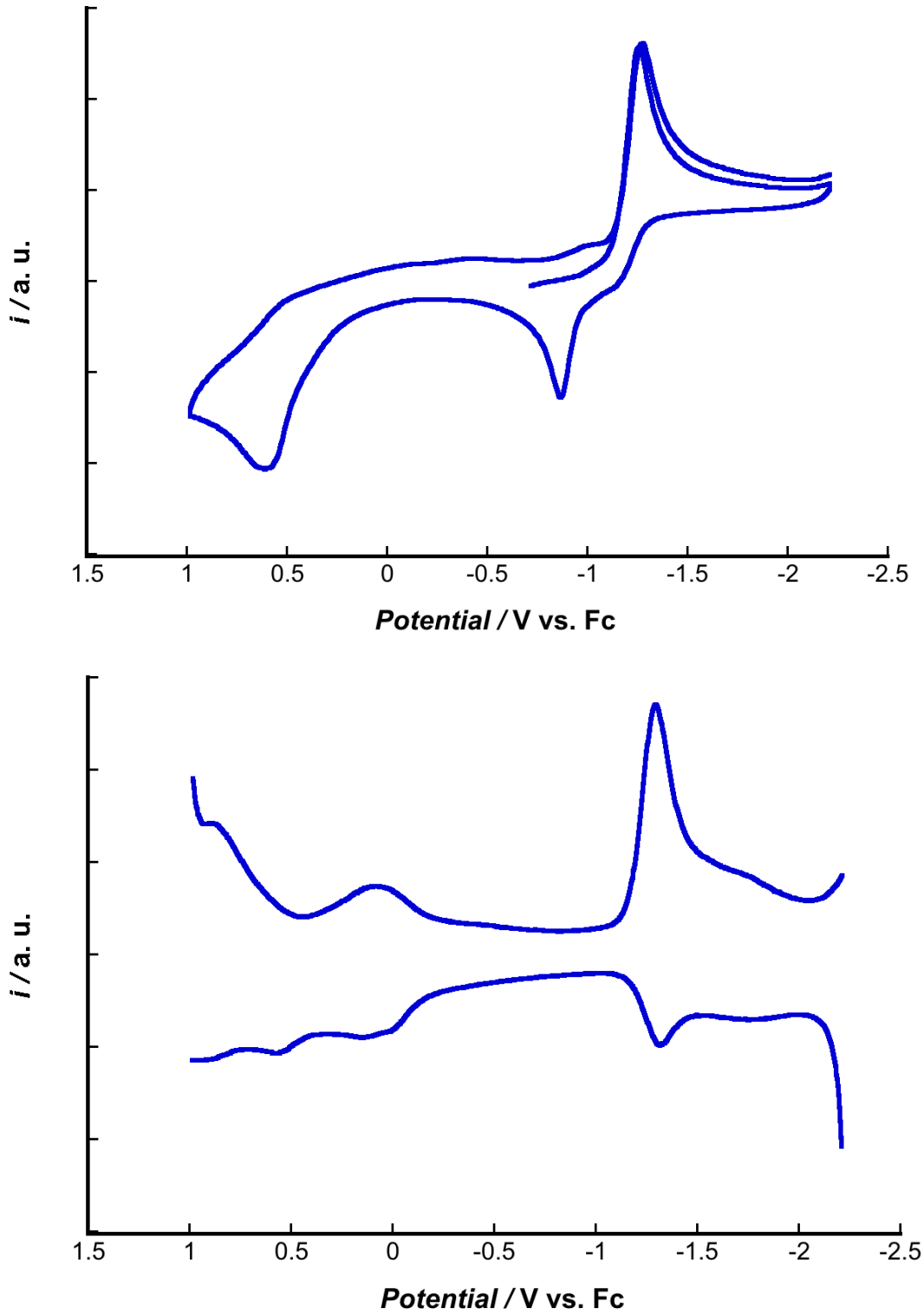

Figure 5.4.26. Cyclic voltammogram (top) and differential pulse voltammogram (bottom) of **5.1-Cl**.

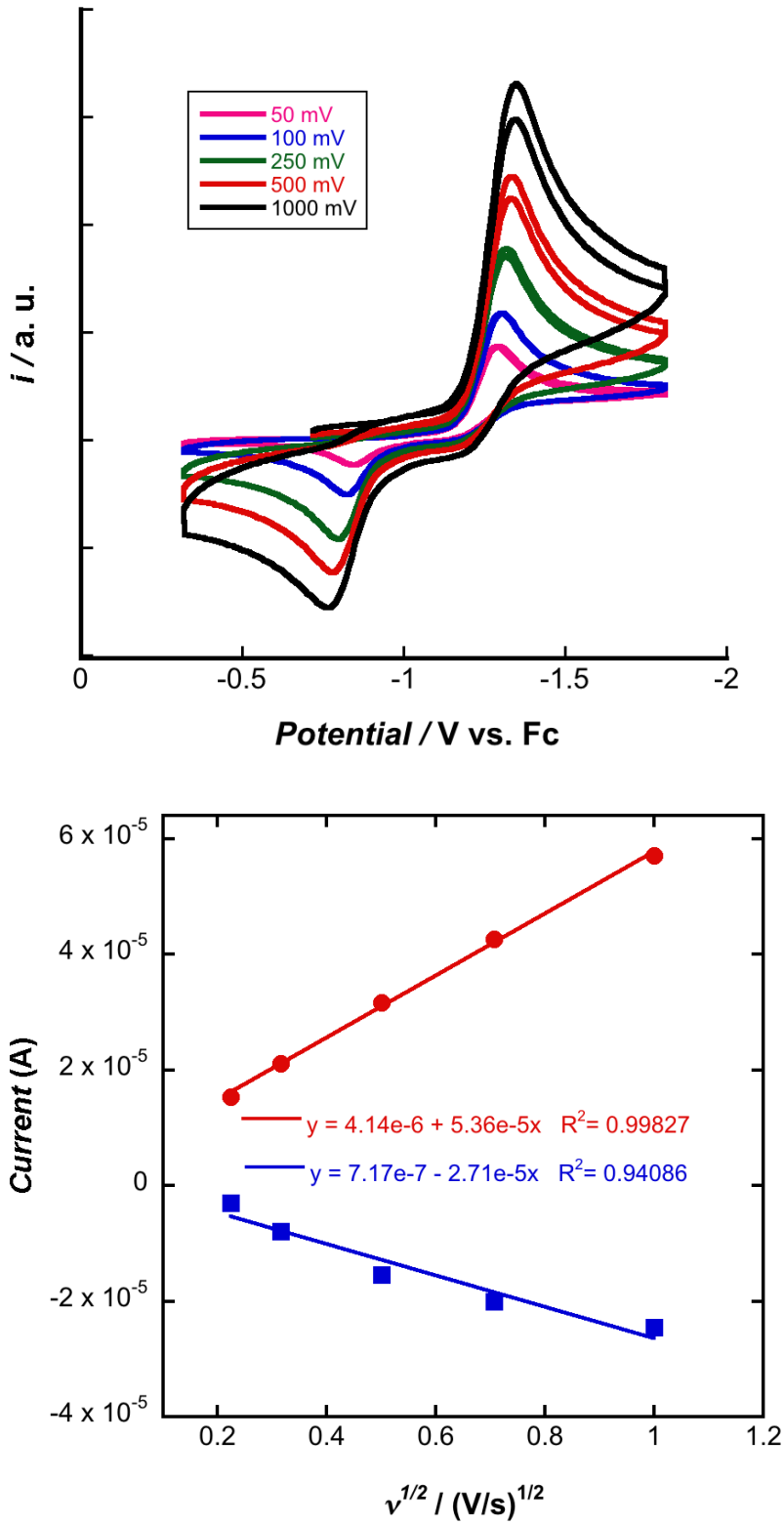

Figure 5.4.27. Scan rate dependence of the $Ce^{IV/III}$ couple of **5.1-Cl**.

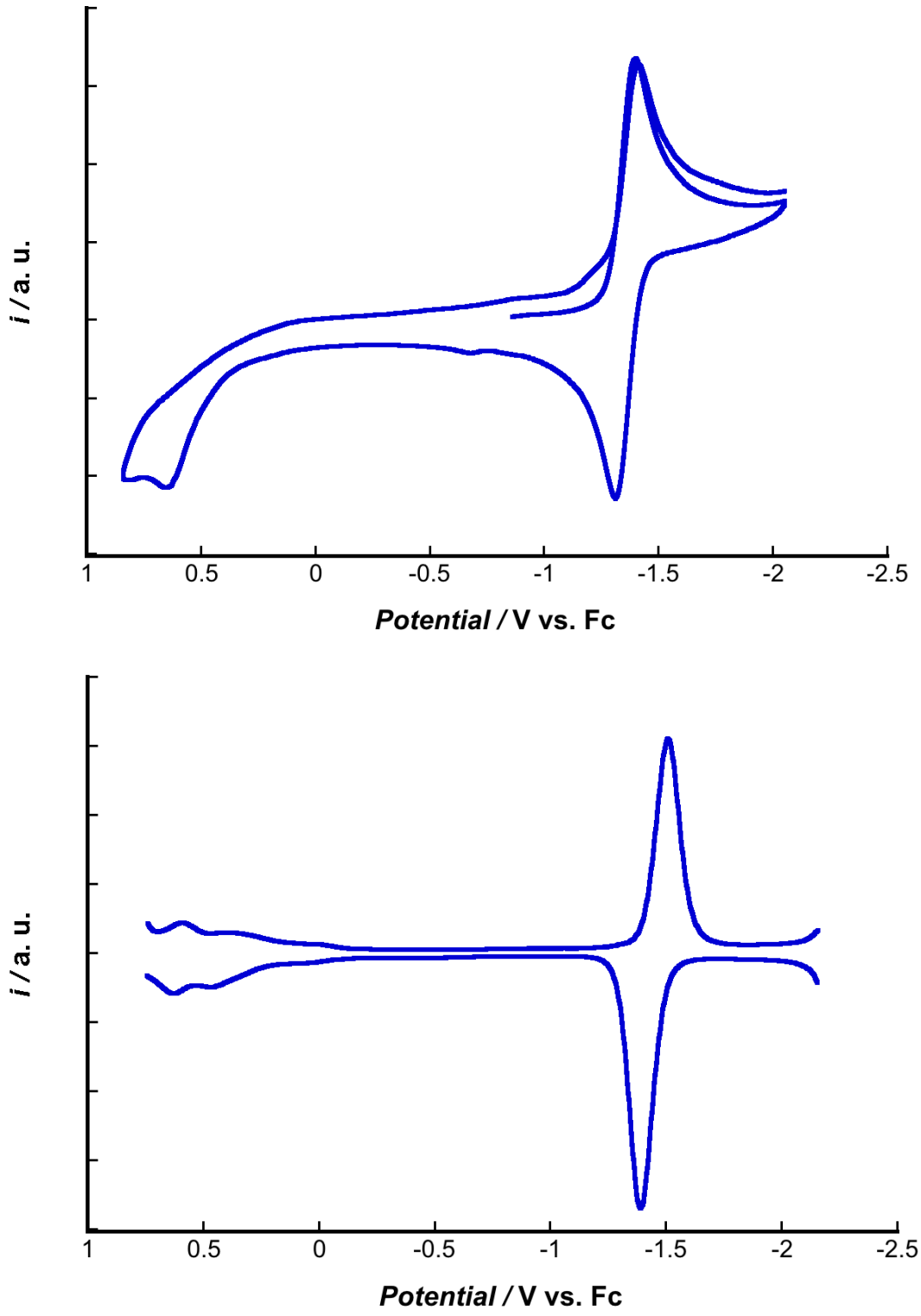

Figure 5.4.28. Cyclic voltammogram (top) and differential pulse voltammogram (bottom) of **5.1-F**.

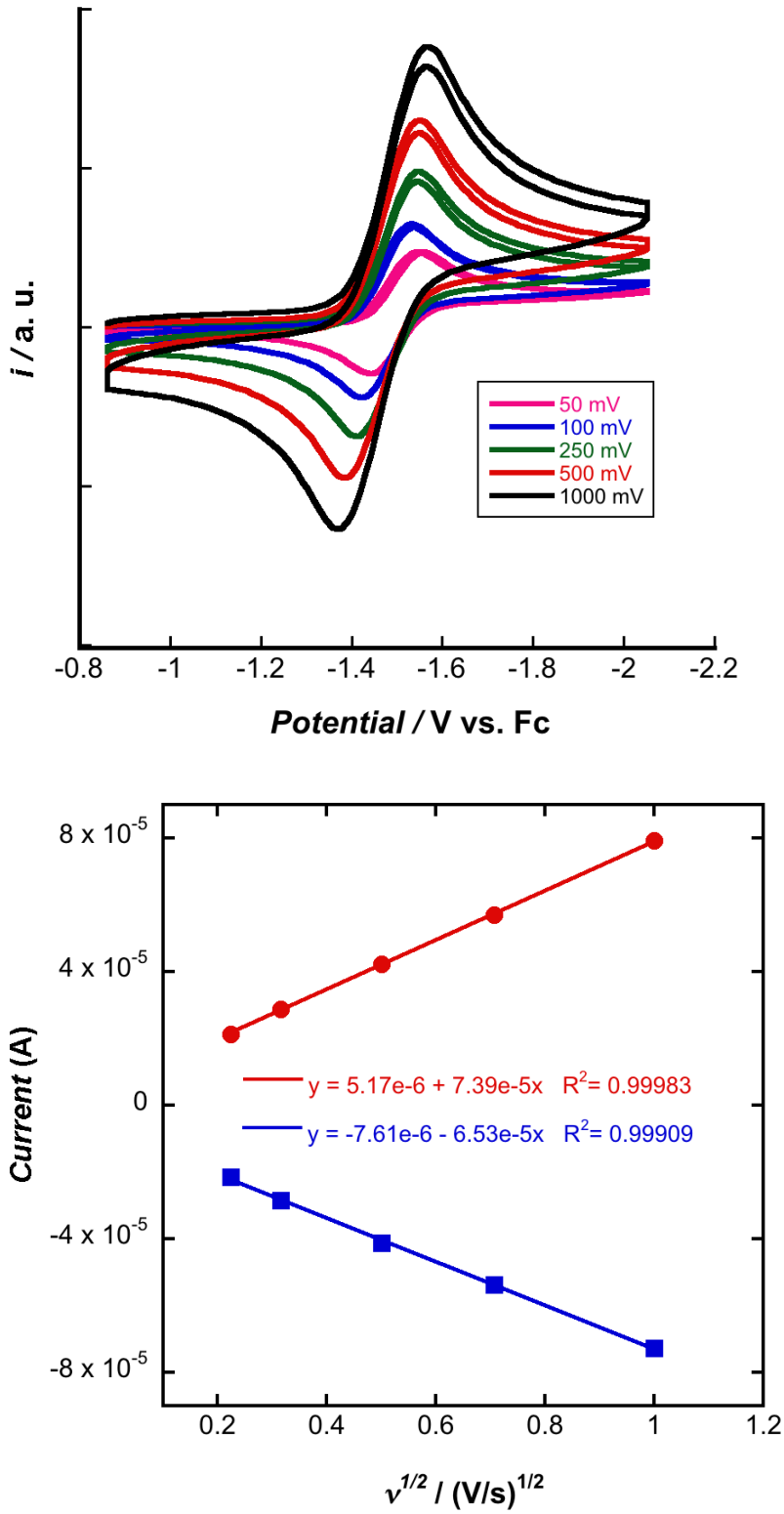

Figure 5.4.29. Scan rate dependence of the $Ce^{IV/III}$ couple of **5.1-F**.

Computational Details. Gaussian 09 Rev. D.01 was used in electronic structure calculations.[31] The B3LYP hybrid DFT method was employed, with a 28-electron small core pseudopotential on cerium with published segmented natural orbital basis set incorporating quasi-relativistic effects,[32] and the 6-31G* basis set on all other atoms.[33] No restraints were imposed other than spin. Frequency calculations were preformed to confirm the geometry was a minimum (no negative frequencies). NBO calculations were run using the NBO6 package.[34] Fragment orbital analysis was performed using the AOMix software.[35] Molecular orbitals were rendered with the Chemcraft v1.6 program.[36]

Table 5.4.5. Optimized coordinates of **4.1-Ce**.

Ce	-0.268488000	-0.140626000	0.736522000
N	-2.139138000	1.093093000	-0.691376000
O	-2.097966000	1.260114000	0.729969000
C	-1.699062000	2.329133000	-1.307828000
C	-0.737393000	2.292261000	-2.337872000
C	-0.339743000	3.504247000	-2.926360000
H	0.388468000	3.477439000	-3.734018000
C	-0.836849000	4.729805000	-2.489794000
H	-0.508114000	5.651612000	-2.961795000
C	-1.739974000	4.759353000	-1.424412000
H	-2.117106000	5.708004000	-1.051014000
C	-2.159241000	3.568875000	-0.837026000
H	-2.829675000	3.578584000	0.012885000
C	-0.099707000	1.002265000	-2.812998000
N	0.930284000	0.434564000	-1.893419000
C	1.461389000	-0.829467000	-2.483550000
C	0.439385000	-1.937970000	-2.639995000

C	-0.020414000	-2.708487000	-1.551555000
N	0.512533000	-2.475031000	-0.222634000
O	-0.581836000	-2.418396000	0.697802000
C	1.533063000	-3.487337000	0.271548000
C	1.981082000	-3.045173000	1.674039000
H	2.298542000	-1.997778000	1.682432000
H	2.827137000	-3.662885000	1.997639000
H	1.173602000	-3.163209000	2.399853000
C	0.938261000	-4.906023000	0.358807000
H	0.009152000	-4.889636000	0.935051000
H	1.647108000	-5.570690000	0.866056000
H	0.735095000	-5.330008000	-0.629891000
C	2.752000000	-3.494910000	-0.665025000
H	2.473603000	-3.710959000	-1.701771000
H	3.445858000	-4.278745000	-0.341203000
H	3.292778000	-2.543887000	-0.630730000
C	-1.052808000	-3.638620000	-1.752152000
C	-1.577350000	-3.866334000	-3.021202000
C	-1.083842000	-3.153628000	-4.116679000
C	-0.092943000	-2.195971000	-3.914277000
H	0.273686000	-1.616443000	-4.758722000
H	-1.479043000	-3.328062000	-5.113677000
H	-2.369102000	-4.599071000	-3.154803000
H	-1.448759000	-4.157439000	-0.888463000
H	2.280902000	-1.150530000	-1.845674000
H	1.892325000	-0.609110000	-3.477302000
C	2.047897000	1.414450000	-1.752566000

C	3.167925000	0.973873000	-0.832250000
C	3.038278000	0.957484000	0.571915000
N	1.809136000	1.416436000	1.190696000
O	1.409727000	0.450657000	2.171192000
C	1.869428000	2.791195000	1.837017000
C	0.470495000	3.100795000	2.394731000
H	-0.302426000	2.997058000	1.626033000
H	0.445480000	4.132997000	2.763533000
H	0.226422000	2.433269000	3.224489000
C	2.231619000	3.844053000	0.777414000
H	3.183248000	3.621221000	0.283796000
H	2.333656000	4.821086000	1.263150000
H	1.449303000	3.935870000	0.017091000
C	2.886221000	2.841342000	2.993456000
H	2.697595000	2.021142000	3.691364000
H	2.779399000	3.788332000	3.534972000
H	3.919540000	2.777812000	2.638079000
C	4.075398000	0.423214000	1.353087000
C	5.260485000	-0.016252000	0.769880000
C	5.424213000	0.057933000	-0.615485000
C	4.377995000	0.539431000	-1.398559000
H	4.486590000	0.568357000	-2.480587000
H	6.347499000	-0.274207000	-1.082250000
H	6.054438000	-0.415705000	1.395709000
H	3.921315000	0.338952000	2.421215000
H	1.605110000	2.344609000	-1.403765000
H	2.477389000	1.615509000	-2.750993000

H	-0.852604000	0.229957000	-2.953951000
H	0.363555000	1.186374000	-3.799580000
C	-3.515205000	0.598190000	-1.102792000
C	-4.629467000	1.570709000	-0.671143000
H	-4.527776000	1.808560000	0.391034000
H	-5.608934000	1.105402000	-0.831070000
H	-4.607371000	2.501157000	-1.247240000
C	-3.563142000	0.398012000	-2.626048000
H	-3.330457000	1.319450000	-3.169367000
H	-4.574501000	0.090214000	-2.914672000
H	-2.876019000	-0.389620000	-2.951351000
C	-3.735843000	-0.757871000	-0.413514000
H	-2.947485000	-1.472295000	-0.673967000
H	-4.693926000	-1.182910000	-0.734377000
H	-3.753088000	-0.645139000	0.672694000
O	-1.622276000	-0.720122000	2.952059000
C	-2.482382000	0.183876000	3.662279000
C	-1.656613000	-1.979283000	3.649414000
C	-3.689409000	-0.677459000	4.049568000
H	-1.956491000	0.564843000	4.550991000
H	-2.710377000	1.007055000	2.983849000
C	-3.077369000	-2.088990000	4.253137000
H	-1.410992000	-2.747274000	2.915275000
H	-0.889677000	-1.970838000	4.436411000
H	-4.414743000	-0.687695000	3.229851000
H	-4.197534000	-0.301292000	4.942810000
H	-3.671296000	-2.854146000	3.745164000

H	-3.028180000	-2.360774000	5.312239000

Lowest Energy Frequencies (in cm^{-1}): 9.2088, 29.5364, 29.7144, 32.5078, 39.1588, 42.2784.

Sum of electronic and thermal Free Energies (in hartrees): –2436.152127.

Table 5.4.6. Optimized coordinates of **[4.1-Ce]$^+$** (cationic portion of **5.1-BAr$^F{}_4$**).

Ce	-0.268488000	-0.140626000	0.736522000
N	-2.139138000	1.093093000	-0.691376000
O	-2.097966000	1.260114000	0.729969000
C	-1.699062000	2.329133000	-1.307828000
C	-0.737393000	2.292261000	-2.337872000
C	-0.339743000	3.504247000	-2.926360000
H	0.388468000	3.477439000	-3.734018000
C	-0.836849000	4.729805000	-2.489794000
H	-0.508114000	5.651612000	-2.961795000
C	-1.739974000	4.759353000	-1.424412000
H	-2.117106000	5.708004000	-1.051014000
C	-2.159241000	3.568875000	-0.837026000
H	-2.829675000	3.578584000	0.012885000
C	-0.099707000	1.002265000	-2.812998000
N	0.930284000	0.434564000	-1.893419000
C	1.461389000	-0.829467000	-2.483550000
C	0.439385000	-1.937970000	-2.639995000
C	-0.020414000	-2.708487000	-1.551555000
N	0.512533000	-2.475031000	-0.222634000
O	-0.581836000	-2.418396000	0.697802000
C	1.533063000	-3.487337000	0.271548000

C	1.981082000	-3.045173000	1.674039000
H	2.298542000	-1.997778000	1.682432000
H	2.827137000	-3.662885000	1.997639000
H	1.173602000	-3.163209000	2.399853000
C	0.938261000	-4.906023000	0.358807000
H	0.009152000	-4.889636000	0.935051000
H	1.647108000	-5.570690000	0.866056000
H	0.735095000	-5.330008000	-0.629891000
C	2.752000000	-3.494910000	-0.665025000
H	2.473603000	-3.710959000	-1.701771000
H	3.445858000	-4.278745000	-0.341203000
H	3.292778000	-2.543887000	-0.630730000
C	-1.052808000	-3.638620000	-1.752152000
C	-1.577350000	-3.866334000	-3.021202000
C	-1.083842000	-3.153628000	-4.116679000
C	-0.092943000	-2.195971000	-3.914277000
H	0.273686000	-1.616443000	-4.758722000
H	-1.479043000	-3.328062000	-5.113677000
H	-2.369102000	-4.599071000	-3.154803000
H	-1.448759000	-4.157439000	-0.888463000
H	2.280902000	-1.150530000	-1.845674000
H	1.892325000	-0.609110000	-3.477302000
C	2.047897000	1.414450000	-1.752566000
C	3.167925000	0.973873000	-0.832250000
C	3.038278000	0.957484000	0.571915000
N	1.809136000	1.416436000	1.190696000
O	1.409727000	0.450657000	2.171192000

C	1.869428000	2.791195000	1.837017000
C	0.470495000	3.100795000	2.394731000
H	-0.302426000	2.997058000	1.626033000
H	0.445480000	4.132997000	2.763533000
H	0.226422000	2.433269000	3.224489000
C	2.231619000	3.844053000	0.777414000
H	3.183248000	3.621221000	0.283796000
H	2.333656000	4.821086000	1.263150000
H	1.449303000	3.935870000	0.017091000
C	2.886221000	2.841342000	2.993456000
H	2.697595000	2.021142000	3.691364000
H	2.779399000	3.788332000	3.534972000
H	3.919540000	2.777812000	2.638079000
C	4.075398000	0.423214000	1.353087000
C	5.260485000	-0.016252000	0.769880000
C	5.424213000	0.057933000	-0.615485000
C	4.377995000	0.539431000	-1.398559000
H	4.486590000	0.568357000	-2.480587000
H	6.347499000	-0.274207000	-1.082250000
H	6.054438000	-0.415705000	1.395709000
H	3.921315000	0.338952000	2.421215000
H	1.605110000	2.344609000	-1.403765000
H	2.477389000	1.615509000	-2.750993000
H	-0.852604000	0.229957000	-2.953951000
H	0.363555000	1.186374000	-3.799580000
C	-3.515205000	0.598190000	-1.102792000
C	-4.629467000	1.570709000	-0.671143000

H	-4.527776000	1.808560000	0.391034000
H	-5.608934000	1.105402000	-0.831070000
H	-4.607371000	2.501157000	-1.247240000
C	-3.563142000	0.398012000	-2.626048000
H	-3.330457000	1.319450000	-3.169367000
H	-4.574501000	0.090214000	-2.914672000
H	-2.876019000	-0.389620000	-2.951351000
C	-3.735843000	-0.757871000	-0.413514000
H	-2.947485000	-1.472295000	-0.673967000
H	-4.693926000	-1.182910000	-0.734377000
H	-3.753088000	-0.645139000	0.672694000
O	-1.622276000	-0.720122000	2.952059000
C	-2.482382000	0.183876000	3.662279000
C	-1.656613000	-1.979283000	3.649414000
C	-3.689409000	-0.677459000	4.049568000
H	-1.956491000	0.564843000	4.550991000
H	-2.710377000	1.007055000	2.983849000
C	-3.077369000	-2.088990000	4.253137000
H	-1.410992000	-2.747274000	2.915275000
H	-0.889677000	-1.970838000	4.436411000
H	-4.414743000	-0.687695000	3.229851000
H	-4.197534000	-0.301292000	4.942810000
H	-3.671296000	-2.854146000	3.745164000
H	-3.028180000	-2.360774000	5.312239000

Lowest Energy Frequencies (in cm^{-1}): 12.1853, 31.3400, 35.5911, 36.6722, 39.5982, 46.4417.

Sum of electronic and thermal Free Energies (in hartrees): –2435.975888.

Table 5.4.7. Optimized coordinates of **5.1-I**.

Ce	0.009626000	0.002666000	0.811141000
N	-0.905758000	2.285590000	-0.036612000
O	-0.129668000	2.152508000	1.141872000
C	-0.108355000	2.991247000	-1.027622000
C	-0.039247000	2.507315000	-2.346251000
C	0.708973000	3.233755000	-3.286325000
H	0.750581000	2.872822000	-4.311365000
C	1.411052000	4.383265000	-2.931526000
H	1.984832000	4.924050000	-3.678805000
C	1.390178000	4.814920000	-1.603688000
H	1.955414000	5.692414000	-1.302016000
C	0.638165000	4.120303000	-0.659402000
H	0.634289000	4.432286000	0.377247000
C	-0.703815000	1.216792000	-2.766710000
N	-0.026393000	-0.011807000	-2.258853000
C	-0.761956000	-1.207860000	-2.762832000
C	-2.203193000	-1.277529000	-2.313782000
C	-2.559599000	-1.583159000	-0.988438000
N	-1.529065000	-1.926355000	-0.021243000
O	-1.777070000	-1.193423000	1.166067000
C	-1.401927000	-3.414939000	0.318908000
C	-0.263657000	-3.567818000	1.337882000
H	0.676783000	-3.156244000	0.958887000
H	-0.104476000	-4.633334000	1.537836000
H	-0.501766000	-3.076690000	2.284457000
C	-2.701126000	-3.965824000	0.934170000

H	-3.004770000	-3.360648000	1.792829000
H	-2.524853000	-4.988222000	1.285873000
H	-3.521109000	-4.001659000	0.210566000
C	-1.051529000	-4.192202000	-0.958716000
H	-1.797070000	-4.052160000	-1.748138000
H	-1.019393000	-5.261342000	-0.722965000
H	-0.065486000	-3.912098000	-1.343347000
C	-3.901963000	-1.498512000	-0.590232000
C	-4.898945000	-1.187884000	-1.511800000
C	-4.563846000	-0.949843000	-2.846385000
C	-3.225556000	-0.986104000	-3.230851000
H	-2.955330000	-0.765402000	-4.260893000
H	-5.334609000	-0.717661000	-3.575851000
H	-5.934478000	-1.134870000	-1.187173000
H	-4.147956000	-1.661216000	0.451435000
H	-0.208608000	-2.083804000	-2.431074000
H	-0.738056000	-1.208249000	-3.867257000
C	1.367423000	-0.046561000	-2.789267000
C	2.160452000	-1.259064000	-2.359215000
C	2.634595000	-1.416762000	-1.044487000
N	2.432209000	-0.357932000	-0.067537000
O	1.947257000	-0.946258000	1.128015000
C	3.660548000	0.500484000	0.251291000
C	3.242524000	1.553970000	1.286918000
H	2.410111000	2.166887000	0.928387000
H	4.089819000	2.222307000	1.476788000
H	2.953113000	1.094475000	2.235134000

C	4.125907000	1.203171000	-1.032936000
H	4.369271000	0.493046000	-1.830007000
H	5.034246000	1.774537000	-0.813305000
H	3.375215000	1.910603000	-1.399909000
C	4.806092000	-0.346221000	0.835409000
H	4.455841000	-0.922981000	1.696007000
H	5.604908000	0.320783000	1.177367000
H	5.238466000	-1.027246000	0.096139000
C	3.246569000	-2.620341000	-0.664477000
C	3.459600000	-3.635050000	-1.594418000
C	3.053725000	-3.461961000	-2.919245000
C	2.402027000	-2.286544000	-3.285018000
H	2.052161000	-2.160872000	-4.307039000
H	3.224351000	-4.242535000	-3.655266000
H	3.943252000	-4.557054000	-1.283788000
H	3.534881000	-2.754732000	0.370310000
H	1.853687000	0.870186000	-2.463383000
H	1.334888000	-0.021349000	-3.893186000
H	-1.733026000	1.178478000	-2.416653000
H	-0.735421000	1.181975000	-3.870447000
C	-2.254770000	2.922789000	0.313466000
C	-2.075084000	4.329537000	0.912875000
H	-1.388879000	4.298233000	1.763699000
H	-3.044568000	4.691311000	1.272220000
H	-1.705078000	5.050631000	0.177752000
C	-3.118824000	2.995130000	-0.954395000
H	-2.636754000	3.565256000	-1.755139000

H	-4.059257000	3.500951000	-0.710754000
H	-3.371205000	1.997094000	-1.326948000
C	-2.945972000	2.023660000	1.348767000
H	-3.079952000	1.004266000	0.974425000
H	-3.939420000	2.431137000	1.567088000
H	-2.384603000	1.979964000	2.285267000
I	0.049242000	0.009623000	3.942659000

Lowest Energy Frequencies (in cm^{-1}): 31.1242, 32.0503, 34.5696, 45.0801, 45.7484, 50.2611.

Sum of electronic and thermal Free Energies (in hartrees): –2215.253275.

Table 5.4.8. Optimized coordinates of **5.1-Br**.

Ce	-0.000662000	0.002321000	1.065954000
N	2.450232000	0.259281000	0.165898000
O	2.118593000	-0.466464000	1.337481000
C	2.924640000	-0.688031000	-0.830636000
C	2.437891000	-0.626341000	-2.148516000
C	2.946045000	-1.532727000	-3.092760000
H	2.584314000	-1.476321000	-4.116833000
C	3.875424000	-2.509228000	-2.743090000
H	4.249066000	-3.200317000	-3.493436000
C	4.298111000	-2.606157000	-1.415685000
H	4.999456000	-3.380671000	-1.117429000
C	3.821877000	-1.703837000	-0.467761000
H	4.123609000	-1.785842000	0.568651000
C	1.355809000	0.343938000	-2.563133000
N	-0.000078000	-0.006060000	-2.052706000

C	-0.982011000	0.993371000	-2.561530000
C	-0.679383000	2.416127000	-2.151971000
C	-0.866056000	2.871611000	-0.834930000
N	-1.450526000	1.990222000	0.163303000
O	-0.658444000	2.070665000	1.335652000
C	-2.913557000	2.265420000	0.521329000
C	-3.345377000	1.223516000	1.564137000
H	-3.228627000	0.202964000	1.187211000
H	-4.404994000	1.372533000	1.800471000
H	-2.773828000	1.319193000	2.490957000
C	-3.095789000	3.673997000	1.115520000
H	-2.414574000	3.823902000	1.957687000
H	-4.121904000	3.777937000	1.484918000
H	-2.930078000	4.461212000	0.373892000
C	-3.775923000	2.109541000	-0.740255000
H	-3.464547000	2.786743000	-1.542173000
H	-4.814874000	2.350558000	-0.490490000
H	-3.759175000	1.080847000	-1.114570000
C	-0.430810000	4.156081000	-0.475422000
C	0.111925000	5.016823000	-1.426189000
C	0.235134000	4.599708000	-2.753167000
C	-0.148764000	3.306384000	-3.099230000
H	-0.019164000	2.962376000	-4.122760000
H	0.646433000	5.266474000	-3.505807000
H	0.435009000	6.011167000	-1.130220000
H	-0.506683000	4.460489000	0.560644000
H	-1.961410000	0.685938000	-2.201436000

H	-1.011854000	0.945439000	-3.665167000
C	-0.376657000	-1.354997000	-2.562878000
C	-1.758180000	-1.804774000	-2.146609000
C	-2.056718000	-2.187558000	-0.826775000
N	-1.000150000	-2.247854000	0.171094000
O	-1.465292000	-1.597073000	1.340490000
C	-0.505928000	-3.650772000	0.534051000
C	0.609717000	-3.498343000	1.578920000
H	1.433435000	-2.883739000	1.203586000
H	1.013869000	-4.488718000	1.816832000
H	0.237004000	-3.051791000	2.504291000
C	0.064030000	-4.321893000	-0.724580000
H	-0.676683000	-4.396461000	-1.527345000
H	0.378194000	-5.340212000	-0.471071000
H	0.944955000	-3.790695000	-1.099269000
C	-1.634095000	-4.512611000	1.129682000
H	-2.101689000	-3.997974000	1.973682000
H	-1.210930000	-5.453883000	1.497203000
H	-2.400987000	-4.760890000	0.389844000
C	-3.385837000	-2.452788000	-0.463531000
C	-4.404540000	-2.418285000	-1.412436000
C	-4.107541000	-2.109662000	-2.741515000
C	-2.796568000	-1.796227000	-3.091705000
H	-2.565847000	-1.517434000	-4.117261000
H	-4.892100000	-2.091423000	-3.492756000
H	-5.426469000	-2.635198000	-1.113580000
H	-3.609154000	-2.666965000	0.573907000

H	0.381239000	-2.051574000	-2.211070000
H	-0.327523000	-1.353510000	-3.666864000
H	1.578770000	1.348125000	-2.208878000
H	1.328926000	0.387875000	-3.667033000
C	3.418867000	1.388153000	0.525995000
C	4.732166000	0.843344000	1.116899000
H	4.524083000	0.176636000	1.958418000
H	5.333474000	1.680743000	1.487571000
H	5.331862000	0.308922000	0.373835000
C	3.710617000	2.217591000	-0.733454000
H	4.141142000	1.612512000	-1.537866000
H	4.437776000	2.997658000	-0.483110000
H	2.809264000	2.716300000	-1.104326000
C	2.731912000	2.276992000	1.573210000
H	1.779388000	2.669706000	1.204837000
H	3.380632000	3.130655000	1.799415000
H	2.546914000	1.734450000	2.503682000
Br	0.000711000	0.009181000	3.843139000

Lowest Energy Frequencies (in cm^{-1}): 27.6027, 32.6249, 35.4415, 42.5388, 48.4044, 49.7060.

Sum of electronic and thermal Free Energies (in hartrees): –4775.244104.

Table 5.4.9. Optimized coordinates of **5.1-Cl**.

Ce	-0.001270000	0.002311000	-1.270446000
N	1.668978000	1.810818000	-0.359987000
O	0.889593000	1.983274000	-1.530076000
C	1.193078000	2.753147000	0.640439000

C	0.959685000	2.323145000	1.958862000
C	0.540985000	3.270408000	2.906955000
H	0.376099000	2.944580000	3.931365000
C	0.309787000	4.599584000	2.561265000
H	-0.017760000	5.310142000	3.314946000
C	0.475792000	4.998850000	1.233437000
H	0.270886000	6.024209000	0.937856000
C	0.910608000	4.079833000	0.281637000
H	1.019699000	4.372617000	-0.754820000
C	1.093301000	0.875132000	2.370700000
N	0.000211000	-0.001336000	1.863293000
C	0.212444000	-1.386363000	2.370428000
C	1.534001000	-1.993132000	1.958151000
C	1.790288000	-2.408048000	0.639161000
N	0.736043000	-2.348705000	-0.361401000
O	1.274141000	-1.755621000	-1.530221000
C	0.088049000	-3.687570000	-0.723835000
C	-0.998311000	-3.412053000	-1.774256000
H	-1.746358000	-2.704222000	-1.404805000
H	-1.514027000	-4.349650000	-2.010410000
H	-0.571716000	-3.016945000	-2.699713000
C	1.112849000	-4.674383000	-1.312948000
H	1.644848000	-4.216755000	-2.151626000
H	0.585094000	-5.558578000	-1.686905000
H	1.839185000	-5.013784000	-0.568295000
C	-0.559420000	-4.286203000	0.534002000
H	0.164515000	-4.436485000	1.341428000

H	-0.980705000	-5.265759000	0.283055000
H	-1.379533000	-3.660850000	0.901459000
C	3.081216000	-2.824505000	0.280047000
C	4.094273000	-2.908512000	1.232016000
C	3.830841000	-2.567544000	2.560276000
C	2.563597000	-2.104833000	2.906326000
H	2.363400000	-1.800525000	3.931056000
H	4.609853000	-2.639733000	3.314025000
H	5.085077000	-3.242381000	0.936096000
H	3.281275000	-3.062597000	-0.756832000
H	-0.619933000	-1.987768000	2.011029000
H	0.157444000	-1.383591000	3.474240000
C	-1.305112000	0.507667000	2.371139000
C	-2.492529000	-0.332088000	1.959829000
C	-2.981741000	-0.346403000	0.641481000
N	-2.404902000	0.537186000	-0.359266000
O	-2.161771000	-0.224474000	-1.528342000
C	-3.240622000	1.768054000	-0.719903000
C	-2.460292000	2.571145000	-1.771453000
H	-1.470018000	2.860155000	-1.406369000
H	-3.011785000	3.489817000	-2.001008000
H	-2.338261000	2.007299000	-2.699695000
C	-3.432533000	2.627856000	0.538315000
H	-3.923295000	2.076157000	1.346665000
H	-4.070135000	3.482956000	0.288813000
H	-2.479638000	3.024465000	0.903543000
C	-4.608826000	1.374221000	-1.306652000

H	-4.479759000	0.682254000	-2.143537000
H	-5.110211000	2.272839000	-1.682731000
H	-5.265850000	0.917608000	-0.560229000
C	-3.988500000	-1.255604000	0.283365000
C	-4.566474000	-2.091250000	1.235812000
C	-4.137937000	-2.033864000	2.563590000
C	-3.103257000	-1.167733000	2.908634000
H	-2.739009000	-1.146156000	3.933157000
H	-4.589488000	-2.672107000	3.317892000
H	-5.351514000	-2.782150000	0.940742000
H	-4.296420000	-1.308892000	-0.753068000
H	-1.408608000	1.530074000	2.013835000
H	-1.273853000	0.552186000	3.475003000
H	2.030888000	0.454781000	2.013351000
H	1.116378000	0.826772000	3.474608000
C	3.153458000	1.916263000	-0.720415000
C	3.497583000	3.294258000	-1.315096000
H	2.838750000	3.521278000	-2.157910000
H	4.528659000	3.277868000	-1.685067000
H	3.424830000	4.097214000	-0.575312000
C	3.993709000	1.660093000	0.539506000
H	3.759988000	2.364721000	1.344212000
H	5.052847000	1.785591000	0.289510000
H	3.862773000	0.638075000	0.909590000
C	3.459798000	0.833151000	-1.765854000
H	3.212450000	-0.166479000	-1.396234000
H	4.531554000	0.848909000	-1.993698000

H	2.912002000	1.005221000	-2.695726000
Cl	-0.005512000	0.003888000	-3.900987000

Lowest Energy Frequencies (in cm^{-1}): 26.8658, 36.4937, 38.6622, 46.1988, 49.4374, 50.8320.

Sum of electronic and thermal Free Energies (in hartrees): –2664.029507.

Table 5.4.10. Optimized coordinates of **5.1-F**.

Ce	0.001500000	0.001073000	-1.390360000
N	1.873408000	-1.617452000	-0.463696000
O	2.033136000	-0.829573000	-1.630657000
C	2.793858000	-1.120840000	0.546274000
C	2.348386000	-0.901042000	1.862467000
C	3.277728000	-0.459159000	2.818173000
H	2.940013000	-0.305245000	3.840480000
C	4.602652000	-0.191609000	2.483319000
H	5.298671000	0.152981000	3.243051000
C	5.015607000	-0.343335000	1.157935000
H	6.037208000	-0.109750000	0.870315000
C	4.115235000	-0.799858000	0.198903000
H	4.417322000	-0.896282000	-0.836140000
C	0.901965000	-1.073666000	2.268383000
N	-0.001956000	-0.003081000	1.763704000
C	-1.381189000	-0.250504000	2.268319000
C	-1.955728000	-1.587982000	1.860063000
C	-2.370021000	-1.858966000	0.543581000
N	-2.338066000	-0.810056000	-0.462519000
O	-1.734898000	-1.341347000	-1.629742000

C	-3.689048000	-0.193882000	-0.823620000
C	-3.440311000	0.881267000	-1.892885000
H	-2.723974000	1.634263000	-1.550222000
H	-4.383648000	1.392876000	-2.114868000
H	-3.066022000	0.440797000	-2.820275000
C	-4.664756000	-1.242351000	-1.389890000
H	-4.203946000	-1.778882000	-2.224100000
H	-5.561489000	-0.735978000	-1.764047000
H	-4.984190000	-1.964265000	-0.632153000
C	-4.289883000	0.464100000	0.427571000
H	-4.421676000	-0.249798000	1.247140000
H	-5.278203000	0.865807000	0.178501000
H	-3.673915000	1.299024000	0.776971000
C	-2.755115000	-3.162078000	0.192248000
C	-2.809845000	-4.173300000	1.147888000
C	-2.469762000	-3.896437000	2.473805000
C	-2.037441000	-2.616776000	2.812456000
H	-1.733864000	-2.404887000	3.835096000
H	-2.519111000	-4.674026000	3.230949000
H	-3.119870000	-5.173450000	0.857122000
H	-2.990818000	-3.371706000	-0.843292000
H	-2.002890000	0.565131000	1.905169000
H	-1.382913000	-0.193063000	3.372399000
C	0.474487000	1.314244000	2.269511000
C	-0.396386000	2.481787000	1.863930000
C	-0.424622000	2.979240000	0.548345000
N	0.467696000	2.430690000	-0.459921000

O	-0.293785000	2.176215000	-1.627490000
C	1.675064000	3.295477000	-0.820275000
C	2.478890000	2.547843000	-1.895351000
H	2.771594000	1.548268000	-1.559168000
H	3.394528000	3.108834000	-2.114283000
H	1.909206000	2.450490000	-2.822720000
C	2.549474000	3.482209000	0.428874000
H	1.998642000	3.947053000	1.253008000
H	3.388877000	4.141136000	0.181007000
H	2.968305000	2.530488000	0.771490000
C	1.251823000	4.666434000	-1.379431000
H	0.550796000	4.538465000	-2.209115000
H	2.136359000	5.190442000	-1.758423000
H	0.792218000	5.301780000	-0.616380000
C	-1.363950000	3.961425000	0.198475000
C	-2.214035000	4.510340000	1.154964000
C	-2.142627000	4.075897000	2.480262000
C	-1.247574000	3.063767000	2.817387000
H	-1.215589000	2.692988000	3.839325000
H	-2.792823000	4.504228000	3.237976000
H	-2.927787000	5.276927000	0.865393000
H	-1.428487000	4.271507000	-0.836665000
H	1.491420000	1.443967000	1.905797000
H	0.526210000	1.285080000	3.373428000
H	0.507138000	-2.020345000	1.906004000
H	0.851604000	-1.103311000	3.372395000
C	2.017657000	-3.095513000	-0.824497000

C	3.415223000	-3.413601000	-1.387382000
H	3.650801000	-2.744345000	-2.219679000
H	3.427529000	-4.442623000	-1.763644000
H	4.197752000	-3.329684000	-0.627190000
C	1.746633000	-3.945810000	0.425683000
H	2.424862000	-3.698403000	1.248756000
H	1.900243000	-5.001884000	0.178104000
H	0.713078000	-3.835779000	0.769432000
C	0.965299000	-3.419205000	-1.896174000
H	-0.046383000	-3.178254000	-1.555182000
H	0.996808000	-4.491845000	-2.118513000
H	1.159986000	-2.873853000	-2.822904000
F	0.001124000	0.002345000	-3.442802000

Lowest Energy Frequencies (in cm^{-1}): 24.5197, 35.5802, 38.6871, 45.9924, 48.7225, 50.6132.

Sum of electronic and thermal Free Energies (in hartrees): –2303.672372.

5.5 References

[1] N. A. Piro, J. R. Robinson, P. J. Walsh, E. J. Schelter, *Coord. Chem. Rev.* **2014**, *260*, 21-36.

[2] a) S. R. Sofen, S. R. Cooper, K. N. Raymond, *Inorg. Chem.* **1979**, *18*, 1611-1616; b) V. Nair, A. Deepthi, *Chem. Rev.* **2007**, *107*, 1862-1891.

[3] a) E. Mamontov, T. Egami, *J. Phys. Chem. Solids* **2000**, *61*, 1345-1356; b) D. Hong, M. Murakami, Y. Yamada, S. Fukuzumi, *Energy Environ. Sci.* **2012**, *5*, 5708-5716; c) D. J. Wasylenko, C. Ganesamoorthy, M. A. Henderson, C. P. Berlinguette, *Inorg. Chem.* **2011**, *50*, 3662-3672.

[4] C. K. Gupta, N. Krishnamurthy, *Int. Mater. Rev.* **1992**, *37*, 197-248.

[5] a) B. D. Mahoney, N. A. Piro, P. J. Carroll, E. J. Schelter, *Inorg. Chem.* **2013**, *52*, 5970-5977; b) J. R. Robinson, P. J. Carroll, P. J. Walsh, E. J. Schelter, *Angew. Chem. Int. Ed.* **2012**, *51*, 10159-10163; c) J. R. Robinson, C. H. Booth, P. J. Carroll, P. J. Walsh, E. J. Schelter, *Chem. Eur. J.* **2013**, *19*, 5996-6004; d) H. B. Lee, J. A. Bogart, P. J. Carroll, E. J. Schelter, *Chem. Commun.* **2014**, *50*, 5361-5363; e) U. J. Williams, P. J. Carroll, E. J. Schelter, *Inorg. Chem.* **2014**, *53*, 6338-6345; f) U. J. Williams, D. Schneider, W. L. Dorfner, C. Maichle-Mossmer, P. J. Carroll, R. Anwander, E. J. Schelter, *Dalton Trans.* **2014**, *43*, 16197-16206; g) D. Werner, G. B. Deacon, P. C. Junk, R. Anwander, *Chem. Eur. J.* **2014**, *20*, 4426-4438; h) D. Schneider, T. Spallek, C. Maichle-Mossmer, K. W. Tornroos, R. Anwander, *Chem. Commun.* **2014**, *50*, 14763-14766; i) A. R. Crozier, C. Schadle, C. Maichle-Mossmer, K. W. Tornroos, R. Anwander, *Dalton Trans.* **2013**, *42*, 5491-5499; j) A. R. Crozier, A. M. Bienfait, C. Maichle-Mossmer, K. W. Tornroos, R. Anwander, *Chem. Commun.* **2013**, *49*, 87-89; k) P. Dröse, A. R. Crozier, S. Lashkari, J. Gottfriedsen, S. Blaurock, C. G. Hrib, C. Maichle-Mössmer, C. Schädle, R. Anwander, F. T. Edelmann, *J. Am. Chem. Soc.* **2010**, *132*, 14046-14047.

[6] a) C. Morton, N. W. Alcock, M. R. Lees, I. J. Munslow, C. J. Sanders, P. Scott, *J. Am. Chem. Soc.* **1999**, *121*, 11255-11256; b) P. Dröse, J. Gottfriedsen, *Z. Anorg. Allg. Chem.* **2008**, *634*, 87-90.

[7] a) L. H. Gade, *Acc. Chem. Res.* **2002**, *35*, 575-582; b) K. M. Wampler, R. R. Schrock, *Inorg. Chem.* **2007**, *46*, 8463-8465; c) W. H. Harman, C. J. Chang, *J. Am. Chem. Soc.* **2007**, *129*, 15128-15129; d) N. A. Piro, M. F. Lichterman, W. H. Harman, C. J. Chang, *J. Am. Chem. Soc.* **2011**, *133*, 2108-2111; e) G. T. Sazama, T. A. Betley, *Organometallics* **2011**, *30*, 4315-4319; f) G. E. Greco, R. R. Schrock, *Inorg. Chem.* **2001**, *40*, 3850-3860; g) E. M. Matson, Y. J. Park, A. R. Fout, *J. Am. Chem. Soc.* **2014**, *136*, 17398-17401; h) T. Taguchi, R. Gupta, B. Lassalle-Kaiser, D. W. Boyce, V. K. Yachandra, W. B. Tolman, J. Yano, M. P. Hendrich, A. S. Borovik, *J. Am. Chem. Soc.* **2012**, *134*, 1996-1999; i) B. M. Gardner, G. Balázs, M. Scheer, F. Tuna, E. J. L. McInnes, J. McMaster, W. Lewis, A. J. Blake, S. T. Liddle, *Angew. Chem. Int. Ed.* **2014**, *53*, 4484-4488; j) P. B. Duval, C. J. Burns, W. E. Buschmann, D. L. Clark, D. E. Morris, B. L. Scott, *Inorg. Chem.* **2001**, *40*, 5491-5496; k) A. J. Lewis, U. J. Williams, J. M. Kikkawa, P. J. Carroll, E. J. Schelter, *Inorg. Chem.* **2011**, *51*, 37-39.

[8] U. J. Williams, J. R. Robinson, A. J. Lewis, P. J. Carroll, P. J. Walsh, E. J. Schelter, *Inorg. Chem.* **2014**, *53*, 27-29.

[9] H. Zheng, S. J. Yoo, E. Münck, L. Que, *J. Am. Chem. Soc.* **2000**, *122*, 3789-3790.

[10] U. J. Williams, J. R. Robinson, A. J. Lewis, P. J. Carroll, P. J. Walsh, E. J. Schelter, *Inorg. Chem.* **2013**, *53*, 27-29.

[11] P. Dröse, J. Gottfriedsen, Cristian G. Hrib, Peter G. Jones, L. Hilfert, Frank T. Edelmann, *Z. Anorg. Allg. Chem.* **2011**, *637*, 369-373.

[12] W. J. Evans, J. M. Perotti, R. J. Doedens, J. W. Ziller, *Chem. Commun.* **2001**, 2326-2327.

[13] R. Shannon, *Acta Crystallogr. Sect. A* **1976**, *32*, 751-767.

[14] The complexes would precipitate too quickly as microcrystalline needles.

[15] O. Eisenstein, P. B. Hitchcock, A. G. Hulkes, M. F. Lappert, L. Maron, *Chem. Commun.* **2001**, 1560-1561.

[16] a) C. H. Booth, M. D. Walter, M. Daniel, W. W. Lukens, R. A. Andersen, *Phys. Rev. Lett.* **2005**, *95*, 267202; b) W. W. Lukens, N. Magnani, C. H. Booth, *Inorg. Chem.* **2012**, *51*, 10105-10110.

[17] M. A. Boreen, J. A. Bogart, P. J. Carroll, E. J. Schelter, *Inorg. Chem.,* **2015**, *Accepted.*

[18] N. G. Connelly, W. E. Geiger, *Chem. Rev.* **1996**, *96*, 877-910.

[19] M. W. Löble, J. M. Keith, A. B. Altman, S. C. E. Stieber, E. R. Batista, K. S. Boland, S. D. Conradson, D. L. Clark, J. Lezama Pacheco, S. A. Kozimor, R. L. Martin, S. G. Minasian, A. C. Olson, B. L. Scott, D. K. Shuh, T. Tyliszczak, M. P. Wilkerson, R. A. Zehnder, *J. Am. Chem. Soc.* **2015**, *137*, 2506-2523.

[20] S. Daniele, L. G. Hubert-Pfalzgraf, M. Perrin, *Polyhedron* **2002**, *21*, 1985-1990.

[21] I. Chávez, A. Alvarez-Carena, E. Molins, A. Roig, W. Maniukiewicz, A. Arancibia, V. Arancibia, H. Brand, J. Manuel Manríquez, *J. Organomet. Chem.* **2000**, *601*, 126-132.

[22] R. R. Schrock, L. G. Sturgeoff, P. R. Sharp, *Inorg. Chem.* **1983**, *22*, 2801-2806.

[23] D. C. Bradley, J. S. Ghotra, F. A. Hart, *J. Chem. Soc., Dalton Trans.* **1973**, 1021-1023.

[24] R. K. Thomson, B. L. Scott, D. E. Morris, J. L. Kiplinger, *C. R. Chimie* **2010**, *13*, 790-802.

[25] C. H. Booth, M. D. Walter, D. Kazhdan, Y.-J. Hu, W. W. Lukens, E. D. Bauer, L. Maron, O. Eisenstein, R. A. Andersen, *J. Am. Chem. Soc.* **2009**, *131*, 6480-6491.

[26] Bruker (2009) SAINT. Bruker AXS Inc., Madison, Wisconsin, USA.

[27] Bruker (2009) SHELXTL. Bruker AXS Inc., Madison, Wisconsin, USA.

[28] Sheldrick, G.M. (2008) TWINABS. University of Göttingen: Göttingen, Germany.

[29] Sheldrick, G.M. (2007) SADABS. University of Göttingen: Göttingen, Germany.

[30] G. Sheldrick, *Acta Crystallogr. Sect. A* **2008**, *64*, 112-122.

[31] Gaussian 09, Revision D.01, Frisch, M. J.; Trucks, G. W.; Schlegel, H. B.; Scuseria, G. E.; Robb, M. A.; Cheeseman, J. R.; Scalmani, G.; Barone, V.; Mennucci, B.; Petersson, G. A.; Nakatsuji, H.; Caricato, M.; Li, X.; Hratchian, H. P.; Izmaylov, A. F.; Bloino, J.; Zheng, G.;

Sonnenberg, J. L.; Hada, M.; Ehara, M.; Toyota, K.; Fukuda, R.; Hasegawa, J.; Ishida, M.; Nakajima, T.; Honda, Y.; Kitao, O.; Nakai, H.; Vreven, T.; Montgomery, Jr., J. A.; Peralta, J. E.; Ogliaro, F.; Bearpark, M.; Heyd, J. J.; Brothers, E.; Kudin, K. N.; Staroverov, V. N.; Kobayashi, R.; Normand, J.; Raghavachari, K.; Rendell, A.; Burant, J. C.; Iyengar, S. S.; Tomasi, J.; Cossi, M.; Rega, N.; Millam, N. J.; Klene, M.; Knox, J. E.; Cross, J. B.; Bakken, V.; Adamo, C.; Jaramillo, J.; Gomperts, R.; Stratmann, R. E.; Yazyev, O.; Austin, A. J.; Cammi, R.; Pomelli, C.; Ochterski, J. W.; Martin, R. L.; Morokuma, K.; Zakrzewski, V. G.; Voth, G. A.; Salvador, P.; Dannenberg, J. J.; Dapprich, S.; Daniels, A. D.; Farkas, Ö.; Foresman, J. B.; Ortiz, J. V.; Cioslowski, J.; Fox, D. J. Gaussian, Inc., Wallingford CT, 2009.

[32] a) X. Cao, M. Dolg, *J. Molec. Struct. (Theochem)* **2002**, *581*, 139-147; b) M. Dolg, H. Stoll, H. Preuss, *J. Chem. Phys.* **1989**, *90*, 1730-1734.

[33] W. J. Hehre, R. Ditchfield, J. A. Pople, *J. Chem. Phys.* **1972**, *56*, 2257-2261.

[34] E. D. Glendening, J. K. Badenhoop, A. E. Reed, J. E. Carpenter, J. A. Bohmann, C. M. Morales, C. R. Landis, F. Weinhold, in *NBO 6.0*, Madison, WI., **2013**.

[35] a) S. I. Gorelsky, A. B. P. Lever, *J. Organomet. Chem.* **2001**, *635*, 187-196; b) S. I. Gorelsky, *AOMix: Program for Molecular Orbital Analysis,* http://www.sg-chem.net/, University of Ottawa, version 6.5, **2011**.

[36] Chemcraft. www.chemcraftprog.com.

Chapter 6

A DFT Study of the Active Site of the XoxF-type Natural, Cerium Dependent Methanol Dehydrogenase Enzyme

Abstract

Rare earth metal cations have recently been demonstrated to be essential cofactors for the growth of the methanotrophic bacterium *Methylacidiphilum fumariolicum* SolV. A reported crystal structure of the rare earth dependent methanol dehydrogenase (MDH) included a cerium cation in the active site. In this current work, the Ce-MDH active site was analyzed through DFT calculations. The results showed the stability of the Ce^{III}-$PQQ^{\bullet-}$ semiquinone configuration, where PQQ = pyrroloquinoline quinone. Calculations on the active oxidized form of this complex indicated a 0.81 eV stabilization of the PQQ^{0} LUMO at cerium versus calcium, supporting the observation that the cerium cation in the active site confers a competitive advantage to *Methylacidiphilum fumariolicum* SolV. Using reported aqueous electrochemical data, a semi-empirical correlation was established based on cerium(IV/III) redox potentials. The correlation allowed for the estimation of +1.35 V versus SCE for the oxidation potential of cerium in the active site. The results are expected to guide the design of functional model complexes and catalysts for the oxidation of alcohols.

6.1 Introduction

Recent work demonstrated the rare earth metals La–Nd were essential elements for the culture of the extremophilic methanotroph *Methylacidiphilum fumariolicum* SolV.[1] The bacterium showed essentially zero growth in the absence of rare earth metal salts, despite the presence of metals, including calcium, that typically have physiological roles. Analysis of mudpot water from its habitat revealed high concentrations of rare earth elements, particularly cerium. The X-ray structure of the XoxF-type methanol dehydrogenase (MDH) enzyme of *M. fumariolicum* SolV, PDB code 4MAE, revealed a heavy atom in the active site bound directly to the pyrroloquinoline quinone (PQQ) ligand cofactor (Figure 6.1.1). Due to the high concentration of cerium (~1.0 μM) in the mudpot water, the anomalous electron density was assigned as a cerium cation. Subsequent growth studies provided evidence that *M. fumariolicum* SolV actively stored cerium.[1]

The discovery of rare earth metals as critical cofactors marked the first known instance of the elements in a physiological role. The cations were presumably useful for methanol dehydrogenase reactivity due to their potent Lewis acidity for substrate activation.[2] Moreover, the cerium cation evidently conferred a competitive advantage to *Methylacidiphilum fumariolicum* SolV.[3] Compared to Ca-MDH enzymes, the XoxF-MDH showed: 1) a higher affinity and faster oxidation rate for methanol, 2) activity for a broader range of substrates including formaldehyde, 3) conversion of methanol directly to formate through a formally 4-electron process, 4) optimal activity at pH = 7 and 5) no requirement for ammonium cation for activation. In terms of understanding the competitive advantages of Ce-MDH and for the development of functional model complexes, there was a clear motivation for interrogating the electronic structure of this unusual active site.

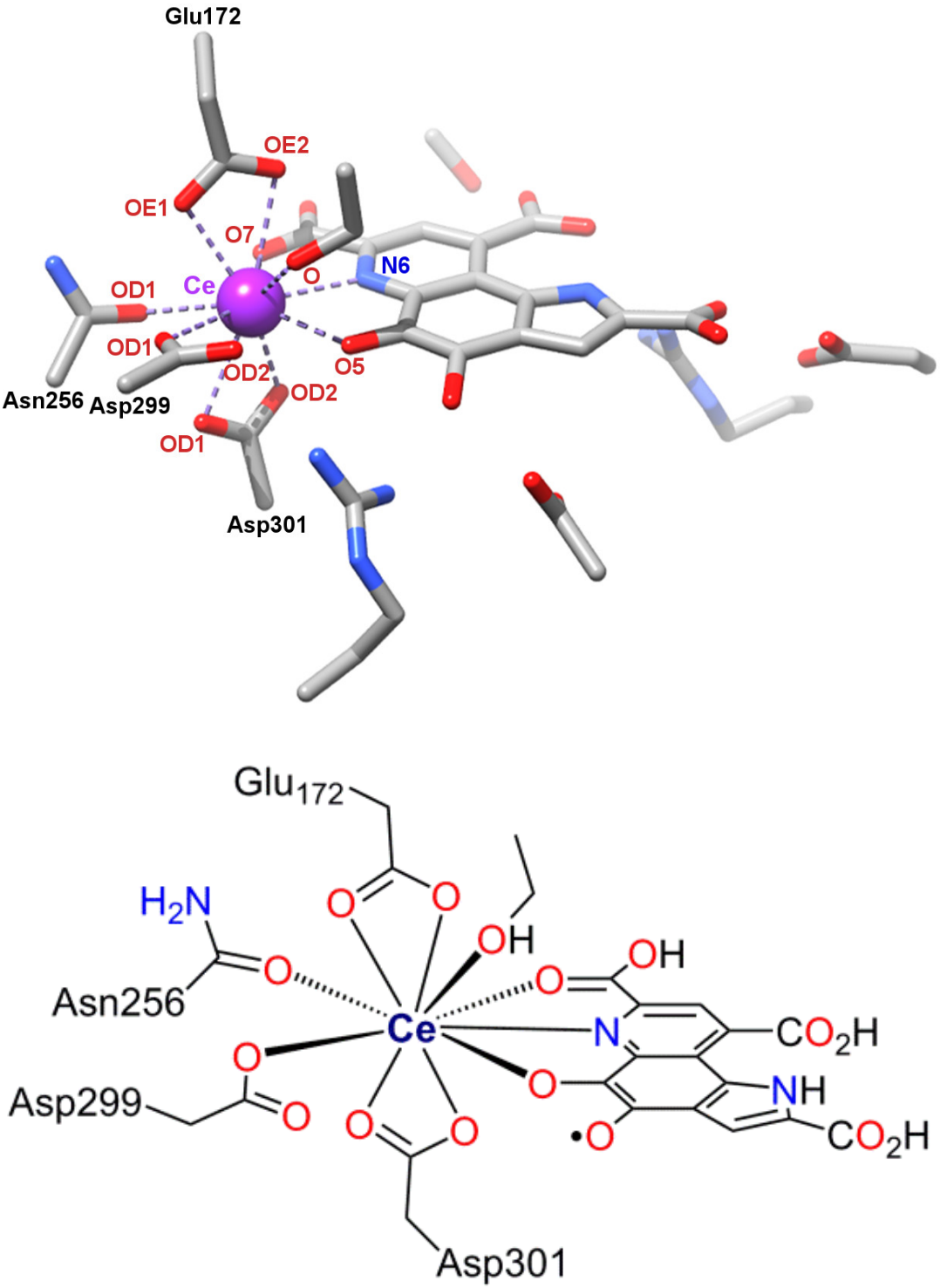

Figure 6.1.1. Partial X-ray structure at 1.6 Å resolution (top) and simplified structural depiction (bottom) of the active site of the methanol dehydrogenase (MDH) enzyme of *Methylacidiphilum fumariolicum* SolV, PDB code 4MAE.[1] Figure reprinted with permission of John Wiley & Sons © 2015.

Density functional theory (DFT) has proven to be a powerful tool for studying the electronic structure of lanthanide and actinide containing systems,[4] and has also been used to study the calcium-bound active site of the MDH enzyme.[5] To the best of our knowledge, however, prior to this work, DFT had not yet been applied to the electronic structure of the rare earth containing MDH metalloenzyme. Herein, we describe the electronic structure of the active site of MDH using DFT, based on the reported Ce-containing crystal structure. Our interrogation of this system yielded several important findings. We demonstrated that the cerium(III) cation conferred a 0.81 eV stabilization of the redox-active PQQ LUMO when directly compared with calcium(II) in the MDH active site of *M. fumariolicum* SolV. We provided evidence supporting the 3+ oxidation state of the cerium cation. And, critically, we predicted the cerium(IV/III) redox potential of cerium within the active site using an experimentally-validated correlation of related cerium compounds.

6.2 Results/Discussion

6.2.1 Aqueous Correlation of $Ce^{IV/III}$ Redox Potentials

As mentioned in Chapter 3, typical probes of metalloenzyme active sites and biomimetic model complexes involve optical transitions, or vibrational modes of carbonyl or cyanide moieties such as those found in iron hydrogenases.[6] However, due to the ionic nature of the bonding between 4f-block metals and ligands,[7] no such environmentally sensitive probes exist for rare earth metal complexes. An extensive examination of a library of cerium complexes, however, revealed the potential of the cerium(IV/III) redox couple was extraordinarily sensitive to its crystal field.[8] Extrapolating from those findings, we showed that combined structural, electrochemical and computational studies could be used to study cerium complexes in new and unusual ligand environments. Moreover, we were able to organize the complexes into a crystal field series for the cerium cation in general. We believed that we could gain insight into the electronics of cerium within the MDH active site by using a similar approach. This necessitated, however, the development of a similar correlation under aqueous conditions.

Towards this goal, we looked in the literature for reported Ce complexes with well-defined aqueous electrochemistry. A series of complexes was chosen based on the large range in

reported aqueous redox potentials, including the homoleptic catecholate, $Na_4[Ce(o\text{-}O_2C_6H_4)_4]$ (**Ce(o-BQ)**),[9] the hydroxypyridinonate, $Ce(HOPO)_2$ (HOPO = hydroxypyridinone) (**Ce(HOPO)**),[10] the EDTA complex, $Ce(OH_2)_3(EDTA)$ (**Ce(EDTA)**),[11] and ceric ammonium nitrate, $[NH_4]_2[Ce(NO_3)_6]$ (**CAN**) (Figure 6.2.1.1).[12]

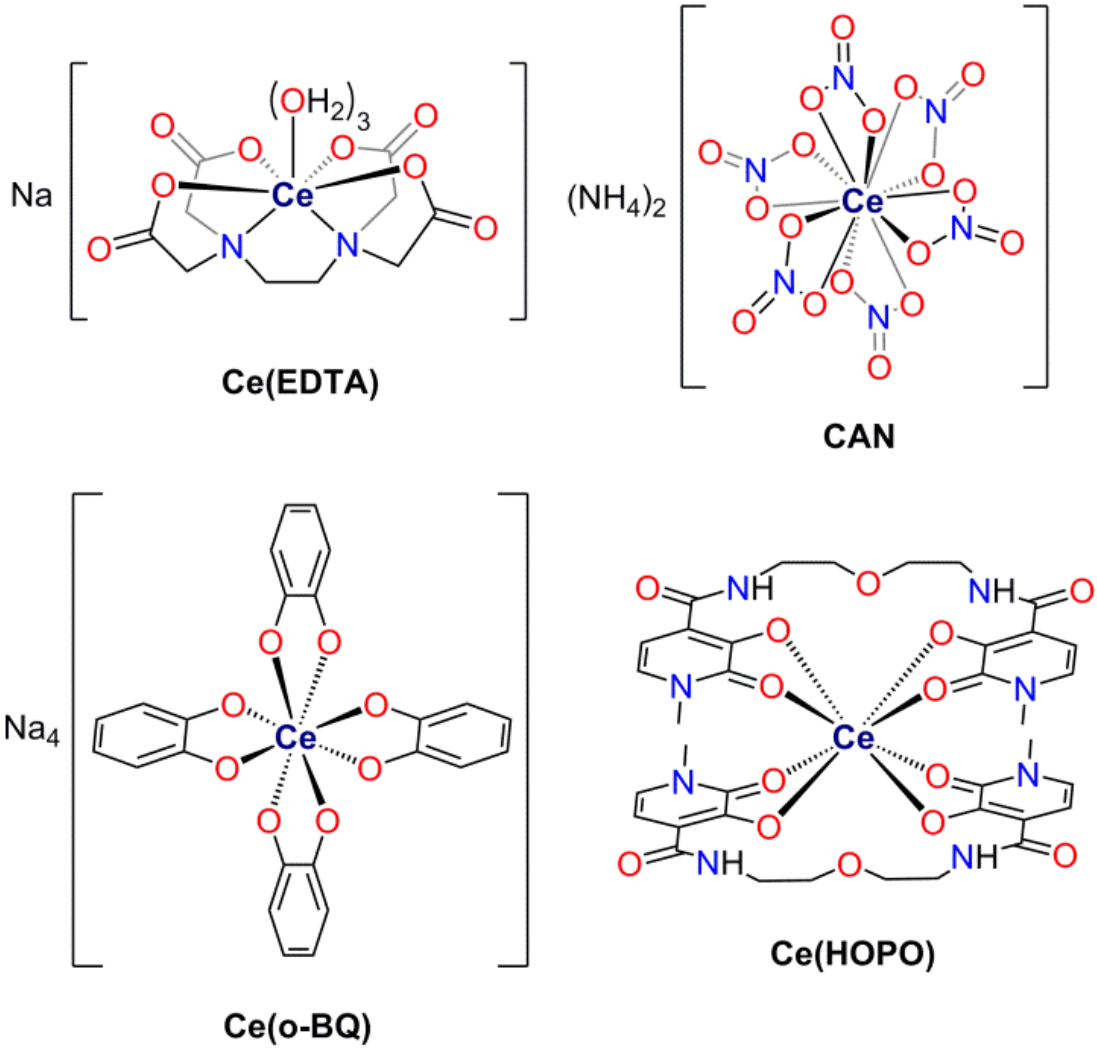

Figure 6.2.1.1. Model complexes used to establish the correlation. Figure reprinted with permission of John Wiley & Sons © 2015.

Each complex was optimized at an identical level of theory using a CPCM model for the dielectric. The two ammonium ions and four sodium ions were included in the calculations of **CAN** and **Ce(o-BQ)**, respectively, in order to accurately model ion pairing effects. Using the approach established for the non-aqueous correlation as described in Chapter 3, the $Ce^{IV/III}$ redox potentials

of these complexes were then computed versus ferrocene and plotted against their experimental values. Excellent agreement of the calculated and experimental redox potentials was obtained over the 2 V range (Figure 6.2.1.2). These results established the validity of using DFT to predict the redox potentials of aqueous cerium complexes. As such, we next turned to applying this method to the cerium cation within the MDH protein framework.

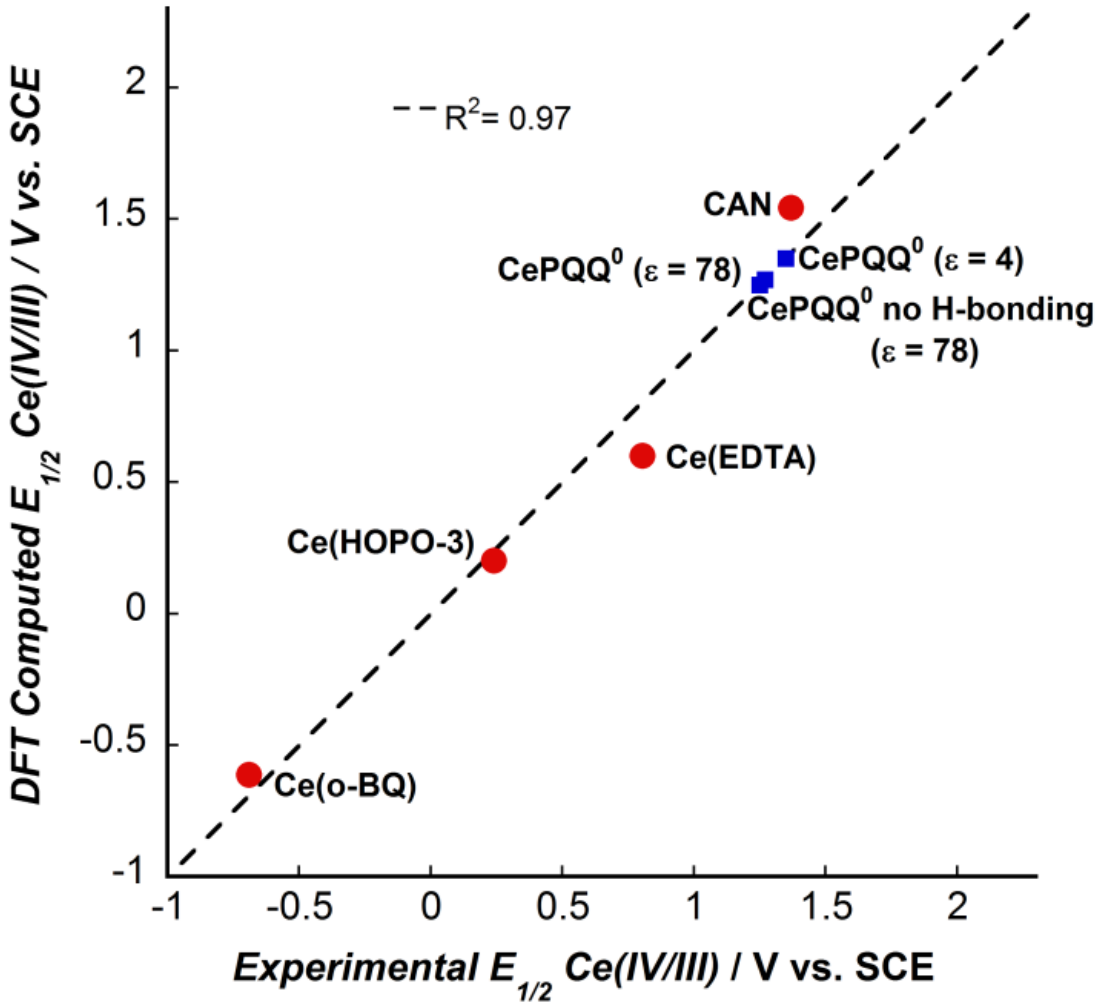

Figure 6.2.1.2. Correlation between DFT calculated and experimental aqueous reduction potentials for a series of reported cerium complexes. Figure reprinted with permission of John Wiley & Sons © 2015.

6.2.2 Electronic Structure Studies

To initiate our study of the Ce-MDH enzyme we began with a computational examination of the active site, whose key components included a 9-coordinate cerium cation complexed by a pyrroloquinoline quinone (PQQ) cofactor (Figure 6.1.1). To guide the effort, we used a modified approach of a reported mechanistic study of Ca^{II}-MDH from *Methylophilus methylotrophus* W3A1.[5]

Table 6.2.2.1. Bond distances in the primary metal coordination sphere of the MDH active site. Table reprinted with permission of John Wiley & Sons © 2015.

	Ce-X Bond Lengths (Å)			
	Exp[a]	**Ce^{III}-$PQQ^{\cdot-}$**	**Ce^{III}-PQQ^{0}**	**Ce^{IV}-PQQ^{0}**
Glu172 OE1	2.7	2.603	2.524	2.519
Glu172 OE2	2.9	2.889	2.671	2.521
Asn256 OD1	2.7	2.559	2.501	2.339
Asp301 OD1	2.8	2.666	3.843	3.756
Asp301 OD2	2.5	2.617	2.360	2.242
Asp299 OD1	2.9	2.429	2.348	2.201
PQQ O5	2.6	2.550	2.864	2.734
PQQ N6	2.8	2.798	2.952	2.875
PQQ O7	2.7	2.724	2.688	2.583
Substrate O	2.8	2.697	2.628	2.560
MAD[b]	–	0.115	0.294	0.340

[a]From reference [1]. [b]Mean absolute deviation.

Starting from the 1.6 Å resolution X-ray structure of the Ce-MDH, we probed three possible electronic structures, namely the Ce^{III}-$PQQ^{\cdot-}$, Ce^{III}-PQQ^{0}, and Ce^{IV}-PQQ^{0} forms. The Ce^{III}-PQQ^{0} electronic configuration calculation also probed the valence tautomer Ce^{IV}-$PQQ^{\cdot-}$ but the Ce^{III}-PQQ^{0} form was found to be lower in energy (*vide infra*). The Ce-X bond distances obtained from these calculations are tabulated in Table 6.2.2.1 and compared to the experimentally determined bond distances. The results of the active site optimization for a Ce^{III}-$PQQ^{\cdot-}$ electronic configuration showed the best agreement.

The electronic structure of the resting state of the active site comprised a singlet diradical with two singly occupied molecular orbitals (SOMOs) as indicated by the spin density plot shown in Figure 6.2.2.1.[13] The higher energy SOMO was a PQQ-based orbital and the lower energy SOMO was a Ce 4f based orbital, calculated to be 0.35 eV lower in energy. The PQQ based orbital had electron density delocalized over the extended aromatic system. This result suggested that single electron oxidation of the resting state of the active site would preferentially remove an electron from the PQQ cofactor to access the catalytically active Ce^{III}-PQQ^{0} configuration.

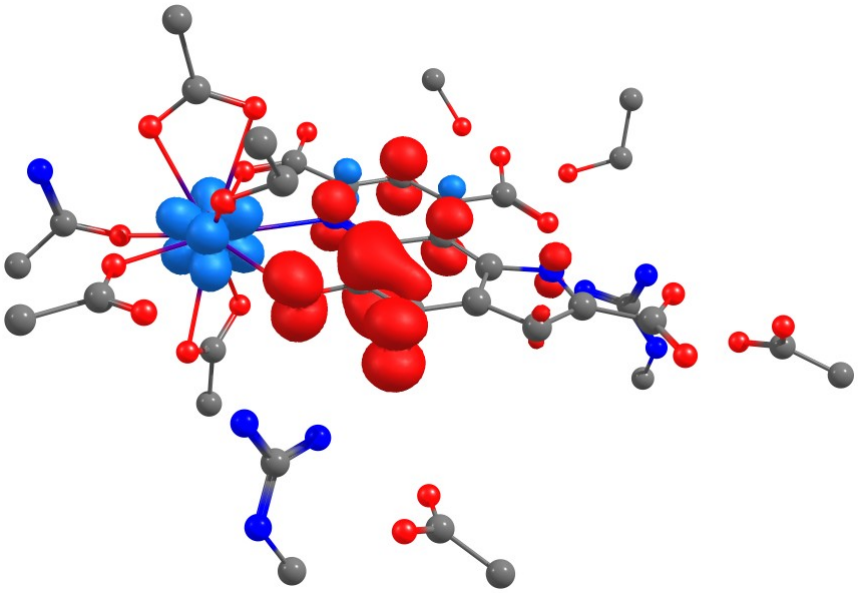

Figure 6.2.2.1. Spin density plot of Ce^{III}-$PQQ^{\cdot-}$; blue = α, red = β. Figure reprinted with permission of John Wiley & Sons © 2015.

In the mechanism of methanol oxidation to formaldehyde by the Ca^{II}-dependent MDH enzymes, the PQQ cofactor was proposed to undergo a $2e^-$ reduction starting from its neutral quinone form.[14] The Ce^{III}-dependent MDH enzyme was expected to undergo similar $2e^-$ redox chemistry starting from an oxidized form of the complex, namely the Ce^{III}-PQQ^0 configuration. It was noteworthy that the LUMO of the $Ce^{III}PQQ^0$ electronic state was the same PQQ based molecular orbital as the higher energy SOMO in the reduced Ce^{III}-$PQQ^{\cdot-}$ form.

Having determined the probable electronic configurations for the active site in its resting and catalytically active forms, we turned to comparison of the Ce^{III}-PQQ^0 form with a Ca^{II}-PQQ^0 analog. *M. fumariolicum* SolV shows only poor growth in the presence of Ca^{II} sources.[1] We performed calculations on the Ce^{III}-PQQ^0 active site with replacement of the Ce^{III} cation with Ca^{II}. Interestingly, despite the nearly identical ionic radii of the two metal ions (1.180 for Ca^{2+}, 1.196 for Ce^{3+} with CN = 9),[15] the ethanol substrate dissociated from the Ca^{II} cation during the course of the optimization, suggesting reduced substrate affinity with calcium in the active site. We postulate that the additional Asp residue (Asp301, Figure 6.1.1) in the primary coordination sphere of the (XoxF-type) MDH coordinatively saturated the Ca^{2+} ion and reduced its affinity for the alcohol substrate.

We hypothesized that the lower Lewis acidity of Ca^{II} compared to Ce^{III} also affected the redox cycling of the PQQ cofactor. A weaker Lewis acidity for the metal cation would result in a higher energy PQQ-based, quinone-type virtual orbital, making the $2e^-$ reduction less favorable for Ca^{II}-MDH. Indeed, the energy of the LUMO was determined to be significantly lower for Ce^{III}-PQQ^0 compared to Ca^{II}-PQQ^0, at –3.00 eV and –3.81 eV respectively (Figure 6.2.2.2).

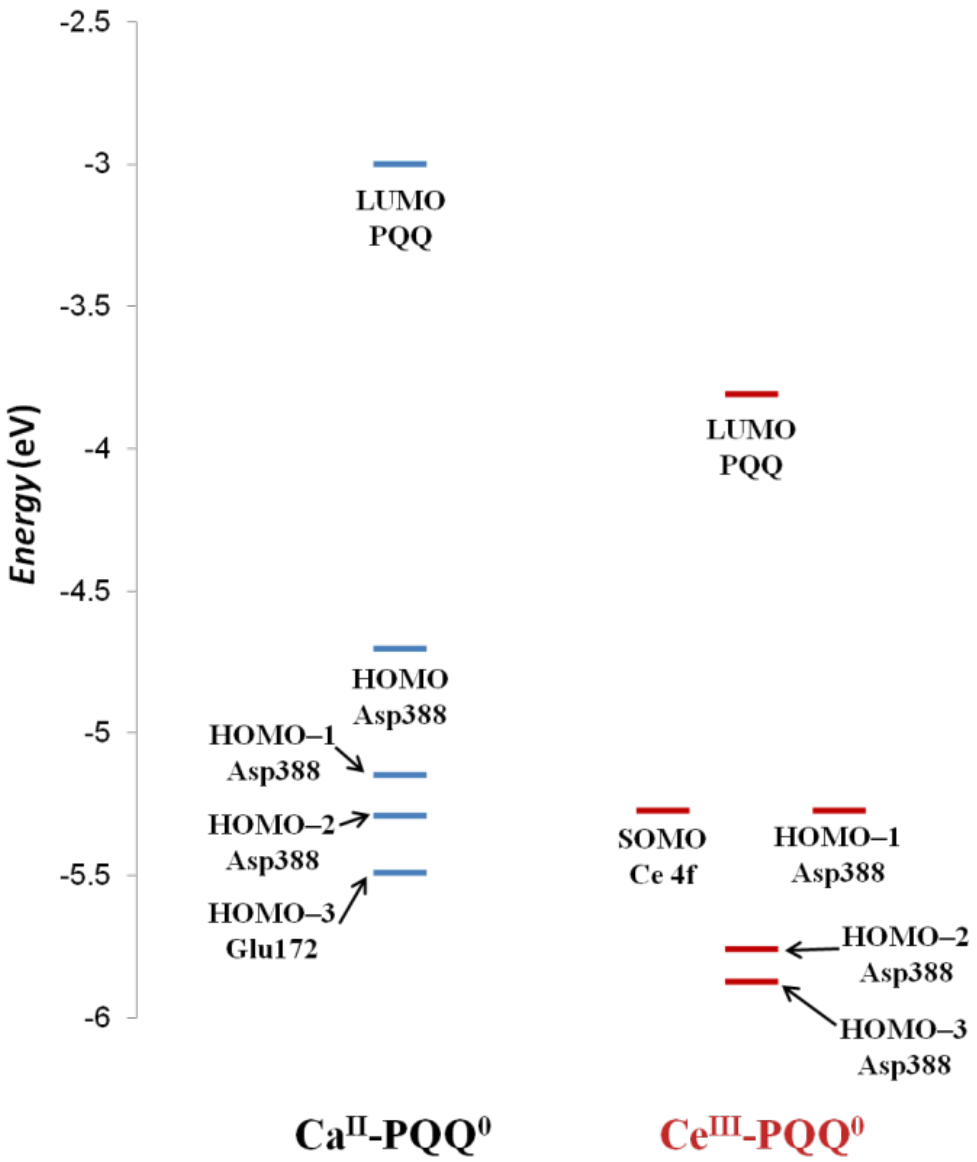

Figure 6.2.2.2. MO diagram of $Ca^{II}PQQ^0$ (left) and $Ce^{III}PQQ^0$ (right). The notation for each MO indicates the primary locations of electron density. Figure reprinted with permission of John Wiley & Sons © 2015.

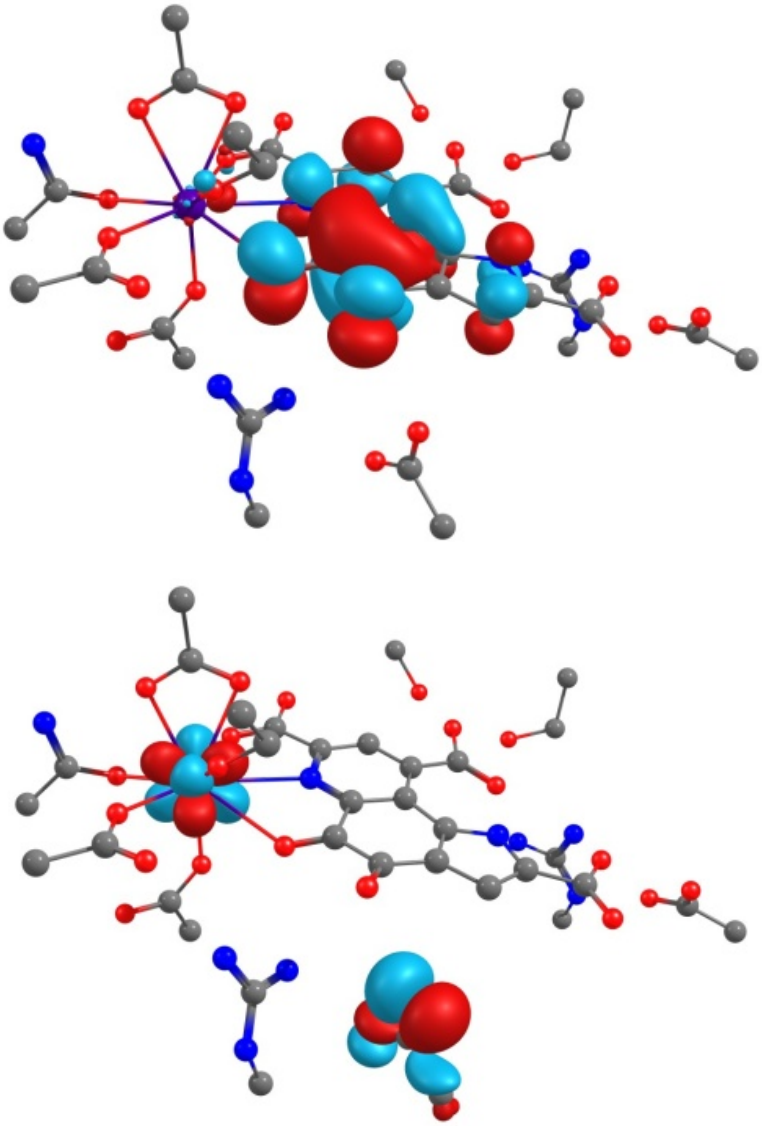

Figure 6.2.2.3. LUMO (top) and SOMO (bottom) of $Ce^{III}PQQ^{0}$. Figure reprinted with permission of John Wiley & Sons © 2015.

Another possible electronic configuration for the Ce-MDH active site in its catalytically active form that was considered was Ce^{IV}-$PQQ^{\bullet-}$. It has been demonstrated that hard, anionic oxygen donor ligands including hydroquinone anions, strongly stabilize the tetravalent state for cerium.[8, 16] The presence of the quinone-based PQQ ligand suggested the possibility of a Ce^{IV} configuration since *p*-benzoquinone is an established oxidant in cerium chemistry.[17] In particular, coordination of *p*-benzoquinone to two equivalents of the electron rich

$[Li_3(THF)_4][(BINOLate)_3Ce(THF)]$ complex caused a shift in the benzoquinone reduction potential, inducing oxidation of the Ce^{III} cations.[18] The oxidation state of the Ce cation in the MDH active site was of interest considering the increased Lewis acidity of Ce^{IV} relative to Ce^{III} could have a significant effect on enzyme activity as well as mechanistic implications. Consideration of the possible valence tautomers, including Ce^{IV}-$PQQ^{\bullet-}$ and Ce^{III}-PQQ^0, showed that the Ce^{III}-PQQ^0 was the ground state configuration. Because both Ce^{IV}-$PQQ^{\bullet-}$ and Ce^{III}-PQQ^0 have the same overall charge and multiplicity and only differ by location of the unpaired spin, performing an unrestricted calculation on this redox form of the active site explored both electronic configurations. In this case, the SCF converged to the Ce^{III}-PQQ^0 form as determined by the spin density plot, and a stability check confirmed that the wavefunction was stable. In fact, the spin density was completely localized in a Ce 4f orbital, indicating qualitatively that the framework energetically favored a Ce^{III} cation (Figure 6.2.2.4).

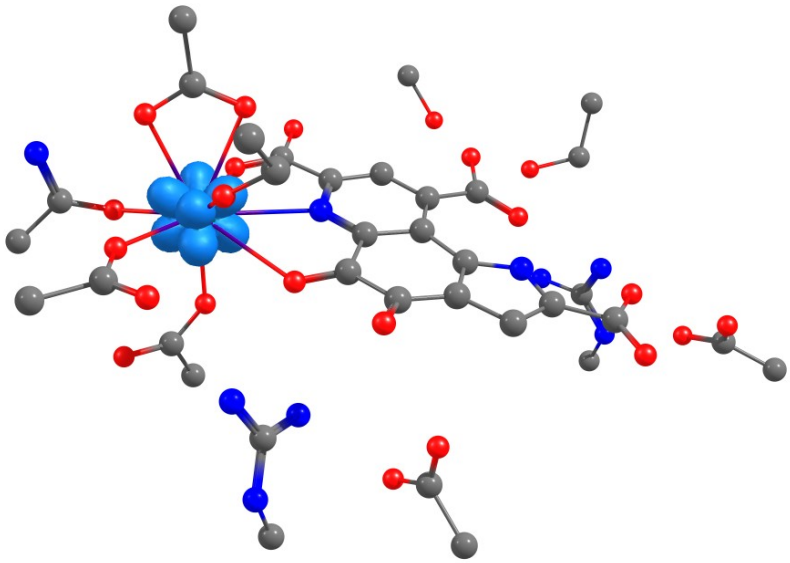

Figure 6.2.2.4. Spin density plot of Ce^{III}-PQQ^0; blue = α, red = β. Figure reprinted with permission of John Wiley & Sons © 2015.

One can also envision the formation of a doubly oxidized form of the active site, namely the Ce^{IV}-PQQ^0 configuration, through oxidation with an external oxidant. In that case, the stronger Lewis acidity of Ce^{IV} compared to Ce^{III} would stabilize the relevant PQQ based unoccupied orbital and make the $2e^-$ reduction of the quinone even more favorable. Establishment of the metal

oxidation potential for the active site, which could be correlated to the energy difference between the Ce^{IV}-PQQ^0 and Ce^{III}-PQQ^0 redox forms, also provided an experimental metric for targeted synthesis of model complexes.

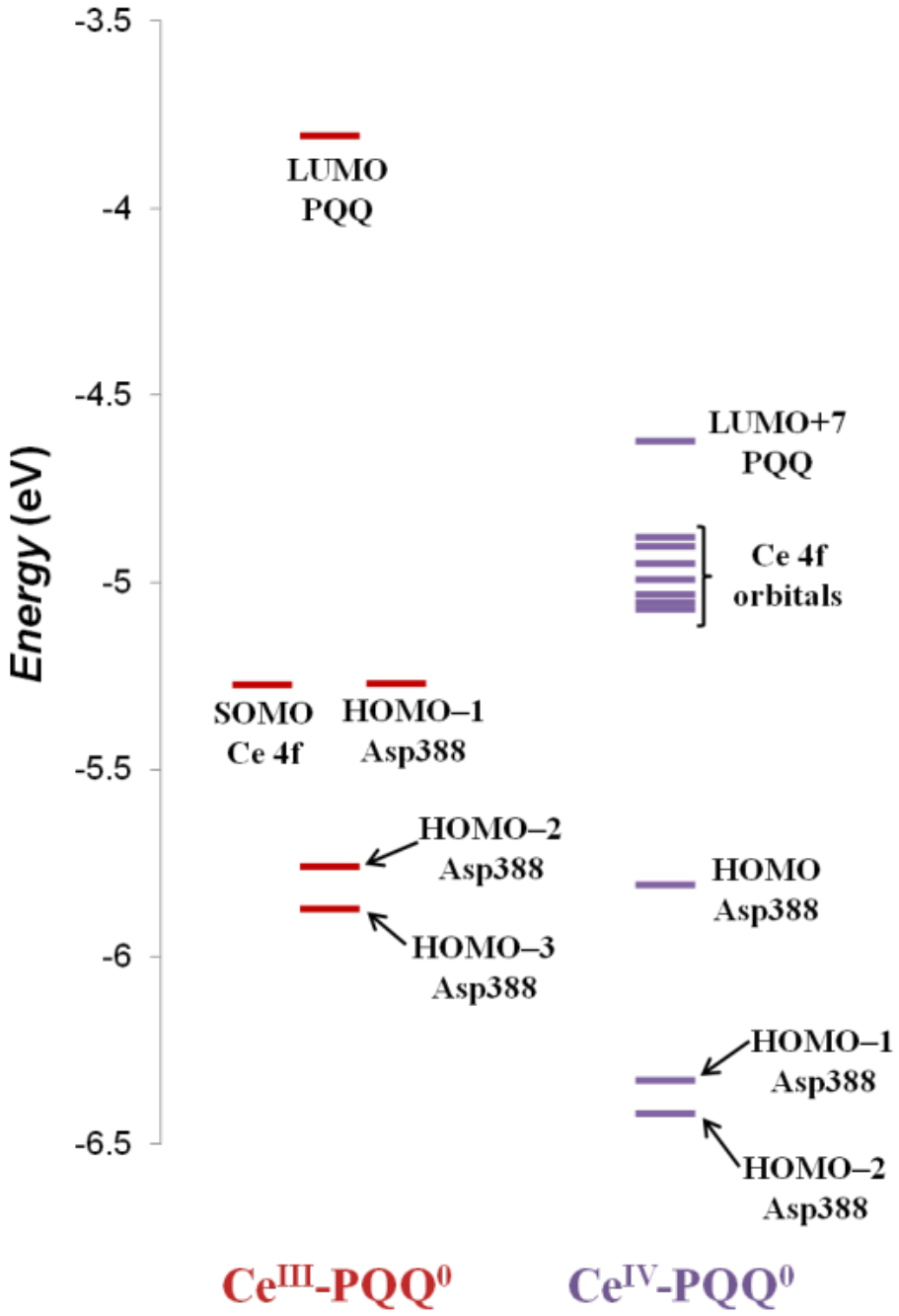

Figure 6.2.2.5. MO diagram of $Ce^{III}PQQ^0$ (left) and $Ce^{IV}PQQ^0$. The notation for each MO indicates the primary locations of electron density. Figure reprinted with permission of John Wiley & Sons © 2015.

As expected, the relevant PQQ based unoccupied orbital decreased in energy from –3.81 eV to –4.62 eV upon oxidation from Ce^{III} to Ce^{IV} (Figure 6.2.2.5). Interestingly, however, according to the calculations, the ligand framework imposed by the enzyme active site strongly favored the +3 oxidation state of Ce despite the coordination of anionic carboxylate ligands and the electron deficient PQQ cofactor. The estimated redox potential of Ce^{IV}-PQQ^0 was calculated to be 1.35 V versus SCE, which was similar to the thermodynamic reduction potential for **CAN** (Figure 6.2.1.2). **CAN** is a potent oxidant and is widely used in organic- and inorganic chemistry.[19]

Another point of interest from the active site results was the effect of the solvent dielectric. Reported DFT treatments of the Ca^{II}-MDH active site have used a dielectric of 4 (compared to 78 for water)[20] to model the hydrophobic enzyme cavity.[5] Our model of the active site structure suggested that the dielectric of the protein interior had only a minimal effect on the redox potential of the Ce^{III} cation (Figure 6.2.1.2). In fact, we observed only an 80 mV shift towards more negative potentials between the active site in a dielectric of 4 compared to a dielectric of 78. Furthermore, removing the hydrogen-bonding residues produced only an additional 20 mV shift in the potential, using a dielectric of 78. This was surprising because bioinorganic proteins are typically quite sensitive to solvent dielectric.[21] We postulate that this insensitivity to protein dielectric in our computed results is due to the coordinative saturation of the cerium cation. We also propose that the sterics of the protein secondary structure maintained the MDH active site in a configuration that favors the +3 oxidation state. Overall, the results of the redox correlation study for the Ce^{III}-MDH active site indicated a strong preference for the Ce^{III}-PQQ^0 electronic configuration.

6.3 Conclusions

We have used DFT to assess the electronic structure of the active site of the first natural, rare earth metal containing metalloenzyme. Our key findings from this study were that the rare earth cation exhibited stronger association with substrate and more significant activation of the PQQ ligand toward reduction than an analogous Ca^{II}-MDH. This finding supported the observation that rare earth metals are essential cofactors for the growth of *M. fumariolicum* SolV, even in the

presence of calcium(II) sources. Computation of the cerium(IV/III)-MDH redox potential demonstrated a strong preference for the +3 oxidation state through a semi-empirical correlation developed from aqueous electrochemical data. This finding discounted the possibility of cerium redox chemistry in the dehydrogenation mechanism.

It is our assertion that functional model complexes for MDH reactivity comprising rare earth cations and quinone ligands should be guided by the redox energetics computed here. Efforts toward developing such compounds as active catalysts for alcohol dehydrogenase reactivity are currently underway in our group. We are also working to develop a similar correlation for Ce^{III}-quinone complexes for the purposes of establishing the Ce-$^{III}PQQ^{0}$/Ce^{III}-$PQQ^{\cdot-}$ redox thermodynamics as an elementary step in the dehydrogenase mechanism.

6.4 Experimental Section

Computational details. Gaussian '09 Rev. D.01 was used in electronic structure calculations.[22] All calculations were performed using the B3LYP DFT method. A 28 electron core pseudopotential and a segmented basis set incorporating quasi-relativistic effects were used for Ce and a 6-31g* basis set was used for C, H, N, Na and O.[23] Solvent effects were modeled in water using the conductor like polarizable continuum model (CPCM) with the default UFF radii.

The coordinates from the X-ray crystal structure, PDB code 4MAE, were used as the starting point for the active site geometry optimization. In order to simplify the structure, the residues Asp299, Asp301, Asp388, Glu55, and Glu172 were truncated to CH_3COO^- groups, the residues Arg110 and Arg326 were truncated to $CH_3NHC(NH_2)_2^+$ groups, and the residues Asn256, Ser169, and Thr154 were truncated to CH_3CONH_2, CH_3OH, and CH_3CH_2OH, respectively. The truncated residues were incorporated to reproduce the hydrogen bonding network at the PQQ ligand for a more accurate representation of the secondary structure and electrostatic environment within the active site. The coordinated polyethylene glycol substrate present in the crystal structure was modeled as a CH_3CH_2OH molecule.

A dielectric constant of 4 was specified to reproduce the electronic properties of the interior of the protein. For mimicking the sterics imposed by the secondary protein structure, approaches

include freezing a hydrogen or a carbon of each residue at its crystallographic position.[5, 24] We opted for freezing the anchoring carbon of each residue at its crystallographic position because, at the resolution of the crystal structure, the positions of the carbon atoms were more precisely determined.

The frequency calculations of the optimized structures with the Ce in both the +3 and +4 oxidation state contained a few small negative frequencies (< –35 cm^{-1}) attributed to vibrational modes that move the restricted protein residues, which would be unfavorable within the expanded protein network (Figure 6.4.1). Thus, we expect these structures accurately describe the lowest energy conformation of the active site of the MDH enzyme.

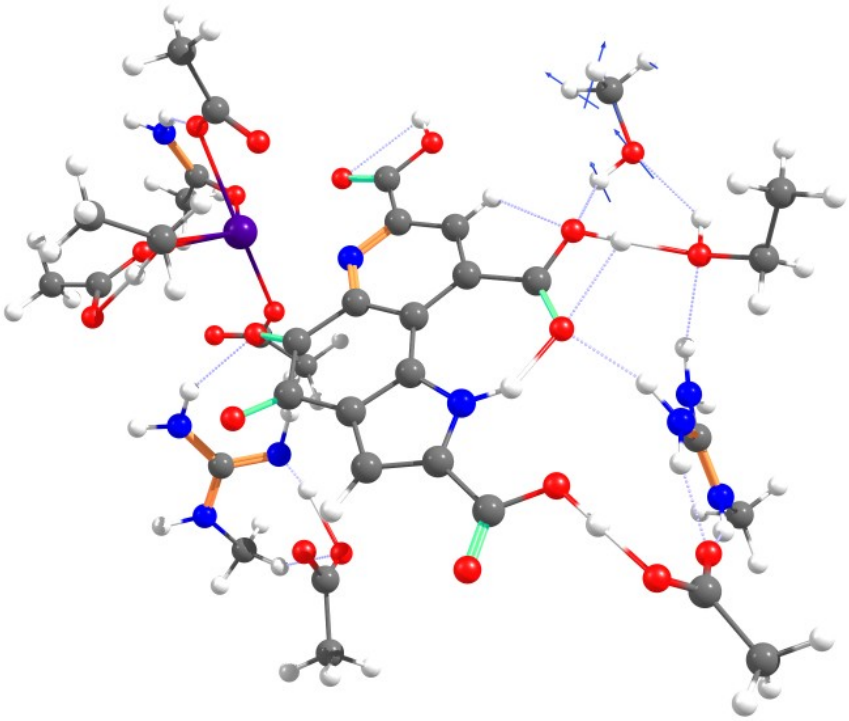

Figure 6.4.1. Vector depiction of the lowest energy negative frequency vibrational mode of Ce^{III}-PQQ^0 corresponding to the H-bond of Ser168 to the PQQ carboxylic acid moiety and Thr154. Figure reprinted with permission of John Wiley & Sons © 2015.

The free energy (G) values for the complexes with the Ce in the +3 and +4 oxidation states and those of the Ce-PQQ^0 active site were obtained from the frequency calculations. From the $\Delta G_{Ce}^{IV/III}$ values, we determined the E^{abs} $Ce^{IV/III}$, which were referenced to ferrocene using the

calculated E^{abs} Fc/Fc^{+} value of 5.08 V. Due to systematic errors inherent to the calculations from using ferrocene as a reference for Ce, an empirical correction factor of 0.75 V was added to the computed redox potentials for each complex to systematically scale the results to match their experimental values.

Table 6.4.1. Optimized coordinates of Ce^{III}-PQQ$^{\bullet-}$ MDH.

C	-10.253330121	2.855579689	0.972746753
C	-8.880081028	2.184470079	1.054144089
O	-8.206917878	2.376967569	2.107698594
O	-8.519039002	1.465893699	0.074001046
C	-8.161633111	0.166403942	-3.749678717
N	-7.875205395	0.133837162	-2.321799037
C	-7.037792347	-0.730783261	-1.739705698
N	-6.354977744	-1.637605250	-2.468582069
N	-6.885762263	-0.697857106	-0.407295483
C	-7.099568869	-4.369687251	-0.323858810
O	-5.760609351	-4.154002452	-0.843651783
C	-7.115846626	-5.361128736	0.828756735
C	-2.484275100	-6.880294698	-0.738099819
O	-3.332771702	-5.922853190	-1.381146434
C	4.902492079	-3.396281767	3.544233662
C	4.344506637	-2.746228009	2.268017107
O	5.175471406	-2.447825546	1.338948570
O	3.121160452	-2.483380278	2.175706655
C	7.598246141	-1.620967161	-2.735242390
C	6.702199989	-2.007165167	-1.576659065
O	5.469482910	-1.830379182	-1.658923997
N	7.277071006	-2.536126512	-0.488097696

C	7.619463820	1.972244872	0.481733621
C	6.182549571	1.548771149	0.744337199
O	5.841753231	0.416635898	0.267566589
O	5.435212757	2.307679143	1.415644377
C	3.192534815	0.953293658	-4.241938640
C	3.313781669	0.373161427	-2.818598830
O	4.039898809	0.987016372	-1.978595718
O	2.681379528	-0.683543883	-2.509695394
Ce	3.756944606	-0.783397709	-0.071902026
N	-3.277729024	0.772645674	1.476382908
C	-3.507867913	2.024538178	1.977396216
C	-4.883302043	2.494987384	2.253851731
O	-5.791807736	1.565069930	1.969498521
O	-5.117859197	3.615366186	2.685012261
C	-2.290906463	2.685791681	2.087772325
C	-1.300650504	1.798662219	1.616729668
C	-1.943323017	0.592251425	1.232834916
C	0.131764438	2.018703565	1.476522283
O	0.710535198	3.050816444	1.860928426
C	0.854153761	0.917875322	0.818573370
O	2.081440893	1.062612840	0.466145264
C	0.190129760	-0.350487116	0.563897717
N	1.017751823	-1.315813777	0.136769294
C	0.538212675	-2.527719240	-0.140080759
C	1.564207921	-3.499824498	-0.594632866
O	2.746425149	-3.223386045	-0.739867340
O	1.079597816	-4.726570431	-0.845747669

C	-0.816155728	-2.834624201	-0.034675685
C	-1.729590427	-1.849463113	0.375518642
C	-3.169132375	-2.237095926	0.337341201
O	-3.374907467	-3.554503135	0.214991772
O	-4.125837294	-1.467949812	0.368044408
C	-1.243955036	-0.555307715	0.724914511
O	3.991454351	0.277383618	2.396711707
C	3.059721253	0.533634006	3.449683610
C	3.774550206	0.814476564	4.769129061
C	1.898363870	5.634771424	-3.075620421
N	2.784814429	5.116019533	-2.037192690
C	2.495368211	4.025332686	-1.298039374
N	1.443337170	3.258882953	-1.608669060
N	3.301621731	3.693617668	-0.277233484
C	-1.951900568	6.577145510	-1.188933323
C	-0.771110764	5.602713761	-1.116436273
O	-0.910106381	4.523436526	-1.789027955
O	0.239094904	5.954335850	-0.466564671
H	7.158804600	-1.985863481	-3.667407588
H	7.631214201	-0.527148842	-2.789853652
H	8.618015944	-2.002719131	-2.636853697
H	7.795011070	2.046119392	-0.597797182
H	7.844087920	2.932236675	0.952129309
H	8.303677620	1.207678232	0.866799144
H	5.671313389	-4.134858041	3.297390970
H	5.373163920	-2.617228386	4.156150361
H	4.103592794	-3.863088746	4.125324495

H	4.408930866	-0.032456094	5.054896227
H	4.409613161	1.704891307	4.687674104
H	3.047954590	0.989194688	5.572392910
H	2.444559110	-0.366356415	3.530955800
H	2.410757119	1.375550543	3.179282492
H	2.769047731	0.219164699	-4.931851081
H	2.536261172	1.830481425	-4.205423272
H	4.173656957	1.283523259	-4.596239604
H	1.372519569	4.805021334	-3.546923575
H	1.170746237	6.326948178	-2.648711819
H	2.507758796	6.143276099	-3.829156298
H	-2.908404665	6.047640329	-1.116584337
H	-1.889464648	7.334658931	-0.402421223
H	-1.940955208	7.088078950	-2.161340229
H	-8.590522382	-0.781494327	-4.097116432
H	-8.893316228	0.954955793	-3.927494967
H	-7.263683985	0.393364388	-4.336199216
H	-6.761004282	-6.347764794	0.508383592
H	-6.482311337	-5.013480794	1.651555706
H	-8.137607829	-5.477750458	1.207244047
H	-7.743266002	-4.703865102	-1.145990674
H	-7.437943588	-3.382077422	-0.003544624
H	-2.818650096	-7.870675108	-1.057225329
H	-1.434918230	-6.751024475	-1.033655176
H	-2.553087177	-6.821625716	0.356770525
H	-11.035926862	2.087437086	0.964424298
H	-10.416751539	3.526193226	1.818736103

H	-10.341574608	3.415783081	0.035359608
H	-3.012820877	-5.044330410	-1.117967384
H	-4.353321206	-3.700287667	0.058604592
H	-5.390169031	-4.998491595	-1.174246924
H	-5.956620784	-2.449982912	-1.999157853
H	-6.567940418	-1.750077932	-3.448582217
H	-6.033438852	-1.094605870	-0.020968977
H	-7.314506856	0.113932105	0.069277350
H	-8.309230013	0.814774083	-1.690157335
H	-1.159943771	-3.824608342	-0.289720812
H	-6.770689231	1.924615734	2.056839697
H	1.829549533	-5.277754082	-1.141746900
H	-3.994208851	0.101222565	1.229874074
H	-2.140484406	3.694682786	2.441629415
H	3.062725736	2.858881331	0.254787731
H	4.273666436	3.968078724	-0.255443896
H	1.417850274	2.396985503	-1.075174063
H	0.499373669	3.746536510	-1.739022784
H	3.375896785	5.799390529	-1.582471992
H	8.282310290	-2.582409159	-0.409323019
H	6.696797407	-2.654352409	0.350580477
H	4.429307106	1.131879846	2.132029450

Lowest Energy Frequencies (in cm^{-1}): –36.6589, –28.2941, –18.8969, –11.1129, –8.1889, 9.3455.

Sum of electronic and thermal Free Energies (in hartrees): –3991.285343

Table 6.4.2. Optimized coordinates of Ce^{III}-PQQ^{0} MDH.

C	10.311065106	-2.743457227	0.910070481
C	8.930625340	-2.095556226	0.982274632
O	8.262227643	-2.293592693	2.043013391
O	8.553489923	-1.380363680	0.009693145
C	8.183704565	-0.061794788	-3.800673443
N	7.903007997	-0.034531091	-2.371916795
C	7.070021305	0.827697661	-1.783198337
N	6.376022859	1.731094984	-2.507061811
N	6.931901651	0.793807663	-0.448483307
C	7.080848377	4.452829077	-0.359382473
O	5.734733800	4.214370876	-0.860973675
C	7.094133743	5.433302004	0.801821978
C	2.439115437	6.916913552	-0.758327048
O	3.329394080	5.984523031	-1.386492177
C	-4.904118770	3.344068128	3.525844578
C	-4.431896429	2.750902417	2.212101916
O	-5.316463054	2.483266346	1.327897338
O	-3.213902633	2.477676916	2.023269195
C	-7.592040744	1.559948362	-2.754608849
C	-6.784687398	1.988475124	-1.551525082
O	-5.534446826	1.901790398	-1.571777738
N	-7.441275711	2.471571539	-0.491769430
C	-7.570723632	-2.042995701	0.451444685
C	-6.149438210	-1.615554688	0.751619451
O	-5.815806718	-0.467019861	0.292922433
O	-5.390395889	-2.359602851	1.421022654

C	-3.162473399	-0.964408719	-4.276664119
C	-3.965909378	-0.848700785	-2.975890052
O	-5.108698144	-1.311635409	-2.919058103
O	-3.340384695	-0.270567421	-1.982619609
Ce	-3.900581494	0.861488253	0.010883273
N	3.330802237	-0.816629876	1.479572936
C	3.613181467	-2.059191006	1.973392779
C	5.015035104	-2.494535244	2.208375079
O	5.882143796	-1.542222723	1.912950175
O	5.268979095	-3.615271855	2.625201188
C	2.418223143	-2.748454893	2.136832961
C	1.394562924	-1.878817999	1.715462204
C	1.992579010	-0.658500469	1.294097173
C	-0.031965653	-2.096996339	1.683430597
O	-0.655856832	-3.022545551	2.176617047
C	-0.806398657	-0.984475438	0.956714805
O	-1.972449965	-1.163012581	0.632701771
C	-0.136608816	0.317472112	0.638366185
N	-0.976227538	1.231790341	0.173582368
C	-0.503470076	2.436515298	-0.158773259
C	-1.516617302	3.385160393	-0.694292780
O	-2.682195927	3.077320593	-0.901617864
O	-1.029427124	4.601169610	-0.946856402
C	0.848718745	2.741667962	-0.046527545
C	1.771097948	1.786461836	0.398505596
C	3.210700449	2.209543598	0.359766708
O	3.372177452	3.510701737	0.135903676

O	4.177351848	1.464951346	0.479702173
C	1.282045897	0.496578957	0.784494503
O	-3.933977188	-0.328487937	2.353832998
C	-3.162060196	-0.450692099	3.552715844
C	-4.046005107	-0.735804147	4.762196760
C	-1.818217192	-5.635630596	-3.126563558
N	-2.492158217	-5.270518208	-1.878814797
C	-2.382198894	-4.057667861	-1.317252620
N	-1.383146592	-3.254866588	-1.704774253
N	-3.280645135	-3.660933702	-0.402968423
C	2.044737032	-6.543900213	-1.249014209
C	1.307631559	-5.208821226	-1.019596715
O	0.915951218	-4.609951243	-2.088085640
O	1.107848922	-4.827330240	0.150456211
H	-7.342607544	2.206595552	-3.602668726
H	-7.284738625	0.542462000	-3.016269705
H	-8.670592138	1.594220315	-2.583590912
H	-7.708385125	-2.109303732	-0.633612559
H	-7.803938502	-3.006642161	0.909256586
H	-8.267101736	-1.282047940	0.820001084
H	-5.678400765	4.096278924	3.349458926
H	-5.351485803	2.545255380	4.129467699
H	-4.073823298	3.781350335	4.085127503
H	-4.780054868	0.064589747	4.906142354
H	-4.588491322	-1.679861239	4.635007098
H	-3.436570068	-0.814544785	5.670202434
H	-2.639768686	0.502503173	3.666641572

H	-2.414678957	-1.246223920	3.433956880
H	-2.741348376	0.006897716	-4.559217898
H	-2.321014939	-1.650842952	-4.124359419
H	-3.794156086	-1.342985907	-5.082986114
H	-2.140329092	-4.976732355	-3.941336763
H	-0.733474191	-5.572322741	-3.013566096
H	-2.105081331	-6.660942844	-3.367338058
H	2.702015753	-6.487177651	-2.123156751
H	2.623145324	-6.831642671	-0.366495402
H	1.306437999	-7.332266839	-1.447258378
H	8.606984874	0.888892363	-4.146831206
H	8.918346417	-0.846246943	-3.983737624
H	7.284454510	-0.291607382	-4.383918515
H	6.713519831	6.415115458	0.497068267
H	6.482707479	5.064216293	1.631949785
H	8.119496685	5.568025028	1.163835579
H	7.699784142	4.808302005	-1.190803272
H	7.444692715	3.469350149	-0.055272421
H	2.847160193	7.914741021	-0.934927556
H	1.432641561	6.865354331	-1.193023647
H	2.369049152	6.750855773	0.324960117
H	11.073908983	-1.987829936	1.135546239
H	10.402642562	-3.556337051	1.633440308
H	10.506795229	-3.115047565	-0.100372538
H	2.955191300	5.099852591	-1.251977585
H	4.349605922	3.701823943	-0.008279546
H	5.345068788	5.055892456	-1.178785238

H	5.988956530	2.548702473	-2.036934843
H	6.588318928	1.845542788	-3.487341165
H	6.083822718	1.182794936	-0.047709517
H	7.366714690	-0.017988676	0.021692579
H	8.344963924	-0.714928729	-1.745783606
H	1.191275166	3.724605357	-0.329580751
H	6.902096801	-1.874437459	1.988468954
H	-1.755671335	5.149877675	-1.303512798
H	4.024669654	-0.116760261	1.228109432
H	2.300671841	-3.769643035	2.462460197
H	-3.083409873	-2.869667599	0.198054915
H	-4.172781958	-4.117261596	-0.281365039
H	-1.442421894	-2.295468325	-1.391773557
H	-0.419366506	-3.687382458	-1.866624152
H	-3.172298278	-5.907340359	-1.490042692
H	-8.450233894	2.474496418	-0.462684099
H	-6.908826242	2.663256091	0.359749094
H	-4.379858170	-1.194998695	2.134694969

Lowest Energy Frequencies (in cm^{-1}): –33.7543, –25.0338, –20.8349, –12.9262, –7.6574, –5.2625.

Sum of electronic and thermal Free Energies (in hartrees): –3991.140962

Table 6.4.3. Optimized coordinates of Ce^{IV}-PQQ^0 MDH.

C	10.359933672	-2.799073824	1.082345082
C	8.960133375	-2.181022601	1.045477769
O	8.134380695	-2.565630509	1.930419205

O	8.721095968	-1.303662057	0.166450931
C	8.309839942	-0.066562053	-3.633443585
N	8.002491150	-0.024904620	-2.210800299
C	7.158285318	0.837500611	-1.641799805
N	6.470741935	1.737554196	-2.376561431
N	6.996172821	0.808651370	-0.307899230
C	7.197511799	4.429920603	-0.171578971
O	5.843728068	4.210326152	-0.680133553
C	7.204673790	5.377086552	1.016702539
C	2.578876763	6.930795353	-0.608301710
O	3.917116082	6.595459805	-1.007909724
C	-4.841805243	3.379578097	3.558733192
C	-4.521505563	2.636836917	2.260362082
O	-5.461489529	2.152013675	1.544382994
O	-3.319782856	2.444809908	1.884986300
C	-7.465471547	1.662437543	-2.767440376
C	-6.801364472	1.906732437	-1.436769265
O	-5.537361376	1.873766383	-1.342490734
N	-7.553786097	2.160543409	-0.373677021
C	-7.509369076	-1.964616845	0.411129460
C	-6.076445775	-1.654309037	0.785064189
O	-5.525020116	-0.637275328	0.161870888
O	-5.466498562	-2.307685430	1.641868043
C	-3.035888782	-0.882663783	-4.254515913
C	-3.959517901	-0.554488755	-3.061645823
O	-5.159626231	-0.775358935	-3.126742727
O	-3.382113417	-0.038058621	-1.962164987

Ce	-3.922800017	0.865237817	0.017242047
N	3.229145351	-0.885956811	1.282893173
C	3.492472189	-2.137283720	1.761642413
C	4.883417424	-2.630363661	1.977967463
O	5.792589066	-1.725487991	1.673931469
O	5.078964283	-3.762272754	2.395652596
C	2.282915823	-2.798033430	1.951875982
C	1.271127986	-1.900078044	1.564641852
C	1.889327348	-0.689351878	1.134894346
C	-0.157585256	-2.093113025	1.555399104
O	-0.798990673	-3.016996794	2.031647817
C	-0.922020219	-0.954179887	0.865001921
O	-2.106337535	-1.102726862	0.568701032
C	-0.234978780	0.323035771	0.538486667
N	-1.073614112	1.245531561	0.087846127
C	-0.592783307	2.433028205	-0.287810223
C	-1.635887826	3.344895936	-0.814535879
O	-2.813336935	2.998708005	-0.924624930
O	-1.196558307	4.541997857	-1.169842767
C	0.771493200	2.724081809	-0.209392654
C	1.686614398	1.766416137	0.246290150
C	3.139623906	2.172218298	0.223831480
O	3.317686394	3.478663552	0.103356295
O	4.083852086	1.391536358	0.276790392
C	1.190530714	0.479719617	0.645805433
O	-3.901962239	-0.260946613	2.315708286
C	-3.076169871	-0.314904952	3.496670131

C	-3.912901095	-0.571066216	4.743140960
C	-1.739527402	-5.572108794	-3.123664730
N	-2.416538862	-5.291846998	-1.857667414
C	-2.313796967	-4.110026870	-1.242575651
N	-1.342708247	-3.273673611	-1.632791912
N	-3.215703857	-3.752845763	-0.306297719
C	2.093495361	-6.522683698	-1.206255459
C	1.269584254	-5.248476224	-0.944318907
O	0.960974179	-4.566320388	-1.992225657
O	0.923069265	-4.987609292	0.224657739
H	-7.147507565	2.439574609	-3.470388792
H	-7.100230235	0.703591065	-3.147401431
H	-8.554926427	1.659921808	-2.698200290
H	-7.587343502	-2.118832616	-0.669950907
H	-7.856445056	-2.849689052	0.945447441
H	-8.140740082	-1.106048683	0.665127573
H	-5.714902777	4.021119848	3.415167743
H	-5.087878988	2.640881202	4.329734776
H	-3.982057709	3.966088452	3.886917698
H	-4.660631284	0.216082840	4.885319372
H	-4.433140710	-1.532983722	4.675660161
H	-3.265511951	-0.597818079	5.626759734
H	-2.568574020	0.650040370	3.547762713
H	-2.325124969	-1.103755863	3.372620829
H	-2.447629788	-0.003544891	-4.537721316
H	-2.333785658	-1.672704275	-3.965191094
H	-3.648788053	-1.214653396	-5.092524751

H	-2.049864114	-4.847597628	-3.884719364
H	-0.654867810	-5.529908338	-3.004528336
H	-2.038084174	-6.571726576	-3.444181119
H	2.809123737	-6.372257551	-2.020927152
H	2.618635040	-6.842073972	-0.301997049
H	1.415545516	-7.331012371	-1.510829431
H	8.743333531	0.878854363	-3.981572442
H	9.044165558	-0.855950529	-3.795039780
H	7.420067557	-0.298095606	-4.230191238
H	6.797047126	6.356702597	0.740786076
H	6.607765028	4.972716561	1.840839170
H	8.229855225	5.525502672	1.373782800
H	7.815011747	4.811207950	-0.992755088
H	7.559580588	3.437253474	0.102339873
H	2.279681105	6.185276633	0.131127549
H	2.532454064	7.925634029	-0.147895067
H	1.880963982	6.893004001	-1.455066373
H	11.068201118	-2.057176751	1.470419080
H	10.386127999	-3.682163463	1.723837143
H	10.683529952	-3.060776200	0.070089434
H	4.207940838	7.266550750	-1.644518840
H	4.297786964	3.668045993	0.007030051
H	5.452573739	5.070471231	-0.942647622
H	6.088550229	2.558818590	-1.907597409
H	6.706775626	1.857232912	-3.351058671
H	6.126381481	1.175254134	0.065114483
H	7.439181969	0.009365383	0.172100717

H	8.445536864	-0.691222213	-1.569409945
H	1.131234837	3.695307406	-0.521320481
H	6.805711769	-2.097649656	1.790633357
H	-1.946868886	5.067481322	-1.513582296
H	3.931790177	-0.201432300	1.010051649
H	2.148402993	-3.820250541	2.267208773
H	-2.945389847	-3.075743417	0.398355924
H	-3.984985578	-4.365552128	-0.074617693
H	-1.400061044	-2.338806799	-1.257136661
H	-0.361457879	-3.699291015	-1.789692294
H	-3.060413830	-5.975239833	-1.486103465
H	-8.561719158	2.192264643	-0.438868141
H	-7.100216212	2.305522703	0.529253281
H	-4.356863471	-1.138232634	2.186007641

Lowest Energy Frequencies (in cm^{-1}): –30.3451, –10.3137, –7.6742, 10.8955, 13.3905, 16.2371.

Sum of electronic and thermal Free Energies (in hartrees): –3990.938417

Table 6.4.4. Optimized coordinates of Ca^{II}-PQQ^{0} MDH.

C	-9.932873027	-3.578664463	-0.880947333
C	-8.569790170	-2.880893311	-0.909310038
O	-7.777205049	-3.186732154	-1.845670002
O	-8.343218644	-2.017602083	-0.008674207
C	-8.030734610	-0.622502499	3.761400099
N	-7.788514308	-0.585776561	2.327055857
C	-7.049618294	0.339601595	1.711345354
N	-6.436549200	1.320459011	2.402526095

N	-6.928980434	0.299194921	0.372639471
C	-7.534573947	3.955924639	0.263965393
O	-6.134656437	3.751879247	0.619910102
C	-7.690150682	4.917363399	-0.902433559
C	-3.194006537	6.941892412	0.508482000
O	-3.848463816	5.686767587	0.719294542
C	4.411556305	4.207849883	-3.881684707
C	5.027792896	3.410695709	-2.724767538
O	6.270454008	3.472318272	-2.567258216
O	4.201486495	2.751573689	-2.011051900
C	7.423082650	2.809095717	2.348700138
C	6.810925170	3.102871382	0.990792576
O	5.597903963	3.382404597	0.892599557
N	7.596429052	3.045516421	-0.093890345
C	7.752931689	-0.802637382	-0.829856450
C	6.339189265	-1.005668002	-0.273148945
O	5.517488230	-0.049262182	-0.361359877
O	6.071173106	-2.140619092	0.230214950
C	3.351139630	-0.197601926	3.988502680
C	3.491569100	0.516588126	2.652924874
O	4.542004149	1.171824848	2.438649486
O	2.565545343	0.394259890	1.770770487
Ca	3.976918805	1.710618036	0.063938126
N	-3.015779793	-0.983354826	-1.542188104
C	-3.146912873	-2.199763090	-2.160674063
C	-4.469792182	-2.861475506	-2.287373839
O	-5.438117993	-2.138972377	-1.734910505

O	-4.600764345	-3.938720023	-2.847201252
C	-1.888731478	-2.615933627	-2.570554482
C	-0.979357368	-1.613552228	-2.170843072
C	-1.714072511	-0.589876398	-1.524541117
C	0.462346114	-1.569125496	-2.317242000
O	1.148203630	-2.384034785	-2.912431862
C	1.144058405	-0.364193339	-1.622651934
O	2.357470621	-0.290000893	-1.578902623
C	0.283227063	0.716626764	-1.009361702
N	0.978955976	1.729803739	-0.516710056
C	0.328276528	2.768853665	0.014074452
C	1.213899202	3.815075616	0.600099140
O	2.425020145	3.698456820	0.694128391
O	0.548805513	4.896998034	1.025479144
C	-1.064060346	2.843805749	0.022280045
C	-1.823896502	1.776457000	-0.470058380
C	-3.313171961	1.916683033	-0.363441960
O	-3.745568618	3.165317002	-0.539400276
O	-4.086177201	1.002769064	-0.105370696
C	-1.148086248	0.632215436	-0.986675545
O	7.969833241	-4.130154021	0.159079689
C	7.718014669	-4.795519586	-1.068635190
C	6.366606044	-5.510029741	-1.090791846
C	2.534182944	-5.004009024	2.902234558
N	2.971039126	-4.252001326	1.729512262
C	2.592984755	-2.970968979	1.529643868
N	1.463188767	-2.521093671	2.094452335

N	3.345536500	-2.177421359	0.766189209
C	-1.236142935	-6.372708780	1.118702279
C	-0.748299224	-4.907915214	1.116934716
O	-0.503112871	-4.411859317	2.275345281
O	-0.587346698	-4.337053880	0.019453408
H	7.287734880	3.680834577	2.997292049
H	6.859840304	1.980585076	2.787542634
H	8.486684893	2.559880347	2.300388451
H	7.698400767	-0.713076556	-1.921466843
H	8.170338501	0.135739173	-0.451957380
H	8.404235797	-1.639430679	-0.570557820
H	5.181806171	4.687144546	-4.490966384
H	3.802136179	3.549977849	-4.511442681
H	3.741909109	4.977570763	-3.478746495
H	6.296805554	-6.224833638	-0.262423133
H	5.550768293	-4.784528421	-0.990788628
H	6.221589305	-6.055172797	-2.031975431
H	8.528126881	-5.524120620	-1.201030310
H	7.776481452	-4.096016934	-1.919513079
H	2.303466109	-0.311788628	4.278757597
H	3.781824113	-1.201896377	3.895734776
H	3.903405046	0.336934051	4.765283202
H	2.896897139	-4.547116789	3.832822475
H	1.444326583	-5.067636789	2.924310860
H	2.945140287	-6.013167607	2.823814131
H	-1.860175471	-6.583735565	1.993523232
H	-1.787474904	-6.605150575	0.202670378

H	-0.365187388	-7.039924772	1.168013132
H	-8.509860529	0.299571501	4.111983032
H	-8.705759194	-1.453479503	3.967640708
H	-7.104319770	-0.785100771	4.324736035
H	-7.291941786	5.908014319	-0.654093894
H	-7.166273831	4.543612101	-1.788288805
H	-8.750501448	5.033800534	-1.153082644
H	-8.068856116	4.312874258	1.151851032
H	-7.904638233	2.959442937	0.014217778
H	-3.561479977	7.628315209	1.275180859
H	-2.105575366	6.848570839	0.613705784
H	-3.422336550	7.364213745	-0.479339558
H	-10.713837679	-2.852969829	-1.137908222
H	-9.970192141	-4.408065656	-1.590350611
H	-10.148487779	-3.943106617	0.128849805
H	-3.505481879	5.062540092	0.060001782
H	-4.721445095	3.214627246	-0.314179047
H	-5.732389916	4.607876911	0.878364382
H	-6.139330607	2.157745940	1.902068073
H	-6.620245779	1.427095233	3.388988646
H	-6.081994834	0.706049823	-0.013245657
H	-7.286888143	-0.565846565	-0.067097229
H	-8.161215009	-1.323116566	1.719629406
H	-1.557475585	3.713492037	0.435877015
H	-6.377601077	-2.599544918	-1.793690144
H	1.202930776	5.515259918	1.405643742
H	-3.773463038	-0.495302982	-1.075044113

H	-1.653100867	-3.543438689	-3.069299150
H	3.056133215	-1.203941864	0.735280712
H	4.359783741	-2.321422882	0.608755977
H	1.286070412	-1.531166401	1.954353172
H	0.638250274	-3.178587386	2.179014966
H	3.861422595	-4.507528986	1.324327080
H	8.566984789	2.776803432	-0.022434700
H	7.152813255	3.155154401	-1.025401705
H	7.294444371	-3.410990423	0.235751448

Lowest Energy Frequencies (in cm^{-1}): –27.4138, –24.3216, –12.5696, –5.4449, 7.6578, 11.4081.

Sum of electronic and thermal Free Energies (in hartrees): –4193.687857

Table 6.4.5. Optimized coordinates of Ce^{III}-PQQ^{0} MDH (ε = 78).

C	-10.312853196	-2.776674090	-0.873621959
C	-8.910651228	-2.179400487	-0.950928828
O	-8.245001865	-2.418717559	-2.010875758
O	-8.507434304	-1.465518973	0.006836024
C	-8.189657386	-0.043873274	3.809528844
N	-7.915493088	-0.017033540	2.379009765
C	-7.094700968	0.851632305	1.782500527
N	-6.413861943	1.771375263	2.491193061
N	-6.956070816	0.804686208	0.445007774
C	-7.100438149	4.439938642	0.323849696
O	-5.739372833	4.190957942	0.779316361
C	-7.144896711	5.412452155	-0.843467529
C	-2.464968973	6.919695913	0.695972521

O	-3.496678264	6.149237387	1.329962786
C	4.885002268	3.324351164	-3.557781832
C	4.412051271	2.752912979	-2.235605302
O	5.295210713	2.495668212	-1.345172975
O	3.194376056	2.482325209	-2.041573225
C	7.581225049	1.608298446	2.738063868
C	6.767961798	2.037139513	1.539344777
O	5.517905328	1.919659502	1.553755686
N	7.415046618	2.549287034	0.490106217
C	7.567313244	-2.025679248	-0.432806550
C	6.149692903	-1.596611540	-0.751042478
O	5.813054467	-0.445057234	-0.303737164
O	5.394461558	-2.345130425	-1.421582974
C	3.159095348	-0.912557096	4.287296745
C	3.992085141	-0.838386401	3.003373666
O	5.137799014	-1.303660210	2.994668414
O	3.394822365	-0.297149600	1.976349133
Ce	3.879460458	0.886115532	-0.022739526
N	-3.328462310	-0.839522142	-1.463369291
C	-3.604408338	-2.069945571	-2.001428156
C	-4.998126436	-2.528715178	-2.225263893
O	-5.886483843	-1.612810370	-1.894396347
O	-5.232304339	-3.648148934	-2.667336662
C	-2.404800271	-2.730759455	-2.214807578
C	-1.382968661	-1.862343917	-1.774180220
C	-1.992489230	-0.671095237	-1.300195094
C	0.043072650	-2.067838424	-1.747072062

O	0.670609574	-2.986440005	-2.253710784
C	0.809406220	-0.974277367	-0.981155306
O	1.971432643	-1.167364440	-0.649183674
C	0.131258287	0.313723610	-0.631804297
N	0.962579195	1.231203986	-0.151372304
C	0.473010639	2.420537548	0.207283174
C	1.482589019	3.374715275	0.746855019
O	2.659027372	3.076011567	0.915401593
O	0.981632581	4.570620001	1.036137531
C	-0.884288728	2.716051851	0.101819120
C	-1.787926308	1.757415366	-0.371433221
C	-3.237317398	2.167202639	-0.343476613
O	-3.398493919	3.473295541	-0.283413154
O	-4.180930816	1.380651897	-0.325608027
C	-1.283792399	0.483641764	-0.768906492
O	3.941591948	-0.309087901	-2.367289897
C	3.175100589	-0.434008776	-3.570795274
C	4.063283114	-0.731573121	-4.774026655
C	1.826238434	-5.598188131	3.183477021
N	2.522683044	-5.259592565	1.939081249
C	2.444717027	-4.051171147	1.363553947
N	1.442973387	-3.230455922	1.709354292
N	3.374192252	-3.670363149	0.474006850
C	-2.035460090	-6.534622255	1.317217276
C	-1.203203191	-5.273734965	1.016067304
O	-0.920255852	-4.544875316	2.034344034
O	-0.833292763	-5.075646093	-0.159982998

H	7.327613042	2.247180277	3.590896411
H	7.288264374	0.585643488	2.994910571
H	8.658410795	1.656564247	2.564255516
H	7.695130399	-2.084087452	0.653911984
H	7.803330477	-2.993991068	-0.879194000
H	8.270340777	-1.270279651	-0.799981108
H	5.660410115	4.078053869	-3.393568210
H	5.330673791	2.515636647	-4.149343660
H	4.055562715	3.754630652	-4.123532050
H	4.802849791	0.063171045	-4.920726871
H	4.599335021	-1.678580085	-4.639955921
H	3.456973206	-0.811435329	-5.683890291
H	2.658195379	0.520716831	-3.692324497
H	2.422279763	-1.223722494	-3.450623042
H	2.733705596	0.067404728	4.530810917
H	2.319080304	-1.600995731	4.136451833
H	3.768993231	-1.267516653	5.120654163
H	2.169106741	-4.957612679	4.004382892
H	0.746776558	-5.491048630	3.061838899
H	2.064860299	-6.635958534	3.421213488
H	-2.757013324	-6.355474589	2.121076238
H	-2.557335894	-6.887169134	0.422671302
H	-1.363489689	-7.335277275	1.654147950
H	-8.623731905	0.902233673	4.153192155
H	-8.912489801	-0.837763977	3.997989288
H	-7.283951633	-0.257153876	4.388453527
H	-6.746687867	6.392880382	-0.557914680

H	-6.563088128	5.032535800	-1.689905573
H	-8.180817268	5.552778479	-1.172199474
H	-7.686165819	4.807500175	1.173570128
H	-7.484855098	3.458697441	0.038748289
H	-2.932489114	7.446435295	-0.139009976
H	-2.035712010	7.658778832	1.384364112
H	-1.660279246	6.283888284	0.305941978
H	-11.043797739	-2.008160158	-1.154485567
H	-10.422673826	-3.622151381	-1.556517303
H	-10.540709722	-3.087985568	0.149943703
H	-3.087514261	5.662420565	2.062247227
H	-4.361179642	3.691181416	-0.085870866
H	-5.327800412	5.028411948	1.081622422
H	-6.011308131	2.574405464	2.006841380
H	-6.628545395	1.906009158	3.468747728
H	-6.104084491	1.194955678	0.051755244
H	-7.352686571	-0.028476005	-0.011040056
H	-8.346629403	-0.710163896	1.763474657
H	-1.252484526	3.684220221	0.410127526
H	-6.904351202	-1.972429920	-1.961059192
H	1.697777513	5.134453021	1.390935562
H	-4.021842355	-0.159542613	-1.154504025
H	-2.282057995	-3.729987730	-2.602720315
H	3.211754787	-2.877650148	-0.135315623
H	4.250067850	-4.160578654	0.364031108
H	1.512988506	-2.280686018	1.369001599
H	0.477351151	-3.650333689	1.843353106

H	3.239165750	-5.889845177	1.606911282
H	8.423456414	2.599546072	0.471533562
H	6.881885934	2.749549607	-0.358294603
H	4.381290531	-1.175704633	-2.141950031

Lowest Energy Frequencies (in cm^{-1}): –29.3886, –19.8737, –12.8612, –11.4042, 6.2731, 11.2220.

Sum of electronic and thermal Free Energies (in hartrees): –3991.177505

Table 6.4.6. Optimized coordinates of Ce^{IV}-PQQ^0 MDH (ε = 78).

C	-10.368769874	-2.801402797	-1.047170141
C	-8.954080222	-2.214819548	-1.034731973
O	-8.152330969	-2.614853487	-1.938367627
O	-8.678734694	-1.349558992	-0.158033443
C	-8.310345942	-0.049645563	3.653770114
N	-7.990249164	-0.012350674	2.232996564
C	-7.156328156	0.861802341	1.665055812
N	-6.490237830	1.776347381	2.394716370
N	-6.984992311	0.825926335	0.330084845
C	-7.203518226	4.432392649	0.171465098
O	-5.851108133	4.194683509	0.673588683
C	-7.202260953	5.388135879	-1.010146339
C	-2.583922388	6.934579552	0.589949716
O	-3.937852273	6.607242095	0.941094641
C	4.829281010	3.365435676	-3.575078721
C	4.531173272	2.626373263	-2.271072174
O	5.477822109	2.125051766	-1.578079710

O	3.333703748	2.451209312	-1.866513670
C	7.463614664	1.674171901	2.753621341
C	6.804830953	1.918897407	1.421231679
O	5.538560862	1.877327497	1.324696673
N	7.556269949	2.181007408	0.362799837
C	7.501737070	-1.965982287	-0.410008639
C	6.067127705	-1.658949165	-0.779189078
O	5.519109259	-0.637706439	-0.163897205
O	5.451381397	-2.323337731	-1.625495097
C	3.036356734	-0.864311207	4.258778536
C	3.960087656	-0.561798661	3.059099946
O	5.156996458	-0.808740627	3.125112077
O	3.390149756	-0.043592311	1.961699930
Ce	3.924262118	0.881395610	-0.023083686
N	-3.230942045	-0.886442908	-1.307078060
C	-3.495745134	-2.134679480	-1.805534739
C	-4.879387893	-2.634154888	-2.018768728
O	-5.799718142	-1.741854158	-1.707327591
O	-5.077010481	-3.767608390	-2.440286252
C	-2.288394898	-2.788229993	-2.007831338
C	-1.274176497	-1.895012876	-1.606159855
C	-1.894250718	-0.694484056	-1.160864635
C	0.152768701	-2.091328597	-1.588778700
O	0.790801211	-3.020515167	-2.061802147
C	0.916947690	-0.959211092	-0.884579775
O	2.098500848	-1.115005971	-0.583297598
C	0.228072934	0.315255937	-0.545561524

N	1.064377202	1.233695125	-0.078562091
C	0.578368275	2.412830113	0.310770018
C	1.618131416	3.321363694	0.858960706
O	2.794815583	2.969916329	0.965209973
O	1.173009867	4.505913371	1.231989851
C	-0.784379179	2.706162926	0.228401335
C	-1.694628771	1.751992209	-0.245835402
C	-3.150237752	2.157158982	-0.228863847
O	-3.328052785	3.460933225	-0.113254106
O	-4.092091757	1.372459502	-0.281850850
C	-1.192858453	0.474993887	-0.654626066
O	3.906786854	-0.261249473	-2.325904849
C	3.081240463	-0.309123715	-3.507021203
C	3.915912595	-0.572199809	-4.753476453
C	1.737600636	-5.558273191	3.149513160
N	2.438335752	-5.267961181	1.897931590
C	2.359877028	-4.077490783	1.295805066
N	1.371919535	-3.243007916	1.652244785
N	3.289137366	-3.708024292	0.395631187
C	-2.098749641	-6.516352198	1.242641983
C	-1.273189761	-5.250774525	0.950389554
O	-0.986367680	-4.531986204	1.975371531
O	-0.910223456	-5.036942682	-0.225103823
H	7.146199228	2.454142716	3.453737706
H	7.096142976	0.716715946	3.134418951
H	8.552873431	1.669111606	2.686187702
H	7.583939464	-2.116057436	0.671328525

H	7.848358116	-2.853360002	-0.940834105
H	8.131190709	-1.107495268	-0.668669679
H	5.713128816	3.996003106	-3.450157573
H	5.048415076	2.624807771	-4.352184152
H	3.969478901	3.963045757	-3.882248556
H	4.670987071	0.207841516	-4.895038257
H	4.426937181	-1.539311343	-4.686771793
H	3.267979261	-0.591449245	-5.636908401
H	2.579898398	0.658834893	-3.558409981
H	2.323285411	-1.091318912	-3.383773901
H	2.459594120	0.025026630	4.533314598
H	2.323723649	-1.648935178	3.981075979
H	3.646464218	-1.194734646	5.099581213
H	2.053503176	-4.861410546	3.934064089
H	0.656796286	-5.487856580	3.014302123
H	2.003863440	-6.573083175	3.448864242
H	-2.825700272	-6.342974364	2.042911535
H	-2.613569666	-6.868969458	0.344203002
H	-1.424171820	-7.313692770	1.581982540
H	-8.760304721	0.891609641	3.990574806
H	-9.033480887	-0.849566006	3.813395002
H	-7.421909253	-0.261916811	4.258953234
H	-6.780616649	6.359609580	-0.727157947
H	-6.612202497	4.981867994	-1.838369299
H	-8.226732285	5.552446949	-1.362643735
H	-7.813867031	4.814862189	0.996949236
H	-7.577376343	3.445993599	-0.108923816

H	-2.295295173	6.250998807	-0.211133130
H	-2.501079135	7.966017979	0.224895425
H	-1.899337762	6.797086867	1.437030144
H	-11.065192640	-2.046719087	-1.432259484
H	-10.427145057	-3.689074512	-1.680815970
H	-10.684874644	-3.047282836	-0.028731107
H	-4.211173418	7.216593772	1.644362627
H	-4.307894335	3.654374212	-0.016836847
H	-5.455865116	5.048153228	0.951572419
H	-6.103527215	2.594779608	1.922127357
H	-6.726590298	1.899820647	3.368949725
H	-6.117462145	1.204181095	-0.038284716
H	-7.398767485	0.014477200	-0.147272365
H	-8.421832952	-0.686396323	1.595980834
H	-1.146082487	3.673404066	0.550039390
H	-6.797089725	-2.125071743	-1.812707874
H	1.914138585	5.036257176	1.589456508
H	-3.926462775	-0.198009716	-1.020721672
H	-2.153785567	-3.802805033	-2.346444906
H	3.051394856	-3.009374515	-0.299459791
H	4.082438357	-4.301470737	0.196565315
H	1.435136812	-2.304243873	1.286377022
H	0.400214330	-3.657575226	1.793763795
H	3.138035226	-5.921004986	1.574098932
H	8.564247408	2.219928495	0.429919489
H	7.106247139	2.326021331	-0.541628710
H	4.349638736	-1.142335991	-2.190420714

Lowest Energy Frequencies (in cm^{-1}): –33.6721, –21.2364, 2.1490, 8.1136, 10.7349, 17.2742.

Sum of electronic and thermal Free Energies (in hartrees): –3990.977882

Table 6.4.7. Optimized coordinates of Ce^{III}-PQQ^{0} MDH no H-bonding residues (ε = 78).

C	-2.748436335	2.570013562	3.509698390
C	-2.355258919	1.736415253	2.278336042
O	-3.292027266	1.343044598	1.496612301
O	-1.152190330	1.433784716	2.064209104
C	-5.886975396	0.884066812	-2.586131905
C	-4.956742473	1.145328578	-1.430938616
O	-3.735008177	0.905951350	-1.568004614
N	-5.463301115	1.618386453	-0.290699819
C	-5.911337552	-2.674854958	0.668746801
C	-4.468283032	-2.303890922	0.977454420
O	-3.986207538	-1.332358715	0.304141887
O	-3.835377856	-2.956545496	1.847661180
C	-1.714214378	-1.931663877	-4.309491106
C	-1.659427631	-1.368443714	-2.879535902
O	-2.195938181	-2.032911450	-1.940294250
O	-1.119253507	-0.236721636	-2.663358577
Ce	-1.965978265	-0.117661480	-0.189197072
N	5.581069194	-0.203695030	-0.056532240
C	6.205506709	-1.427101160	-0.030116487
C	7.664248832	-1.575561128	0.033376956
O	8.290118141	-0.379966582	0.055518522
O	8.239110588	-2.647237854	0.061736658

C	5.237269033	-2.417061800	-0.077135419
C	3.992691901	-1.756622193	-0.135174731
C	4.236766811	-0.359002420	-0.119261661
C	2.669168515	-2.328242373	-0.209200442
O	2.396159775	-3.519628608	-0.229648894
C	1.535583353	-1.286813789	-0.263417357
O	0.376302756	-1.662231857	-0.305523440
C	1.866594793	0.180782034	-0.257512846
N	0.786997913	0.947178200	-0.341123329
C	0.932709303	2.272253293	-0.348059082
C	-0.335331744	3.039405784	-0.514124999
O	-1.411370858	2.502774814	-0.728369884
O	-0.170175692	4.357995741	-0.432326335
C	2.180888957	2.874181888	-0.237120963
C	3.341550361	2.095041394	-0.140973165
C	4.629608061	2.864786394	-0.018470471
O	4.414915036	4.177615039	0.117332553
O	5.763646140	2.412212907	-0.037219944
C	3.208044678	0.674432144	-0.170907047
O	-1.597415259	-1.607950993	1.820363683
C	-0.675162747	-1.784503817	2.898380693
C	-1.341864263	-1.594732368	4.255885948
H	-5.458650441	1.311569071	-3.496707898
H	-5.959331918	-0.199577348	-2.730863057
H	-6.891096476	1.286744054	-2.431706828
H	-6.547568100	-1.786948039	0.746994558
H	-5.982452307	-3.032977371	-0.364834481

H	-6.276865308	-3.451384068	1.344196590
H	-3.382211161	3.409220156	3.205493620
H	-3.334871959	1.946840649	4.194537641
H	-1.862624244	2.941308483	4.028981443
H	-1.748066153	-0.581894776	4.343394931
H	-2.160125555	-2.310570345	4.394789679
H	-0.614970423	-1.748515129	5.062002575
H	0.113934559	-1.042135755	2.754981707
H	-0.218535089	-2.781832383	2.827984423
H	-2.676379015	-1.659329680	-4.759915186
H	-0.914605335	-1.512530900	-4.925241472
H	-1.646963639	-3.022510589	-4.290077789
H	5.287087917	4.614556905	0.179756111
H	2.255252913	3.951747304	-0.230119926
H	9.251517207	-0.547361044	0.095670167
H	-1.037352644	4.788579294	-0.569113944
H	6.029356832	0.716275544	-0.044043322
H	5.409656988	-3.482978236	-0.072474448
H	-6.455603603	1.774544648	-0.186444956
H	-4.848936499	1.690450038	0.526507059
H	-2.404102292	-2.211895563	1.919688755

Lowest Energy Frequencies (in cm^{-1}): –16.8531, 2.2547, 14.0802, 20.1486, 20.7053, 28.9493.

Sum of electronic and thermal Free Energies (in hartrees): –2773.212782

Table 6.4.8. Optimized coordinates of Ce^{IV}-PQQ^{0} MDH no H-bonding residues (ε = 78).

C	-3.299494333	1.336593969	4.072087348
C	-2.851706291	1.011943949	2.644640244
O	-3.674653353	0.509549901	1.805187176
O	-1.647395204	1.198559973	2.277949214
C	-5.444707467	1.064209929	-2.649170160
C	-4.938276452	0.994260925	-1.236924054
O	-3.702667361	1.168260951	-1.022210041
N	-5.768299513	0.757381900	-0.230972978
C	-4.949620414	-3.265871400	-0.583770005
C	-3.672139322	-2.817286354	0.086427047
O	-3.190785292	-1.668386263	-0.330263985
O	-3.119823274	-3.484780397	0.969766115
C	-0.614621113	-0.241948128	-4.458631299
C	-1.679671190	-0.390842149	-3.359202217
O	-2.799312272	-0.814148194	-3.624885238
O	-1.307984165	-0.042619119	-2.130392123
Ce	-1.936668217	0.102306886	0.020731041
N	5.429072343	-0.229035069	-0.068954965
C	6.014860392	-1.461922161	-0.205293976
C	7.470473542	-1.661768161	-0.179275974
O	8.132808562	-0.499358065	-0.011364961
O	8.007505581	-2.746214235	-0.296193983
C	5.016603342	-2.411665240	-0.358956987
C	3.792783241	-1.715307198	-0.308589984
C	4.079324249	-0.336410091	-0.126775970
C	2.451745141	-2.241987254	-0.401108991

O	2.136398131	-3.410644342	-0.562990003
C	1.354146048	-1.173811179	-0.257417980
O	0.177922961	-1.503657217	-0.297334983
C	1.726367060	0.267310933	-0.085073967
N	0.665492975	1.064406984	-0.026936962
C	0.846155977	2.384359086	0.061509045
C	-0.413266128	3.170983135	0.024182042
O	-1.505029204	2.631374083	-0.146141971
O	-0.251190128	4.473424238	0.162384052
C	2.115551066	2.946602139	0.129384050
C	3.256002160	2.134820093	0.093288047
C	4.573156258	2.861688156	0.184955054
O	4.410967230	4.187000257	0.158621052
O	5.680252357	2.358871131	0.285060062
C	3.082994162	0.722167980	-0.031537963
O	-1.497247166	-1.572695236	1.829346181
C	-0.494083087	-1.785693244	2.840430254
C	-1.090153129	-2.410295295	4.094315354
H	-5.239295485	2.063676006	-3.046304192
H	-4.866819441	0.346395877	-3.239437208
H	-6.513517555	0.855413901	-2.728542170
H	-4.797038404	-3.323418405	-1.666511086
H	-5.264904431	-4.236185478	-0.197786975
H	-5.731854494	-2.520267350	-0.405067991
H	-4.305243411	1.764051990	4.059584351
H	-3.334059323	0.403698896	4.646320394
H	-2.595109285	2.021880026	4.546547389

H	-1.866288193	-1.767672255	4.522081387
H	-1.530965149	-3.389634375	3.876405338
H	-0.305843065	-2.552384303	4.846216412
H	-0.074959064	-0.800300165	3.053029272
H	0.299470980	-2.421748284	2.429370225
H	-0.274603095	0.797862954	-4.514249305
H	0.257951961	-0.859452169	-4.219491280
H	-1.036786138	-0.548119154	-5.416326368
H	5.294815312	4.597951297	0.236011058
H	2.220138065	4.019357222	0.205708056
H	9.089283634	-0.697581072	-0.003111960
H	-1.122413198	4.916752263	0.110174048
H	5.906179397	0.664776003	0.076635045
H	5.157316362	-3.474406321	-0.487565998
H	-6.759676576	0.626216879	-0.378599989
H	-5.387265488	0.697122899	0.713456093
H	-1.968299194	-2.424157305	1.597883163

Lowest Energy Frequencies (in cm^{-1}): 19.3514, 21.1560, 24.7997, 31.3100, 35.3041, 36.7100.

Sum of electronic and thermal Free Energies (in hartrees): –2773.013880

Table 6.4.9. Optimized coordinates of $[Ce^{III}(HOPO\text{-}3)_2]^-$.

Ce	-0.046722029	0.698009356	0.056594726
O	0.544120902	2.563297552	1.703488310
O	2.228902616	1.599803113	-0.121404567
O	6.284478211	2.856197313	-0.012602304
O	5.092392240	-1.463948682	-1.043868430

O	3.039019691	-4.955146728	1.833968332
O	1.349569147	-1.161833670	0.922182973
O	-0.886192575	-0.430641512	2.169255006
O	0.859955327	-0.302007798	-2.094079826
O	-1.341440418	-1.179523441	-0.887329057
O	-3.080712122	-4.829127596	-2.183989666
O	-4.669414562	-1.594296458	1.309337388
O	-6.422037572	2.801512337	-0.256026322
O	-2.377878448	1.524391630	0.077480833
O	-0.555007115	2.667022891	-1.493697360
N	2.134008573	3.975368363	2.555091410
N	4.766564229	1.455531181	-0.993210228
N	3.189240354	-3.096544931	0.508591771
N	-0.890130596	-2.322730960	3.458797439
N	0.942042609	-2.128248489	-3.471695590
N	-3.241812769	-3.071992519	-0.731315735
N	-5.023459288	1.224171935	0.599270707
N	-2.063817243	4.193406879	-2.289667431
C	1.141752880	4.480266796	3.512477142
C	1.730633409	3.009981333	1.677528906
C	2.700069370	2.489246356	0.703079154
C	4.020519285	2.956948168	0.753153716
C	4.359403728	3.961574173	1.704496943
C	3.434186273	4.454688670	2.570574025
C	5.122366559	2.428551747	-0.112800182
C	5.729865105	0.734156549	-1.801659961
C	6.194483894	-0.572865773	-1.165536704

C	5.460035827	-2.683298182	-0.409602213
C	4.251477182	-3.605376341	-0.338302416
C	2.623877604	-3.831039994	1.504951462
C	1.437727002	-3.216862321	2.181653517
C	0.891868117	-1.974719860	1.825377320
C	-0.338927838	-1.527870748	2.496326234
C	-2.152213662	-1.879683897	4.065993555
C	-0.321854037	-3.532941310	3.823809496
C	0.807354389	-3.975997153	3.209251699
C	2.196680421	-1.614586394	-4.036981851
C	0.396719675	-3.319492640	-3.925024159
C	-0.748170353	-3.806257163	-3.374763240
C	-1.411826855	-3.120084857	-2.316840535
C	-0.870343537	-1.914553391	-1.849834670
C	0.354274412	-1.398955836	-2.478661858
C	-2.644779757	-3.750936111	-1.746365642
C	-4.393267913	-3.580013976	-0.010672479
C	-5.345162664	-2.467167652	0.403757325
C	-5.274945024	2.340508855	-0.129016158
C	-4.097721806	2.971400110	-0.804033590
C	-2.783172630	2.499696035	-0.682259914
C	-1.737430088	3.123294999	-1.506386707
C	-0.993205566	4.800370517	-3.090265465
C	-3.358744812	4.681210505	-2.360658898
C	-4.354781873	4.088767814	-1.649783307
C	-5.526165679	-0.705941225	2.023983463
C	-6.093077446	0.433880871	1.180837113

H	-4.910606430	-0.297638634	2.831823842
H	-6.359002402	-1.265395218	2.474873563
H	-6.717460508	1.063521369	1.827045509
H	-6.755252760	0.045095894	0.394777350
H	0.276052094	4.873923619	2.975546229
H	0.808591933	3.671083407	4.166989531
H	1.598643665	5.270599463	4.107187469
H	3.643751047	5.219665592	3.306259509
H	5.378625452	4.327013503	1.729975361
H	3.796972933	1.142627584	-0.947937151
H	6.600603778	1.377349756	-1.952071630
H	5.284099383	0.524026348	-2.780488040
H	6.628167510	-0.369499001	-0.174031810
H	6.981256584	-1.026055588	-1.790753570
H	5.845290040	-2.481931427	0.602318139
H	6.259284135	-3.180880983	-0.982658444
H	4.560146827	-4.570653519	0.069166605
H	3.875196994	-3.774023315	-1.357336119
H	2.751575473	-2.197504757	0.306332869
H	1.239838979	-4.929106191	3.487676541
H	-0.837969065	-4.077429022	4.603212705
H	-2.416222520	-2.568798921	4.867913351
H	-2.941407079	-1.871176753	3.309049872
H	-2.034982338	-0.871671999	4.468502688
H	2.036253300	-0.617891232	-4.454063896
H	2.958140711	-1.549062149	-3.254696198
H	2.531372198	-2.292590183	-4.821714278

H	0.939740804	-3.811187608	-4.721066241
H	-1.169487324	-4.738014905	-3.731843396
H	-2.773025080	-2.222038447	-0.416015076
H	-4.080108405	-4.130927202	0.888715967
H	-4.918999964	-4.283851045	-0.661198056
H	-6.223091110	-2.910708914	0.897121202
H	-5.690484157	-1.915764646	-0.481927845
H	-4.062014592	0.884117989	0.608200796
H	-5.369766126	4.459924847	-1.720545523
H	-3.505212496	5.533745190	-3.010295442
H	-1.387684244	5.682838710	-3.593192426
H	-0.162649739	5.084377956	-2.440837126
H	-0.627815401	4.085633894	-3.832076589

Lowest Energy Frequencies (in cm^{-1}): 12.0697, 13.0152, 16.1095, 19.5993, 22.1439, 27.4794.

Sum of electronic and thermal Free Energies (in hartrees): –3362.128213

Table 6.4.10. Optimized coordinates of $Ce^{IV}(HOPO\text{-}3)_2$.

Ce	-0.039885114	0.629405436	0.036339841
O	0.339391959	2.424206879	1.650707414
O	2.119688814	1.474016522	-0.007694377
O	6.093602549	3.004866210	0.117148401
O	5.082480750	-1.469995326	-0.902258486
O	2.917053262	-4.950414863	1.867621587
O	1.238898525	-1.166938431	0.840045483
O	-0.947785092	-0.386560932	2.037396217
O	0.922192625	-0.286292852	-1.995177636

O	-1.266813456	-1.145052829	-0.861571281
O	-2.976662651	-4.823829034	-2.163451249
O	-4.691685082	-1.550245262	1.223567260
O	-6.213403886	2.923584691	-0.422911925
O	-2.222749846	1.459944710	0.002641275
O	-0.325966926	2.562046683	-1.415798876
N	1.805027279	3.969009092	2.519765664
N	4.713416672	1.429119971	-0.801648794
N	3.110344429	-3.120628697	0.508673629
N	-1.019786547	-2.256461337	3.374414332
N	1.058952701	-2.112641533	-3.384083803
N	-3.176894733	-3.068418927	-0.713851277
N	-4.932497947	1.239286052	0.411834392
N	-1.731248355	4.163519440	-2.274282365
C	0.743082689	4.462291523	3.409810506
C	1.502570435	2.948956322	1.672034982
C	2.528931591	2.440301916	0.778890765
C	3.816331158	2.976620687	0.835469735
C	4.059547186	4.040812952	1.745191964
C	3.072204423	4.517495606	2.555609178
C	4.976485912	2.477783493	0.018790135
C	5.735874389	0.748786749	-1.574820073
C	6.181431102	-0.567011597	-0.945263430
C	5.427052685	-2.699775164	-0.274307947
C	4.220474819	-3.627354718	-0.278629413
C	2.519858164	-3.835137943	1.500815625
C	1.314093887	-3.204768758	2.140797668

C	0.772782710	-1.974548327	1.760845985
C	-0.440305435	-1.499925517	2.404880574
C	-2.282239254	-1.778339839	3.960314789
C	-0.470849402	-3.461803044	3.764725062
C	0.663644802	-3.933019266	3.173133204
C	2.324515838	-1.591850802	-3.925213473
C	0.527453673	-3.304092079	-3.837841557
C	-0.627778714	-3.797398381	-3.306673215
C	-1.314353824	-3.111788892	-2.268134378
C	-0.779216939	-1.906315255	-1.811285689
C	0.442808206	-1.394952467	-2.407067431
C	-2.560822844	-3.745815051	-1.715156562
C	-4.350311204	-3.571822476	-0.022312304
C	-5.328076748	-2.458168622	0.322970374
C	-5.103150884	2.391633241	-0.278253069
C	-3.872557929	2.988246558	-0.899572732
C	-2.583015850	2.475816435	-0.746547843
C	-1.491464369	3.074356084	-1.495354500
C	-0.598969061	4.745863276	-3.010652785
C	-3.000455947	4.694576628	-2.389100413
C	-4.050517158	4.127405120	-1.730895082
C	-5.576685860	-0.629001557	1.859008539
C	-6.060297561	0.495830584	0.947516254
H	-5.007864065	-0.208508901	2.694125477
H	-6.447924976	-1.160907329	2.267378586
H	-6.701353782	1.168122957	1.529210847
H	-6.680971938	0.099814779	0.132051454

H	-0.103714687	4.808779768	2.814052430
H	0.409004730	3.655995997	4.066214418
H	1.139458283	5.284051095	4.004417834
H	3.213970987	5.325619672	3.260382356
H	5.053026977	4.468952600	1.788833905
H	3.771200202	1.046941589	-0.774507960
H	6.598718849	1.413934187	-1.653211883
H	5.353284847	0.559170111	-2.584251955
H	6.560156962	-0.384371696	0.072253083
H	7.003329837	-0.997262165	-1.539913764
H	5.761654529	-2.516010823	0.758451960
H	6.254447455	-3.183595186	-0.817605092
H	4.507069412	-4.593619478	0.141677629
H	3.898345927	-3.790370722	-1.315953501
H	2.698411564	-2.219594685	0.276785430
H	1.080827036	-4.884416527	3.478281899
H	-1.001335808	-3.987503646	4.547083404
H	-2.552157677	-2.432579304	4.788386747
H	-3.065573144	-1.796815417	3.197905007
H	-2.152969840	-0.756663060	4.321027217
H	2.166279410	-0.589531613	-4.327738032
H	3.072787370	-1.542687685	-3.129689096
H	2.666298903	-2.258632022	-4.715780179
H	1.085968607	-3.799494235	-4.620399964
H	-1.034973394	-4.733459789	-3.667822601
H	-2.733883796	-2.211977866	-0.388026533
H	-4.060547644	-4.092032473	0.901790577

H	-4.841112074	-4.299409480	-0.673243988
H	-6.217455849	-2.895866386	0.799854333
H	-5.647215503	-1.939546449	-0.591534067
H	-4.000047444	0.833836524	0.441730614
H	-5.046195648	4.538907435	-1.838018009
H	-3.091477836	5.561941342	-3.028838734
H	-0.940546963	5.643459403	-3.524171589
H	0.200463799	4.998388701	-2.311689942
H	-0.219622287	4.023923307	-3.737412727

Lowest Energy Frequencies (in cm^{-1}): 12.2784, 14.9046, 17.3091, 19.6131, 21.8294, 23.4487.

Sum of electronic and thermal Free Energies (in hartrees): –3361.967827

Table 6.4.11. Optimized coordinates of $Na_4[Ce^{III}(o\text{-}BQ)_4]^{-}\cdot 14H_2O$.

Ce	-0.090787583	-0.010878116	-0.163048112
Na	-1.672926122	3.125094625	-2.165253558
Na	1.974624333	1.921254262	2.112571317
Na	-2.796688272	-2.049515323	0.031200295
Na	3.179798874	-0.648116435	0.518192868
O	-1.073579197	1.769361373	1.428756289
O	-2.579800532	0.376569178	-0.371637180
O	-0.980014193	-1.679368845	1.412220637
O	1.674237323	-1.496837672	-1.161512718
O	0.063600693	1.670159345	-1.956538854
O	1.342895322	-0.381782347	1.875825962
O	-0.976185860	-1.837053632	-1.663597304
O	2.041964974	1.364658054	-0.126928691
O	-3.243595350	1.512017598	-2.725721978

O	-3.635291974	-2.162223129	-2.292205339
O	5.300126452	0.428962877	1.083644127
O	0.408291745	3.948178162	1.367354916
O	-4.691749076	-1.673164120	1.407893904
O	3.862387444	-2.952962971	0.879767861
O	-2.168304127	5.354827452	-2.904975977
O	4.142567477	1.868691732	3.168631826
O	-4.343819776	-4.929751465	-2.072844404
O	5.788024701	-1.775385368	-0.656635140
O	-1.700018616	4.713819461	-0.276230885
O	0.275828602	1.812256952	3.811298169
O	-2.539420243	-4.455499417	0.016601226
O	3.921846540	-0.543563483	-2.265547728
C	-2.403997546	1.967900893	1.406290471
C	-3.191572607	1.215476955	0.468251230
C	-4.585950610	1.415056054	0.453043025
C	-5.210867723	2.337614774	1.312643058
C	-4.442312764	3.078043539	2.204998166
C	-3.047416226	2.892048473	2.244470752
C	-0.406043501	-1.836868308	2.598584355
C	1.270274735	-2.652415128	-1.712987025
C	1.250279191	2.233940241	-2.203797236
C	0.839490127	-1.151153243	2.848355329
C	-0.134877998	-2.825354476	-1.978110489
C	2.295831177	2.084591017	-1.221534743
C	-0.945179376	-2.634226327	3.622642807
C	2.158589486	-3.679346240	-2.065369018

C	1.525648743	2.959931855	-3.373973633
C	1.459062084	-1.305278503	4.100784599
C	-0.555812772	-4.032712005	-2.566418253
C	3.540756433	2.691399600	-1.470576405
C	-0.305232575	-2.774257073	4.866961176
C	1.709481575	-4.879913276	-2.646005691
C	2.780847404	3.553774034	-3.599629270
C	0.895443080	-2.113179034	5.108971607
C	0.353350383	-5.054977292	-2.896561064
C	3.788134594	3.423358407	-2.648535476
H	-5.176487961	0.865687105	-0.280037270
H	-6.289239854	2.468865639	1.269157002
H	-4.908117736	3.796329496	2.874852922
H	-2.442390584	3.459630343	2.949658143
H	-1.885097772	-3.150671111	3.429589395
H	3.224299971	-3.521184632	-1.905420723
H	0.738887626	3.044716030	-4.123583772
H	2.409314682	-0.799425541	4.271413458
H	-1.610245940	-4.147416016	-2.809521143
H	4.315737869	2.605246565	-0.709804479
H	-0.754585738	-3.399936461	5.635518675
H	2.426665240	-5.655834795	-2.903086730
H	2.957930639	4.106679797	-4.519496759
H	1.402524554	-2.214108440	6.065976215
H	-0.012529785	-5.971861989	-3.353024607
H	4.763118211	3.879017796	-2.805020454
H	-2.648068202	-2.065755757	-2.272367156

H	-3.813149115	-3.119366901	-2.379455951
H	-4.185410778	-5.651422145	-2.703299865
H	-5.285286671	-4.994303940	-1.841784481
H	-1.703849346	-4.463074298	-0.487030629
H	-3.204032085	-4.761071581	-0.639654541
H	-4.742923818	-0.698633790	1.342243582
H	-4.418507996	-1.838385777	2.325220617
H	-0.343692149	1.724180161	3.039458300
H	0.473253389	0.885989408	4.050002877
H	-0.184653923	3.131861977	1.409736224
H	0.266796163	4.404059573	2.214146514
H	4.576855064	2.731127513	3.284481146
H	4.157093900	1.459428212	4.050384795
H	-0.853360609	4.617746664	0.225312339
H	-2.369184790	4.327920095	0.319542077
H	-2.089573549	5.477614830	-1.933953389
H	-3.117492073	5.444668731	-3.088056404
H	-4.150031940	1.821444570	-2.571475753
H	-3.029407430	0.966098080	-1.914394834
H	4.623541737	-2.710191335	0.289741247
H	3.206231626	-3.344065948	0.277052016
H	5.200263694	-1.319406758	-1.314308775
H	5.934153717	-1.091790536	0.026722411
H	5.434192133	1.158822609	0.457360306
H	5.008172448	0.874570626	1.914198414
H	3.843802511	0.424909739	-2.161528970
H	3.039777023	-0.899673080	-1.948431028

Lowest Energy Frequencies (in cm^{-1}): 22.3635, 23.7255, 26.4210, 30.7255, 33.6119, 35.3023.

Sum of electronic and thermal Free Energies (in hartrees): –3720.614906

Table 6.4.12. Optimized coordinates of $Na_4[Ce^{IV}(o\text{-}BQ)_4]\cdot 14H_2O$.

Ce	0.113459449	0.010346036	-0.132251554
Na	1.558528738	-3.251142746	-2.059669472
Na	-2.297684027	-1.763682576	2.079578989
Na	3.019867311	1.842654962	0.109570863
Na	-3.177506155	0.882516587	0.435587948
O	0.814437172	-1.716124718	1.470701259
O	2.447726357	-0.540705486	-0.292061919
O	1.059780541	1.540330502	1.341938591
O	-1.475306868	1.482471981	-1.172089246
O	-0.013846531	-1.532974557	-1.874585221
O	-1.306000312	0.471291304	1.757698905
O	1.145320741	1.596588224	-1.602813216
O	-1.998638164	-1.183730791	-0.165907278
O	3.179423671	-1.712085784	-2.659698793
O	3.891819880	1.722735428	-2.155365256
O	-5.339735846	-0.086662003	0.918857268
O	-0.806609545	-3.845642286	1.377221447
O	4.810154136	1.350081861	1.560652046
O	-3.768913754	3.174527025	0.828208094
O	1.648247867	-5.514474248	-2.804870993
O	-4.458066577	-1.570587613	3.097762414
O	4.763668704	4.432837062	-2.053532181

O	-5.689773684	2.156926716	-0.810928028
O	1.304976523	-4.808514332	-0.174587786
O	-0.646922388	-1.745940295	3.814600256
O	2.918327241	4.225942845	0.037266087
O	-3.835695399	0.803893987	-2.364751534
C	2.124409430	-2.039557049	1.518608220
C	2.991347388	-1.401036016	0.582261390
C	4.361603936	-1.711827201	0.599354032
C	4.879427259	-2.644957375	1.515029537
C	4.028556884	-3.273951905	2.420666497
C	2.655045869	-2.972449712	2.419370066
C	0.478451964	1.816285478	2.514281509
C	-0.991292416	2.610468555	-1.729073707
C	-1.213249574	-2.032472016	-2.223104622
C	-0.811701130	1.242395540	2.736614944
C	0.415846725	2.660854542	-1.969301498
C	-2.275900187	-1.867918191	-1.281528711
C	1.052547720	2.620487923	3.506387720
C	-1.794336010	3.695378839	-2.100700881
C	-1.458325898	-2.693742691	-3.432840057
C	-1.477756144	1.495946903	3.945298750
C	0.957275256	3.805156321	-2.576914415
C	-3.538775156	-2.403962875	-1.581466137
C	0.373116488	2.863527174	4.711740032
C	-1.232076372	4.836764782	-2.696518845
C	-2.730506778	-3.217317773	-3.718584542
C	-0.885625345	2.306200278	4.931297657

C	0.138664836	4.889658493	-2.935864228
C	-3.765016734	-3.078567716	-2.795072652
H	5.014254383	-1.242550748	-0.135252724
H	5.942142177	-2.871897610	1.507306672
H	4.417925303	-3.996047647	3.133161006
H	1.989618422	-3.454419857	3.132486083
H	2.035109060	3.053057970	3.328036429
H	-2.869158631	3.634979315	-1.942650788
H	-0.649766986	-2.785493681	-4.155920995
H	-2.469869229	1.074200245	4.098270102
H	2.021285024	3.827706834	-2.798824365
H	-4.337433919	-2.304251667	-0.849382868
H	0.835534628	3.489070976	5.471293120
H	-1.873513621	5.668651257	-2.975483892
H	-2.902350200	-3.726090916	-4.663570572
H	-1.416473534	2.494368659	5.861120272
H	0.583069427	5.763318738	-3.405728634
H	-4.750496244	-3.485395316	-3.006418256
H	2.909769815	1.661957204	-2.216975400
H	4.116350379	2.662132473	-2.312222257
H	4.707002668	5.133139989	-2.724411772
H	5.699510228	4.404955597	-1.793202449
H	2.081345044	4.334979521	-0.449886448
H	3.604314340	4.453753883	-0.629437557
H	4.808781196	0.373544086	1.545977876
H	4.566923492	1.578779605	2.472720483
H	0.011185695	-1.650869649	3.081408974

H	-0.779500493	-0.829302438	4.119518103
H	-0.182721374	-3.063826404	1.424352947
H	-0.715676298	-4.292690411	2.235859371
H	-4.958265953	-2.398127330	3.201043991
H	-4.478324684	-1.151743720	3.974859125
H	0.457287533	-4.627968919	0.299669818
H	1.995134000	-4.542727878	0.459000619
H	1.574469525	-5.644275606	-1.834926815
H	2.561687689	-5.764522828	-3.019037799
H	4.081541349	-2.027872476	-2.493116769
H	2.970877071	-1.131436771	-1.881206049
H	-4.519899822	3.009055950	0.199025025
H	-3.108261936	3.658641931	0.305195403
H	-5.107786996	1.676376786	-1.452637291
H	-5.904325901	1.473129690	-0.145990897
H	-5.568686817	-0.810800899	0.314087128
H	-5.159454682	-0.535357320	1.779039348
H	-3.869964299	-0.170164004	-2.310652230
H	-2.924481858	1.034490456	-2.041016191

Lowest Energy Frequencies (in cm^{-1}): 8.1992, 23.3869, 26.1132, 29.4310, 31.4695, 36.8316.

Sum of electronic and thermal Free Energies (in hartrees): –3720.484424

Table 6.4.13. Optimized coordinates of $[Ce^{III}(EDTA)(H_2O)_3]^-$.

Ce	-0.032084616	-0.301752812	-0.843261319
O	-0.197668144	-1.740110143	1.085462349
O	-2.328089721	-0.613805762	-1.376897490

O	2.437717102	-0.682249796	-0.423107357
O	0.058763969	2.028781957	-1.200150458
O	-1.064186132	-2.403325751	3.052073652
O	-4.482913127	0.041600223	-1.368393109
O	4.378580995	-0.167047434	0.598692407
O	0.432764524	4.176126940	-0.638731360
O	0.224306163	-2.679452254	-1.962484245
O	1.723932157	0.124432861	-2.879291428
O	1.772519503	-3.395302853	0.102504271
N	-1.842381219	0.535201249	1.045987509
N	1.130874933	1.161733549	1.235384143
C	-1.265686202	1.631127459	1.857530193
H	-1.271601658	2.541470864	1.252666071
H	-1.892099448	1.834197323	2.741218204
C	0.153783135	1.330232841	2.339187171
H	0.153516812	0.412664309	2.932672125
H	0.469100675	2.140944261	3.014930595
C	-2.182352830	-0.641327815	1.879525784
H	-2.998706143	-1.182526453	1.388403131
H	-2.553082700	-0.337330414	2.867786331
C	-1.056429716	-1.675459839	2.059380304
C	-3.024297498	0.982238923	0.281822694
H	-2.809063701	1.972507497	-0.136002387
H	-3.918529763	1.081600672	0.912809535
C	-3.337655310	0.053695754	-0.912249141
C	2.332067229	0.435944196	1.699558089
H	2.001680113	-0.408712535	2.313925318

H	2.984719787	1.067646411	2.317196338
C	3.149732382	-0.160403519	0.538764396
C	1.513882927	2.469014962	0.651501788
H	2.503768329	2.361438482	0.192130330
H	1.603461734	3.243250718	1.425495117
C	0.580977563	2.965199454	-0.468320669
H	2.409743644	-0.121299117	-2.216446070
H	1.732162234	1.097438408	-2.893563809
H	2.325689728	-2.606734452	-0.084840853
H	1.095771452	-3.013473046	0.711017707
H	0.787465553	-3.147086501	-1.279429840
H	-0.612493328	-3.171635378	-1.998034288

Lowest Energy Frequencies (in cm^{-1}): 7.6132, 29.9278, 38.1768, 46.1264, 56.0503, 66.6906.

Sum of electronic and thermal Free Energies (in hartrees): –1804.244422

Table 6.4.14. Optimized coordinates of $[Ce^{IV}(EDTA)(H_2O)_3]$.

Ce	0.010192470	-0.224834708	-0.794807083
O	0.705853234	-1.380915734	1.028079188
O	-1.896093143	-1.303252855	-1.175634321
O	2.129588493	0.532091296	-0.774725531
O	-0.980904968	1.723978534	-1.100211095
O	0.514496124	-2.376469005	3.029806630
O	-4.058553381	-1.866605604	-0.939102860
O	4.001096808	0.448213082	0.453377087
O	-1.387356858	3.922088332	-0.874339248
O	1.430581146	-2.128031833	-1.864915062

O	0.548660751	-0.021271663	-3.293582142
O	3.255305778	-2.336179487	0.049697821
N	-1.757329052	-0.165209620	1.243385022
N	0.638136930	1.662575151	1.109516947
C	-1.650912640	1.115490194	1.993218129
H	-2.121807984	1.895834921	1.391724391
H	-2.215711931	1.055125914	2.934853261
C	-0.209471804	1.490575114	2.320027769
H	0.242065072	0.715114640	2.942387099
H	-0.216833728	2.410763998	2.921360141
C	-1.441716252	-1.335345222	2.102941116
H	-1.982817209	-2.206535892	1.717302556
H	-1.783515838	-1.179062681	3.132855041
C	0.037762956	-1.734141108	2.107651053
C	-3.100616796	-0.318089736	0.639231612
H	-3.427375593	0.657016354	0.263037610
H	-3.848052630	-0.661604602	1.363817625
C	-3.067608878	-1.261919000	-0.567152945
C	2.076470554	1.502330146	1.423791437
H	2.189711982	0.872620756	2.308822716
H	2.562870003	2.458825093	1.653829978
C	2.830920981	0.793634304	0.296371104
C	0.384323798	2.957185451	0.434004146
H	1.273643446	3.221525246	-0.147887048
H	0.214819306	3.764312135	1.156991232
C	-0.770181724	2.915012474	-0.570602710
H	1.002717755	0.783428290	-3.597197727

H	1.199718522	-0.748975745	-3.358865496
H	3.746888667	-1.486706209	0.057570630
H	2.544783587	-2.188958566	0.708599584
H	2.215748259	-2.261262641	-1.242973185
H	1.011116898	-3.000162899	-1.962219339

Lowest Energy Frequencies (in cm^{-1}): 27.5545, 38.7630, 49.0029, 51.7020, 66.2766, 78.3043.

Sum of electronic and thermal Free Energies (in hartrees): –1804.069393

Table 6.4.15. Optimized coordinates of $[NH_4]_2[Ce^{III}(NO_3)_6]^-$.

Ce	-0.000646677	-0.000899339	-0.000705402
O	-0.721071117	0.678607437	2.462049487
O	-2.070848924	-0.738512424	1.523360687
O	-2.523332181	0.038575617	3.518439843
N	-1.786051793	-0.000212086	2.537658311
O	2.074254629	0.951825493	1.402183563
O	0.716484071	2.470183020	0.651666537
O	2.527721156	3.069299690	1.717832527
N	1.787373519	2.198831511	1.268826726
O	2.077876816	-1.698949615	0.120531984
O	0.716585679	-1.790274828	1.808708226
O	2.519170842	-3.025845506	1.803940667
N	1.786386635	-2.199120288	1.268417794
O	0.723502793	-0.677595761	-2.462626083
O	2.073281965	0.737306355	-1.520897981
O	-2.075685117	-0.950992462	-1.401612094
O	-0.716989817	-2.470029321	-0.654144435

O	-2.077640279	1.699506039	-0.120289779
O	-0.717185607	1.792066612	-1.809443957
N	1.789185411	0.000319760	-2.536272189
N	-1.788512382	-2.198238763	-1.270059318
N	-1.787201854	2.199495120	-1.268632735
O	2.527721759	-0.038228186	-3.516291055
O	-2.528942825	-3.068243145	-1.719599085
O	-2.521513991	3.024750125	-1.804191566
N	4.272341191	-0.000582006	0.001768358
N	-4.272093462	0.002123910	0.002285383
H	5.293493269	-0.001742011	0.005693406
H	3.877738087	0.430043296	-0.850909931
H	3.872903264	-0.952624339	0.053648144
H	3.871364729	0.522652454	0.798260292
H	-3.872349300	-0.520979913	-0.794904573
H	-3.877325080	-0.428909271	0.854563513
H	-5.293265087	0.003791019	-0.000619198
H	-3.872162226	0.954017128	-0.049704643

Lowest Energy Frequencies (in cm^{-1}): 37.5895, 38.8348, 40.5153, 44.2656, 45.1746, 49.3895.

Sum of electronic and thermal Free Energies (in hartrees): –2271.657404

Table 6.4.16. Optimized coordinates of $[NH_4]_2[Ce^{IV}(NO_3)_6]$.

Ce	-0.000044738	-0.000839092	0.000314302
O	0.645386684	-0.698333540	2.335874654
O	1.981950924	0.735622534	1.432191041
O	2.383628011	0.008355982	3.458263214

N	1.694648869	0.012021823	2.456973661
O	-1.989834168	-0.866258823	1.347355302
O	-0.656102153	-2.372945801	0.566150800
O	-2.408576734	-2.982883965	1.722895483
N	-1.709168567	-2.118141627	1.232917288
O	-1.979420478	1.608888600	0.066924071
O	-0.654710242	1.674084549	1.769662369
O	-2.397107373	2.994270833	1.710342563
N	-1.701617853	2.132541074	1.209279268
O	-0.643993784	0.697748778	-2.336697022
O	-1.981381530	-0.735651988	-1.433271467
O	1.989226032	0.866731203	-1.348812672
O	0.657321208	2.373326264	-0.563994138
O	1.982211708	-1.610233165	-0.068991482
O	0.652986199	-1.676928777	-1.768230659
N	-1.694999486	-0.009709746	-2.457157952
N	1.710408630	2.119156779	-1.230114664
N	1.701701897	-2.134523087	-1.210595977
O	-2.387010443	-0.001711052	-3.456242518
O	2.412064578	2.984020178	-1.716673507
O	2.396542577	-2.995683779	-1.713362016
N	-4.352167674	0.007622397	-0.002432607
N	4.349693061	-0.005789113	-0.002589656
H	-5.374422832	-0.011303376	0.021241415
H	-3.983086614	-0.478428615	-0.830666911
H	-3.992105769	0.970880980	-0.026321928
H	-3.942918955	-0.450874434	0.824058763

H	3.928876517	0.458772067	-0.820164918
H	4.001975533	0.480995395	0.833852294
H	5.371422821	0.001938466	-0.045202841
H	3.977913764	-0.964906849	0.023947051

Lowest Energy Frequencies (in cm^{-1}): 46.5047, 49.7141, 54.4489, 55.1424, 59.4084, 65.2465.

Sum of electronic and thermal Free Energies (in hartrees): –2271.447697

6.5 References

[1] A. Pol, T. R. M. Barends, A. Dietl, A. F. Khadem, J. Eygensteyn, M. S. M. Jetten, H. J. M. Op den Camp, *Environ. Microbiol.* **2014**, *16*, 255-264.

[2] a) S. J. Franklin, *Curr. Opin. Chem. Biol.* **2001**, *5*, 201-208; b) S. Lim, S. J. Franklin, *Cell. Mol. Life Sci.* **2004**, *61*, 2184-2188.

[3] J. Keltjens, A. Pol, J. Reimann, H. M. Op den Camp, *Appl. Microbiol. Biotechnol.* **2014**, *98*, 6163-6183.

[4] a) B. Vlaisavljevich, P. Miró, D. Koballa, T. K. Todorova, S. R. Daly, G. S. Girolami, C. J. Cramer, L. Gagliardi, *J. Phys. Chem. C* **2012**, *116*, 23194-23200; b) K. Arumugam, U. Becker, *Minerals* **2014**, *4*, 345-387.

[5] M. Leopoldini, N. Russo, M. Toscano, *Chem. Eur. J.* **2007**, *13*, 2109-2117.

[6] a) S. Muhammad, S. Moncho, E. N. Brothers, M. Y. Darensbourg, D. J. Darensbourg, A. A. Bengali, *Inorg. Chem.* **2012**, *51*, 7362-7369; b) M. T. Olsen, B. E. Barton, T. B. Rauchfuss, *Inorg. Chem.* **2009**, *48*, 7507-7509.

[7] D. A. Atwood, *The Rare Earth Elements: Fundementals and Applications*, John Wiley & Sons, **2012**.

[8] N. A. Piro, J. R. Robinson, P. J. Walsh, E. J. Schelter, *Coord. Chem. Rev.* **2014**, *260*, 21-36.

[9] S. R. Sofen, S. R. Cooper, K. N. Raymond, *Inorg. Chem.* **1979**, *18*, 1611-1616.

[10] J. Xu, E. Radkov, M. Ziegler, K. N. Raymond, *Inorg. Chem.* **2000**, *39*, 4156-4164.

[11] A. Abbaspour, M. A. Mehrgardi, *Talanta* **2005**, *67*, 579-584.

[12] T. A. Beineke, J. Delgaudio, *Inorg. Chem.* **1968**, *7*, 715-721.

[13] The triplet diradical spin state was also calcualted but was found to be isoergonic with the singlet diradical spin state.

[14] Y.-J. Zheng, T. C. Bruice, *P. Natl. Acad. Sci.* **1997**, *94*, 11881-11886.

[15] R. Shannon, *Acta Crystallogr. Sect. A* **1976**, *32*, 751-767.

[16] a) J. R. Robinson, Z. Gordon, C. H. Booth, P. J. Carroll, P. J. Walsh, E. J. Schelter, *J. Am. Chem. Soc.* **2013**, *135*, 19016-19024; b) J. R. Robinson, P. J. Carroll, P. J. Walsh, E. J. Schelter, *Angew. Chem. Int. Ed.* **2012**, *51*, 10159-10163; c) B. D. Mahoney, N. A. Piro, P. J. Carroll, E. J. Schelter, *Inorg. Chem.* **2013**, *52*, 5970-5977.

[17] A. Sen, H. A. Stecher, A. L. Rheingold, *Inorg. Chem.* **1992**, *31*, 473-479.

[18] J. R. Robinson, C. H. Booth, P. J. Carroll, P. J. Walsh, E. J. Schelter, *Chem. Eur. J.* **2013**, *19*, 5996-6004.

[19] a) N. G. Connelly, W. E. Geiger, *Chem. Rev.* **1996**, *96*, 877-910; b) V. Nair, A. Deepthi, *Chem. Rev.* **2007**, *107*, 1862-1891.

[20] D. R. Lide, *CRC Handbook of Chemistry and Physics*, 86th ed., CRC Press, Boca Raton, Fl, **2005-2006**.

[21] I. Bertini, H. B. Gray, E. I. Stiefel, J. S. Valentine, in *Biological Inorganic Chemistry: Structure and Reactivity*, University Science Books, Sausalito, California, **2007**, pp. 229-235.

[22] Gaussian 09, Revision D.01, Frisch, M. J.; Trucks, G. W.; Schlegel, H. B.; Scuseria, G. E.; Robb, M. A.; Cheeseman, J. R.; Scalmani, G.; Barone, V.; Mennucci, B.; Petersson, G. A.; Nakatsuji, H.; Caricato, M.; Li, X.; Hratchian, H. P.; Izmaylov, A. F.; Bloino, J.; Zheng, G.; Sonnenberg, J. L.; Hada, M.; Ehara, M.; Toyota, K.; Fukuda, R.; Hasegawa, J.; Ishida, M.; Nakajima, T.; Honda, Y.; Kitao, O.; Nakai, H.; Vreven, T.; Montgomery, J. A., Jr.; Peralta, J. E.; Ogliaro, F.; Bearpark, M.; Heyd, J. J.; Brothers, E.; Kudin, K. N.; Staroverov, V. N.; Kobayashi, R.; Normand, J.; Raghavachari, K.; Rendell, A.; Burant, J. C.; Iyengar, S. S.; Tomasi, J.; Cossi, M.; Rega, N.; Millam, N. J.; Klene, M.; Knox, J. E.; Cross, J. B.; Bakken, V.; Adamo, C.; Jaramillo, J.; Gomperts, R.; Stratmann, R. E.; Yazyev, O.; Austin, A. J.; Cammi, R.; Pomelli, C.; Ochterski, J. W.; Martin, R. L.; Morokuma, K.; Zakrzewski, V. G.; Voth, G. A.; Salvador, P.; Dannenberg, J. J.; Dapprich, S.; Daniels, A. D.; Farkas, Ö.; Foresman, J. B.; Ortiz, J. V.; Cioslowski, J.; Fox, D. J. Gaussian, Inc., Wallingford CT, 2009.

[23] a) M. Dolg, H. Stoll, H. Preuss, *J. Chem. Phys.* **1989**, *90*, 1730-1734; b) X. Cao, M. Dolg, *J. Molec. Struct. (Theochem)* **2002**, *581*, 139-147.

[24] C. Lambertz, P. Chernev, K. Klingan, N. Leidel, K. G. V. Sigfridsson, T. Happe, M. Haumann, *Chem. Sci.* **2014**, *5*, 1187-1203.